ol. 162, August 1, 1984
ompiete in one issue

ISSN 0003-2670

ANALYTICA CHIMICA ACTA

International journal devoted to all branches of analytical chemistry

ELSEVIER

ANALYTICA CHIMICA ACTA

International journal devoted to all branches of analytical chemistry
Revue internationale consacrée à tous les domaines de la chimie analytique
Internationale Zeitschrift für alle Gebiete der analytischen Chemie

PUBLICATION SCHEDULE FOR 1984

	J	F	M	A	M	J	J	A	S	O	N	D
Analytica Chimica Acta	156	157/1	157/2	158/1 158/2	159	160	161	162	163	164	165	166

Scope. *Analytica Chimica Acta* publishes original papers, short communications, and reviews dealing with every aspect of modern chemical analysis, both fundamental and applied.

Submission of Papers. Manuscripts (three copies) should be submitted as designated below for rapid and efficient handling:

Papers from the Americas to: Professor Harry L. Pardue, Department of Chemistry, Purdue University, West Lafayette, IN 47907, U.S.A.

Papers from all other countries to: Dr. A. M. G. Macdonald, Department of Chemistry, The University, P.O. Box 363, Birmingham B15 2TT, England. Papers dealing particularly with computer techniques to: Professor J. T. Clerc, Universität Bern, Pharmazeutisches Institut, Baltzerstrasse 5, CH-3012 Bern, Switzerland.

Submission of an article is understood to imply that the article is original and unpublished and is not being considered for publication elsewhere. Upon acceptance of an article by the journal, authors will be asked to transfer the copyright of the article to the publisher. This transfer will ensure the widest possible dissemination of information.

Information for Authors. Papers in English, French and German are published. There are no page charges. Manuscripts should conform in layout and style to the papers published in this Volume. Authors should consult Vol. 160 for detailed information. Reprints of this information are available from the Editors or from: Elsevier Editorial Services Ltd., Mayfield House, 256 Banbury Road, Oxford OX2 7DH (Great Britain).

Reprints. Fifty reprints will be supplied free of charge. Additional reprints (minimum 100) can be ordered. An order form containing price quotations will be sent to the authors together with the proofs of their article.

Advertisements. Advertisement rates are available from the publisher.

Subscriptions. Subscriptions should be sent to: Elsevier Science Publishers B.V., Journals Department, P.O. Box 211, 1000 AE Amsterdam, The Netherlands. Tel: 5803 911, Telex: 18582.

Publication. *Analytica Chimica Acta* appears in 11 volumes in 1984. The subscription for 1984 (Vols. 156–166) is Dfl. 2145.00 plus Dfl. 231.00 (p.p.h.) (total approx. U.S. $914.00). All earlier volumes (Vols. 1–155) except Vols. 23 and 28 are available at Dfl. 215.00 (U.S. $82.70), plus Dfl. 15.00 (U.S. $6.00) p.p.h., per volume.

Our p.p.h. (postage, packing and handling) charge includes surface delivery of all issues, except to subscribers in Australia, Brazil, Canada, China, Hong Kong, India, Israel, Japan, Malaysia, New Zealand, Pakistan, Singapore, South Africa, South Korea, Taiwan and the U.S.A. who receive all issues by air delivery (S.A.L. — Surface Air Lifted) at no extra cost. For the rest of the world, airmail and S.A.L. charges are available upon request.

Claims for issues not received should be made within three months of publication of the issues. If not they cannot be honoured free of charge.

For further information, or a free sample copy of this or any other Elsevier Science Publishers journal, readers in the U.S.A. and Canada can contact the following address: Elsevier Science Publishing Co., Inc., Journal Information Center, 52 Vanderbilt Avenue, New York, NY 10017, U.S.A., Tel: (212) 867-9040.

ANALYTICA CHIMICA ACTA
VOL. 162 (1984)

ANALYTICA CHIMICA ACTA

International journal devoted to all branches of analytical chemistry

ELSEVIER Amsterdam–Oxford–New York–Tokyo

0003-2670/84/$03

Printed in The Netherlands

Analytica Chimica Acta, 162 (1984) 1—8
Elsevier Science Publishers B.V., Amsterdam — Printed in The Netherlands

THE APPLICATION OF STRONGLY REDUCING AGENTS IN FLOW INJECTION ANALYSIS
Part 4. Uranium(III)

R. C. SCHOTHORST, M. VAN SON and G. DEN BOEF*

Laboratory for Analytical Chemistry, University of Amsterdam, Nieuwe Achtergracht 166, 1018 WV Amsterdam (The Netherlands)

(Received 16th March 1984)

SUMMARY

The application of uranium(III) in acidic medium as a powerful reducing reagent in flow injection analysis is described in detail. Results of the determination of a number of organic and inorganic substances are presented. With spectrophotometric detection based on the absorption by uranium(III) at 350 nm, limits of determination were of the order of 10^{-5} mol l^{-1}. For nitrate and nitrite, similar limits of determination were achieved with amperometric detection. This limit of determination is lower than in the case of chromium(II) and vanadium(II).

Previous parts of this work [1—3] described the application of chromium(II)—EDTA and vanadium(II)—EDTA as powerful reducing agents in flow injection analysis (f.i.a.). The present paper deals with the application of trivalent uranium. The normal potential of the half-reaction $U^{4+} + e^- \rightleftharpoons U^{3+}$ is —0.61 V. This normal potential is even lower than the corresponding values for Cr^{3+}/Cr^{2+} and V^{3+}/V^{2+}. In the past, uranium(III) has been used only very occasionally for analytical purposes, probably because of its instability. An application in f.i.a., however, seems attractive because of the very short residence time of the reagent in the flow system.

Chromium(II)—EDTA can only be applied in the pH range 8—10, as at higher pH values the reaction becomes too slow and at lower pH the instability of chromium(II)—EDTA causes problems. Vanadium(II)—EDTA allows a pH range of 5—10 to be used. Both chromium(II) and vanadium(II) have been applied in acidic medium [4]. Because of the low molar absorptivity of the aqueous ions, spectrophotometric detection is not sensitive. However, amperometric detection could be applied.

Uranium(III) shows a high molar absorptivity; therefore uranium(III) seems a welcome extension to the range of reducing agents for flow analysis, as it can be applied directly in acidic solution with spectrophotometric detection.

The normal potentials for some half-reactions involving uranium are

0003-2670/84/$03.00

$UO_2^{2+} + e^- \rightleftharpoons UO_2^+$ ($E^0 = +0.05$ V)

$UO_2^{2+} + 4H^+ + 2e^- \rightleftharpoons U^{4+} + 2H_2O$ ($E^0 = +0.33$ V)

$UO_2^+ + 4H^+ + e^- \rightleftharpoons U^{4+} + 2H_2O$ ($E^0 = +0.62$ V)

$U^{4+} + e^- \rightleftharpoons U^{3+}$ ($E^0 = -0.61$ V)

Of these four oxidation states of uranium, uranium(V) in strongly acidic medium is unstable, and there is disproportionation to uranium(VI) and uranium(IV). Thus if uranium(III) is oxidized by a reducible species, the end product of the oxidation can be either uranium(IV) or uranium(VI).

The quantitative reduction in acidic solution of uranium(VI) to uranium(III) has been described by Kennedy [5]. The reaction is possible in a Jones reductor. The reduction is quantitative in 1 mol l^{-1} hydrochloric acid for uranium(VI) concentrations below 10^{-2} mol l^{-1}.

Detection can be done spectrophotometrically at 350 nm, where uranium(III) absorbs strongly [6] (E_{350} = 1440 l mol^{-1} cm^{-1}), or polarographically. The polarographic behaviour of the oxidation states of uranium in perchloric and hydrochloric acid medium has been investigated by Kritchevsky and Hindman [7]. The halfwave potential of the reaction $U^{4+} + e^- \rightleftharpoons U^{3+}$, which appears to be reversible at a DME, is −0.89 V (vs. SCE) in 1 mol l^{-1} hydrochloric acid.

In the present paper, the analytical applications of uranium(III) in acidic medium in f.i.a. are extensively studied and compared with those of chromium(II)—EDTA and vanadium(II)—EDTA. The inorganic and organic substances tested were the same as for chromium(II)—EDTA and vanadium(II)—EDTA.

EXPERIMENTAL

The instrumentation for both the spectrophotometric and the polarographic part of the work was described earlier [1, 2]. The dimensions of the flow system (Fig. 1) were the same as before [1, 3], with the exception of the buffer stream, which was removed. The uranium(VI) acetate concentration entering the Jones reductor (zinc, with a 5% degree of amalgamation) was 10^{-3} mol l^{-1} in 10^{-1} mol l^{-1} hydrochloric acid for both detection methods.

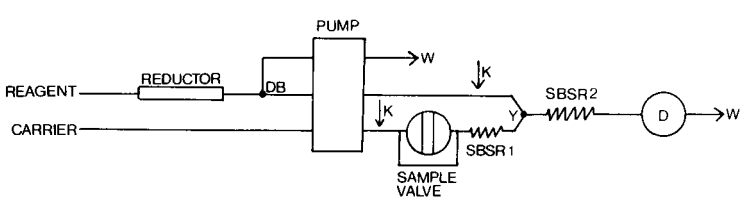

Fig. 1. Flow diagram. Length of single bead string reactors (SBSR): (1) 0.2 m; (2) 0.4 m. DB, debubbler; K, damping device; D, detector; W, waste. All connecting and SBSR tubing is 1 mm i.d. nylon. SBSRs are packed with 0.6 mm glass beads.

The carrier stream was distilled water. The sample solution was introduced by means of an injection valve (Rheodyne) with a loop volume of 33 μl. All solutions were carefully deaerated with nitrogen, because oxygen interferes with the determinations.

RESULTS

Spectrophotometric detection

To compare the practical performance of uranium(III) in acidic medium with vanadium(II)—EDTA and chromium(II)—EDTA in alkaline medium, the same test substances were investigated. Results of these experiments are presented in Table 1. There is a linear response of the absorbance (A) to changes in concentration of the analyte in the sample solution (C) over about one decade. When compared with the results obtained for chromium(II)—EDTA and vanadium(II)—EDTA, the limit of determination, which is defined as the analyte concentration for which the absorbance change equals ten times the peak-to-peak noise, for all substances was lower, by a factor of about 5 with respect to vanadium(II)—EDTA and by a factor of about 20 with respect to chromium(II)—EDTA.

Maleic acid, which could not be determined with chromium(II)—EDTA or vanadium(II)—EDTA could be determined with a limit of determination of 1.5×10^{-5} mol l^{-1}. Pyridine-2,6-dicarboxylic acid, which was inactive towards

TABLE 1

Calibration lines for the flow-injection system with spectrophotometric detection (reagent concentration, 10^{-3} mol l^{-1})

Sample	Concentration range (mol l^{-1})	Regression line	Regression coefficient, r	Limit of determination[a] (mol l^{-1})
KIO_3	10^{-5}—10^{-4}	$A = (2520 \pm 80)C$	0.9983	4×10^{-6}
$NaNO_3$	10^{-5}—10^{-4}	$A = (1960 \pm 50)C$	0.9990	5×10^{-6}
$NaNO_2$	10^{-5}—10^{-4}	$A = (1060 \pm 20)C$	0.9994	9×10^{-6}
NH_2OH	5×10^{-5}—5×10^{-4}	no signal	—	—
NH_2NH_2	5×10^{-5}—5×10^{-4}	no signal	—	—
$VOSO_4$	5×10^{-5}—5×10^{-4}	$A = (780 \pm 20)C$	0.9981	10^{-5}
$UO_2(H_3C_2O_2)_2$	5×10^{-5}—5×10^{-4}	$A = (840 \pm 10)C$	0.9996	10^{-5}
NH_4VO_3	5×10^{-5}—5×10^{-4}	$A = (1180 \pm 20)C$	0.9998	8×10^{-6}
$K_3Fe(CN)_6$	10^{-4}—5×10^{-4}	$A = (290 \pm 10)C$	0.9989	3×10^{-5}
Methyl red	2.5×10^{-5}—2.5×10^{-4}	$A = (1160 \pm 20)C$	0.9993	8×10^{-6}
o-Nitrophenol	10^{-5}—10^{-4}	$A = (1760 \pm 10)C$	0.9998	5×10^{-6}
Maleic acid	5×10^{-5}—5×10^{-4}	$A = (600 \pm 20)C$	0.9985	2×10^{-5}
Formaldehyde	2×10^{-3}—2×10^{-2}	no signal	—	—
Pyridine-2,6-dicarboxylic acid	2×10^{-4}—10^{-3}	$A = (230 \pm 5)C$	0.9996	4×10^{-5}

[a]See text.

chromium(II)—EDTA and vanadium(II)—EDTA, could be determined with a limit of determination of 3.9×10^{-5} mol l^{-1}. Polarographic studies showed that uranium(IV) forms a yellow complex with pyridine-2,6-dicarboxylic acid.

Amperometric detection

Apart from the working potential of the amperometric flow-through detector, the experimental set-up was identical with that in the paper on chromium(II) [2]. As in the case of chromium and vanadium, a working potential set along the limiting current of the reducing agent, uranium(III) in this case, is not very attractive. The oxidation of uranium(III) gives a very large current and excessive pump pulsation results in a very uneven baseline. A working potential on the limiting current of the uranium(IV) reduction wave is therefore more suitable.

Reductions in the Jones reductor produce zinc ions, which in acidic medium produce a reversible polarographic wave with a halfwave potential of —0.76 V, corresponding to the reaction $Zn^{2+} + 2e^- \rightleftharpoons Zn(Hg)$. This potential is very close to the potential at which the reaction $U^{4+} + e^- \rightarrow U^{3+}$ occurs. To establish whether or not the zinc wave interferes with the uranium(IV) wave under the experimental conditions, a polarogram in a flow of the reagent solution was recorded. This should produce adequate information as the half-reaction $U^{4+} + e^- \rightleftharpoons U^{3+}$ is reversible at mercury under the experimental conditions. Figure 2 presents this polarogram. In the figure, wave I corresponds to the reaction $U^{3+} \rightarrow U^{4+} + e^-$, wave II to the reaction $Zn^{2+} + 2e^- \rightarrow Zn(Hg)$ and wave III to the reaction $2H^+ + 2e^- \rightarrow H_2$.

Attempts to separate the uranium(III)/uranium(IV) and zinc waves by adding complexing agents were not successful. Baker and Sawyer [8] studied

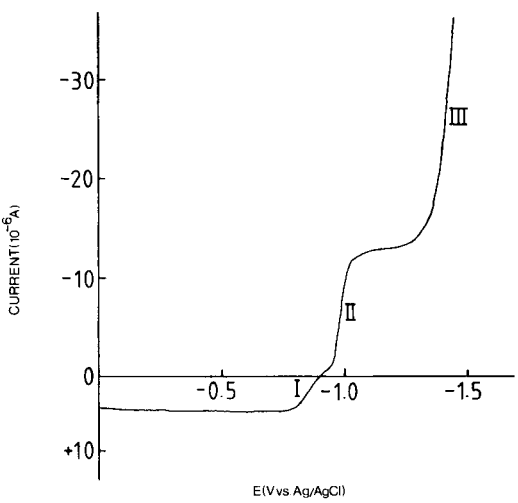

Fig. 2. Polarogram obtained in a flow of the reagent solution. For explanation of I, II and III, see text.

the electrochemical behaviour of the uranium oxidation states in the presence of excess of EDTA. Their results were in good agreement with the present experiments; the uranium(III) oxidation wave, the uranium(IV) reduction wave and the zinc reduction wave disappeared in the hydrogen wave. Thus no suitable working potential for the flow-through detector could be selected. Diethylenetriaminepentaacetic acid showed the same behaviour as EDTA. Other complexing agents like ammonia, tartrate and triethylenetetramine all caused precipitations in the flow system (probably uranium hydroxide) or the oxidation of uranium(III) to uranium(IV). No suitable complexing agent could be found, and so a noncomplexing acidic medium was used for all detections.

For the selection of the working potential of flow-through detectors, the same procedure as for vanadium(II) was applied. Four polarograms in flow were recorded: (A) a polarogram of the reagent solution, uranium(III); (B) a polarogram of the background current, by introducing 10^{-1} mol l^{-1} hydrochloric acid into the Jones reductor instead of the uranium(VI) solution; (C) a polarogram of the products of the reaction of the analyte under investigation with uranium(III) by replacing the water in the carrier stream by a solution of the particular analyte in excess; and (D) a polarogram of the analyte itself by introducing 10^{-1} mol l^{-1} hydrochloric into the Jones reductor and replacing the water in the carrier stream by a solution of the analyte under investigation.

Figure 3 presents the four polarograms obtained for sodium nitrate as the analyte. In polarograms C and D, the concentration of the analyte in the carrier stream was 10^{-2} mol l^{-1}. Polarograms A and B (Fig. 3) show that no reducible forms of uranium are present, so that the reduction efficiency in the Jones reductor must be very close to 100%. The same batch titration procedure as for vanadium(II) [3] also showed a reduction efficiency very close to 100% for flows through the Jones reductor from 0.1 to 0.7 ml min^{-1}. As polarograms B and D coincide, it can be concluded that sodium nitrate itself is not electroactive under the conditions used; the wave starting at about −1.0 V is the zinc wave. Information about the end products of the reaction of sodium nitrate with uranium(III) can be found in polarogram C. The uranium(III) oxidation wave has disappeared. Before the zinc wave, a reduction wave appears with the same halfwave potential as for the uranium(III) oxidation wave; this wave must be ascribed to the reaction $U^{4+} + e^- \rightarrow U^{3+}$ in agreement with results obtained by Kritchevsky and Hindman [7]. To date, there is no satisfactory explanation for the oxidation wave in polarogram C, which starts at about −0.3 V. As this wave does not interfere at the working potential, no further work was done to explain this wave.

The conclusion from these experiments is that a working potential of −0.91 V is suitable for the amperometric detector; at this potential, the reduction of uranium(IV) is very near its limiting current, the contribution of zinc to the current is very small, and the noise in the baseline is also minimal. However, care must be taken to keep the experimental conditions

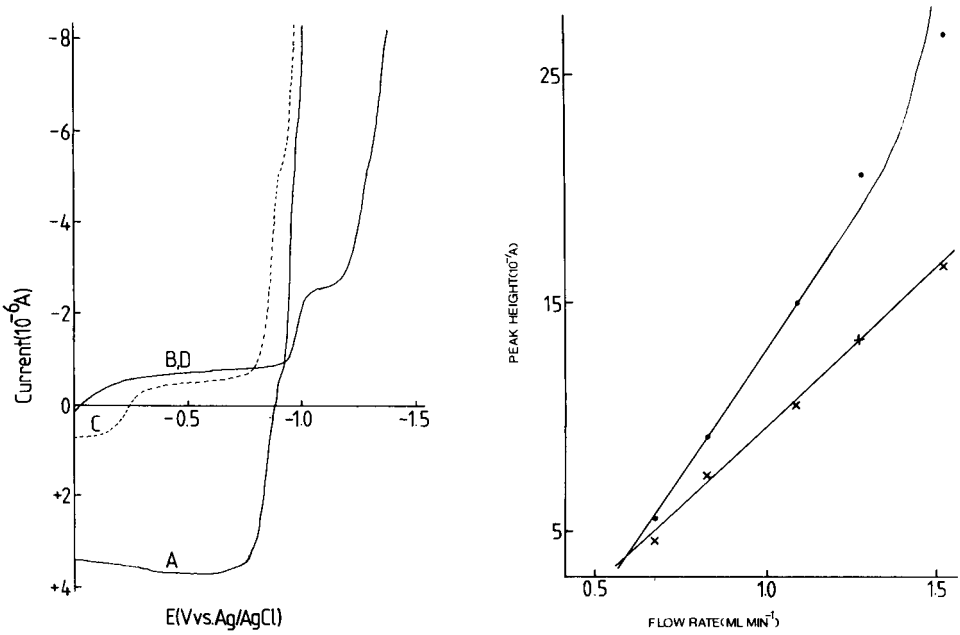

Fig. 3. Polarograms in flow for nitrate. For explanation of A, B, C and D, see text.

Fig. 4. Peak height as a function of the flow rate for the amperometric measurement of: (•) 10^{-4} mol l^{-1} sodium nitrate; (×) 10^{-4} mol l^{-1} sodium nitrite.

constant as the working potential is in the rising part of the *i*—*E* curve. The same procedure was applied for all the species determined in this part of the work.

With nitrite, in contrast to the oxidation of vanadium(II)—EDTA and chromium(II)—EDTA, the oxidation of uranium(III) was not quantitative, polarogram C still having a small anodic wave corresponding to uranium(III). Nitrite itself is not electroactive. The same working potential as in the case of nitrate was suitable. Hydrazine and hydroxylamine showed no reaction at all with uranium(III) and were not electroactive.

Dependence of the signal on the flow rate

As the peak height is dependent on the flow rate in a non-predictable way [2], the dependence of the signal on the flow rate must be evaluated experimentally for every analyte. For nitrate and nitrite, peak heights resulting from the injection of a 10^{-4} mol l^{-1} sample solution were recorded at different flow rates. For both species the resulting peak height as a function of the flow rate is presented in Fig. 4.

Although the graphs of peak height vs. flow rate for nitrate and nitrite are different, for both species the peak height increases with rising flow rate. For both nitrate and nitrite, the highest obtainable flow rate (about 1.5 ml min^{-1}) for the given pump and pump tubes was applied.

Determination of nitrate and nitrite

Results for the determinations of nitrate and nitrite are summarized in Table 2. The correlations for the current (I) and the concentration of the analyte in the sample solution (C) show good linearity for nitrate and nitrite in the concentration range 2×10^{-5}—10^{-4} mol l^{-1}. The maximum sampling rate is $S_{max} = 3600/4\sigma_t = 375$ h^{-1} for $\sigma_t = 2.4$ s (σ_t is the standard deviation in time units (s)). From the moments of a peak resulting from the injection of 10^{-4} mol l^{-1} sodium nitrate, the number of tanks to which the flow system corresponds can be calculated. The mean equals 11 s and the variance 6 s^2, so that the number of tanks is 21. In comparison with the spectrophotometric detection, the limit of determination with amperometric detection is about the same.

DISCUSSION

When the results of the determinations with chromium(II) and vanadium(II) in alkaline medium and with uranium(III) in acidic medium are compared, the conclusion is that in the case of spectrophotometric detection, determinations with uranium(III) achieve lower limits of determination for all substances tested; this must be ascribed to the high molar absorptivity of uranium(III). With regard to the substances determined, hydroxylamine can be determined only by means of vanadium(II), and maleic acid and pyridine-2,6-dicarboxylic acid only by means of uranium(III).

For the substances determined with amperometric detection, nitrate and nitrite can better be determined with uranium(III), because the limit of determination in that case is lower. Hydrazine can only be determined by using vanadium(II) in slightly acidic medium. For amperometric detection, the limits of determination are in all cases equal or superior to those for spectrophotometric detection. The limiting factor for amperometric detection is the flow pulsations. By eliminating these pump pulsations, lower limits of determination can be expected.

The experimental set-up for chromium(II)—EDTA [2], vanadium(II)—EDTA [3] and uranium(III) is easily interchangeable by changing the

TABLE 2

Calibration lines for the flow-injection system with amperometric detection (reagent concentration 10^{-3} mol l^{-1})

Sample	Concentration range (mol l^{-1})	Regression line	Regression coefficient, r	Limit of determination (mol l^{-1})
$NaNO_3$	10^{-5}—10^{-4}	$I = (26.5 \pm 0.5)10^{-3}\ C$	0.9993	4×10^{-6}
$NaNO_2$	2×10^{-5}—10^{-4}	$I = (16.8 \pm 0.1)10^{-3}\ C$	0.9999	6×10^{-6}
NH_2NH_2	10^{-4}—10^{-3}	no signal	—	—
NH_2OH	10^{-4}—10^{-3}	no signal	—	—

reagent solution and introducing or disconnecting the buffer stream. In this way the three reagents can be used in the same experimental set-up. The choice of the reagent depends only on the nature of the analyte under investigation and on the presence of other substances in the sample solution.

The authors thank Mr. W. Ozinga for experimental aid with the spectrophotometric part of the work.

REFERENCES

1 R. C. Schothorst, J. M. Reijn, H. Poppe and G. den Boef, Anal. Chim. Acta, 145 (1983) 197.
2 R. C. Schothorst and G. den Boef, Anal. Chim. Acta, 153 (1983) 133.
3 R. C. Schothorst, J. J. F. van Veen and G. den Boef, Anal. Chim. Acta, 161 (1984) 27.
4 A. Berka, J. Vulterin and J. Zýka, Massanalytische Oxidations- und Reduktionsmethoden, Akademische Verlagsgesellschaft, Geest u. Porlig K.-G, Leipzig, 1964.
5 J. H. Kennedy, Anal. Chem., 32 (1960) 150.
6 C. J. Rodden, Analytical Chemistry of the Manhattan Project, McGraw-Hill, New York, 1950, p. 542.
7 E. S. Kritchevsky and J. C. Hindman, J. Am. Chem. Soc., 71 (1949) 2096.
8 B. C. Baker and D. T. Sawyer, Inorg. Chem., 9 (1970) 197.

Analytica Chimica Acta, 162 (1984) 9—18
Elsevier Science Publishers B.V., Amsterdam — Printed in The Netherlands

DETERMINATION OF WATER BY FLOW INJECTION ANALYSIS WITH THE KARL FISCHER REAGENT

Minimization of Effects Caused by Differences in Physical Properties of the Samples

INGRID NORDIN-ANDERSSON*, OVE ÅSTRÖM and ANDERS CEDERGREN
Department of Analytical Chemistry, University of Umeå, S-901 87 Umeå (Sweden)
(Received 17th February 1984)

SUMMARY

In the previously described flow-injection method for the spectrophotometric determination of water with the Karl Fischer reagent, problems can arise from the rather large variation between the calibration curves for different types of samples. Different combinations of flow-injection arrangements and detector types are described here, to establish a system which levels out this undesirable spreading between the calibration curves. One necessary condition for attaining a low spread is shown to be the use of a spectrophotometric detector especially constructed to minimize refractive index effects. The best results, including samples with large differences in refractive indices and viscosities, were obtained by a combination of peak area measurements and the use of this detector. For example, the relative mean deviation for a sample containing 0.1% water was about 2%.

In two previous papers [1, 2] a method was described for the spectrophotometric determination of water by flow injection analysis (f.i.a.) with the Karl Fischer reagent. A principal feature of the f.i.a. approach, when compared with the conventional Karl Fischer batch titration method, is the expected small influence of side-reactions. The reason for this is that, in a flow-injection system, effects from such reactions can be minimized by using a short reaction time. The main disadvantage with the method was the rather large variation between the calibration curves for different types of samples (organic solvents).

According to the theories on which the f.i.a. is based, the extent of dispersion of the sample is determined by, among other parameters, the molecular diffusion of the sample [3, 4]. This means that a variation in peak shapes is expected for samples having different molecular diffusivities or viscosities. Because most flow-injection methods are based on spectrophotometric detection, the differences in refractive indices between the sample matrix and the carrier stream [5] may also affect the peak shape. Differences in absorptivities between samples constitute another potential source of error. In those cases, where the flow-injection method is based on a chemical reaction, variations in the results can occur as a consequence of a change in reaction

0003-2670/84/$03.00

rate with type of sample matrix. It should be mentioned that the present theory for dispersion in f.i.a. only takes into consideration the case for which the sample is dissolved in the same solvent as that of the carrier stream. Numerous applications of f.i.a. in non-aqueous systems are foreseeable and so there is a real need for fundamental studies of systems where the fluid cannot be assumed to have constant viscosity and density.

The aim of this paper was to investigate whether the flow-injection system could be designed in such a way as to level out the above-mentioned undesirable spreading between the calibration curves. The test samples selected were organic solvents with large differences in viscosities and refractive indices.

EXPERIMENTAL

Samples and carrier solutions

All organic liquids were of analytical grade; 100 ml of 2-propanol, isopropyl acetate, propyl acetate, and methanol (all from Merck) were stored with about 30 g of molecular sieves (3 Å, Union Carbide) in the bottle and were used as samples. The mixtures of water and the organic solvents were standardized coulometrically [6]. The Karl Fischer carrier solution contained 4.57 g of iodine (Riedel de Haen), 50 g of sulphur dioxide (Fluka) and 80 ml of dried pyridine (Merck) diluted to 1 l with dried methanol. Before use, the reagent was calibrated by amperometric titration and adjusted to 6.0 mM by addition of iodine. The physical properties of the solvents and a Karl Fischer reagent are given in Table 1.

Instrumentation and procedure

The flow-injection manifolds used are outlined in Fig. 1.

TABLE 1

Physical properties of the solvents and a Karl Fischer reagent

Solvent	Refractive index[a]	Viscosity[a] ($g\ cm^{-1}\ s^{-1}$)	Kinematic viscosity[a] ($cm^2\ s^{-1}$)	Absorbance measured[b]
2-Propanol	1.375	2.3×10^{-2}	2.9×10^{-2}	−0.1070
Isopropyl acetate	1.375	0.569×10^{-2}	0.654×10^{-2}	−0.1099
Propyl acetate	1.384	0.585×10^{-2}	0.700×10^{-2}	−0.1100
Methanol	1.324	0.597×10^{-2}	0.754×10^{-2}	−0.1023
Karl Fischer reagent	1.36	0.7×10^{-2} (25°C)	0.824×10^{-2} (25°C)	—

[a]At 20°C. [b]At 546 nm with detector D, and the two-line manifold, L = 200 cm, at a flow rate of 3.3 ml min^{-1}.

A four-channel peristaltic pump (Gilson Minipuls 2) equipped with silicone rubber tubings was used. The spectrophotometric detector, D_1, is a Beckman absorbance detector (Model 160) supplied with a mercury lamp and a filter assembly for monitoring at 546 nm. The flow cell has a volume of 18.5 μl and standard 10-mm optical path length. The internal configuration is especially designed to minimize band spreading and refractive index sensitivity. The reference cell is operated dry. The original metallic cell was replaced by a teflon cell in order to withstand the very reactive Karl Fischer reagent. The teflon was etched with a solution containing a compound of metallic sodium and naphthalene in tetrahydrofuran; this eliminated problems with air bubbles staying in the cell. The detector, D_2, is a homemade spectrophotometer consisting of a small grating monochromator, a halogen lamp, an u.v.-enhanced photodiode and a flow-through cuvette in etched teflon (volume 20 μl, light path 10 mm). An integrator (Hewlett-Packard 3388) was used for recording and evaluation of the peaks. Generally, a Vitatron recorder was coupled in parallel with the integrator.

Teflon tubing (0.5 mm i.d.) was used for connection and as coiled reactors. Information about the single bead string reactor (SBSR) [7] is given in Table 2. A standard liquid chromatographic inlet slide valve injected the sample (10 μl) into the carrier stream. The change in the absorbance was measured with detector D_1 at 546 nm and detector D_2 at 525 nm.

RESULTS AND DISCUSSION

Studies with modified Karl Fischer reagent

For all experiments with the single-line mode, the reactor length was 200 cm, because this length had earlier been found to be suitable when a conventional Karl Fischer reagent was used. Figures 2—4 show the results obtained with a Karl Fischer reagent without any sulfur dioxide in single-line arrangements. The single effect from the solvent could easily be studied by means of such a reagent because the rate of the main reaction was zero. Comparison of Fig. 2(a) and (b) shows that there is much less spreading in

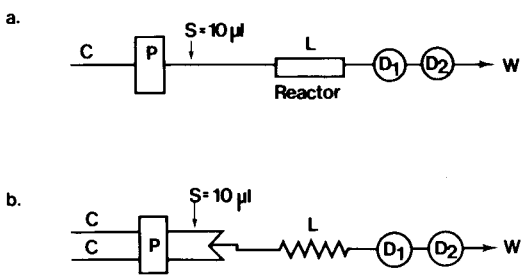

Fig. 1. The manifolds used in the various experiments. (a) Single-line arrangement; (b) two-line manifold with mixing point. C, carrier stream; P, pump; reactor, coil or SBSR; L, 200 cm; D_1, Beckman Model 160; D_2, homemade detector; W, waste.

TABLE 2

Geometric constants for the single bead string reactor (SBSR)

Tube diameter, d_t	0.08 cm
Particle diameter, d_p	0.05 cm
Void fraction, ϵ	0.67
Number of particles/unit length, N/L	25 cm^{-1}
Open volume/unit length, V_0/L	0.50×10^{-2} cm^2
Void volume/unit length, $\epsilon V_0/L$	0.34×10^{-2} cm^2

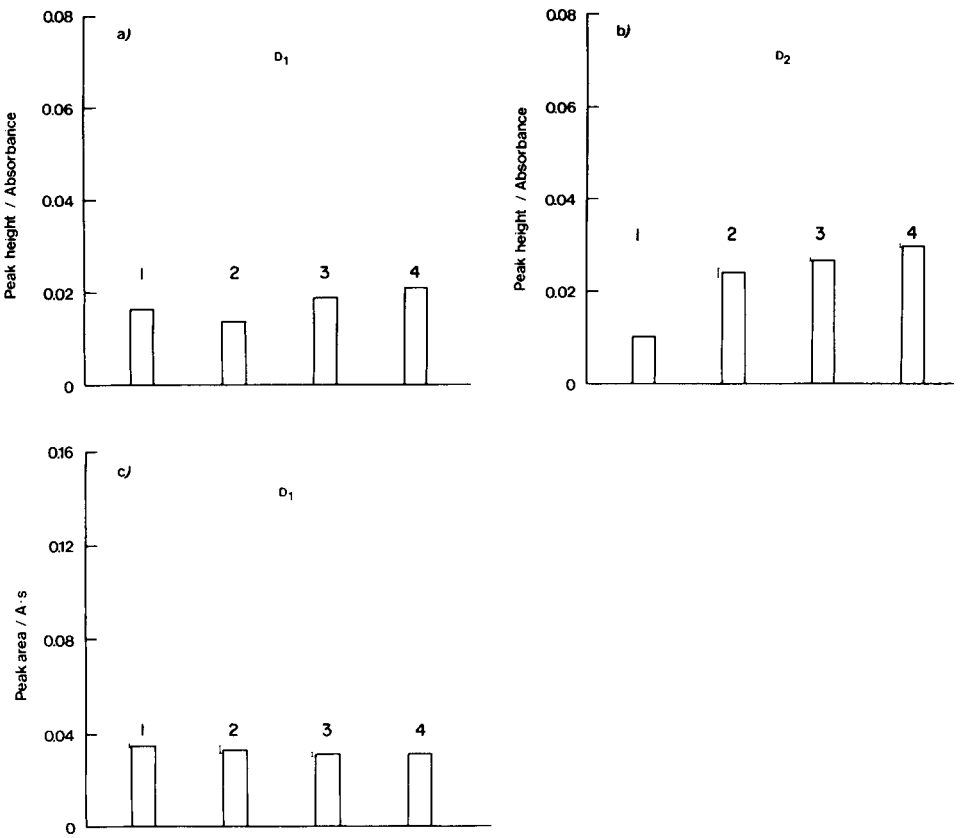

Fig. 2. Peak height (a, b) and peak area (c) blank values from dried solvents: (1) methanol; (2) 2-propanol; (3) isopropyl acetate; (4) propyl acetate by using a modified 5.9 mM Karl Fischer reagent (no SO_2 added) as carrier stream. Single-line mode with a 200-cm coil reactor. Flow rate 3.0 ml min^{-1}. Baseline absorbance was 0.32. Detectors D_1 and D_2 were used as indicated.

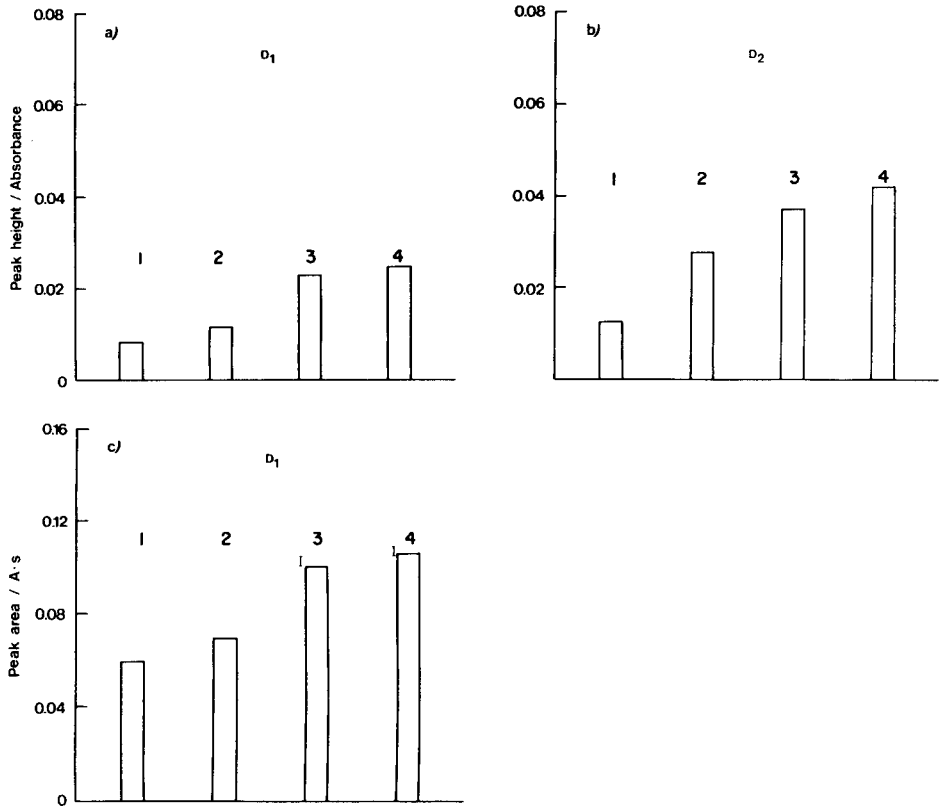

Fig. 3. Peak height and peak area blank values obtained from the same solvents under the same conditions as those given in Fig. 2, except for the flow rate which was 1.5 ml min^{-1}.

the peak height values for the various solvents when detector D_1 is used. This improvement can be ascribed to a decrease in the influence of the refractive index for this detector in view of the fact that 2-propanol, isopropyl acetate and propyl acetate have similar refractive indices, which differ very much from that of methanol. The very low variation seen for the peak area results (Fig. 2c) indicates that there is no significant influence from the refractive index effect under these experimental conditions. Peak areas for detector D_2 are not included in Fig. 2 because the integrator used could not adequately evaluate the very badly shaped peaks obtained in those experiments. The peak heights and peak areas should not be affected by the differences in absorptivities between the solvents as these are very small (see Table 1). Comparison of the results given in Figs. 2 and 3 shows that the variations in peak height as well as peak area are much larger when the flow rate is reduced to 1.5 ml min^{-1}. The peak area results given in Fig. 3(c) indicate an increased influence from the refractive index effect when the flow rate is decreased. Considering the peak height results (peak areas should not be affected), the

decreased flow rate could also produce differences in molecular diffusion between the samples. Calculations carried out according to Tijssen's model [8] showed that the differences in dispersion between the various solvents were much smaller for a flow rate of 3 ml min^{-1} than for 1.5 ml min^{-1}.

Comparison between the results obtained with a coil reactor and a single bead string reactor (SBSR) using detector D_1 is shown in Fig. 4. The SBSR was included because it is supposed to be effective in levelling out differences in dispersion owing to differences in the physical properties of the samples [7]. As can be seen, there are no major discrepancies between the solvents for peak area measurements. For peak height measurements, the situation is somewhat more favourable when the SBSR arrangement is used mainly because of the increased sensitivity.

Karl Fischer reagent with a single-line arrangement

Figures 5–7 summarize the results obtained with the Karl Fischer reagent in the single-line mode. Compared to the results given in Figs. 2—4, these

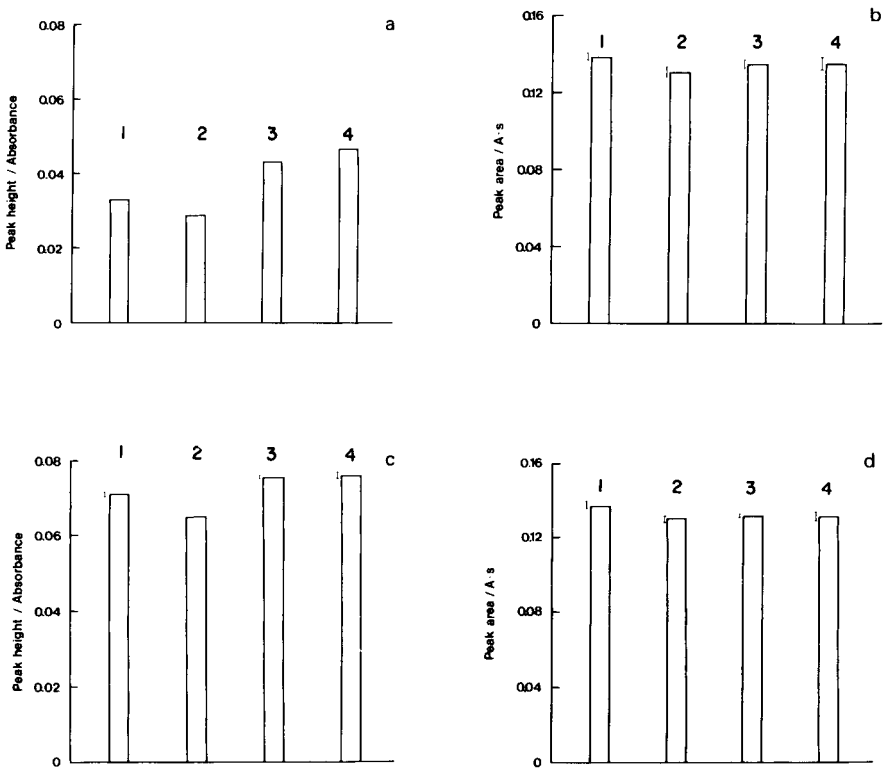

Fig. 4. Peak height and peak area blank values from the same solvents as in Fig. 2, by using a modified 12.0 mM Karl Fischer reagent (no SO_2 added) and detector D_1 for coil and SBSR, respectively. Coil and SBSR lengths, 200 cm. Flow rates: (a) and (b) 3.0 ml min^{-1} (coil); (c) and (d) 2.9 ml min^{-1} (SBSR). Baseline absorbance level was 1.06.

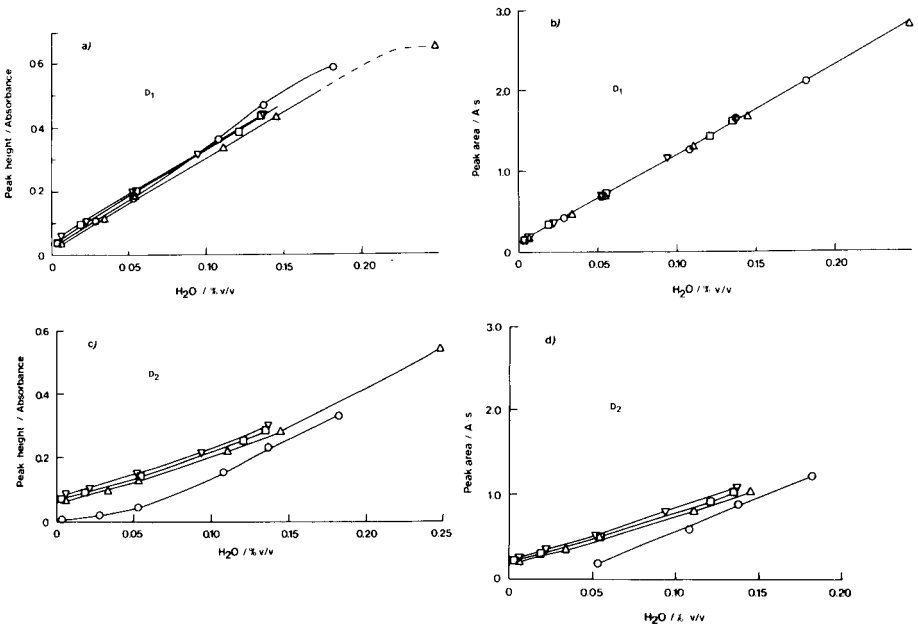

Fig. 5. Calibration graphs for the determination of water in different solvents: (○) methanol; (△) 2-propanol; (□) isopropyl acetate; (▽) propyl acetate. (a) Peak heights and (b) peak areas with detector D_1; (c) peak heights and (d) peak areas with detector D_2. Single-line mode; coil reactor, 200 cm; carrier stream, 6.1 mM Karl Fischer reagent; flow rate, 3.0 ml min^{-1}.

figures should reflect the additional effects caused by the chemical reaction involving water. Generally, the spreading patterns seen for the solvents in Fig. 5 are in very good agreement with those of Fig. 2. No significant effect of the chemical reaction on the results can be discerned; this is most obvious from the results seen in Fig. 5(b). Furthermore, an improved sensitivity is noticed when detector D_1 is used; this is clear by comparing parts (a—d) of Fig. 5. The results represented in Fig. 5(b) are encouraging for future work in developing a Karl Fischer flow-injection method which can be used without any need for standardizing against the same type of sample as that to be analyzed. The results for the lower flow rate (1.5 ml min^{-1}) (Fig. 6) show a larger deviation than those given in Fig. 5; this is in line with what could be predicted based on the information given in Fig. 3.

One obvious advantage of the SBSR arrangement (Fig. 7) is that negligible variation between the solvents can be maintained at the lower flow rate (1.5 ml min^{-1}). A comparison of the extent of spreading between the calibration graphs for various combinations of flow-injection arrangements and detectors is shown in Table 3.

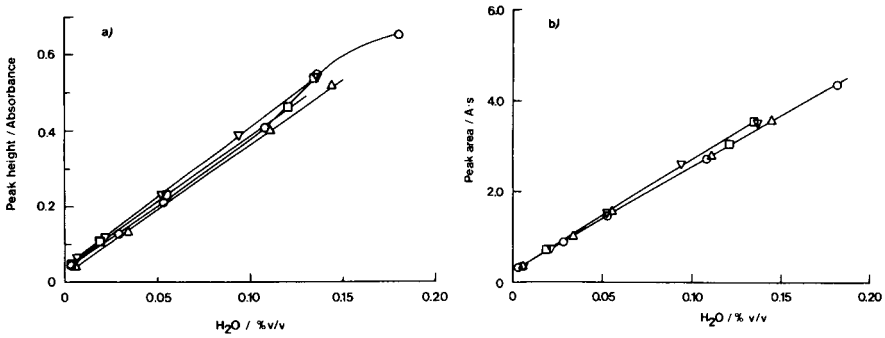

Fig. 6. Calibration graphs for the determination of water with detector D_1: (a) peak heights; (b) peak areas. The solvents and conditions are the same as given in Fig. 5 except for the flow rate (1.5 ml min^{-1}).

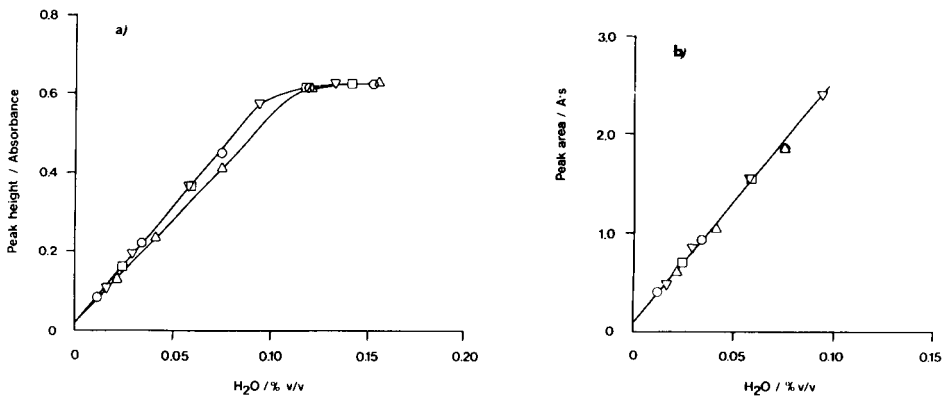

Fig. 7. Calibration graphs for determination of water with detector D_1 and the SBSR: (a) peak heights; (b) peak areas. Reactor length, 200 cm; carrier stream, 6.1 mM Karl Fischer reagent; flow rate, 1.5 ml min^{-1}. Symbols as in Fig. 5.

Karl Fischer reagent with the two-line manifold

Use of the two-line manifold offers two advantages in principle. The first is the one pointed out by Růžička and Hansen [9], namely, the ability of such flow-injection arrangements to suppress matrix interference effects. Secondly, mixing between the sample and carrier (the reagent) will be very effective, which must be advantageous when chemical reactions are involved.

Calibration graphs (peak height evaluation) for the determination of water obtained by using the Karl Fischer reagent and the two-line configuration are shown in Fig. 8. Comparison of the results in Fig. 8(a) and (b) shows that there is less variation between the solvents at the higher flow rate. No significant improvement can be seen for an increase in the coil length from 100 to 200 cm (compare Fig. 8b and c). As is evident from a direct comparison between Figs. 8(c) and 5(a), there is no essential improvement with respect

TABLE 3

Comparison of the spreading between the calibration graphs for various flow-injection arrangements for water determinations with 6 mM Karl Fischer reagent

Arrangement[a]	Peak evaluation	Relative deviation (%) at 0.075% H_2O[b]				Mean deviation[c] (% H_2O)
		Methanol	2-Propanol	Isopropyl acetate	Propyl acetate	
Single-line, coil, 3.0 ml min^{-1}, detector D_2	Height	40.5	1.3	−10.0	−17.2	0.0156
	Area	40.5	0	−8.3	−18.4	0.0117
Single-line, coil, 3.0 ml min^{-1}, detector D_1	Height	−4.0	9.8	−2.2	−4.4	0.0042
	Area	0.3	3.4	−0.7	−3.1	0.0019
Single-line, SBSR, 1.5 ml min^{-1}, detector D_1	Height	−0.1	9.3	−2.5	−3.7	0.0021
	Area	3.2	3.8	−2.3	−2.8	0.0017
Two-line, coil, 3.0 ml min^{-1}, detector D_1	Height	−2.5	8.3	−1.4	−4.7	0.0035
	Area	−0.7	2.0	0.6	−2.4	0.0022

[a]The coil or SBSR was 200 cm long in all cases. [b]The deviation (in % H_2O) of the actual calibration curve from the regression line, computed from all data points at the point corresponding to 0.075% H_2O. [c]Calculated from the deviation of each data point from the regression line.

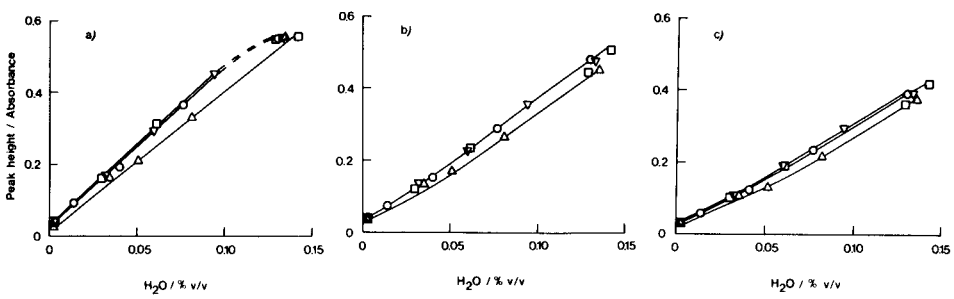

Fig. 8. Calibration graphs for determination of water obtained with the two-line arrangement including coil reactor and detector D_1. Peak height evaluation. Solvents: (○) methanol; (△) 2-propanol; (□) isopropyl acetate; (▽) propyl acetate. (a) Coil length 100 cm, flow rate 1.0 ml min^{-1}; (b) coil length 100 cm, flow rate 3.0 ml min^{-1}; (c) coil length 200 cm, flow rate 3.0 ml min^{-1}. Carrier stream is Karl Fischer reagent with a baseline absorbance level of 0.48 (original 6.1 mM reagent).

to peak height measurements by use of the two-line configuration instead of the single line. The integrated peak values for the experiment represented in Fig. 8 are given in Fig. 9. As can be seen, the variation is very small even for low flow rates. This indicates that the influence from the refractive index effect is very small in this case. There are two general conclusions from these

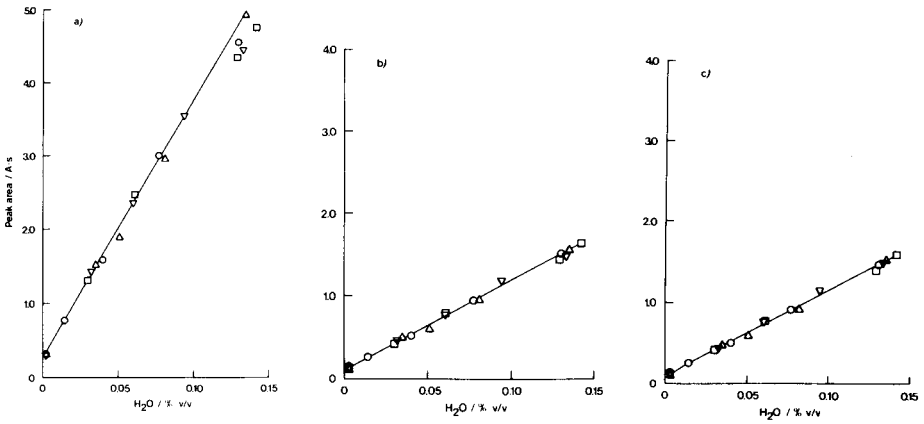

Fig. 9. Calibration graphs for determination of water by peak area evaluation for the same runs as shown in Fig. 8.

experiments with the two-line configuration: first, variations in the peak height values cannot be reduced further by using the two-line mode compared with the single-line mode; secondly, for peak area measurements the usable range of flow rates will include low rates. This latter conclusion is of course especially important when slow kinetics is involved.

Conclusions

As shown in Table 3, the use of a spectrophotometric cell which minimizes the refractive index effect (i.e., D_1) is necessary for attaining small spreads between the calibration graphs for different solvents. The best results were obtained by combining peak area measurements with the use of this detector. The prerequisite for obtaining precise results with peak height measurements appears to be the use of the single bead string reactor (SBSR). However, it is attractive to keep the system as simple as possible and so the single-line arrangement including a coil reactor is recommended in combination with a high flow rate of the Karl Fischer reagent stream.

REFERENCES

1 I. Kågevall, O. Åström and A. Cedergren, Anal. Chim. Acta, 114 (1980) 199.
2 I. Kågevall, O. Åström and A. Cedergren, Anal. Chim. Acta, 132 (1981) 215.
3 G. Taylor, Proc. Soc. London, Ser. A, 219 (1953) 186; 223 (1954) 446.
4 C. G. Painton and H. A. Mottola, Anal. Chim. Acta, 154 (1983) 1.
5 D. Betteridge, E. L. Dagless, B. Fields and N. F. Graves, Analyst (London), 103 (1978) 897.
6 A. Cedergren, Talanta, 21 (1974) 367.
7 J. M. Reijn, W. E. van der Linden and H. Poppe, Anal. Chim. Acta, 126 (1981) 1.
8 R. Tijssen, Sep. Sci. Technol., 13 (1978) 681.
9 J. Růžička and E. H. Hansen, Flow Injection Analysis, Wiley, New York, 1981, p. 59.

Analytica Chimica Acta, 162 (1984) 19—32
Elsevier Science Publishers B.V., Amsterdam — Printed in The Netherlands

ON-LINE ELECTROCHEMICAL REAGENT PRODUCTION FOR DETECTION IN LIQUID CHROMATOGRAPHY AND CONTINUOUS FLOW SYSTEMS

W. TH. KOK*, U. A. TH. BRINKMAN and R. W. FREI

Department of Analytical Chemistry, Free University, De Boelelaan 1083, 1081 HV Amsterdam (The Netherlands)

(Received 23rd February 1984)

SUMMARY

The on-line electrochemical production of bromine as a reagent for detection in liquid chromatography is studied. For detection, the excess of bromine after reaction with an analyte in the column effluent is measured amperometrically. Phenolic ethers are used as model compounds. The relations between generating current, reaction time, rate constant, signal and noise are investigated. Rate constants were measured in batch experiments with rotating ring-disk electrodes. Lower and upper limits of detection are predicted. Under favourable conditions, detection limits are shown to be in the subnanogram range. The optimal generating current, with respect to sensitivity and selectivity, is discussed in detail. The determination of opiates (morphine, codeine, noscapine and papaverine) is used as an example of the efficacy of the method.

In the search for more sensitive and selective detection in liquid chromatography, post-column reaction systems are becoming increasingly popular. In such systems, a reagent is added to the column effluent to increase the detectability of the analyte. Takata and Muto [1] were the first to point out the possibility of electrochemical generation of the reagent. With electrochemical generation, it is possible to use unstable reagents because the time between generation and detection is short.

Two different methods can be used. In the first, reagent is produced off-line, and then mixed with the column effluent. This is the more widely applicable method because the solution in which the reagent is produced may be optimized for this purpose, and the separation can be optimized independently. In the second method, the reagent is produced on-line, i.e., in the column effluent itself. When it is possible to find a solvent suitable for both the separation and the reagent production, this method is preferable because less equipment is required and an extra source of noise, peak dilution and possibly band broadening is eliminated. It might then even be worthwhile to generate reagents which are stable on storage.

Though the detection can be done in various ways, electrochemical detection is logical when the reagent is produced electrochemically. A scheme for such a detection system is presented in Fig. 1. Reagent is produced from a

0003-2670/84/$03.00

precursor of the reagent in the mobile phase. The excess of reagent after the reaction with the analyte can be monitored with an amperometric detector. The presence of an analyte in the column effluent is shown as a dip in the detector current. King and Kissinger [2] have shown that such a system can be used satisfactorily. They determined phenols and unsaturated compounds with electrochemically generated bromine. However, various problems have to be solved before the method becomes adequate for routine purposes. Two aspects are of particular importance: first, the signal obtained is basically a difference value, so that optimization of signal-to-noise ratios is essential to obtaining reasonable sensitivity; secondly, the region of linear response is inherently limited and so requires careful evaluation.

In this work, the on-line generation of bromine was studied for the detection of phenolic ethers. These compounds are generally difficult to oxidize directly at an electrode, whereas the rate of the homogeneous reaction with bromine is reasonably fast [3]. Many compounds of pharmaceutical importance have phenolic ether moieties. The performance of the system was investigated with simple methoxybenzenes as model compounds. The determination of opiates was used as an application.

EXPERIMENTAL

Chemicals and equipment

Doubly-distilled demineralized water and analytical-grade methanol (J. T. Baker Chemicals) were used as solvents. Morphine, codeine and papaverine were used in the hydrochloride form. Noscapine hydrochloride was a gift from Roter (Hilversum, The Netherlands). Other chemicals were of analytical-grade quality.

For chromatography, the mobile phase was delivered at a flow rate of 1 ml min^{-1} with a Perkin-Elmer 601 pump. Samples were injected with a Rheodyne 7120 valve with 20-μl and 1-ml loops. The amperometric detector was a Metrohm (Herisau, Switzerland) 1096/2 cell, with a platinum working electrode operated generally at +0.4 V vs. a Ag/AgCl/1 M LiCl in methanol—water (1:1) reference electrode. The coulometric cell, made in our workshop, is outlined in Fig. 2 (see below). The potentiostats and amplifiers used were custom-made.

Columns were packed with LiChrosorb-RP materials (Merck) in the laboratory or obtained from Supelco (Bellefonte, PA, U.S.A.).

Ring-disk measurements

Two platinum ring-disk electrodes were used, one for first-order measurements of slow ($k_2 < 10^5$ mol^{-1} l s^{-1}) reactions and one for second-order measurements of fast reactions. Table 1 gives some data on these electrodes. The electrodes, embedded in a Kel-F shaft, were driven by a servomotor with tachogenerator. The rotation speed was variable from 0 to 80 rps. A Tacussel, model Bi-pad, bipotentiostat/galvanostat was used. When phenol

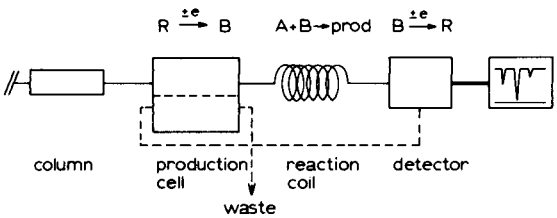

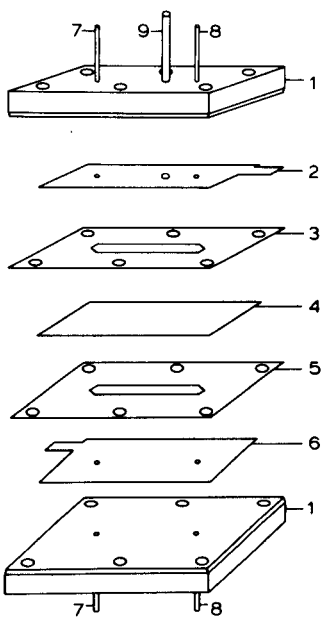

Fig. 1. Scheme of on-line electrochemical reagent production and detection.

Fig. 2. Coulometric cell: (1) stainless-steel support with PTFE insulation; (2) Pt working electrode; (3) spacer; (4) ion-exchange membrane; (5) spacer; (6) stainless-steel counter electrode; (7) inlet; (8) outlet; (9) channel to reference electrode (optional).

TABLE 1

Characteristics of the ring-disk electrodes

Parameter[a]	Electrode 1	Electrode 2
r_1 (mm)	2.011	2.017
r_2 (mm)	2.100	2.147
r_3 (mm)	2.201	3.028
N_0 (calc.)	0.160	0.463
N_0 (exp. ± s.d.)	0.165 ± 0.002	0.465 ± 0.003
Technique	first order	second order

[a] r_1, disk radius; r_2, inner ring radius; r_3, outer ring radius. N_0, collection efficiency.

was present in the solution, the electrodes had to be polished after each experiment. Otherwise, this was not necessary.

For the calculation of reaction-rate constants (see [4]), the kinematic viscosity, ν, of the solution and the diffusion coefficients, D, of the species involved must be known. The viscosities of solutions containing 0.1 M potassium nitrate, 0.01 M potassium bromide, 0.001 M nitric acid and variable amounts of methanol were measured with an Ubbelohde viscosimeter. The

diffusion coefficient of bromine was evaluated from limiting currents at a disk electrode. The diffusion coefficients of the analytes were assumed to be the same as that of bromine. The values of ν and D used in calculations are given in Table 2. All experiments were done at ambient temperature (20 ± 1°C).

RESULTS AND DISCUSSION

Construction of the coulometric cell

An electrochemical cell for on-line production of reagent should have certain characteristics. First, the working electrode must be separated physically from the counter-electrode compartment, to prevent re-conversion of the reagent produced or interference from other counter-electrode products. Accumulation of such products, which may diffuse to the working electrode compartment in the long term, must be avoided. Second, though a conversion of 100% of the reagent precursor is usually not necessary, a high coulometric yield is desirable. This can be important when a high precursor concentration is incompatible with the separation system, or when (partial) passivation of the working electrode may occur. In the system studied here, the advantage of a high yield is that the bromide concentration can be kept low, so that tribromide formation is prevented; tribromide usually reacts much more slowly than bromine. Third, the contribution to band-broadening of the production cell should be small. Finally, the cell should be able to resist some back-pressure from a reaction capillary.

The cell developed here (Fig. 2) meets these requirements. It has a thin-layer configuration, with the working- and counter-electrode compartments separated by a polymeric ion-exchange membrane. Two versions of the cell were tested, one with a connection to a reference electrode and one without. The reference electrode can be used to monitor the potential of the working electrode; its position ensures a negligible ohmic drop. However, when reaction capillaries with a long residence time were used, the back-pressure caused problems with the sealing of the reference electrode, and then the cell without reference channel was used. With this cell, back-pressures up to 4 bar could be tolerated.

The maximum coulometric yield Y of the cell can be calculated from the

TABLE 2

Viscosities and diffusion coefficients of bromine

Methanol (% v/v)	ν (10^{-2} cm^2 s^{-1})	D (10^{-5} cm^2 s^{-1})
0	0.92	1.21
20	1.37	1.04
40	1.67	0.93

theory developed by Stephen [5] for heat transfer, and adapted by Lankelma and Poppe [6] for diffusion-controlled currents in thin-layer cells

$$Y = 1 - \exp(-2.43\,DWL/b\Phi) \quad (1)$$

where Φ is the volumetric flow rate and W, L and b are the width, length and thickness of the electrode compartment. For the cell used in this study, with W = 0.5 cm, L = 3 cm and b = 50 μm, the calculated maximum conversion is 32%.

The coulometric yield of the production cell was measured under potentiostatic conditions by injection of 1-ml plugs of bromine solutions in 40% methanol. By applying Faraday's Law to the current maxima measured, a yield of 27% was found. The value calculated from the screening effect on the amperometric cell downstream was 29%. In practice, the fraction of precursor converted was much lower (<2%) than the maximum yield.

Band-broadening contributions

The various parts of the system will, of course, all contribute to band broadening. The expression for band broadening in a straight tube with inner radius r and length L was derived by Taylor [7] and Aris [8]; the contribution to the second moment of a peak is

$$\sigma_t^2 = \pi\, r^4 L/24\, D\, \Phi \quad (2)$$

When the tubing is coiled, the band broadening is reduced by secondary flow patterns with a factor κ, for which Tijssen [9] and van den Berg et al. [10] have given empirical expressions. For the reaction coils used here, with an inner diameter of 0.33 mm and a coil diameter of 3 cm, κ is about 0.2 at a flow rate of 1 ml min^{-1}.

Following the method of Aris [8], an equation for the band broadening in thin rectangular channels was derived. Neglecting side-wall effects this yielded

$$\sigma_t^2 = b^3\, W\, L/105\, D\, \Phi \quad (3)$$

This expression can be used to calculate the band broadening in the working electrode compartment.

The band broadening caused by the various parts of the system was measured experimentally from the peak width at half height in the amperometric detector after injection of 20-μl samples of bromine solutions. The results of calculations based on Eqns. 2 and 3 and the experimental data (Table 3) are in reasonable agreement. The band broadening in the coulometric cell is fairly small, and is caused mainly by the connecting tubing.

Finally, the kinetics of the reaction between reagent and analyte can be a source of band broadening. When the reaction is slow, any part of the analyte spending more time in the reactor will react more completely than a more rapidly eluting part, which will affect the final peak shape. With (near)

TABLE 3

Contributions to band broadening

System part	σ_t^2 (s^2)	
	Calculated	Experimental
Injector and detector	—	1.0
Coulometric cell		
inlet and outlet	0.5[a]	0.5
electrode compartment	0.01[b]	
Reaction coil (20 s)	5.0[a]	5.8
Total	—	7.3

[a]Calculated from Eqn. 2. [b]Calculated from Eqn. 3.

Gaussian reactors such as long narrow tubing or (non-retaining) packed beds, the effect will be smaller than with reactors behaving as mixing chambers, (e.g., short wide tubing). The theoretical contribution of the reaction kinetics effect to the moments of a peak was derived. The results are given in Table 4. Though the experimental precision was too low for quantitative verification of the theory, it was clearly seen that in flow-injection experiments with very short reaction coils the peak maxima of slowly reacting analytes appeared later and their widths were greater than those for fast reacting analytes. The conclusion is therefore that band-broadening contributions in a system such as that used here should be measured with quickly reacting analytes.

Optimization of the generating current

In acidic solutions, bromine can be generated with 100% current efficiency, and the bromine concentration in the column effluent can easily be controlled by the generating current. As can be seen in Fig. 3A, the detector

TABLE 4

Effect of reaction kinetics on peak shape[a]

Reactor type	Moment		
	Zero	First	Second
Gaussian reactor			
fast reaction	1	t_r	σ_t^2
slow reaction	$k_1 t_r$	$t_r(1 + \sigma_t^2/t_r^2)$	$\sigma_t^2(1-\sigma_t^2/t_r^2)$
Mixing chamber reactor			
fast reaction	1	t_r	t_r^2
slow reaction	$k_1 t_r$	$2t_r$	$2t_r^2$

[a]t_r, mean residence time, V/Φ; σ_t^2, second moment for non-reacting compound; k_1, (pseudo-) first-order reaction rate constant.

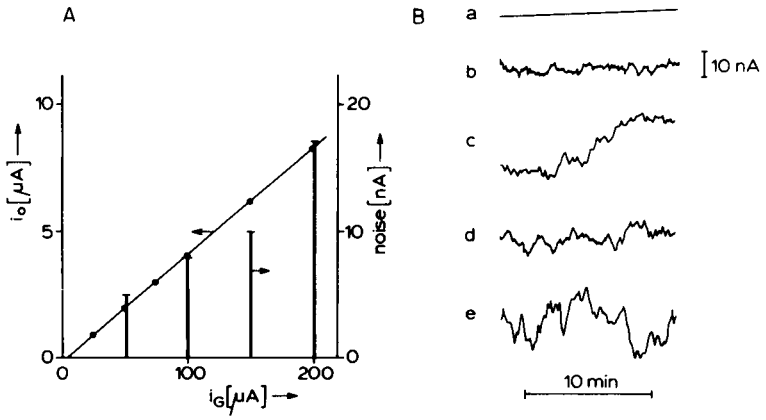

Fig. 3. (A) Dependence of detector current (i_0) and noise on the generating current (i_G). Solvent: 40% (v/v) methanol, 0.1 M KNO_3, 0.01 M KBr, 0.001 M HNO_3. (B) Noise patterns for different i_G: (a) 0; (b) 50; (c) 100; (d) 150; (e) 200 μA.

current i_0, and thus the bromine concentration, is linear with the generating current i_G; the small intercept ($i_G = 4 \pm 2$ μA) is caused by traces of oxidizable compounds in the mobile phase, mostly coming from the methanol used. King and Kissinger [2] corrected for a similar phenomenon by adding some bromine to the mobile-phase stock solution. However, the problem is more easily dealt with by correcting the generation current for the intercept.

The noise measured with the downstream detector also increases linearly with i_G (Fig. 3A). In general, the noise can be described by $N = \phi i_0$. At a flow rate of 1 ml min^{-1}, a value of $\phi = 0.002$ was found independently of the length of the reaction tubing and the mobile-phase composition. The noise could not be damped electronically, because its frequency was of the same order as that of expected chromatographic peaks (Fig. 3B).

The influence of the reaction time and the concentration of bromine produced on the signal of the phenolic model compounds was investigated in flow-injection experiments. The results are presented in Fig. 4. Some of the compounds investigated can react with more than one equivalent of bromine. However, the first step is usually by far the fastest and therefore the most important in optimization studies. In the following, only this first step is considered.

For a second-order reaction between reagent and analyte, the signal S, which is proportional to the amount of reagent reacted, can be written as

$$S = q\,\{A_0B_0 - A_0B_0 \exp[k_2t_r(A_0 - B_0)]\}/\{B_0 - A_0 \exp[k_2t_r(A_0 - B_0)]\} \quad (4)$$

where A_0 and B_0 are the original concentrations of analyte and reagent, respectively, k_2 is the second-order rate constant, t_r the residence time in the reactor coil and q a proportionality constant determined by the effi-

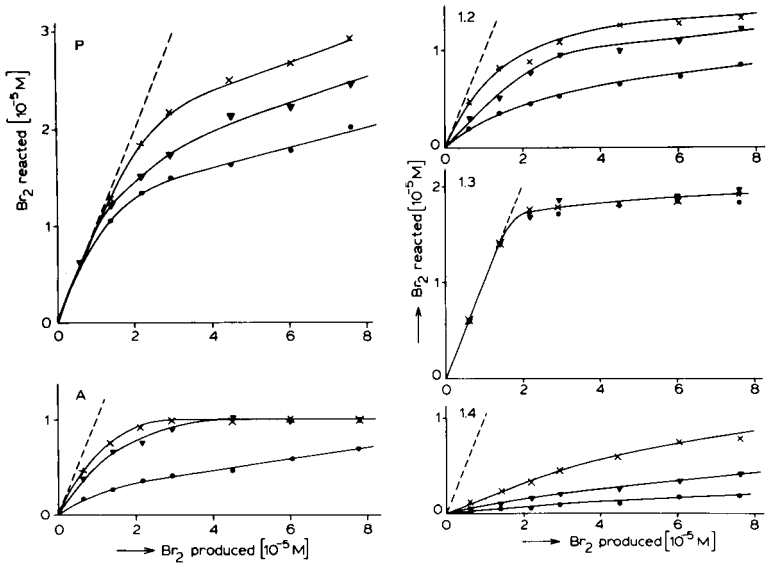

Fig. 4. Dependence of the signal of phenol (P), anisole (A) and 1,2-, 1,3-, and 1,4-dimethoxybenzenes on the bromine concentration. Plug injections (1 ml) of 10^{-5} M solutions in 20% methanol. Residence time, t_r: (○) 2; (▾) 6; (×) 18 s.

ciency of the amperometric detector and the amplifier setting. For optimization of sensitivity, S/N rather than S is important. From the above, the noise can be written as

$$N = q\ \phi\ B_0 \tag{5}$$

Detection limits were calculated from Eqns. 4 and 5, setting S/N = 2. The results of these calculations for various values of $k_2 t_r$ are presented in Fig. 5. The behaviour of the curves in this figure in the extreme regions is easily explained. With low B_0 or $k_2 t_r$ values, the reaction of the analyte will be far from complete, and for small values of A_0 one can write

$$S = q\ A_0 B_0\ k_2 t_r \tag{6}$$

Because the noise is also proportional to the reagent concentration, the detection limit is independent of B_0, and $A_{min} = 2\phi/k_2 t_r$. In contrast, with high B_0 or $k_2 t_r$ values, the analyte will react completely and $S = q\ A_0$. Then the detection limit increases with the noise: $A_{min} = 2\phi\ B_0$.

Because the amount of reagent available is limited, there is obviously an upper limit of linear response for the analyte concentration. This upper limit was defined as the analyte concentration where the sensitivity (S/A_0) is 97% of its correct value as measured from the slope. Maximum analyte concentrations can be calculated numerically from Eqns. 4 and 5; the values found are also included in Fig. 5. Again the extremes of the curves can be explained easily. With low B_0 or $k_2 t_r$ values, a 3% deviation of the signal

from its pseudo-first order value will be found when approximately 6% of the reagent reacts, thus $A_{max} = 0.06/k_2 t_r$. When the value of B_0 or $k_2 t_r$ is high, the analyte will react completely as long as reagent is available, i.e., $A_{max} = B_0$. The range of linear response is larger with high B_0 and $k_2 t_r$ values ($A_{max}/A_{min} = 250$ for $\phi = 0.002$) than with low values ($A_{max}/A_{min} = 15$). Given a certain rate constant and reaction time, which is limited by the band broadening and back-pressure caused by the reaction coil, a generating current can be chosen such that it fits the range of analyte concentrations expected.

It is tempting to use very small generating currents in order to obtain the lowest detection limits, but this is not advisable from the point of view of selectivity. When the reagent concentration is decreased, the sensitivity for a certain analyte will reach a maximum value. But then, as can be seen in Fig. 5, the sensitivity for interfering compounds which react more quickly or are oxidized directly on the generating electrode, is still increasing. Of course, when the reagent concentration is increased, the interference of more slowly reacting compounds will become more important. In practice, the nature of the real sample must be taken into account, but in general it is a reasonable compromise to choose a generating current such that $B_0/k_2 t_r \approx 1$, i.e.,

$$i_{G,opt} = nF\Phi/k_2 t_r \qquad (7)$$

In that case the detection limit is only slightly higher than its absolute minimum, and the selectivity for the analyte considered is approximately optimal with respect to interferences which react more slowly or more quickly. When a wide linear range is more important than a low detection limit, the generating current chosen should be somewhat higher than that suggested in Eqn. 7.

Selection of the separation system

Rate constants, which obviously have to be known for optimization, can be evaluated from curves such as are shown in Fig. 4. However, it is less time-consuming and more accurate to measure them in batch experiments with a rotating ring-disk electrode. The second-order rate constants for the reaction of phenol, anisole and two dimethoxybenzenes with bromine were measured in solutions with various methanol concentrations. Phenol is the only compound which is itself electroactive on platinum in the potential range employed, but interference from direct oxidation on the disk was not encountered; in the second-order measuring technique used with phenol, penetration of the analyte to the disk does not occur. The results of the ring-disk measurements are given in Fig. 6. Each point in this figure represents the means of at least 8 measurements at different analyte concentrations and rotation speeds; standard deviations were 5—10%. The rate constant for 1,3-dimethoxybenzene measured experimentally was very high ($>10^7$ mol^{-1} l s^{-1}), but the value found depended on the concentration and the rotation

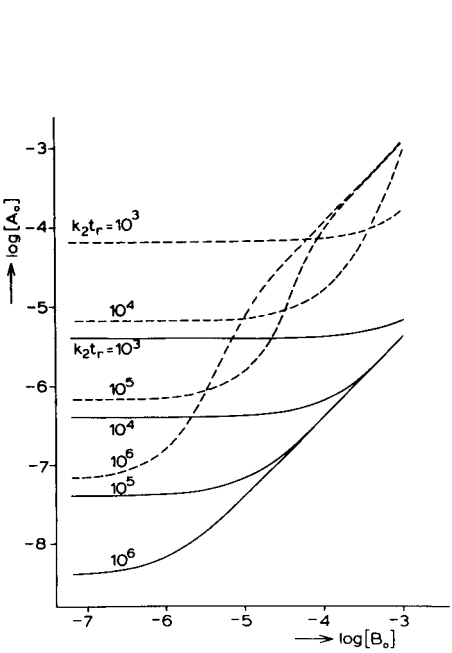

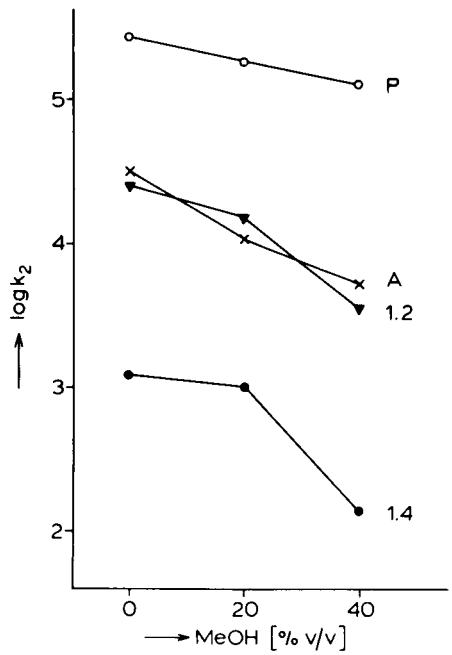

Fig. 5. Calculated detection limits (—) and upper limits of linear response (---) for ϕ = 0.002. For further explanation, see text.

Fig. 6. Reaction-rate constants measured with the ring-disk electrodes for phenol (P), anisole (A) and 1,2- and 1,4-dimethoxybenzene. The water/methanol mixtures contained 0.1 M KNO_3, 0.01 M KBr and 0.001 M HNO_3.

speed; this may be caused by a reaction with a second molecule of bromine with a rate constant of the same order of magnitude as the first one (cf. Fig. 4).

The reactions are strongly retarded by adding methanol to the solution, though not to the same extent for every solute. Therefore, in choosing the stationary and mobile phases, this effect on sensitivity should also be considered. The retention behaviour of the model compounds on two columns, a LiChrosorb RP-2 and a LiChrosorb RP-8 column, is depicted in Fig. 7. As expected, the compounds can be eluted with a mobile phase containing less methanol from the RP-2 column than from the RP-8 column; the separation on the RP-2 column with 30% methanol is about the same as that on the RP-8 column with 40% methanol. What this change of separation system does to the sensitivity can be seen by comparing the peaks in Fig. 8.

Determination of opiates

Many papers have appeared on the h.p.l.c. of opiates; recent reviews are available [11]. In reversed-phase h.p.l.c., the poor column efficiency for opiates is often a problem. The best separations are obtained with ion-

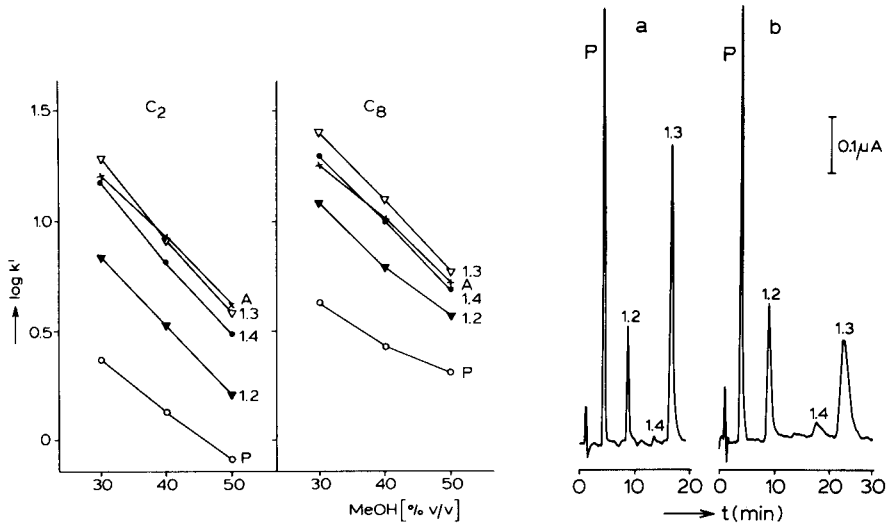

Fig. 7. Retention behaviour of the model compounds in reversed-phase h.p.l.c. on columns packed with 5-μm LiChrosorb RP-2 (C_2) or LiChrosorb RP-8 (C_8), with aqueous methanol as mobile phase. (For abbreviations, see Fig. 4.)

Fig. 8. Separation of phenol (**P**) and the three dimethoxybenzenes (1 nmol of each compound injected). Column (100 × 4.6 mm): (a) LiChrosorb RP-8 and mobile phase with 40% methanol; (b) LiChrosorb RP-2 and mobile phase with 30% methanol. i_G = 100 μA, t_r = 20 s.

pairing agents such as heptanesulfonic and camphorsulfonic acids. For detection, ultraviolet absorbance measurement is still most frequently used; the native fluorescence of the opium alkaloids is weak [12]. Sometimes, more specific methods have been recommended. For morphine, a post-column derivatization method has been developed [13]. Morphine can also be detected by electrochemical oxidation, but codeine and other opiates cannot or only at high potentials [14—16].

The major constituents of raw opium contain phenolic or phenolic ether groups. Four of these compounds were tested here: morphine (**M**), codeine (**C**), noscapine (**N**) and papaverine (**Pa**). A Supelco LC-8 column was used;

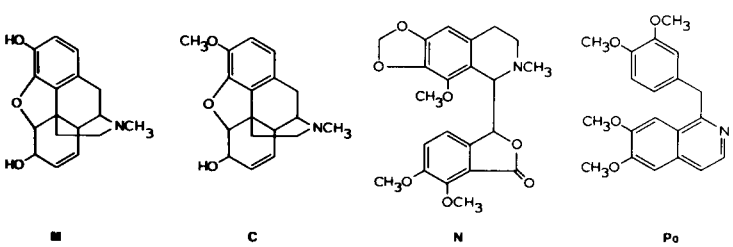

the mobile phase contained 40% (v/v) methanol, 1% (v/v) glacial acetic acid, 0.1 M KNO_3, 0.01 M tetramethylammonium bromide and 2.5 mM heptane-

sulfonic acid. The heptanesulfonic acid acted as ion-pairing agent. Addition of the quaternary ammonium salt, which decreased the retention of the opiates, was necessary to obtain good column efficiency. Capacity factors ranged from 0.30 for morphine to 3.0 for papaverine.

The rates of reaction with bromine were measured with the ring-disk electrode technique in the solvent mixture described above. The results are given in Table 5. From the rate constants, optimal generating currents were calculated for a 20-s reaction coil. The current was then optimized for codeine (i_G = 3 μA) and for noscapine (i_G = 100 μA). The changes in sensitivity can be seen in Fig. 9. Lower detection limits were measured experimentally in

TABLE 5

Detection of opiates[a]

Compound	k_2 (mol^{-1} l s^{-1})	$i_{G,opt}$ (μA)	Experimental detection limit (ng)	
			i_G = 3 μA	i_G = 100 μA
Morphine	1.1 × 10^5	1.5	0.4	5
Codeine	5.9 × 10^4	3	0.5	8
Noscapine	1.7 × 10^3	100	20	30
Papaverine	1.4 × 10^2	(1300)	300	300

[a] t_r = 20 s; for details see text.

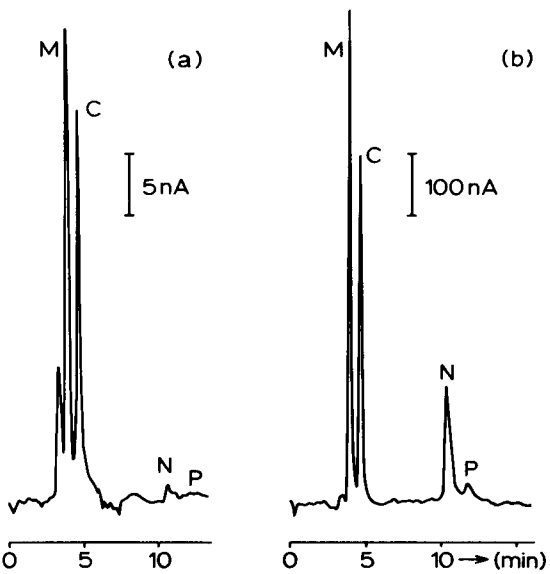

Fig. 9. H.p.l.c. separation of opiates: (a) i_G = 3 μA with 0.1 nmol of each component injected; (b) i_G = 100 μA with 1 nmol of each component injected. t_r = 20 s; for further details see text.

the two systems; the results are included in Table 5. These detection limits compare well with those observed with u.v. detection (10—100 ng) and with direct amperometric detection (0.1—1 ng for morphine) [11]. The range of linear response was measured for codeine and noscapine. As Fig. 10 shows, this range is wider at high generating currents, as predicted in the earlier discussion on A_{max}/A_{min} values.

Incompleteness of the reaction can introduce an extra source of peak height variation, e.g., when the temperature is not constant; this was confirmed in practice. For instance, with a generating current of 100 μA, the relative standard deviation on the peak height for codeine (1 nmol) was 2.1% (n = 10), while for noscapine (2 nmol) it was 3.6% (n = 10). The detection system could be used for several months without significant changes in sensitivity.

The noscapine content of a commercial cough syrup was measured. The syrup was diluted (1 + 49) with the mobile phase and filtered before injection. The chromatogram obtained is shown in Fig. 11. The noscapine concentration measured was 2.93 ± 0.09 mg ml^{-1}, compared to a value of 3 mg ml^{-1} given by the manufacturer.

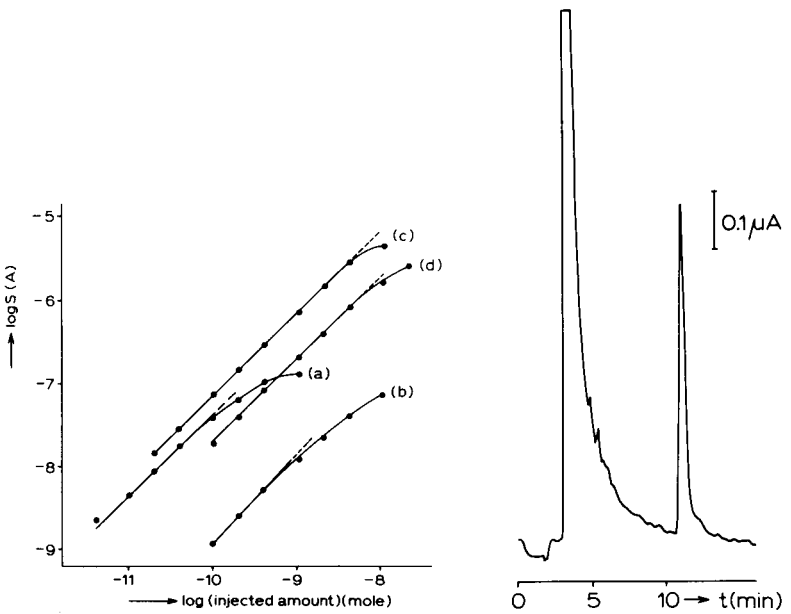

Fig. 10. Linearity of response for the opiates in the h.p.l.c. system used in Fig. 9: (a) i_G = 3 μA, codeine; (b) i_G = 3 μA, noscapine; (c) i_G = 100 μA, codeine; (d) i_G = 100 μA, noscapine.

Fig. 11. H.p.l.c. of noscapine-containing cough syrup. i_G = 100 μA, t_r = 20 s; for details, see text.

Conclusions

On-line generation of reagents for detection in h.p.l.c. is possible with negligible band broadening and satisfactory noise level and long-term stability. When the detection is achieved by amperometric measurement of the excess of reagent, the sensitivity is poorer than in direct electrochemical detection, but under favourable conditions detection limits in the subnanogram range can be obtained. Linearity of response is a weak point when the highest sensitivity is pursued. Otherwise, linear ranges of over two orders of magnitude are possible. Optimization of the system, with respect to sensitivity, selectivity and/or linear range, should be done on the basis of experimentally determined reaction-rate constants, rather than by trial and error.

The conclusions on optimization drawn in this study should be capable of extension to all post-column reaction detection systems where the noise is proportional to the (excess) concentration of reagent.

Reaction rates and reaction times are decisive for the sensitivity of the system. The use of heated reaction coils and segmented-flow or packed-bed reactors, which was not attempted in this work, may be a way to improve sensitivity with other reactions. However, it must be kept in mind that some selectivity will then be lost, because the number of sample components giving an appreciable signal will increase.

Thanks are due to W. H. Voogt for technical assistance and to D. J. van Iperen for building the production cell.

REFERENCES

1 Y. Takata and G. Muto, Anal. Chem., 45 (1973) 1864.
2 W. P. King and P. T. Kissinger, Clin. Chem., 26 (1980) 1484.
3 J. E. Dubois and J. J. Aaron, J. Chim. Phys., 66 (1969) 1109.
4 W. J. Albery and M. L. Hitchman, Ring-Disk Electrodes, Clarendon Press, Oxford, 1971.
5 K. Stephen, Chem. Ing. Tech., 32 (1960) 401.
6 J. Lankelma and H. Poppe, J. Chromatogr., 125 (1976) 375.
7 G. Taylor, Proc. R. Soc. London, Ser. A, 219 (1953) 186.
8 R. Aris, Proc. R. Soc. London, Ser. A, 235 (1956) 67.
9 R. Tijssen, Anal. Chim. Acta, 114 (1980) 71.
10 J. H. M. van den Berg, R. S. Deelder and H. G. M. Egberink, Anal. Chim. Acta, 114 (1980) 91.
11 T. A. Gough and P. B. Baker, J. Chromatogr. Sci., 20 (1982) 289; 21 (1983) 145.
12 L. A. King, J. Chromatogr., 218 (1981) 113.
13 P. E. Nelson, S. L. Nolan and K. R. Bedford, J. Chromatogr., 234 (1982) 407.
14 R. G. Peterson, B. H. Rumack, J. B. Sullivan and A. Makowski, J. Chromatogr., 188 (1980) 420.
15 R. S. Schwartz and C. R. Benjamin, Anal. Chim. Acta, 141 (1982) 365.
16 D. A. Meinsma, D. M. Radzik and P. T. Kissinger, J. Liq. Chromatogr., 6 (1983) 2311.

Analytica Chimica Acta, 162 (1984) 33—46
Elsevier Science Publishers B.V., Amsterdam — Printed in The Netherlands

INTERCOMPARISON OF FIVE METHODS FOR THE DETERMINATION OF TRACE METALS IN SEA WATER

R. BONIFORTI
ENEA-CREA, C.P. 316, 19100 La Spezia (Italy)
R. FERRAROLI, P. FRIGIERI and D. HELTAI
CISE S.p.A., C.P. 12081, 20134 Milano (Italy)
G. QUEIRAZZA
ENEL-CRTN, Via Rubattino 54, 20134 Milano (Italy)
(Received 14th February, 1984)

SUMMARY

Trace elements (Mn, Fe, Co, Zn, Ni, Cu and Cr) were preconcentrated from sea water by retention on Chelex-100 resin, APDC/8-quinolinol complexation followed by extraction with 4-methyl-2-pentanone or Freon-113, or coprecipitation with $Mg(OH)_2$ or $Fe(OH)_2$. After consideration of analytical blanks, extraction efficiency, precision, preconcentration factor, and suitability for operation on board ship, the best results were obtained by preconcentrating Mn, Fe, Co, Zn, Ni and Cu on Chelex-100 resin and coprecipitation of chromium(III) and (VI) with $Fe(OH)_2$. Graphite-furnace atomic absorption spectrometry and inductively-coupled plasma atomic emission spectrometry were used for the final measurements. The accuracy of the method was tested by using the reference sea water sample NASS-1.

The determination of trace elements in sea water is complicated by various factors, the most important of which are the very low element concentrations, the high salt content of the matrix, and contamination or loss of elements from the samples during sampling, preservation and pretreatment. The first two factors are dictated by the sea water medium and cannot be controlled, but loss or contamination during pretreatment is determined by the care taken in handling the samples and by the method chosen. In order to find the preconcentration method that gives the greatest recovery of trace elements from sea water and, at the same time, results in the least contamination, five preconcentration methods were compared, in preparation for a study of trace elements in water in the Taranto Gulf (Ionian Sea). The results of that study will be reported later.

At present, the most widely used methods of preconcentration for the determination of trace elements in sea water areas are: (a) retention on chelating resins containing iminodiacetic [1, 2] or dithiocarbamate [3—5] chelating groups; (b) complexation with, for example, 8-quinolinol, ammonium pyrrolidinedithiocarbamate (APDC), diethylammonium diethyldithiocarbamate (DDTC), sodium diethyldithiocarbamate (Na-DDCT), or dithizone

0003-2670/84/$03.00

[6—14] followed by extraction into 4-methyl-2-pentanone (MIBK) [9, 14—17], 1,1,2-trichloro-1,2,2-trifluoroethane (Freon-113) [18, 19], chloroform [20—22], or carbon tetrachloride [23]; (c) coprecipitation with inorganic hydroxides, such as those of Fe(II) [24, 25], Fe(III) [25—27], aluminium [28], indium [29], magnesium [30], lanthanum [31], or bismuth [32—34], or with organic reagents such as thionalide [35, 36], APCD and molybdenum [10], or Na-DDTC [37].

In this paper, an experimental comparison is made of APDC/8-quinolinol complexation followed by extraction with MIBK or Freon-113, coprecipitation with magnesium or iron(II) hydroxide, or chelating by batch treatment with Chelex-100. From these five preconcentration methods, two were chosen which have the advantage of being rapid, reproducible and easily used in the sometimes severe working conditions at sea. Included in the discussion are the possible instrumental problems that can arise from matrix components which may remain after the preconcentration and separation procedure. The suitability of the procedures for treating several samples simultaneously will also be discussed. The latter is important because, if at least some of the steps in the pretreatment can be done immediately after sampling, there is less risk of element loss. The comparisons were made with reference to interferences, recovery, precision, accuracy and detection limits.

EXPERIMENTAL

Reagents

Purification of reagents and treatment of the samples were done in a class 100 clean air laboratory. Concentrated nitric and hydrochloric acids (Carlo Erba, RPE) were purified by sub-boiling in a quartz still, and stored in FEP (fluorinated ethylene propylene) teflon vessels. The water used for all rinsing and solution preparation was Milli-Q grade (Waters Associates).

Sea-water samples were filtered through 0.45-μm Nuclepore polycarbonate membrane filters fitted to Millipore holders. The filtrates were acidified to pH 2 with sub-boiling distilled hydrochloric acid. Filters were precleaned by washing with 100 ml of 6 M hydrochloric acid and rinsed with 20 ml of water. Filters used for filtering precipitates obtained by the coprecipitation methods were additionally rinsed twice with 2 ml of 1 M ammonium acetate (pH 8) in order to avoid the risk of precipitate dissolution from residual acidity.

The plasticware consisted of polyethylene bottles and cylinders (Kartell), polypropylene pipets and flasks (Kartell), and fluorinated ethylene propylene (FEP) teflon bottles and separatory funnels (Nalgene). This ware was filled with 1 M nitric acid and shaken for 5 days, then rinsed twice with water. Sampling bottles were kept filled with 0.01 M nitric acid until used. Prior to filling with a given reagent, vessels were rinsed with the same reagent.

Standard solutions were prepared by diluting stock solutions (BDH laboratory reagents) with water, and used to prepare spiked water and sea water samples, and for instrumental calibration.

Chelex-100 resin (200–400 mesh, Na form; Bio-Rad) was purified by pouring about 100 ml of resin into a polypropylene column (i.d. 30 mm) fitted with a porous polyethylene frit (35-μm pore size), washing five times with 250 ml of 2.5 M nitric acid in order to eliminate trace metals present in the resin, and removing the excess of acid by rinsing thrice with 50 ml of water. Finally, the resin was transformed into the ammonium form by adding three 50-ml aliquots of 2 M ammonia. The column was rinsed with 150 ml of water in order to remove the excess of ammonia.

Ammonium acetate buffer was prepared by diluting 60 ml of glacial acetic acid with ca. 640 ml of water, and adjusting the pH to the required value ($4 < pH < 9$) with ammonia. The solution was diluted to 1 l and purified by adding about 5 ml of Chelex-100 resin.

The MIBK (Carlo Erba, RPE) was purified by sub-boiling distillation in a quartz still and stored in a precleaned quartz bottle. Freon 113 (Carlo Erba, RPE) was purified by extracting twice with nitric acid and finally rinsing with water. A fresh 5% solution of APDC (Spectrosol, BDH) was filtered through a 0.22-μm membrane filter, and metal impurities were eliminated by repeated extractions with distilled MIBK. The reagent was stabilized by adjusting the pH to ca. 9 with ammonia [9]; this solution was prepared weekly.

The iron(II) solution was prepared by dissolving 0.7 g of $Fe(NH_4)_2(SO_4)_2 \cdot 6H_2O$ (Carlo Erba, RPE) in water and diluting to 100 ml. This solution was prepared daily. The solution of 2% ammonium nitrate (Carlo Erba, RPE) was purified by adding about 5 ml of Chelex-100. Ammonia was purified by isopiestic distillation. 8-Quinolinol (AnalaR, BDH Chemicals) and ammonia were not purified because their contribution to the blanks was negligible. Also the iron(II) solution was not purified because this reagent was used only in the final procedure for the coprecipitation of chromium, and its blank contribution of this element was negligible. However, the unpurified reagents were always analyzed before use in order to verify that the impurity content was very low.

Apparatus

A Varian AA-1475 atomic absorption spectrometer, fitted with a GTA-95 graphite tube atomizer, a Pye-Unicam Model SP9 flame atomic absorption spectrometer, and a PlasmaTherm ICP-2500 plasma source coupled with a Jobin-Yvon monochromator VHR-1000 were used for the instrumental determinations. The instrumental conditions for graphite-furnace atomic absorption spectrometry are given in Table 1. Plasma emission measurements were made at 257.610 nm (Mn), 221.647 nm (Ni), 205.552 nm (Cr), 324.754 nm (Cu), 238.892 nm (Co), 213.856 nm (Zn) and 238.204 nm (Fe). In all cases, the bandwidth was 0.004 nm, the incident power was 1.25 kW, the coolant flow was 17–20 l min^{-1} and the nebulizer gas flow rate was 0.7 l min^{-1}. Spiked solutions were analyzed using this technique.

TABLE 1

Instrumental conditions used for graphite-furnace a.a.s. for analyser of NASS-1 reference material[a]

Element	Pretreatment steps												Atomization steps (L'vov platform)								λ	BW
	T	*R*	*T*	*R*	*T*	*H*	*T*	*R*	*T*	*H*	*T*	*H*	*T*	*R*	*T*	*H*	*T*	*H*	*T*	*H*		
Mn	65	10	110	30	110	10	800	10	800	10	800	1[b]	2400	0[b]	2400	2[b]	—	—	—	—	279.5	0.2
Ni	65	10	110	30	110	10	800	10	800	10	800	1[b]	2400	0[b]	2400	2[b]	—	—	—	—	232.0	0.2
Cr	70	5	110	40	110	10	1000	10	1000	10	1000	1[b]	2700	0[b]	2700	2[b]	—	—	—	—	357.9	0.2
Cu	75	5	110	40	110	10	700	10	700	10	700	1[b]	2300	0[b]	2300	2[b]	—	—	—	—	324.7	0.5
Co	70	5	110	40	110	10	800	10	800	10	800	1[b]	2400	0[b]	2400	2[b]	—	—	—	—	240.7	0.2
Zn	65	15	90	20	90	15	120	25	120	5	400	10	400	5[b]	2100	0[b]	2100	3[b]	—	—	213.9	1
Fe	65	15	90	20	90	20	120	20	120	5	500	3	500	10	500	3[b]	2500	0[b]	2500	1[b]	248.3	0.2

[a] *T* = temperature in °C; *R* = ramp time (s); *H* = hold time (s); λ = wavelength (nm); BW = bandwidth (nm).
[b] Decreased gas flow.

Liquid—liquid extraction

Sturgeon et al. [9] showed that the manganese—APDC chelate could not be extracted and therefore used a double chelate system consisting of APDC and 8-quinolinol. This system was also used here. MIBK or Freon-113 was used as solvent, and trace elements were stripped from the organic phases by back-extraction with nitric acid or solvent evaporation. The detailed procedure was as follows.

A weighed aliquot of acidified sea water (about 100 g) was placed in a separatory funnel and 2.5 M ammonia was added to neutralize the sample. Then 2 ml of pH 4 ammonium acetate buffer was added, followed by 0.5 ml of 5% APDC and 15 ml of organic solvent (Freon-113 or MIBK). The mixture was shaken for 3 min and the phases were allowed to separate. The organic phase contained Fe(III), Co(II), Zn, and Cr(VI) (organic phase 1) and the aqueous phase contained Cr(III) and Mn(II). The aqueous phase was transferred to a separatory funnel and heated in an oven at 90°C for 20 min in order to increase the complexation rate of chromium(III). The aqueous phase was allowed to cool to room temperature, and 15 ml of organic solvent was added. The mixture was shaken for 3 min and the phases were allowed to separate. The organic phase (organic phase 2) contained chromium(III). The aqueous phase was mixed with 0.5 ml of 8-quinolinol to complex manganese and adjusted to pH 9.2 with aqueous ammonia. This solution (organic phase 3) contained the manganese(II). The organic phases were stripped by one of two methods. In one method, each organic phase was shaken with 0.3 ml of 14 M nitric acid for 1 min, 3 ml of water was added and the shaking was continued for another 2 min. In the second method, each organic phase was evaporated at about 50°C in the presence of 1—2 ml of concentrated nitric acid. After 2—3 additions of acid, the organic phases were completely decomposed and the residues were diluted to 10 ml with water.

Chelating ion-exchange

Preconcentration with Chelex-100 resin was done by a batch method. The batch method has the advantages that some non-labile complexes may also be chelated by the resin [38] and that it can be applied on board ship. During the development of the method, two critical parameters were tested, the effect on the loss of trace elements of the pH of the ammonium acetate buffer used to elute the alkaline earth metal ions, and the amount of acid necessary to elute the trace metals of interest [9, 28]. The first parameter was investigated by extracting spiked sea-water samples by the batch method, pouring the resin into a polypropylene column, and eluting with 40 ml of pH 5.5—6.6 ammonium acetate. Eight successive 5-ml fractions were collected. The trace elements of interest were determined by inductively-coupled plasma atomic emission spectrometry (i.c.p.-a.e.s.) and the alkali and alkaline-earth elements by i.c.p.-a.e.s. or flame atomic absorption spectrometry (a.a.s.). The elution of the macro constituents was almost complete within the pH range investigated. Additional tests showed that the loss of manganese (which

is the first element that can be eluted by the buffer) occurred only at pH <5.5.

The second parameter was investigated by continuously measuring by flame a.a.s. the eluate obtained by passing 2.5 M nitric acid at a flow rate of 0.5 ml min^{-1}. The finding that elution was complete after passing 10 ml of the acid did not agree with that reported by Sturgeon et al. [9], who found that complete elution required 30 ml. This was probably due to the slower elution rate used in the present investigation. Based on the above tests, the following procedure was adopted.

The acidified sea-water sample (1 kg) was weighed in a precleaned polyethylene bottle and the pH was adjusted to 5.0—5.5 by adding 1 M ammonia. Chelex-100 (5—6 ml) and 10 ml of 1 M ammonium acetate buffer (pH 5.8) were added to the sample and the slurry was shaken for 24 h. The resin was collected in a polypropylene column (i.d. 8 mm) fitted with a porous polyethylene frit and washed with 30 ml of 1 M ammonium acetate buffer in order to elute the alkali and alkaline earth metal ions. Trace metals were eluted with 10 ml of 2.5 M nitric acid (0.3—0.5 ml min^{-1}) and collected in preweighed 10-ml polyethylene cylinders.

Coprecipitation with magnesium hydroxide

The acidified sea-water sample (1 kg) was weighed in a polyethylene bottle and 5 ml of 16 M ammonia was added; ammonia was used instead of sodium hydroxide because of its higher purity. In order to decrease the formation of soluble hydroxide complexes of trace elements, the pH was kept between 9.8 and 10.0. This resulted in only partial precipitation of magnesium hydroxide. After shaking for 24 h, the precipitate was filtered off on a 0.8-μm Nuclepore filter. The filter was washed with a few ml of ammonium acetate (pH 8) buffer and the residue was dissolved with 3 ml of 6 M hydrochloric acid or 3 ml of 7 M nitric acid. The solution was transferred to a preweighed polyethylene cylinder, about 7 ml of water was added, and the cylinder was re-weighed.

Coprecipitation with iron(II) hydroxide

The acidified sea-water sample (ca. 500 g) was weighed in a polyethylene bottle and the pH was adjusted to 8.0 with aqueous ammonia. A 500-μl aliquot of 1 mg Fe(II) ml^{-1} was added and the mixture was shaken for 24 h. The precipitate was filtered off on a 0.22-μm Nuclepore filter and, after washing with a few ml of ammonium acetate buffer (pH 8.5—9.0), it was dissolved with 3 ml of 6 M hydrochloric acid. The solution was transferred to a preweighed polyethylene cylinder, an additional 7 ml of water was passed through the filter and the cylinder was re-weighed. The coprecipitation with iron(II) was mainly investigated as a means for preconcentrating chromium-(III) and (VI). In addition, the use of iron(II) avoids the adverse affects of magnesium when optical spectroscopy is used.

Recovery efficiency

The chemical recovery for each procedure was calculated as follows (Fig. 1). A sea-water sample was divided into 2 sets of 5 sub-samples each (sets A and B). Trace metals (10 $\mu g\ l^{-1}$ each) were added to set A sub-samples and both set A and set B sub-samples were preconcentrated by the methods described above. Two sets of solutions, each consisting of 5 equal aliquots, were thus obtained (sets C and D, respectively). Set D solutions were divided into 2 equal aliquots (sets E and F). Trace elements were added to set E solutions in amounts equal to a half of those added to set A sub-samples. These solutions, designated set G, contain in principle the trace elements of interest in concentrations equal to those of set C solutions. The average signal obtained by analyzing set F solutions was subtracted from the signals obtained by analyzing set C and set G solutions. The recoveries were calculated by comparing these two sets of net signals. Trace elements were added to the sea water samples prior to any pH adjustment and allowed to equilibrate for 24 h before processing. Other recovery tests were done on a natural sea-water sample certified by the National Research Council of Canada (NASS-1).

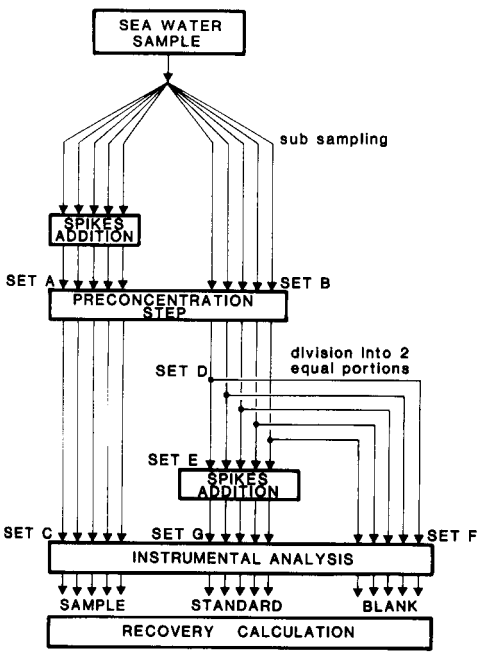

Fig. 1. Experimental scheme used for the calculation of recovery efficiency in sea-water samples.

RESULTS AND DISCUSSION

Instrumental measurements

The trace elements were quantified by graphite-furnace a.a.s. or by i.c.p.-a.e.s. The determination of trace elements in aqueous solutions stripped from either Freon-113 or MIBK did not present serious problems, provided that the ashing time was long enough to eliminate both the salt residue (mainly sodium) and the residual organic phase (solvent and APDC). The residual organic phase was more abundant with MIBK than with Freon-113. The residual amounts of Na, K, Ca and Mg in acidic solutions obtained by using Chelex-100 resin were low and therefore did not pose any problems. In this part of the study, a thermal program was chosen that would eliminate nitric acid, the main component responsible for a matrix effect.

The solution obtained by the coprecipitation with magnesium hydroxide showed a severe matrix effect. As Table 2 shows, the residual concentrations of alkali and alkaline earth metals were also rather high. The determination of Zn, Mn, and Co in the solutions obtained by dissolution of the precipitate in hydrochloric acid was possible only by chemical modification of the matrix by adding 1% (w/v) ammonium nitrate solution. Also in this case, however, a relatively long ashing time had to be used in order to eliminate the salt residue. In contrast, the determination of Zn, Mn and Co was possible without matrix modification in the solution obtained by dissolution in nitric acid. The solutions obtained after coprecipitation with iron(II) and dissolution did not exhibit instrumental difficulties.

Blank levels

The blank levels contributed by the methods investigated are reported in Table 3, along with the concentrations of the corresponding elements in the

TABLE 2

Total residual amount (mg) of alkali and alkaline earth metal ions in preconcentrated solutions (initially 100 g of sea water, 10 g of preconcentrated solution)

Preconcentration method	Residual amount of element (mg)			
	Na	K	Mg	Ca
Chelex-100[a]	0.025	0.002	0.010	0.042
APDC/MIBK	2.5	0.14	0.25	0.12
APDC/Freon-113	0.1	0.01	0.01	0.05
Coprecipitation with Mg(II)	0.9	0.10	15	0.12
Coprecipitation with Fe(II)	0.1	0.04	0.003	0.03

[a]The total residual amounts of alkali and alkaline earth metal ions were nearly equal when either 100-g or 1000-g sea-water samples were used.

TABLE 3

Blanks of the methods and trace element concentrations in the reference material NASS-1 and in typical coastal sea waters [39]

Element	Concentration of element ($\mu g\ l^{-1}$)[a]				
	Chelex-100	APDC	Copptn. with $Mg(OH)_2$	NASS-1[c]	Coastal water
Cr	—	0.01 ±0.001	0.01[b] ±0.001	0.184 ±0.016	0.28—0.5
Mn	0.005 ±0.001	0.005 ±0.002	0.006 ±0.002	0.022 ±0.007	0.18—0.9
Fe	0.06 ±0.02	0.20 ±0.06	0.20 ±0.08	0.192 ±0.036	0.2—2
Co	<0.001	0.003 ±0.0006	0.005 ±0.001	0.004 ±0.001	0.02
Ni	0.020 ±0.002	0.020 ±0.002	0.030 ±0.004	0.257 ±0.027	0.3—0.6
Cu	0.030 ±0.006	0.040 ±0.016	0.050 ±0.018	0.099 ±0.010	0.11—0.9
Zn	0.14 ±0.02	0.30 ±0.06	0.50 ±0.14	0.159 ±0.028	0.20—0.6

[a]Mean and 2× standard deviation for $n = 4$ unless otherwise stated. [b]The same value was obtained by coprecipitation with iron(II) hydroxide. [c]$n = 6$.

reference sample NASS-1 and in typical coastal waters [39]. To make the comparison straightforward, the blank levels are given as the contribution of trace elements to 1 l of sea water from reagents and sample handling. The Table shows that the procedure that gave least contamination was that based on Chelex-100. Even though the zinc blank of the Chelex method was close to the analyte content, it was still possible to determine this element owing to the small standard deviation of the blank.

Liquid—liquid extraction efficiency

The recoveries of spikes added to pure water and sea water are shown in Table 4. They show that the recoveries from pure water were generally higher than from sea water, and that APDC/8-quinolinol (8-Q) complexation did not present particular problems for back-extraction of Mn, Fe, Cu, Ni and Zn. The recovery efficiency for cobalt was 80 ± 20% for extraction with MIBK followed by solvent evaporation, and 80 ± 5% for extraction with Freon-113 followed by stripping into nitric acid. Thus the recovery was acceptable by both methods, but considerably less than when Chelex-100 resin was used (see Table 5). For chromium, only the values obtained by solvent evaporation are reported because the recoveries obtained by back-extraction were only a few per cent. The recovery of chromium(III) was unsatisfactory on extraction with MIBK or Freon-113, whereas the recovery

TABLE 4

Recovery (%) of added metal ions (10 $\mu g\ l^{-1}$ each) by liquid—liquid extraction

Matrix	System	Recovery (%) of metal ion[a]								Ref
		Cr(III)	Cr(VI)	Mn(II)	Fe(III)	Co(II)	Ni(II)	Cu(II)	Zn(II)	
Q-grade water	APDC/8-Q MIBK	90 ± 5[b]	72 ± 5[b]	96 ± 5[b]	100 ± 5[b]	85 ± 5[c]	95 ± 5[b]	100 ± 3[b]	100 ± 15[b]	This wor
Sea water	APDC/8-Q MIBK	60 ± 5[c]	80 ± 5[c]	84 ± 4	96 ± 5	80 ± 20[c]	100 ± 4[c]	92 ± 4[c]	109 ± 15[b]	
Sea water	APDC/8-Q Freon-113	54 ± 7[c]	34 ± 3[c]	78 ± 6[b]	97 ± 3[b]	80 ± 5[b]	100 ± 5[b]	90 ± 4[b]	110 ± 15[b]	
Demineralized water	APDC/8-Q MIBK	90[d]	—	90	100	90[d]	95	100	90	[9]
Sea water	APDC/8-Q MIBK	17[d] 73[e]	—	89	76	12[d] 71[e]	87	75	27	[9]
Sea water	DDTC $CHCl_3$	—	—	—	95	—	104	101	100	[20

[a]Mean ±2 × std. dev. of 5 replicate determinations. [b]Stripped by back-extraction. [c]Removed by solvent evaporation. [d]In organic phase. [e]In aqueous phase.

TABLE 5

Recovery (%) of added metal ions (10 $\mu g\ l^{-1}$ each) by Chelex-100 resin

Matrix	Recovery (%) of metal ion[a]								Ref.
	Cr(III)	Cr(VI)	Mn(II)	Fe(III)	Co(II)	Ni(II)	Cu(II)	Zn(II)	
Q-grade water	30 ± 10	≈0	95 ± 5	95 ± 5	98 ± 3	100 ± 4	100 ± 3	100 ± 10	This worl
Sea water	25 ± 10	≈0	86 ± 2.5	90 ± 15	92 ± 2.5	95 ± 6	88 ± 3	100 ± 5	
Sea water	—	—	95 ± 1	90 ± 10	107 ± 2	100 ± 3	97 ± 2	117 ± 2	[2]
Demineralized water	36	—	94	94	80	100	100	100	[2]
Sea water	8	—	44	57	86	85	77	96	[9]

[a]Mean ± 2 × std. dev. of 5 replicate determinations.

of chromium(VI) was 80 ± 5% on extraction with MIBK followed by solvent evaporation. Therefore, the recovery of chromium by Freon-113 was too low for this solvent to be an effective preconcentrator for chromium, whereas MIBK provides a fairly efficient recovery for chromium(VI) but a poor recovery for chromium(III).

A comparison with the recoveries reported by Sturgeon et al. [9] and McLeod et al. [20] shows that the agreement is good, with the exception of zinc for which Sturgeon et al. calculated a recovery of 27% from sea water. As far as chromium is concerned, Sturgeon et al. [9] took into account only the chromium(III), and obtained a nearly quantitative recovery, even though it was shared between the organic solvent (73%) and the back-extracted solution (17%).

Chelating ion-exchange efficiency

The efficiencies of recovery of spikes added to purified Q-grade water and sea water with Chelex-100 are summarized in Table 5. They show that the preconcentration yields for Q-grade water were higher than those for sea water. With the exception of chromium, the recoveries were very satisfactory. The present results and those obtained by Kingston et al. [2] are in good agreement, whereas significantly lower recoveries were obtained by Sturgeon et al. [9] for spiked sea water. The low recoveries for iron and manganese obtained by these authors could have been due to the washing of the resin and possibly to losses by hydrolysis.

Coprecipitation efficiency

Table 6 reports the recoveries obtained by coprecipitation with magnesium hydroxide and iron(II) hydroxide. The results show that coprecipitation with magnesium hydroxide allowed good recoveries to be obtained for all the ions considered with the exception of chromium(VI). Coprecipitation with iron(II) gave good recoveries only for chromium(III) and (VI). The recoveries of nickel and copper were low, and manganese and zinc suffered from contamination from impurities in the iron(II) solution.

Precision

Tables 4—6 show the precision of the methods tested as determined by using spiked sea-water samples. For liquid—liquid extraction, the standard deviation of a result ranged from 3% to 7% with the exception of zinc and cobalt. The large standard deviation for zinc was due to the relatively large and variable blank obtained, whereas the large standard deviation (20%) for cobalt occurred only with solutions obtained by evaporating MIBK. The

TABLE 6

Recovery (%) of added metal ions (10 $\mu g\ l^{-1}$ each) by coprecipitation with magnesium or iron(II) hydroxide

Matrix	Agent	Recovery (%) of metal ion[a]							
		Cr(III)	Cr(VI)	Mn(II)	Fe(III)	Co(II)	Ni(II)	Cu(II)	Zn(II)
Sea water	$Mg(OH)_2$	96 ± 10	≈0	89 ± 3	98 ± 4	87 ± 2	81 ± 7	84 ± 7	100 ± 10
Q-grade water	$Fe(OH)_2$	90 ± 7	95 ± 5	80 ± 10	—	85 ± 3	<50	<50	—
Sea water	$Fe(OH)_2$	80 ± 3	80 ± 3	—	—	—	—	—	—
Sea water[b]	$Fe(OH)_2$	—	—	48 ± 7	—	—	—	—	106 ± 2

[a]Mean ±2 × std. dev. of 5 replicate determinations. [b]Taken from Chakravorty and Van Grieken [27].

precision was much better for all other treatments. For chelating ion exchange, the precision depended on the element determined and ranged from 2.5% to 15% for sea water. The large standard deviation for chromium was due to poor and variable recovery. For coprecipitation, the precision was of the same order of magnitude as for the other methods and ranged from 2% to 10%. The precision found by the Chelex-100 method for the reference material NASS-1 is given in Table 7. It can be seen that the 100-fold lower trace metal concentrations in NASS-1 sample than in spiked sea water samples resulted in about a 4-fold decrease in the precision.

Choice of method

A preconcentration factor of 100 could be achieved with Chelex-100 or by coprecipitation. The use of volumes larger than 100 ml for liquid—liquid extraction was impractical and it was thus difficult to obtain a preconcentration factor higher than 40—50, which is not sufficient for the determination of cobalt and manganese in unpolluted waters when spectrometric techniques are used.

The procedures based on Chelex-100 and coprecipitation are easily done on board ship, whereas liquid—liquid extraction is obviously less suitable. In addition, the use of Chelex-100 allows the simultaneous processing of several samples which makes it possible to standardize the time at which the preconcentration of trace metals is begun, thus avoiding possible differences caused by physicochemical or biological processes which may perturb the composition of natural water samples.

Based on all the above considerations, the Chelex-100 resin method is the most appropriate among those tested for the preconcentration of Fe, Co, Zn, Cu, Ni and Mn, whereas preconcentration of Cr(III) and (VI) is achieved only by coprecipitation with iron(II) hydroxide. Because it is possible to treat many samples simultaneously in a short time, it is concluded that a suitable operating scheme for the determination of all these elements can be achieved by running pairs of samples, one by the Chelex-100 method and one by the iron(II) coprecipitation method.

TABLE 7

Experimental and certified values for the reference material NASS-1

Metal	Metal present ($\mu g\ l^{-1}$)		Metal	Metal present ($\mu g\ l^{-1}$)	
	Found[a]	Certified		Found[a]	Certified
Fe	0.19 ± 0.06	0.192 ± 0.036	Cu	0.122 ± 0.018	0.099 ± 0.010
Co	0.0036 ± 0.0007	0.004 ± 0.001	Cr	0.184 ± 0.017	0.184 ± 0.016
Zn	0.170 ± 0.068	0.159 ± 0.027	Mn	0.025 ± 0.013	0.022 ± 0.007
Ni	0.233 ± 0.014	0.257 ± 0.027			

[a]Mean ±2 × std. dev. of a result, n = 4. Coprecipitation with iron(II) hydroxide for chromium; preconcentration on Chelex-100 resin for all other metals.

Accuracy

After selection of these two methods which gave the best compromise for the parameters considered (analytical blanks, extraction efficiency, precision, preconcentration factor, and suitability for shipboard operation), the accuracy of the determination of Fe, Co, Zn, Mn, Ni, Cu and Cr was tested by analyzing four samples of the reference material NASS-1 by the standard addition method. The results are reported in Table 7, which shows that the agreement between experimental and certified values is excellent for Fe, Co, Cr and Mn, and satisfactory for Zn and Ni, whereas some uncontrolled factors increase the bias for the determination of copper to 23%.

REFERENCES

1 J. P. Riley and D. Taylor, Anal. Chim. Acta, 40 (1968) 479.
2 H. M. Kingston, I. L. Barnes, T. J. Brady and M. A. Rains, Anal. Chem., 50 (1978) 2064.
3 J. Zu-cheng and R. M. Barnes, ICP Inf. Newsl., 8 (1982) 45.
4 A. Miyazaki and R. M. Barnes, Anal. Chem., 53 (1981) 364.
5 W. B. Kerfoot and R. L. Crawford, ICP Inf. Newsl., 20 (1977) 289.
6 H. Armannsson, Anal. Chim. Acta, 110 (1979) 21.
7 R. Guevremont, Anal. Chem., 53 (1981) 911.
8 E. C. Kuehner, R. Alvarez, P. J. Paulsen and T. J. Murphy, Anal. Chem., 44 (1972) 2050.
9 R. E. Sturgeon, S. S. Berman, A. Desaulniers and D. S. Russell, Talanta, 27 (1980) 85.
10 J. W. Mitchell, Anal. Chem., 50 (1978) 194.
11 H. J. Patrick, F. W. Schulze and N. K. Kammenga, Mikrochim. Acta, 2 (1981) 277.
12 R. C. Hughes, P. C. Murau and G. Gundersen, Anal. Chem., 43 (1971) 691.
13 A. R. Knott, At. Abs. Newsl., 14 (1975) 126.
14 K. S. Subramanian and J. C. Meranger, Anal. Chim. Acta, 124 (1981) 31.
15 T. K. Jan and D. R. Young, Anal. Chem., 50 (1978) 1250.
16 R. E. Sturgeon, S. S. Berman, J. A. H. Desaulniers, A. P. Mykytiuk, J. W. McLaren and D. S. Russell, Anal. Chem., 52 (1980) 1585.
17 H. Bergmann and K. Hardt, Fresenius Z. Anal. Chem., 297 (1979) 381.
18 L. Rasmussen, Anal. Chim. Acta, 125 (1981) 117.
19 L. G. Danielsson, B. Magnusson and S. Westerlund, Anal. Chim. Acta, 98 (1978) 47.
20 C. W. McLeod, A. Otsuki, K. Okamoto, N. Haraguchi and K. Fuwa, Analyst (London), 106 (1981) 419.
21 K. W. Bruland, R. P. Franks, G. A. Knauer and J. H. Martin, Anal. Chim. Acta, 105 (1979) 233.
22 A. Sugimae, Anal. Chim. Acta, 121 (1980) 331.
23 J. D. Kinrade and J. C. Van Loon, Anal. Chem., 46 (1974) 1894.
24 R. H. Smillie, K. Hunter and M. Loutit, Water Res., 15 (1981) 1351.
25 R. E. Cranston, Geol. Surv. Can., 78-1A (1978) 337.
26 A. J. Pik, J. M. Eckert and K. L. Williams, Anal. Chim. Acta, 124 (1981) 351.
27 R. Chakravorty and R. Van Grieken, Int. J. Environ. Anal. Chem., 11 (1982) 67.
28 M. Hiraide, Y. Yoshida and A. Mizuike, Anal. Chim. Acta, 81 (1976) 185.
29 M. Hiraide, T. Ito, M. Baba, H. Kawaguchi and A. Mizuike, Anal. Chem., 52 (1980) 804.
30 B. Andersen and B. Salbu, Radiochem. Radioanal. Lett., 52 (1982) 19.
31 M. Thompson, B. Pahlavanpour and L. T. Thorne, Water Res., 15 (1981) 407.
32 E. Makayama, T. Kuwamoto, S. Tsurubo, M. Tokozo and T. Fujinaga, Anal. Chim. Acta, 130 (1981) 289.
33 E. Nakayama, T. Kuwamoto, H. Tokoro and T. Fujinaga, Anal. Chim. Acta, 131 (1981) 247.

34 E. Nakayama, T. Kuwamoto, S. Tsurubu and T. Fujinaga, Anal. Chim. Acta, 130 (1981) 401.
35 A. T. Ellis, D. E. Leyden, W. Wegscheider, B. B. Jablonski and W. B. Bodnar, Anal. Chim. Acta, 142 (1982) 73.
36 R. Panayappan, D. L. Venetzy, J. V. Gilfrich and L. S. Birks, Anal. Chim. Acta, 50 (1978) 1125.
37 J. Smits, J. Nelissen and R. Van Grieken, Anal. Chim. Acta, 111 (1979) 215.
38 P. Figura and B. McDuffie, Anal. Chem., 52 (1980) 1433.
39 P. G. Brewer, D. W. Spencer, in T. M. Church (Ed.), Marine Chemistry in the Coastal Environment, ACS Symp. Ser. 18, Am. Chem. Soc., Washington, DC, 1975, p. 80.

Analytica Chimica Acta, 162 (1984) 47—55
Elsevier Science Publishers B.V., Amsterdam — Printed in The Netherlands

COMBINATION COLLECTORS IN ADSORPTION COLLOID FLOTATION FOR MULTIELEMENT DETERMINATION IN WATERS BY NEUTRON ACTIVATION

XI FENG and D. E. RYAN*

Trace Analysis Research Centre, Department of Chemistry, Dalhousie University, Halifax, Nova Scotia, B3H 4J1 (Canada)

(Received 28th January 1984)

SUMMARY

A method is described for the collection of small amounts of both anions and cations in water samples by adsorption colloid flotation with a combination collector, prior to quantitation by neutron activation. In the presence of 20 mg of iron(III) and 2 ml of 0.1 M ammonium pyrrolidinedithiocarbamate, As(V), Cd(II), Co(II), Cu(II), Hg(II), Mo(VI), Sn(IV), Sb(III), Te(VI), Ti(IV), U(VI), V(V) and W(VI) are quantitatively collected from 1-l samples at a pH 5.8 ± 0.1; sodium dodecyl sulfate and sodium oleate are used as surfactant. Recoveries for all the elements tested are greater than 90%. Results for a number of elements in sea water and an NBS water standard, SRM 1643a, are given.

An earlier paper [1] described the use of adsorption colloid flotation (a.c.f.), with hydrous iron oxide as collector, for the successful preconcentration of arsenic, molybdenum, uranium and vanadium in sea water prior to their quantitation by neutron activation. The a.c.f. method has the particular merit of providing quick, simple preconcentration and separation of traces from large solution volumes; it therefore has considerable potential in the determination of very small amounts of materials in solution. Direct multielement determinations of the elements collected can then be done by neutron activation.

According to Kim and Zeitlin [2], the hydrous iron oxide has a positive charge in acidic solution and adsorbs anions, while in basic solution the hydrous iron oxide has a negative charge and adsorbs cations. Therefore, both anions and cations are not collected at the same pH. A pH >7 has been recommended [3] to collect cations but, from sea waters, a high background is observed in activation measurements because of adsorbed sodium. Direct measurements of several heavy metals by neutron activation, after a.c.f. collection at pH >9 [4], is also hampered by high background from magnesium and by handling problems caused by the relatively large amount of basic salts collected. Collection from acidic solution, therefore, is preferred.

The present study was concerned with expansion of the application of a.c.f. by simultaneous collection of a large number of elements in acidic

0003-2670/84/$03.00

solution. A reagent which reacts with ions over a wide pH range to form products which can be floated by a.c.f. is required. Ammonium pyrrolidinedithiocarbamate (APDC) is such a broad spectrum reagent [5] which has been widely used for concentration or separation of trace metals before measurement by atomic absorption spectrometry (a.a.s.) [6] or x-ray fluorescence (x.r.f.) [7]; co-precipitation of divalent and trivalent metal ions with APDC has been reported to be particularly well suited for preconcentration [8, 9]. The APDC—metal precipitates do not exhibit any colloidal properties and cannot be floated by themselves but, in the presence of a colloidal precipitate such as hydrous iron oxide, the APDC—metal complexes are floated and collected. The anions are also collected by the hydrous iron oxide under the same conditions.

Conditions of collection and flotation for cations and anions in acidic solution, prior to determination by neutron activation, are described in this paper.

EXPERIMENTAL

Apparatus

All samples were irradiated in the Dalhousie University SLOWPOKE reactor at a flux of 5×10^{11} n cm^{-2} s^{-1}. The activated samples were counted with a Canberra Ge(Li) detector having a 9.5% relative efficiency and 1.9-keV resolution at 1332 keV in conjunction with a TN-11 pulse height analyser (Tracor Northern). The ^{197}Hg nuclide was counted at 77 keV in a low energy photon detector (LEPD; Aptec) with a resolution of 0.560 keV, connected to a Jupiter multichannel analyser (Canberra). Conditions of measurement by neutron activation are shown in Table 1.

The flotation apparatus has been described previously [1]. A fine porosity frit was used to produce the fine bubbles of nitrogen gas used to float the precipitate. A Nuclepore filter funnel assembly, with a Gelman Metricel membrane filter (0.45-μm pore size, 47-mm diameter) was used to collect the floated precipitate.

Chemicals

A 0.1 M iron(III) solution was prepared by dissolving reagent-grade iron(III) chloride in 0.1 M hydrochloric acid. A solution which was 0.5% in both sodium dodecyl sulfate and sodium oleate was used as surfactant. The aqueous 0.1 M APDC solution, containing 1—2 drops of concentrated ammonia, was freshly prepared and filtered before use; traces of APDC complexes in 20 ml of the aqueous APDC solution can be removed by two extractions with 5 ml of methyl isobutyl ketone, if necessary. Potassium hydroxide (10% w/v) was used to adjust the pH.

The saturated solution of potassium chloride, added to help prevent formation of a colloidal suspension with fresh-water samples was prepared from reagent-grade potassium chloride and deionized-distilled water.

TABLE 1

Conditions used in neutron activation measurements

Element	Nuclide	Half-life	Energy Peak (keV)
5-min irradiation	*2-min decay*	*15-min counting*	
Co	^{60m}Co	10.47 min	59
Cu	^{66}Cu	5.0 min	1039
Sn	^{125m}Sn	9.5 min	332
Te	^{131}Te	25.0 min	150
Ti	^{51}Ti	5.78 min	320
U	^{239}U	23.5 min	74
V	^{52}V	3.75 min	1434
16-h irradiation	*72-h decay*	*15-min counting*	
As	^{76}As	26.4 h	559
Cd	^{115}Cd	2.22 d	336
Hg	^{197}Hg	2.67 d	77
Mo	^{99}Mo	2.76 d	140
Sb	^{122}Sb	2.70 d	564
W	^{187}W	23.9 h	686

Artificial sea water was prepared with analytical-grade chemicals and distilled water [10]. Natural sea water from the Northwest Arm, Halifax, Nova Scotia was collected directly from the taps in an oceanography laboratory of the university; the water is filtered through a sand bed before entering the building.

Except for mercury(II), appropriate concentrations of standard solution were prepared by dilution of atomic absorption spectrometry standards (Alfa Products Ventor). The standard solution (1000 mg l^{-1}) of mercury(II) was obtained by dissolution of mercury(II) chloride in deionized-distilled water.

Procedures

Flotation. Water samples (1 l), acidified to pH 3 with 6 M hydrochloric acid, were collected; for fresh water, 6 ml of a saturated potassium chloride solution were added to prevent formation of colloidal suspensions of hydrous iron oxide. Iron(III) chloride solution (4 ml) was added and the pH was adjusted to 5.5 with 10% potassium hydroxide. The mixture was stirred continuously for 10 min and 2 ml of 0.1 M APDC solution was added with stirring for at least 3 min at pH 5.8 ± 0.1. A portion (1 ml) of a mixture containing 0.6 ml of 0.5% sodium dodecyl sulfate and 0.4 ml of 0.5% sodium oleate was added and nitrogen was bubbled through the stirred solution. Stirring was stopped as soon as foams were formed on the surface of the solution. The nitrogen flow was controlled so that the bubbles just broke the surface. Most of the precipitate was floated and the solution became

clear within a few minutes. The precipitate was then transferred to the membrane filter and nitrogen was bubbled through the solution again with stirring to ensure complete recovery. The precipitates were washed with deionized-distilled water, dried with filter paper, and then folded for transfer into a polyethylene vial. The filter with precipitate in the vial was dried completely in vacuum at room temperature.

Standards used for calculating recovery were obtained by precipitation of hydrous iron oxide and APDC-iron complex from 1 l of deionized-distilled water according to the above procedure. Four or five drops of concentrated nitric acid and standard solution were then added to the collected precipitates in the vial and, after standing for 6 h to ensure uniform geometry, the content of the vial was dried under an infrared lamp.

The precipitates obtained by a similar procedure, but without addition of standards and acid, were used to quantify reagent blanks.

Irradiation and measurements. Two sets of irradiation, decay, and counting conditions were selected according to the half-lives of the nuclides used. For isotopes with half-lives of less than 60 min, 5-min irradiation, 2-min decay and 15-min counting were used, while 16-h irradiation, 3-days decay and 15-min counting were selected for nuclides with half-lives longer than 20 h. It is not possible, of course, to choose measurement conditions which are optimal for all isotopes in each group, but the above conditions provided simultaneous determination of the studied elements with adequate sensitivities and detection limits. Table 1 shows the conditions used.

It was necessary to correct the fission interference of ^{235}U by measurement of ^{99}Mo and ^{115}Cd when sea water was assayed. This contribution was obtained by measurement in artificial sea water containing 3 μg of uranium (the quantity expected from 1 l of sea water). The counts at 140 keV of ^{99}Mo and 336 keV of ^{115}Cd were then used to correct the interference.

RESULTS AND DISCUSSION

Selection of flotation conditions

Attempts to float the black precipitates of the iron-APDC complex at pH <4 were not successful even in the presence of large amounts of surfactant. However, the precipitate begins to float at pH 4 and flotation becomes easy with increasing pH. The colour of the precipitate changes gradually from black to brown and then becomes lighter in colour at pH's greater than 7. This results from competition between hydroxyl and APDC radicals; with increasing hydroxide ion concentration, the precipitate of hydrous iron oxide and APDC—iron changes completely into hydrous iron oxide. Over the pH range 4—7, both hydrous oxide and APDC-iron complex exist in the solution and the hydrous iron oxide plays a decisive role both in the flotation and adsorption/collection of APDC-metal complexes.

Selection of surfactant

The flotation ability of both anion and cation surfactants was examined. It was found that only anion surfactants, such as sodium dodecyl sulfate and sodium oleate could float the precipitate; cation surfactants (C_{12}-, C_{14}- or C_{16}-trimethylammonium bromides) were ineffective. These results suggest that the hydrous iron oxide with APDC—metal complexes still has a positive charge.

It was difficult to float the precipitate completely if only sodium dodecyl sulfate was used for flotation and sodium oleate was more effective. Sodium oleate, with its longer chain structure (C_{17}), produces a finer foam than the sodium dodecyl sulfate, but the dodecyl sulfate is very effective in hard water because its calcium and magnesium salts are soluble. A combined sodium dodecyl sulfate and sodium oleate mixture was therefore used for flotation. A portion (1 ml) of solution consisting of 0.6 ml of 0.5% sodium dodecyl sulfate and 0.4 ml of 0.5% sodium oleate is used in the recommended procedure.

Effect of pH on collection

Although the precipitate of hydrous iron oxide and APDC—metal complexes is successfully floated at pH >4 using the combined surfactant, complete recovery of various ions is pH-dependent. Table 2 shows the optimum pH range for collection of both anions and cations. Cadmium(II), Co(II), Hg(II), Sb(III) and U(VI) are more sensitive to pH change but good recovery is obtained for most elements in the pH range 5.5—6.3; to collect as many elements as possible under the same conditions, a pH of 5.8 ± 0.1 was selected in further studies.

The behaviour of uranium(VI), tungsten(VI), molybdenum(VI), vanadium(V) and arsenic(V) in flotation, using the hydrous iron oxide/APDC system, is similar to that described previously [1] and implies that the nature of collection of these anions is still one of adsorption onto the hydrous iron oxide precipitate. Over the pH ranges for better recovery of a number of cations [Co(II), Cd(II), Hg(II) and Sb(III)], both APDC and

TABLE 2

Optimum pH for collection

Element	pH	Element	pH
As	4.0 ≈ 8.0	Sb	5.5
Cd	5.0 ≈ 6.3	Te	5.0 ≈ 7.5
Co	5.5 ≈ 6.5	Ti	4.0 ≈ 7.5
Cu	5.5 ≈ 7.5	U	5.8 ≈ 6.5
Hg	5.8 ≈ 6.3	V	4.0 ≈ 7.5
Mo	4.5 ≈ 6.0	W	4.0 ≈ 6.5
Sn	4.0 ≈ 7.5		

hydroxide ions exist in the solution and the iron oxide collects both anions and metal complexes.

Cadmium(II) and Hg(II) show a decreased collection at pH 7 or 7.5. Here, the hydrous iron oxide has insufficient negative charge to collect completely positively charged cations and there is insufficient formation of iron—APDC to collect other APDC complexes. As the pH increases, however, the excess of hydroxide ions provide sufficient negative charges for cations to be completely collected by the hydrous iron oxide precipitate. It is difficult to determine the exact nature of the collection process, but the introduction of APDC into acidic solutions containing hydrous iron oxide plays an important role in the collection of cations at characteristic pH values.

Effect of the amount of APDC and iron(III) added on collection

Figure 1 shows the effect of the amount of APDC on the collection using hydrous iron oxide/APDC. No effect is observed for Mo(VI), As(V), Sb(III), W(VI) and Ti(IV), at a pH of 5.8 ± 0.1, on increasing the amount of 0.1 M APDC from 0 to 4 ml. Nor was an effect observed in the collection of V(V), Sn(IV) and U(VI) when up to 2 ml of 0.1 M APDC was present; a slightly lower recovery was obtained when 4 ml of 0.1 M APDC was added. For these seven elements, the nature of collection is still adsorption of anions onto positively charged hydrous iron oxide even in the presence of APDC.

In contrast to the above elements, the collection of Cd(II), Hg(II), Co(II), Cu(II) and Te(VI) was improved in the presence of APDC. The collecting efficiencies, in the presence of 2 ml of 0.1 M APDC, were 8.3, 7.5, 2.4, 1.5 and 1.3 times greater for Hg(II), Cd(II), Co(II), Cu(II) and Te(VI), respectively, than in its absence.

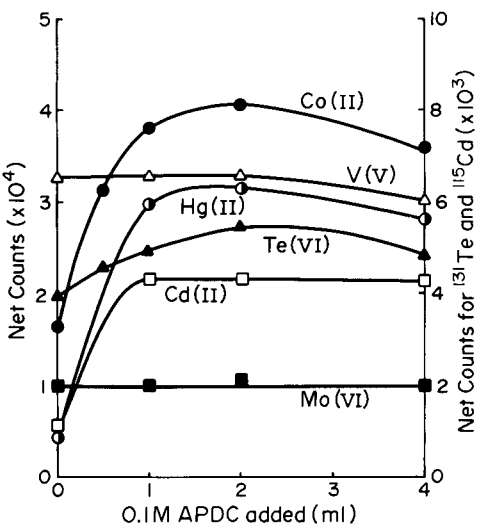

Fig. 1. Effect of amount of APDC on the collection of a number of ions. The Mo(VI) curve is also representative of As(V), Sb(III), Ti(IV), W(VI) whilst Sn(IV) and U(VI) are similar to V(V); Cu(II) is like Co(II).

Variation in the amount of APDC (from 1 to 4 ml) has no effect on quantitative collection of Cd(II) but efficiencies for collection of Hg(II), Co(II), Cu(II) and Te(VI) decrease with an increase in the amount of APDC. Collection of these elements depends on adsorption by hydrous iron oxide as well as on the role of APDC; with an increased amount of APDC, more hydrous iron oxide becomes converted to the APDC complex and the collection of the species dependent on the hydrous iron oxide surface is less effective. In the procedure described here, 2 ml of 0.1 M APDC is therefore recommended.

Studies of the effect of variation in the amount of iron(III) (from 2.5 mg to 20 mg) show that, except for Ti(IV), V(V) and W(VI), at least 10 mg of iron(III) is needed for quantitative collection. Better recovery, however, is obtained for Co(II), U(VI) and Sb(III) with 20 mg of iron(III). More than 20 mg of iron(III) results in higher backgrounds (from ^{56}Mn produced from the reaction ^{56}Fe(n,p)^{56}Mn). Studies of recovery in artificial sea water show that the 20 mg of iron(III) is sufficient to collect quantitatively all the elements investigated.

Stirring for 3 min after addition of APDC and the use of potassium hydroxide to adjust the pH are also recommended.

Results for different waters

Recoveries from artificial sea water and the relative standard deviation (r.s.d.) for seven samples are shown in Table 3; 90% or more recovery was obtained for all elements studied. Relative standard deviations were, in general, less than 5%; the r.s.d. for Te(VI), W(VI) and Sb(III) were higher but were still less than 10%.

The results for sea water are given in Table 4; they were obtained by standard addition. Sensitivities and counting statistics detection limit based on 2(background)$^{1/2}$ are given in Table 5.

The standard-addition calibration graphs show good linearity over all concentration ranges studied. Apparent recoveries at higher concentration

TABLE 3

Recovery and reproducibility from artificial sea water

Element	Conc. (μg l^{-1})	Recovery (%)	R.s.d. (%)	Element	Conc. (μg l^{-1})	Recovery (%)	R.s.d. (%)
As	5	90	±5	Sb	5	91	±9
Cd	25	90	±4	Te	10	102	±8
Co	5	92	±5	Ti	10	101	±4
Cu	25	93	±3	U	1	91	±4
Hg	25	90	±4	V	1	94	±2
Mo	25	90	±4	W	5	98	±3
Sn	5	99	±3				

TABLE 4

Results of determination for several elements in sea water and SRM 1643a

Element	Conc. in sea water ($\mu g\ l^{-1}$)		Conc. in SRM 1643a ($\mu g\ l^{-1}$)	
	This work	Ref.	This work	Certified[a]
As	1.20 ± 0.06	1.04 ± 0.01 [1]	75.1 ± 0.8	77.3 ± 7.1
Cd	<0.4	0.02—0.17 [11]	9.8 ± 1.7	10.2 ± 1.1
Co	0.75 ± 0.08	0.04—0.7 [11]	18.3 ± 1.4	19.3 ± 2.0
Cu	1.10 ± 0.17	1—20 [11]	18.8 ± 2.4	18.3 ± 2.0
Mo	11.0 ± 0.3	10.3 ± 0.4	103 ± 4.5	96.6 ± 6.1
Sb	0.16 ± 0.02	0.2 [11]	—	—
U	3.00 ± 0.09	3.10 ± 0.05 [1]	—	—
V	1.43 ± 0.11	1.22 ± 0.02 [1]	50.0 ± 1.3	53.9 ± 3.0
W	0.11 ± 0.01	0.1 [11]	—	—

[a]N.B.S. certified value.

TABLE 5

Sensitivities and detection limits for the elements collected in sea water

Element	Isotope	Sensitivity (counts μg^{-1})	Detection limit (μg)	Element	Isotope	Sensitivity (counts μg^{-1})	Detection limit (μg)
As	^{76}As	1.06×10^5	0.016	Sb	^{122}Sb	1.30×10^5	0.014
Cd	^{115}Cd	6.7×10^2	0.40	Te	^{131}Te	4.9×10^2	0.53
Co	^{60m}Co	5.8×10^3	0.060	Ti	^{51}Ti	1.3×10^2	1.4
Cu	^{66}Cu	1.9×10^2	0.66	U	^{239}U	3.06×10^5	0.010
Hg	^{197}Hg	3.7×10^3	0.071	V	^{52}V	1.32×10^5	0.0082
Mo	^{99}Mo	1.4×10^3	0.28	W	^{187}W	3.3×10^3	0.048
Sn	^{125m}Sn	2.0×10^2	0.93				

for Mo(VI), W(VI), Sb(III) and As(V) were slightly lower; it is therefore advisable to interpolate from curves corresponding to the concentration range of the elements in the samples at higher element concentrations.

Samples (100 ml) of SRM 1643a were taken for assay and were diluted to 1000 ml with deionized-distilled water. The results are also listed in Table 4.

The results for As(V), U(VI), Mo(VI) and V(V) in sea water agree with those found earlier [1]. The results for all other elements are within the range of concentrations given in the literature [11] except for cobalt; the cobalt result is near the upper limit of the concentration range. The results for As(V), Cd(II), Co(II), Cu(II), Mo(VI) and V(V) in SRM 1643a agree with certified values.

This work was supported by a grant from the Natural Sciences and Engineering Research Council of Canada.

REFERENCES

1 R. S. Shreedhara Murthy and D. E. Ryan, Anal. Chem., 55 (1983) 682.
2 Y. S. Kim and H. Zeitlin, Anal. Chim. Acta, 46 (1969) 1.
3 Y. S. Kim and H. Zeitlin, Sep. Sci., 7 (1972) 1.
4 M. Hiraide, Y. Yoshida and A. Mizuike, Anal. Chim. Acta, 81 (1976) 185.
5 W. J. Price, Spectrochemical Analysis by Atomic Absorption, Heyden, London, 1979, pp. 148—149.
6 A. W. Morris, Anal. Chim. Acta, 42 (1968) 797.
7 P. R. Brooks, B. J. Presly and I. R. Kaplan, Talanta, 14 (1967) 809.
8 E. A. Boyle and J. M. Edmond, Adv. Chem. Ser., 147 (1975) 44.
9 K. V. Krishnamurty and M. M. Reddy, Anal. Chem., 49 (1977) 222.
10 K. Grasshoff, Methods of Seawater Analysis, Verlag Chemie, Weinheim, 1976, Appendix Table 3.
11 J. P. Riley and G. Skirrow, Chemical Oceanography, Vol. 2, Academic Press, London, 1965, pp. 343—360.

Analytica Chimica Acta, 162 (1984) 57—65
Elsevier Science Publishers B.V., Amsterdam — Printed in The Netherlands

DETERMINATION OF FLUORINE IN GEOLOGICAL MATERIALS BY FAST NEUTRON ACTIVATION BASED ON THE $^{19}F(n,2n)^{18}F$ REACTION

M. ESPRIT, C. VANDECASTEELE and J. HOSTE*

Institute for Nuclear Sciences, Rijksuniversiteit Gent, Proeftuinstraat 86, B-9000 Gent (Belgium)

(Received 7th March 1984)

SUMMARY

The determination of fluorine in geological materials by fast neutron activation analysis based on the $^{19}F(n,2n)^{18}F$ reaction is described. Fast neutrons are produced by irradiation of a thick beryllium target with 14.5 MeV deuterons. A rotating sample holder allows simultaneous irradiation of samples and standards. Fluorine-18 is separated by steam distillation of hexafluorosilicic acid or by extraction with triphenylantimony(V) dichloride and the annihilation radiation is measured with γ—γ coincidence equipment. The nuclear interference of recoil protons that induce the $^{18}O(p,n)^{18}F$ reaction is evaluated by means of synthetic samples: for a rock containing 43.4% of oxygen and 0.5% of hydrogen, the interference corresponds to 4.4 $\mu g\ g^{-1}$ fluorine. The method was applied to USGS and NIMROC reference rocks: for concentrations between 6000 and 50 $\mu g\ g^{-1}$, the relative standard deviation ranged from 2 to 10%.

For the determination of fluorine in geological materials, titrimetry with thorium nitrate, potentiometry with a fluoride-selective electrode and spectrophotometric methods utilizing zirconium/eriochrome cyanine R and alizarin fluorine blue have been used. Results for fluorine in reference rocks show that the accuracy of these methods is questionable. For the reference sample NIM-L, for example, the results obtained ranged from 1950 to 8000 $\mu g\ g^{-1}$ [1]; for lower concentrations the picture was even worse, results for NIM-N ranging from 10 to 530 $\mu g\ g^{-1}$ [1].

Fluorine can also be determined by activation analysis with photons [2], protons [3] or neutrons [4—7]. The present paper describes the determination of fluorine by means of the $^{19}F(n,2n)^{18}F$ reaction (threshold = 10.9 MeV) induced by fast neutrons. Fluorine-18 is a pure β^+-emitter with a 109.8-min half-life. Fast neutrons are obtained by irradiation of a thick beryllium target with 14.5-MeV deuterons. This yields a neutron spectrum up to 18 MeV with a maximum around 7 MeV. Under these conditions, the highest sensitivity for fluorine is not obtained but the extent of nuclear interferences is limited.

No direct nuclear interferences occur, but there are two kinds of secondary interferences. In the first type, fast neutron irradiation of materials con-

0003-2670/84/$03.00

taining both hydrogen and oxygen yields ^{18}F, formed by the $^{18}O(p,n)^{18}F$ reaction induced by recoil protons; the threshold is 2.59 MeV. A similar interference was observed by Gilmore and Hull [8] for the determination of nitrogen with fast neutrons. When small amounts of fluorine are determined in materials containing both oxygen and hydrogen, this interference must be corrected for. The interference was studied as a function of the hydrogen and oxygen concentrations. For this purpose, a synthetic geological matrix was prepared from pure magnesium oxide, silicon dioxide, iron(III) oxide and aluminium oxide, in relative amounts close to those of dunite, a rock with a low fluorine content. Oxalic acid was added as a source of hydrogen atoms. Samples enriched in ^{18}O were prepared by adding potassium nitrate enriched in ^{18}O. To simulate a real sample, reduction of the particle size and homogenizing was required. The brittle-fracture technique [9] was used and the particle size distribution and homogeneity were checked by scanning electron microscopy. Homogeneous samples with particle sizes less than 10 μm were obtained.

Another sort of secondary interference is caused by fast neutron irradiation of lithium; tritons are produced by the $^{6}Li(n,\alpha)^{3}H$ reaction ($Q > 0$) and induce the $^{16}O(^{3}H,n)^{18}F$ reaction ($Q > 0$). To evaluate this source of interference, lithium carbonate was irradiated. The ^{18}F formed was compared to the activity of a fluorine standard. For an oxygen content of 65.0%, which is larger than that of rocks (ca. 45.0%), 100 μg of lithium induces the same ^{18}F activity as 0.28 μg of fluorine. As the lithium content of geological material is generally below 100 $\mu g\ g^{-1}$, this interference can be neglected in nearly all cases.

EXPERIMENTAL

Samples and standards

Synthetic rock samples were prepared from pro analysi reagents: magnesium oxide (43.7%), silicon dioxide (39.0%), iron(III) oxide (17.0%) and aluminium oxide (0.3%). The oxides were heated at 1000°C and cooled in a desiccator. To prepare samples of approximately 1 g, appropriate amounts of the oxides were weighed into the steel vessel used for the homogenization. For the preparation of the ^{18}O-enriched samples, potassium nitrate containing 21.2 atom-% of ^{18}O (Prochem, Great Britain) was added. The contents of the vessel were pulverized by means of a steel ball: the vessel was cooled in liquid nitrogen and shaken for 15 s over an amplitude of 10 mm, at a frequency of 50 Hz with a Mikro-Dismembrator. This cycle was repeated five times. After the mixture had been dried at 110°C, the necessary amount of oxalic acid, ground in an agate mortar, was added. The whole was shaken during 12 h in a Turbula Mixer. A blank was prepared from the oxides mixed in the same way. A 1-g sample was weighed into an aluminium container (12 mm internal diameter).

The NIMROC geochemical reference materials (NIM-G, NIM-S, NIM-L,

NIM-N, NIM-P) and USGS standard materials (DTS-1, PCC-1, GSP-1, G-2) were dried for 2 h at 110°C and packed in aluminium containers. A 100-mg sample was used when the separation was done by extraction. When steam distillation was applied, samples of 0.5—1 g were used, depending on the fluorine content expected.

Potassium fluoride was used as the standard, because no spectral interference occurs when the annihilation radiation is measured. The potassium fluoride was dried at 125°C for 12 h. For standardization, 200-μl portions of 0.075 M potassium fluoride in 0.1 M potassium hydroxide were spotted on Whatman 41 filter papers (47 mm diameter) and dried at 110°C. The filter papers were each packed in two blank filter papers and pressed to a pellet (12 mm diameter). Blank pellets were also prepared. The blank amounted to 4% of the ^{18}F activity in the standard.

Irradiation

Fast neutrons were produced by irradiating a 1-mm thick beryllium target with 14.5-MeV deuterons. A rotating holder was used for the simultaneous irradiation of samples and standards; two samples, a standard and a blank rotated close to the beryllium disk with the sample axes coinciding successively with the target axis (Fig. 1). The mean flux amounted to about 46% of the flux corresponding to the position closest to the beryllium disk. Irradiation times ranged from 30 min to 2 h and the deuteron beam intensity was 20 μA. An aluminium foil (50 μm thick, 12 mm diameter) was placed on each side of the samples and the standards. The ^{24}Na activity from the $^{27}Al(n,\alpha)^{24}Na$ reaction ($t_{1/2}$ = 15.03 h; E_γ = 1.369 MeV) was used to correct for differences in neutron flux between the samples and the standards.

Radiochemical separation by steam distillation

After the sample has been fused and dissolved, fluorine is steam-distilled as hexafluorosilicic acid from the acidic solution and precipitated as calcium fluoride, together with calcium carbonate to obtain a precipitate that can be filtered easily. As the separation is not quantitative, the yield must be determined. A known amount of sodium fluoride is therefore added before the separation and the fluorine content of the precipitate is determined by neutron activation with an isotopic neutron source by means of the $^{19}F(n,\alpha)^{16}N$ reaction [10].

Procedure. After the irradiation, transfer the sample to a nickel crucible and mix it with a ten-fold amount of sodium peroxide and 400 mg of sodium fluoride. Heat the mixture on a Bunsen burner until fusion is complete. Cool the melt and dissolve in water. Transfer the solution to a pyrex distillation flask and add 20 ml of concentrated nitric acid and 25 ml of phosphoric acid (85%). Heat to 130°C, introduce steam and collect 200 ml of distillate; this takes 60—90 min. Adjust the pH to 7 and add about 15 ml of a 1 M sodium carbonate solution. Heat to 80°C, and stir in 25 ml of 1 M calcium chloride. Filter off the calcium fluoride/calcium carbonate precipitate on a membrane

filter paper and wash with hot water. Pack the precipitate in mylar foil and transfer it to an aluminium container for counting.

Radiochemical separation by liquid—liquid extraction

As the distillation/filtration procedure is relatively slow, usually taking 2—3 h in all, and a separate yield determination is needed, a liquid—liquid extraction procedure with triphenylantimony(V) dichloride [11] was used. In aqueous solution, mainly the hydroxyfluoride of triphenylantimony is formed, which is soluble in carbon tetrachloride. Tracer experiments showed that extraction is quantitative between pH 2 and 11.5 (Fig. 2).

The efficiency of the fluoride extraction is influenced by silicon(IV), aluminium(III) and iron(III) that form fluoro complexes. A complexing agent that forms strong complexes with aluminium(III) and iron(III) is essential. The masking of aluminium by ethylenediaminetetraacetic acid (EDTA) and *trans*-1,2-diaminocyclohexanetetraacetic acid (CDTA) during the extraction of fluoride was studied by tracer experiments. The results obtained with CDTA were far more satisfactory, especially at pH 6 (Fig. 3). Adding more than two equivalents of CDTA did not improve the extraction. The addition of CDTA provided 90% extraction yields even in the presence of 15 mg of aluminium (Fig. 4). Iron(III) could be masked completely by adding two equivalents of CDTA.

Silicon was removed from the solution, before the extraction of fluoride, by precipitation with zinc sulfate at pH > 10 [12]. The zinc silicates formed were filtered off and washed.

The yield of the separation of fluoride from a geological matrix was

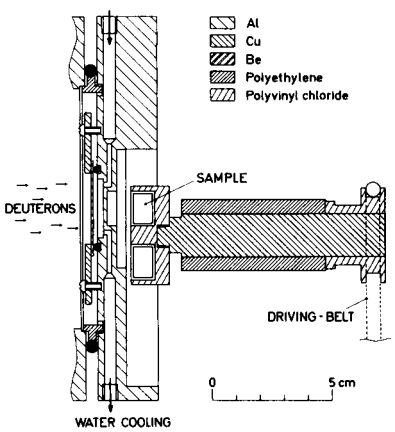

Fig. 1. Beryllium target with rotating sample holder.

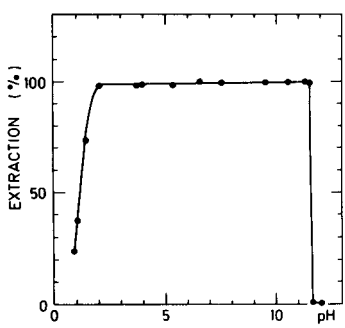

Fig. 2. Extraction of fluoride as a function of pH. (3×10^{-4} M fluoride; 10^{-2} M triphenylantimony(V) dichloride; 20-ml phases.)

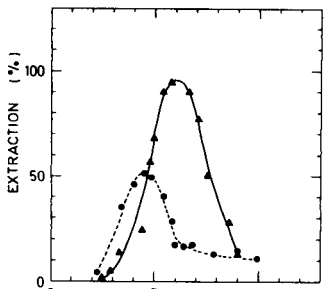

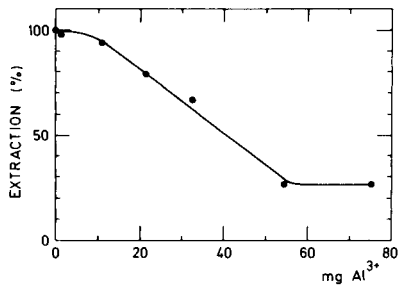

Fig. 3. Extraction of fluoride as a function of pH in the presence of aluminium, with EDTA (•) and CDTA (▲) as complexing agent. (3×10^{-4} M fluoride; 2×10^{-2} M aluminium, 4×10^{-2} M complexing agent; 10^{-2} M triphenylantimony(V) dichloride; 20-ml phases.)

Fig. 4. Extraction of fluoride as a function of the amount of aluminium in the aqueous phase (pH 6) with CDTA (2 equivalents) as complexing agent. (3×10^{-4} M fluoride; 10^{-2} M triphenylantimony(V) dichloride; 20-ml phases.)

determined by tracer experiments. Carrier-free ^{18}F, obtained by irradiation of lithium carbonate in a nuclear reactor, was added to an inactive sample and the separation was applied. The mean yield was 98.8 ± 0.9% (mean and standard deviation of 5 experiments).

Procedure. Transfer the sample to a nickel crucible and fuse with 2.5 g of sodium peroxide. After cooling to room temperature, dissolve the melt in 50 ml of 6 M nitric acid. Add 10 ml of 1 M zinc sulfate and adjust the pH to about 10 with 6 M ammonia: a mixed precipitate of zinc silicate and zinc aluminate is formed. Filter and wash with 1% (w/v) sodium sulfate solution. Add 1 g of CDTA, dissolved in sodium hydroxide and adjust the pH to 6. Extract fluoride with three 50-ml portions of 0.01 M triphenylantimony(V) dichloride in carbon tetrachloride after stirring the solutions mechanically for 10 min. Combine the organic phases and extract the fluoride back into 100 ml of 2 M ammonia. Collect the aqueous phase in a polyethylene bottle for counting. This procedure takes about 1.5 h.

Measurements

The annihilation radiation was measured with γ—γ coincidence equipment with two NaI(Tl) detectors (7.6 × 7.6 cm) in a 180° geometry.

The standards and the calcium fluoride/calcium carbonate precipitates were centred in a poly(vinyl chloride) holder to ensure complete annihilation. The solutions obtained from the fluoride extraction were measured in polyethylene containers. A correction factor was applied for the different detection efficiencies of samples and standards. For this purpose, a copper foil was irradiated with thermal neutrons in a nuclear reactor. The ^{64}Cu activity, formed via the $^{63}Cu(n,\gamma)^{64}Cu$ reaction (β^+-emitter; $t_{1/2}$ = 12.8 h)

was measured in the geometry of the standard and, after dissolution, in the geometry of the sample.

Repeated activity measurements for the standards and the samples with measuring times ranging from 10 to 30 min were started 2—3 h after the irradiation. The half-life, determined from a series of measurements, was in agreement with the literature value of 109.8 min. The radiochemical purity was checked by Ge(Li) γ-spectrometry: a pure annihilation spectrum was always obtained.

For flux monitoring, the 1.369 MeV γ-ray of ^{24}Na ($t_{1/2}$ = 15.03 h) from the $^{27}Al(n,\alpha)^{24}Na$ reaction was measured with a Ge(Li)γ-spectrometer.

RESULTS AND DISCUSSION

Interference from the ^{18}O (p,n)^{18}F reaction

Figure 5 shows the apparent fluorine concentration as a function of the hydrogen concentration determined by means of synthetic samples using steam distillation to separate ^{18}F. The fluorine concentration ($\mu g\ g^{-1}$) corresponding to the observed ^{18}F activity in samples containing 43.4% of oxygen is given as a function of the hydrogen concentration. The ^{18}F activity increases with the hydrogen concentration. The slope of the regression line corresponds to 7.65 ± 0.70 $\mu g\ g^{-1}$ (% H)$^{-1}$ and the intercept is not significantly different from zero at the 95% confidence level.

The results for samples enriched in ^{18}O are given in Fig. 6. For synthetic samples containing 1.00% of hydrogen, the original amount of ^{18}O was

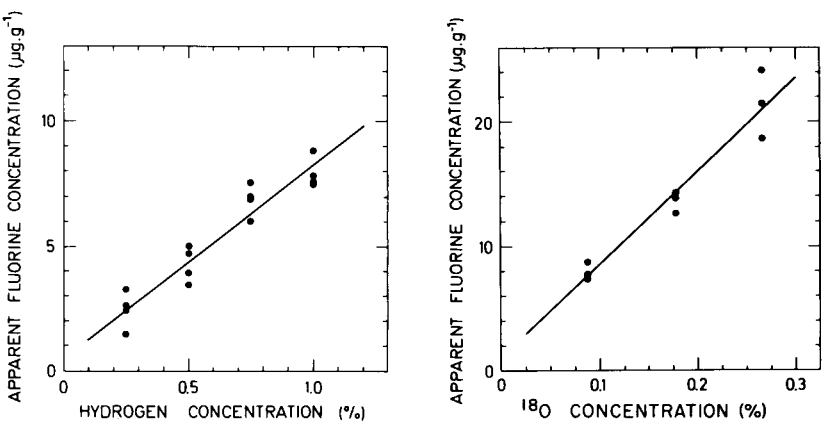

Fig. 5. Apparent fluorine concentration ($\mu g\ g^{-1}$) in synthetic rock samples (43.4% of oxygen) as a function of the hydrogen concentration (%); experimental data and regression line.

Fig. 6. Apparent fluorine concentration ($\mu g\ g^{-1}$) in synthetic rock samples (1.00% of hydrogen) as a function of the ^{18}O concentration (%); experimental data and regression line.

doubled and tripled and the ^{18}F activity induced was determined. The slope of the regression line corresponds to 75.2 ± 1.6 $\mu g\ g^{-1}$ (% $^{18}O)^{-1}$ and the intercept is not significantly different from zero at the 95% confidence level. The straight line through the origin confirms that the interference is due to the $^{18}O(p,n)^{18}F$ reaction induced by recoil protons. It indicates that the particle sizes are sufficiently small and that the ^{18}O-containing potassium nitrate is sufficiently well mixed with the oxides and the oxalic acid. Otherwise the increase of the ^{18}F activity obtained would be much lower than the ^{18}F activity in the original sample. The curves determined can be used to correct for the interference when fluorine determinations are to be carried out in the presence of hydrogen.

Hydrogen concentrations in geological materials after drying at 110°C, range from 0.03 to 0.50%. For a geological material containing 43.4% of oxygen and 0.5% of hydrogen, the interference corresponds to 4.4 $\mu g\ g^{-1}$ of fluorine. When fluorine has to be determined at the $\mu g\ g^{-1}$ level, the amount of ^{18}F formed via the interfering reaction is therefore no longer negligible and a correction has to be applied.

The results obtained in fluorine determinations can be corrected for the interference in two different ways: (1) the amount of hydrogen from literature data is used to correct for the interference by means of Fig. 5; or (2) the amount of ^{18}O originally present in the sample is doubled by adding ^{18}O-enriched potassium nitrate. The increase of the ^{18}F activity corresponds to the ^{18}F activity from the $^{18}O(p,n)^{18}F$ reaction in the original sample. The results obtained in this way are independent of literature values for the hydrogen concentration.

Results for fluorine

Table 1 shows the results for the determination of fluorine in NIMROC reference materials, compared with literature data. The interference of lithium was negligible in all cases. For SARM 4 NIM-N and SARM 5 NIM-P,

TABLE 1

Fluorine concentrations in NIMROC reference materials

SARM[a] standard	Fluorine content ($\mu g\ g^{-1}$)		
	This work[b]	Literature data [13]	[1]
SARM 1 NIM-G	5410 ± 250 (4.6)	4000	7547
SARM 2 NIM-S	135.5 ± 8.1 (6.0)	200	151.5
SARM 3 NIM-L	5500 ± 230 (4.2)	4000	4382
SARM 4 NIM-N	59.4 ± 5.0 (8.4)	300	132.5
SARM 5 NIM-P	57.0 ± 5.5 (9.5)	200	93.5

[a]South African Reference Material. [b]Average of 2 determinations ± standard deviation (standard deviation in %).

the results were corrected for the interference from $^{18}O(p,n)^{18}F$. The agreement with Flanagan's values [13] is very poor. However, Flanagan's values were only estimated "magnitudes". The results for fluorine from different laboratories were reported by the National Institute for Metallurgy (NIM) [1]. The means of the laboratory means are given in Table 1. Recommended values were suggested only for SARM 1 NIM-G (4200 $\mu g\ g^{-1}$) and for SARM 3 NIM-L (4400 $\mu g\ g^{-1}$).

Table 2 gives the results for the USGS standard rocks GSP-1 and G-2. The results obtained by steam distillation and by extraction of the fluoride are compared. The means are not significantly different at the 95% confidence level; the standard deviation is smaller for the extraction method. The results obtained are in reasonable agreement with the values from Flanagan [13] and in good agreement with the "usable values" from Abbey [14].

The results for USGS DTS-1 and USGS PCC-1 are given in Table 3. Because of the low apparent concentrations in DTS-1, twice the original ^{18}O amount was added to determine the interference, whereas in the case of PCC-1, the amount of ^{18}O was only doubled. The interference deduced from the hydrogen content is also given and does not differ significantly (95%

TABLE 2

Fluorine concentrations in USGS standard rocks (comparison between separation by steam distillation and separation by extraction)

USGS standard	Fluorine content ($\mu g\ g^{-1}$)			
	This work[a]		Literature	
	Steam distillation	Extraction	[13]	[14]
USGS-GSP-1	3590 ± 170 (4.8)	3741 ± 78 (2.1)	3200	3800
USGS-G-2	1393 ± 79 (5.7)	1302 ± 52 (4.0)	1290	1300

[a]Average of 3 determinations ± standard deviation (standard deviation in %).

TABLE 3

Fluorine concentrations in USGS standard rocks with 95% confidence limits for n determinations

USGS standard	Apparent fluorine concentration ($\mu g\ g^{-1}$)	Interference	Fluorine concentration ($\mu g\ g^{-1}$)
USGS-DTS-1	2.74 ± 0.47 (n=5)	1.06 ± 0.86[a]	1.68 ± 0.98[a]
		1.78 ± 0.31[b] (n=3)	0.96 ± 0.79[b]
USGS-PCC-1	8.4 ± 1.6 (n=3)	5.44 ± 0.41[a]	3.0 ± 1.7[a]
		6.2 ± 3.2[b] (n=2)	2.2 ± 4.7[b]

[a]Obtained from the literature hydrogen content and Fig. 5. [b]Obtained by addition of ^{18}O.

confidence) from the value determined by adding ^{18}O. Upper limits (95% confidence) were 2.47 and 1.59 $\mu g\ g^{-1}$ for USGS-DTS-1 and 4.12 and 5.66 $\mu g\ g^{-1}$ for USGS-PCC-1.

We thank K. Strijckmans for helpful comments and suggestions and the NFWO and IIKW for financial support. C. Vandecasteele is a research associate of the National Fund for Scientific Research, Belgium.

REFERENCES

1 T. W. Steele, South African National Institute of Metallurgy, Report 1945 (1978).
2 J. S. Hislop, A. G. Pratchett and D. R. Williams, Analyst (London), 96 (1971) 117.
3 M. A. Chaudhri, G. Burns, E. J. Reen, J. L. Rouse and B. M. Spicer, Radioanal. Chem., 37 (1977) 243.
4 R. Henkelmann, H. Staerk and H.-J. Born, Radiochim. Acta, 11 (1969) 101.
5 G. Weber and M. Guillaume, J. Radioanal. Chem., 5 (1970) 379.
6 J. Wing and M. A. Wahlgren, J. Radioanal. Chem., 3 (1969) 37.
7 A. N. Gorbachev, A. M. Karpunin and L. F. Matukanis, Z. Angew. Geol., 17 (1971) 436.
8 J. T. Gilmore and D. E. Hull, Anal. Chem., 34 (1962) 187.
9 G. V. Iyengar, Radiochem. Radioanal. Lett., 24 (1976) 35.
10 C. Vandecasteele, F. Adams and J. Hoste, Anal. Chim. Acta, 76 (1975) 27.
11 H. Chermette, C. Martelet, D. Sandino, M. Benmalek et J. Tousset, Anal. Chim. Acta, 59 (1972) 373.
12 Chia-Chen Chu and J. L. Schafer, Anal. Chem., 27 (1955) 1429.
13 F. J. Flanagan, Geochim. Cosmochim. Acta, 37 (1973) 1189.
14 S. Abbey, Geol. Surv. Canada Pap., 74—41 (1975) 1.

Analytica Chimica Acta, 162 (1984) 67—73
Elsevier Science Publishers B.V., Amsterdam — Printed in The Netherlands

SUBSTOICHIOMETRIC EXTRACTION OF TANTALUM WITH DIANTIPYRYLMETHANE

R. CALETKA* and V. KRIVAN

Sektion Analytik und Höchstreinigung, Universität Ulm, D-7900 Ulm-Donau (West Germany)

(Received 24th February 1984)

SUMMARY

Diantipyrylmethane is used for substoichiometric extraction of tantalum from 1—4 M hydrofluoric acid into 1,2-dichlorethane. The selectivity of the method is good, niobium and antimony(V) being the main interferences. The stoichiometric composition of the tantalum/diantipyrylmethane complex is 1:1. The method was used for the determination of trace amounts of tantalum ($0.52 \pm 0.05\ \mu g\ g^{-1}$) in a lake sediment (Bodensee/Lake Constance) by neutron activation/γ-spectrometry. Tantalum was determined in niobium samples by an isotope dilution procedure after separation of the matrix on a polyurethane foam column loaded with diantipyrylmethane.

Neutron activation/γ-spectrometry based on the reaction $^{181}Ta(n,\gamma)^{182g}Ta$ provides a highly sensitive method for the determination of tantalum in various matrices [1]. The half-life of the indicator radionuclide ^{182g}Ta is 115.1 d and several suitable γ-rays are emitted, so that in many cases, the analysis can be completed instrumentally. However, when other long-lived radionuclides (e.g., ^{46}Sc, ^{59}Fe, ^{60}Co, ^{65}Zn) are produced simultaneously at higher activity, radiochemical separations are needed.

Substoichiometric separations lead to a significant increase in the selectivity of the radiochemical isolation of the elements [2], which is an important feature. For the determination of tantalum, substoichiometric extractions with methyl violet [3] and triphenylguanidine [4] have been reported. The displacement reaction based on the substoichiometric exchange extraction in the system $(C_6H_5)_4AsTaF_6$—$AuCl_4^-$, has also been recommended for the determination of traces of tantalum [5].

For a substoichiometric separation by liquid—liquid extraction, it is necessary to use a reagent which forms a very stable, readily-extractable complex with the element concerned. Diantipyrylmethane forms a strong complex with hexafluorotantalate ions [6, 7], which can be extracted into 1,2-dichlorethane. This principle was used here for the substoichiometric extraction of tantalum. Applications to activation and isotope dilution procedures are outlined.

EXPERIMENTAL

Chemicals

Diantipyrylmethane (Fluka) was used as received. 1,2-Dichlorethane was purified by distillation. Hydrofluoric acid solutions were prepared by dilution of the analytical-grade 40% acid (Merck), and were standardized by titration with potassium hydroxide solution (phenolphthalein indicator).

A stock solution of tantalum was prepared by dissolution of high-purity metal (Max-Planck-Institute of Metallforschung, Stuttgart) in hydrofluoric/nitric acid mixture. The resulting solution was evaporated to dryness several times with hydrofluoric acid, to remove nitrogen oxides. The residue was dissolved in 1 M hydrofluoric acid to give a final tantalum concentration of 1.3826 mg ml^{-1}. Part of this solution was labelled with ^{182g}Ta. Solutions of other elements were prepared from the metals or compounds of highest available purity by dissolution in hydrofluoric acid so that the resulting concentration of each metal ion was 20 mg ml^{-1} in 4 M hydrofluoric acid.

Procedures

Irradiation and radioactivity measurements. Samples of lake sediment (ca. 50 mg) and standard, containing 0.1 μg of tantalum, were sealed in quartz ampoules and irradiated simultaneously in the FRG-2 reactor, Geesthacht, at a thermal neutron flux of 8×10^{13} cm^{-2} s^{-1} for 24 h.

Niobium samples for the determination of tantalum by the instrumental technique were wrapped in aluminium foil and irradiated together with tantalum standards in polyethylene ampoules for 10 min in the FRM reactor, Garching, at a flux of 1×10^{13} n cm^{-2} s^{-1}. Possible surface contaminations were removed by post-irradiation etching with a mixture of hydrofluoric and nitric acids.

An automatic sample changer (Type 530, Berthold, Wildbad) with a 3 × 3 in. well-type NaI(Tl) crystal and a high-resolution γ-spectrometer consisting of a Ge(Li) detector (Ortec) and a Canberra 8180 multichannel analyzer were used for counting.

Procedure for neutron activation. The irradiated metal or geological sample was dissolved in about 2 ml of a mixture (1 + 1) of hydrofluoric acid and nitric acid by heating under an infrared lamp with periodic stirring. Then 1 ml of tantalum carrier solution containing 1.38 mg of tantalum and 1—2 drops of concentrated sulphuric acid were added and the solution was evaporated almost to dryness. The residue was dissolved in two or three stages with 10 ml of 4 M hydrofluoric acid, and the solution was transferred to a 20-ml disposable syringe [8] and shaken for 3 min with 5 ml of 5×10^{-4} M diantipyrylmethane in dichlorethane. The aqueous phase was discarded (or retained for the determination of other elements), and the organic phase was scrubbed with about 5 ml of 4 M hydrofluoric acid. An aliquot (4 ml) of the organic phase was taken for counting with the scintillation counter/NaI(Tl) detector. The standard (run simultaneously) was

extracted and counted under the same conditions as the sample. The amount of tantalum (m) was calculated from the equation $m = m_s\, a/a_s$, where m_s is the amount of tantalum in the standard, and a and a_s are the measured activities in the sample and standard, respectively.

Procedure for isotope dilution. The sample, containing 20—200 μg of tantalum, was dissolved in the acid mixture as described above. To the resulting solution, the standard solution containing an exactly known amount of tantalum (200—250 μg) labelled with ^{182g}Ta, was added. This mixture was evaporated to dryness, after which 1-ml portions of the 40% hydrofluoric acid were added and repeatedly evaporated in order to remove nitrogen oxides. The residue was dissolved in 3 ml of 2 M hydrofluoric acid and the tantalum was extracted substoichiometrically with 1 ml of 5×10^{-4} M diantipyrylmethane in dichlorethane for 5 min in 5-ml disposable syringes. The activity of 0.7 ml of the resulting organic phase was measured. From the radioactivity obtained in the sample, a, and in the standard, a_s, done simultaneously, the amount of tantalum originally present in the sample was calculated from the equation $m = m_s(a_s/a - 1)$.

RESULTS AND DISCUSSION

Extraction method

The extraction technique in disposable syringes [8] enables the lighter or the heavier phase to be drawn in first, as required, to prevent losses of the solution and to decrease the risk of contamination. Volumes down to 1 ml can be extracted without difficulty. A further advantage of the polypropylene syringes, in this case, was their resistance to the hydrofluoric acid. The time necessary to reach extraction equilibrium was tested earlier [7]; the rate of extraction was very rapid. The extraction time of about 3 min used in this work was quite sufficient.

Two species were predicted [7] for the extractable complexes of tantalum with 1:1 and 1:2 ratios of diantipyrylmethane to tantalum. For the determination of the ratio of the complexes occurring under substoichiometric conditions, a solution of 1.137×10^{-3} M tantalum in 1 M hydrofluoric acid was extracted with 10^{-3}—10^{-5} M diantipyrylmethane (DAM) in dichlorethane. The volume of both the aqueous and organic phases was 5 ml. From the activity distribution, the ratio of DAM:Ta in the organic phase was calculated. The results in Fig. 1 show that at diantipyrylmethane concentrations above 5×10^{-5} M, only the 1:1 complex was extracted, the estimated average ratio being 1.06 ± 0.05.

Effect of hydrofluoric acid concentration

The influence of the concentration of hydrofluoric acid on the substoichiometric extraction of tantalum was checked on a series of 10-ml hydrofluoric acid solutions (0.25—4 M) containing different amounts of tantalum labelled with ^{182g}Ta. The solutions were extracted with 5 ml of

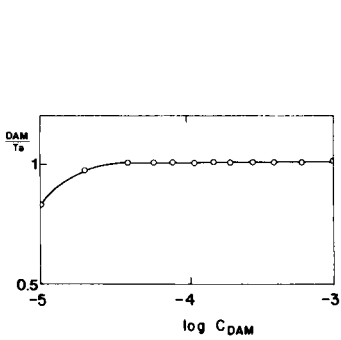

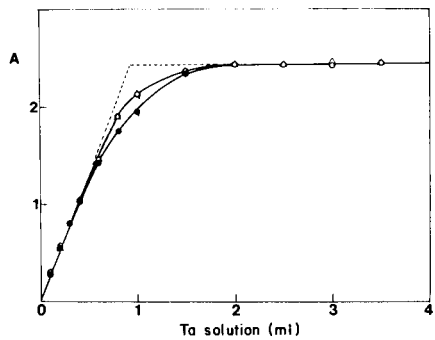

Fig. 1. The estimated DAM:Ta ratio in the organic phase after extraction of tantalum in 1 M HF with DAM in dichlorethane. C_{DAM} is the molar concentration of DAM in the organic phase before extraction. The original concentration of tantalum was 1.137×10^{-3} M and the phase ratio was 1.

Fig. 2. Extraction of tantalum with a substoichiometric amount of organic reagent. A is the radioactivity of the extracts (10^3 cpm); $C_{DAM} = 5 \times 10^{-4}$ M; $C_{Ta} = 1.3836$ mg ml^{-1}: $V_0 = 5$ ml; $V_w = 10$ ml. Curves: (•) 0.25 M HF; (△) 1 M HF; (○) 4 M HF.

5×10^{-4} M diantipyrylmethane. The results summarized in Fig. 2 show that the changes in the added acid had little significant effect.

In another series of experiments, the applicability of this substoichiometric extraction for the determination of traces of tantalum by a radioisotopic dilution procedure was investigated. For this purpose, variable amounts of inactive tantalum (23—236 μg) were added to a series of 1-ml 2 M hydrofluoric acid solutions containing 237.1 μg of tantalum labelled with ^{182g}Ta. After dilution to 3 ml with 2 M hydrofluoric acid, the extraction was done with 1 ml of 5×10^{-4} M diantipyrylmethane in 5-ml syringes. The results are given in Table 1.

TABLE 1

Substoichiometric isotope dilution analysis for tantalum by liquid-liquid extraction with DAM in 1,2-dichlorethane

Activity of the organic phase[a]	Tantalum (μg)	
	Taken	Found
21 256 ± 156[b]	—	—
19 242 ± 264	23.3	24.8 ± 0.4
17 742 ± 123	47.1	46.9 ± 0.8
14 304 ± 82	116.9	115.2 ± 1.9
10 763 ± 62	236.3	231.1 ± 4.0

[a] Average from three experiments. [b] Activity of the standard solution containing 237.1 μg of inactive tantalum in 3 ml of 2 M hydrofluoric acid.

Selectivity

The effects of various elements on the substoichiometric extraction of tantalum were examined. For this purpose, different amounts of Co, Fe, Mo, Nb, Sb, Ti, V or Zr were added to 1-ml portions of tantalum solution (1.3826 mg ml^{-1}), labelled with ^{182g}Ta. After dilution to 10 ml with 4 M hydrofluoric acid, extraction was done with 5 ml of 5×10^{-4} M diantipyrylmethane. The radioactivity of 3 ml of the organic phase was measured in each case and compared with the radioactivity of an equal volume of the organic extract obtained without interfering ions. In the case of antimony(V), the degree of co-extraction was also examined by means of labelling with ^{122}Sb. As shown in Table 2, most of the investigated metals caused only negligible interference, even at relatively high concentrations. Niobium and antimony were the exceptions.

The niobium metal used here contained 150 $\mu g\, g^{-1}$ tantalum. For amounts of niobium between 25 and 100 mg, the error found varied in the range −0.9 to −7.6%. After correction for the tantalum present in the niobium, the errors found for the four different masses of niobium processed became −0.63, −2.01, −2.45 and −6.7%, respectively. These results indicate that interferences caused by niobium concentrations below 2—3 mg ml^{-1} can be neglected in the substoichiometric extraction of tantalum in the range considered. Therefore, the approximate content of niobium in the system to be examined must be known, especially if the substoichiometric separation is applied with isotope dilution. If necessary, niobium can be separated from tantalum by extraction chromatography on a polyurethane foam column loaded with 0.01 M diantipyrylmethane in dichlorethane from 1—2 M

TABLE 2

Extraction of tantalum with diantipyrylmethane in the presence of other elements

Other element	Mass (mg)	Activity of org. phase (cpm)	Error (%)	Other element	Mass (mg)	Activity of org. phase (cpm)	Error (%)
None	—	77140	(±0.49)	Ti	50	78065	+1.20
Co	50	77857	+0.93		100	74617	−3.27
	100	77996	+1.11	V	50	75905	−1.60
Fe	50	75288	−2.40		100	76369	−1.00
	100	80086	+3.82	Zr	50	78196	+1.37
Mo	50	78235	+1.42		100	79400	+2.93
	100	79230	+2.71	Sb	1	53149	−31.1
Nb[a]	25	76445	−0.90		2	32013	−58.5
	50	75165	−2.56		None	(8631)[b]	(29.5)
	75	74617	−3.27		1	(5910)[b]	(20.2)
	100	71308	−7.56		2	(5178)[b]	(17.7)

[a]Tantalum content was 150 $\mu g\, g^{-1}$. [b]^{122}Sb activity added to the solution (100% = 29 258 cpm).

hydrofluoric acid [9]. Tantalum is eluted with 1 M nitric acid/0.3% hydrogen peroxide, and the eluate is evaporated with hydrofluoric acid and extracted as outlined above.

The results given in Table 2 also show that antimony(V) at any concentration is strongly extracted with diantipyrylmethane from hydrofluoric acid solutions. This is not surprising as tantalum and antimony in hydrofluoric acid solutions behave very similarly in the extraction of ion-pairs (ketones, TBP, or basic extractants) as well as in anion exchange [10]. Traces of antimony do not interfere in the substoichiometric neutron activation method for tantalum. In the isotope dilution method, however, antimony must be removed before the extraction of tantalum with diantipyrylmethane if it is present at the same concentration level as tantalum. Distillation as antimony tribromide [10, 11] or extraction with diisopropyl ether from a hydrochloric acid medium [10] should be suitable procedures for the separation.

Application of the method

The method can be applied to the determination of tantalum by both the neutron activation and the isotope dilution procedures. It can be used for the determination of traces of tantalum in various geological samples, glasses and metals. The determination of tantalum in niobium and its products is of practical importance. The main advantage of the proposed method is its speed and simplicity. The aqueous phase after the extraction of tantalum can be used for the determination of other elements.

A sample of lake sediment (Lake Constance), analysed by the substoichiometric neutron activation procedure, was found to contain 0.52 ± 0.05 $\mu g\ g^{-1}$ tantalum; this was in good agreement with the value of 0.54 ± 0.09 $\mu g\ g^{-1}$ measured instrumentally; these values are the averages of three measurements with corresponding average deviation. Under the conditions described, the limit of detection was 0.2 ng of tantalum.

The substoichiometric isotope dilution procedure was applied to the determination of tantalum in three different niobium samples. In this case, the matrix was removed by a preliminary separation on a polyurethane foam column, pretreated with diantipyrylmethane [9]. The results shown in Table 3

TABLE 3

Tantalum content found in different niobium samples by the isotope dilution procedure (n = 6) and comparison with results obtained by instrumental neutron activation

Niobium sample	Tantalum found ($\mu g\ g^{-1}$)	
	Isotope dilution	Instrumental
Nb 1	153 ± 7	147 ± 7
Nb 2	1466 ± 57	1474 ± 43
Nb 3	1527 ± 73	1507 ± 37

are the means from six separate determinations and are in good agreement with results obtained by the instrumental neutron activation method.

Financial assistance was provided by the Bundesministerium für Forschung und Technology, Bonn. The authors thank the FRM Reaktorstation Garching and the Forschungszentrum Geesthacht GmbH., for making the irradiation facilities available.

REFERENCES

1 V. Krivan, Pure Appl. Chem., 54 (1982) 787.
2 J. Růžička and J. Starý, Substoichiometry in Radiochemical Analysis, Pergamon Press, Oxford, 1968.
3 W. Zmijevska, Chem. Anal. (Warsaw), 15 (1970) 471.
4 G. N. Bilimovich, I. P. Alimarin and T. V. Tikhonova, J. Anal. Chem. USSR, 26 (1971) 104.
5 G. N. Bilimovich and N. N. Churkina, J. Radioanal. Chem., 8 (1971) 53.
6 V. P. Zhivopistsev and B. I. Petrov, Utsch. Zap. Perms-ogo Univ., (1974) 252.
7 R. Caletka, J. Inorg. Nucl. Chem., 43 (1981) 1619.
8 R. Caletka, Fresenius Z. Anal. Chem., 311 (1982) 124.
9 R. Caletka and V. Krivan, Fresenius Z. Anal. Chem., in press.
10 O. G. Koch and G. A. Koch-Dedic, Handbuch der Spurenanalyse (2. Auflage), Springer Verlag, Berlin, 1974.
11 K. Samsahl, Sci. Total Environ., 1 (1972) 65.

Analytica Chimica Acta, 162 (1984) 75—83
Elsevier Science Publishers B.V., Amsterdam — Printed in The Netherlands

DETECTION OF TOLUENE DIISOCYANATE WITH A COATED QUARTZ PIEZOELECTRIC CRYSTAL
Part 3. Practical Coatings for a Humidity-Corrected Detector

J. J. McCALLUM, P. R. FIELDEN, M. VOLKAN[a] and J. F. ALDER*

Department of Instrumentation and Analytical Science, UMIST, Manchester M60 1QD (Great Britain)

(Received 14th March 1984)

SUMMARY

Dithizone and tri-n-octylphosphine oxide (TOPO) were tested as coatings for quartz piezoelectric crystals to be used in a detector for toluene diisocyanate (TDI). Cobalt(II) chloride and polyethylene glycol (PEG) with molecular weights of 400 and 1540 were tested for suitability as coatings for detecting humidity variations so that correction for humidity could be obtained from a two-crystal system. Sensitivities for TDI of 12 and 75 Hz ppm^{-1} were found with dithizone and TOPO, respectively, between 0 and 1 ppm TDI. Cobalt chloride-coated crystals showed a sensitivity for water of 0.053 Hz ppm^{-1} at 8000 ppm water and about 40 Hz ppm^{-1} for TDI at the 2 ppm level. PEG-400 and PEG-1540 provided sensitivities to water of 0.038 and 0.051 Hz ppm^{-1} respectively, and the response was linear over the range 9000—13 000 ppm water. All coatings showed irreversible behaviour towards TDI.

Toluene diisocyanate (TDI) is widely used in the production of polyurethane foams and urethane paints. It is poisonous, lachrymatory, and a respiratory irritant. Persons exposed to TDI can become sensitized to its effects and may suffer asthmatic attacks when subsequently exposed to even very low concentrations for short periods. Both its threshold limit value (TLV) and ceiling value have been set at 0.02 ppm (0.14 mg m^{-3}) TDI which, although an apparently arbitrary level, corresponds to the practical limit of detection of the Marcali method [1]. The saturated vapour pressure of TDI at ambient temperature (15—25°C) corresponds to 10—15 ppm TDI. The work described in this series of papers has been aimed only at the development of a man-portable detector for use on board ships which carry the monomer. The goal is a detector which can be used by a person during operations in tanks or enclosed spaces, to assess whether a hazard exists from TDI in the atmosphere.

The requirements of such a detector are that it be rapid in response and sure of detecting TDI near the worker's face. The single consequence of an

[a]Present address: Chemistry Department, Middle East Technical University, Inonu Bulvari, Ankara, Turkey.

0003-2670/84/$03.00

alarm would be the exit from the location of an exposed person until the tank had been ventilated thoroughly. It would be unreasonable to expect anyone to work for more than 6 h before leaving the tank, so that the operational lifetime of the sensor need only be of that order, although a long shelf-life is desirable. These requirements can be met by the use of a coated quartz piezoelectric crystal detector, if a suitable specific TDI-sensitive coating can be found and the response to atmospheric humidity fluctuations removed. This paper describes the choice of crystal coatings for this application and Part 4 [2] describes the automatic instrument designed for the sampling and determination of TDI.

Requirements for a TDI-sensitive coating

Under the expected working conditions, the maximum concentration of TDI encountered would be about 15 ppm. In practice, in a ventilated tank, the maximum level would be rather less. For a long-term monitor, a completely reversible adsorption on the crystal coating is required, but irreversible adsorption is acceptable for detection purposes, where the presence of vapour above a defined concentration is all that is required. This is of particular consequence in TDI detection because TDI can hydrolyse and self-polymerize on any surface, yielding solid products. In this work, these particular properties were used to advantage and, as long as there is not gross contamination of the crystal surface by TDI adsorption products, the crystal can still be useful after several exposures to low TDI concentrations.

The coating itself needs to have a low vapour pressure to minimize bleed, to be of low polarity and ideally to have lyophilic characteristics, thus decreasing water vapour response and ensuring maximum adsorption of TDI. The vapour pressure of TDI held in the coating could be diminished by the formation of donor—acceptor complexes between delocalized molecular orbitals on the isocyanate groups and groups on the coating molecule; such bonding would not be available to water which has no such tendency.

Two compounds were chosen, which posssessed most of the characteristics presumed to lead to a good coating: dithizone (diphenylthiocarbazone) and tri-n-octylphosphine oxide. Dithizone was chosen from its physical characteristics (involatile, conjugated unsaturated system, insoluble in water) and the belief that it may form a loose addition compound with TDI and show some reversibility. Tri-n-octylphosphine oxide (TOPO) is known to react reversibly with isocyanates [3] in solution yielding R—N=C=N—R species and regenerating TOPO. The possibility of the coating regenerating itself made this a particularly attractive compound and it also fulfilled the other requirements outlined above.

Requirements for a water-sensitive coating

The relative humidity in marine environments is usually high and the air temperature can vary over the range −10 to 35°C during the course of the year. The range of water vapour concentration to which the detector may be

exposed is therefore very large. It is accepted that at very high relative humidities, with water condensing on the crystals, the detector will not work, although the exact upper limit of relative humidity which can be tolerated has not yet been assessed.

The aim of continuous monitoring of the water vapour concentration is to permit correction for humidity change to the response of the TDI detector crystal. High sensitivity is therefore less important than a known and reproducible response to water vapour. PEG 400 (polyethylene glycol, molecular weight 400) and PEG 1540 were used to model the system initially, as previous work had given experience with PEG [4]. Cobalt(II) chloride was chosen as a coating for humidity correction to be used with TOPO based on work here and on experience elsewhere with hydrated metal salts [5].

Performance criteria

Janghorbani and Freund [6] described the response characteristics of a liquid-coated quartz piezoelectric crystal in terms of a partition detector for vapour dissolved in a gas stream. From this approach:

$$\Delta f_y / C_g = \Delta f_x K_{yx} / n\rho \qquad (1)$$

where Δf_x is the incremental frequency on first coating the crystal with material of density ρ. The term $\Delta f_y / C_g$ can be termed the sensitivity of the crystal, where Δf_y is the frequency change observed on exposing the crystal to a gas-phase concentration of y equal to C_g. This is a useful equation because Δf_x can be measured readily, and there is no term in the equation relating Δf to a mass change Δm, so that inhomogeneities in sensitivity over the crystal surface are hidden both for the coating and, since one assumes that the analyte gas is adsorbed only onto the coating material, for the gas. The term K_{yx} is the ratio of the concentration of component y, in the liquid phase of the coating (x), to the concentration in the gas phase.

Assuming no density change on adsorption, ρ can readily be measured for liquids and possibly waxes. The value of n can be measured because in practical terms it is the numerical ratio of the carrier gas flow rate to the cell volume. Edmonds and West [7] derived similar equations to Eqn. 1, and to those of Janghorbani and Freund [6]. They also measured a sensitivity (the inverse of that described here), and commented on the usefulness of measuring the frequency decrease on coating the crystal. They produced results for chloroform on various substrates to support this theoretical approach.

The sensitivity of the crystal, i.e., the gradient of the response—concentration graph, can therefore be directly related to an intrinsic property of the coating, K_{yx} and, when the respective gradients are compared, is a direct measure of that parameter.

It should not be forgotten, however, that this theory is applicable only to coatings where the 'dominant mechanism of solute pick-up is dissolution' and not other mechanisms such as substrate adsorption [6].

For TOPO, the coating eventually chosen for this work, it was found, as

expected, that adsorption is irreversible to the extent of 20—60%. There is no doubt that the partition model is invalid for the irreversible part of the process. It is convenient and reasonable, therefore, to separate the process into reversible and irreversible steps, and to consider the reversible part in terms of partition theory. The irreversibly adsorbed material, however, will modify the coating, and it is generally observed that there is a decrease in sensitivity for the first few exposures and then a steadying of sensitivity for some considerable number of exposures. For detection purposes, it is possible to exploit the full sensitivity of the coating, but if a monitor were required, the decreased sensitivity of the contaminated coating would have to be considered.

EXPERIMENTAL

Equipment

Frequency measurement was by either a Racal 9905 or a Venner 7737 counter-timer through a digital-analog converter to a strip-chart recorder. The crystals were 9.9-MHz AT-cut quartz with gold electrodes in an HC6/U holder (Quartz Crystal Co., New Malden, Surrey, and Senator Crystals, London SW16). They were used to control the frequency of a TTL oscillator giving a 10-MHz square-wave output.

Generation of atmospheres

It is difficult to handle TDI at low gas-phase concentrations, particularly if the concentration is to remain stable for a period of time. The low vapour pressure and the ability of TDI to self-polymerize and hydrolyse on surfaces means that losses from the vapour phase can be considerable and rapid. To overcome this, a dynamic system with continuous monitoring of the TDI entrained in the air by the Marcali method [1] was employed. This system has been described fully in previous work [4].

The authors' laboratory is air-conditioned with a relative humidity of about 48—53% at 18—23°C (8—10.5 g m^{-3} water). The laboratory air, therefore, provides a stable reservoir of air the humidity of which can be accurately determined by a wet and dry bulb hygrometer. The laboratory air can easily be diluted with dry air (dried over molecular sieve and silica gel) to give known mixtures of humid air. It is known from other work that air bubbled quickly through water at ambient temperatures becomes about 85% saturated and this air can be diluted to give intermediate values which are measured by an in-line wet and dry bulb hygrometer. These methods of humid air preparation proved adequate for the present study.

Mass sensitivity of the coatings

According to Sauerbrey's equation [8], the mass sensitivity of a 10-MHz quartz crystal oscillating in a shear mode will be of the order of 1 Hz ng^{-1}. This assumes the coating to be equivalent to an increment in thickness of the

quartz having the same mass. The response of the crystals to mass loading with the chromatographic coating material SE-30 was measured (Fig. 1). The material was coated on one side of the crystal only, and the mass added was measured on a microbalance (<2% r.s.d. above 100 μg). The sensitivity was found to be approximately 0.18 Hz ng^{-1} over the initial part of the curve; in concurrent work on loading identical crystals with copper(II) sulphate pentahydrate, the mass sensitivity was found to be about 0.3 Hz ng^{-1}. The reason for the difference between the theoretical and observed sensitivities is not certain, but may be related to the evenness of coating of the crystal, different parts of the crystal surface showing different sensitivity to added mass.

Testing of coatings

Dithizone. Solutions of 1% (w/v) dithizone (analytical reagent grade, BDH) in chloroform were spotted onto the crystal in 1—5-μl aliquots and the solvent was allowed to evaporate. The coated crystal was exposed to TDI in the dynamic gas rig described earlier [4]. Alternately, dry air and dry air contaminated with TDI were passed over the crystal. Later, moist air and dry air were passed alternately over the crystal. The steady frequency change after exposure of the crystal to TDI was measured to obtain the response. The sensitivity to TDI was found to be 12 ± 4.4 Hz ppm^{-1} over the range 0.2—14 ppm TDI (Fig. 2). The sensitivity to water was constant at 0.012 ± 0.003 Hz ppm^{-1} (15 measurements) over the range 2—14 g m^{-3} water. A typical sensitivity of an uncoated crystal to water is 0.01 Hz ppm^{-1}.

The results show that dithizone is a useful coating with about 1000 times greater sensitivity to TDI than water vapour, but the sensitivity to TDI was not adequate for the present work. Reversibility of the coated crystal to water was complete, but to TDI it was about 50%.

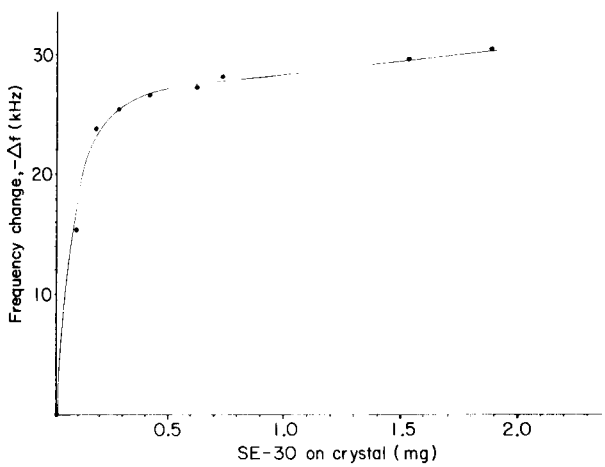

Fig. 1. Effect of mass loading on the frequency of a crystal coated with SE-30.

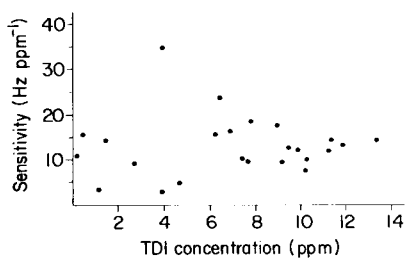

Fig. 2. Sensitivity of a dithizone-coated crystal with respect to exposure concentration.

Tri-n-octylphosphine oxide. To determine whether any reaction occurred when the TDI vapour was passed over tri-n-octylphosphine oxide (TOPO), a solution of TOPO in carbon tetrachloride was allowed to evaporate on the surface of one plate of an infrared (i.r.) gas cell. The cell was assembled and the i.r. spectrum was obtained. The cell was next flushed with 10 ppm TDI and at 0.5-h intervals the i.r. spectrum of the TOPO film was obtained again. New bands appeared in the spectrum, but could not be rigorously assigned to any particular group. The observed changes in the spectrum were 20—60% reversible on flushing the cell with clean air, depending on the conditions employed. Humidified air passed through the gas cell did not change the TOPO spectrum after the cell had been dried.

To measure the response of a TOPO-coated crystal to TDI, a total of 10.8 μg of TOPO was applied to both sides of the crystal by spotting on a solution in chloroform. The crystal was exposed to dry TDI atmospheres (air dried over molecular sieve 5A and silica gel prior to passage over TDI in the Nielson and Booth cell [4]) followed by clean, dry air. The frequency decrease was measured when it became steady after 2 min. The decrease never reached a plateau, owing to continuous adsorption, but attained a steady slow increase after an initial rapid rise. Care was taken not to over-expose the crystal to high concentrations of TDI for any longer than was necessary, in order to minimize the irreversible adsorption. The crystal was allowed to desorb to a steady state between exposures, which could take 3—5 min. The frequency decrease after exposure was plotted against the measured TDI concentration and these data, acquired in an irregular order of concentration over a week, were used to obtain the data in Fig. 3. The same crystal was later exposed alternately to dry and moist air to determine the water sensitivity.

The water sensitivity of TOPO-coated crystals is flow-rate dependent at low flow rates, increasing from 0.016 Hz ppm^{-1} at 100 ml min^{-1} to a plateau value of about 0.024 Hz ppm^{-1} above 1 l min^{-1}. An uncoated crystal exposed to dry air gives a similar response profile. In this work with TOPO, the flow rates used for TDI and water exposure were 1—1.2 l min^{-1}, and the sensitivity to water vapour was steady at 0.024 Hz ppm^{-1}.

In a series of experiments, the response of the TOPO crystal to TDI in humid air (49% relative humidity at 21°C, 8.99 g m^{-3}) was measured. The response had the same nature in all cases, typically as shown in Fig. 4. The frequency initially increased on passing the humid air over the TDI in the bubbler, which may be due to partial desiccation of the air by the TDI. Once an equilibrium humidity had been re-established, the expected frequency change in the negative direction was apparent. The sensitivity was about 32 Hz ppm^{-1} at the 2-ppm level, compared to that observed in dry air (Fig. 3). It must be emphasised that the response shown in Fig. 4 was obtained in the flow rig and some of the response shape is almost certainly due to alterations in the loss of TDI to the walls and partial desiccation of the air. The observed frequency increase of 20 Hz at a sensitivity of 0.02 Hz

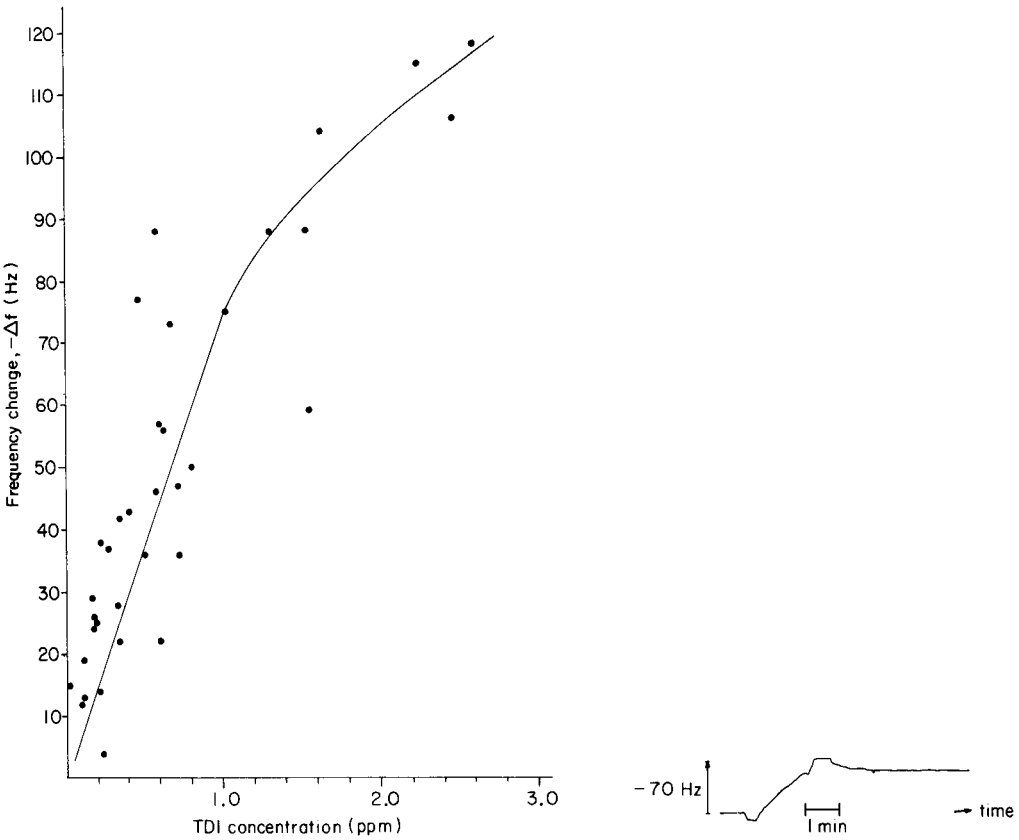

Fig. 3. Calibration graph for TDI in dry air obtained from a tri-n-octylphosphine oxide-coated crystal.

Fig. 4. Response of a TOPO-coated crystal to TDI in moist air (2.22 ppm TDI at 49% relative humidity and 21°C).

ppm^{-1} water corresponds to a drop of 1000 ppm in the water content of the air stream. At 9 mg l^{-1} with a flow rate of 1 l min^{-1}, this would correspond to a loss of about 1 mg min^{-1} to the TDI, which seems not unlikely.

It would seem that TOPO is a useful and sensitive coating for the determination of TDI in air; the irreversible adsorption is a nuisance as far as long-term monitoring is concerned in that it will cause baseline drift and alteration to the coating, but for a detector, this same phenomenon acts beneficially in increased sensitivity and decreasing response time when a coating is exposed to TDI for the first time.

Polyethylene glycols (PEG). The response of PEG-400 to TDI has previously been characterized; PEG-400 is known to behave reversibly and linearly to water [4]. Solutions of PEG-400 or PEG-1450 in chloroform

were spotted onto one electrode of separate crystals. For the pair of crystals for which data are presented, and which were used in the characterization of the detection instrument, the loadings were about 0.9 μg of PEG. It was observed that with mass loadings of about 5 μg, PEG-400 showed a degree of irreversibility on exposure to different water vapour concentrations, but this effect was not noticeable at the 0.9-μg loading.

From eight measurements over the range 9000—13 000 ppm water (30—70% relative humidity) the sensitivity to water and standard deviation were constant at 0.038 ± 0.003 Hz ppm^{-1} and 0.051 ± 0.002 Hz ppm^{-1} for PEG-400 and PEG-1540, respectively. The behaviour of PEG coatings towards TDI is described in Part 4 [2].

Cobalt chloride. Cobalt(II) chloride was employed as a coating to be used for humidity correction to the TOPO-coated crystal in the portable monitor to be described [2]. The important requirement is that the coating must have response characteristics different from TOPO towards water and TDI. The sensitivity of the coating was found to average about 40 Hz ppm^{-1} at the 2-ppm exposure level. The sensitivity, however, was not reproducible and could vary over a range, from 25 to 125 Hz ppm^{-1} for different crystals; the reason for this is not understood. The sensitivity to water vapour showed an increase with water vapour concentration, varying from 0.024 Hz ppm^{-1} between 1000 and 4000 ppm water to 0.053 Hz ppm^{-1} between 4000 and 9000 ppm water after 1-min equilibration.

DISCUSSION

The data presented above might suggest that the adsorption of water vapour is much more a physical than a chemical phenomenon and that it cannot be related to solubility or reactivity considerations. The reactivity of the TDI with adsorbed water may also be considered to make a greater contribution to the overall sensitivity of the coatings than the loose addition-complex formation hoped for with dithizone, or even the chemical reaction predicted with TOPO.

The curvature of the TDI calibration graphs obtained with TOPO and dithizone may be attributed to the coating becoming contaminated with a "TDI/polymer/hydrolysate". The crystal coating seems to recover after exposure to TDI, even though there is considerable chemisorption.

The response of a TOPO crystal to 1 ppm TDI is about 75 Hz, which corresponds to a mass increment of about 0.4 μg. As the total mass of TOPO on the surface is 10.8 μg, the mass increment of 4% ppm^{-1} suggests that the change in sensitivity as the concentration increases is caused by the coating becoming saturated. Notwithstanding these results and comments, the crystal for which data are presented here was used in the portable monitor over a period of several months with exposure to TDI several times per week. The sensitivity at the 1—2 ppm level remained 70—75 Hz ppm^{-1}.

This work has shown that TOPO is a stable and reasonably sensitive coating

for the detection of TDI in the atmosphere. Dithizone is also useful but does not give the sensitivity required. Although the behaviour of TOPO is not completely reversible, its response is reasonably predictable and steady over a period of time. The nature of the adsorption of TDI onto TOPO appears to involve chemical change and it is probable that the actual absorber is a product of TDI with TOPO and water.

Cobalt(II) chloride, although its behaviour is far from ideal, does have a sufficiently different response from TOPO to be used as the second crystal in a water-response correction system for a portable TDI monitor.

The two polyethylene glycols proved to be useful coatings with which to characterise the monitor, and their behaviour towards water vapour is predictable. It is clear from this work, however, that an ideal coating for TDI, showing high sensitivity and minimal response to water vapour, has yet to be found.

Murvet Volkan was supported by the British Council, John McCallum by SERC in collaboration with Panocean Anco Ltd (now PAL Shipping Services) under the CASE scheme. We are grateful to David Owen (ex-Panocean Anco, now of Safety Survey Services, Ltd.) for many helpful discussions.

REFERENCES

1 K, Marcali, Anal. Chem., 29 (1957) 558.
2 P. R. Fielden, J. J. McCallum, T. Stanios and J. F. Alder, Anal. Chim. Acta, 162 (1984) 85.
3 S. Patai (Ed.), The Chemistry of Cyanates and their Derivatives, Wiley, New York, 1977.
4 J. F. Alder and C. A. Isaac, Anal. Chim. Acta, 129 (1981) 163, 175.
5 P. S. Daley and D. A. Lundgren, Am. Ind. Hyg. Assoc. J., 36 (1975) 791.
6 M. Janghorbani and H. Freund, Anal. Chem., 45 (1973) 325.
7 T. E. Edmonds and T. S. West, Anal. Chim. Acta, 117 (1980) 147.
8 G. Z. Sauerbrey, Z. Physik, 155 (1959) 206.

Analytica Chimica Acta, 162 (1984) 85—96
Elsevier Science Publishers B.V., Amsterdam — Printed in The Netherlands

DETECTION OF TOLUENE DIISOCYANATE WITH A COATED QUARTZ PIEZOELECTRIC CRYSTAL

Part 4. A Portable Automatic Detector With Humidity Correction

P. R. FIELDEN, J. J. McCALLUM, T. STANIOS and J. F. ALDER*

Department of Instrumentation and Analytical Science, University of Manchester, Institute of Science and Technology, Manchester M60 1QD (Great Britain)

(Received 14th March 1984)

SUMMARY

Microcomputer-controlled measurement of the frequency of two differently-coated quartz piezoelectric crystals and subsequent data processing permits the immediate correction of instrumental response for fluctuations in water vapour concentration and the display of the corrected toluene diisocyanate concentration in air. Crystal pairs with coatings of polyethylene glycol 400 or 1540 or tri-n-octylphosphine oxide and cobalt(II) chloride were used to illustrate the performance of the instrument. Toluene diisocyanate can be detected over the range 0.1—15 ppm in atmospheres with relative humidities ranging from 30 to 60% without significant interference from changes in water concentration.

Previous work [1, 2] has shown the problems that are associated with the detection and monitoring of toluene diisocyanate (TDI) in the atmosphere. Parallel to the search for a specific and sensitive coating for TDI has been the development of suitable instrumentation for practical portable use on board ship. The threshold limit value and ceiling value for TDI are so low (0.02 ppm) that any TDI which can be detected by the instrument will be too much in operational terms. Nonetheless, this work was aimed at quantifying TDI, for which purpose humidity correction is a pre-requisite.

One of the major anticipated advantages of gas monitors based on coated piezoelectric crystals is that the instrumental hardware will be the same, no matter which gas is being monitored. It must be emphasized that the instrument described below is equally suitable for any gas-monitoring application requiring humidity correction, provided that a suitable coating for the quartz crystal is available. Several workers have developed quartz crystal-based portable vapour and aerosol monitors. Most of these devices, however, suffer from interference from other airborne species because of the lack of selectivity of the crystal coatings. Attempts to employ a reference crystal have offered only marginal improvement.

0003-2670/84/$03.00

Mercury vapour monitors have been the most successful portable instruments based on quartz crystals mainly because of the high selectivity of the gold film electrodes towards mercury; unlike most other chemical coatings, their sensitivity to water vapour is low. Bristow [3] described a portable mercury vapour sensor for monitoring soil gases. A quartz crystal (15-MHz, AT-cut) with gold electrodes was used as the analyser; a reference crystal with aluminium electrodes served to compensate for environmental temperature and pressure changes. The reference crystal was found to be sensitive to water vapour and so was replaced by a sealed unit which presented a further problem in that a time lag was observed between the crystals in the attainment of thermal equilibrium. Scheide and Warner [4] reported a direct-reading, hand-held (weight 315 g) mercury monitor which used two 9-MHz crystals; the analyser crystal again had gold electrodes. They claimed that the reference crystal eliminated any water vapour interference and compensated for temperature changes. Carpenter and Brenchley [5] described an aerosol-measuring instrument based on a 10-MHz AT-cut crystal as the mass analyser with a sealed reference crystal to subtract ambient changes. Daley and Lundgren [6] later presented an in-depth study of temperature and humidity effects on an aerosol monitor. It was concluded that a reference crystal could not be used successfully to compensate for either humidity or temperature changes, because the local environments of the two crystals were not equivalent.

Karmarkar et al. [7] developed a sulphur dioxide detector based on a quartz crystal (9-MHz, AT-cut) coated with *N,N,N',N'*-tetrakis(2-hydroxypropyl)ethylenediamine as the sensing element. Sampled air was injected into a nitrogen carrier stream passing over the crystal. Four layers of hydrophobic membrane filter were used to eliminate water vapour interference. Later, Ho and Guilbault [8] described a portable monitor for continuous toluene determination; a crystal (9-MHz, AT-cut) coated with Carbowax-550 was used as the toluene sensor, but interferences were observed from benzene, alkylbenzenes and water vapour. It was suggested that perm-selective membrane tubing (Nafion; Du Pont) could be used to eliminate water interference, but results to support this supposition were not presented.

All the previously reported instruments based on coated piezoelectric crystals have adopted simple methods of data acquisition and processing; mainly, direct or heterodyne frequency measurement has been used, sometimes followed by frequency–voltage conversion. Correction of water vapour interference is difficult with such systems and the prior removal of water by absorbents has been only partly successful. The advent of fast, cheap devices which can do this task digitally has now rendered possible a much easier approach to the problem.

This work exploits the ability of an on-line microcomputer to acquire the frequency signals from two oscillating crystals which have different responses to water and TDI. The data and previously input response characteristics of the crystals are manipulated mathematically to calculate correction factors

for the rapid instrument response so that a TDI concentration reading, corrected for humidity changes, is output.

THEORETICAL BASIS

The equations which are generally accepted to describe best the response of coated quartz crystals are due to Sauerbrey [9]. These have been extensively reported [10]. For small mass loadings, the decremental frequency change (Δf) on loading a crystal (characterized by a constant, M) by adsorption of a mass ΔW of gas is given by $\Delta f = M\Delta W$. This linear response was found in practice to be true for frequency changes up to 2% of the unloaded crystal frequency [11]. It has been shown, however, that the mass of gas adsorbed is not linear with gas-phase concentration to that extent [2], and the relationship $\Delta f = A[\text{gas}]$, where A is constant and [gas] represents the concentration of analyte in the gas phase, is only true over relatively small frequency and concentration changes, possibly because of saturation of the coating by the adsorbate. For the purpose of toxic gas detection (rather than monitoring at intermediate or high levels) the responses of the coated crystals are initially approximately linear and indeed show their highest sensitivity.

Janghorbani and Freund [12], reporting the use of coated quartz crystals for chromatographic detection, stated that although theoretically a coated crystal "should be additive towards gas streams containing two partitionable gases if the said gases behave ideally . . . in all cases studied so far, we have been unable to confirm the theoretical predictions. The frequency response to composite samples is invariably greater than the sum of frequency shifts due to each component when introduced separately". However, Edmonds and West [13] considered the analysis of binary mixtures of chloroform and hexane in nitrogen; they assumed no synergic effects and obtained results which were in good agreement with the known concentrations.

It was assumed for the purpose of this work that the responses to both TDI and water vapour over limited concentration ranges would be linear, and that the responses to the different vapours were additive. The observed frequency changes, Δf_a and Δf_r, for two similar crystals (10-MHz, AT-cut gold electrodes) coated with analyser (a) and reference (r) coatings are given by

$$\Delta f_a = \pm A[\text{TDI}] \pm B[\text{water}] \quad (1)$$

$$\Delta f_r = \pm C[\text{TDI}] \pm D[\text{water}] \quad (2)$$

where the square brackets represent concentrations in the gas phase, and A and B are the response coefficients (Hz ppm^{-1}) for the analyser crystal, and C and D are the response coefficients for the reference crystal, to TDI and water vapour concentrations, respectively.

A parameter, α, may be defined to relate the responses of the two crystals to water vapour such that $\alpha = B/D$. Substitution into Eqn. 2 yields

$$\alpha\Delta f_r = \pm\alpha C[\text{TDI}] \pm B[\text{water}] \quad (3)$$

Manipulation of Eqns. 1 and 3 gives $\Delta f_a - \alpha \Delta f_r = \pm A[\text{TDI}] \pm \alpha C[\text{TDI}]$. Rearrangement, with $\beta = (A - \alpha C)$, gives

$$[\text{TDI}] = (\pm \Delta f_a \pm \alpha \Delta f_r)/\beta \quad (4)$$

Thus, the response to water vapour is eliminated. The coefficients A, B, C and D and hence α and β, were obtained by measuring the response characteristics of the crystals to known water and TDI concentrations (see Part 3 [2]).

Two further parameters are defined for convenience; $X = 16/\alpha$ and $Y = 1.28\beta$, and the equation multiplied by a scaling factor of 100 (see below). Equation 4 then becomes

$$[\text{TDI}] = 128/Y(\Delta f_a \pm 16\, \Delta f_r/X) \quad (5)$$

Equation 5 is the form implemented by the instrument, where X and Y lie in the range 0—255. This form is particularly suitable in programming terms because it requires only integer arithmetic to provide the correction for water vapour interferences. As a consequence of the values of X and Y used in these equations, the TDI concentration in Eqn. 5 is displayed in increments of 0.01 ppm.

Unsigned arithmetic routines may be used if a truth table is drawn up for the possible combinations of the absolute signs of Δf_a and Δf_r with respect to the baseline. A general case is assumed where the baseline conditions represent zero TDI concentration and a finite concentration of water vapour. The truth table shown in Table 1 was utilized by the microcomputer program to allow correction under all conditions of concentration changes of TDI and water vapour, regardless of direction.

EXPERIMENTAL

Sensor head design

The quartz crystals used were 10-MHz, fundamental mode, AT-cut with gold electrodes (Quartz Crystal Co., New Malden, Surrey). The remote sampling head was constructed in a die-cast aluminium alloy box and connected to the instrument belt pack via a flexible hose containing the aspiration tube and data lines. The crystals were mounted one behind the other with the coated face of the analyser crystal perpendicular to the influent air

TABLE 1

Truth table to define the arithmetic operations required to correct for absolute sign frequency changes

Absolute sign		
Δf_a	Δf_r	Unsigned arithmetic operation
—	—	Difference
+	—	Forbidden
—	+	Sum
+	+	Difference

stream (flow rate 1200 ml min^{-1}). This configuration was chosen on practical rather than scientific grounds. It was considered that with a linear flow rate of 11 m min^{-1} and with the air being aspirated from between the crystals via the tube to the pump, both crystals would receive similar good exposure to the air. As mentioned below, this may not be the case and the geometry of the sensor head requires close investigation. The influent air was passed through a fine nylon gauze (1.2 cm diameter) to remove dust particles and grit, and to protect the crystals from draughts.

The HC6/U crystal holders were soldered to a double-sided circuit board on which the oscillators were mounted. These both gave square-wave outputs from a single TTL integrated circuit (type 74LSO4, Texas Instruments). A logic-based oscillator design was adopted because it requires few external components and is relatively immune to minor fluctuations in supply voltage.

The instrument main module (belt pack) housed the signal processing and display circuits, the sampling pump (Vinten Instruments), alarm and battery. It weighed 1.86 kg. Instrument signal processing and control was done by an 8-bit, single-chip C-MOS microcomputer unit (HD6301VP, Hitachi). Supporting circuitry was constructed from CMOS devices with the exception of the high-frequency section (>5 MHz) where a low-power Schottky TTL was employed. The unit was powered from a single 5-V supply, obtained by regulating a 9-V rechargeable 1.2-A h nickel-cadmium battery and consumed 180 mA; the battery was recharged after running for 6 h.

Figure 1 is a block diagram of the microcomputer-based instrumentation. The incoming crystal frequencies from the remote sensing head were selectable

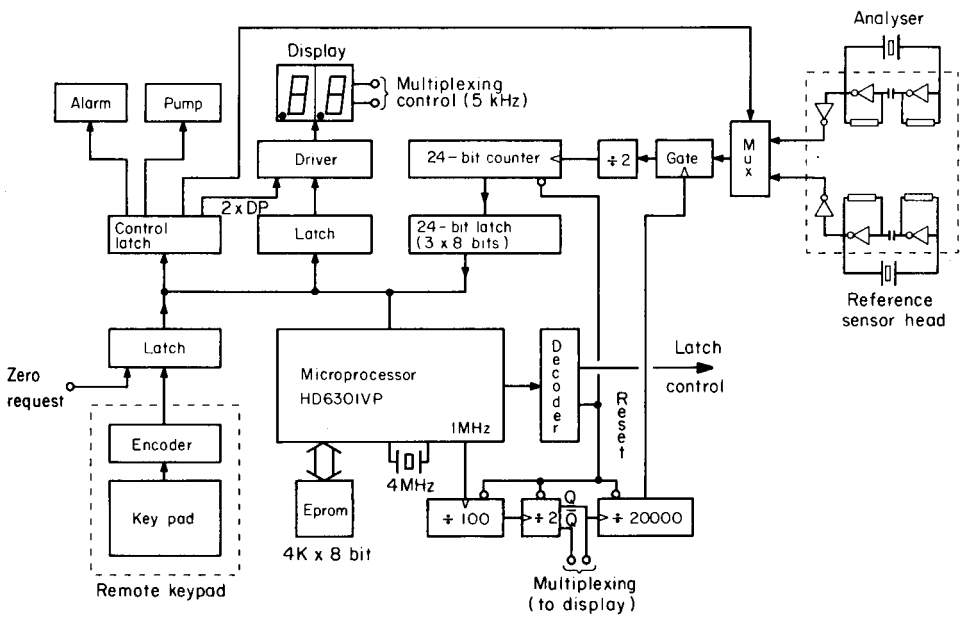

Fig. 1. Block diagram of the microcomputer-based instrument.

via a multiplexer which was controlled by the microcomputer through a control latch. A gate was used to sample the frequency for 2 s. During this period, the frequency was divided by 2 to allow the use of slower CMOS counters (ca. 5-MHz maximum operating frequency) which provided a resolution of ±1 Hz to a maximum of 2^{24} counts.

Precise timing was achieved through the 4-MHz crystal clock of the microcomputer, which provided a 1-MHz buffered output. The 1-MHz signal was divided down to 0.25 Hz to give the required 2-s gate time. An intermediate frequency of 5-kHz was used to multiplex the instrument display (2 digit LED × 2 cm height) to decrease power consumption.

Data were acquired from the counter as three sequential bytes via three 8-bit tri-state latches into port 1 of the microcomputer. The latches were selected by using three outputs of the control decoder. Readout was given as a two-digit value but illumination of decimal points offered a readout range of 0.00—99. Output data were latched into the display drivers from port 1 of the microcomputer. The pump and alarm were controlled by logic levels held at the output of the control latch. A further latch was used to interface a zero request facility and a remote demountable keypad into the microcomputer.

System operation

The operation of the system was controlled by a machine-code program contained in a 4K × 8-bit EPROM. The timing diagram for a typical data cycle with a zero request is shown in Fig. 2. A reset pulse generated by the microcomputer clears the counter and opens the gate. During the following 2 s, the frequency of the analyser crystal is measured, with a negative transition on the gate signalling the microcomputer to take in the datum, select the reference crystal and reset the counters. After a further 2 s, the second datum is acquired and the new TDI concentration value is computed and displayed. This cycle is repeated until interrupted by a zero request, where new baseline values for the two crystals are taken and the cycle is repeated as before.

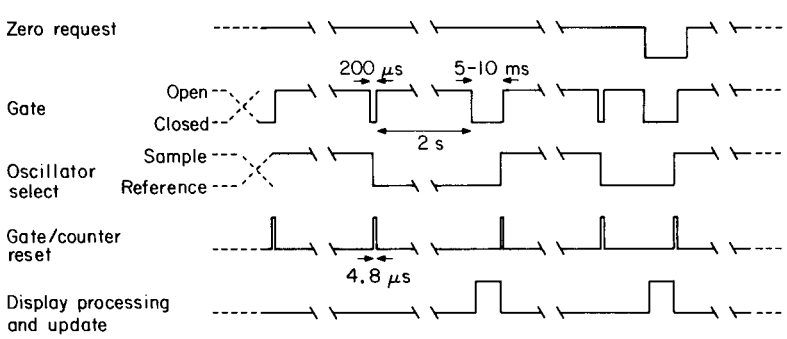

Fig. 2. Timing diagram of a typical data cycle with a zero request.

Software

The control program was developed by using an HP64000 (Hewlett Packard) microprocessor development system equipped with a 6800 series assembler (Manchester University Microprocessor Development Unit) and blown directly into the EPROM (TMS 2516, Texas Instruments). A flow diagram of the control program is given in Fig.3. At power-on, the instrument utilizes a self-test routine to check the operation of the alarm and display. The two parameters X and Y and a further parameter Z, the alarm threshold, are either entered via the remote keypad or are contained within the EPROM. This option provides flexibility so that the parameters may easily be changed during laboratory tests and calibration procedures. If the keypad is connected, the microcomputer reads in the values entered for the parameters. The display is then blanked to indicate that a zero request is required. The operator provides a TDI baseline by sampling a TDI-free atmosphere or by temporarily placing a charcoal filter over the sensing head to remove TDI from the sample stream. The zero request button is then pressed and baseline frequencies for the two crystals are measured. Subsequent readings will be relative to these

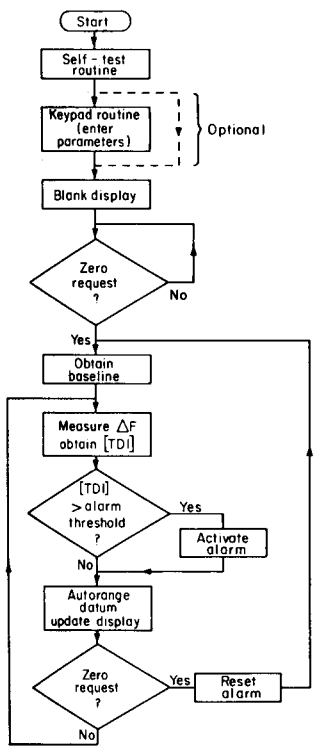

Fig. 3. Flow diagram of control program.

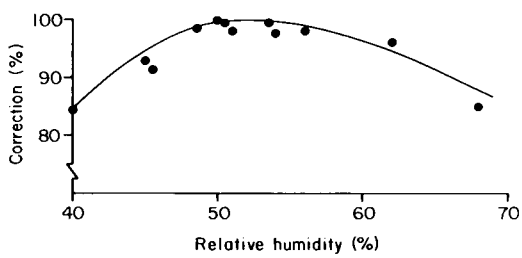

Fig. 4. Plot to show % correction for humidity achieved by the instrument at 20° C.

baseline values. A program cycle to obtain updated crystal frequencies and to compute a new value for TDI concentration is entered. Each value for TDI concentration is compared with the alarm threshold, which is activated when exceeded. The TDI datum is then processed by an autoscaling routine and the display is updated to read TDI concentration directly in ppm with a theoretical resolution of 0.01 ppm. The alarm may only be reset by a zero request and will continue to operate even if the TDI concentration falls to below the threshold value.

RESULTS AND DISCUSSION

The prototype instrument was assessed for its ability to correct for humidity changes in a specially-constructed flow rig based on an analyser crystal coated with PEG-400 (polyethylene glycol, molecular weight 400) and a reference crystal coated with PEG-1540. Relative humidities over the range 30—80% at ambient temperatures (18—23°C) could be attained rapidly (<5 min) and reproducibly. Dry air (2 l min^{-1}) was passed through a Drechsel bottle containing a sintered frit humidifier, with a variable flow by-pass; the humidified air was then passed to a 2 l round-bottomed flask in which the sensor head was placed. Alternatively, the humidified air could be passed over TDI in a round-bottomed flask maintained at a known temperature in a water bath, to generate a TDI-laden atmosphere; the TDI atmosphere took about 10 min to stabilize in concentration after being brought on-line). The outlet stream was split between the sensor head (1 l min^{-1}) and a bubbler (for determination of TDI by the Marcali method) and an on-line wet-and-dry bulb hygrometer.

Parameter X = 28 was found to be optimum for the PEG-400 and PEG-1540 crystal combination (by calibration and experimental iteration). Parameter Y was set at 128 to give a readout equivalent to 10^{-2} Hz. Measurements were made (with the TDI generator by-passed), by varying the humidity every 15 min and taking data when the instrument and hygrometer readings were stable.

Figure 4 shows the instrumental correction for humidity changes. The data are presented to show % correction as a function of humidity. The prototype instrument is clearly able to correct for both positive and negative humidity changes and correction is optimum at around 50% relative humidity.

Exposure of PEG-400/PEG-1540 crystals to TDI

Although it was known from earlier work that the PEG crystals had inadequate sensitivity to TDI, a series of tests with the PEG crystals was done over a period of five days. Exposure to TDI-laden air, (30% relative humidity) was effected in the gas rig described above. Figure 5 shows the results from the five daily exposures, the response being normalized to account for the differing TDI concentrations. The concentration of TDI was measured by using the Marcali method at each datum point after the first 10

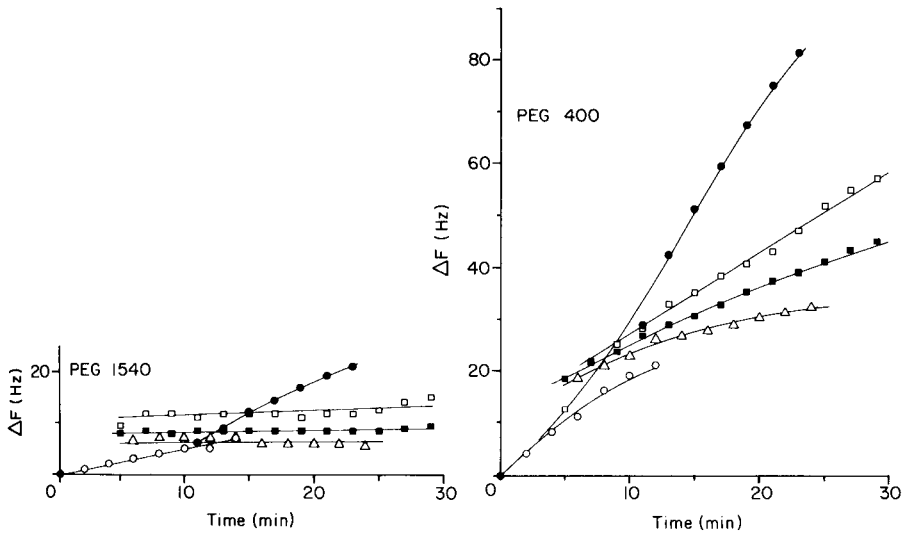

Fig. 5. Graphs to show the normalized response of PEG-1540 and PEG-400-coated crystals to TDI (1 ppm). Exposure number (•) 1; (○) 2; (□) 3; (■) 4; (△) 5.

min and was steady at the value stated for the rest of the period (±0.05 ppm) (at $T = 0$, $\Delta f = 0$, the concentration of TDI is zero). It is unfortunate that the values of concentration were not all the same, but it is difficult to reproduce desired concentrations of TDI on a day-to-day basis, hence the need for continuous calibration. It is clear from the plots, however, that the sensitivity of the response decreases as the crystal is re-exposed to TDI, that the chemisorption of TDI on the PEG-400 crystal is continuous (the absolute oscillation frequency at point zero on each run is lower than the preceding one), and that the PEG-1540 crystal eventually reaches a plateau value. Although "sensitivity" has little strict meaning in this context, an approximate description of the response for the PEG-400 crystal can be obtained by looking at the frequency change from zero TDI at the earliest time that the gas-phase TDI concentration became constant, which is generally 10 min. There is a gradual trend downwards from 29 Hz ppm^{-1} (10 min) through 19, 27, 25 and 23 Hz ppm^{-1} (10 min) for runs 1—5, respectively. (Although there was a temptation to reject the data for run 2, re-examination revealed no justification for that.) The corresponding values for the PEG-1540 coating were 5.6, 5.0, 11, 8.5 and 7.2 Hz ppm^{-1} (10 min). In this series of experiments, the relative humidity was constant so that the value of the humidity correction remained unproven. It was obvious, however, that the PEG-400/PEG-1540 combination could be used successfully to detect TDI at levels below 1 ppm at ca. 50% relative humidity with no interference from relative humidity changes over the range 40--70%.

As the sensitivity obtained with the PEG crystals was inadequate, the TOPO/$CoCl_2$ combination was investigated under more realistic conditions.

A simulation test with the portable instrument was done in a glove box, 0.5 m^3, with two side-arms, one of ca. 10-l capacity and the other about 1 l (Faircrest Engineering). The side-arms could be shut off from the main glove box and also from the laboratory air. The instrument was so arranged that the sensing head was inside the main chamber connected to the instrument "belt pack" outside, in the laboratory. The main chamber could be maintained at various humidities with ease and the relative humidity monitored with a hair hygrometer accurate to 2%. Different TDI atmospheres and humid TDI atmospheres could be maintained in the side-arms or the main box. The air was sampled continuously for determination of TDI levels by the Marcali method.

The coefficients measured and chosen for the TOPO and cobalt chloride crystals as described in Part 3 [3] were used initially to program the instrument (Tables 2 and 3). Slow alteration of the humidity of the atmosphere being monitored caused baseline drift, indicating that the coefficients were incorrect. As the parameter $\alpha = B/D$ is the ratio of the water coefficients, this was altered by small increments until the baseline remained steady with changing relative humidity. An initial period of 5 min was required to allow the instrument to stabilize after switch-on. This was due to alterations in battery voltage and to stabilization of the oscillators and pump. Figure 6 shows the effect of changing the atmosphere from 30% to 46% relative humidity, leaving for 30 min and returning to the 30% value. It can be seen that the device, although not operating perfectly, copes well with real conditions and changing humidity.

TABLE 2

Data for the correction parameters obtained by measurement [2]

Crystal coating	Calibration vapour	Parameter	Value (Hz ppm^{-1})
Tri-n-octylphosphine oxide	TDI	A	76
	WATER	B	0.024
Cobalt(II) chloride	TDI	C	40
	WATER	D	0.053

TABLE 3

Coefficients calculated from the data in Table 2 compared with the coefficients which give optimal results

Parameter	Calculated value	Empirical value
α	0.45	0.8
β	58	106
X	36	20
Y	74	136

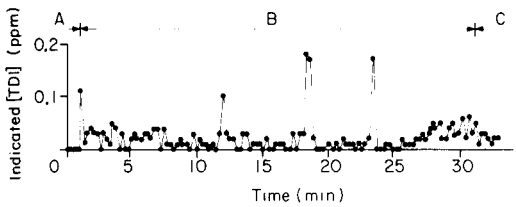

Fig. 6. Effect of changing relative humidity of air on the baseline of the TOPO/$CoCl_2$ crystal combination: (A) baseline checked for 1 min at 30% humidity; (B) exposure for 30 min to 46% humidity; (C) return to air at 30% humidity.

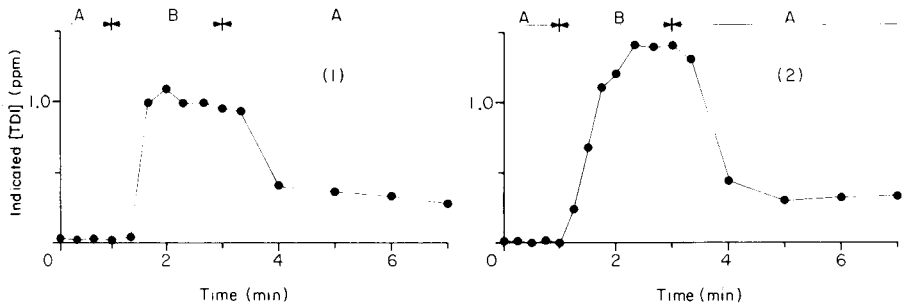

Fig. 7. Typical exposure to TDI and "wet" air at 22°C. Relative humidity: (A) box air at 23%; (B) laboratory air at 50%. TDI concentration by Marcali = (1) 0.97; (2) 0.96 ppm.

Next, the TDI response was measured with the calculated value of Y, obtained from the measured data in Part 3 [3] (Table 3). This was initially done at constant humidity, the sensor being passed from a clean atmosphere to one containing TDI. The sensor was allowed to stabilize in clean air and transferred to the TDI-contaminated side-arm for 2 min. The steady TDI concentration displayed was noted and compared to the known TDI concentration in the side arm, measured by the Marcali method. The sensor was allowed to stabilize and desorb the TDI for 10 min, and the process was repeated. The initial tests with the measured coefficient $\beta = 41$ ($Y = 52$) gave displayed results that were far too high. The coefficient was altered stepwise until the readings obtained corresponded reasonably with the Marcali results.

These optimized parameters $X = 20$, $Y = 136$ were used in a further experiment in which the change in relative humidity was from 20—35% in the glove box to 50—60% in the side-arm contaminated with TDI. Two typical responses are shown in Fig. 7. The effect of chemisorption of TDI can be clearly seen. There is a linear correlation between measured and true TDI concentration. The gradient is 0.97 with a standard deviation of 0.24 (15 results).

The results obtained in this work are encouraging, but indicate that the prediction of the characteristic responses of the coated crystals is far from easy. There is no question that TDI is a difficult material to handle and not

the best with which to optimize an instrument or develop a technique. However, it is possible to establish coefficients for the correction and display algorithm. The empirical α-factor for the humidity correction is reasonably close to the value predicted by measurement. The fact that the β-factors are so different is disappointing and not understood. Although the original assumption was that only the effects of water vapour were being corrected for, it may be that other so far unobserved factors contribute to the empirical parameters and that a more complex correction algorithm is needed.

The portable instrument itself works well. Since its construction it has worked almost daily for over a year with neither maintenance nor repair. The battery life, at 6 h is quite acceptable and the freedom from electromagnetic interference in an electrically very noisy environment is excellent.

Further work is needed on the coatings and to test them over wider TDI and humidity ranges and at low temperature. It is not certain how stable TDI will be in very humid atmospheres, in view of its reactivity with water. With a sensitivity of 76 Hz ppm^{-1}, a limit of detection of around 0.1 ppm is attainable with this system. A crystal sufficiently sensitive to monitor below the TLV of 0.02 ppm would require a sensitivity which has been hitherto unobtainable, unless major signal recovery techniques are employed, as in the earlier work [2].

This work has shown that coated piezoelectric crystals have a major role to play in portable equipment for toxic gas detection. The instrumentation to monitor and display the crystal behaviour is now in an advanced stage of development and has been shown to operate under conditions of changing humidity. The practical behaviour of the coated crystals is becoming better understood, but as yet is far from being controlled precisely.

John McCallum was supported by SERC in collaboration with Panocean Anco Ltd (now PAL Shipping Services) under the CASE Scheme.

REFERENCES

1 J. F. Alder and C. A. Isaac, Anal. Chim. Acta, 129 (1981) 163, 175.
2 J. J. McCallum, P. R. Fielden, M. Volkan and J. F. Alder, Anal. Chim. Acta, 162 (1984) 75.
3 Q. Bristow, J. Geochem. Explor., 1 (1972) 55.
4 E. P. Scheide and R. B. J. Warner, Am. Ind. Hyg. Assoc. J., 39 (1978) 745.
5 T. E. Carpenter and D. L. Brenchley, Am. Ind. Hyg. Assoc. J., 33 (1972) 503.
6 P. S. Daley and D. A. Lundgren, Am. Ind. Hyg. Assoc. J., 36 (1975) 518.
7 K. H. Karmarkar, L. M. Webber and G. G. Guilbault, Anal. Chim. Acta, 81 (1976) 265.
8 M. H. Ho and G. G. Guilbault, Anal. Chim. Acta, 52 (1980) 1489.
9 G. Sauerbrey, Z. Phys., 155 (1959) 206.
10 See, e.g., J. F. Alder and J. J. McCallum, Analyst (London), 108 (1983) 1169.
11 O. Lewis and C. Lu, Proceedings of the 29th Annual Symposium on Frequency Control, (1975) 5.
12 M. Janghorbani and H. Freund, Anal. Chem., 45 (1973) 325.
13 T. E. Edmonds and T. S. West, Anal. Chim. Acta, 117 (1980) 147.

Analytica Chimica Acta, 162 (1984) 97—102
Elsevier Science Publishers B.V., Amsterdam — Printed in The Netherlands

A COATED PIEZOELECTRIC CRYSTAL DETECTOR FOR PHOSGENE

A. SULEIMAN and G. G. GUILBAULT*
Department of Chemistry, University of New Orleans, New Orleans, LA 70148 (U.S.A.)
(Received 27th September 1983)

SUMMARY

A piezoelectric quartz crystal coated with methyltrioctylphosphonium dimethylphosphate was found to be a good detector for phosgene in air. The coating is sensitive to phosgene in the $\mu g\ l^{-1}$ range and has a reasonably long lifetime. The response curve is linear over the concentration range 5—140 $\mu g\ l^{-1}$. The coated crystal can be used for more than six weeks without significant loss in sensitivity, provided that high ammonia concentrations are not encountered.

There has been considerable interest in recent years in the application of piezoelectric crystal resonators for monitoring thin films and for studying absorption processes. The linear relationship between the mass added to the crystal surface and the change in frequency can be derived from the Sauerbrey equation [1]

$$\Delta F = 2.3 \times 10^6\ F^2\ M_s/A \qquad (1)$$

where ΔF is the frequency change (Hz), F is the basic frequency of the quartz crystal (MHz), M_s is the mass of the deposited material (g), and A is the area of the quartz crystal (cm^2).

Piezoelectric crystal detectors have become increasingly useful for the detection for organophosphorus pesticides, and inorganic gases such as H_2S, SO_2, CO and NH_3 in the atmosphere [2, 3]. Other applications include a sorption detector for gas chromatography and a moisture detector [4]. In this study, the selective detection of phosgene in air was accomplished by using methyltrioctylphosphonium dimethylphosphate as the coating. The detector exhibited good sensitivity in the $\mu g\ l^{-1}$ range. The proposed detector is the first portable device described for monitoring phosgene in air, and has several advantages (sensitivity, cost) compared with other methods.

EXPERIMENTAL

Apparatus and crystal coating

A schematic diagram of the experimental set-up is shown in Fig. 1. The piezoelectric crystal used was a 9-MHz quartz crystal with gold-coated metal electrodes. The crystal was driven by a low-frequency-transistor oscillator

0003-2670/84/$03.00

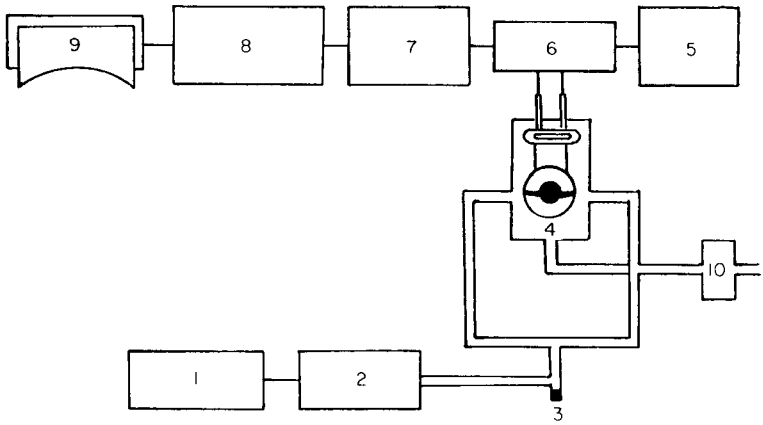

Fig. 1. Block diagram of the experimental set-up. (1) Carrier gas; (2) drying tube; (3) injection port; (4) piezoelectric crystal; (5) power supply; (6) oscillator; (7) frequency counter; (8) digital-to-analog converter; (9) recorder; (10) flow meter.

type OT-13 (International Crystal Manufacturing Company, OK). The oscillator was powered by a Heathkit 1—30 VDC regulator power supply (Model IP-28) set at 9 V d.c. The frequency of the vibrating crystal was monitored by a frequency counter (Systron Donner Model 8050) which was modified by a digital-to-analog converter (DAC). The output of the converter was connected to a recorder. The design of the detector cell is essentially the same as described earlier [5]. The carrier gas used was nitrogen. The volume of sample injected was usually 2.5 ml.

The coating used was methyltrioctylphosphonium dimethylphosphate (K & K Labs) which was dissolved in chloroform. The coated crystals were prepared by dropping a solution of the substrate onto both sides of the electrode of the piezoelectric crystal using a syringe and spreading the solution with a glass rod. The coated crystal was placed in a desiccator for 2 h to allow the solvent to evaporate, leaving a film of coating on the surface. The crystal was then placed in an oven at 70°C for 2 h to ensure complete evaporation of the solvent. The amount of coating applied to the crystal was determined by noting the frequency change of the crystal.

Procedure

The syringe dilution method described by Karasek and Tiernay [6] and Guilbault and Karmarkar [5] was used to obtain the desired concentrations of the sample gas. The sample gas (2.5 ml) was injected into the carrier gas stream at the injection port. Each response reported is the average for five separate injections. In the interference study, the flask dilution method (Fig. 2) was used to prepare mixtures of different known concentrations.

In this method, the flasks were first evacuated to 10^{-3} torr, and then carrier gas was allowed to fill the flasks to 1 atm. The stopcock between the

two flasks was closed and a known volume of pure gas was injected into the first flask. The mixture was then stirred sufficiently to obtain a homogeneous mixture. If a more dilute mixture was desired, then a known volume of the mixture from the first flask was withdrawn and injected into the second flask. Heating tapes were wrapped around the flask to prevent the sample gas from being adsorbed onto the glass walls of the flasks. The volume of each flask was 2 l.

RESULTS AND DISCUSSION

Optimum coating and effect of flow rate

The first set of experiments was done to establish the optimum amount of substrate to be applied to the crystal. It is evident from the results listed in Table 1 that the net response increases as the amount of coating increases, because of an increased probability of interaction of the coating substrate with the phosgene molecules. However, at high amounts of coating, it is difficult to obtain a uniform dry film and thus poor precision is observed. The relative standard deviation (RSD) is relatively high when a large amount of coating is applied. It is concluded that for better reproducibility, small amounts (15—20 μg) of coatings should be used.

Flow rate showed a marked effect on the sensitivity of the detector (Table 2). This effect on the detector response was probably due to a rather

TABLE 1

Effect of amount of coating on the response to phosgene[a]

Amount of coating (μg)	Response (Hz)	RSD (%)	Amount of coating (μg)	Response (Hz)	RSD (%)
1.35	2	0.5	38.12	129	18.0
4.43	9	1.2	43.73	148	15.13
9.06	16	1.9	45.02	160	20.0
9.73	17	2.1	48.82	174	18.5
12.17	26	3.2	55.45	221	21.9
16.03	48	6.3	56.36	226	21.0
19.24	60	5.69	59.64	245	26.8
31.70	111	12.1	66.97	305	36.2
35.54	113	14.0			

[a]Sample size, 2.5 ml; concentration, 50 μg l^{-1} flow rate, 10 ml min^{-1}.

TABLE 2

Effect of flow rate on the response to phosgene[a]

Flow rate (ml min^{-1})	0	5	7.5	10	15	20	40	60	70
Response (Hz)	0	21	25	26	19	15	11	5	0

[a]Sample size, 2.5 ml; concentration, 50 μg l^{-1}; amount of coating, 17.95 μg.

weak adsorption of phosgene by the substrate. At high flow rates, phosgene was desorbed easily from the substrate surface and the net response decreased significantly. Maximum sensitivity was obtained at low flow rates (5—10 ml min^{-1}).

Reversibility of adsorption

Reversibility is the ability of the detector crystal to reattain the baseline frequency after it has been exposed to a gas sample, and is one of the most important factors in evaluating a piezoelectric detector. If complete reversibility is not achieved, the reproducibility will be very poor and in most cases further measurements cannot be performed. Completeness with which adsorbed analyte is removed is governed by the type of interaction between the substrate and the analyte and is highly affected by the flow rate. Table 3 shows that complete removal of the analyte can be accomplished in shorter times at higher flow rates (e.g., 70 ml min^{-1}). All further measurements were done with an initial flow rate of 10 ml min^{-1}; then the flow rate was increased to 70 ml min^{-1} to achieve rapid removal of analyte.

Interferences

Interferences from various gases which would be expected to exist in the atmosphere as potential pollutants were tested; the results are listed in Table 4. At very high concentrations, hydrogen chloride, ammonia and hydrogen sulfide gave a relatively high response. The response to ammonia is irreversible and if the substrate is exposed to large doses of ammonia, the response to phosgene is irreversible and increases markedly. The response for 4 injections of 50 $\mu g\ l^{-1}$ phosgene alternated with 5-ml doses of pure ammonia were 270, 266, 267, 268 Hz, which is much higher than the response to phosgene in the absence of ammonia. However, the decrease in frequency after each exposure to ammonia was about 5000 Hz and the crystal ceased to vibrate after several exposures. Thus, prior exposure to ammonia makes the coated crystal useless for the determination of phosgene. Although it is

TABLE 3

Effect of flow rate on desorption of phosgene from the detector

Flow rate (ml min^{-1})	Response[a] (Hz)	Time (min)	Amount removed (%)
		5	69
		10	77
10	26	15	82
		20	87
		30	98
15	19	5	90
		10	98

[a] Concentration, 50 $\mu g\ l^{-1}$; amount of coating, 17.95 μg.

TABLE 4

Detector response to potential interferences[a]

Interference	Response (Hz)	Interference	Response (Hz)	Interference	Response (Hz)
SO_2	4	NH_3	21, 17, 11	CO_2	0
NO_2	2	HCl	16	H_2NNH_2	0
CO	0	H_2S	18	Air	14
C_2H_3Cl	3				

[a]Interferent concentration, 320 mg l^{-1}; flow rate, 10 ml min^{-1}; amount of coating, 17.95 μg.

not expected that these pollutants will exist in such high concentrations in air, an additional set of experiments was done to evaluate their effects on the measurements of phosgene. A glass column (7 mm internal diameter, 15 cm long) filled with phosphorus pentoxide was placed before the injection port. As shown in Table 5, the presence of these pollutants did not then affect the accurate measurement of phosgene.

Calibration curve and lifetime

The response curve for phosgene is shown in Fig. 3. This plot was linear over the concentration range 5—140 μg l^{-1}. The relative standard deviation was 2.5% for 100 μg l^{-1} and 12% for 5 μg l^{-1}. Reproducibility at lower concentrations could be improved by using a better dilution method, e.g., a permeation device, for the generation of the desired phosgene concentrations.

The coating was found to have a reasonably long lifetime. When 50 μg l^{-1} phosgene samples were tested (flow rate 10 ml min^{-1}; coating, 17.95 μg), the response decreased from 26 Hz to 25 Hz after 3 weeks, 24 Hz after 5 weeks and 23 Hz after 6 weeks, i.e., the loss in sensitivity was only about 12.5% after 6 weeks. The lifetime of the coating is limited only by exposure to moisture or high concentrations of ammonia. It is necessary to protect the

TABLE 5

Effect of interferences on the response of the phosgene detector to 50 μg l^{-1} phosgene

Gas	Concentration added	Response (Hz)
—	—	25
H_2S	100 mg l^{-1}	25
HCl	100 mg l^{-1}	25
NH_3	100 mg l^{-1}	22
NH_3	pure	6

[a]Flow rate, 10 ml min^{-1}; amount of coating, 16.4 μg.

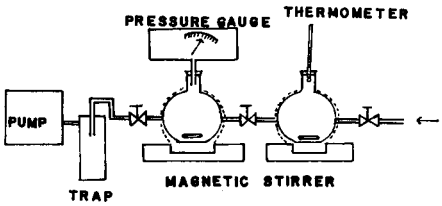

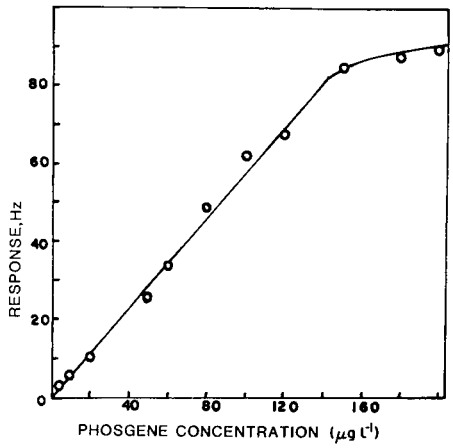

Fig. 2. Apparatus for flask dilution method.

Fig. 3. Response of the detector to phosgene in air.

coating from moisture by keeping the coated crystal in a desiccator when not in use.

This work was supported by the Army Research Office through Grant No. DAAG29-77-G-0226-DR.

REFERENCES

1 G. Z. Sauerbrey, Z. Phys., 155 (1959) 206.
2 G. G. Guilbault, Int. J. Environ. Anal. Chem., 10 (1981) 89.
3 G. G. Guilbault and J. Hlavay, Anal. Chem., 49 (1977) 1890.
4 W. H. King, Jr., Anal. Chem., 36 (1964) 1735; Res. Dev., 20(4) (1969) 28; Res. Dev., 20(5) (1969) 28.
5 G. G. Guilbault and K. H. Karmarkar, Anal. Chim. Acta, 71 (1974) 419.
6 F. W. Karasek and J. P. Tiernay, J. Chromatogr., 89 (1974) 31.

Analytica Chimica Acta, 162 (1984) 103—111
Elsevier Science Publishers B.V., Amsterdam — Printed in The Netherlands

STANDARD pH VALUES FOR POTASSIUM HYDROGENPHTHALATE REFERENCE BUFFER SOLUTIONS IN 10, 30 AND 50% (w/w) 1,4-DIOXANE/WATER MIXED SOLVENTS AT TEMPERATURES FROM 288.15 TO 318.15 K

TORQUATO MUSSINI*, MAURIZIO CICOGNINI, PAOLO LONGHI and SANDRA RONDININI

Department of Physical Chemistry and Electrochemistry, University of Milan, Via Golgi 19, I-20 133 Milano (Italy)

ARTHUR K. COVINGTON

Electrochemistry Research Laboratories, Department of Physical Chemistry, The University, Newcastle-upon-Tyne NE1 7RU (Great Britain)

(Received 23rd March 1984)

SUMMARY

Standard pH(S) values for 0.05 mol kg^{-1} potassium hydrogenphthalate (KHPh) reference buffer solutions in 10, 30 and 50% (w/w) 1,4-dioxane/water solvent mixtures within the temperature range 288.15—318.15 K are determined from e.m.f. measurements of the cell without transference $Pt|H_2|KHPh + KCl|AgCl|Ag|Pt$. The consistency of the results is analysed by a recently described method of multilinear regression of the quantity $p(a_{H\gamma Cl})$ as a function of both solution composition and temperature. The standard pH(S) determined can be reproduced to within ±0.01 by the equation $pH(S) = 4.004 + 3.309w + 0.408z + 1.037w^3 - 14.95zw^2 + 27.1zw^3$, where w is the weight fraction of dioxane in the solvent mixture, $z = (T - \theta)/\theta$, and $\theta = 298.15$ K. Values of the first ionization constant of phthalic acid (H_2Ph; benzene-1,2-dicarboxylic acid) in the above solvent mixtures are also determined from e.m.f. measurements of the cell without transference $Pt|H_2|H_2Ph + KHPh + KCl|AgCl|Ag|Pt$.

Standardization of pH measurements in aqueous solutions, based on the universally accepted operational definition [1] of pH, quite recently came to a conclusive stage with the official IUPAC proposal of the buffer solution of molality 0.05 mol kg^{-1} of potassium hydrogenphthalate (KHPh) as the reference value standard (RVS) for the aqueous pH scale [1, 2]. This has provided an impetus for parallel, and long overdue, pH standardization in nonaqueous and mixed solvents, for which there have hitherto been data only for a few buffer materials, other than KHPh, in methanol/water, ethanol/water and dimethyl sulfoxide/water mixtures [3—8]. The desirability and appropriateness of extending the RVS role of the KHPh buffer to the contiguous, and nearly unlimited, domain of water-rich solvent mixtures was reassessed recently [9]. In this context, standard pH data for KHPh have been recently determined over a range of temperatures in dimethyl sulfoxide/water [8]

and in methanol/water [10]. The present paper extends these data for the 0.05 mol kg^{-1} KHPh buffer to solvent mixtures of water with the nonpolar aprotic 1,4-dioxane over the temperature range 288.15—318.15 K, and supersedes the data at 298.15 K available in a preliminary communication [11].

To this end, the reversible e.m.f. E_A of the cell (A)

$$\mathrm{Pt} \mid \mathrm{H_2}\ (1\ \mathrm{atm}) \mid \begin{matrix}\mathrm{KHPh}\ (m = 0.05\ \mathrm{mol\ kg^{-1}}) + \mathrm{KCl}\ (m_1) \\ \text{in 1,4-dioxane/water mixtures}\end{matrix} \mid \mathrm{AgCl} \mid \mathrm{Ag} \mid \mathrm{Pt} \qquad \text{(A)}$$

as measured within the above temperature range at various molalities m_1 of KCl ($0.01 < m_1 < 0.07$ mol kg^{-1}) in 1,4-dioxane/water mixtures at 10, 30 and 50% (w/w) dioxane, that have corresponding relative permittivities (dielectric constants) of the orders of 70, 53 and 35, respectively, which ensure the negligibility of ionic association for the present purposes. Supplementary data for the first ionization constant, K_1, of phthalic acid (H_2Ph; benzene-1,2-dicarboxylic acid) in the same solvent mixtures and within the same temperature range, were also determined from the reversible e.m.f. (E_B) of the cell (B)

$$\mathrm{Pt} \mid \mathrm{H_2}\ (1\ \mathrm{atm}) \mid \begin{matrix}\mathrm{H_2Ph}\ (m_2) + \mathrm{KHPh}\ (m_3) + \mathrm{KCl}\ (m_4) \\ \text{in 1,4-dioxane/water mixtures}\end{matrix} \mid \mathrm{AgCl} \mid \mathrm{Ag} \mid \mathrm{Pt} \qquad \text{(B)}$$

at various molalities of the mixed electrolyte ($0.004 < m_2 \approx m_3 \approx m_4 < 0.04$ mol kg^{-1}).

EXPERIMENTAL

The hydrogen electrodes in cells (A) and (B) were based on smooth platinum ribbon supports [12] which were washed in concentrated nitric acid and rinsed in triply-distilled water before each experiment; the high-purity hydrogen (99.999%) bubbled into the electrode compartment was presaturated with a solution identical to that under study. The silver/silver chloride electrodes were prepared by the electrolytic method [13]. The potentiometric and thermostatic apparatus were described earlier [14]. The e.m.f. values were mostly measured in duplicate (cf. Tables 1 and 2) and their values were corrected to 1 atm (101 325 Pa) pressure of hydrogen, making use of vapour pressure data available in the literature [15]. The solutions were made up by weight from triply-distilled water and reagent-grade Carlo Erba chemicals (1,4-dioxane, potassium hydrogenphthalate, phthalic acid and potassium chloride). Before use, potassium chloride and potassium hydrogenphthalate were dried at 110°C [1]; 1,4-dioxane was distilled over sodium in a nitrogen atmosphere and used immediately for preparation of the above solutions.

RESULTS AND DISCUSSION

From the values for the e.m.f., E_A, of cell (A) collected in Table 1, one obtains the function

$$p(a_H\gamma_{Cl}) = -\log(a_H\gamma_{Cl}) = pH + p\gamma_{Cl} = (E_A - E^0)/k + \log m_1 \quad (1)$$

where $k = RT(\ln 10)/F$, E^0 is the standard e.m.f. of the cell (the required values are available in the literature [16]), a and γ are the ionic activities and activity coefficients (to simplify printing, the ions involved are denoted by the subscripts without the charge numbers). It is clear that $p(a_H\gamma_{Cl})$ for the KHPh/KCl mixed electrolyte can be determined in thermodynamically exact terms, whereas pH requires an appropriate extrathermodynamic convention for $p\gamma_{Cl}$. Linear regression analysis of $p(a_H\gamma_{Cl})$ values against m_1 to $m_1 = 0$ gives the $p(a_H\gamma_{Cl})^0$ value for 0.05 mol kg^{-1} KHPh, a value which is now free from the influence of the KCl added to KHPh, but still differs from the sought pH^0 standard value

$$pH^0 = pa_H^0 = p(a_H\gamma_{Cl})^0 - p\gamma_{Cl}^0 \quad (2)$$

by the single Cl^- ionic activity coefficient term $p\gamma_{Cl}^0$. This can be calculated, by an extrathermodynamic convention, from the Debye—Hückel equation

$$p\gamma_{Cl}^0 = AI^{1/2}/(1 + a_0BI^{1/2}) \quad (3)$$

at the actual ionic strength of the 0.05 m KHPh buffer solution, given the same conventional value [4] of the ion-size parameter a_0 fixed by the Bates—Guggenheim convention [17], internationally endorsed for aqueous standard buffers. Thus, at each temperature T:

$$(a_0B)_T = 1.5[(\epsilon^w\rho^s)/(\epsilon^s\rho^w)]_T^{1/2} \quad (4)$$

where ϵ^w, ϵ^s, ρ^w and ρ^s are the relative permittivities and the densities of water and the dioxane/water mixture, respectively; the relevant data are available from the literature [15, 18—21]. The ionic strength of the KHPh buffer solution is given by

$$I = (m_K + m_{HPh} + 4m_{Ph} + m_H)/2 \quad (5)$$

Now, the molality m_H of H^+, which is required by Eqn. 5 for I can be calculated from I as

$$pm_H = p(a_H\gamma_{Cl})^0 - 2AI^{1/2}/(1 + a_0BI^{1/2}) \quad (6)$$

but I depends in turn on m_H through Eqn. 5. Therefore the calculation must proceed by successive iterations, using appropriate equations for the molalities m_{HPh} and m_{Ph} for the hydrogenphthalate and phthalate ion, respectively, in terms of the first ionization constant K_1 of phthalic acid; these equations and the iterative calculation steps were described in previous papers [10, 11]. Two or three iterations suffice to attain constancy of the I value; through it, $p\gamma_{Cl}^0$ can then be obtained from Eqn. 3 for insertion into

TABLE 1

Values of e.m.f. E_A of cell (A) at various molalities m_1 of KCl in 0.05 m potassium hydrogen standard e.m.f.s E^0 and Debye—Hückel constants A and B

	Weight percent of 1,4-dioxane in mixtures with water					
	10					30
T (K)	288.15	298.15	308.15	318.15	T (K)	288.15
m_1 (mmol kg^{-1})	E_A (mV)	E_A (mV)	E_A (mV)	E_A (mV)	m_1 (mmol kg^{-1})	E_A (mV)
10.018	586.54	592.87	599.01	605.26	10.029	608.58
10.018	586.32	592.85	599.04	605.12	10.029	608.67
20.018	568.87	—	—	—	20.020	590.94
—	—	—	—	—	20.020	590.91
30.043	558.75	564.05	569.44	575.02	30.015	579.90
30.043	559.24	564.56	569.83	574.68	30.015	580.05
39.942	550.93	556.16	561.40	566.30	40.020	572.59
39.942	551.34	556.37	561.43	566.28	40.020	572.55
50.021	544.94	549.79	554.62	559.16	50.049	566.22
50.021	545.17	549.80	554.62	559.13	50.049	565.98
60.033	540.61	545.32	550.08	554.66	60.041	561.22
60.033	540.67	545.36	550.12	554.13	60.041	560.96
70.015	536.47	540.89	545.57	549.62	70.019	557.00
70.015	536.58	541.00	545.20	549.58	70.019	556.93
E^0 (mV)[a]	219.58	213.02	205.92	197.94		198.38
A (mol$^{-1/2}$ kg$^{1/2}$)[b]	0.5926	0.6023	0.6139	0.6270		0.89
a_0B (mol$^{-1/2}$ kg$^{1/2}$)[b]	1.5910	1.5892	1.5896	1.5917		1.83

[a]From Ref. [16]. [b]Calculated from densities and dielectric constants interpolated from data i

Eqn. 2 to give finally the sought standard pH^0 value from $p(a_H\gamma_{Cl})^0$. Table 3 collects these pH^0 values for 0.05 mol kg^{-1} KHPh for the various solvent mixtures (including pure water [2, 22, 23] to facilitate comparison) and temperatures examined, together with values of $p(a_H\gamma_{Cl})^0$ and the relevant values of I and pK_1. The latter were obtained separately from the e.m.f. E_B of cell (B) (see Table 2), expressed by the equation

$$E_B - E^0 = k(pm_1 + pm_4) + k(p\gamma_H + p\gamma_{Cl}) \quad (7)$$

which can be combined with the expression for K_1

$$K_1 = m_H\gamma_H m_{HPh}\gamma_{HPh}/m_{H_2Ph}\gamma_{H_2Ph} \quad (8)$$

to define the extrapolation function

hthalate for various dioxane/water solvent mixtures at different temperatures, T, with relevant

				50			
98.15	303.15	318.15	T (K)	288.15	298.15	308.15	318.15
E_A (mV)	E_A (mV)	E_A (mV)	m_1 (mmol kg^{-1})	E_A (mV)	E_A (mV)	E_A (mV)	E_A (mV)
13.86	618.70	623.72	10.023	623.80	626.63	629.88	632.67
13.81	618.77	—	10.023	623.74	626.71	629.63	632.20
95.36	599.65	603.98	20.008	605.86	608.42	610.85	613.10
95.21	599.32	—	20.008	605.66	608.31	610.69	612.69
84.15	588.25	592.20	30.022	594.84	596.98	599.27	601.21
84.21	588.16	—	30.022	594.71	597.15	598.65	600.68
76.60	580.20	583.77	40.029	587.18	589.14	590.87	592.56
76.22	579.55	—	40.029	586.57	588.69	590.57	591.94
70.15	573.67	576.78	50.063	580.95	582.64	584.06	585.47
69.48	573.09	—	50.063	—	582.15	583.84	—
64.92	568.40	571.41	60.052	576.13	577.66	579.02	580.29
64.19	567.95	—	60.052	575.93	577.00	—	579.91
60.50	563.52	566.57	70.041	571.69	573.04	574.26	575.30
—	563.17	—	70.041	571.34	—	—	574.83
90.23	181.12	171.43		165.20	151.72	138.11	124.46
0.9200	0.9455	0.9737		1.6277	1.6781	1.7335	1.7932
1.8401	1.8446	1.8510		2.2495	2.2564	2.2646	2.2742

efs. [15, 18—21]. [c]See Eqn. 4.

$$\Phi = [(E_B - E^0)/k] + \log[(m_2 - m_H)m_4/(m_3 + m_H)]$$
$$= pK_1 - (b_{Cl} - b_{HPh})I \quad (9)$$

where the standard e.m.f. E^0 is the same as for cell (A), γ_{H_2Ph} is put equal to unity, b_{Cl} and b_{HPh} are the specific interaction parameters in the extended Debye—Hückel equations for $p\gamma_{Cl} = AI^{1/2}/(1 + a_0BI^{1/2}) - b_{Cl}I$ and for $p\gamma_{HPh} = AI^{1/2}/(1 + a_0BI^{1/2}) - b_{HPh}I$. The additive contribution of the second ionization of H_2Ph, which has an equilibrium constant K_2 in water lower than K_1 by about three orders of magnitude [22, 23], can be neglected safely. Thus for the mixed electrolyte in cell (B) one can write $m_{Cl} = m_4$, $m_{HPh} = m_3 + m_H$, $m_{H_2Ph} = m_2 - m_H$ and, for the ionic strength,

$$I = m_3 + m_4 + m_H \quad (10)$$

TABLE 2

Values of e.m.f. E_B of cell (B) at various molalities of the mixed electrolyte H_2Ph (m_2) + KHPh (m_3) + KCl (m_4) and various temperatures T, in different dioxane/water solvent mixtures

	Weight percent of 1,4-dioxane in mixtures with water													
	10[a]					30[a]					50[b]			
T/K	288.15	298.15	308.15	318.15	T/K	288.15	298.15	308.15	318.15	T/K	288.15	298.15	308.15	318.15
m_2 (mmol kg^{-1})	E_B (mV)	E_B (mV)	E_B (mV)	E_B (mV)	m_2 (mmol kg^{-1})	E_B (mV)	E_B (mV)	E_B (mV)	E_B (mV)	m_2 (mmol kg^{-1})	E_B (mV)	E_B (mV)	E_B (mV)	E_B (mV)
—	—	—	—	—	4.004	547.63	—	—	—	—	—	—	—	—
—	—	—	—	—	4.004	548.77	—	—	—	—	—	—	—	—
—	—	—	—	—	8.009	530.12	534.59	535.65	536.30	7.989	537.31	537.23	537.10	536.79
—	—	—	—	—	8.009	531.43	533.27	534.67	535.72	7.989	536.58	537.18	537.00	536.63
15.018	510.00	513.02	514.75	517.37	14.935	515.74	—	—	518.08	14.994	521.80	521.36	520.58	519.60
15.018	509.33	512.92	514.94	517.42	14.935	514.76	—	—	518.17	14.994	521.52	521.10	519.73	519.40
20.015	501.99	—	507.38	508.82	19.985	509.55	511.52	510.78	511.84	20.000	514.55	513.91	512.76	511.49
20.015	501.67	—	507.38	508.74	19.985	—	510.27	510.88	—	20.000	514.38	513.46	512.45	510.93
27.074	494.50	497.08	499.57	501.11	29.943	502.45	502.97	503.23	502.95	29.977	505.10	504.24	502.81	500.92
27.074	493.48	497.23	499.53	500.08	29.943	501.89	502.38	502.39	502.35	29.977	503.57	502.50	502.12	500.18
35.010	488.34	490.53	493.06	494.34	—	—	—	—	—	—	—	—	—	—
35.010	487.84	490.51	492.64	492.91	—	—	—	—	—	—	—	—	—	—
40.003	484.62	487.01	487.99	490.21	40.003	494.96	495.35	495.51	495.19	40.008	497.79	496.49	495.16	493.28
40.003	484.61	486.88	488.32	490.03	40.003	494.56	495.26	495.27	495.12	40.008	497.78	496.18	494.54	492.38

[a] $m_2 = m_3 = m_4$. [b] $m_3 = 0.9999\, m_2$, $m_4 = 1.0002\, m_2$.

TABLE 3

Reference value standards pH^0 of 0.05 *m* potassium hydrogenphthalate buffers (with corresponding standard errors) in various 1,4-dioxane/water solvent mixtures at various temperatures T, together with the relevant values of $p(a_H\gamma_{Cl})^0$, of the first ionization constant K_1 of phthalic acid, and of the actual ionic strength I of the buffers

Weight per cent of 1,4-dioxane		0	10	30	50
T = 288.15 K	pH^0	3.998 ± 0.001[a]	4.323 ± 0.003	5.042 ± 0.002	5.784 ± 0.003
	$p(a_H\gamma_{Cl})^0$	4.084 ± 0.001[a]	4.423 ± 0.003	5.186 ± 0.002	6.028 ± 0.003
	pK_1	2.936 ± 0.001[b]	3.178 ± 0.006	3.654 ± 0.011	4.393 ± 0.004
	I/mol kg^{-1}	0.05310[a]	0.05255	0.05137	0.05111
T = 298.15 K	pH^0	4.005 ± 0.001[a]	4.327 ± 0.003	5.023 ± 0.003	5.789 ± 0.003
	$p(a_H\gamma_{Cl})^0$	4.093 ± 0.001[a]	4.428 ± 0.003	5.170 ± 0.003	6.040 ± 0.003
	pK_1	2.950 ± 0.001[b]	3.191 ± 0.002	3.663 ± 0.013	4.408 ± 0.002
	I/mol kg^{-1}	0.05314[a]	0.05258	0.05145	0.05111
T = 308.15 K	pH^0	4.018 ± 0.001[a]	4.335 ± 0.003	5.014 ± 0.003	5.792 ± 0.003
	$p(a_H\gamma_{Cl})^0$	4.107 ± 0.001[a]	4.438 ± 0.003	5.165 ± 0.003	6.051 ± 0.003
	pK_1	2.967 ± 0.001[b]	3.178 ± 0.016	3.636 ± 0.015	4.412 ± 0.003
	I/mol kg^{-1}	0.05316[a]	0.05248	0.05141	0.05110
T = 318.15 K	pH^0	4.038 ± 0.001[a]	4.356 ± 0.004	5.019 ± 0.002	5.790 ± 0.003
	$p(a_H\gamma_{Cl})^0$	4.129 ± 0.001[a]	4.461 ± 0.004	5.174 ± 0.002	6.058 ± 0.003
	pK_1	2.989 ± 0.001[b]	3.170 ± 0.004	3.615 ± 0.012	4.421 ± 0.003
	I/mol kg^{-1}	0.05316[a]	0.05232	0.05132	0.05110

[a]From [2]. [b]From [22, 23].

It is clear that m_H and I are interrelated, and iterative calculation is again necessary to obtain the appropriate I and m_H pairs for each concentration of the mixed electrolyte ($m_2 + m_3 + m_4$) at which E_B was measured. This is described in previous papers [10, 11]. The intercept at $I = 0$ of the Φ vs. I plot gives pK_1. Inspection of results in Table 3 shows that both $p(a_H\gamma_{Cl})^0$ and pH^0 are continuous and smooth functions of solution composition and temperature. Because, in contrast to pH, $p(a_H\gamma_{Cl})$ is not affected by anything extrathermodynamic, it is useful to analyse the internal consistency of the $p(a_H\gamma_{Cl})$ results in terms of the recently described multilinear regression [10, 24] having weight fraction w of dioxane, temperature T and molality m_1 of KCl as independent variables; this scheme leads to the regression equation (11), where $z = (T - \theta)/\theta$ with θ = 298.15 K

$$p(a_H\gamma_{Cl})_{T,w} = A + Bm_1 + Cz + Dw + Em_1w + Fw^2z + Gz^2 + Hw^3z + Jw^3 \quad (11)$$

Calculation with the SPSS package [25] resulted in the following parameters (with corresponding estimated standard errors, n = 263): A = 4.0962 ± 0.0008, B = −0.718 ± 0.030, C = 0.357 ± 0.017, D = 3.4059 ± 0.055, E = −0.785 ± 0.101, F = −15.37 ± 0.70, G = 3.045 ± 0.299, H = 29.6 ± 1.4, J = 1.892 ± 0.022. The above A value is of course that for $p(a_H\gamma_{Cl})$ at w = 0

and 298.15 K, i.e., $p(a_H\gamma_{Cl})^0$, and is identical to the observed value in Table 3. There is good agreement (standard error of fit ±0.0054; maximum error 0.011) between the smoothed values of $p(a_H\gamma_{Cl})^0$ calculated from Eqn. 11 and the corresponding observed values in Table 3 determined by extrapolation of Eqn. 1 to $m_1 = 0$. An independent multilinear regression of the pH^0 results in Table 3 as a function of w, T and z led to the equation

$$pH^0 = pH(S) = 4.004 + 3.309w + 0.408z + 1.037w^3 - 14.95zw^2 + 27.1zw^3 \quad (12)$$

which reproduces the observed pH^0 values with a standard error of fit of ±0.007 (maximum error 0.011); the identification $pH^0 = pH(S)$ is in terms of the operational equation for pH and related endorsed terminology [1].

Finally, it must be pointed out that each standard pH^0 value quoted in Table 3 or interpolated from Eqn. 12 is valid only for the pH scale in the single solvent of composition considered, and could be conveniently identified by left-hand superscript s as ${}^spH^0$. In fact, the corresponding standard ${}^s_wpH^0$ value for an "intersolvent" pH scale having ultimate reference to water (subscript w) is linked to ${}^spH^0$ by the fundamental relation

$${}^s_wpH^0 = {}^spH^0 + ({}^wE^0_H - {}^sE^0_H)/k \quad (13)$$

where ${}^wE^0$ and ${}^sE^0$ are the absolute standard potentials (i.e., referred to an electrode having standard potential invariant with varying composition of the solvent) in water (w) and in the solvent mixture (s), respectively, and their difference (the, so-called, primary medium effect [26]) is a measure of the Gibbs energy of transfer of H^+ from water to that solvent mixture. Although a selection of such transfer energy values was recently published [27], a reliable, IUPAC-recognized, system of intersolvental ${}^s_wpH^0$ values cannot yet be safely set up and standardized.

The financial support granted by the National Research Council of Italy (CNR) is gratefully acknowledged.

REFERENCES

1 A. K. Covington, Pure Appl. Chem., 55 (1983) 1467.
2 H. P. Bütikofer and A. K. Covington, Anal. Chim. Acta, 108 (1979) 179.
3 R. G. Bates, Pure Appl. Chem., 18 (1969) 421.
4 R. G. Bates, Determination of pH. Theory and Practice, 2nd edn., Wiley, New York, 1973, pp. 243—253.
5 C. L. De Ligny, P. F. M. Luykx, M. Rehbach and A. A. Wienecke, Rec. Trav. Chim. Pays-Bas, 79 (1960) 713.
6 M. Paabo, R. A. Robinson and R. G. Bates, J. Am. Chem. Soc., 87 (1965) 415.
7 R. G. Bates, H. P. Bennetto and M. Shankar, Anal. Chem., 52 (1980) 1598.
8 M. J. Taylor, J. Chem. Eng. Data, 24 (1979) 230.
9 T. Mussini, A. K. Covington, P. Longhi and S. Rondinini, Criteria for Standardization of pH Measurements in Water-Rich Mixed Solvents, Report to IUPAC Commission on Electroanalytical Chemistry, 32nd IUPAC Meeting, Lyngby, 1983.

10 T. Mussini, A. K. Covington, F. Dal Pozzo, P. Longhi, S. Rondinini and Z.-Y. Zou, Electrochim. Acta, 28 (1983) 1593.
11 T. Mussini, A. K. Covington, M. Cicognini, P. Longhi and S. Rondinini, Ann. Chim. (Rome), 72 (1982) 639.
12 P. Giammario, P. Longhi and T. Mussini, Chim. Ind. (Milan), 53 (1971) 347.
13 D. J. G. Ives and G. J. Janz, Reference Electrodes, Academic Press, New York, 1961, pp. 204, 207.
14 T. Mussini and A. Pagella, J. Chem. Eng. Data, 16 (1971) 49.
15 F. Hovorka, R. A. Schaefer and D. Dreisbach, J. Am. Chem. Soc., 58 (1936) 2264.
16 M. M. Elsemongy, A. Fouda and M. F. Emira, J. Chem. Soc., Faraday Trans. I, 77 (1981) 1157.
17 R. G. Bates and E. A. Guggenheim, Pure Appl. Chem., 1 (1960) 1163.
18 F. E. Critchfield, J. A. Gibson and J. L. Hall, J. Am. Chem. Soc., 75 (1953) 1991.
19 G. Akerlöf and O. A. Short, J. Am. Chem. Soc., 58 (1936) 1241.
20 N. C. Das and P. B. Das, J. Chem. Soc., Faraday Trans. I, 74 (1978) 22.
21 H. S. Harned and C. Calmon, J. Am. Chem. Soc., 60 (1938) 334.
22 W. J. Hamer, G. D. Pinching and S. F. Acree, J. Res. Nat. Bur. Stand., 35 (1945) 539.
23 R. A. Robinson and R. H. Stokes, Electrolyte Solutions, 2nd rev. edn., Butterworths, London, 1965, pp. 520, 529.
24 A. K. Covington and Z.-Y. Zou, Electrochim. Acta, 28 (1983) 1587.
25 Statistical Programs for Social Science (SPSS), Michigan Terminal System (MTS) Version H, October 1981.
26 B. B. Owen, J. Am. Chem. Soc., 54 (1932) 1758.
27 Y. Marcus, Pure Appl. Chem., 55 (1983) 977.

Analytica Chimica Acta, 162 (1984) 113—122
Elsevier Science Publishers B.V., Amsterdam — Printed in The Netherlands

CRITICAL STUDY OF METALLOCHROMIC INDICATORS FOR CALCIUM

J. CACHO*, A. GARNICA[a] and C. NERÍN[a]
Department of Analytical Chemistry, Faculty of Sciences, University of Zaragoza (Spain)
(Received 21st November 1983)

SUMMARY

The visual clarity of the colour changes at the end-points in the complexometric titration of calcium is discussed for the metallochromic indicators, arsenazo-III, calcein, calcon, eriochrome blue black B, methylthymol blue, murexide, phthalein complexone, and thymolphthalein complexone. The colour changes were specified with the help of CIE chromaticity diagrams. The sharpness of the colour changes of the indicators was studied by varying the optical (or colour) concentration. Thymolphtalein complexone and phthalein complexone are shown to be the most appropriate indicators for the visual titration of calcium with EDTA.

The selection of the best indicator for any visual titrimetric method remains a difficult problem. Not only a great variety of indicators but also lists of indicators for different types of titration are offered by many chemical firms. A multitude of indicators has been described [1] but the information given about their properties is rarely extensive enough to allow an objective selection. At best, the guides available comprise a description of their properties, the colours before and after the equivalence point, and the values of the equilibrium constants. Therefore, when an indicator for any particular titration is needed, a fairly detailed investigation with different indicators may be required to establish which is the most appropriate.

With reference to metallochromic indicators, Ringbom [2] introduced the concept of the pM of transition as a guide to estimate their sensitivity. Although this concept is important and has been widely accepted [3], the possible successive formation of complexes between the metal and the indicator is not considered. Fortuin et al. [4] and Flaschka and Khalafalla [5] did a mathematical treatment from which the basic equations of colour change were derived. Based on these, Reilley and Schmid [6] established some "end-point indices", and other workers [7, 8] established general equations in which the staggered formation of metal—indicator complexes and the indicator concentration used were considered.

[a]Present address: Department of Chemistry, Escuela Técnica Superior de Ingenieros Industriales, University of Zaragoza (Spain).

0003-2670/84/$03.00

These processes of determining the sensitivity of indicators do not consider the quality of the colour (i.e., the perceptibility to the human eye) and there are various examples of quite sensitive substances (according to the above criteria) which have sharp colour changes occurring practically at the equivalence point, but which are useless in practice because the colours of the transition are difficult to distinguish visually. Reilley et al. [9] approached this problem from the optical point of view; working with the CIE chromaticity diagram and basing their work on McAdam's studies [10], they introduced the concepts of complementary colour coordinates (Q_x, Q_y), effective absorptivity (E) and optical or colour concentration (J). This feature J may be described as an "effective absorbance" which takes into account not only the absolute absorbance but also the ability of the eye to see the colour. Later, Kotrly et al. [11—13] introduced a new constant K, which connects the optical concentration with the absorbance, and studied precision in colour specification. In these papers, the colours of the indicator at the beginning and end of a titration are given more emphasis than the sharpness or perceptibility of the colour change at the equivalence point.

Several authors have tried to solve this problem. Bhucher et al. [14, 15] used a so-called specific colour discrimination method and, for acid—base indicators, reported results that appear to be correct but have many errors of interpretation. Vytras et al. [16], working with metallochromic indicators, proposed the "perceptibility of colour changes" as a criterion. Cacho et al. [17] proposed a method of evaluating indicators based on the variation of optical concentration throughout the titration. Recently, an IUPAC Commission of Analytical Reactions and Reagents [18] recommended that the greatest possible amount of data on chromaticity should be specified in all new work on indicators; they also suggested that existing indicators be evaluated chromatically.

It is well known that the indicators used to determine calcium compleximetrically do not show colour changes with perfect precision and that practice is needed to obtain results free of error. Accordingly, most analysts, once they have become used to one indicator, will not readily change to another, even though they may realize that their choice is not the most appropriate. In an attempt to solve this problem, and to follow the IUPAC recommendations, the chromatic transitions of the most commonly used indicators in the titration of calcium with EDTA are described in this paper. The transitions were studied throughout the titrations, with special attention to the parts closest to the equivalence point. The method used was to monitor the variation of the optical concentration during the titration. This method enables the quality of the chromatic transition to be evaluated and a scale of perceptibilities to colour changes in these indicators to be presented. Thus the most appropriate indicators may finally be decided. The following indicators were examined.

Arsenazo-III [19, 20]. 2,7-Bis(arsenophenylazo)-1,8-Dihydroxynaphthalene-3,6-disulphonic acid has the following pK_a values: pK_{a7} = 6.27, pK_{a8} = 9.05, pK_{a9} = 11.98, pK_{a10} = 15.1. Used in the titration of calcium, it forms a 1:1 complex with the metal ion. At pH 9, the value of pM_{trans} is 5.3.

Calcein [21, 22]. Calcein 2′,7-bis[*N*,*N*-di(carboxymethyl)-aminomethyl]-fluorescein or fluorescein complexone, has been used as an indicator for the titration of calcium in the presence of magnesium above pH 12. The acidity constants are $pK_{a1} < 4$, $pK_{a2} = 5.4$, $pK_{a3} = 9.0$, $pK_{a4} = 10.5$ and $pK_{a5} = 12.0$.

Calcon [23, 24]. This dye, 1-(2-hydroxy-1-naphthylazo)-2-naphthol-4-sulfonic acid, is also known as erichrome blue black R. It forms 1:1 complexes with calcium, the stability constant being 5.3. The value of pM_{trans} at pH 12 is 3.8; and $pK_{a1} = 7.3$ and $pK_{a2} = 13.5$.

Eriochrome blue black B [23]. This dye is the 1-hydroxy analogue of calcon and also forms 1:1 complexes with calcium. The stability constant is 5.7; pK_{a1} and pK_{a2} are 6.2 and 12.5, respectively, and $pM_{trans} = 4.0$ at pH 11.

Methylthymol blue [25—28]. This is the sodium salt of 3′,3″-bis[(carboxymethyl)-aminomethyl]thymolsulphophthalein. The values of pK_{a1}, pK_{a2}, pK_{a3} and pK_{a4} are 4.5, 7.2, 11.2 and 13.5, respectively. At pH 10.5, $pM_{trans} = 6.3$.

Murexide [29—31]. This, the ammonium salt of purpuric acid, with $pK_{a2} = 9.2$ and $pK_{a3} = 10.9$, forms 1:1 complexes with calcium. At pH 12, $pM_{trans} = 5.0$.

Phthalein complexone [30—32]. This indicator, 3,3′-dimethyl-5,5′-[*N*,*N*-di(carboxymethyl)-aminomethyl]-phenolphthalein, is also known as metalphthalein or *o*-cresolphthalein complexone. It has been studied extensively in titrations of alkaline earth metals with EDTA. The acidity constants are $pK_{a1} = 2.2$, $pK_{a2} = 2.9$, $pK_{a3} = 7.0$, $pK_{a4} = 7.8$; $pK_{a5} = 11.4$, $pK_{a6} = 12.0$; the value of pM_{trans} is 4.5 at pH 10.

Thymolphthalein complexone [33—35]. This dye, 3,3′-bis[*N*,*N*-di(carboxymethyl)-aminomethyl]thymolphthalein, has been used in the titration of calcium at pH 10.5—12. The acidity constants are $pK_{a1} = 7.4$ and $pK_{a2} = 12.3$.

EXPERIMENTAL

Apparatus and reagents

A Pye-Unicam SP8-100 spectrophotometer with 1-cm silica cells, an Orion Research pH meter (Model 901) and a PDP-11/55 computer were used.

Reagents of analytical purity (Sigma) were used.

The stock indicator solutions were all 3.86×10^{-4} M in the dye. Arsenazo-III, methylthymol blue and murexide were dissolved in water. Calcon and eriochrome blue black B were dissolved in methanol. Calcein, phthalein complexone and thymolphthalein complexone were dissolved in water with the minimal amount of sodium hydroxide.

The stock calcium solution (0.025 M) was prepared by dissolving calcium carbonate in diluted hydrochloric acid, boiling to eliminate CO_2, and diluting appropriately with distilled water. Working calcium solutions (0.0025 M) were prepared by diluting this stock immediately before use.

The EDTA (disodium salt) solution was 0.005 M. Buffer solutions were ammoniacal ammonium chloride for pH 10—10.5, Tris—nitric acid for pH 9, and borax—sodium hydroxide for pH 11.

TABLE 1

Chromaticity coordinates for the colour change of some metallochromic indicators for calcium

L/M[a]	J	D	Y	P_x	P_y	Q_x	Q_y	λ_d (nm)	e
Arsenazo-III									
0.00	1.6523	0.058	0.1499	0.202	0.200	0.391	0.389	519.8	0.500
0.95	1.4905	0.021	0.1727	0.251	0.223	0.353	0.379		
0.96	1.4793	0.012	0.1764	0.263	0.223	0.341	0.381		
0.97	1.4616	0.008	0.1798	0.274	0.224	0.332	0.384		
0.98	1.4312	−0.017	0.1818	0.286	0.224	0.326	0.385		
0.99	1.3822	0.010	0.1946	0.316	0.226	0.306	0.391		
1.00	1.3276	0.077	0.2141	0.350	0.228	0.285	0.397	476	0.409
1.01	1.3277	0.066	0.2108	0.344	0.225	0.289	0.399		
1.02	1.3287	0.065	0.2102	0.344	0.225	0.289	0.399		
Calcein									
0.00	0.7222	0.681	0.8416	0.399	0.386	0.081	0.215	485.5	0.426
0.95	0.6635	0.444	0.8063	0.398	0.366	0.077	2.243		
0.96	0.6489	0.393	0.7992	0.398	0.360	0.073	0.258		
0.97	0.6354	0.381	0.7893	0.397	0.356	0.073	0.273		
0.98	0.6215	0.372	0.7800	0.396	0.351	0.073	0.281		
0.99	0.6077	0.371	0.7745	0.395	0.346	0.071	0.292		
1.00	0.5847	0.535	0.8033	0.390	0.351	0.067	0.293	490.8	0.295
1.01	0.5882	0.507	0.7823	0.394	0.348	0.066	0.296		
1.02	0.5912	0.472	0.7707	0.395	0.342	0.066	0.313		
Calcon									
0.00	1.1040	0.241	0.3028	0.362	0.265	0.278	0.374	507.5	0.155
0.95	1.0512	0.080	0.3089	0.284	0.265	0.332	0.383		
0.96	1.0596	−0.004	0.3128	0.262	0.262	0.350	0.385		
0.97	1.0756	0.026	0.2925	0.248	0.251	0.373	0.387		
0.98	1.0890	0.066	0.2738	0.229	0.234	0.392	0.389		
0.99	1.1008	0.113	0.2756	0.212	0.229	0.416	0.391		
1.00	1.1396	0.156	0.2820	0.192	0.224	0.450	0.393	483.5	0.314
1.01	1.1414	0.161	0.2857	0.197	0.224	0.453	0.392		
1.02	1.1406	0.158	0.2847	0.196	0.223	0.452	0.393		
Eriochrome blue black B									
0.00	0.911	−0.021	0.2998	0.284	0.206	0.324	0.444	558	0.188
0.95	0.8834	0.117	0.3303	0.220	0.224	0.428	0.417		
0.96	0.8799	0.125	0.3363	0.219	0.226	0.431	0.416		
0.97	0.8760	0.139	0.3407	0.218	0.227	0.436	0.414		
0.98	0.8748	0.142	0.3452	0.216	0.227	0.440	0.414		
0.99	0.8738	0.159	0.3487	0.212	0.228	0.449	0.413		
1.00	0.8604	0.181	0.3744	0.207	0.238	0.465	0.402	484	0.166
1.01	0.8564	0.187	0.3755	0.206	0.237	0.465	0.403		
1.02	0.8548	0.182	0.3765	0.207	0.238	0.467	0.403		

TABLE 1 (continued)

L/M[a]	J	D	Y	P_x	P_y	Q_x	Q_y	λ_d (nm)	e
Methylthymol blue									
0.00	0.9005	0.176	0.3563	0.200	0.220	0.478	0.426	497	0.517
0.95	0.7678	0.117	0.4121	0.254	0.266	0.395	0.371		
0.96	0.7544	0.112	0.4238	0.261	0.270	0.376	0.361		
0.97	0.7392	0.109	0.4330	0.269	0.278	0.374	0.367		
0.98	0.7227	0.108	0.4448	0.276	0.283	0.364	0.361		
0.99	0.7083	0.108	0.4577	0.284	0.289	0.352	0.354		
1.00	0.6899	0.122	0.4757	0.293	0.297	0.339	0.344	472.5	0.08
1.01	0.6824	0.124	0.4810	0.294	0.298	0.337	0.342		
1.02	0.6847	0.122	0.4793	0.294	0.298	0.337	0.343		
Murexide[b]									
0.00				0.373	0.272	0.143	0.452	499	0.283
0.95				0.353	0.260	0.197	0.467		
0.96				0.345	0.253	0.218	0.478		
0.97				0.331	0.244	0.253	0.493		
0.98				0.318	0.236	0.284	0.509		
0.99				0.310	0.231	0.305	0.518		
1.00				0.295	0.224	0.341	0.534	558.5	0.345
1.01				0.293	0.223	0.345	0.539		
1.02				0.293	0.223	0.345	0.536		
Phthalein complexone									
0.00	1.0624	0.121	0.2972	0.263	0.163	0.408	0.548	563.5	0.516
0.95	0.3292	0.120	0.5860	0.287	0.243	0.393	0.530		
0.96	0.3086	0.120	0.6251	0.290	0.255	0.389	0.536		
0.97	0.2683	0.102	0.6628	0.293	0.264	0.387	0.531		
0.98	0.2146	0.129	0.7180	0.296	0.275	0.386	0.524		
0.99	0.1558	0.135	0.7854	0.300	0.287	0.382	0.515		
1.00	0.0672	0.113	0.9035	0.307	0.305	0.361	0.484	563.5	0.032
1.01	0.0620	0.138	0.9121	0.307	0.307	0.363	0.476		
1.02	0.0563	0.165	0.9195	0.308	0.307	0.358	0.477		
Thymolphthalein complexone									
0.00	1.1629	0.150	0.2938	0.188	0.217	0.465	0.409	481.5	0.561
0.95	0.4285	0.132	0.5324	0.250	0.261	0.427	0.405		
0.96	0.4138	0.120	0.6180	0.264	0.284	0.412	0.402		
0.97	0.3958	0.119	0.6081	0.274	0.285	0.404	0.395		
0.98	0.3670	0.117	0.6538	0.279	0.289	0.392	0.388		
0.99	0.3122	0.112	0.6875	0.288	0.294	0.384	0.385		
1.00	0.2281	0.105	0.7693	0.300	0.305	0.356	0.366	481.5	0.052
1.01	0.2290	0.103	0.7699	0.300	0.305	0.355	0.367		
1.02	0.2276	0.103	0.7693	0.300	0.305	0.355	0.366		

[a]Ligand/metal ratio. [b]Approximate values (see text).

Procedure

Add 20 ml of the working solution of calcium, 10 ml of the appropriate buffer solution, 5 ml of indicator solution, and different quantities of EDTA solution to 50-ml calibrated flasks, and dilute to 50 ml with distilled water. Measure the absorbances of each of these solutions at specified wavelengths to determine the chromaticity coordinates. The absorbances are treated with a linear computer program in BASIC [17].

RESULTS AND DISCUSSION

Table 1 shows the chromaticity parameters, optical concentration (J), dichromatism (D), luminosity (Y), true coordinates (P), complementary coordinates (Q), dominant wavelength (λ_d) and spectral purity (e) of the colours obtained in the titration of calcium with EDTA at different points of the titration for each of the indicators studied.

Figure 1 shows the chromatic transitions in the C.I.E. chromaticity diagram, between the initial and final point of the titration with each indicator, using coordinates of true colour; the McAdam ellipses are also shown. Figure 2 shows the progress of the colour intensity vs. the EDTA/Ca ratio for each indicator.

Behaviour of individual indicators

Arsenazo-III. Arsenazo-III, at the optimum pH of titration, is bluish in colour, with a maximum in the absorption spectrum at 538 nm. Its calcium complex is reddish (λ_{max} = 598 nm). The chromatic transition in this titration, in true colour coordinates, is shown in Fig. 1. As can be seen, the transition travels through an area of the chromaticity diagram in which the McAdam ellipses show almost identical sizes but not identical orientation. As the length of transition is large, several tones are seen, but because the direction of the transition becomes less perpendicular to the longer axes of the ellipses, the ease of perception becomes less. Figure 2 shows that the variation of the optical concentration at the end-point of the titration is not very sharp.

Calcein. This indicator at pH $\geqslant$ 12 is brown in colour (λ_{max} = 503 nm) while its complex with calcium is yellow-green (λ_{max} = 493 nm). The transition between these two colours is very short, and the area covered has relatively large ellipses; the transition is almost parallel to the longer axis of the ellipse. Therefore, the colour changes of this indicator are difficult to see although the initial and final points of the titration may be distinguished perfectly. The graphic representation of the variation of the optical concentration (Fig. 2) clearly illustrates this. Of course, calcein is more widely used as a fluorescent indicator at lower pH.

Calcon. At the optimum pH for the titration, the calcon complex with calcium is red (λ_{max} = 550 nm) while calcon itself is blue (λ_{max} = 638 nm). The chromatic transition is therefore relatively long and its direction tends to be perpendicular to the longer axis of the ellipses in an area with rather

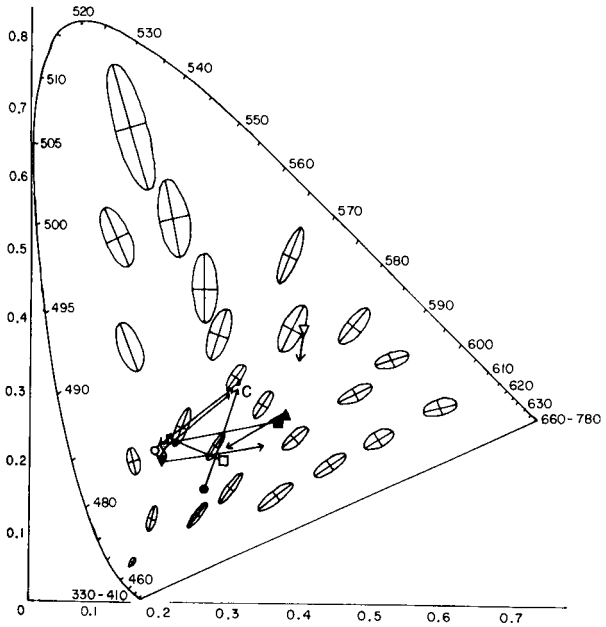

Fig. 1. Chromatic transitions of the indicators in the complexiметric titration of calcium. (▼) arsenazo-III; (▽) calcein; (■) calcon; (□) eriochrome blue black B; (×) methylthymol blue; (▲) murexide; (●) phthalein complexone; (○) thymolphthalein complexone.

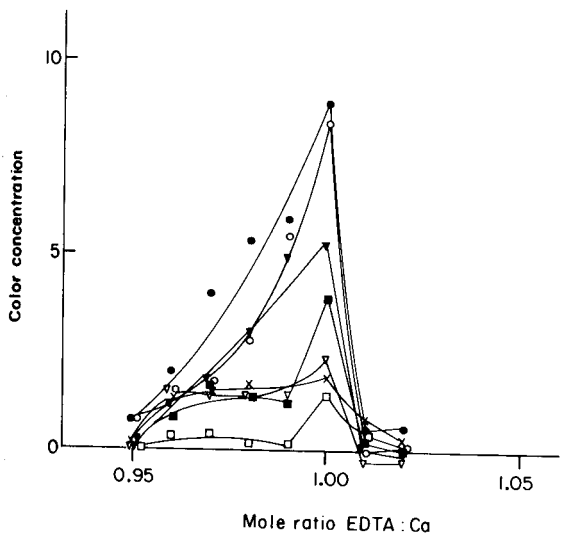

Fig. 2. Progress of colour concentration vs. the EDTA/Ca ratio for the indicators (symbols as in Fig. 1) in the vicinity of the end-point of the titration.

small ellipses (Fig. 1). As a result, it should be possible to see the colour change clearly. Unfortunately, because of the unfavourable value of the formation constant of the complex, the chromatic transition is gradual and some experience is needed to estimate the real end-point of the titration (cf. Fig. 2).

Eriochrome blue black B. Solutions of this dye at pH 11 are blue (λ_{max} = 635 nm) whereas the calcium complex is red (λ_{max} = 557 nm). The chromatic transition between the initial and final points of the titration of calcium is short (Fig. 1) and the formation constant of the calcium/indicator complex is unfavourable; thus the colour change is difficult to observe. The optical concentration is low and, although the direction of the transition is almost parallel to the minor axes of the ellipses, the transition is gradual (cf. Fig. 2).

Methylthymol blue. The calcium/indicator complex is blue (λ_{max} = 612 nm) at pH 10, whereas the free indicator solution is greyish (λ_{max} = 602 nm). Consequently, its chromatic transition (Fig. 1) follows a line towards the achromatic point. This transition is of medium length, it does not quite reach the achromatic point, and it is almost perpendicular to the minor axis of the relevant ellipses. For all these reasons, a very good visual memory would be necessary to perceive the colour transition at the end-point of the titration. The variation of the optical concentration during this process clearly indicates that the perceptibility of the colour change is slight.

Murexide. The calcium/murexide complex is salmon-pink at pH 12 (λ_{max} = 503 nm) and the free indicator is blue-violet (λ_{max} = 548 nm). The solution of the free indicator at pH 12 decomposes rapidly, so that the true chromaticity of the colours obtained during the titration cannot be established exactly. Only approximate values of the true and complementary chromaticity coordinates are shown in Table 1.

Although these data are not totally reliable, conclusions can be drawn: the chromatic transition of murexide (Fig. 1) is situated in an area of the diagram in which the ellipses are of medium size, and is parallel to their major axis. Consequently, the colour variation is gradual and only experienced eyes will be able to distinguish the different tones.

Phthalein complexone. The indicator solution at pH 10 is colourless (λ_{max} = 572 nm) whereas the calcium complex is red (λ_{max} = 572 nm). The chromatic transition (Fig. 1) is long and ends almost at the achromatic point of the diagram. Consequently, the colour change of this indicator is characterized only by a diminution in the colour intensity. The final direction of the transition is almost parallel to the major axis of the ellipse, thus the colour decrease is not very sudden although it is quite perceptible. The plot of the variation of the optical concentration at the end-point of the titration shows a high sharp peak, which indicates easy perceptibility.

Thymolphthalein complexone. The calcium complex is blue (λ_{max} = 608 nm) and the free indicator is practically colourless (λ_{max} = 593 nm) at pH 11. The chromatic transition (Fig. 1) is long and almost reaches the achromatic point. Unlike phthalein complexone, the direction of this transition is much

more perpendicular to the major axes of the ellipses, so that the end-point of the titration can be seen more clearly. The peak for this indicator in Fig. 2 is high and sharp.

Conclusions

Table 2 lists the values of the $\Delta J/\Delta(L/M)$ breaks between the ligand: metal ratios of 1 and 1.01, obtained from Fig. 2. When they are represented on the same scale, these data are perfectly comparable. The bandwidths at half height are also indicated. A study of Table 2 clearly shows that thymolphthalein complexone is the indicator that best shows the colour transition. Next best is phthalein complexone and then arsenazo-III.

In the middling bracket of colour transitions are calcon and calcein. Calcon is clearly better than calcein. From the transitions studied, methylthymol blue and eriochrome blue black B are frankly bad; these substances, therefore, are not recommended for the visual titration of calcium. As has already been indicated, the results obtained for murexide are somewhat subjective, owing to the quick decomposition of the indicator, but its transition is similar to that of calcon if titrations are done quickly.

On the above basis of colour transitions, the order of efficiency for the indicators studied is as follows: thymolphthalein complexone > phthalein complexone > arsenazo-III > calcon = murexide > calcein > methylthymol blue = eriochrome blue black B. If this sequence is compared with the values of pM_{trans}, it is clear that selection of an indicator for a visual titration on the basis of pM_{trans} alone can lead to errors in the titration because the end-point is not clearly perceptible.

As the chromatic transitions of thymolphthalein complexone, methylthymol blue and phthalein complexone go towards the achromatic point, it should be possible to obtain a more perceptible colour change if these indicators were mixed with inert dyes with a dominant wavelength of 583 nm for thymolphthalein complexone, and methylthymol blue, or 563 nm for phthalein complexone. This aspect will be described in a later paper.

TABLE 2

Height (h) and half-bandwidth (σ) of the peaks in Fig. 2

Indicator	h	σ	Indicator	h	σ
Arsenazo-III	5.46	2.7	Eriochrome blue black B	1.34	1.1
Calcein	2.3	2.4	Methylthymol Blue	1.84	4.5
Calcon	3.88	1.5	Phthalein Complexone	8.86	2.4
			Thymolphthalein complexone	8.41	2.1

REFERENCES

1 E. Bishop (Ed.), Indicators, Pergamon Press, Oxford 1972.
2 A. Ringbom, Complexation in Analytical Chemistry, Wiley, New York, 1963.
3 I. M. Kolthoff, E. B. Sandell and E. J. Meehan, Quantitative Chemical Analysis, Macmillan, New York, 1969.
4 J. M. M. Fortuin, P. Karsten and H. L. Kies, Anal. Chim. Acta, 10 (1954) 356.
5 H. Flaschka and S. Khalafalla, Z. Anal. Chem., 156 (1957) 401.
6 C. N. Reilley and R. W. Schmid, Anal. Chem., 31 (1959) 887.
7 M. Tanaka and G. Nakagawa, Anal. Chim. Acta, 32 (1965) 123.
8 O. Yamauchi, M. Tanaka and T. Uno, Talanta 15 (1968) 459.
9 C. N. Reilley, H. Flaschka, S. Laurent and B. Laurent, Anal. Chem., 32 (1960) 1218.
10 D. L. McAdam, J. Opt. Soc. Am., 32 (1942) 2, 247, 675; 33 (1943) 18.
11 S. Kotrly and K. Vytras, Talanta, 18 (1971) 253.
12 S. Kotrly, K. Vytras, J. Oharek and E. Vondruskova, Sb. Ved. Pr. Vys. Sk. Chemikotechnol. Pardubice, 22 (1970) 19.
13 K. Vytras, S. Kotrly, E. Vondruskova and B. Vorac, Collect. Czech. Chem. Commun., 35 (1970) 3379.
14 V. M. Bhuchar and S. R. Das, J. Opt. Soc. Am., 54 (1964) 817.
15 V. M. Bhuchar, V. P. Kukreja and S. R. Das, Anal. Chem., 43 (1971) 1847.
16 K. Vytras, S. Kotrly and J. Vitrasova, Collect. Czech. Chem. Commun., 40 (1975) 3815.
17 J. Cacho, C. Nerín, L. Ruberte and E. Rivas, Anal. Chem., 53 (1982) 1446.
18 IUPAC Analytical Chemistry Division, Commission on Analytical Reactions and Reagents, Pure Appl. Chem., 51(b) (1979) 1357.
19 S. B. Savvin, Dokl. Akad. SSSR, 127(6) (1959) 1231; Talanta, 8 (1961) 673; Talanta, 11 (1964) 7.
20 V. Michaylova and P. Ilkova, Anal. Chim. Acta, 53 (1971) 194.
21 H. Diehl and J. L. Ellingboe, Anal. Chem., 28 (1956) 882.
22 B. M. Tucker, Analyst (London), 82 (1957) 284.
23 G. Schwarzenbach and W. Biedermann, Helv. Chim. Acta, 31 (1948) 678.
24 G. P. Hildebrand and C. N. Reilley, Anal. Chem., 29 (1957) 258.
25 J. Körbl and R. Pribil, Chem. Listy, 51 (1957) 1061.
26 J. Körbl, Chem. Listy, 51 (1957) 1304.
27 F. Buben, J. Körbl and R. Pribil, Chem. Listy, 51 (1957) 1307.
28 J. Körbl and B. Kabac, Chem. Listy, 51 (1957) 1680, 2259.
29 G. Schwarzenbach, W. Biedermann and F. Bangenter, Helv. Chim. Acta, 29 (1946) 811.
30 G. Schwarzenbach and H. Gysling, Helv. Chim. Acta, 32 (1949) 1108, 1314, 1489.
31 G. Schwarzenbach, Complexometric titrations, Interscience, New York, 1957, p. 37.
32 G. Anderegg, H. Flaschka, R. Sallmann and G. Schwarzenbach, Helv. Chim. Acta, 37 (1954) 113.
33 J. Körbl and R. Pribil, Chem. Listy, 51 (1957) 1804.
34 J. Körbl and R. Pribil, Collect. Czech. Chem. Commun, 23 (1958) 1213.
35 A. Bezdekova and B. Budesinsky, Collect. Czech. Chem. Commun., 30 (1965) 818.

Analytica Chimica Acta, 162 (1984) 123—132
Elsevier Science Publishers B.V., Amsterdam — Printed in The Netherlands

INVESTIGATION OF ION-SELECTIVE ELECTRODES BASED ON QUATERNARY PHOSPHONIUM SALTS
Part 2. A Tetrachlorothallate(III) Ion-Selective Electrode[a]

A. V. KOPYTIN, P. GÁBOR-KLATSMÁNYI, V. P. IZVEKOV and E. PUNGOR*
Institute for General and Analytical Chemistry, Technical University of Budapest, 1111 Budapest (Hungary)
G. A. YAGODIN
Mendeleev University, 125047 Moscow (U.S.S.R.)
(Received 14th March 1984)

SUMMARY

A tetrachlorothallate(III)-selective electrode based on the tetradecylphosphonium tetrachlorothallate(III) ion-pair complex in a PVC membrane is described. The mechanism of the influence of the hydrochloric acid content of sample solutions is discussed in detail. Electrode membranes made with and without dibutyl phthalate as plasticizer were investigated. The membranes without plasticizer are better with regard to selectivity and limit of detection (2×10^{-7} mol l^{-1}).

Ion-selective electrodes based on extraction have been dealt with in many papers. Quaternary salts have been suggested as electroactive material [2—5], in the form of liquid-membrane or PVC-membrane electrodes. The electroactive material may, in some cases, serve as plasticizer as well, thus making any other plasticizer such as dibutyl phthalate unnecessary. Investigations in this field have led to the development of ion-selective electrodes which show reasonable selectivity for chloro complexes of some metal ions [6, 7].

In an earlier paper [1], a new electrode sensitive for trichloromercurate(II) ion was described which has a better performance than other similar electrodes described in the literature [5, 7]. This paper deals with a new ion-selective electrode of the type described above, which is sensitive for tetrachlorothallate(III) ion. The electroactive material is the tetradecylphosphonium tetrachlorothallate(III) salt.

EXPERIMENTAL

Reagents and membranes

Electroactive material. The tetradecylphosphonium tetrachlorothallate(III), $(C_{10}H_{21})_4P[TlCl_4]$, was prepared by a process analogous to that described

[a]For Part 1, see ref. 1.

0003-2670/84/$03.00

earlier [1]. The extraction was done with a solution of thallium(III) chloride containing hydrochloric acid. The ratio of the organic and aqueous phase was 1:1. After the evaporation of the chloroform, the quaternary salt was left as a transparent, viscous liquid. The composition and structure of the compound thus obtained was checked by far-infrared spectrometry (Fig. 1). The intense absorptions at 90 and 284 cm^{-1} can be ascribed to the $[TlCl_4]^-$ ion [8]. There was no band characteristic of any other Tl(III)-Cl^- complexes, indicating that under the given conditions $[TlCl_4]^-$ is the only extractable species.

Preparation of electrode membranes. Two types of membranes were prepared: (1) PVC with dibutyl phthalate and the electroactive material; (2) PVC with only the electroactive material. The composition and some electrochemical characteristics of these membranes are summarized in Table 1.

Electrodes and equipment

The far-infrared spectra of the membranes were measured in the range 40—400 cm^{-1} with a Fourier-transform spectrometer (Type IS-3; Grubb-Parsons, U.K.). A PVC film without plasticizer was used as reference.

A double-junction silver/silver chloride electrode (Radelkis, OP-08203) was used as reference. The membrane discs of the $[TlCl_4]^-$-selective electrode were made in the usual manner [1, 5]. Potentials were measured with a digital pH meter (Radelkis, OP-208). The potentiometric cell used was as follows

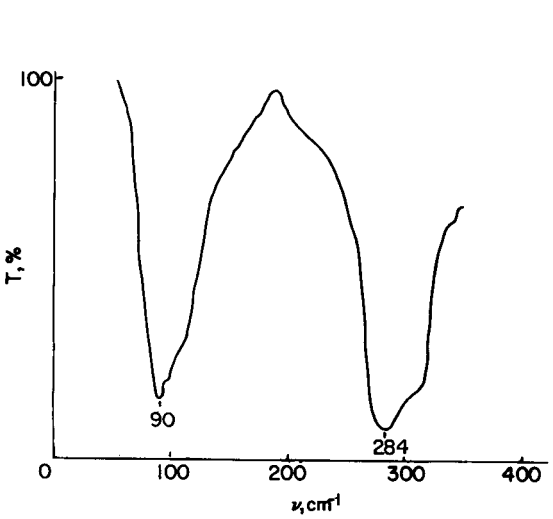

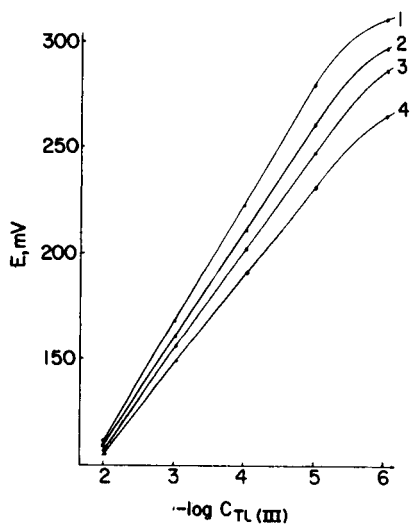

Fig. 1. The far-infrared spectrum of tetradecylphosphonium tetrachlorothallate(III).

Fig. 2. Calibration curves for the $[TlCl_4]^-$-selective electrode made with dibutyl phthalate as plasticizer. The hydrochloric acid concentration in the calibration solutions was: (1) 0.01; (2) 0.1; (3) 1.0; (4) 4.0 mol l^{-1}.

TABLE 1

Composition of the membranes and some electroanalytical parameters of the tetrachlorothallate(III) ion-selective electrodes

Sample no.	$(C_{10}H_{21})_4$ $TlCl_4$ (%)	PVC (%)	Slope (mV/pTl^{3+})	Lower detection limit[a] (mol l^{-1} Tl^{3+})
1	70[b]	30	57	3.5×10^{-6}
2	70[c]	30	57	5.0×10^{-6}
3	60	40	58	2.1×10^{-7}
4	50	50	56	3.0×10^{-7}
5	40	60	55	5.0×10^{-7}

[a]The lower detection limit was determined at 0.01 mol l^{-1} HCl. [b]The active material was put into the membrane as a 10^{-3} mol l^{-1} solution in dibutyl phthalate. [c]The active material was put into the membrane as a 10^{-2} mol l^{-1} solution in dibutyl phthalate.

Ag/AgCl 3 mol l^{-1} KCl	0.1 mol l^{-1} KCl 0.1 mol l^{-1} HCl 0.1 mol l^{-1} $TlCl_3$	membrane	sample soln.	3 mol l^{-1} KCl	AgCl/Ag

The $[TlCl_4]^-$-selective electrodes were conditioned in 10^{-3} mol l^{-1} $TlCl_3$/0.1 mol l^{-1} HCl solution for 24 h.

RESULTS AND DISCUSSION

The complex ions formed between the thallium(III) and chloride ions are as follows: $[TlCl]^{2+}$, $[TlCl_2]^+$, $[TlCl_4]^-$ and $[TlCl_5]^{2-}$. If the solution contains 0.1 mol l^{-1} hydrochloric acid, then only $[TlCl_4]^-$ is extractable with the quaternary phosphonium cation into the organic phase [9]. The present results based on the far-infrared spectra of membranes also prove this. Hence, the electrode is expected to be selective for tetrachlorothallate(III) ions. According to the literature data [10], large dye cations are also suitable for the preparation of tetrachlorothallate(III)-selective electrodes. However, some tests with such materials were unfavourable and the tetradecylphosphonium cation, which had already been used successfully [5], was therefore selected.

The PVC/dibutyl phthalate/$(C_{10}H_{21})_4P[TlCl_4]$ membrane electrode

The calibration curves of the electrode were measured in the presence of different hydrochloric acid concentrations (Fig. 2). The electrode membrane had the composition shown in Table 1 as sample no. 1. The shift of the calibration curve towards more negative potentials with increasing hydrochloric acid content is similar to that observed in the case of trichloromercurate(II) [1] and other electrodes [5, 11]. This phenomenon is connected with a change in the boundary phase of the membrane caused by the increasing acid concentration at the surface.

Based on the calibration curves obtained at hydrochloric acid concentrations below 0.1 mol l^{-1}, it can be assumed that the anions act as charge carriers within the membrane because they are more mobile than the tetradecylphosphonium cation.

Morf [2] describes the diffusion potential, E_D, in the membrane phase by

$$E_D = -RTF^{-1} \ln [\sum u_i a_i(o) / \sum u_i a_i(d)] \quad (1)$$

where u_i is the mobility of the anions in the membrane phase, $a_i(o)$ is the activity of the anions in the boundary layer of the membrane at the side of the sample solution, and $a_i(d)$ is the activity of anions in the membrane boundary layer close to the inner reference solution (cf. Fig. 3); RTF^{-1} is the usual Nernst factor. When i (= $[TlCl_4]^-$) and j (= Cl^-) ions are present both in the sample and in the inner reference solution, then if hydrochloric acid enters the membrane, charge will be carried by both $[TlCl_4]^-$ and Cl^- ions; hydrochloric acid can enter the membrane as a hydrated ion-associate with esters, e.g., dibutyl phthalate according to the hydrate-solvate mechanism [13]. Thus Eqn. 1 can be rewritten as

$$E_D = -RTF^{-1} \ln [u_i' a_i'(o) + u_j' a_j'(o) / u_i a_i(d) + u_j a_j(d)] \quad (2)$$

It has been proved [14, 15] that the potential of ion-selective electrodes of the liquid ion-exchanger type is influenced by hydration of the ions present in the membrane phase. The equations used explained satisfactorily the

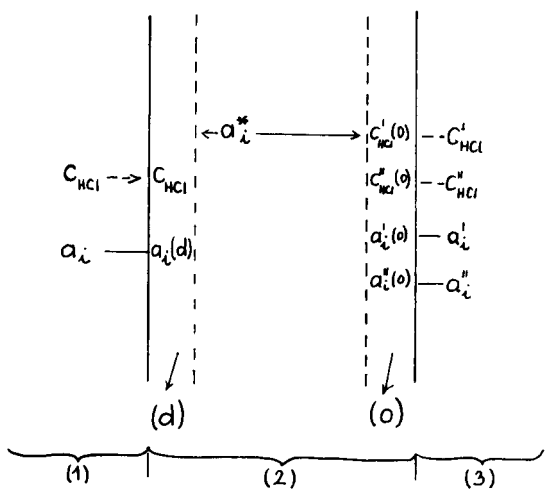

Fig. 3. Scheme for the electrode membrane: (1) inner reference solution, where a_i and c_{HCl} are the activity of the ion measured and the hydrochloric acid concentration in the inner reference solution, respectively, both being constants; (2) membrane, where a_i^* is the activity in the middle of the membrane (for the meaning of d and o, see text); (3) sample solution with different hydrochloric acid concentration; (") first sample solution; (') second sample solution.

results of measurements in presence of a practically constant water activity, a_w, because the hydration number of the ions present in the membrane is then also constant. But in solutions with high electrolyte concentrations, the activity of water, a_w, changes considerably and therefore the hydration in the organic phase will also change [13]. The change in activity of the extracting ion as a function of hydration [13] is taken into consideration by the equation

$$a_i = a_i^* \exp(-h) \tag{3}$$

where a_i^* is the activity of the extracting ion in the pure organic solvent, a_i is the activity of the extracting ion in the organic solvent which is in equilibrium with water, and h is the degree of hydration of ion i in the solvent. Among other examples, the quaternary ammonium bases [16, 17] illustrate the usefulness of Eqn. 3. Insertion of Eqn. 3 into Eqn. 2 yields

$$E_D = -RTF^{-1} \ln \{[u_i' a_i^* \exp(-h'(o)) + u_j' a_j'(o)] / [u_i a_i^* \exp(-h(d)) + u_j a_j(d)]\} \tag{4}$$

where u_j is the mobility of ion j. If the hydrochloric acid concentration c' changes to c'', then the activities of ions i and j in the membrane boundary layer change because of the change in the degree of hydration caused by the penetration of hydrochloric acid into the membrane. In this case

$$\Delta E_D = -RTF^{-1} \ln \{[u_i'' a_i^* \exp(-h''(o)) + u_j'' a_j''(o)] / [u_i' a_i^* \exp(-h'(o)) + u_j' a_j'(o)]\} \tag{5}$$

if the mobility of ions remains constant or if there is a negligible change with the alteration in the degree of hydration, then

$$\Delta E_D = -RTF^{-1} \ln \{[a_i^* \exp(-h''(o)) + K a_j''(o)] / [a_i^* \exp(-h'(o)) + K a_j'(o)]\} \tag{6}$$

where $K = u_j/u_i$ (for $u_j' = u_j''$, $u_i' = u_i''$).

Hence, the reason for the change in diffusion potential in the membrane is the penetration of hydrochloric acid (i.e., the $a_j(o)$ changes) or an alteration in the degree of hydration of the active material in the membrane boundary layer. If the acid concentration is not high or the acid is in a strongly associated form (i.e., $a_i \gg a_j$), then E_D will be a function of the degree of hydration of the phosphonium salts

$$\Delta E_D = -RTF^{-1} \ln \{[a_i^* \exp(-h''(o))] / [a_i^* \exp(-h'(o))]\} = RTF^{-1}[h'(o) - h''(o)] \tag{7}$$

As the hydration influences the activity of the active component of the membrane, there will be a change in the potential between the two phases. If at the boundary only one ion i acts as charge carrier, namely $K_j/K_i \to 0$, then the potential differences between the two phases, E_B, can be given [12] by

$$E_B = -RTF^{-1} \ln [K_i a_i'/a_i'(o)] + RTF^{-1} \ln [K_i a_i/a_i(d)] \quad (8)$$

where K_i is the distribution coefficient of the ion i between the aqueous and the membrane phase [(2) and (3) on Fig. 3].

The composition of the inner reference solution is constant, consequently a_i and $a_i(d)$ are also constant

$$\Delta E_B = -RTF^{-1} \ln [K_i a_i''/a_i''(o)] + RTF^{-1} \ln [K_i a_i'/a_i'(o)] \quad (9)$$

which can be rearranged to

$$\Delta E_B = RTF^{-1} \ln [a_i''(o)/a_i'(o)] - RTF^{-1} \ln (a_i''/a_i') \quad (10)$$

Insertion of Eqn. 3 and then Eqn. 7 into Eqn. 10 gives

$$\Delta E_B = RTF^{-1} [h'(o) - h''(o)] - RTF^{-1} \ln (a_i''/a_i) \quad (11)$$

This means that the membrane potential is a function of the activity of the ion to be measured and of the degree of hydration of the ions in the boundary layer of the membrane phase. The total change in membrane potential, ΔE_{MB}, can be given by combining Eqns. 6 and 11

$$\Delta E_{MB} = \Delta E_B + \Delta E_D = -RTF^{-1} \ln (a_i''/a_i') + RTF^{-1} [h'(o) - h''(o)]$$
$$- RTF^{-1} \ln \{[a_i^* \exp(-h''(o)) + Ka_j''(o)]/[a_i^* \exp(-h'(o)) + Ka_j'(o)]\} \quad (12)$$

When the penetration of acid into the membrane is negligible, i.e., for $a_i(o) \gg Ka_j''(o)$, then

$$\Delta E_{MB} = -RTF^{-1} \ln (a_i''/a_i') \quad (13)$$

The electrode potential is not a function of the degree of hydration of the active component and of the water activity in the sample solution (if the transference number of the anion $t \to 1$). At high ionic strengths, when the solution components do not penetrate the membrane, the change in the potential of the cell can be ascribed solely to the change in liquid junction potential at the reference electrode, although the activity of water changes appreciably.

At high acid concentrations, the acid penetrates into the membrane, and $a_i(o)$ and $Ka_j(o)$ become comparable, because the final term in Eqn. 12 is greater than the penultimate term, $RTF^{-1} [h'(o) - h''(o)]$. If $a_j''(o) > a_j'(o)$, then the electrode potential is shifted towards more negative potentials, as is observed in practice [1, 5, 18] (Figs. 2 and 4).

In the deduction of Eqn. 12, it was assumed that the hydrated/solvated hydrogen ion complexes produced within the membrane by penetration of acid do not take part in the charge transfer. In this case, the slopes of the calibration curves measured in a series of solutions with different acid concentrations remain constant (Fig. 4) as mentioned earlier [1, 11]. In the case of the tetrachlorothallate(III)-selective electrode, the change in slope (Fig. 2) is probably due to extraction processes leading to changes in the ionic mobilities in the organic phase (e.g., in 0.1 mol l^{-1} hydrochloric acid the slope decreases from 57 mV/decade to 47 mV/decade if the change in liquid junction potential at the reference electrode is not considered).

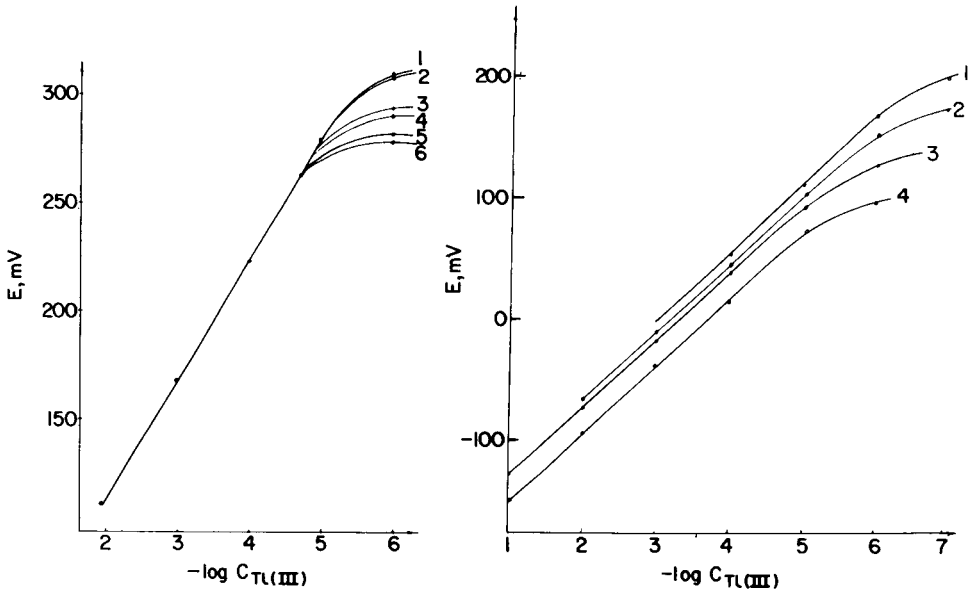

Fig. 4. Calibration curves for the $[TlCl_4]^-$-selective electrode made with plasticizer in the presence of interfering ions: (1) no interfering ion; (2) acetate; (3) nitrate; (4) oxalate; (5) phosphate; (6) sulphate. (Measured by the mixed solution method with a fixed concentration of interfering ion, 10^{-1} mol l^{-1}.)

Fig. 5. Calibration curves for a $[TlCl_4]^-$-selective electrode made without plasticizer at different concentrations of hydrochloric acid: (1) 0.01; (2) 0.1; (3) 1.0; (4) 4.0 mol l^{-1}.

TABLE 2

Selectivity coefficients for the $[TlCl_4]^-$-selective electrode made with dibutyl phthalate as plasticizer

Ion, X	Acetate	NO_3^-	Oxalate	PO_4^{3-}	SO_4^{2-}
$K_{Tl^{3+}/X}$	1.1×10^{-4}	1.0×10^{-4}	8.0×10^{-5}	1.0×10^{-5}	7.5×10^{-5}

Interferences of other ions were studied by the mixed-solution method; the results are summarized in Fig. 4 and Table 2. The selectivity of the electrode in the presence of a series of anions is very high, but as expected, iodide and bromide have a strong effect on the electrode potential because of competitive complex formation with the thallium(III) ion. These iodo or bromo complexes are extracted into the organic phase in the same way as the chloro complex, so the electrode loses its selectivity.

The stability of the electrode potential was satisfactory. In solutions with different Tl^{3+} concentrations, the change did not exceed 2 mV during a 24-h period. The lifetime of the electrode was at least 1 month if it was stored in a 10^{-3} mol l^{-1} Tl(III)/0.1 mol l^{-1} HCl solution. The response time of the

electrode in the lower concentration ranges ($<10^{-3}$ mol l^{-1} $[TlCl_4]^-$) was $\leqslant$3 min and decreased with increasing ion concentration.

The PVC/$(C_{10}H_{21})_4P[TlCl_4]$ membrane electrode

Electrode membranes of this type made with different compositions (Table 1) were investigated. The best electrode parameters were found with membranes containing 60% active compound to 40% PVC (no. 3 in Table 1). All the results shown below were obtained with this electrode.

The calibration curves measured at different hydrochloric acid concentrations in the solutions are shown in Fig. 5. The detection limit for Tl^{3+} decreases with increasing acidity of the solution, probably because of a change in the solubility of the electroactive material. Further, the unfavourable change in the detection limit at high chloride concentrations may be connected to a decrease in the $[TlCl_4]^-$ concentration caused by a shift of the complex equilibrium towards $[TlCl_5]^{2-}$. The detection limits are summarized in Table 3. The best detection limit, 2.1×10^{-7} mol l^{-1} at 0.01 mol l^{-1} hydrochloric acid is an order of magnitude better than that of the electrode made with dibutyl phthalate plasticizer.

As shown in Fig. 5, a change in the hydrochloric acid concentration causes a parallel shift of the calibration curves. This behaviour can be attributed to a change in the diffusion potential within the membrane caused by the penetration of acid. It should be noted that in this case the penetration of acid and a change in the degree of hydration of the membrane components does not affect the ionic mobilities within the membrane, i.e., the slope of the linear portion of the calibration curve remains constant at a value of about 57 mV/decade, if the liquid junction potential at the reference electrode is neglected.

The infrared spectra of membranes stored in hydrochloric acid solution (0.1—3 mol l^{-1}) for 3 days (in contrast to the case described earlier [1]) did not show any appreciable change; they were in agreement with the spectrum shown in Fig. 1.

The response time at lower concentrations ($<10^{-3}$ mol l^{-1} Tl^{3+}) was $\leqslant$5 min and at higher concentrations 1—2 min. The calibration curves of the electrode in the presence of interfering ions are shown in Fig. 6 and the selectivity data are summarized in Table 4. The interfering ions in the order of decreasing interference are: $Hg^{2+} > Cu^{2+} > Co^{2+} > Zn^{2+}$; and $ClO_4^- > NO_3^- > SO_4^{2-}$. The effects of bromide and iodide are, of course, the same as for the electrodes made with plasticizer.

TABLE 3

Influence of the concentration of hydrochloric acid on the lower detection limit of the $[TlCl_4]^-$-selective electrode without plasticizer

HCl (mol l^{-1})	0.01	0.1	1.0	3.0
Detection limit (mol l^{-1})	2.1×10^{-7}	7.0×10^{-7}	2.0×10^{-6}	3.5×10^{-6}

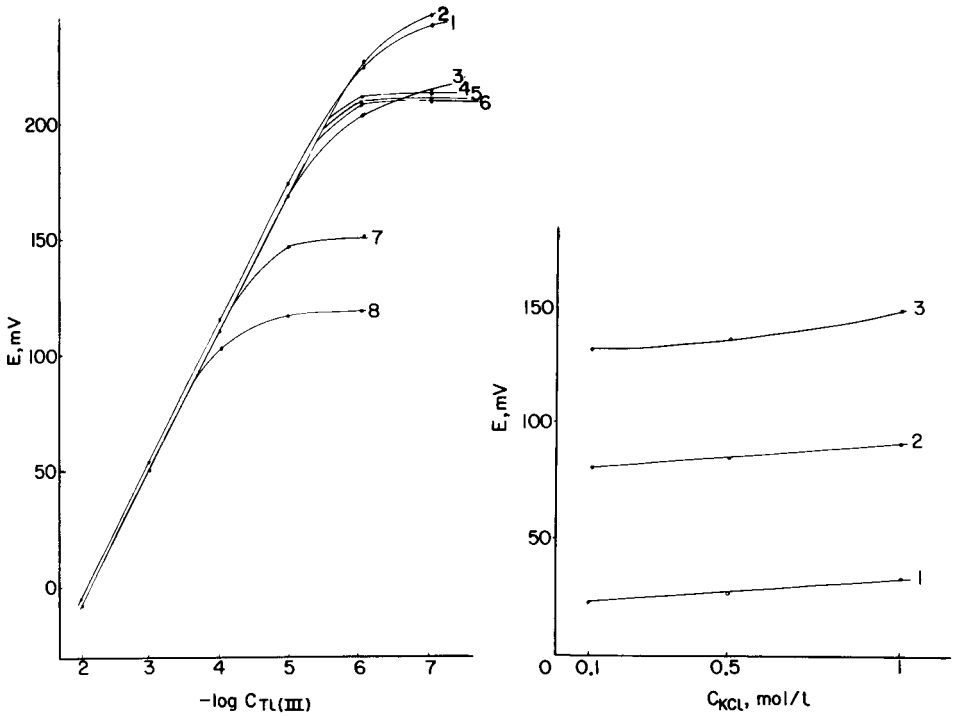

Fig. 6. Calibration curves for a $[TlCl_4]^-$-selective electrode made without plasticizer in the presence of interfering ions: (1) no interfering ion; (2) sulphate; (3) copper(II); (4) zinc(II); (5) cadmium(II); (6) nitrate; (7) perchlorate; (8) mercury(II).

Fig. 7. Influence of the concentration of chloride ions on the potential of the $[TlCl_4]^-$-selective electrode. Tl^{3+} concentration: (1) 10^{-3}; (2) 10^{-4}; (3) 10^{-5} mol l^{-1}. The hydrochloric acid concentration was constant at 10^{-2} mol l^{-1} in all solutions.

TABLE 4

Selectivity coefficients for the $[TlCl_4]^-$-selective electrode made without plasticizer

Ion, X	$K_{Tl^{3+}/X}$	Ion, X	$K_{Tl^{3+}/X}$
Perchlorate	2.2×10^{-3}	Mercury(II)	5.4×10^{-3}
Nitrate	2.3×10^{-5}	Copper(II)	2.7×10^{-4}
Sulphate	1.8×10^{-6}	Cadmium(II)	2.4×10^{-4}
		Zinc(II)	2.0×10^{-4}

The influence of chloride ions on the electrode potential is shown in Fig. 7. If the concentration of potassium chloride is in excess of 0.1 mol l^{-1}, then the potential of the electrode increases because the concentration of $[TlCl_4]^-$ ions decreases, as the equilibrium $[TlCl_4]^- + Cl^- \rightleftharpoons [TlCl_5]^{2-}$ is driven to the right. This is in good agreement with the distribution of thallium(III) chloro complexes calculated from the stepwise complex formation constants.

Finally, it can be concluded that the sensitivity for tetrachlorothallate(III) ions can be increased by using the electroactive material with plasticizer. This also reduces the effect of the hydrochloric acid content of the solutions. The lifetime of the electrodes without plasticizer was longer, at least 3 months, than that of membranes made with plasticizer. The response time and the stability of the electrode potential were almost the same.

The electrode is suitable for measuring thallium(III) ion concentrations in aqueous solutions containing hydrochloric acid if the ratio of different thallium(III) chloro complexes can be kept constant by maintaining a constant chloride concentration.

REFERENCES

1 A. V. Kopytin, P. Gábor-Klatsmányi, V. P. Izvekov and E. Pungor, Anal. Chim. Acta, 148 (1983) 35.
2 C. J. Coetzee and H. Freiser, Anal. Chem., 41 (1969) 1128.
3 M. Matsui and H. Freiser, Anal. Lett., 3 (1970) 161.
4 H. J. Nielsen and E. H. Hansen, Anal. Chim. Acta, 85 (1976) 1.
5 A. V. Kopytin, A. F. Zhukov, Yu. I. Urusov, L. A. Kopytina and A. V. Gordievskii, Zh. Anal. Khim., 34 (1979) 356.
6 R. W. Cattrall and C. P. Pui, Anal. Chim. Acta, 87 (1976) 419; 88 (1977) 185; 116 (1980) 391.
7 R. W. Cattrall and C. P. Pui, Anal. Chem., 48 (1976) 552.
8 D. M. Adams and D. M. Morris, J. Chem. Soc. A, (1968) 694.
9 D. L. Horrocks and A. F. Voigt, J. Am. Chem. Soc., 79 (1957) 2440.
10 F. Seeley and D. Crouse, J. Chem. Eng. Data, (II) (1966) 424.
11 A. V. Kopytin, P. Gábor-Klatsmányi, V. P. Izvekov and E. Pungor, Magy. Kem. Foly., 88 (1982) 122.
12 W. E. Morf, The Principles of Ion-Selective Electrodes and of Membrane Transport, Akadémiai Kiadó, Budapest, 1981, pp. 49 and 219.
13 The Principles of Solvent Extraction, G. A. Yagodin (Ed.), Khimiya, Moscow, 1981, p. 69 and 105.
14 O. D. Bonner and D. C. Lunney, J. Phys. Chem., 70 (1966) 1140.
15 G. J. Hills, in D. J. G. Ives and G. J. Janz (Eds.), Reference Electrodes, Theory and Practice, Academic Press, New York, 1961, p. 418.
16 Yu. G. Frolov, V. V. Sergievskii and A. P. Zuev, Russ. Atom. Energ., 35 (1973) 106.
17 Yu. G. Frolov and V. V. Sergievskii, Zh. Fiz. Khim., 52 (1978) 1321.
18 E. A. Materova, Z. S. Alagova and V. P. Zhesko, Elektrokhimiya, 10 (1974) 1568.

Analytica Chimica Acta, 162 (1984) 133—140
Elsevier Science Publishers B.V., Amsterdam — Printed in The Netherlands

INVESTIGATION OF ION-SELECTIVE ELECTRODES BASED ON QUATERNARY PHOSPHONIUM SALTS
Part 3. An Ion-Selective Electrode for Hexafluorophosphate

A. V. KOPYTIN, P. GÁBOR-KLATSMÁNYI, V. P. IZVEKOV and E. PUNGOR*

Institute for General and Analytical Chemistry, Technical University of Budapest, 1111 Budapest (Hungary)

E. G. ILYIN

Institute for General and Inorganic Chemistry, U.S.S.R. Academy of Sciences, Leninsky Prospect 31, Moscow (U.S.S.R.)

(Received 14th March 1984)

SUMMARY

A hexafluorophosphate-selective electrode based on the tetradecylphosphonium hexafluorophosphate(V) ion-pair complex in a PVC membrane is described. The active material is a white powder; its solution in dibutyl phthalate was used for the electrode membranes. The composition of the tetradecylphosphonium hexafluorophosphate was identified as its infrared and ^{31}P-n.m.r. spectra. The calibration curves for the electrode were investigated and interpreted with respect to the hydrogen fluoride concentration of the sample solution. It is shown that the hydrolysis of hexafluorophosphate depends on the hydrofluoric acid content of the solution. The lifetime of the electrodes is about one month and the limits of detection vary from about 10^{-7} mol l^{-1} to 10^{-6} mol l^{-1} with 0—1 mol l^{-1} hydrofluoric acid present.

Several recent papers [1—5] have dealt with new ion-selective electrodes of the ion-pair type, which are sensitive to chloro complexes of metal ions. These electrodes have been applied successfully to the determination of the appropriate metal ions in solutions containing hydrochloric acid.

An ion-selective electrode sensitive to hexafluorophosphate(V) ion is described in this paper. The electrode is suitable for the simple direct determination of phosphorus(V) often occurring in hydrofluoric acid.

EXPERIMENTAL

Electroactive material

The active material of the ion-selective electrode was the ion-pair of tetradecylphosphonium with hexafluorophosphate. The compound was prepared according to the reaction

$$(C_{10}H_{21})_4PBr + LiPF_6 \rightarrow (C_{10}H_{21})_4P[PF_6] + LiBr$$

0003-2670/84/$03.00

by the following procedure. Solutions of tetradecylphosphonium bromide (5×10^{-2} mol l^{-1} in chloroform) and lithium hexafluorophosphate (aqueous 10^{-1} mol l^{-1} solution) were shaken vigorously for 5 min in a separatory funnel at a 1:1 phase ratio. This extraction was repeated three times, each with a fresh lithium salt solution. The organic phase was then washed twice with distilled water. The complete replacement of bromide by hexafluorophosphate was monitored by potentiometric titrations of the combined aqueous phases and of the wash water with standard silver nitrate solution in the usual manner. After the evaporation of chloroform (the solution was allowed to stand at room temperature in a Petri dish), a white amorphous powder was obtained. This compound was identified by its ^{31}P-n.m.r. spectrum (Fig. 1a) with phosphoric acid as standard. The separated ion-pair complex, $(C_{10}H_{21})_4P[PF_6]$, was also characterized by its infrared spectrum in the range 400—4000 cm^{-1} (Fig. 1b).

The pure ion-pair complex was dissolved in dibutyl phthalate to give a 10^{-3} mol l^{-1} solution and this solution was mixed with PVC dissolved in cyclohexanone. The membranes and the electrodes were made as described earlier [1]. Before use, the electrodes were conditioned in aqueous 10^{-3} mol l^{-1} lithium hexafluorophosphate for 24 h.

All the chemicals were of analytical grade.

Electrodes and equipment

The ^{31}P-n.m.r. spectra were measured with a JEOL FX-100 spectrometer; the standard was phosphoric acid. The infrared spectra were measured with a UR-10 Zeiss spectrometer with PVC film as reference.

A double-junction silver/silver chloride electrode (Radelkis, OP-08203) was used as reference. Potentials were measured with a digital mV meter (Radelkis, OP-208). The potentiometric cell used was as follows

Ag/AgCl	0.1 mol l^{-1} KCl 10^{-3} mol l^{-1} $LiPF_6$	membrane	sample soln.	0.1 mol l^{-1} KCl	AgCl/Ag

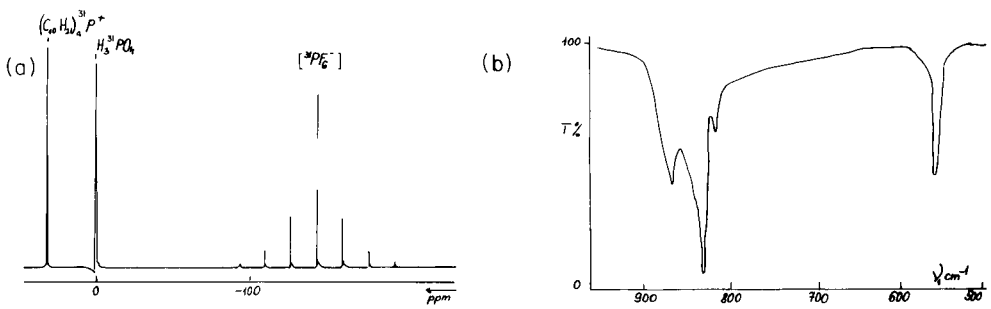

Fig. 1. Spectra of the separated tetradecylphosphonium hexafluorophosphate: (a) ^{31}P-n.m.r.; (b) infrared.

RESULTS AND DISCUSSION

Composition of the ion-pair complex

The singlet at δ = 30.4 ppm on the ^{31}P-n.m.r. spectrum (Fig. 1a) represents the tetradecylphosphonium cation, while the septet at δ = −144.7 ppm and the J_{P-F} = 712.9 Hz show the presence of the hexafluorophosphate anion in the system [6]. The data prove that hexafluorophosphate extracted into the organic phase. The i.r. spectrum (Fig. 1b) of the ion-pair complex show two intense absorptions at 560 and 835 cm^{-1}. The structure of the hexafluorophosphate ion is octahedral and has an O_h symmetry. Six vibrations belong to this type of symmetry, only two of which are i.r.-active, the $\nu_{3(F_{1U})}$ and the $\nu_{4(F_{1U})}$ [7]. The most intense absorption band at 835 cm^{-1} can be assigned to the ν_3 stretching vibration of the P—F bond. The band at 560 cm^{-1} is due to the F—P—F (ν_4) bending vibration [8].

The absence of signals of tetracoordinated oxofluorophosphates, $[PO_2F_2]^-$ and $[PO_3F]^{2-}$ in the ^{31}P-n.m.r. spectrum, and the absence of the bands characteristic of the P=O and P—O bonds between 1350 and 1200 cm^{-1} in the i.r. spectrum, clearly show that hydrolysis of tetradecylphosphonium hexafluorophosphate did not occur either in air or in chloroform saturated with water.

The i.r. and ^{31}P-n.m.r. spectra show that the phosphorus(V) was transferred from the aqueous solution to the organic phase as the $[PF_6]^-$ ion-pair with tetradecylphosphonium ion. The easy extraction of hexafluorophosphate indicates that it is weakly hydrated in aqueous solutions. It is therefore to be expected that the electrode will show good selectivity for hexafluorophosphate in the presence of more strongly hydrated ions such as chloride, sulphate and fluoride.

Characteristics of the hexafluorophosphate-selective electrode

The calibration curves of the ion-selective electrode measured in a series of aqueous lithium hexafluorophosphate solutions in the presence and absence of hydrogen fluoride are shown in Fig. 2. The reason for the use of the total concentration of phosphorus(V) instead of the hexafluorophosphate concentration was the possibility of hydrolytic processes

$$LiPF_6 + 2H_2O \rightleftharpoons H[PO_2F_2] + LiF + 3HF$$

$$H[PO_2F_2] + H_2O \rightleftharpoons H_2[PO_3F] + HF$$

$$H_2[PO_3F] + H_2O \rightleftharpoons H_3PO_4 + HF$$

which would mean that $[PO_2F_2]^{2-}$, $[PO_3F]^-$ and PO_4^{3-} ions could also occur in the sample solution.

The calibration curves in Fig. 2 show that the detection limit of the electrode decreases with increasing concentration of hydrofluoric acid. Because of this, the hydrolysis of the hexafluorophosphate that actually establishes the potential of the ion-selective electrode was investigated in detail. The

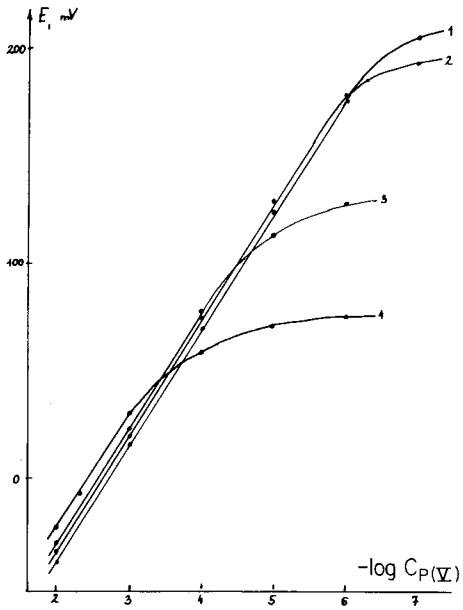

Fig. 2. Calibration curves for the hexafluorophosphate-selective electrode as a function of the total phosphorus(V) concentration at different concentrations of hydrofluoric acid: (1) none; (2) 0.1; (3) 1.0; (4) 4.0 mol l^{-1}.

literature indicates that hexafluorophosphate has good stability in alkaline media, but hydrolysis may occur in the acidic range [9].

Figure 3 shows the ^{31}P-n.m.r. spectra of 0.1 mol l^{-1} lithium hexafluorophosphate containing hydrofluoric acid in concentrations similar to those in the calibration solutions (see Fig. 2). The ^{31}P-n.m.r. spectrum of an aqueous lithium hexafluorophosphate solution containing 0.1 mol l^{-1} hydrofluoric acid (Fig. 3b) shows a triplet from the $[PO_2F_2]^-$ ion (δ = —12.7 ppm and J_{P-F} = 960.7 Hz), a doublet from $[PO_3F]^{2-}$ (δ = —2.4 ppm and J_{P-F} = 909.4 Hz), and a very minor singlet from phosphoric acid in the range of tetracoordinated phosphorus compounds, in addition to the septet of hexafluorophosphate (δ = —143 ppm and J_{P-F} = 709 Hz). It can be seen from the ^{31}P-n.m.r. spectra (Fig. 3a—d) that there is a change in the intensity of signals of the tetracoordinated phosphorus compounds with increasing concentration of hydrofluoric acid. Table 1 lists the compositions of these solutions on the basis of the integral intensities of the ^{31}P-n.m.r. spectra. As can be seen from the data, the concentration of hexafluorophosphate decreases as the hydrofluoric acid content increases up to 1 mol l^{-1} while the concentration of phosphoric acid increases. Summing up the data of Fig. 3 and Table 1, it may be concluded that the concentration of hexafluorophosphate, which is of prime interest from the point of view of the proposed electrode, changes along a minimum curve with the hydrogen fluoride content of the solution. The data for 4 mol l^{-1} hydrofluoric acid (Table 1) indicate suppres-

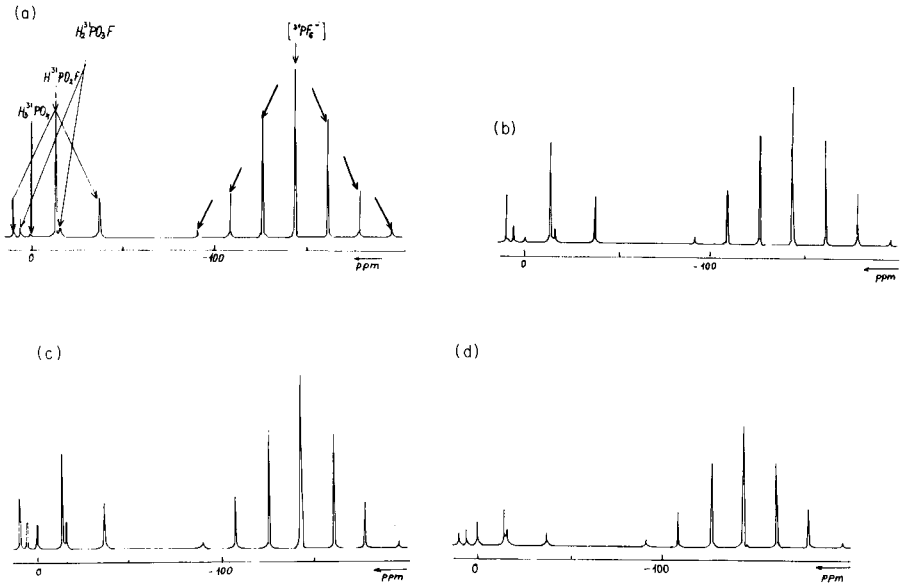

Fig. 3. ^{31}P-n.m.r. spectra of lithium hexafluorophosphate solutions (10^{-1} mol l^{-1}) at different concentrations of hydrofluoric acid: (a) none; (b) 0.1; (c) 1.0; (d) 4.0 mol l^{-1}.

sion of the hydrolysis described by the above equations. Further investigations are needed to describe the kinetics in more detail.

It follows from what has been said above that the fact that the detection limit for phosphorus(V) (as hexafluorophosphate) decreases as the hydrogen fluoride concentration increases cannot be explained by assuming hydrolysis of the primary ion. To explain the data, it is necessary to consider that with alteration of the acid concentration, not only is there a change in detection limit but other characteristics important in electrochemical measurements (e.g., activity of different components, permittivity of solutions) also change. These characteristics may affect the distribution of components between the

TABLE 1

Compositions of $LiPF_6/HF/H_2O$ systems at different HF concentrations, calculated from the data in Fig. 3

Ion	Content (%) of ion in different media			
	H_2O	HF (mol l^{-1})		
		0.1	1.0	4.0
$[PF_6]^-$	75	70	65	81
$[PO_2F_2]^-$	23	24	21	10
$[PO_3F]^{2-}$	2	3	6	5
PO_4^{3-}	0.5	3	8	4

aqueous and organic phases [10]. The change of the detection limit with hydrofluoric acid concentration can be interpreted in terms of the distribution of hexafluorophosphate between the aqueous solution and the membrane.

On the basis of the percentage of hexafluorophosphate present in the solution (known from the ^{31}P-n.m.r. spectrum, Fig. 3), the calibration curve for hexafluorophosphate can be drawn (Fig. 4). It can be seen that at $c_{HF} \leqslant 1$ mol l^{-1}, the electrode potential is practically independent of the hydrofluoric acid concentration over quite a wide range of hexafluorophosphate concentrations, although the calibration curve is shifted. This is in agreement with earlier conclusions [3, 4] that above a given hydrofluoric acid content, the acid can enter the membrane and change the $E^{0'}$ value of the potentiometric cell. In the present case (Fig. 4, curve 4), the shift is towards positive potentials; this is not in agreement with the results obtained with the ion-selective electrodes for trichloromercurate(II) and tetrachlorothallate(III) [1—5]. The opposite shift of $E^{0'}$ can be interpreted as follows. The membrane of the hexafluorophosphate indicator electrode differs from the others in that it

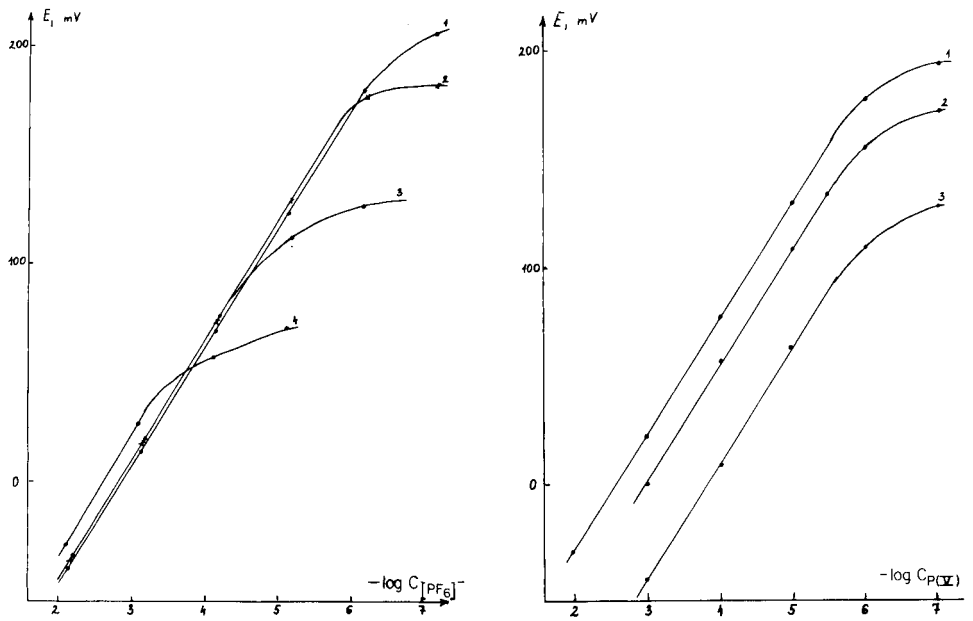

Fig. 4. Calibration curves for the hexafluorophosphate-selective electrode (calculated from the data in Table 1) at different concentrations of hydrofluoric acid: (1) none; (2) 0.1; (3) 1.0; (4) 4.0 mol l^{-1}.

Fig. 5. Calibration curves for the hexafluorophosphate-selective electrode as a function of the total phosphorus concentration of the sample at a constant level of hydrofluoric acid (1.0 mol l^{-1}) and different concentrations of sulphuric acid: (1) none; (2) 1.0; (3) 3.0 mol l^{-1}.

TABLE 2

Lower detection limits for the hexafluorophosphate-selective electrode as a function of the concentration of hydrofluoric acid

HF (mol l^{-1})	0	0.1	1.0	4.0
Detection limit (mol l^{-1})	1.2×10^{-7}	4.2×10^{-7}	6.0×10^{-6}	1.5×10^{-4}

TABLE 3

Selectivity coefficients for the hexafluorophosphate-selective electrode

Interfering ion	$K_{i,j}^{pot}$	Interfering ion	$K_{i,j}^{pot}$
Cl^-	1.7×10^{-6}	NO_3^-	4.7×10^{-5}
Br^-	1.5×10^{-5}	ClO_4^-	8.5×10^{-2}
I^-	1.2×10^{-3}	$[AsF_6]^-$	3.7

also contains dibutyl phthalate. As is known, in solvents with low permittivity, e.g., dibutyl phthalate (ϵ = 6.1), hydrogen fluoride will be present predominantly in an associated form, so that it cannot influence the potential drop within the membrane. The $E^{0\prime}$ value also contains the diffusion potential, and the latter may be responsible for the change in electrode potential with the hydrofluoric acid concentration of the solution. It should be noted that when the level of hydrofluoric acid was kept constant at 1 mol l^{-1}, and a constant concentration of sulphuric acid (0.1 or 3.0 mol l^{-1}) was maintained in the series of calibration solutions, the calibration curves were shifted in the negative direction with increasing concentration of sulphuric acid (Fig. 5). This is in agreement with earlier results.

Data on the limit of detection were calculated from Fig. 4, with the results given in Table 2. The response time of the electrode in the lower concentration ranges was $\leqslant$5 min and decreases with increasing concentration of hexafluorophosphate. Some data on selectivity coefficients are listed in Table 3.

The potential stability and lifetimes were studied in the usual calibration solutions. The potential of an electrode remained within ±0.1 mV for at least a month. If the electrodes were stored in 10^{-3} mol l^{-1} lithium hexafluorophosphate solution, then the slope of the calibration curve decreased by 2—3 mV during this time.

REFERENCES

1 A. V. Kopytin, P. Gábor-Klatsmányi, V. P. Izvekov and E. Pungor, Anal. Chim. Acta, 148 (1983) 35 (Part 1).
2 A. V. Kopytin, P. Gábor-Klatsmányi, V. P. Izvekov and E. Pungor, Anal. Chim. Acta, 162 (1984) 123 (Part 2).

3 A. V. Kopytin, A. F. Zhukov, Yu. I. Urusov, L. A. Kopytina and A. V. Gordievskii, Zh. Anal. Khim., 34 (1979) 465.
4 A. V. Kopityin, P. Gáborné-Klatsmányi, V. P. Izvekov and E. Pungor, Magy. Kem. Foly., 88 (1982) 122.
5 A. V. Kopityin, P. Gáborné-Klatsmányi, E. Pungor and G. A. Yagodin, Magy. Kem. Foly., 89 (1983) 42.
6 D. P. Ames, S. Ohashi, C. F. Callis and J. R. Van Wazer, J. Am. Chem. Soc., 81 (1959) 6350.
7 K. Nakamoto, Infrared and Raman Spectra of Inorganic and Coordination Compounds, Wiley, New York, 1978, p. 153.
8 H. G. Mayfield and W. E. Bull, J. Chem. Soc. A, (1971) 2280.
9 J. R. Van Wazer, Phosphorus and Its Compounds, Vol. 1., Chemistry, Interscience, New York, 1958, p. 810.
10 D. Midgley, Ion-Selective Electrode Rev., (1981) 43.

Analytica Chimica Acta, 162 (1984) 141—151
Elsevier Science Publishers B.V., Amsterdam — Printed in The Netherlands

ION-SELECTIVE ELECTRODES IN TITRATIONS INVOLVING AZO-COUPLING REACTIONS

Part 2. Titrations with Diazonium Salts Derived from 1-Aminonaphthalenes and 1-Amino-9,10-anthraquinone

K. VYTŘAS*, J. KALOUS and T. ČAPOUN[a]

Department of Analytical Chemistry, College of Chemical Technology, 532 10 Pardubice (Czechoslovakia)

(Received 3 February 1984)

SUMMARY

Lipophilic arenediazonium salts derived from 1-aminonaphthalene, 1-amino-4-bromonaphthalene, 1-amino-4-nitronaphthalene and 1-amino-9,10-anthraquinone were tested as titrants for determination of aromatic hydroxy compounds, amines, and compounds containing active methylene groups, usually at the 10^{-2} M level. The potentiometric titrations were monitored with indicator electrodes selective for organic cations which were based on PVC membranes plasticized with 2-nitrophenyl alkyl ethers (where alkyl is n-octyl or 2-ethylhexyl). Titrations of 11 compounds ranging from 1,2-diaminotoluene to 1-phenyl-3-methyl-5-pyrazolone were examined; 4-bromo-1-naphthalenediazonium chloride seemed to be the most widely applicable titrant.

In Part 1 of this series [1], organic cation-selective plastic membrane electrodes were used for monitoring titrations of sixteen different aromatic hydroxy compounds, amines, and compounds containing active methylene groups, with 4-methyl-, 4-bromo-, or 4-nitro-benzenediazonium chloride solutions as the titrant. These electrodes were also found useful in titrations of 2,4-diaminotoluene, resorcinol and 1-phenyl-3-methyl-5-pyrazolone with a 4-(*N*-acetyl)-benzenediazonium salt [2]. However, when different organic cations were titrated with an oppositely charged reagent to form ion-pairs (e.g., with sodium tetraphenylborate, $NaBPh_4$), the titration curves obtained with plastic membrane electrodes showed a steepness and an overall potential break which increased with increasing mass of the cation because of its more lipophilic character [3]. This was also observed in titrations of arenediazonium salts with $NaBPh_4$ [4].

Subsequently, further experiments were made in which more lipophilic arenediazonium salts were examined as titrants for determinations based on azo-coupling reactions. The experience gained and the results obtained with

---

[a]Present address: Research Institute of Civil Defence, 113 84 Prague (Czechoslovakia).

0003-2670/84/$03.00

diazonium salts derived from three 1-aminonaphthalenes and 1-amino-9,10-anthraquinone are described below.

EXPERIMENTAL

Preparation of titrants and their standardization

1-Naphthalenediazonium chloride. 1-Naphthylamine (ca. 7.2 g) is mixed with distilled water (300 ml) and heated on a water bath until the amine melts. Then 100 ml of hydrochloric acid (1 + 3, i.e. 10%) is added (very carefully to avoid precipitating the 1-naphthylamine hydrochloride), and the solution is transferred to a 1-l volumetric flask and, after cooling, diluted to the mark. For diazotization, 50 ml of this ca. 0.05 M solution is transferred to a 150-ml beaker and 30 ml of concentrated hydrochloric acid (38%) is added. The beaker with the hydrochloride suspension is cooled in ice to 0°C and the solution is titrated with 1 M sodium nitrite until the potential of the platinum indicator electrode shows a small permanent increase; the potential change is about 80 mV for the first drop of nitrite in excess and diazotization is quick. This solution is quantitatively transferred to a 250-ml volumetric flask and diluted with water to the mark, giving a ca. 0.01 M 1-naphthalenediazonium chloride solution.

This solution must be kept in an ice-box and is not stable for longer than 8 h. The slightly orange solution becomes deep red on ageing as a result of an auto-azo-coupling reaction. This is also why titrations which take a long time suffer from negative errors when the burette is not cooled. When the concentration of the solution was monitored, it was found that 1% of the diazonium salt decomposed during 8 h, 4.6% during 24 h, and ca. 10% during 48 h. It seems best to prepare small portions of the diazonium salt solution as required by titrating aliquots of the stable stock 1-naphthylamine solution. If all the operations are done carefully in the same way, the resulting concentrations of the 1-naphthalenediazonium chloride are surprisingly reproducible.

For standardization, 5 ml of the 1-naphthalenediazonium chloride solution (ca. 0.01 M) is pipetted into a beaker, diluted with water (50 ml) and titrated with standard 0.01 M $NaBPh_4$. The potential break is adequate (170—190 mV), but the relative standard deviation (s_r) on the end-point estimate is 1.55% because the change in potential is not very steep (4—6 mV/0.1 ml). The advantage of this manner of standardization is that the electrode membrane is conditioned simultaneously with the 1-naphthalenediazonium tetraphenylborate formed.

Another standardization procedure involves azo coupling with 0.01 M 2,4-diaminotoluene; for this, 5 ml of the 2,4-diaminotoluene solution is mixed with 70 ml of the desired buffer (pH 10) and titrated with the diazonium salt solution. This manner is more reproducible than the $NaBPh_4$ method (s_r = 0.58%), but the difference in the results of the two standardizations is statistically insignificant.

4-Bromo-1-naphthalenediazonium chloride. As 4-bromo-1-naphthylamine is only slightly soluble in hydrochloric acid, the diazotization is done in its

suspension. About 0.56 g of 4-bromo-1-naphthylamine is weighed into a 100-ml beaker and water (20 ml) and concentrated hydrochloric acid (40 ml) are added. The suspension is cooled to 0°C, stirred vigorously and titrated with 1 M sodium nitrite as described above. In this case, the titration is complete when the permanent increase of the electrode potential is ca. 40 mV. This solution contains small particles of the unreacted amine, and must be filtered through a glass frit (S3), the filtrate being transferred to a 250-ml volumetric flask and diluted with water to the mark. This ca. 0.01 M solution of 4-bromo-1-naphthalenediazonium chloride is stable for at least 14 days when stored in an ice box (the concentration dropped by ca. 0.5% after 25 days).

Both the $NaBPh_4$ and the 2,4-diaminotoluene method can be used for standardization as mentioned above; the latter is more reproducible.

4-Nitro-1-naphthalenediazonium chloride. The titrant is prepared by diazotization of 4-nitro-1-naphthylamine in suspension (ca. 0.47 g for 250 ml of 0.01 M reagent) with water (20 ml) and concentrated hydrochloric acid (40 ml) as in the procedure described above for 4-bromo-1-naphthalenediazonium chloride, inclusive of filtration through a glass frit. The stock solution stored in an ice box is stable (the concentration dropped by ca. 0.7% after 20 days).

The $NaBPh_4$ standardization method is not recommended because the potential jump at the end-point is rather diffuse. Standardization with 2,4-diaminotoluene at pH 9 is much more precise.

9,10-Dioxo-1-anthracenediazonium salt. 1-Amino-9,10-anthraquinone (ca. 2.8 g) is dissolved in concentrated sulfuric acid (30 ml) at 70°C, and glacial acetic acid (to 250 ml) is added carefully with stirring and cooling to obtain a 0.05 M solution. An aliquot (50 ml) of this stock aminoanthraquinone solution is pipetted into a beaker and titrated at 20°C with 1 M sodium nitrite; the potential break after addition of the first drop of nitrite in excess is about 300 mV. This solution is transferred to a 250-ml volumetric flask and diluted to the mark with water to obtain a ca. 0.01 M diazonium salt solution; the concentration is perfectly reproducible. Stored in an ice-box, this solution is stable for ca. 2 days; 1.3% of the diazonium salt decomposes after 4 days, and 5.5% after 6 days.

Potentiometric titration of 2,4-diaminotoluene does not provide curves suitable for standardization and the $NaBPh_4$ procedure is far more precise. The diazonium salt solution (5 ml) is diluted with water (50 ml) and titrated with 0.01 M $NaBPh_4$ at 0°C (cooled externally). Results are somewhat lower than corresponds to the nitrite consumption in diazotization, but are free of systematic errors [2].

Other solutions

Stock solutions of passive compounds (0.01 M) were prepared. Amines were converted with hydrochloric acid to their soluble hydrochlorides, and compounds of acidic character were dissolved as their sodium salts after addition of sodium hydroxide.

Concentrated Britton-Robinson buffers (a 0.4 M H_3PO_4/0.4 M CH_3COOH/0.4 M H_3BO_3 stock solution mixed with the desired volume of 2 M NaOH) were used.

2,4-Diaminotoluene used for standardization was purified by treble recrystallization from water, and dried in air and above phosphorus(V) oxide in vacuum; its purity was checked by determination of melting point (97–97.5°C, theoretically 99°C) and by elemental analysis (theoretical values are given in parentheses): 68.5 (68.8)% C, 8.4 (8.25)% H, 22.9 (22.9)% N.

Sodium tetraphenylborate (0.01 M) solutions prepared from a reagent of guaranteed purity (>98.5%; Jenapharm-Laborchemie Apolda) was standardized by potentiometric titration of thallium(I) nitrate [5, 6].

Instrumentation and electrodes

Potentiometric measurements were done with OP-204 and OP-208 pH meters (Radelkis, Budapest). The diazotization was monitored with platinum and saturated calomel (SCE) electrodes; for monitoring the azo-coupling titrations, the plastic membrane electrode and SCE were used. The electrode membrane was made from poly(vinyl chloride) (PVC) plasticized with either 2-nitrophenyl 2-ethylhexyl ether (NPEHE; electrode working code 179B) [1] or 2-nitrophenyl n-octyl ether (NPOE; 280A). A solution 0.01 M in NaCl and 0.01 M in $NaBPh_4$ was used as the internal electrolyte, and a Ag/AgCl wire served as the internal reference electrode (for other details, see [1]). The electrode membrane was conditioned in a stirred aqueous suspension of the appropriate arenediazonium tetraphenylborate. The pH value of the titrated solutions was checked potentiometrically with glass and saturated calomel electrodes.

General procedure

For the azo-coupling titrations, an appropriate volume of a solution of the passive component to be titrated (usually 5 ml of 0.01 M solution) was pipetted into a 150-ml beaker cooled in ice, 70 ml of concentrated Britton-Robinson buffer was added to adjust the pH value, and the 0.01 M arenediazonium salt titrant was added from a 10-ml burette, the titration solution being stirred magnetically.

RESULTS AND DISCUSSION

The basic criterion for selection of the optimal medium for these determinations of passive components with arenediazonium salt titrants is the shape of the potentiometric titration curve (i.e., the overall potential break and particularly its steepness near the inflexion point, which is the deciding factor for reproducibility). From this point of view, the PVC membrane electrodes are useful. Arenediazonium ions derived from 1-aminonaphthalenes and 1-amino-9,10-anthraquinone are of more lipophilic character than those derived from aminobenzenes, so that titrations could be made with more

TABLE 1

Characteristic values for potentiometric titrations of passive compounds (ca. 0.05 mmol in 75 ml) with 0.01 M arenediazonium salts

Substance determined	pH	Titration curve		Titration time (min)
		Overall potential change (mV)	Steepness near end-point (mV per 0.1 ml)	
With 1-naphthalenediazonium salt[a]				
2,4-Diaminotoluene	6	109	2[b]	3
	7	113	5	3
	8	118	7	3
	9	126	7	3
	10	133—161	10—12	3
2-Naphthol	8	146	22	100
	9	149—169	22—28	50
	10	148	16	30
8-Quinolinol	8	122	8	120
	9	114	9	80
	10	103—146	7—11	30
Resorcinol	8	144	10	60
	9	138—162	21—28	10
	10	141	20	10
Quercetin	8	136	11[c]	120
	9	143	15[c]	90
	10	148—153	28—40[c]	20
Phloroglucinol	7	89	2[b]	40
	8	97	5; 5[d,e]	20
	9	115	6[d]	15
	10	143—165	10—18[d]	10
1-(2',5'-Dichloro-4'-sulfophenyl)-3-carboxy-5-pyrazolone	7	120	8	90
	8	111	6	60
	9	138	20	30
	10	136—160	18—23	15
1-Phenyl-3-methyl-5-pyrazolone	7	94	4	60
	8	104	6	20
	9	117	8	5
	10	146—176	26—41	3
With 4-bromo-1-naphthalenediazonium salt[g]				
2,4-Diaminotoluene	6	183	16	3
	7	208	18	3
	8	198	20	3
	9	216	24	3
	10	216—231	35—46	3
2-Naphthol	7	212	29	240
	8	257	60	80
	9	217—260	64—95	30
	10	179	12	20
8-Quinolinol	7	113	7	180
	8	144	28	90
	9	170	37	60
	10	148—172	38—49	15

TABLE 1 (continued)

Substance determined	pH	Titration curve		Titration time (min)
		Overall potential change (mV)	Steepness near end-point (mV per 0.1 ml)	
8-Quinolinol-5-sulfonic acid	9	161	?[b]	140
	10	139—147	14—24	80
Resorcinol	8	163	6; 20[d,e]	190
	9	153	25[d]	120
	10	171—173	52—56[d]	20
Quercetin	8	148	10	80
	9	172—187	8; 8; 10[f,e]	80
	10	163—188	20—23[f]	15
Phloroglucinol	7	182	10[f]	80
	8	152	14[f]	60
	9	166	16[f]	40
	10	168—187	19—29[f]	20
Apomorphine	10	158—187	4; 16—23[d,e]	25
1-(2',5'-Dichloro-4'-sulfophenyl)-3-carboxy-5-pyrazolone	6	120	7[b]	80
	7	151	10	60
	8	134	32	40
	9	165—178	44—56	40
	10	153	33	40
With 4-nitro-1-naphthalenediazonium salt[a]				
2,4-Diaminotoluene	6	162	5	3
	7	167	20	3
	8	164	31	3
	9	172—178	41—51	3
	10	167	29[b]	3
2-Naphthol	6	176	5[b]	90
	7	183	20	60
	8	192	27	30
	9	196—214	27—35	5
	10	197	15[b]	5
2-Naphthol-3,6-disulfonic acid, disodium salt (R-salt)	8	219	8	90
	9	199—210	25—28	60
	10	200—219	21—31[b]	30
With 9,10-dioxo-1-anthracenediazonium salt[a]				
2,4-Diaminotoluene	8	144	4	30
	9	162—182	9—15	30
	10	171	8	30
2-Naphthol	8	196	4	60
	9	191—234	15—19	60
	10	179	8	60
Resorcinol	8	192	5	40
	9	192	9	40
	10	182—210	12—25	40

TABLE 1 (continued)

Substance determined	pH	Titration curve		Titration time (min)
		Overall potential change (mV)	Steepness near end-point (mV per 0.1 ml)	
1-Phenyl-3-methyl-5-pyrazolone	6	116	8	10
	7	146	10	3
	8	165	16	3
	9	173	25	3
	10	177—203	44—56	3

[a]Data for 179B electrode vs. SCE. [b]The potential break does not correspond to any stoichiometry expressed by a whole number. The potential break corresponds to a formation of the [c]tetrakis-, [d]bis-azo compound; [e]bis- or tris-azo compounds are formed in a stepwise manner, [f]tris-azo compound. [g]Data for 280A electrode vs. SCE.

TABLE 2

Statistical evaluation of titration results for pure passive compounds

Substance determined	pH	Taken (mg)	Found[a] (mg)	Lord's test	
				u_0	u'_0
With 1-naphthalenediazonium salt					
2,4-Diaminotoluene	10	6.109	6.110 ± 0.042 (5)	0.51	0.01
8-Quinolinol	10	7.258	7.247 ± 0.051 (4)	0.72	0.15
Resorcinol	9	2.202	2.204 ± 0.016 (4)	0.72	0.06
Quercetin	10	3.022	3.022 ± 0.011 (5)	0.51	0.00
With 4-bromo-1-naphthalenediazonium salt					
2,4-Diaminotoluene	10	6.970	6.982 ± 0.017 (5)	0.51	0.36
8-Quinolinol	10	7.258	7.251 ± 0.022 (5)	0.51	0.16
Resorcinol	10	2.752	2.750 ± 0.005 (5)	0.51	0.20
Quercetin	10	6.045	6.054 ± 0.010 (5)	0.51	0.45
With 4-nitro-1-naphthalenediazonium salt					
2,4-Diaminotoluene	9	3.665	3.658 ± 0.012 (4)	0.72	0.39
2-Naphthol-3,6-disulfonic acid,	9	10.448	10.414 ± 0.087 (4)	0.72	0.28
disodium salt (R-salt)	10	10.448	10.587 ± 0.107 (4)	0.72	0.93
With 9,10-dioxo-1-anthracenediazonium salt					
2,4-Diaminotoluene	9	6.109	6.083 ± 0.196 (4)	0.72	0.10
Resorcinol	10	5.506	5.485 ± 0.153 (4)	0.72	0.10

[a]Given as a reliability interval $\bar{x} \pm u_0 R$ for the significance level $\alpha = 0.05$ (95% probability); the u'_0 values were calculated from the arithmetic means $\bar{x}$, values taken μ and range R by the formula $u'_0 = (|\bar{x} - \mu|)/R$. The number of replicates is given in parentheses.

dilute solutions (0.01 M instead of 0.1 M [1]), providing titration curves for which end-point readings and the overall shapes were reproducible. Characteristic values are given in Tables 1 and 2.

The sometimes slow reaction rate and the resulting delay time of the electrode response bring problems in their wake. Excessive titration times are obviously inconvenient for practical applications, and the less stable arenediazonium salt solutions may decompose during such titrations. In agreement with theoretical considerations, the reaction rate depends strongly on the substituents on the aromatic ring of the diazonium salt. Arenediazonium salts containing electronegative substituents are generally more reactive, which appears as a shorter titration time. As shown in Table 3, the time necessary for completion of titration decreases in the direction of diagonals towards higher pH values and more electronegative substituents.

However, the titration time is shortened significantly only for cases in which the same reaction product, the monoazo compound, is produced. The more reactive arenediazonium cations can bond into more than one position of the passive component to form bis-, or tris-azo dyes, so that longer times are then needed to complete such titrations. For example, when resorcinol is titrated with 1-naphthalenediazonium chloride, the potential break of the titration curve corresponds to the formation of the monoazo compound; but when the 4-bromo-1-naphthalenediazonium salt is used as titrant, a bisazo compound is formed with resorcinol and the titration time is longer even though buffering is done to the same pH. Similarly, in titrations of phloroglucinol, the titration time increases when 4-bromo-1-naphthalenediazonium chloride is used as titrant and a trisazo compound is formed, whereas the bisazo compound only is formed with the 1-naphthalenediazonium salt.

The reaction rate of the azo-coupling is significantly influenced by the pH value of the medium. Some examples are shown in Fig. 1. In agreement with theoretical considerations [7], the reaction time decreased with increasing

TABLE 3

Effect of naphthalene ring substituents (X) on the titration times for 2-naphthol and R-salt at different pH values[a]

X	Titration time (min)					
	2-Naphthol			R-salt		
	pH 8	pH 9	pH 10	pH 8	pH 9	pH 10
4-H-	100	50	30	180	130	90
4-Br-	80	30	20	180	90	60
4-NO_2-	30	5	5	90	60	30

[a] 5 ml of 0.01 M passive component mixed with 70 ml of buffer solution was titrated at 0° C with 0.01 M 4-X-1-naphthalenediazonium chloride.

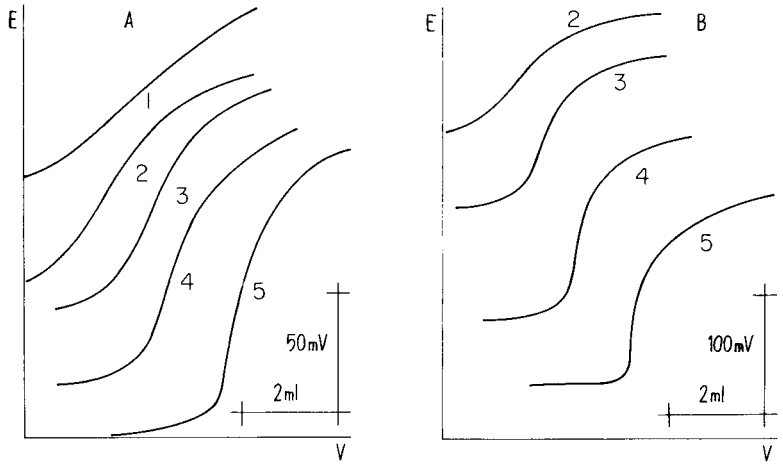

Fig. 1. Effect of pH on the shapes of titration curves: (A) 2,4-diaminotoluene with 1-naphthalenediazonium chloride; (B) 8-quinolinol with 4-bromo-1-naphthalenediazonium chloride. The sample solutions were buffered to: (1) pH 6; (2) pH 7; (3) pH 8; (4) pH 9; (5) pH 10. The curves are displaced for clarity; conditions as outlined under Experimental.

pH value in titrations of all the aromatic hydroxy compounds (phenols), but was constant in titrations of 2,4-diaminotoluene (the pH value was higher than the pK_a of the corresponding ammonium cation). The determinations were usually done at pH 10, but this pH is not universally satisfactory, especially for titrations with 4-nitro-1-naphthalenediazonium chloride, which is partially hydrolyzed to form diazotate analogously to the 4-nitrobenzenediazonium ion [8]. The results of such titrations at pH 10 suffer from significant errors. 2-Naphthol gives the best developed titration curves at pH 9 with all the diazonium salts.

Quite different dependences of the reaction time on pH were observed in titrations with the 9,10-dioxo-1-anthracenediazonium salt; the titration time was almost constant in the pH range 7—10. It is to be supposed that the 9,10-dioxo-1-anthracenediazonium cation is sufficiently electrophilic, but it appears that steric influences predetermine the reaction rate instead of polar influences. Steric factors are probably also the reason that the determination of 1-(2′,5′-dichloro-4′-sulfophenyl)-3-carboxy-5-pyrazolone is slower with 4-bromo-1-naphthalenediazonium than with 1-naphthalenediazonium titrant, and that quercetin forms a tetrakisazo compound with 1-naphthalenediazonium, but only a trisazo compound with 4-bromo-1-naphthalenediazonium cations at the appropriate pH (Fig. 2). However, titrations of 1-phenyl-3-methyl-5-pyrazolone with 9,10-dioxo-1-anthracenediazonium salt are surprisingly out of line with these considerations; the titration time is short (3 min) and the reproducibility of the end-point readings is very good (with a relative standard deviation of 0.10% compared to 1.6—2.2% in titrations of 2,4-diaminotoluene, 2-naphthol and resorcinol with the same titrant).

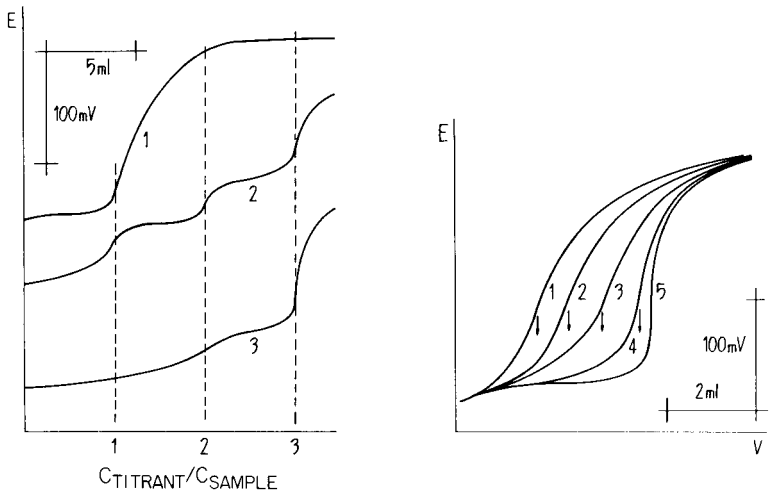

Fig. 2. Potentiometric titration curves for quercetin titrated with 4-bromo-1-naphthalenediazonium chloride at different pH values: (1) pH 8; (2) pH 9; (3) pH 10. Curve 1 shows clean formation of the monoazo compound, whereas curves 2 and 3 show the stepwise formation of a trisazo compound.

Fig. 3. Time dependence of the shape of the potentiometric titration curves for 2-naphthol titrated with 4-bromo-1-naphthalenediazonium chloride at pH 8. The potentials were read at different times: (1) 3 min after each addition of titrant; (2) 5 min after each addition of titrant; (3) after half the time needed to establish equilibrium; (4) 10 min after each titrant addition; (5) after establishment of the equilibrium potential.

It is absolutely essential to wait for as long as is needed for stabilization of the equilibrium potentials after each addition of the titrant. Figure 3 shows how the titration curves can be deformed and their inflexion points shifted when titrations are done in a hurry. This is particularly important from the standpoint of automatic titrators. For practical use, the stability of the stock solutions of the arenediazonium salt titrants is a point of significance. 4-Bromo- and 4-nitro-1-naphthalenediazonium, and even 9,10-dioxo-1-anthracenediazonium salt solutions stored in an ice box, are stable for several days and can be recommended. 4-Bromo-1-naphthalenediazonium chloride seems to be the most widely useful. This selection represents a compromise of the titrant properties mentioned above.

With regard to the indicator electrode, the membrane plasticizer is a good solvent for the azo dyes formed if they are not charged. Then the membrane becomes gradually saturated with the azo compound and the potential breaks become smaller and smaller when the titrations are repeated. In that case, the electrode membrane must be reconditioned in a suspension of the arenediazonium tetraphenylborate (this can be done during a titration of arenediazonium cation with $NaBPh_4$). When the membrane is refreshed in this way, the electrode can again be used to monitor the azo-coupling reactions.

REFERENCES

1 K. Vytřas, J. Kalous, Z. Kalábová and M. Remeš, Anal. Chim. Acta, 141 (1982) 163.
2 K. Vytřas, J. Latinák, T. Čapoun and H. Svobodová, Chem. Prum., 32 (1982) 81.
3 K. Vytřas, Collect. Czech. Chem. Commun., 42 (1977) 3168.
4 K. Vytřas, M. Remeš and H. Kubešová-Svobodová, Anal. Chim. Acta, 124 (1981) 91.
5 K. Vytřas, V. Říha and S. Kotrlý, Sb. Ved. Pr. Vys. Sk. Chemickotechnol. Pardubice, 35 (1976) 41.
6 W. Selig, Talanta, 27 (1980) 914.
7 J. B. Conant and W. D. Peterson, J. Am. Chem. Soc., 52 (1930) 1220.
8 V. Štěrba, in S. Patai (Ed.), The Chemistry of Functional Groups — The Chemistry of Diazonium and Diazo Groups Pt. 1, Ch. 2, Wiley, Chichester, p. 71, 1978.

Analytica Chimica Acta, 162 (1984) 153—159
Elsevier Science Publishers B.V., Amsterdam — Printed in The Netherlands

SOLID-STATE ELECTROCHEMICAL DETECTOR FOR CARBON MONOXIDE AT SUB-ppm CONCENTRATIONS

KUNIO NAGASHIMA* and SHIGETAKA SUZUKI

Department of Industrial Chemistry, Faculty of Technology, Tokyo Metropolitan University, Setagaya-ku, Tokyo 158 (Japan)

(Received 2nd December 1983)

SUMMARY

Carbon monoxide reacts with iodine pentoxide at 42°C to produce iodine vapor, which is detected by a solid-state electrochemical detector, essentially a Pt/AgI/Ag galvanic cell. The response begins to rise steeply 3.7 s after a 1.1-ml gas sample is introduced and reaches a maximum after a further 1.2 s. The response is linearly related to the concentration of carbon monoxide up to 2 ppm from the detection limit of 0.03 ppm. Interferences such as H_2S and C_2H_4 are removed by 5A molecular sieve; H_2 (1%), CH_4 (5%) and C_2H_6 (5%) are without effect.

Carbon monoxide is one of the most widespread poisons related to human life and activity. The common methods of determination of carbon monoxide in air are spectrophotometric [1] and dispersive or nondispersive infrared [2] methods, use of oxidation catalysts like hopcalite [3] and gas chromatography by reduction to methane [4]. The iodine pentoxide method of estimating carbon monoxide as triiodide has also been reported and has been used in several ways [4—6] to provide a sensitive means of detecting carbon monoxide. Nelson et al. [5] determined the triiodide spectrophotometrically; the method could be used to determine sub-ppm concentrations of carbon monoxide because of the reasonably large molar absorptivity of triiodide and the large volume of sample that could be handled. Other, interfering gases may also liberate iodine from iodine pentoxide, and must be removed before determination of carbon monoxide.

The present authors have developed a galvanic, solid-state detector [7] for continuous monitoring of ozone and nitrogen dioxide. The detector is a galvanic cell, essentially Pt/AgI/Ag, which has a platinum gauze as the working electrode, silver as the counter electrode and silver iodide as the solid electrolyte. The detector (13 mm diameter, 1.2 mm thick) is thermostated at 90 ± 0.1°C. When iodine vapor at 20 ml min^{-1} impinges on the platinum cathode, the current flowing in the external circuit is linearly related to the concentration of iodine vapor up to 1 ppm from the detection limit of 0.1 ppb [8]. In this paper, a sensitive but simple and inexpensive detector is described for carbon monoxide, based on the reduction of iodine pentoxide

0003-2670/84/$03.00

by carbon monoxide to iodine vapor; the iodine vapor produced is detected with the solid-state galvanic detector.

EXPERIMENTAL

Apparatus

The instrumentation consisted of the galvanic solid-state detector, thermostated detector holder (78°C), flow control system for carrier gas (15 ml min^{-1}), six-way cock for injection of sample (sample size 1.1 ml), heated iodine pentoxide reactor (42°C), external 100-kohm resistance, voltmeter and recorder. The experimental setup is shown schematically in Fig. 1.

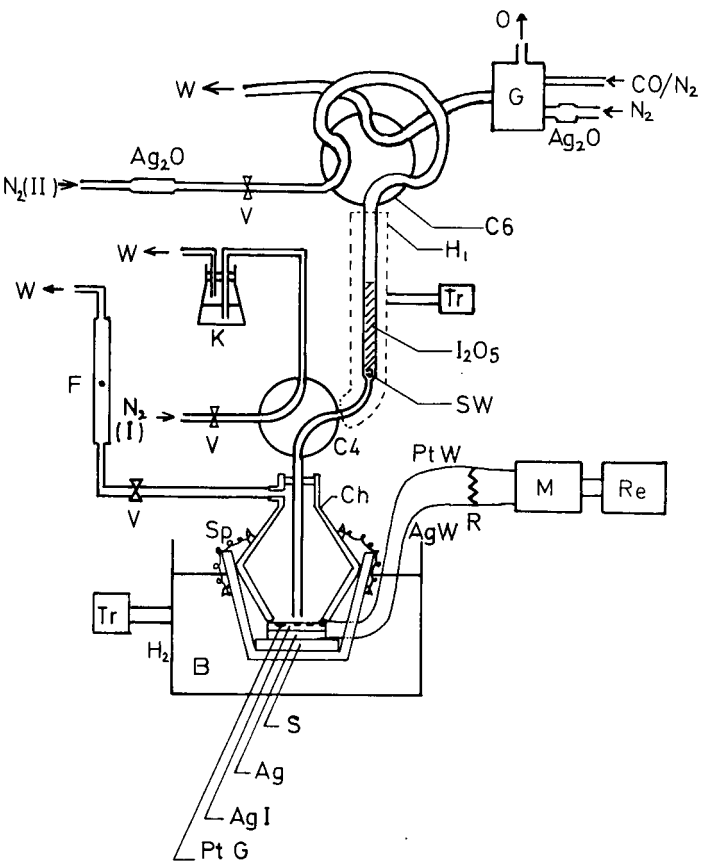

Fig. 1. Schematic diagram of gas flow system and cell assembly: (○) overflow; (G) standard CO generator; (W) waste; (C6) six-way cock; (H1) heater for I_2O_5 reactor; (V) flow control valve; (Tr) thermo-regulator; (SW) silica wool; (K) KI aqueous solution; (Ch) cell holder; (C4) four-way cock; (F) flow meter; (PtW) Pt wire; (AgW) Ag wire; (R) resistance; (M) voltmeter; (Re) recorder; (Sp) spring; (B) silicone oil bath; (H2) heater for oil bath; (S) silicone rubber; (Pt G) Pt gauze.

The construction of the cell is also shown in Fig. 1. The cell was prepared as follows [7]. The detector was constructed by using silver iodide (Kanto Chemical Co.) as the solid electrolyte. Commercial silver iodide was powdered in an agate mortar and dried under vacuum for 24 h; 1 g of silver powder was placed in a die (13 mm i.d.) and levelled off, and a pressure of 700 kg cm^{-2} was applied. Any residual silver powder on the surface of the plunger and on the inner wall of the die was removed with a clean tissue. Silver iodide powder (0.2 g) was placed on top of the silver disk. A pressure of 700 kg cm^{-2} was again applied. Finally, platinum gauze (55 mesh) was placed on the disk and again a pressure of 7000 kg cm^{-2} was applied for 15 min. The thickness of the Pt/AgI/Ag disk was about 1.2 mm. After removal from the die, about 3 mm of the platinum wire was very carefully pulled from the gauze. A pad of silicone rubber was placed in the bottom of a pyrex glass holder. A silver wire was placed on this pad and the other end of the wire was threaded through a tiny hole in the cell holder. The cell was placed on this silver wire over the pad, and the other contact was made by attaching the platinum mesh wire to a platinum wire threaded through another hole in the cell holder. The two tiny holes for these connections were sealed with silicone adhesive. The holder was held together with springs. The lower half of the cell holder was immersed in an oil bath at 78 ± 0.1°C.

Generation of carbon monoxide standards

The standard concentrations of carbon monoxide were prepared by controlling the flow rates (SGGU-72; Stec Co.) of streams of primary standard 0.508% carbon monoxide (N_2 Balance, Takachiho Co.) and nitrogen. Various concentrations of carbon monoxide (32 ppb to 10.2 ppm) were obtained by adjusting the dilution ratio. The nitrogen in a cylinder generally contains 0.2—0.5 ppm carbon monoxide as an impurity. Carbon monoxide is known to be oxidized quantitatively by silver oxide at room temperature [9]. The nitrogen used both for a reference stream (or carrier, II in Fig. 1), and for dilution of the primary carbon monoxide mixture, was passed through a column packed with granular silver oxide.

Iodine pentoxide reactor

The iodine pentoxide reactor was filled with 0.4 g of iodine pentoxide powder (ca. 100 mesh) held in by silica wool at each end. The reactor was a 4.2 cm long, 4 mm i.d. pyrex tube. After filling, the reactor was conditioned by heating at 90°C for 2 weeks and then at 42°C for 2 more days while sweeping continuously with purified nitrogen. When the reactor was not in use, nitrogen was passed at a rate of 10 ml min^{-1} through the reactor maintained at 42°C at all times.

Procedure

The nitrogen (I in Fig. 1) flowed at 15 ml min^{-1}, and the flow rate of the nitrogen (II in Fig. 1) was increased to 15 ml min^{-1} from 10 ml min^{-1}. The

temperature of the oil bath was 78° C. The baseline for the detector became constant about 1.5 h after heating began and remained constant for 10 h to within 0.4 nA. The baseline was about 3.5 nA at 78° C. The current produced by the detector was converted to a voltage via an external 100-kohm resistance, and the voltage was recorded. The nitrogen carrier gas (II) was passed through the four-way cock to the detector, which showed a response (ca. 20 nA) which was due to blank generation of iodine vapor from the iodine pentoxide. Samples (1.1 ml) were injected by changing the position of the six-way cock. The sample gas was carried through the iodine pentoxide reactor to produce iodine vapor, which impinged on the detector. The peak height was measured. When the detector was not in use, the flow rate of nitrogen (I) was 0 ml min^{-1}, that of nitrogen (II) was 10 ml min^{-1}, the latter being passed through the reactor to waste via the four-way cock. The heater for the oil bath was turned off.

RESULTS AND DISCUSSION

Iodine pentoxide/carbon monoxide reaction

The reaction of carbon monoxide with iodine pentoxide is

$$5CO + I_2O_5 \rightarrow 5CO_2 + I_2$$

The reaction proceeds rapidly at 65° C or above, but slowly at room temperature [10]. As the temperature of the reactor is increased, the extent of reaction is also increased. As the amount of iodine pentoxide in the reactor is increased, the extent of the reaction is again increased. However, as both the reaction temperature the amount of iodine pentoxide are increased, the baseline caused by iodine vapor generated by the thermal decomposition of iodine pentoxide is increased. Exposure to large amounts of iodine vapor decreases the sensitivity of the detector and shortens its lifetime. Therefore the optimum temperature and the optimum amounts of iodine pentoxide are a compromise between these two effects. The effect of the temperature of the iodine pentoxide reactor on the response is shown in Fig. 2. As the temperature of the reactor increases, the temperature of the carrier gas is increased, but above 45° C, the response is decreased because hot carrier gas decreases the adsorption efficiency for iodine vapor on the working electrode of the detector. Therefore, the optimum temperature is 42° C for a reactor containing 0.4 g of iodine pentoxide. The carrier gas, nitrogen (II), was also preheated to this temperature before introduction into the heated reactor.

Detection of iodine vapor by the galvanic cell

Iodine vapor produced from the reactor is adsorbed on the working electrode of the detector and reacts with silver ions to produce silver iodide at the three-phase contact area, I_2 (vapor)/Ag^+/Pt [11]. The reactions $I_2 + 2e^- \rightarrow 2I^-$ and $I^- + Ag^+ \rightarrow AgI$ proceed at the platinum cathode while the reaction at the silver anode is $Ag \rightarrow Ag^+ + e^-$. The activity of silver ions at the working

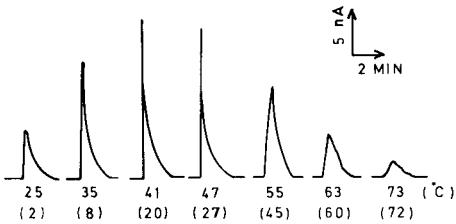

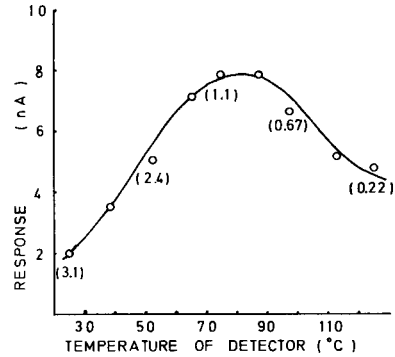

Fig. 2. Effect of temperature of iodine pentoxide reactor on response. (5.1 ppm CO, 1.1-ml sample, cell temperature 78°C. Flow rate of carrier gas 15 ml min^{-1}; the numbers in parentheses indicate the baseline current in nA.)

Fig. 3. Effect of detector temperature on response. Flow rate of carrier gas 15 ml min^{-1}, reactor temperature 42° C, 1.1 ml of 2.1 ppm CO; the numbers in parentheses indicate detector resistance in k ohm.

electrode side of the solid electrolyte becomes less than that on the opposite side. The e.m.f. of the cell is based on the difference of the silver ion activities at the two sides of the solid electrolyte layer; silver ions pass through this layer from the silver anode to the platinum cathode, and the current flowing through the external circuit is proportional to the concentration of iodine vapor.

As the detector temperature is increased, the silver ion conductivity is increased. Therefore the sensitivity of the detector to iodine vapor is proportional to the temperature [7]. But as the detector temperature is increased, the adsorption and/or reaction efficiency of iodine vapor at the three-phase contact area is decreased. Therefore the optimum detector temperature is a compromise between the two effects. The effect of temperature of the detector on the response is shown in Fig. 3. Maximum response was obtained between 70 and 86° C. Therefore it was concluded that the optimum temperature of the detector is 78° C. The detector resistance at each temperature is also shown in Fig. 3. The electrical resistance of the detector at each temperature was measured with an a.c. (1000 Hz) bridge.

Effect of carrier gas flow rate

Figure 4 shows the effect of carrier gas flow rate on the response of the detector to 4.4 ppm carbon monoxide. As the flow rate increased, the response decreased because the efficiency of the reaction between carbon monoxide and iodine pentoxide decreased, and possibly because of a decrease in the adsorption efficiency of iodine vapor at the detector. At flow rates less than 10 ml min^{-1}, it was difficult to control the flow rate with precision; the optimum flow rate was therefore taken as 15 ml min^{-1}.

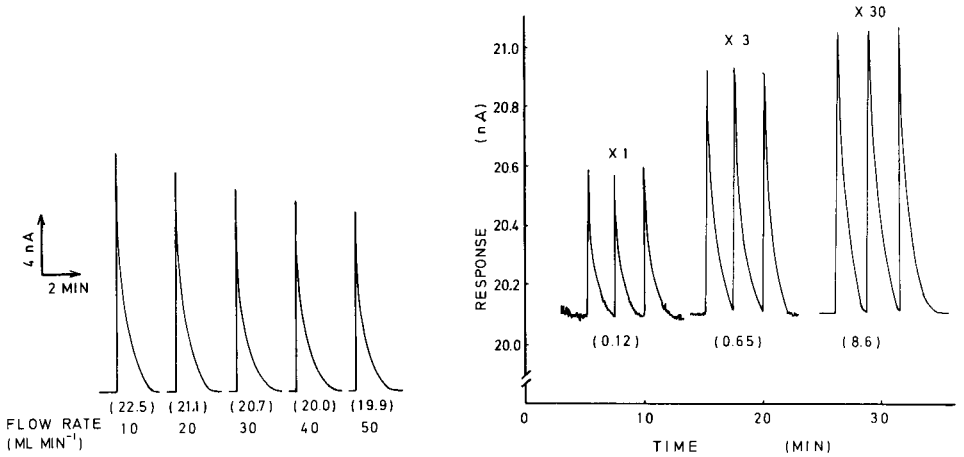

Fig. 4. Effect of carrier gas flow rate on response. Reactor temperature 42°C, detector temperature 78°C, 1.1 ml of 4.4 ppm CO; the numbers in parentheses indicate the baseline current in nA.

Fig. 5. Detector response to 1.1 ml of various concentrations of carbon monoxide. Temperatures as in Fig. 4, carrier gas flow rate 15 ml min^{-1}; the numbers in parentheses indicate the CO concentration in ppm.

Analytical performance

Typical detector responses to various concentrations of carbon monoxide at the optimum experimental conditions are shown in Fig. 5. Typically, the current begins to rise steeply 3.7 s after carbon monoxide has been introduced, and reaches a maximum after a further 1.2 s. The baseline for the detector is constant at ca. 20 nA to within 1.6 nA for 3 h. The relative standard deviations (n = 6) are 3.7% and 0.94% for 0.3 and 0.9 ppm carbon monoxide, respectively. The lowest concentration determined was 32 ppb, for which the signal-to-noise ratio was 3.6. The detection limit for carbon monoxide is therefore 30 ppb (signal:noise = 3). The relationship between concentration of carbon monoxide and detector sensitivity is shown in Table 1. The calibration graph was linear up to ca. 2 ppm. The calibration graph for iodine vapor had previously been found to be linear up to about 20 ppm, but the sensitivity to carbon monoxide began to decrease above 2 ppm, mainly because of incomplete reaction between carbon monoxide and iodine pentoxide.

TABLE 1

Relationship between concentration of carbon monoxide and detector sensitivity (experimental conditions as in Fig. 5)

Concentration of CO (ppm)	0.06	0.23	0.58	3.4	9.7
Sensitivity (na ppm^{-1})	3.9	3.8	3.8	3.5	3.3

The lifetime of the detector depended strongly on its exposure time to the iodine vapor. Under the experimental conditions used, the response decayed to ca. 10% of its original value after 30—50 h of exposure.

It is necessary to remove other reducing gases which will react with iodine pentoxide to produce iodine vapor. Hydrogen sulfide and ethylene were removed effectively by using 5A molecular sieve. Hydrogen, methane and ethane were not removed by molecular sieve 5A; therefore the detector responses to those gases were determined under the same experimental conditions as for Fig. 5. The system gave no response to 1% hydrogen, 5% methane or 5% ethane (v/v) in nitrogen.

The detector is inexpensive, small and very sensitive for reducing gases, so it should find use in gas chromatography.

REFERENCES

1 R. G. Smith, R. J. Bryan, M. Feldstein, B. Levadie, F. A. Miller, E. R. Stephens and N. G. White, Health Lab. Sci., 7 (1970) 75.
2 Methods of Air Sampling and Analysis, 2nd edn., Am. Pub. Health Assoc., Washington, DC, 1977, p. 348.
3 C. J. Bossart, Ind. Res., 1976 (1976) 96.
4 K. A. Rao, K. K. Pushpa, H. Mohan and R. M. Iyer, J. Chromatogr. Sci., 16 (1978) 306.
5 K. H. Nelson, M. D. Grimes, D. E. Smith and B. J. Heinrich, Anal. Chem., 29 (1957) 181.
6 Japanese Industrial Standards (JIS) K0515, 1976.
7 S. Suzuki and K. Nagashima, Anal. Chim. Acta, 144 (1982) 261.
8 K. Nagashima and S. Suzuki, Bunseki Kagaku, 32 (1983) 541.
9 R. C. Robbins, K. M. Borg and E. J. Robinson, Air Pollut. Control Assoc., 18 (1968) 106.
10 P. G. Stecher (Ed.), The Merck Index, 8th edn., Merck & Co. Inc, NJ, 1968, p. 570.
11 A. J. Bard (Ed.), Electroanalytical Chemistry, Vol. 6, M. Dekker, New York, 1973, p. 162.

Analytica Chimica Acta, 162 (1984) 161—173
Elsevier Science Publishers B.V., Amsterdam — Printed in The Netherlands

EVALUATION OF ELECTROCHEMICAL CHARGE-TRANSFER RATES BY USING (REAL) LAPLACE SPACE ANALYSIS

Single Potential-Step Chronoamperometry of Hexacyanoferrate(III)/(II) and Europium(III)/(II) Couples

EDWARD D. MOORHEAD*, VITAUTAS E. DAUYOTIS[a] and MICHAEL M. STEPHENS

Department of Chemical Engineering, University of Kentucky, Lexington, KY 40506-0046 (U.S.A.)

(Received 19th March 1984)

SUMMARY

The one-electron hexacyanoferrate(III)/(II) and europium(III)/(II) redox couples were evaluated by using single-pulse chronoamperometry at a planar glassy carbon electrode (and also a mercury-pool electrode for europium) to test Wijnen's method for calculating heterogeneous electron-transfer rate constants by using (real-axis) Laplace space analysis. The k^0 values obtained for the former couple in potassium or lithium chloride supporting electrolytes agreed well with published constants obtained by diverse real-time techniques. Transfer coefficients (α^0) obtained from $(\partial \ln k^a/\partial \eta)_{\eta=0}$ for LiCl electrolyte were 0.4—0.5, rather than 0.22 previously reported. The cathodic rate values calculated for europium(III) reduction (in $NaClO_4/HClO_4$) on both glassy carbon and mercury agreed very well with each other and with published values obtained by d.c. polarography and faradaic impedance measurements. Owing to several factors, including its ability to utilize virtually any set of recorded $i(t)$ data points, Wijnen's Laplace technique offers an attractive alternative to conventional single-pulse analysis in real-time.

Kinetic parameters for totally irreversible electrochemical charge-transfer reactions can readily and accurately be determined by using Tafel analyses [1], whereas moderately fast electrode processes controlled by mixed mass-transport and electron-transfer rates constitute a conceptually different problem in terms of deriving convenient expressions for the calculation of charge-transfer rates from experimentally observed data [2—6]. Thus, efforts to obtain apparent forward (k_f^a) and backward (k_b^a) rates for such processes have employed various real-time techniques based on permutations of parameters such as electrode geometry, current, potential, frequency and phase [2, 4—7]. The corresponding boundary value problems have been solved by an assortment of mathematical routes, sometimes involving expansions and/or approximations, resulting in real-time equations which often differ in

[a]Present address: Department of Chemistry, Vilnius University, Vilnius, Lithuania (U.S.S.R.).

0003-2670/84/$03.00

their exactness, or are severely restrictive and complex even for simple processes. Partially as a result of this, compiled rate parameters for a given process obtained by different techniques may vary widely for otherwise identical measurement conditions [8].

Some of the restrictions which accompany real-time rate analyses are exemplified by the nominally simple, single potential-step chronoamperometric technique [1, 4, 6]. This involves stepping (pulsing) the magnitude of the working electrode potential from a fixed value (E_1) at the foot of the S-shaped current—potential ($i - E$) curve where the faradaic current is zero to a second potential (E_2) which induces current flow (associated with either reduction or oxidation). For the case of reduction with only bulk oxidant (C_0^b) present at $t = 0$, and for a pulse amplitude $\Delta E = (E_2 - E_1)$ one first observes a current spike caused by the combined effects of double-layer charging and large surface flux, after which the current decays more or less rapidly depending on transport geometry and the rates of electron transfer. For the schematic, simple, single-step, quasi-reversible first-order reduction process $Ox + ne \underset{k_b}{\overset{k_f}{\rightleftharpoons}} Red$, a planar geometry produces a time decay of faradaic current that can be described by

$$i(t) = nFAk_f^a C_0^b \exp[Q^2 t] erfc[Qt^{1/2}] \tag{1a}$$

or by

$$i(t) = nFAk_f^a C_0^b g(Q, t) \tag{1b}$$

$$\text{where } g(Q, t) = \exp[Q^2 t] erfc[Qt^{1/2}] = g[(Q_f + Q_b), t] \tag{1c}$$

$$\text{and } Q = [k_f^a/D_0^{1/2} + k_b^a/D_r^{1/2}] \tag{1d}$$

where all terms have their usual electrochemical significance; the form of the $g(Q, t)$ function occurs frequently in electrochemical theory [1—6].

While Eqn. 1 is simplified if $Q_f \gg Q_b$, or vice versa, it can be solved conventionally for k only by expansion of $g(Q, t)$ for very short times (depending on the ratio $k/D^{1/2}$), a restriction which results in neglect of $i - t$ data that otherwise could improve the accuracy and precision for the rate constants. (Long times are usually avoided because of the small slope of the $i(t)$ curve and the uncertain onset of natural convection.) However, currents at very short times following the leading edge of the pulse necessitate experimental correction for contributions from double-layer charging, instrument and cell time constants, etc. [1, 2, 6, 9—11]; also, during this time interval, transport occurs exclusively by semi-infinite linear diffusion regardless of the actual shape of the working electrode [6], and hence geometry effects cannot be discerned.

In recent studies of solid cylindrical electrodes [12—14], it was desirable to be able to measure rate parameters quickly, precisely and for a wide range of k, time, radius, Q, etc. For this task, the method of (Real) Laplace Space Analysis (RLSA) originated in 1960 by Wijnen [15] was chosen for

evaluation. The literature revealed no cases in which the RLSA method had been critically applied to working electrochemical systems. Hence, it was decided to test the validity of the method by using planar electrodes and two mechanistically simple 1-electron transfer reactions, viz., the europium and hexacyanoferrate couples, for which real-time data exist.

THEORY

That one can, in principle, bypass the formal applicational restraints of Eqn. 1 was suggested in 1960 by Wijnen [15], and reviews and extensions of Wijnen's approach were later published by Pilla [9], and more recently in a lucid account by MacDonald [6]. Neither these nor other workers have carefully examined the real-axis technique for actual systems. Wijnen recognized that while Eqn. 1 and similar expressions satisfy the intrinsic need to relate observed current, i.e., $i(t)$, to "real time", the concessions attached to its practical use render it inconvenient for measuring electron-transfer rates, which he suggested is most efficiently done in Laplace (or frequency) space itself. This can be accomplished by transforming recorded chronoamperometric $i(t)$ data according to

$$\bar{i}(p) = \int_0^\infty i(t) \exp(-pt)\mathrm{d}t \tag{2}$$

to obtain the Laplace current $\bar{i}(p)$. (This integral converges if the time change in $i(t)$ is less than $\exp(-pt)$, a condition satisfied by most electrochemical $i(t)$ functions.) The Laplace variable p must be a positive real or complex number. In the RLSA method, real rather than complex values of p are used, and k values are obtained from $\bar{i}(p)$ vs. p real-axis analysis, whereby $\bar{i}(p)$ retains its real-time relationship to k and D. (Imaginary-axis analysis is also possible, but this is tantamount to single-sided Fourier transformation [9].)

To implement the transform to Laplace space, one first chooses a fixed real p. Afterwards, the recorded i at time t is multiplied by $\exp(-pt)$ to yield a product L. A plot of L vs. t for each i yields an area $S = \bar{i}(p)$. At this point, a table of results would show one area (S) for the chosen value of p; moreover, it would embody the fact that S reflects all the recorded $i(t)$ data that were chosen, and that no additional experimental data are required to obtain k. By iterating the above procedure over a selected range of increasing p values, one obtains a table of $\bar{i}(p)$ (areas) vs. p; by rearranging the Laplace transform of Eqn. 2, one obtains [6] (for the forward process) the following dependence for planar diffusion

$$[1/\bar{i}(p)p^{1/2}] = [nFA(k_f^a/Q)C_0^b]^{-1} + [nFAk_f^aC_0^b]^{-1}(p^{1/2}) \tag{3}$$

Equation 3 embodies the simplifying construction of a linear dependence of $[1/\bar{i}(p)p^{1/2}]$ on $p^{1/2}$, with the resulting plot providing k_f^a from the slope and D_0 from the intercept (for $Q_f \gg Q_b$), both obtained from a single potential

pulse and all, or any practical portion, of the resulting real-time $i - t$ decay curve.

The aim of the present study was to assess the ability of the RLSA method to obtain kinetic parameters precisely and rapidly. For simplification, planar diffusion was used and the classic one-electron transfer associated with the hexacyanoferrate(III)/(II) and europium(III)/(II) couples were selected for study. Their rates reportedly differ by a factor of about 10, and their constituents are fairly immune to aqueous supporting electrolyte composition; moreover, the reductions occur at potentials positive and negative relative to Ag/AgCl as reference.

EXPERIMENTAL

Stock and test solutions were prepared with water double-distilled from tin, then distilled twice more, once from acidic permanganate, and then neat. Reagent-grade potassium salts of hexacyanoferrate(III) and hexacyanoferrate(II) were used as received. Because of its storage instability, lithium hexacyanoferrate(III) was initially prepared by passing the potassium analog through a thoroughly pre-washed column of Bio-Rad AG-50W-X12 ion-exchange beads previously converted to the lithium form with concentrated lithium chloride. Aliquots of the effluent were vacuum-dried to straw-colored crystals and stored in vacuo protected from light. Portions were weighed as needed and introduced directly into the pre-purified and degassed cell solution. Current/time curves for such solutions displayed unacceptable scatter near $t = 0$, a problem possibly derived from resin-associated debris which may have served to catalyze self-decomposition of lithium hexacyanoferrate(III) as discussed by Peter et al. [16]. To circumvent this, results for the $Li_3Fe(CN)_6/Li_4Fe(CN)_6$ system were obtained by adding millimolar levels of potassium hexacyanoferrate(III) or hexacyanoferrate(II) to 1 M solutions of lithium chloride as supporting electrolyte. The other materials used were of reagent grade or better.

Additionally, all supporting electrolytes were potentiostatically pre-purified under nitrogen. These 4-h pre-purifications were done in a custom-built cell (Kontes Glass). Aliquots of prepared electrolyte were pipeted into a water-jacketed (25 ± 0.1°C) 3-electrode measurement cell (Metrohm EA 876-20), followed by addition of the redox salt itself, plus final degassing to remove residual oxygen.

The cell was controlled by a custom-built, 3-electrode operational amplifier-based potentiostat which housed a digital PC board for generation of the potential pulse, the amplitude and period of which could be controlled by two panel-mounted 10-turn potentiometers. The pulse was derived from three cascaded 555 IC timer chips, two of which were used to "debounce" the momentary trigger switch. The 555 chip combination controlled a CMOS 4066 digital switch which applied the chosen potential step to a summing point resistor connected to the potential control amplifier of the potentiostat.

The glassy carbon electrode (GCE) was constructed from a cylindrical plug of glassy carbon epoxy-mounted flush with the end of a glass tube. The GCE surface was treated to a mirror finish by rotary polishing on soft tissue paper soaked with laboratory detergent, followed by dry polishing with soft paper tissue. The GCE used for the hexacyanoferrate measurements was 0.0856 cm^2 in area, while that used for europium measurements was 0.230 cm^2. The mercury electrode used for several comparative europium studies consisted of a mercury-filled glass U-tube with arms of length 13.5 cm and 2.5 cm (internal diameter 3.5 mm). When immersed in electrolyte, the hemiellipsoidal dome of mercury projecting from the short arm of the U-tube was 0.562 cm^2 in area.

The fairly fast decay of charging current, ca. 0.95 ms, associated with the supporting electrolyte alone, as well as the slower decay recorded during the reaction were either captured by computer (Cromemco CS-2) via an integral multichannel 12-bit A/D converter (California Data Systems), or captured by the 4 kbyte memory of a Nicolet 2090 12-bit precision digital storage scope with floppy disk storage. The digital expansion capabilities of the storage scope enabled automatic subtraction of the two signals to produce corrected input to a FORTRAN data analysis program. The use of a sampling time delay (t_d) eliminated the traditional need to measure and correct for surface charging separately; subtracted background was due mostly to instrument noise.

The silver/silver chloride/saturated sodium chloride reference electrode (Ag/AgCl) used for rate measurements was calibrated by using it as a reference electrode to obtain an ordinary polarogram for reduction of thallium(I) to the amalgam from 0.1 M sodium nitrate; that $E_{1/2}$ = −0.460 V vs. the saturated calomel electrode (SCE) for this reaction is well established [17].

RESULTS AND DISCUSSION

As mentioned previously, the RLSA offered a rather attractive possibility for obtaining precise electrochemical rate parameters not only because of its speed but also because all data contribute to k, not just those recorded at short times.

Pilla [9] has thoroughly discussed the problems which result from the fact that a working electrode can never experience a perfectly rectangular potential pulse because of instrumentation and double-layer time constants. He advocated that rates should be analyzed via an impedance function derived from Laplace transform of both the effective $E - t$ pulse and the resulting $i - t$ decay. However, digitizing fast, $E - t$ pulses with sufficient sampling frequency to yield a 10—12 bit precision Laplace transform would appear to be costly and instrumentation-intensive.

There are theoretical grounds [15] for believing that the faradaic $i(t)$ function near $t = 0$ should, in Laplace space, be a simple extension of the $i(t)$ data recorded for longer times. Accordingly, the procedure adopted here

did not correct for, but simply ignored, current/time behavior at very short times; i.e., no effort was made to correct for surface charging. This was accomplished by introducing a sample acquisition time delay t_d (ca. 2.0 ms) after application of the ΔE pulse (442 ms) to accommodate charging of the double layer, circuit ringing, etc. Starting precisely at t_d, $i(t)$ data were captured over a fairly large $i(t)$ data window, Δt, of 440 ms at an adjustable A/D sample rate. This window yielded sufficient data, though an arbitrarily longer Δt could have been chosen, short of the onset of natural convection.

Because the integration of Eqn. 2 must logically commence at zero time, it was necessary to obtain an accurate value of $i(t)$ at $t = 0$ which, in turn, required extrapolation backward (i.e., upward) from t_d over an interval varying in width between 0.5 to 2.0 ms using a function $i(t)_{ext}$. It was recognized that the extent of the error [11] introduced by this procedure would depend on the particular ratio $k/D^{1/2}$. The choice of $i(t)_{ext}$ was guided by recognition that backward extrapolation of $1/\bar{i}(p)p^{1/2}$ vs. $p^{1/2}$ must yield D as intercept (assuming neglect of the backward term Q_b). Both an exponential function and a quadratic function of the general type $i(t)_{ext} = a + bt + ct^2$, were evaluated for this purpose and produced rate parameters differing by only a few tenths of a percent. The latter function was chosen because it produced D values essentially congruent with literature values for both the hexacyanoferrate and europium systems tested. An expanded version of Eqn. 1(a) could have been used, but any successful arbitrary function would be suitable.

In assessing the results, it was necessary to adhere to some guidelines in selecting the p parameter to assure reasonable accuracy and precision. Because, in development of the RLSA expressions, k and $(pD)^{1/2}$ occur together in ratios, sums, etc. [6], p values should be chosen such that these two quantities are about the same order of magnitude, for otherwise the error in k can become large [11]. Secondly, p should be "neither too large nor too small". For large p, $\exp(-pt)$ could possibly be sufficiently small that the $L(t)$ vs. t function (see above) would converge to zero virtually instantly subtending a very small, inaccurately measurable area and intercept. Overly small p values, in contrast, result in slow convergence and an area S at the end of the time period which falls short of the true area; a longer time period would of course more truly approximate this area, but this risks the onset of natural convection.

The hexacyanoferrate(III)/hexacyanoferrate(II) system

Reduction of potassium hexacyanoferrate(III) in 1.0 M KCl. Values (Table 1) were obtained for k_f^a and (k_f^a/Q) for reduction of hexacyanoferrate-(III) for five applied potentials and hexacyanoferrate(III) concentrations of 2.0, 4.0, and 6.0 × 10^{-3} M (in 1.0 M KCl). Each set of rate parameters was obtained from a negative-going potential pulse which started at +0.490 V vs. Ag/AgCl, i.e., in advance of the foot of the reduction wave. As expected, the rate values increased with increase in E_{app}, and were only slightly affected by

TABLE 1

Potential and concentration dependence of the electron transfer rate constant (k_f^a) and $(k_f^a/Q)^2$ ratio for reduction of potassium hexacyanoferrate(III) in 1.0 M KCl supporting electrolyte[a]

E_{app} [b,c]	Hexacyanoferrate(III) concentration, C_0^b (10^{-3} M)					
	2.0		4.0		6.0	
	k_f^a [d]	$(k_f^a/Q)^2$ [e]	k_f^a [d]	$(k_f^a/Q)^2$ [e]	k_f^a [d]	$(k_f^a/Q)^2$ [e]
0.260	0.760	2.98	0.790	2.74	0.660	3.11
0.230	1.27	5.55	1.20	5.44	1.12	5.91
0.200	1.94	7.52	1.89	7.11	1.74	7.67
0.170	3.11	8.01	2.78	8.10	2.77	8.23
0.140	5.03	8.12	4.37	8.26	4.50	8.66

[a]Planar, glassy carbon electrode (A = 8.56 × 10^{-2} cm^2). [b]Potential in V vs. Ag/AgCl. Negative-going potential pulse applied from +0.490 V vs. Ag/AgCl. [c]$E^{0'}$[$Fe(CN)_6^{3-}$/$Fe(CN)_6^{4-}$] = +0.273 V vs. Ag/AgCl. [d]In units of 10^{-2} cm s^{-1}. [e]In units of 10^{-6} cm^2 s^{-1}.

the increase of C_0^b. Predictably, the ratio k_f^a/Q proved to be substantially dependent on E_{app} near the foot of the voltammogram; i.e., for small potential perturbations the ratio reflects a contribution from k_b^a/Q_b. For $E_{app} \leqslant$ +0.170 V vs. Ag/AgCl, viz., in the region of negligible backward rate, k_f^a/Q is essentially insensitive to changing E_{app}. For each concentration, the potential dependence of ln k_f^a proved linear with a correlation coefficient $r \geqslant 0.999$ which correlated with a one-electron process with kinetics following the usual Butler—Volmer expression [6].

Combining data for all three concentrations yielded an intercept (at $E^{0'}$ = 0.273 V vs. Ag/AgCl), slope, and r value of 3.60, —15.0 and 0.994. Transforming these results to E^0 vs. NHE yielded $k_f^0 = 6.16 \times 10^{-3}$ cm s^{-1} and α_c^0 = 0.39.

Oxidation of hexacyanoferrate(II) in 1.0 M KCl. Oxidation of hexacyanoferrate(II) at the GCE was studied in a reverse experiment symmetrical to the one described above. The k_b^a rate data shown in Table 2 were obtained for four hexacyanoferrate(II) concentrations of 2.0, 4.0, 6.0 and 8.0 × 10^{-3} M, respectively. The positive-going potential step in this case commenced at +0.040 V vs. Ag/AgCl. Processing of the lumped ln k_b^a vs. E_{app} data yielded intercept, slope, and r equal, respectively, to —6.04, 20.2, and 0.990, from which one calculates $k_b^0 = 5.98 \times 10^{-3}$ cm s^{-1}, and α_a^0 = 0.52.

Electron transfer in 1.0 M LiCl. Peter et al. [16—18] studied the extent to which heavy alkali metal cations catalyze the hexacyanoferrate(III)/(II) charge transfer, an effect which increases with cation atomic number. Because there is only a small difference in rates between the K^+ and Li^+ forms of the redox couple, a comparison of the k^0 values offered a test of the RLSA approach.

TABLE 2

Potential and concentration dependence of the electron transfer rate constant (k_b^a) and $(k_b^a/Q)^2$ ratio for oxidation of potassium hexacyanoferrate(II) in 1.0 M KCl supporting electrolyte[a]

E_{app}[b]	Hexacyanoferrate(II) concentration, C_R^b (10^{-3} M)							
	2.0		4.0		6.0		8.0	
	k_b^a[c]	$(k_b^a/Q)^2$[d]	k_b^a[c]	$(k_b^a/Q)^2$[d]	k_b^a[c]	$(k_b^a/Q)^2$[d]	k_b^a[c]	$(k_b^a/Q)^2$[d]
0.270	0.61	1.32	0.56	1.37	0.55	1.39	0.54	1.42
0.300	1.21	3.31	1.06	3.25	1.00	3.43	1.04	3.33
0.330	1.93	5.40	1.89	5.04	1.60	5.52	1.53	5.49
0.360	3.91	6.41	4.01	6.44	3.34	6.65	3.36	6.50
0.390	9.79	6.93	11.60	6.92	8.46	7.11	—	—

[a]Glassy carbon electrode (A = 8.56 × 10^{-2} cm^2). [b]Potential in V vs. Ag/AgCl. [c]In units of 10^{-2} cm s^{-1}. [d]In units of 10^{-6} cm^2 s^{-1}.

Moreover, Müller and Dietzsch [19] recently studied this couple in lithium chloride, using potentiodynamic voltammetry at a rotating pyrographite electrode, and confined their attention to the Tafel region, viz., a potential window extending from η = 100 mV to η = 150 mV either side of E^0. Their study of ln i vs. η for the anodic and cathodic branches produced four points (see Fig. 1 [19]) which were then fitted to straight lines and extrapolated to η = 0. From the line slopes, the authors calculated an unexpectedly low value of 0.22 for both the anodic (α_a^0) and cathodic (α_c^0) transfer coefficients, a result which was potentially significant from our point of view because it could imply a less than straightforward one-electron transfer mechanism in the Tafel region. Müller and Dietzsch asserted [19, 20] that the $Fe(CN)_6^{3-}$/$Fe(CN)_6^{4-}$ one-electron exchange occurs via two "partial transfers" of charge.

Müller and Dietzsch's study was exactly repeated using RLSA-processed data; measurements were confined to the same Tafel range, and again a value of exactly 0.22 was obtained for both α_a^0 and α_b^0. Because in both cases a long extrapolation to η = 0 was employed, it was decided to use the RLSA method to collect rate data closer to η = 0 (i.e., closer to E^0). The resulting ln k^a (not ln i) vs. η plot exhibited considerable curvature in the anodic and cathodic regions close to η = 0. These data were found to fit the quadratic equation ln $k^a = C_0 + C_1\eta + C_2\eta^2$ with high correlation. This enabled the rate constants to be measured and also the α^0 values from the derivative evaluated at η = 0. The α values so obtained were in better agreement with expectation (see below).

Reduction of hexacyanoferrate(III) in 1.0 M LiCl. Measurements of k_f^a vs. E_{app} were done for each of four lithium hexacyanoferrate(III) concentrations (2.5, 5.0, 7.5, and 10.0 × 10^{-3} M, see Experimental). The quadratic equation mentioned in the preceding discussion was used to fit the combined body of results with a correlation coefficient r = 0.999. The resulting equation

TABLE 3

Potential and concentration dependence of the electron transfer rate constant (k_f^a) and $(k_f^a/Q)^2$ ratio for reduction of potassium hexacyanoferrate(III) in 1.0 M LiCl supporting electrolyte[a]

E_{app} [b]	Hexacyanoferrate(III) concentration, C_o^b (10^{-3} M)							
	2.50		5.0		7.5		10.0	
	k_f^a [c]	$(k_f^a/Q)^2$ [d]	k_f^a [c]	$(k_f^a/Q)^2$ [d]	k_f^a [c]	$(k_f^a/Q)^2$ [d]	k_f^a [c]	$(k_f^a/Q)^2$ [d]
0.260	1.23	1.00	1.22	0.82	1.23	0.70	1.21	0.79
0.230	2.19	2.01	2.13	1.83	2.04	1.95	2.03	2.07
0.200	3.43	3.39	3.30	3.57	3.24	3.37	3.21	3.58
0.170	4.96	5.28	5.02	4.88	4.74	4.82	4.85	4.91
0.140	7.23	5.94	7.21	5.66	6.99	5.62	7.01	5.79
0.110	10.16	6.38	10.39	6.21	10.14	6.18	9.97	6.40

[a]Supporting electrolyte pre-electrolyzed at −1.50 V vs. Ag/AgCl. Glassy carbon electrode (A = 8.56 × 10^{-2} cm²) as in Table 1. [b]Potential in V vs. Ag/AgCl. All potential steps commenced at +0.500 V vs. Ag/AgCl. [c]In units of 10^{-3} cm s^{-1}. [d]In units of 10^{-6} cm² s^{-1}.

parameters (three significant figures) were found to be: C_0 = −3.76, C_1 = −5.02 and C_2 = −24.1. Table 3 lists the rate data which yield k_f^0 = 1.2 × 10^{-3} cm s^{-1}, with α_c^0 = 0.46.

Oxidation of hexacyanoferrate(II) in 1.0 M LiCl. Measurement of the electron transfer rate for oxidation of lithium hexacyanoferrate(II) at the GCE mirrored the above procedures used for the potassium salt with the exception that an anodic pulse was imposed on the GCE. The data again agreed with a quadratic expression with a correlation r = 0.999; the coefficients for the equation were: C_0 = −12.1, C_1 = +26.9 and C_2 = −18.7. The k_b^0 value was calculated (Table 4) to be 1.9 × 10^{-3} cm s^{-1}, with α_a^0 = 0.44.

Any attempt to explain why transfer coefficients obtained in the Tafel region equal 0.22, whether measured by Müller and Dietzsch's technique [19, 20] or the single-pulse method used here, is beyond the goal of the present paper.

The europium(III)/europium(II) system

Reduction of europium(III) in 1.0 M $NaClO_4$/0.1 M $HClO_4$ media at the GCE. While the RLSA method produced rate parameters for the hexacyanoferrate(III)/(II) couple in good agreement with those obtained by other authors [8] using various real-time methods and different electrodes, a further test of the method was desirable using a chemically different but still uncomplicated one-electron redox system. For this purpose, the Eu(III)/Eu(II) half-reaction was selected for the following reasons [21, 22]: (1) k_f^0 and k_b^0 are reportedly [8, 21–24] smaller than for the hexacyanoferrate(III)/(II) couple by about one order of magnitude; (2) E^0 for the Eu(III)/Eu(II) couple in acidified perchlorate media places it in an accessible range of

TABLE 4

Potential and concentration dependence of the electron transfer rate constant (k_b^a) and $(k_b^a/Q)^2$ ratio for oxidation of potassium hexacyanoferrate(II) in 1.0 M LiCl supporting electrolyte[a]

E_{app}[b]	Hexacyanoferrate(II) concentration, C_R^b (10^{-3} M)							
	2.50		5.00		7.50		10.0	
	k_b^a[c]	$[k_b^a/Q]^2$[d]	k_b^a[c]	$[k_b^a/Q]^2$[d]	k_b^a[c]	$[k_b^a/Q]^2$[d]	k_b^a[c]	$[k_b^a/Q]^2$[d]
0.260	1.75	1.31	1.82	0.99	1.75	1.12	1.74	1.09
0.290	3.25	2.31	2.96	2.64	2.95	2.85	2.92	2.76
0.320	4.87	3.86	4.82	3.89	4.66	4.15	4.62	4.23
0.350	7.69	4.61	7.02	5.09	7.09	5.06	6.87	5.33
0.380	10.85	5.27	10.31	5.55	10.48	5.47	10.14	5.78
0.410	16.05	5.38	15.79	5.60	16.24	5.51	15.17	5.88

[a] All results were obtained using pre-electrolyzed supporting electrolytes, the separate $i - t$ decay values of which were subtracted from reaction data. [b] All positive-going potential pulses commenced at +0.030 V. All potentials given as V vs. Ag/AgCl. [c] In units of 10^{-3} cm s^{-1}. [d] In units of 10^{-6} cm^2 s^{-1}.

potentials virtually free of proton reduction, and (3) the solvated Eu(III) and Eu(II) mononuclear cations are similar in structure and not strongly prone to hydrolyze, and exhibit weak tendencies to complex with simple anions.

The variation of k_f^a with E_{app} for reduction of Eu(III) in sodium perchlorate/perchloric acid media was measured for 2.54, 5.04, and 7.61 × 10^{-3} M europium perchlorate with the results shown in Table 5. The 442-ms cathodic potential pulses which in this case commenced at −0.350 V vs. Ag/AgCl yielded ln k_f^a vs. E_{app} plots which were linear for each concentration, though the data were slightly more scattered than for the hexacyanoferrate system. A least-squares treatment of the combined data yielded slope, intercept, and r equal, respectively, to −11.4, −18.1 and −0.954, from which k_f^0 = 3.06 × 10^{-4} cm s^{-1}, and α_c^0 = 0.47 were calculated.

Reduction of europium(III) from 1.0 M $NaClO_4$/0.1 M $HClO_4$ at a stationary mercury electrode. In determining the rate parameters for reduction of europium(III) at the GCE, slow, single sweep voltammograms revealed the presence of a small faradaic component near the europium step ($E^{0'}$ = −0.690 V vs. Ag/AgCl) which was identified with proton reduction. Correction for these background proton currents was a part of the usual calculational procedure (see above), but the possible electrochemical rate effects of concurrent surface removal of protons were not definable. Raising the pH to effect a negative shift of proton reduction was judged risky because of europium(III) hydrolysis. Because europium(III) is reduced at −0.430 V vs. NHE, the use of a small mercury pool electrode (see Experimental) with its larger hydrogen overpotential permitted the circumvention of proton interference. The general measurement procedures (including pre-electrolysis) used with

TABLE 5

Cathodic electron transfer rate constant (k_f^a) for reduction of Eu(III) to Eu(II) in 1.0 M $NaClO_4$/0.1 M $HClO_4$ [a]

E_{app} [b]	Values of k_f^a (10^{-4} cm s^{-1}) for various Eu(III) concs. (10^{-3} M)		
	2.54	5.04	7.61
−0.600	—	0.582	0.476
−0.630	—	0.955	0.924
−0.660	2.112	1.505	1.404
−0.690	3.362	2.585	—
−0.720	4.970	3.944	—
−0.750	11.42	7.391	—

[a] Glassy carbon electrode (A = 0.23 cm^2). Four-hour pre-electrolysis of supporting electrolyte at −1.10 V vs. Ag/AgCl. [b] All potentials in V vs. Ag/AgCl. All potential pulses commenced at −0.350 V.

the GCE were followed; however, the mercury electrode provided the added advantage of an easily renewable, clean surface.

Charge-transfer rate data were obtained for three europium perchlorate concentrations (2.69, 9.24 and 13.6 × 10^{-3} M). As in the case with the GCE, the ln k_f^a vs. E_{app} results showed some scatter because of the lower currents (k values) involved, and this was especially noticeable at the lowest concentration (2.69 × 10^{-3} M). This is partly due to the fact that, for both the GCE and mercury electrode, instrument noise itself constitutes a fairly large fraction of the baseline and reaction signals toward the end of the pulse, and obtaining an accurate difference between the two is thus more difficult. A regression analysis of the combined ensemble of data produced a slope, intercept, and r equal to −13.8, −21.46 and −0.975, respectively. The results given in Table 6 yielded k_f^0 = 2.70 × 10^{-4} cm s^{-1} and α_c^0 = 0.55, which agree moderately well with the parameters obtained with the GCE (see above). They are in close agreement (mercury electrode) with similar raw data (i.e., no Frumkin or activity corrections) yielding k_f^0 = 2.5 ± 0.5 × 10^{-4} cm s^{-1}, α_c^0 = 0.60 for 1.0 M $NaClO_4$/pH 3 solutions obtained by Timmer et al. [23] using d.c. polarography, and with k_f^0 = 2.9 ± 0.05 × 10^{-4} cm s^{-1}, α_c^0 = 0.59 obtained [24] from separate impedance measurements, also using the mercury electrode.

CONCLUSIONS

Wijnen's 1960 data analysis technique [15] for the calculation of electrochemical rate parameters in real-axis Laplace space was evaluated in its planar diffusion form using digitally captured, computer-analyzed $i(t)$ data from single potential pulse chronoamperograms obtained for the one-electron Eu(III)/Eu(II) couple in sodium perchlorate/perchloric acid solutions and for

TABLE 6

Variation of k_f^a for Eu(III) reduction from 1.0 M $HClO_4$ at a stationary Hg electrode[a]

E_{app}[b]	Values of k_f^a (10^{-4} cm s^{-1}) for various Eu(III) concs. (10^{-3} M)		
	2.69	9.24	13.64
−0.630	—	—	0.70
−0.660	—	1.49	—
−0.670	1.58	—	—
−0.690	3.33	2.21	2.57
−0.710	6.70	—	—
−0.720	—	4.97	4.62
−0.750	9.07	10.5	8.44

[a]Hg pool electrode (A = 0.562 cm^2). Four-hour pre-electrolysis of supporting electrolyte at −0.950 V vs. Ag/AgCl. [b]All potentials in V vs. Ag/AgCl. Potential pulses applied starting at −0.350 V.

TABLE 7

Summary of kinetic parameters for (K^+, Li^+) hexacyanoferrate(III)/(II) and europium-(III/(II) couples

Electroactive component	Rate constant (cm s^{-1})		Transfer coefficient		Standard rate constant (cm s^{-1})	Standard exchange current density[a] (A cm^{-2})
	k_f^0	k_b^0	α_c^0	α_a^0	k_s^0	o_i
$K_3Fe(CN)_6$[b]	6.16×10^{-3}		0.39		6.07×10^{-3}	5.86×10^{-1}
$K_4Fe(CN)_6$[b]		5.98×10^{-3}		0.52		
$Li_3Fe(CN)_6$[c]	1.20×10^{-3}		0.46		1.55×10^{-3}	1.50×10^{-1}
$Li_4Fe(CN)_6$[c]		1.90×10^{-3}		0.44		
Eu(III)[d]	3.06×10^{-4}	—	0.47		—	2.95×10^{-2}
Eu(III)[c]	2.70×10^{-4}	—	0.55		—	2.61×10^{-2}

[a]Calculated from $o_i = nFC^b k_s^0$ (see [8]); or k_f^0 in the case of Eu(III). [b]1.0 M KCl supporting electrolyte. [c]1.0 M LiCl supporting electrolyte. [d]1.0 M $NaClO_4$/0.1 M $HClO_4$ supporting electrolyte. Stationary glassy carbon electrode (A = 0.230 cm^2). [e]Hg-pool electrode, hemi-ellipsoidal (A = 0.562 cm^2); 1 M $NaClO_4$/1.0 M $HClO_4$ supporting electrolyte.

the hexacyanoferrate(III)/(II) couple in neutral LiCl and KCl solutions. The fairly large 442-ms pulse widths allowed collection and utilization of a larger number of data points than is conventionally possible by using the short-time expanded form of the corresponding real-time equations (Eqns. 1). Because the linear RLSA approach offers the possibility of utilizing all of the faradaic $i - t$ decay, double-layer charging currents near $t = 0$ were ignored. The resulting raw k^0, α, and ^0i values uncorrected for double-layer ϕ_2 potentials or activities are summarized in Table 7. The present RLSA-obtained rate parameters for both couples agreed well with real-time measurements obtained by others [8] using a variety of techniques and electrodes, and for the hexacyanoferrate system correctly reflected, on the one hand, Müller and

Dietzsch's [19, 20] predicted alkali cation catalytic rate enhancement of K^+ over Li^+, and on the other hand, the as-yet unresolved low values of α obtained in the Tafel region.

We gratefully acknowledge the National Science Foundation (ENG 7725654), the University of Kentucky Research Foundation, and the IREX Exchange Scholar Program (1982/1983) for providing financial support in aid of this research.

REFERENCES

1 J. O'M. Bockris and A. K. N. Reddy, Modern Electrochemistry, Vol. 2, Plenum/Rosetta, New York, 1970.
2 P. Delahay, New Instrumental Methods in Electrochemistry, Interscience Publishers, New York, 1954.
3 K. J. Vetter, Electrochemical Kinetics, Academic Press, New York, 1967.
4 R. N. Adams, Electrochemistry at Solid Electrodes, M. Dekker, New York, 1969.
5 H. R. Thirsk and J. A. Harrison, A Guide to the Study of Electrode Kinetics, Academic Press, New York, 1972.
6 D. D. MacDonald, Transient Techniques in Electrochemistry, Plenum Press, New York, 1977.
7 D. T. Sawyer and J. L. Roberts, Jr., Experimental Electrochemistry for Chemists, Wiley-Interscience, New York, 1974.
8 R. Tamamushi, Kinetic Parameters of Electrode Reactions of Metallic Compounds, Butterworths, London, 1975.
9 A. A. Pilla, in J. S. Matteson, H. B. Mark, Jr. and H. C. MacDonald, Jr. (Eds.), Computers in Chemistry and Instrumentation, Ch. 6, M. Dekker, New York, 1972.
10 Information Chemistry: Computer Assisted Chemical Research and Design. S. Fujiwara and H. Mark (Eds.), University of Tokyo Press, Tokyo, 1975, pp. 181—193.
11 W. Lorentz and K. D. Schulze, J. Electroanal. Chem., 65 (1975) 141.
12 E. D. Moorhead, M. M. Stephens and G. A. Bhat, Anal. Lett., 13 (1980) 167.
13 E. D. Moorhead, G. A. Bhat and M. M. Stephens, J. Chem. Technol. Biotechnol., 31 (1981) 259.
14 E. D. Moorhead, M. M. Stephens and G. A. Bhat, Anal. Lett., 14 (1981) 219.
15 M. D. Wijnen, Rec. Trav. Chim., 79 (1960) 1203.
16 L. M. Peter, W. Dürr, P. Bindra and H. Gerischer, J. Electroanal. Chem., 71 (1976) 31.
17 I. M. Kolthoff and J. J. Lingane, Polarography, Vol. 2, Interscience Publishers, New York, 1952.
18 P. Bindra, H. Gerischer and L. M. Peter, J. Electroanal. Chem., 57 (1974) 435.
19 L. Müller and S. Dietzsch, J. Electroanal. Chem., 121 (1980) 255.
20 L. Müller, J. Electroanal. Chem., 101 (1979) 363.
21 S. P. Sinha, Europium, Springer-Verlag, Berlin, 1967.
22 Encyclopedia of Electrochemistry of the Elements, Vol. 6, A. J. Bard (Ed.), M. Dekker, New York, 1976, pp. 33—62.
23 B. Timmer, M. Sluyters-Rehbach and J. H. Sluyters, J. Electroanal. Chem., 14 (1967) 181; see also the early results of L. Gierst and R. Cornelissen, Coll. Czech. Chem. Commun., 25 (1960) 3004.
24 C. W. Kreuk, M. Sluyters-Rehbach and J. H. Sluyters, J. Electroanal. Chem., 28 (1970) 391.

Analytica Chimica Acta, 162 (1984) 175—187
Elsevier Science Publishers B.V., Amsterdam — Printed in The Netherlands

A SWEPT-POTENTIAL ELECTROCHEMICAL DETECTOR FOR FLOW STREAMS

PATRICIA A. REARDON, GERALD E. O'BRIEN and PETER E. STURROCK*
School of Chemistry, Georgia Institute of Technology, Atlanta, GA 30332 (U.S.A.)
(Received 26th March 1984)

SUMMARY

An instrument has been designed, constructed, and evaluated for electrochemical measurements in flow streams. The instrument is basically a computer-controlled potentiostat with features which are necessary for measurements in flow streams. These features include real-time graphics display, rapid transfer of data to disk storage, automated compensation for IR drop, and automated d.c. current offset. The instrument can be programmed to operate in several modes, but the primary mode of operation is rapid-sweep square-wave voltammetry. Programs are available for post-run processing of the data and display of any desired voltammogram or current vs. time plot. Any alphanumeric or graphics display can be copied on a dot-matrix printer. Performance evaluations in unstirred solutions indicate limits of detection of less than 1×10^{-9} M in favorable cases.

This is the second in a series of papers concerning the design and applications of a swept-potential electrochemical detector. This paper discusses the capabilities of the instrument and the basic design of the hardware and software. The advantages of the detector were illustrated in the first paper [1] which dealt with application to the chromatography of a mixture of nitrophenols.

The purpose of the instrument is to obtain voltammograms, with high sensitivity, from a flow stream such as in high-performance liquid chromatography (h.p.l.c.), flow injection systems or ion chromatography. A detector suitable for these applications must be able to acquire voltammograms at a high repetition rate and with enough points that eluted samples are adequately defined on both the potential and time axes. The large volume of data generated at high repetition rates must be stored so that the data can be retrieved and processed numerically and figures generated after the run. A visual display of data during the experiment is essential for the operator to monitor performance of both the detector and the flow stream. The primary mode of operation is square-wave voltammetry. However, other modes of operation, such as stair-case voltammetry, may be indicated in some cases, and the instrument must be flexible enough to accommodate these alternative modes.

0003-2670/84/$03.00

The above requirements dictate a potentiostat controlled by a programmable computer with disk storage and graphics capability. The fundamental questions in designing such an instrument have to do with the distribution of logic capability and the assignment of tasks to the various logic centers. If a single processor is required to handle all the timing, control, data acquisition, data storage, and data display, it can do so only at a relatively slow rate. Some instruments [2] simplify the problem by limiting the amount of data to the size of the available memory and by limiting the display to post-run mode. Others [3] use a slave microprocessor to handle the timing, control, and data acquisition. The approach used in this work was to design a "smart" potentiostat with considerable logic capability, but not including a microprocessor. In addition, a bit-mapped graphics terminal, including a second processor, is used for display. Figure 1 is a block diagram showing the major components of the detector system connected to a simple chromatograph. Once an experiment is started with this system, the central computer has only to supply the potentiostat with the next potential, accept the current value from the potentiostat, and send the current value to the disk controller and graphics terminal. The result is an instrument that can operate with a square wave of up to 500 Hz until over 125 000 points have been taken.

For rapid pulse-type experiments in solutions of high resistance, such as are often encountered in h.p.l.c., a means of IR compensation is essential. For reproducibility, the adjustment of this compensation should be done automatically by the instrument, rather than by operator estimation. Therefore, the instrument requires the capability to measure the actual cell resistance and set the IR compensation accordingly. One method [2] uses measurements of current versus time following a potential pulse in a region with no faradaic current. Although the present instrument can be programmed to use this method, it normally uses an alternative method in which a potential pulse is made to a region where faradaic current will flow. The current

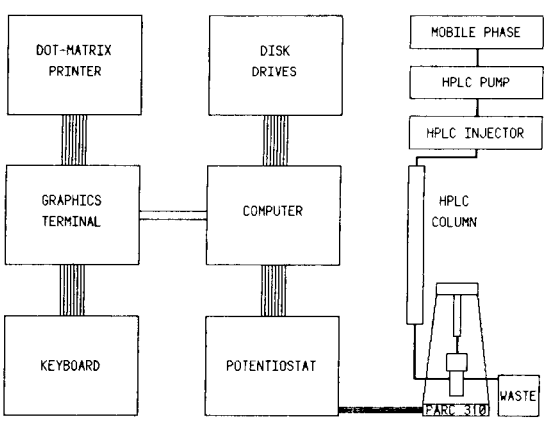

Fig. 1. Block diagram of detector system connected to simple chromatograph.

and potential are measured at a set time after the potential pulse. Then the current is interrupted and the potential measured again. The cell resistance is calculated from these three measurements.

EXPERIMENTAL

Hardware

The following description of the various components is intended to afford the reader with a basic understanding of the design and operation of the instrument. If a reader needs more detail than is provided here, the authors will be pleased to provide it on request.

Computer. After surveying the microcomputers available commercially, it was decided to capitalize on past experience and use an updated version of a laboratory computer designed and constructed in these laboratories. Although this entailed considerable effort, the advantages were that the system could be tailored to our needs, and the intimate knowledge of the hardware and software gained makes it simple to modify either if necessary. Finally, maintenance is easier, thus reducing instrument down time. The computer is named LAMPS II for Laboratory Applications MicroProcessor System, Model II.

The LAMPS II uses a Z80A processor operating at 4 MHz. The single-board computer has 64 kbytes of random access memory (RAM), 2 kbytes of EPROM, a 16-bit programmable real-time clock, a 60-Hz clock, 4 general-purpose parallel I/O ports, 2 EIA-RS232 serial I/O ports, and a controller for two 5.25-in., double-sided, double-density, floppy-disk drives. Two direct memory access (DMA) channels are provided. One channel is used by the disk controller while the other channel is available to the user. An expansion bus is also available.

Graphics terminal. The graphics terminal is based on a second Z80A microprocessor with 64 kbytes of RAM and 8 kbytes of EPROM on a single board. A 12-in. long-persistence green-screen CRT (Dotronix BHD 1200) is fed a composite video signal of 12.5 MHz. The keyboard (Cherry CB 12-AA) has full upper/lower case letters, numerical keypad, and 24 programmable keys. Baud rate is selectable from 300 to 19 200. Separate RAM buffers are used for alphanumerics and graphics. The graphics display is bit mapped and has 481 pixels vertically and 640 pixels horizontally. Alpha graphics and a graphics cursor are also provided. The terminal has an EIA-RS232 port for connection to the computer and a parallel output port for connection to a dot-matrix printer with graphics capability. Either an IDS 460G Paper Tiger or Prism-80 printer is used.

Potentiostat. The potentiostat requires the LAMPS II for operation. Because no user controls are available on the potentiostat, all parameters are controlled by the computer, including cell potential generation, current-to-voltage converter scale factor, positive feedback for IR compensation, direct current offset, timing, and operating modes. In addition, the computer can

zero the control amplifier, determine the uncompensated cell resistance, and control the PARC-310 electrode stand via the potentiostat.

Figure 2 is a simplified diagram of the potentiostat. The configuration of the analog circuits is conventional. The reference electrode (RE) is connected to a voltage follower (A1); the control amplifier (A2), in an adder circuit, drives the counter electrode (CE). The working electrode (WE) is connected to the summing point of the current-to-voltage converter (A3), which is followed by an inverting amplifier (A4) to increase the magnitude of the current signal. As in previous instruments constructed in this laboratory [4], the final stage in the analog current-signal path is a gated integrator (A6) which amplifies the signal and serves to filter out high-frequency noise. The current-to-voltage converter has three gain settings, selected by relays controlled by the computer. The gain of the inverting amplifier (A4) is set by an 8-bit digital-to-analog converter (DAC 4) controlled by the computer. Gain is selectable in a binary sequence from 1 to 256. The combined relative gain of A3 and A4 is selectable in a binary sequence from 1 to 16,384, and the absolute sensitivity ranges from 1.638 mA to 0.10 μA per volt. These values are augmented by the gated integrator (A6) which has a time constant of 1 ms.

Positive feedback for IR compensation is controlled in 10-Ω increments by an 8-bit DAC (DAC 3) between the output of the current to voltage converter (A3) and the summing point of the control amplifier (A2). This signal is adjusted by a noninverting amplifier (A5), or an associated resistance and switching network, to maintain a constant calibration regardless of the gain setting of A3. The current-interrupt switch (S3) is operated at the same time as S1, which connects a feedback loop around the control amplifier to maintain its voltage output while the counter electrode is isolated.

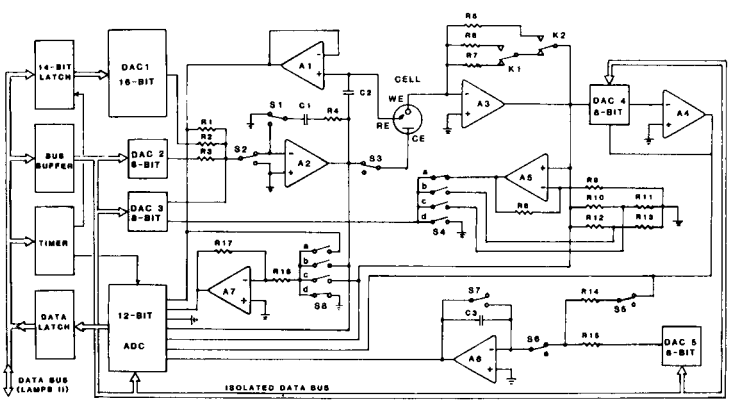

Fig. 2. Simplified diagram of potentiostat. Amplifiers A1—A3, AD381LH; amplifiers A4—A6, AD544LH; amplifier A7, ADOP07EH. DAC 1, DAC72-COB-V; DAC 2—DAC 5, AD7524LN; ADC, AD572AD. Multiplexer, AD362K. See text for details of operation.

The cell potential is set via a 16-bit DAC (DAC 1). The two least significant bits are set to 0, leaving 14 bits selectable. The effective range of cell potential is ±4.096 V in 0.50 mV steps. An additional 8-bit DAC (DAC 2) is provided to compensate for any offset in the control amplifier.

Analog signals from the potentiostat are selected and converted to digital by an 8-channel analog multiplexer and a 12-bit ADC. The multiplexer can select the outputs of amplifiers A1 through A4 and A6. A gain-of-16 inverting amplifier (A7) can also be selected. The input of A7 can be switched between amplifiers A1 through A3. This capability is used in zeroing A2 and in precise measurements of the uncompensated cell resistance. The ADC is usually set to a 5-V range, but a 20-V range can also be selected. Using the 5-V range, the resolution is 1.22 mV per step.

The potentiostat also contains considerable timing and control logic, which minimizes the work of the computer. In spite of the close relationship between the potentiostat and the computer, no time-critical operations are required of the computer during data acquisition for square-wave voltammetry. Three 16-bit timers (in an Intel 8253 module) provide time delays during the square-wave cycles. Each counter is operated as a digital oneshot with the count decremented by a 1-MHz clock when the channel is enabled. When the count reaches zero, the channel is disabled and the potentiostat hardware starts the next timer channel. Timer channel 0 determines the time between potential change and the start of current integration. Timer channel 1 determines the time between the start of integration and the start of conversion to digital. Timer channel 2 determines the post-integration delay which must be at least 10 μs. The summation of the three times determines the square-wave half-cycle time.

The potentiostat can be operated in a single-cycle mode, or more commonly in an autocycle mode. (Here, one cycle refers to the operations in one-half of a square-wave cycle.) In the autocycle mode, a new cycle is started whenever timer channel 2 reaches zero, until a stop command is issued by the computer. In this mode, the computer must update the input latch (two bytes) of DAC 1 with the next potential and acquire the current output (two bytes) of the ADC from the previous cycle at some time during each half cycle. Double buffering is used with both the 14-bit DAC 1 and the 12-bit ADC. This arrangement allows a new cycle to start while data from the previous conversion are being transferred. Any one of three methods can be used to transfer ADC data from the potentiostat to the computer: polled operation, input interrupts, or DMA transfer.

The potentiostat interfaces to the computer via Z80A parallel I/O ports. One port is operated in bidirectional mode and is used to transfer data to and from the potentiostat. A second port is operated in bit mode with four bits for input and four bits for output. The output bits define the register of the potentiostat which will receive the data output by the computer. The input bits indicate status of the PARC-310, current or voltage limit, data error (not read in time and the latch cleared), and data available. User

programs need only load interrupt vectors in the control ports for the bidirectional port and enable interrupts when required. Interrupts are not available from the bit-mode port.

An internal bus is used to set the various parameters such as gain, IR compensation, current offset, and control amplifier zero. After these parameters have been set, the internal bus is grounded, thereby minimizing digital noise in the analog portions of the potentiostat.

PARC-310 electrode stand. A PARC-310 electrode stand and flow cell are used when the detector is used for reduction reactions. The stand is modified slightly for operation with the potentiostat. These modifications are transparent when used with other PARC equipment and consist of sense lines for indicator lights on the potentiostat front panel to indicate stir, purge, dislodge and dispense. In addition, a relay is installed to switch the 5-V line to a back panel connector so that the 5-V supply in the potentiostat is used rather than the 15-V supply. The reference electrode signal is routed directly to the potentiostat rather than through the voltage follower in the PARC-310 stand. A modified valve seat described previously [5] can be used, although the new model capillary is satisfactory for most cases.

Chromatographic equipment. The standard chromatographic equipment was described previously [1].

Software

The software used with the detector system consists of a number of separate programs ranging from those resident in the EPROMs of the computer and graphics terminal, through the disk operating system, the instrument control and data acquisition programs, maintenance programs, to the programs written in BASIC or FORTRAN for processing and display of the acquired data. Program listings are not included in this paper but will be provided by the authors on request.

Computer resident program. The computer resident program (RPG) is stored in the 2-K EPROM of the computer. The RPG serves to initialize the computer and to establish communication with the terminal and also allows access to any address in RAM and to all of the computer registers and ports. This capability is extremely important when tracing problems in either hardware or software. A modified version of RPG can be installed in the terminal for evaluation of hardware problems.

Terminal resident program. The terminal resident program (TRPG) is much more extensive than the RPG, using 6-K of EPROM. In addition to initialization and communication functions, TRPG also contains the routines for storage and display of alphanumerics, graphics, alpha graphics, and graphics cursor. The TRPG also includes a screen-dump routine by which a graphics display on the CRT can be copied on the printer/plotter.

The terminal can be operated in the alphanumeric or graphics mode. A keyboard switch allows toggling between the two modes which can also be selected programmatically. In addition, a split-screen mode, selected

programmatically, displays 12 lines of alphanumerics on the lower third of the CRT screen and graphics on the upper two thirds.

In alphanumeric mode, 37 lines of 80 characters are displayed on the CRT. The buffer for alphanumerics has two bytes for each screen location. One byte is used for the ASCII code of the character and the other byte is used for attributes such as intensity, underscoring, blinking, and positive or negative video. Scrolling and a cursor are provided.

The protocol for graphics display is similar to that of a Tektronix 4010. Usually, *XY* values are passed in a four-byte sequence: Hi*Y*, Lo*Y*, Hi*X*, Lo*X*. Shorter sequences are possible if some of the bytes are unchanged from the previous point. Positive values between 0 and 1023 are accepted. However, only 0 to 480 vertically and 0 to 639 horizontally are displayed. Individual points may be displayed or straight lines can be drawn between successive points.

Alphagraphics are generated from a table of offset values referenced to the lower-left corner of the character cell. Larger characters (2X and 4X standard) can be selected. Character positions can be input as absolute values on the 481 by 640 grid or derived from the location of the graphics cursor.

Disk operating system. The disk operating system (LITE) is similar to CP/M. An operator familiar with CP/M would have no trouble in using the system to load and run programs, transfer data files, etc. The disks are formatted with 253 kbytes of user space on each double-sided, double-density disk. In addition, the operating system can be stored on each disk. The disk heads are not loaded unless the disk is being accessed. The drive motor stops if the disk has not been accessed for 10 s. These features minimize wear on the disks and heads and decrease the chance of damage to the disk files from power transients.

Control and data acquisition. Several versions of the control and data acquisition program have been written in Z80 assembly language, one for each mode of operation of the instrument, such as square-wave voltammetry with the PARC-310 (POLAR), or with a solid electrode cell (OXIDTN), or triangular sweep voltammetry (CPOLAR), etc. These programs are modular in nature and the differences between the various programs are minor. New versions can be generated quickly as needed and stored on a floppy disk. The programs have a foreground section for interaction with the potentiostat and a background section for interaction with the disk drives and graphics terminal. The foreground and background are linked by interrupt service routines.

When the program is loaded and started by the disk operating system, a menu of parameters, allowable ranges of each parameter, and default values are displayed on the CRT. Figure 3 is an example of the parameter display. Parameters may be changed in any sequence by keyboard entries, or parameters from a previous run can be loaded from the parameter file of the previous run.

After entry of a file name, the setup routine is entered. The setup routine checks to see that each parameter is within the allowable limits, that there is

```
Feb. 17, 1984

Item Parameter                Range                  Selected

F    File Name  X10
R    Remark  1 X 10-6 M PB & CD
     Created

0    Initial Potential        +- 4000 mV             -  170 mV
1    Pulse Size               +-  100 mV             -   60 mV
2    Step Size                +-   25 mV             -    5 mV
3    Number of Steps            1-255                  81

4    Drop Settle Delay        2-32000 msec            400 msec
5    1st Sweep Delay            0-18 min                0 min
6    Number of Sweeps           0-1200                 25

7    Pre-Integration Time     20-65000 micro-sec      1000 micro-sec
8    Integration Time         2-65000 micro-sec      15647 micro-sec

     Current Gain             1-16384                  512
     Auto Offset                                         0
     IR Compensation   @  +     0 mV,  0% Comp  -        0 ohms

Commands:
     Item#,Value         To Select Values for above Items
     A,Y/N               Auto-Offset (Yes or No)
     C,+-mV,n            IR Compensate @ mV and "n"%
     M,n                 Manual IR Compensate, "n" ohms
     P,name              Parameters from file "name"
     U,@                 Up Gain x2, "@" times
     D,@                 Decrease Gain x2, "@" times
     S                   Setup and Await Signal
Cmd>
```

Fig. 3. Example of parameter selection menu from instrument CRT.

sufficient disk space for the new files, and creates the parameter file and data file. The setup routine also downloads all necessary parameters to the potentiostat. If requested, the cell resistance and direct current are measured and the compensation circuits set. The system then waits for a keyboard entry to initiate the experiment. At any time prior to initiation, the setup routine can be exited and parameters changed.

Upon initiation of the experiment, the foreground routine is activated and the terminal switches to the split-screen mode with a simplified parameter display on the bottom third of the CRT. Experimental data appear as acquired on the upper part of the CRT in the form of a 3D-type display. In this display, one vertical pixel is equivalent to 16 ADC levels. Each voltammogram is offset from the previous one by one pixel horizontally and vertically. When any part of the display reaches the upper limit of the CRT screen, the screen is cleared and the display continues from that point, starting at the bottom of the graphics display area. The display helps the operator to evaluate system performance but does not provide the detail available during post-run work-up of the data.

The experiment terminates at the end of the last programmed voltammogram or at the end of the voltammogram during which an ESC is entered on the keyboard. At this time the potentiostat is switched to standby and the files are closed. If desired, the display remaining in the graphics buffer can be dumped to the printer/plotter at this time.

During the setup routine, all of the potential values for the voltammogram(s) are calculated and stored in a RAM buffer. The initial potential is then loaded into the potentiostat DAC. On experiment initiation, the next potential value is loaded into the potentiostat DAC latch and the interrupt vector set. The computer can then return to the background routine until the potentiostat interrupt signifies that a current value is ready. The computer

transfers the current value to a RAM buffer and updates the potentiostat DAC latch before resetting the interrupt vector and returning to background again. In the background routine, the computer transfers current values (or calculates and transfers difference-current values) to the disk file and to the graphics terminal. When the last current value for the voltammogram is acquired, the initial potential is reset in the potentiostat and the next voltammogram can be started or the experiment terminated. If the potentiostat is at current or voltage limit at the end of a voltammogram, the experiment is terminated and an error message appears on the CRT.

Maintenance program. The DP82 TEST is a menu-driven diagnostic program for the potentiostat and the LAMPS II I/O channels. It also provides hardware configuration control and display required for potentiostat calibration.

Post-run processing. Programs for post-run processing and display are written in BASIC because it is easy to develop and evaluate ideas in an interactive language and because real-time operations are unnecessary. Future plans call for the use of FORTRAN, which should execute more rapidly. A program, SEEVOLTA, obtains and displays any desired voltammogram from the data file; SEECHROM does the same for any constant-potential chromatogram, and SEE3D displays all data in a region bounded by specified potentials and voltammograms. A program, SEEDC, calculates and displays a pseudo-d.c. chromatogram by adding the points in a voltammogram between specified potential limits and SEEAV calculates and displays the average of multiple voltammograms. A program AVCHROM does the same for multiple constant-potential chromatograms and SUBVOLTA allows the subtraction of one voltammogram (e.g., a baseline) from another.

These programs obtain the number of voltammograms and number of points in each voltammogram by accessing the parameter file. Except for SEE3D, the display may be set to full scale vertically via an autorange routine or the desired scaling may be specified after the vertical range of the data has been reported by the program. The graphics cursor is used to obtain X and Y values, scaled appropriately. Routines are also available for smoothing (11-point sliding box) or integrating the area below the displayed curve and between cursor points. Any display may be labeled with alpha graphics and dumped to the printer/plotter.

The location and quantification of peaks in a swept-potential chromatogram might proceed as follows, although shortcuts are often possible. First, SEEDC is run and the cursor is used to identify the voltammograms of each peak. Then SEEVOLTA is used to examine each of these voltammograms and the cursor is used to obtain the potentials of each peak. If necessary, SUBVOLTA can be used at this step. Finally, constant-potential chromatograms are displayed, via SEECHROM, for each peak, and the cursor or autoranging report is used to quantify the peak heights. Of course, the entire procedure could be combined in one automated sequence. However, at this stage in the development of the detector system, interaction with an operator is highly desirable.

RESULTS AND DISCUSSION

Voltammetry in unstirred solution

A series of experiments was run to demonstrate the performance of the instrument for voltammetry in unstirred solutions. Figure 4 shows a set of twenty-five voltammograms of micromolar concentrations of lead and cadmium. No filtering, smoothing or averaging was used on the curves shown in this figure. The peak currents have relative standard deviations of 0.3%, indicating satisfactory reproducibility of the mercury-drop surface area.

Figure 5 shows the average of ten voltammograms of copper, lead, and cadmium, which can be directly compared with Fig. 7 of reference [6], which shows an average of thirty voltammograms. In the present work, the voltammograms appear to have less noise and the baseline is significantly lower. Probably these improvements can be attributed to three factors: lower resistance in the PARC electrode capillary as compared to a DME capillary, initiation of current sampling with a shorter delay after potential change, and the use of a gated integrator as a sampling device to increase the magnitude of the signal as compared to the electronic noise level. Yarnitzky et al. [7] described another instrument to which comparison can be made. Their instrument shows improved signal-to-noise ratio over that of the earlier instrument [6], but is restricted to square-wave voltammetry at a slowly-growing DME with a fixed set of pulse parameters.

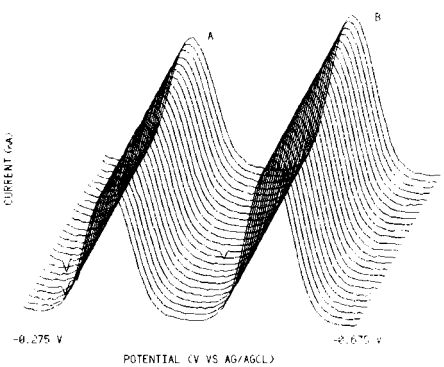

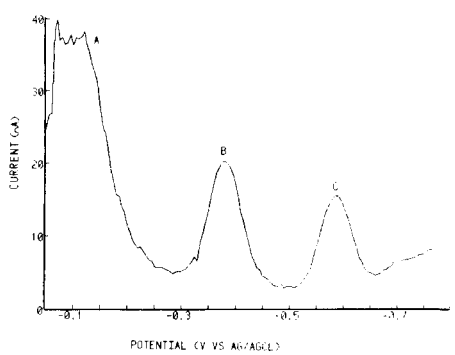

Fig. 4. Square-wave voltammetry: A, 1.0×10^{-6} M Pb^{2+}; B, 1.2×10^{-6} M Cd^{2+} in 0.1 M KNO_3. Square wave is 60 mV at 30 Hz. Step size is −5 mV. Potential range from −0.275 to −0.675 V vs. Ag/AgCl. Each voltammogram was run on a new medium-sized drop of the PARC-310 electrode stand.

Fig. 5. Square-wave voltammetry of 2.2×10^{-7} M Cu^{2+}, 2.4×10^{-7} M Pb^{2+}, and 2.1×10^{-7} M Cd^{2+} in 0.1 M HCl. Medium-sized drop on PARC-303 electrode stand. Average of 10 voltammograms with 60-mV, 30-Hz square waves and −5-mV steps. No positive feedback or filtering. Delay of 2.0 ms between pulse application and start of current integration.

The importance of short time delays between pulse application and current sampling was discussed earlier [4]. The effect can be seen in Fig. 6. Only when current sampling was initiated at less than 1 ms did the baseline increase substantially. Even then, the increased faradaic response prevented a serious deterioration in signal-to-noise ratio. Of course, such early sampling is feasible only with a low resistance cell unless the resistance is compensated by a positive-feedback loop. The effect of positive feedback can be seen in Fig. 7. The application of 50-Ω feedback resulted in oscillation. Figure 8 shows a comparison of a voltammogram with a 4-ms sampling delay and no positive feedback with a voltammogram having 500-μs delay and 40-Ω positive feedback. Most commercial instruments use fixed sampling delays of 33 to 50 ms, a truly excessive time, which leads to great loss of sensitivity and increases the time for obtaining the voltammogram.

Limits of detection can be estimated in various ways. The usual calculation is based on twice the standard deviation of the baseline. In this case, however, a base surface rather than a baseline is available, and the standard deviation can be examined in either axis of that surface, with or without averaging and/or filtering. Figure 9 shows the results when sets of ten baselines and ten voltammograms are averaged and smoothed with a digital filter. One method of calculation uses only the ten unfiltered voltammograms. The standard deviation for the current at one potential is calculated for the ten voltammograms. Selecting potentials on each side of and between the two peaks, limits of detection of 6.0×10^{-8} and 8.0×10^{-9} M were calculated for lead and cadmium, respectively. Instead of using single points for current, it is possible to average four adjacent current values centered on the points selected before. When these averaged values are processed for the set of ten voltammograms,

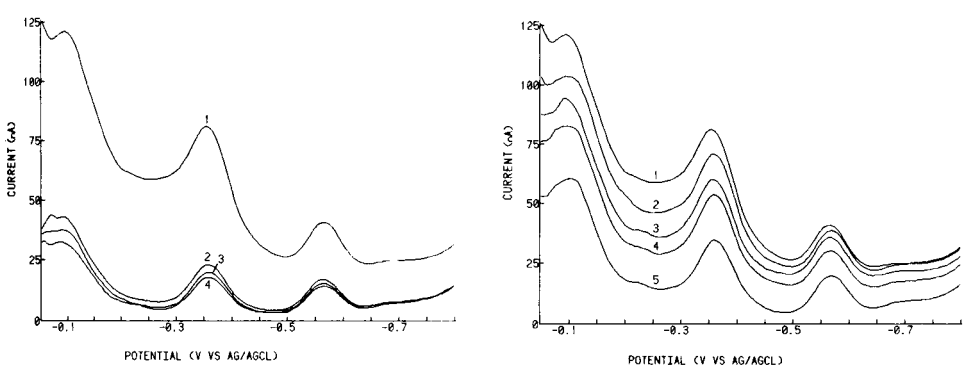

Fig. 6. Variation of pre-integration delay time: curve 1, 0.5 ms; curve 2, 1.0 ms; curve 3, 2.0 ms; curve 4, 4.0 ms. Solution and cell as in Fig. 5. Each curve is the average of 10 voltammograms smoothed by 11-point digital filter.

Fig. 7. Variation of positive feedback: curve 1, 0 Ω; curve 2, 10 Ω; curve 3, 20 Ω; curve 4, 30 Ω; curve 5, 40 Ω. Pre-integration delay was 0.5 ms. Solution, cell and processing as in Fig. 6.

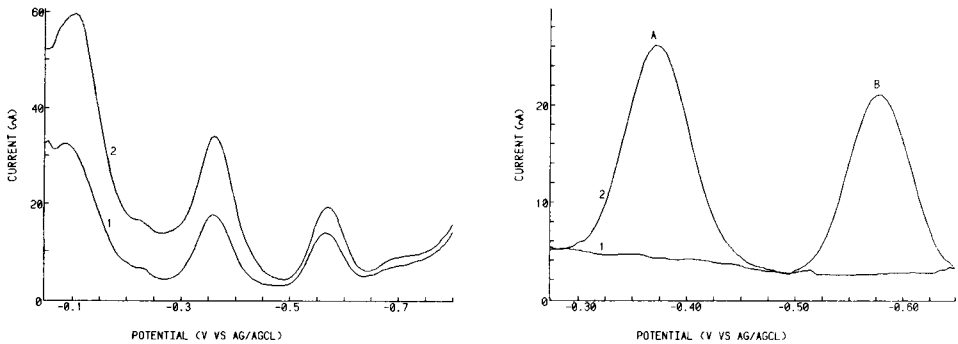

Fig. 8. Comparison of pre-integration delay and positive feedback: curve 1, 4.0 ms delay and 0 Ω feedback; curve 2, 0.5 ms delay and 40 Ω feedback. Solution, cell, and processing as in Fig. 6.

Fig. 9. Square-wave voltammetry of 0.1 M HCl (curve 1) and 2.4×10^{-7} M Pb^{2+} and 2.1×10^{-7} M Cd^{2+} in 0.1 M HCl (curve 2). Average of 10 voltammograms with 60-mV, 30-Hz square wave and −5-mV steps with no positive feedback. Curves smoothed with 11-point digital filter. Large-sized drop on PARC-303 electrode stand.

limits of detection of 8.5 and 4.4×10^{-9} M are calculated. Still lower limits of detection are calculated if the averaged and smoothed baseline (Fig. 9) is used for comparison to the peak height. Taking five values from the smoothed baseline directly under each peak and treating them as sets of replicates, 3.6×10^{-9} and 9.0×10^{-10} M are calculated as limits of detection for lead and cadmium.

Voltammetry in a flow cell

Applications of the swept-potential detector to h.p.l.c. have been reported [1]. In that work, the detector was used for reduction reactions with a PARC-310 flow cell. Work is continuing on applications to several types of compounds and future papers will deal with applications to oxidation reactions using a wall-jet cell and to a flow-injection system. A point of interest is the variation in current as a function of solution flow rate. Samuelsson and Osteryoung [8] reported that with the PARC-310 cell, no significant increase in current was observed until the flow rate was increased above about 1 ml min^{-1}. Their experiments were with differential pulse at a fixed base potential. We have observed the same response behavior with swept-potential square-wave voltammetry, extending the range of flow rates up to 5 ml min^{-1} with large drops, 6 ml min^{-1} with medium drops, and 7 ml min^{-1} with small drops.

In contrast to the present results and those of Samuelsson and Osteryoung [8], Lloyd [9] indicated a significant increase in current response as the flow rate is increased from 0.2 to 0.4 ml min^{-1}. The reason for this difference is not certain, but it can probably be attributed [10] to the thicker diffusion layer associated with the d.c. technique used by Lloyd or to the distortion of the drop area as the flow rate is changed [9]. While no increase in pulse

response was observed here at flow rates below 1 ml min^{-1}, an increase in d.c. current was observed because of oxygen in the flow stream at flow rates as low as 0.1 ml min^{-1}. In our early experiments, steel tubing was used all the way from the pump to the detector cell as suggested by Lloyd [9]. However, considerable electronic noise was found with this configuration. When the steel tubing was grounded, it acted as an electrode and introduced changes in the detector response. For this reason, steel tubing is now used up to the injection port of the PARC-310 stand and teflon tubing from that point to the cell body. Nitrogen from the purge system of the PARC-310 flows around the teflon tubing and prevents oxygen absorption.

This work was supported by Cooperative Agreement CR-808565 between the School of Chemistry of the Georgia Institute of Technology and the Analytical Chemistry Branch of the Environmental Research Laboratory, United States Environmental Protection Agency. The instrument described in this paper is subject to pending patent.

REFERENCES

1 J. Scanlon, P. Flaquer, G. Robinson, G. O'Brien and P. Sturrock, Anal. Chim. Acta, 158 (1984) 169.
2 P. He, J. Avery and L. Faulkner, Anal. Chem., 54 (1982) 1313A.
3 P. Baecklund and R. Danielsson, Anal. Chim. Acta, 154 (1983) 61.
4 P. Sturrock and R. Carter, CRC Crit. Rev. Anal. Chem., 5 (1975) 201.
5 P. Sturrock and K. Williams, Anal. Chem., 54 (1982) 2629.
6 J. Turner, J. Christie, M. Vukovic and R. Osteryoung, Anal. Chem., 49 (1977) 1904.
7 C. Yarnitzky, R. Osteryoung and J. Osteryoung, Anal. Chem., 52 (1980) 1174.
8 R. Samuelsson and J. Osteryoung, Anal. Chim. Acta, 123 (1981) 97.
9 J. B. F. Lloyd, Anal. Chim. Acta, 154 (1983) 121.
10 J. Osteryoung, private communication.

Analytica Chimica Acta, 162 (1984) 189—196
Elsevier Science Publishers B.V., Amsterdam — Printed in The Netherlands

THEORETICAL AND EXPERIMENTAL ASPECTS OF THE RESPONSE OF STRIPPING VOLTAMMETRY IN FLOW INJECTION SYSTEMS

JOSEPH WANG* and HOWARD D. DEWALD
Department of Chemistry, New Mexico State University, Las Cruces, NM 88003 (U.S.A.)
(Received 13th February 1984)

SUMMARY

The coupling of stripping voltammetry with flow injection systems offers significant advantages over conventional stripping methods. Equations solved for conventional stripping voltammetry, with steady-state deposition current, are not applicable to flow injection systems. Theoretical equations for the peak current under flow injection conditions are derived. As the total charge passed during the deposition step, $\int i\,dt$, is independent of the shape of the sample plug, the stripping peak current is independent of the degree of dispersion. As a result, precise control of the dispersion or deposition period may not be required. The peak current is predicted to be directly proportional to the sample volume. Experimental results are incorporated to support the theoretical conclusions. The effects of experimental variables such as flow rate, length of tubing, deposition period, or sample volume are presented using cadmium ion as test species.

Stripping voltammetry is a very useful technique for determining heavy metals [1—3]. Increased use of the technique is due to its ability to determine several metals simultaneously at concentration levels ranging down to the fractional parts-per-billion range with relatively inexpensive instrumentation. Recent work [4—7] has indicated that significant advantages are obtained by combining anodic stripping measurements with the manifold of flow injection systems. In flow injection systems, a small volume of the sample is introduced into an unsegmented carrier stream [8, 9]. The injected sample forms a zone that disperses on its way to the detector. Besides the obvious advantages of enhanced sample throughput, small sample volumes, and simplicity that characterize flow injection systems, their coupling with stripping voltammetry offers versatility in performing certain stripping procedures. For example, the manifold of a stripping voltammetry/flow injection system possesses the characteristics of the medium-exchange method [4—6]. In this case, the deposition occurs while the sample is flowing through the detector, and the stripping (measurement) step is effected after the sample volume has passed the detector. By suitable choice of the carrier solution, the problems of overlapping peaks or oxygen interference can be minimized. The flow injection manifold can be used to achieve subtractive stripping voltammetry that yields lower detection limits [7]. For this

0003-2670/84/$03.00

purpose, the carrier solution voltammogram is subtracted from the sample voltammogram yielding a response related only to the species of interest.

While the future of stripping voltammetry/flow injection systems seems very promising, better understanding of their behavior is necessary for optimizing their performance. It is usually the case in flow injection systems that the concentration of the metal ion in the stream passing through the detector is not a steady-state function. For small sample volumes, a peak-shaped concentration profile is observed. Experimental parameters such as flow rate, length of tubing or sample volume affect the degree of dispersion and the resulting current transient. As a result, equations for stripping voltammetry, solved rigorously for batch and flow systems with steady-state deposition currents [1—3], are not applicable to stripping voltammetry/flow injection systems. At present, no theoretical treatment of stripping voltammetry under flow injection conditions seems to be available. In this paper, the effect of dispersion on the response in stripping voltammetry/flow injection systems is examined, and expressions for the corresponding stripping peak currents are derived. Experimental results are shown to support the theoretical conclusions.

THEORY

One must distinguish between stripping voltammetry and most other detection schemes used in flow injection systems, in that in stripping voltammetry the detector response is not recorded directly and continuously during the passage of the sample plug. Instead, the stripping peak current (or time signal in the potentiometric stripping mode) is usually obtained after the plug has passed completely through the detector. Consider a flow-through mercury film electrode, with the deposition potential being applied during the passage of the entire sample plug, under conditions of laminar flow. For tubing of small inner diameter and low flow rates, the solution is homogeneous in the cross-section [10].

For the mercury film electrode, using the linear-scan stripping mode, the stripping peak current, i_p, is given [2] by

$$i_p = 1.116 \times 10^6 n^2 A C_E l v \quad (1)$$

where C_E is the concentration of the metal in the mercury, A and l are the surface area and the thickness of the mercury film, respectively, and v is the potential scan rate. For the same electrode, using a differential-pulse stripping waveform, i_p is given [2] by

$$i_p = 0.138 Q/t_p \quad (2)$$

where Q is the amount of metal deposited, and t_p is the pulse width.

According to Faraday's law, $C_E = Q/nFAl$, where Q corresponds to the area of the current-time peak during the deposition step (passage of sample plug). According to Meschi et al. [11], this peak area can be obtained from

$Q = \int i(t)dt$, where $i(t)$ is the time-dependent deposition current, given [10] by $i(t) = i_{ss}C(x, d, t)/C_0$, where i_{ss} is the limiting steady-state current, $C(x, d, t)$ is the concentration at any point in the stream (x and d being the axial and radial coordinates) and C_0 is the initial concentration of the sample. The steady-state deposition current is given by $i_{ss} = nFAKC_0U^{\alpha}$, where K is a constant related to the diffusion coefficient and geometric parameters, U is the fluid flow rate, and α is a constant dependent on the electrode geometry.

Careful evaluation of the integral $\int i(t)dt$ has led [11] to the following expression for Q

$$Q = i_{ss}V_s/U \tag{3}$$

where V_s is the sample volume.

By combining Eqns. 1 and 2 with the expressions given for C_E, i_{ss} and Eqn. 3, the stripping peak currents recorded in the linear scan (l.s.) and differential-pulse (d.p.) stripping modes, respectively, are given by

$$i_p(\text{l.s.}) = 1.116 \times 10^6 n^2 AKC_0U^{\alpha-1}V_s v \tag{4}$$

$$i_p(\text{d.p.}) = 0.138nFAKC_0U^{\alpha-1}V_s/t_p \tag{5}$$

EXPERIMENTAL

Apparatus and reagents

The wall-jet electrode was the same as described earlier [12]. Solution flow was directed through the inlet nozzle (0.34-mm diameter) onto the planar glassy carbon disc electrode (2.5-mm diameter). Eight PTFE gaskets (0.005 in. each) separated the plexiglas cell blocks. The reference electrode was Ag/AgCl and the auxiliary electrode was a platinum tube placed in the solution outlet tubing.

The flow injection system was constructed of 250-ml and 400-ml Nalgene sample and carrier reservoirs, respectively, fitted with covers. The sample injection valve was a Rheodyne Model 7010 with 10-μl, 20-μl, 200-μl, and 500-μl sample loops (V_s). All interconnections were made with 1 mm i.d. PTFE tubing sealed in Tygon tubing to prevent oxygen permeation. The lengths of tubing between the valve and the electrochemical cell were 20.5, 99 and 240 cm. The respective retention volumes (V_R) were calculated to be 0.183, 0.89, and 2.2 ml. The two longer lengths of tubing were coiled into four loops. Carrier solution flow was maintained by a variable speed Masterflex pump (Cole-Palmer Instrument Co., No. 7553-10 with head No. 7013-20) located between the carrier reservoir and injection valve. Flow rates were calibrated volumetrically. All data were obtained with a Princeton Applied Research Model 364 polarographic analyzer and Houston Omniscribe strip-chart recorder.

Chemicals and reagents used have been described in detail earlier [5, 12] except as noted. Acetate buffer (0.1 M, pH 4.5) was prepared from anhydrous sodium acetate and glacial acetic acid. Deionized water was used in all

reagent preparations. Aliquots of stock solution were added to the supporting electrolyte contained in the sample reservoir to give the desired concentration.

Procedure

Carrier and sample solutions were purged with nitrogen for 5 min and then continuously throughout the experiment to avoid interference associated with dissolved oxygen. The glassy carbon electrode was coated with a mercury film as a carrier solution containing 5×10^{-5} M Hg^{2+} in supporting electrolyte flowed through the electrochemical cell at a rate of 0.55 ml min^{-1} for 10 min, with a potential of −0.6 V imposed on the working electrode. Next, the potential was changed to −0.1 V and held for 1 min to oxidize and remove contaminants which might have codeposited with the mercury. After this conditioning, the experiment was begun.

As the carrier and sample solutions flowed through the electrochemical cell and sample loop, respectively, the deposition potential (−1.1 V for Cd^{2+} reduction) was applied at the mercury film electrode and the sample was injected into the carrier stream. The deposition time was chosen, depending on the V_s and V_R being used. In all cases, sufficient time was allowed for complete passage of the sample plug through the cell. Two and ten minutes were the shortest and longest times required, respectively, for the flow rate of 0.55 ml min^{-1}.

After deposition, the carrier solution flow was stopped and the injection valve was turned to the LOAD position. After a 30-s equilibration time, the differential pulse scan was commenced at 5 mV s^{-1}. The potential scan was terminated and held at −0.1 V at which time carrier solution flow was resumed for 1 min with repetition of the cycle.

RESULTS AND DISCUSSION

The peak current response of amperometric detectors with flow injection systems strongly depends on the dispersion of the sample plug [10]. In contrast, Eqns. 4 and 5 predict that the stripping peak currents obtained in flow injection systems are independent of the degree of dispersion. To verify this prediction, experimental stripping peaks for the injection of a 6.3×10^{-7} M cadmium solution were recorded using different lengths of connecting tubing, ranging from 20.5 to 240 cm (Fig. 1A). These lengths correspond to volumes (V_R) of 0.183 to 2.2 ml. Figure 1B is the corresponding amperometric response, recorded under the same conditions, for the oxidation of hexacyanoferrate(II). While the amperometric response depends strongly on the tubing length, the stripping peak currents are essentially the same, given the fact that different mercury films were used for recording the three stripping peaks. A series of nine different stripping runs, with three injections at each length and film yielded a mean stripping peak current of 6.26 μA with a range of 5.71—6.91 μA, and a relative standard deviation of 6.3% (condi-

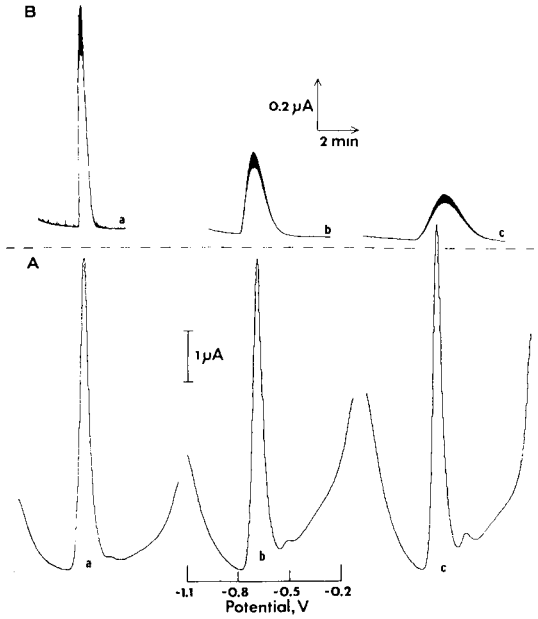

Fig. 1. (A) Stripping voltammograms obtained for a 6.3×10^{-7} M Cd^{2+} solution: (a) V_R = 0.183 ml, deposition time 2 min; (b) V_R = 0.89 ml, deposition time 6 min; (c) V_R = 2.2 ml, deposition time 10 min; sample volume 200 μl; supporting electrolyte 0.1 M acetate buffer, pH 4.5. (B) Amperometric response obtained for a 5×10^{-5} M $K_4Fe(CN)_6 \cdot 3H_2O$ solution: V_R and sample volume as above; applied potential 0.9 V; supporting electrolyte 0.1 M phosphate buffer, pH 7.4. Flow rate (A, B) 0.55 ml min^{-1}.

tions, as in Fig. 1A). Different lengths of tubing may be required in stripping voltammetry, depending on the nature of the sample pretreatment. Other parameters that affect the degree of dispersion and thus the amperometric response (e.g., the curvature of the tubing [10]) will not affect the stripping response.

In stripping voltammetry/flow injection systems, one must distinguish between the apparent deposition period (i.e., the period of applying the deposition potential) and the effective deposition period (i.e., the period of actual deposition during the passage of the sample plug). As indicated by the shape of the amperometric response, the effective deposition period depends on the degree of dispersion. Nevertheless, the stripping peak currents are independent of the effective deposition period and the apparent deposition period, provided that the latter is longer than the passage of the sample plug through the cell. To ensure this requirement, the deposition potential was applied over 2-, 6-, and 10-min periods for the 20.5-, 99-, and 240-cm tubing, respectively. Interestingly, Hu et al. [6] obtained the same expression for the amount of metal deposited, as that of Eqn. 3, by assuming a steady-state deposition current and deposition period of V_s/U. This is due to the fact that the square wave plug (without dispersion) is the product of its amplitude (i_{ss})

and its width (V_s/U). The agreement between the square wave and peak areas is obvious, as the integral over the peak must yield the total mass injected.

The lack of dependence of the stripping peaks on the deposition period is an interesting feature of stripping voltammetry in flow injection systems. Conventional stripping voltammetry, based on steady-state deposition currents, is characterized with stripping peak currents proportional to the deposition period. In stripping voltammetry/flow injection systems, the deposition current decays and approaches zero as the sample plug passes from the detector. Figure 2 shows stripping peak currents for the injection of a 6.3×10^{-7} M Cd^{2+} solution, obtained for different deposition periods (starting from the point of injection). Essentially the same stripping peak currents are observed, once the deposition period becomes longer than the passage of the sample plug (compare curves c—e with periods of 4—8 min). Thus, theoretically, precise control of the deposition period will not be required. In practice, however, such measurements may be subject to errors. As the deposition potential is applied for periods longer than the passage of the sample plug, a larger portion of the carrier solution is "active", thus, trace metal impurities in the carrier solution may deposit and contribute to the stripping signal; the gradual increase in the lead peak at —0.5 V in Figs. 1A and 2 should be noted. Even the ascending and descending portions of the sample peak during deposition are a mixed sample/carrier zone. Thus, highly purified carrier solutions should be used in stripping voltammetry/flow injection systems. To minimize errors caused by impurities in the carrier solution, and to maintain the speed and medium-exchange features that characterize stripping voltammetry/flow injection systems, the deposition step should be terminated as the sample plug passes from the detector.

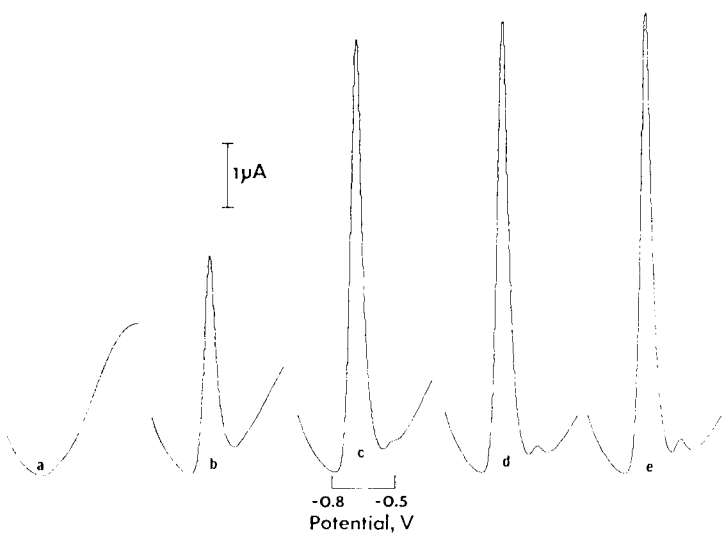

Fig. 2. Stripping voltammograms obtained for cadmium using different deposition times: (a) 0; (b) 2; (c) 4; (d) 6; (e) 8 min. V_R = 0.89 ml; conditions as in Fig. 1A.

Figure 3A shows the dependence of the stripping peak current on the volume of the injected cadmium solution. In agreement with Eqn. 5, the stripping peak current is directly proportional to the sample volume over the 10—500 μl range. Least-squares treatment of these data yielded the equation i_p (μA) = (0.040 ± 0.001) V_s (μl) — 0.012 ± 0.345 μA with S_{yx} = 0.508 μA and r = 0.999.

Unlike stripping voltammetry in systems with steady-state deposition current, in which the peak current increases on increasing the solution flow rate, the flow injection/stripping peak current decreases as the solution flow rate increases (Fig. 3B). The stripping peak current is predicted by Eqn. 5 to be proportional to $U^{\alpha-1}$. For α = 0.75 predicted for the wall-jet cell design [13], the log i_p vs. log U plot should have a slope of —0.25. The data of Fig. 3B yield a straight line with a slope of —0.38 (r = 0.994) over the 0.5—1.6 ml min^{-1} range, that corresponds to an α value of 0.62. Deviations from the theoretical value of α, ranging from 0.50 to 0.75, have been reported [13] for the wall-jet design and attributed to the presence of the nozzle within the boundary layer, resulting in a loss of momentum transfer in the radial flow.

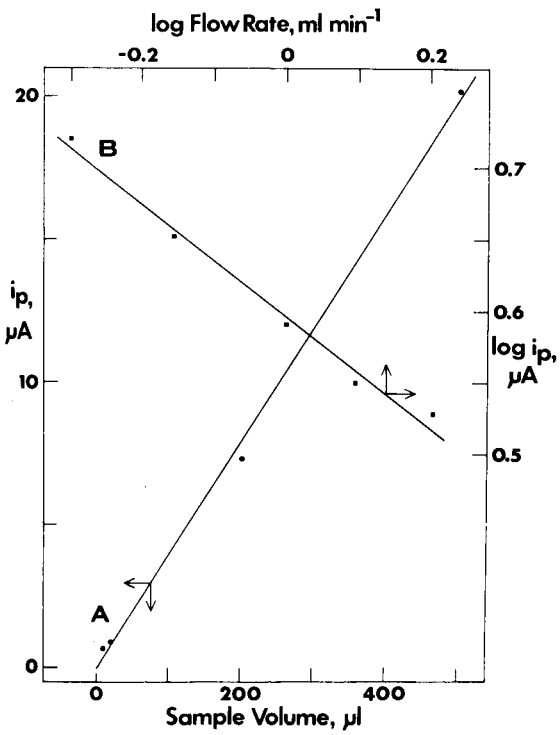

Fig. 3. (A) Dependence of stripping peak current on volume of 7.8 × 10^{-7} M Cd^{2+} solution injected; V_R = 0.89 ml; deposition time 6 min; supporting electrolyte 0.1 M KNO_3. (B) Dependence of stripping peak current on flow rate: sample volume 200 μl. Conditions as above, except supporting electrolyte and Cd^{2+} concentration as in Fig. 1A.

REFERENCES

1 W. D. Ellis, J. Chem. Educ., 50 (1973) A131.
2 T. R. Copeland and R. K. Skogerboe, Anal. Chem., 46 (1974) 1257A.
3 J. Wang, Environ. Sci. Technol., 16 (1982) 104A.
4 L. Anderson, D. Jagner and M. Josefson, Anal. Chem., 54 (1982) 1371.
5 J. Wang, H. D. Dewald and B. Greene, Anal. Chim. Acta, 146 (1983) 45.
6 A. Hu, R. E. Dessy and A. Graneli, Anal. Chem., 55 (1983) 320.
7 J. Wang and H. D. Dewald, Anal. Chem., 56 (1984) 156.
8 K. K. Stewart, Anal. Chem., 55 (1983) 931A.
9 J. Růžička, Anal. Chem., 55 (1983) 1040A.
10 P. L. Meschi and D. C. Johnson, Anal. Chim. Acta, 124 (1981) 303.
11 P. L. Meschi, D. C. Johnson and G. R. Luecke, Anal. Chim. Acta, 124 (1981) 315.
12 J. Wang and H. D. Dewald, Anal. Chim. Acta, 136 (1982) 77.
13 H. Gunasingham and B. Fleet, Anal. Chem., 55 (1983) 1409.

Analytica Chimica Acta, 162 (1984) 197—205
Elsevier Science Publishers B.V., Amsterdam — Printed in The Netherlands

ADSORPTIVE STRIPPING VOLTAMMETRY OF ELECTROACTIVE ORGANIC COMPOUNDS

ROBERT KALVODA

UNESCO Laboratory of Environmental Electrochemistry, J. Heyrovský Institute of Physical Chemistry and Electrochemistry, Czechoslovak Academy of Sciences, Vlašská 9 118 40 Prague (Czechoslovakia)

(Received 7th February 1984)

SUMMARY

Adsorptive stripping voltammetry at a hanging mercury drop electrode is described for various polarographically active compounds. Diazepam, nitrazepam, papaverine and aromatic nitro compounds can be determined at concentrations of 1×10^{-9}—1×10^{-6} M with errors of 5—7%. The effects of changing accumulation potentials and times are considered. Interferences by other surface-active agents may be removed by prior molecular exclusion chromatography.

Adsorptive stripping analysis [1] is becoming important in trace analysis because of its broad scope of application and simple experimental techniques [2—9]. Adsorptive stripping voltammetry allows not only determination of polarographically irreducible organic compounds such as detergents, some polychlorinated biphenyls [10], crude oil components [11], and some alkaloids and drugs but offers possibilities for voltammetric determinations of various electroactive compounds with surface-active properties, e.g., complexed metal ions and organic compounds. Some examples of adsorptive stripping voltammetry of electroactive compounds have been given [1] and polarographic adsorptive analysis and tensammetry of adsorbable molecules have been reviewed [12].

The present paper deals with adsorptive stripping voltammetry of various polarographically reducible organic compounds. Generally applicable conditions for this kind of analysis are discussed.

EXPERIMENTAL

Equipment

A polarographic analyzer (model PA3; Laboratorní přístroje, Prague) was used in the two-electrode configuration for d.c. voltammetry and fast-scan differential pulse voltammetry (d.p.v.); for the latter five polarization pulses (amplitude 50 mV) per second were applied to the mercury electrode and the scan rate was 20 mV s^{-1}. A static mercury drop electrode (SMDE)

0003-2670/84/$03.00

(Laboratorní přístroje, Prague) was used as the working electrode in the hanging mercury drop electrode (HMDE) mode, with a saturated calomel reference electrode.

Preliminary investigations and optimization of parameters

The d.c. voltammetric behaviour of the studied group of organic compounds was first examined at the HMDE in different supporting electrolytes. The supporting electrolyte solution (20 ml) containing 1×10^{-7}—1×10^{-6} mol l^{-1} of the compound studied was transferred to the electrolytic cell and the dissolved oxygen was removed with nitrogen. Then the initial potential was fixed (usually −0.2 V), a new drop of mercury was formed and immediately the voltage scan (20 mV s^{-1}) towards more negative potentials was started. After the voltammetric curve had been recorded, a new drop of mercury was formed and the same initial potential was applied for 60 s to the electrode in the stirred solution. After this accumulation period (t_{acc}), stirring was stopped and after 10 s the voltage was scanned as before. If the compound was surface-active and accumulated on the electrode surface, a substantial increase of the peak current, i_p, was obtained because not only the compound transported by diffusion to the electrode but also the adsorbed compound was reduced during the voltage scan. If the same voltage scan was repeated (on the same mercury drop) immediately after the peak had formed, the peak then obtained was of the same height as in the case without prior accumulation.

To establish the optimal conditions, the most suitable accumulation potential, E_{acc}, was first established by examining the dependence of i_p on E_{acc} (see Fig. 2). The effect of the accumulation time, t_{acc}, was then studied, and the dependence of i_p on concentration was established. Usually, a linear concentration dependence of i_p was obtained over a reasonably wide range. When the method of standard additions was used, three additions of the standard solution were made, to ensure that the measured i_p values corresponded to the linear part of the calibration plot. If the i_p value did not increase linearly with the standard additions, the sample solution was diluted or a shorter accumulation time was applied or the accumulation was done in unstirred solution.

RESULTS

The compounds studied are listed in Table 1.

Diazepam (7-chloro-2,3-dihydroxo-1-methyl-5-phenyl-1H-1,4-benzodiazepin-2-one)

An example of the preliminary tests for Diazepam is given in Fig. 1. Curve 1 was recorded immediately after a new mercury drop had been formed in an acetate-buffered solution; curves 2—5 were obtained after adsorptive accumulation in stirred solution for increasing times. At longer times,

TABLE 1

Accumulation potentials and supporting electrolytes for adsorptive stripping voltammetry of various organic compounds

Compound	Electrolyte	pH	Accumulation potential (V vs. SCE)	Peak potential (V vs. SCE)
Diazepam (Spofa)	Acetate buffer	4.6	−0.50	−0.82
	0.2 M NaOH	—	−0.80	−1.25
Nitrazepam (Spofa)	Acetate buffer	4.6	−0.50	−0.87
	0.2 M NaOH	—	−0.40	−0.72
Papaverine	0.2 M KF	—	−1.10	−1.45
Nitrobenzene	B-R buffer[a]	7	−0.20	−0.55
1,8-Dinitronaphthalene	B-R buffer	8	−0.20	−0.42
4,8-Dinitronaphthalene	B-R buffer	8	−0.20	−0.36, −0.46
2,4-Dinitro-1-naphthol	0.2 M NaOH	—	−0.50	−0.72, −0.77

[a]Britton-Robinson buffer.

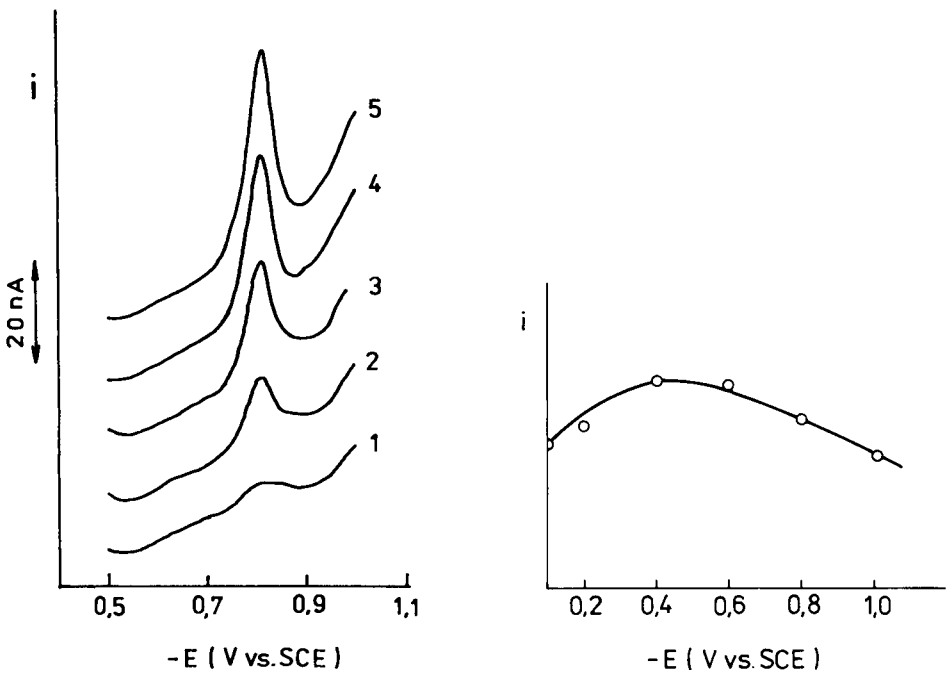

Fig. 1. The influence of preceding adsorptive accumulation on the peak height for 5×10^{-8} M Diazepam in acetate buffer, pH 4.6. Accumulation time: (1) 0 s; (2) 30 s; (3) 60 s; (4) 120 s; (5) 180 s. Conditions: d.p.v., E_{acc} −0.5 V.

Fig. 2. The dependence of the peak height of 2×10^{-6} M Diazepam in acetate buffer pH 4.6 on E_{acc} for a 60-s accumulation time.

i_p reached a limiting value, and the peak was sometimes distorted. The best accumulation potential was −0.50 V vs. SCE (Fig. 2). In unstirred solution, the accumulation effect was less pronounced. The peak current depended linearly on concentration, as can be deduced from Fig. 3. Nevertheless,

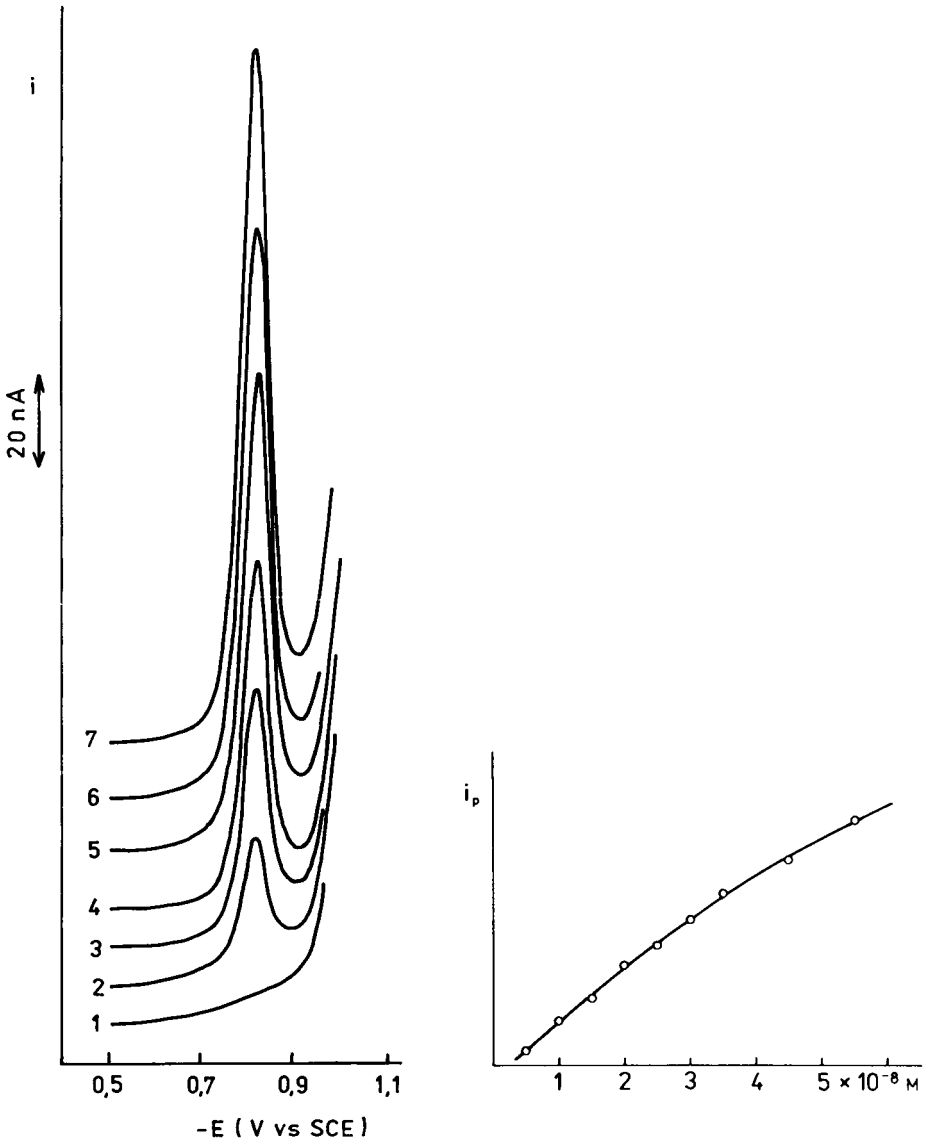

Fig. 3. Voltammograms of Diazepam in acetate buffer, pH 4.6 (E_{acc} = −0.5 V, t_{acc} = 60 s). Concentration of Diazepam: (1) 0, (2) 0.5, (3) 1.0, (4) 1.5, (5) 2.0, (6) 2.5, (7) 3 × 10^{-7} M.

Fig. 4. The concentration dependence of the peak height of Diazepam in acetate buffer, pH 4.6 (t_{acc} = 180 s, E_{acc} = −0.5 V, d.p.v. mode).

i_p—C dependences deviating from linearity were obtained for accumulation times of 3 min or longer (Fig. 4). Good results were also obtained in a 0.2 M sodium hydroxide electrolyte (Table 1).

Nitrazepam (1,3-dihydro-7-nitro-5-phenyl-2H-1,4-benzodiazepin-2-one)

Nitrazepam gave results similar to those obtained for Diazepam. The peak potential in 0.2 M sodium hydroxide was about 500 mV more positive than for Diazepam, so that simultaneous determinations of the two compounds were possible. Peak heights for Nitrazepam were unaffected by 10-fold concentrations of Diazepam in the sample. The stripping process can be evaluated by the d.c. or the d.p.v. mode; the latter offers greater sensitivity but the d.c. mode is preferable when the peak is located in the less negative potential range (e.g., with the nitro compounds). With the d.p.v. method, the baseline becomes complicated at the less negative potentials by relatively big changes in the differential capacity values. The shapes of the curves are compared in Fig. 5.

Papaverine and aromatic nitro compounds

A remarkable accumulation effect was observed with papaverine in 0.2 M potassium fluoride, partly because of the influence of the catalytic depression of hydrogen overvoltage. Figure 6 shows the dependence of the peak height on accumulation time.

Adsorptive stripping voltammetry can be used also for the determination of various aromatic nitro compounds (Table 1). Neutral or alkaline electrolytes are suitable. As the peak potentials of these compounds are mostly at less negative potentials, the d.c. method is preferred for recording the stripping process.

The influence of other surface-active compounds

In practical exploitation of adsorption phenomena in polarography (e.g., polarographic maxima, tensammetric measurements), an important complication is the presence of other surfactants. Competitive coverage of the electrode surface can then hinder or prevent application of the method. Further, surfactants present as impurities in the sample can contribute to full coverage of the electrode surface for long accumulation times, because there is an inverse relationship between the moment of complete coverage and the square of the surfactant concentration [13]. For these reasons, the influence of some surfactants on the peak current in adsorptive stripping voltammetry was studied in an attempt to overcome the difficulties involved. As was shown for mixtures of Diazepam and Nitrazepam, which differ substantially in their E_p values, simultaneous determination is possible if the concentrations are similar. Obviously, the determination of two compounds with similar E_p values is not possible unless an efficient separation (e.g., h.p.l.c.) is applied first [14].

The influence of a surplus of surfactant on the peak height in adsorptive

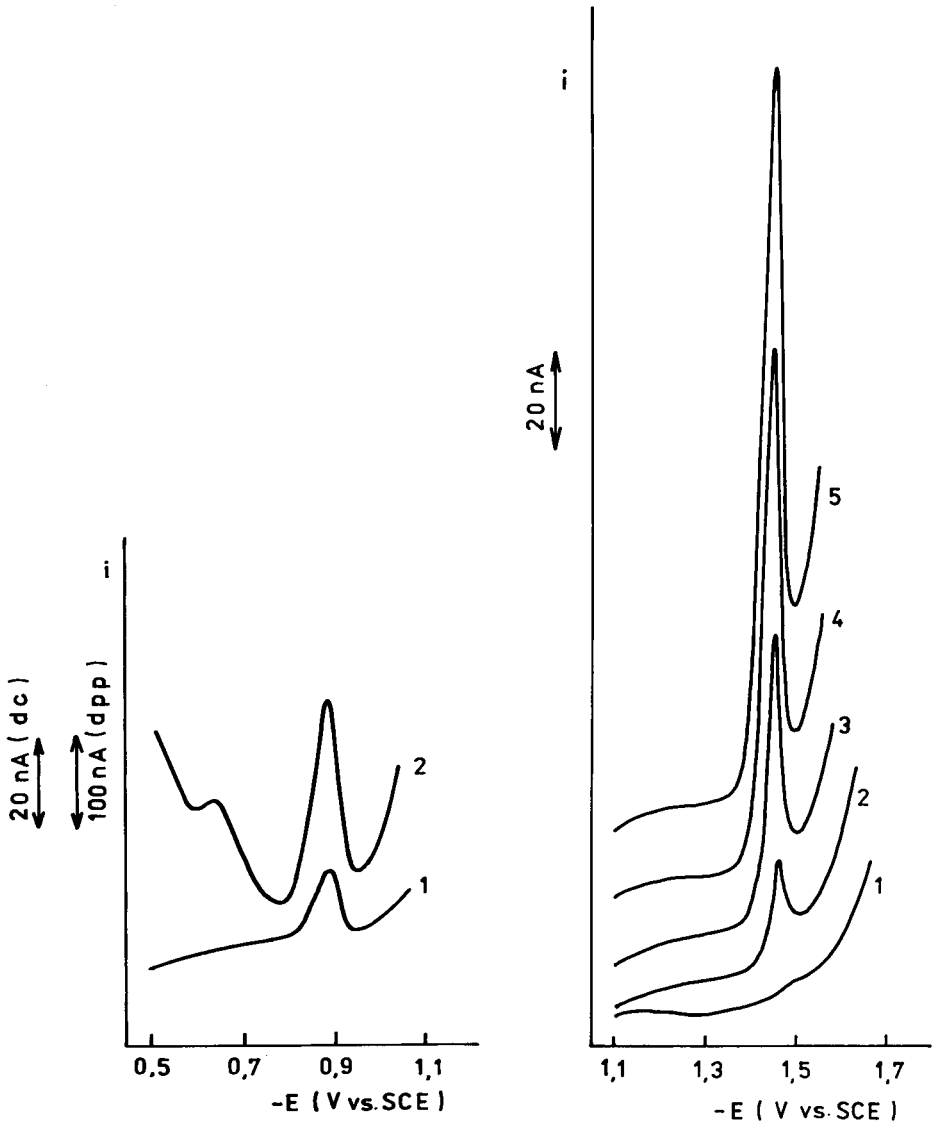

Fig. 5. Voltammograms for 2×10^{-7} M Nitrazepam in acetate buffer, pH 4.6 (E_{acc} = −0.5 V, t_{acc} = 60 s). Mode: (1) d.c.; (2) d.p.v.

Fig. 6. The influence of preceding adsorptive accumulation on the peak height of 1×10^{-6} M papaverine in 0.2 M potassium fluoride. Accumulation time: (1) 0 s; (2) 15 s; (3) 30 s; (4) 60 s; (5) 120 s. (D.c. mode, E_{acc} = −1.1 V.)

stripping voltammetry was studied with the systems Nitrazepam/gelatine and Nitrazepam/dodecylbenzenesulphonate (DBS). The peak of 5×10^{-8} M Nitrazepam in 0.2 M sodium hydroxide at t_{acc} = 15 s was not influenced by up to 5 mg l^{-1} gelatine, but at t_{acc} = 30 s the peak current was decreased

by 40% and at t_{acc} = 60 s the peak was totally suppressed. With a gelatine concentration of 1 mg l^{-1}, the peak current was decreased by 20% at t_{acc} = 60 s. Thus, increases in both gelatine concentration and in accumulation time may decrease the peak heights for Nitrazepam, as indicated in Fig. 7.

The peak current for 1×10^{-7} M Nitrazepam in 0.2 M sodium hydroxide at t_{acc} = 60 s was decreased of about 10% in presence of 1×10^{-6} M DBS. At a DBS concentration of 3×10^{-6} mol l^{-1}, the depression was about 50%.

Separation of interfering surfactants by molecular exclusion chromatography

The use of molecular exclusion chromatography on Sephadex (Pharmacia, Uppsala) for the separation of surfactants (e.g., proteins) which interfere with polarographic determinations of drugs was described earlier [15].

For the present measurements in the Nitrazepam/gelatine system, Sephadex G-25 was used; this gel accumulates compounds with molecular weights up to 1000 whereas compounds with molecular weights higher than 4000 are eluted from the column. A column containing 1.5 g of Sephadex was tested with Nitrazepam/gelatine mixtures. After the sample (about 1 ml) had penetrated into the gel, distilled water was used for elution. The first 5 ml of eluate contained the gelatine and the next 20 ml contained the separated Nitrazepam. This eluate was mixed with the base solution and subjected to adsorptive stripping voltammetry. In this way, it was possible to measure 5×10^{-8} mol l^{-1} Nitrazepam in solutions containing 10 mg l^{-1} gelatine. After the separation, the peak heights for Nitrazepam were nearly the same (with a systematic error of −10%) at various accumulation times as those obtained with test solutions of the same Nitrazepam concentration but without gelatine. To obtain correct results, it is always necessary to test the Sephadex column first by construction of the elution curve. Further studies of such separations are in progress.

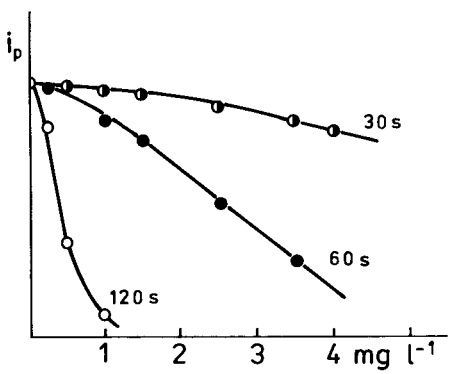

Fig. 7. The influence of gelatine concentration on the peak current for 1×10^{-7} M Nitrazepam in 0.2 M NaOH at various accumulation times. (D.c. mode, E_{acc} = −0.5 V.)

DISCUSSION

From the set of polarographically active compounds studied here, it is evident that adsorptive stripping voltammetry can be used in trace analysis for a broad range of organic compounds. The adsorptive properties of different compounds can vary with the composition of the supporting electrolyte, which must therefore be chosen carefully. Some ions which exhibit specific adsorption (e.g., bromide) can have a negative effect on the required adsorptive accumulation. Of course, the composition of the supporting electrolyte must also be optimal for the electroreduction response. For effective accumulation, it is important to establish the optimal E_{acc}. In most cases, for preliminary tests, potentials of −0.2 to −0.4 V vs. SCE should be adequate in all types of supporting electrolytes, but the dependence of i_p on E_{acc} must be examined. In general, less negative potentials are preferable for accumulation, so as to avoid electrolytic deposition of metal ions which may be present in samples as impurities.

Special consideration must be given to the choice of accumulation time. Frequently, at prolonged accumulation times, the peak height becomes constant, and eventually the peak may disappear because of inhibition of the electrode surface. The presence of other surfactants (possibly present as impurities in the sample) can affect the accumulation process. To overcome such short accumulation times (15—30 s) in stirred solutions are usually preferable, or a separation technique can be used.

The optimal voltammetric mode for the stripping process has to be considered. Of course, the most sensitive method is d.p.v., but in some cases (e.g., Fig. 5) there may be problems with the baseline at less negative potentials; the d.c. mode will then be preferable despite the lower sensitivity. Other parameters of adsorptive stripping voltammetry are similar to those in anodic stripping voltammetry, e.g., the surface area of the mercury electrode, stirring rate, scan rate for stripping and the amplitude and polarity of the voltage pulse.

For the polarographically active organic compounds tested above, adsorptive stripping voltammetry is useful in the concentration range 1×10^{-9}—1×10^{-6} mol l^{-1}. Adsorptive accumulation may be effective at higher concentrations, but direct d.p.p. measurements are then usually possible. The improvement in sensitivity offered by the adsorptive technique is usually about 1—1.5 order, compared with direct voltammetric methods. The error in determinations is usually 5—7%.

REFERENCES

1 R. Kalvoda, Anal. Chim. Acta, 138 (1982) 11.
2 V. Gemmercolos, G. Scollary and R. Neeb, Z. Anal. Chem., 313 (1982) 412.
3 K. H. Lubert, M. Schnurbusch and A. Thomas, Anal. Chim. Acta, 144 (1982) 123.
4 J. M. Séquaris, P. Valenta, H. W. Nürnberg, J. Radiat. Biol., 42 (1982) 407.
5 H. Sawamoto, J. Electroanal. Chem., 147 (1983) 279.

6 J. Wang and B. A. Freiha, Anal. Chem., 55 (1983) 1285; J. Electroanal. Chem., 151 (1983) 273; Anal. Chim. Acta, 148 (1983) 79; Anal. Chim. Acta, 154 (1983) 87.
7 M. Schnurbusch, K. H. Lubert and A. Thomas, Z.f. Chemie, 23 (1983) 194.
8 V. Brabec, V. Glezers and V. Kadysh, Coll. Czechoslov. Chem. Commun., 48 (1983) 1257.
9 N. K. Lam, R. Kalvoda and M. Kopanica, Anal. Chim. Acta, 154 (1983) 79.
10 N. K. Lam and M. Kopanica, Anal. Chim. Acta, 161 (1984) 315.
11 R. Kalvoda and L. Novotný, Vodní Hospodářství, in press.
12 R. Kalvoda, Pure Appl. Chem., in press.
13 J. Koryta, Collect. Czech. Chem. Commun., 18 (1953) 206.
14 A. M. Bond and R. D. Jones, Anal. Chim. Acta, 152 (1983) 13.
15 R. Kalvoda, Abh. Dtsch. Akad. Wiss. Berlin, Kl. Chem. Geol. Biol., (1962) 286.

Analytica Chimica Acta, 162 (1984) 207—214
Elsevier Science Publishers B.V., Amsterdam — Printed in The Netherlands

TENSAMMETRY WITH ACCUMULATION ON THE HANGING MERCURY DROP ELECTRODE

Part 1. The Influence of Preconcentration Potential on the Accumulation of Poly(ethylene glycols) with Various Molecular Weights

HANNA BATYCKA and ZENON ŁUKASZEWSKI*

Institute of General Chemistry, Technical University of Poznań, 60-965 Poznań (Poland)

(Received 4th January 1984)

SUMMARY

The preconcentration of poly(ethylene glycols) (PEG) with various molecular weights on the hanging mercury drop electrode (HMDE) from a stirred solution was studied for the tensammetric determination of trace concentrations of these polymers. Preconcentration was significant in the case of PEGs having m.w. > 1000. The influence of the preconcentration potential on the cathodic tensammetric peak heights was studied in detail for PEG 1500, PEG 4000, PEG 6000, PEG 9000 and PEG 20 000. The concentration of the PEG affects this dependence. With a preconcentration potential of −1.76 V vs. SCE applied for 10 min, the calibration graphs of these PEGs were linear in the concentration range 0.01—0.10 mg l^{-1}.

Preconcentration of surfactants on a mercury electrode in order to improve detection limits has frequently been proposed in combination with d.c. polarography [1], oscillopolarography [2], a.c. polarography [3], the Kalousek commutator technique [4], and, recently, with differential pulse polarography [5]. The method has not found wide application in practical analysis, but has been used for special purposes, e.g., purity checks of supporting electrolytes for accidental contamination with surfactants [6]. Recently, the possibility of determining substances by means of adsorptive preconcentration at a mercury electrode has been considered critically and tested by Kalvoda [5].

As a rule, preconcentration of surfactants at a hanging mercury drop electrode (HMDE) proceeds under conditions that are far from those of an adsorption equilibrium state because of the slow transport of low concentrations of surfactant to the electrode surface. The achievement of adsorption equilibrium by that system actually means the end of surfactant preconcentration on the HMDE. An increased amount of surfactant at the electrode per unit time, and so an acceleration of the attained adsorption equilibrium can be obtained by stirring the solution. It is impossible to describe mathematically the dependence between the amount of accumulated substance

0003-2670/84/$03.00

and the preconcentration time because of the complicated hydrodynamic conditions in an electrochemical cell.

None of the investigators who have tried to preconcentrate surfactants at the mercury surface has reported a detailed study of the influence of the preconcentration potential on the results. Preconcentrations of surfactants were usually done at a potential close to the potential of maximum adsorption [1, 3—11]. Yet the adsorption of a substance at the electrode depends strongly on the electrode potential. Because the adsorption potential is an individual property of different substances, it would be expected that a particular substance would respond differently to a change in preconcentration potential, which could be useful analytically. Unfortunately, the desorption potential also depends on the concentration of a determinable substance. According to the experimental data of Lorenz and Möckel [12] and according to the theoretical considerations of Damaskin and Tedoradze [13], $(E_p - E_m)^2$ changes proportionally to the logarithm of the surfactant concentration; E_p is the peak potential and E_m is the maximum adsorption potential. Breyer and Hacobian [14] showed experimentally that the tensammetric peak potential depends linearly on the logarithm of the concentration of the substance tested. Though the shifts of the peak potential caused by the above features are not large, the effect tends to complicate tensammetric determinations.

The purpose of the work described here was to study the behaviour of the negative tensammetric peaks of substances preconcentrated on the HMDE at different potentials. This was a preliminary step in a more extensive study of surfactant mixtures. Poly(ethylene glycols) (PEG) with different molecular weights were taken as model substances. These substances do not associate, which simplifies the interpretation of results. Another purpose of this work was to explain the influence of the molecular weight on the preconcentration of PEGs on the HMDE and to examine the effect of changes in the preconcentration potential.

The tensammetric properties of PEGs with different molecular weights were investigated by Jehring and coworkers [3, 15—17] and Canterford [18]. The preconcentration of PEG (m.w. 1500) on the HMDE from a stirred solution and its tensammetric determination has been reported previously [19].

EXPERIMENTAL

Apparatus and reagents

An OH-105 polarograph (Radelkis) with a voltage scan rate of 400 mV min^{-1} was used. The applied amplitude of the alternating voltage was 2 mV. Controlled-temperature Kemula electrode equipment (Radiometer) with an additional mercury pool auxiliary electrode was used. The potential was checked with a digital voltmeter N-517 (Mera-Tronic, Poland). The tensammetric peak potentials were read by temporarily fixing the display of the voltmeter at the maximum current value.

Poly(ethylene glycols) of m.w. (nominal mean) 200, 600, 1000, 1500, 4000 and 6000 (Carl Roth) and PEGs of m.w. 9000 and 20 000 (Fluka) were used without additional purification. These substances are indicated below by the abbreviations PEG 200, PEG 600, etc.

The sodium sulphate used for preparation of the supporting electrolyte was purified by double crystallization and heated at 600° C. All solutions were prepared in water thrice-distilled from quartz. Only freshly distilled water was used. Only glass and quartz vessels were used. The supporting electrolyte in all studies was aqueous 0.5 M sodium sulphate.

Typical experiment

A fresh mercury pool and test solution were placed in the measuring cell. Dissolved oxygen was removed by bubbling oxygen-free nitrogen through the solution for 15 min; the nitrogen stream was then directed over the solution surface. Simultaneously, the solution was thermostatted (20 ± 0.5° C). Thorough deaeration was very important because oxygen was found to lower the tensammetric peaks of PEGs. Just before the preconcentration was started, the stirrer was switched on, the required preconcentration potential was set, and a new mercury drop was formed at the HMDE. The preconcentration time was measured from this moment. This procedure avoided any accumulation of surfactant on the mercury drop before the experiment was started. The preconcentration time was usually 10 min, except when it was a variable parameter. After the preconcentration time, stirring was stopped, and after a quiescent period lasting 1 min, the tensammetric peak was recorded from the preconcentration potential to more negative potentials.

Results

The preconcentration of PEGs with different molecular weights (200, 600, 1000, 1500, 4000 and 20 000) on the HMDE was studied at a concentration of 0.1 mg l^{-1}. These PEGs were preconcentrated at −1.20, −1.40, −1.50, −1.60, −1.60 and −1.60 V vs. SCE, respectively. The choice of potential was based on the position of the negative tensammetric peak of the corresponding PEG, as described earlier [19]. Under the experimental conditions, PEG 200 did not exhibit a peak; and the peaks of PEG 600 and PEG 1000 were low, which indicates that these substances are not significantly preconcentrated at the HMDE. It may be inferred that the preconcentration on HMDE is significant for PEGs with m.w. > 1000.

The dependence of the negative tensammetric peak height on the preconcentration time was studied for a 0.05 mg l^{-1} solution of PEG 1500. Over the first 10 min of preconcentration, the peak height increased linearly with increasing preconcentration time; after that, the peak height increase was limited because the system approximated adsorptive equilibrium conditions.

The influence of preconcentration potential on the negative tensammetric peak height was studied for a 0.1 mg l^{-1} solution of PEG 1500. The whole accessible potential range was examined. The dependence of the peak height

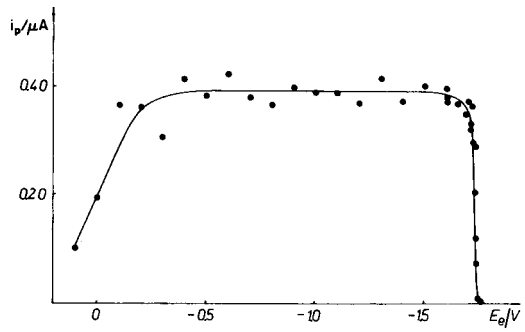

Fig. 1. Dependence of the cathodic tensammetric peak height of PEG 1500 (0.1 mg l^{-1}) on preconcentration potential. Preconcentration time, 10 min.

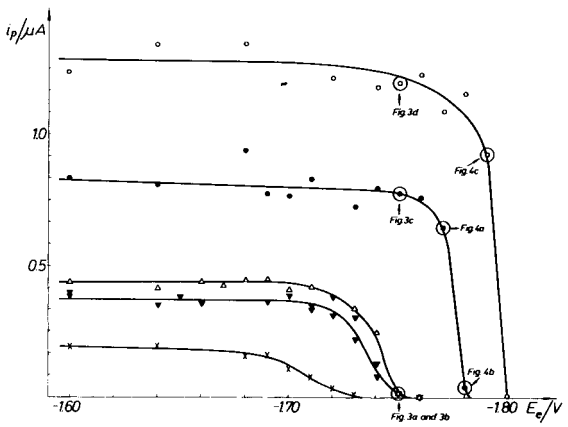

Fig. 2. Dependence of cathodic tensammetric peak height of PEG 1500 on preconcentration potential, at various concentrations of PEG 1500: (×) 0.05; (▼) 0.5; (△) 5; (●) 50; (○) 500 mg l^{-1}. Preconcentration time, 10 min.

on the preconcentration potential is presented in Fig. 1. The range of preconcentration potentials approaching the cathodic desorption peak, i.e., less than −1.60 V vs. SCE, was studied in more detail for 0.05—500 mg l^{-1} concentrations of PEG 1500. The results are summarized in Fig. 2, and typical tensammetric curves obtained at characteristic points (encircled) of the curves in Fig. 2 are given in Figs. 3 and 4. These tensammetric curves in Fig. 3 were recorded after preconcentration of PEG 1500 at the same potential. The preconcentration potential was chosen so that an increase in the PEG concentration was simultaneously associated with a transfer from the lower section of the plot of peak height vs. preconcentration potential to the plateau of that plot. The curves in Fig. 4 were recorded after preconcentration at a potential approximating the tensammetric peak potential. Curve (d) in Fig. 3 and curve (c) in Fig. 4 show a second peak or shoulder located on the cathodic side; this was caused by the presence of impurities. Simultaneously

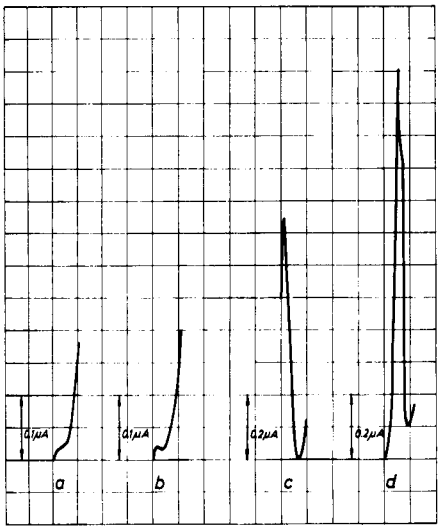

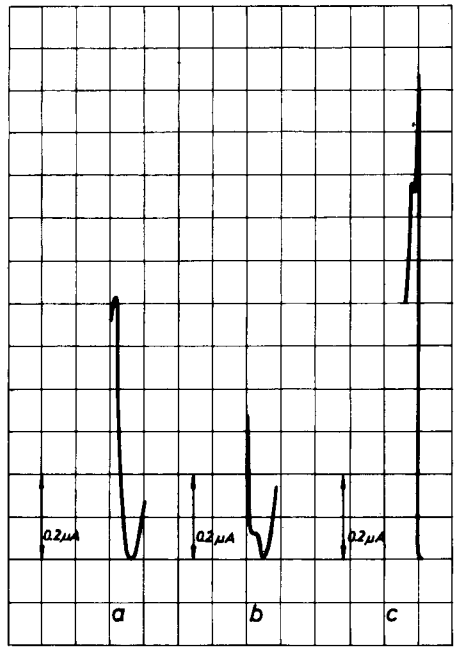

Fig. 3. A.c. polarograms relating to encircled segments of Fig. 2. Concentration of PEG 1500: (a) 0.5, (b) 5, (c) 50, (d) 500 mg l^{-1}; preconcentration potential, −1.75 V vs. SCE; preconcentration for 10 min.

Fig. 4. A.c. polarograms relating to encircled segments of Fig. 2. Concentration of PEG 1500: (a) and (b) 50, (c) 500 mg l^{-1}; preconcentration potential: (a) −1.77 V, (b) −1.78 V, (c) −1.79 V vs. SCE. Preconcentration time of 10 min.

with the measurements of peak height, the peak potentials were recorded. The peak potential of PEG 1500 was shifted systematically but slightly in the cathodic direction as the concentration of PEG 1500 increased. A change of four orders of magnitude in the concentration shifted the peak by 30 mV, which should not cause significant difficulty in the identification of PEG 1500 on the basis of its peak potential.

Studies of the influence of the molecular weight of the PEG on the peak height vs. preconcentration potential relationship were also limited to the range of potentials approximating the negative tensammetric peak potential. For these studies, 0.05 mg l^{-1} solutions were prepared from PEGs having molecular weights of 1500, 4000, 6000, 9000 and 20 000. The results are summarized in Fig. 5. All the curves, except that of PEG 1500, are very similar; in the case of PEG 9000 and PEG 20 000 they are almost identical. In these experiments, both the peak heights and peak potentials were recorded; the latter values are given in Table 1. There is a large difference in peak potential between PEG 1500 and the remaining PEGs. However, even for the remaining PEGs, an increase of m.w. causes small shifts of the peak potential in the cathodic direction.

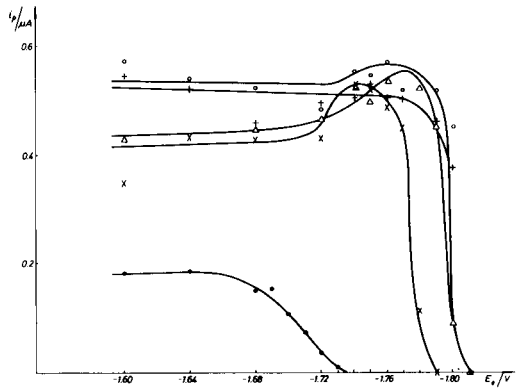

Fig. 5. Dependence of the cathodic peak height on the preconcentration potential for different PEGs: (•) PEG 1500; (×) PEG 4000; (△) PEG 6000; (○) PEG 9000; (+) PEG 20 000. Preconcentration time, 10 min; concentration of the PEG, 0.05 mg l^{-1}.

TABLE 1

The influence of the molecular weight of the PEGs (0.05 mg l^{-1}) on the potential of the cathodic tensammetric peaks

M.w.	1500	4000	6000	9000	20 000
E_p (V)	−1.768	−1.801	−1.811	−1.821	−1.827

The dependence of the peak height on the concentration of PEG 4000, PEG 6000, PEG 9000 and PEG 20 000 was studied for the range 0.01—0.1 mg l^{-1}. The preconcentration potential was −1.76 V vs. SCE. In all cases, the dependence of the peak height on the PEG concentration was linear; this dependence began from the origin of the coordinates. The slopes of the plots were, respectively, 1.04, 1.05, 1.02 and 1.01 μA/0.1 mg l^{-1}. The corresponding dependence for PEG 1500 was also linear for the investigated range of concentration [19].

DISCUSSION

The dependence of the peak height vs. preconcentration potential (Fig. 1) is similar to that between the degree of coverage and the potential [20], which is self-evident. The charging of the electrode with a sufficiently negative potential causes complete disappearance of the tensammetric peak, indicating the disappearance of PEG from the HMDE under these conditions. Thus, as expected, the use of an appropriate potential makes it possible to cause the disappearance of surfactant adsorption at the electrode. However, the tensammetric peak disappears only after a potential approximate to or exceeding the value of the peak potential has been applied to the HMDE. As

follows from Fig. 4, at potentials deviating somewhat from that of the peak, PEG 1500 is preconcentrated on the HMDE and a tensammetric peak is formed. This is in agreement with the observations of Sathyanarayana and Baikerikar [21], who noted an increase in the differential capacity of the HMDE in the presence of camphor at the desorption potential.

The varying values of the potential necessary to prevent completely any adsorption on HMDE for PEG 1500 and for the remaining PEGs (Fig. 5) confirm the assumption that these values are characteristic for the particular substances. Thus, it may be possible to use that characteristic analytically by preconcentrating under conditions that do not allow preconcentration of some substances.

As expected [12—14], the dependence of the desorption potential on the concentration of the test substance was confirmed by the dependences of the peak height of PEG 1500 vs. preconcentration potential, as determined for different concentrations of PEG 1500 (Fig. 2). A detailed knowledge of this dependence is indispensable for studies of the preconcentration on the HMDE of PEG mixtures having different molecular weights if PEG 1500 is present in excess. These studies are described in the next paper.

The capacity for preconcentration on the HMDE, and the tensammetric peak heights then obtained, depend strongly on the molecular weight of the PEG. There is no preconcentration for PEGs with the lowest m.w., but the capacity increases gradually up to m.w. 4000; PEGs with m.w. $\geqslant$ 4000 do not exhibit such a tendency. A similar effect of molecular weight was observed in studies dealing with the inhibition of instantaneous and average currents of In(III), Cd(II) and Pb(II) under the conditions of d.c. polarography [22]. The increase in the adsorptive properties of PEGs with increase in molecular weight may be explained to some extent by the influence of the hydroxyl end-groups, which affect the dipole moment of PEG molecules [23]. However, the differences in the dipole moments of PEGs having m.w. $>$ 1000 are minimal, whereas the difference in peak heights between PEG 1500 and PEG 4000, and even the difference in peak potentials (Table 1), are clear. Between PEG 1500 and PEGs of higher molecular weight, there seems to be a boundary below which PEG behaves as a single molecule and above which molecular fragments of the PEG behave as separate molecules. In the latter case, PEG desorption does not involve displacement of the whole macromolecule by water molecules, but only displacement of individual fragments [20]. Accordingly, the properties of the tensammetric peaks of PEGs with m.w. $\geqslant$ 4000 do not differ very significantly.

Particularly useful from the analytical point of view is the linear dependence of the peak height on the concentration of PEG 1500, PEG 4000, PEG 6000, PEG 9000 and PEG 20 000. This behaviour is not in agreement with the theoretically expected logarithmic dependence suggested by Damaskin and Tedoradze [13], but these workers assumed an adsorptive equilibrium at the electrode; under the conditions used here for preconcentration, adsorptive equilibrium is not attained. The slopes of the calibration graphs of the PEGs

examined are similar; this provides further evidence of the similarities of this group of substances in terms of their participation as macromolecular fragments, rather than whole molecules, in the adsorption-desorption process.

Some of the tensammetric curves showed the presence of a second peak (see Figs. 3 and 4). This is likely due to PEGs with m.w. > 1500. In 0.05% i.e. 5 mg l^{-1} solutions of PEG 1500, higher-molecular-weight PEGs attain a level sufficient to cause the second peak.

This research was supported by the Committee of Analytical Chemistry, Polish Academy of Sciences. Part of this paper was presented at Euroanalysis IV, Helsinki, 1981.

REFERENCES

1 W. Kemula, Z. Kublik and A. Axt, Roczniki Chem., 35 (1961) 1009.
2 R. Kalvoda and G. Budnikov, Collect. Czech. Chem. Commun., 28 (1963) 838.
3 H. Jehring and W. Stolle, Collect. Czech. Chem. Commun., 33 (1968) 1670.
4 B. Ćosović and M. Branica, J. Electroanal. Chem., 46 (1973) 63.
5 R. Kalvoda, Anal. Chim. Acta, 138 (1982) 11.
6 E. Bednarkiewicz, M. Donten and Z. Kublik, J. Electroanal. Chem., 127 (1981) 241.
7 O. V. Meshkova, V. N. Dmitreva and W. B. Bezuglyj, Zh. Anal. Khim. (Moscow), 26 (1971) 1665.
8 O. V. Meshkova, W. B. Bezuglyj, V. N. Dmitreva and W. B. Titova, Zh. Anal. Khim. (Moscow), 27 (1972) 1425.
9 Z. Kozarac, V. Zutić and B. Ćosović, Tenside Deterg., 13 (1976) 260.
10 B. Ćosović and D. Hršak, Tenside Deterg., 16 (1979) 262.
11 B. Ćosović, N. Batina and Z. Kozarac, J. Electroanal. Chem., 113 (1980) 239.
12 W. Lorenz and F. Möckel, Ber. Bunsenges. Phys. Chem., 60 (1956) 507.
13 B. B. Damaskin and G. A. Tedoradze, Electrochim. Acta, 10 (1965) 529.
14 B. Breyer and S. Hacobian, Aust. J. Sci. Res., Ser. A, 5 (1952) 500.
15 H. Jehring, E. Horn, A. Reklat and W. Stolle, Collect. Czech. Chem. Commun., 33 (1968) 1038.
16 H. Jehring and E. Horn, Monatsber. Dtsch. Akad. Wiss. Berlin, 10 (1968) 295.
17 H. Jehring, J. Electroanal. Chem., 20 (1969) 33; Z. Phys. Chem. (Leipzig), 246 (1971) 1.
18 D. R. Canterford, Anal. Chim. Acta, 94 (1977) 377.
19 Z. Łukaszewski, Research Report, Wydawnictwo Politechniki Poznańskiej, Poznań, 1978.
20 H. Jehring, Elektrosorptionanalyse mit der Wechselstrompolarographie, Akademie-Verlag, Berlin, 1974.
21 S. Sathyanarayana and K. G. Baikerikar, J. Electroanal. Chem., 25 (1970) 209.
22 Z. Łukaszewski, Pol. J. Chem., 55 (1981) 1863.
23 J. E. Mark and P. J. Flory, J. Am. Chem. Soc., 88 (1966) 3702.

Analytica Chimica Acta, 162 (1984) 215—225
Elsevier Science Publishers B.V., Amsterdam — Printed in The Netherlands

TENSAMMETRY WITH ACCUMULATION ON THE HANGING MERCURY DROP ELECTRODE

Part 2. The Behaviour of Mixtures of Poly(ethylene glycols) as an Example of Surfactant Mixtures

H. BATYCKA and Z. ŁUKASZEWSKI*

Institute of General Chemistry, Technical University of Poznań, 60-965 Poznań (Poland)

(Received 4th January 1984)

SUMMARY

Model investigations with two-, three- and four-component mixtures of poly(ethylene glycols) (PEG) having different molecular weights (1500—20 000) are described. Three different types of mixture can be distinguished. The first group comprises mixtures of components which have very similar properties and behave additively; such mixtures give only one peak, the height of which depends linearly on the total concentration of PEG. Examples are mixtures of PEG 9000 with PEG 20 000, and PEG 6000 with PEG 9000 or PEG 20 000. The second group consists of mixtures of components with rather different properties; in such cases, a suitable choice of preconcentration potential enables one component to be determined with adequate precision, even in the presence a 100-fold amount of another component. Examples are mixtures of PEG 4000, PEG 9000 or PEG 20 000 with a 100-fold amount of PEG 1500, and multicomponent mixtures consisting of PEGs 6000, 9000 and 20 000 with PEG 1500 in excess; in the latter case, the three PEGs of higher-molecular-weight behave as a single component. The third group comprises mixtures of components which have similar properties, but which behave nonadditively; their properties are too similar for any component to be eliminated by choosing a suitable preconcentration potential, and two very close peaks of dubious usefulness are obtained. Mixtures of PEG 4000, 6000, 9000 and 20 000, or of PEG 4000, 9000 and 20 000 behave in this way.

A principal reason for the relatively limited application of tensammetry for the determination of surfactants is the difficulty of determining their mixtures. Common nonionic surfactants are mixtures of substances differing in the length and degree of alkyl branching, in the degree of oxyethylation, etc. Moreover, they usually contain impurities, e.g., surfactants having an oxyethylene chain are always accompanied by poly(ethylene glycols). To complicate matters further, commercial products generally contain several surfactants in order to obtain maximum desirable properties.

The position of the peaks of differential capacity of individual substances on the potential axis, and therefore the position of the tensammetric peaks, is a function of the concentration of the substances [1]. This makes it difficult to identify substances on the basis of tensammetric peak position.

0003-2670/84/$03.00

The greatest difficulty, however, results from the non-additive character of the differential capacity peaks (and thus the tensammetric peaks) of mixtures. Under conditions of adsorptive equilibrium in accordance with the three parallel-connected condensers model, a two-component mixture should yield a common peak shifted towards a potential farther from the maximum adsorption potential, and higher than the peaks of the components [2]. This is an effect similar to that of an increase in concentration of the individual substances. Such behaviour was confirmed experimentally for mixtures of n-butanol and n-pentanol [2], and of iso-pentanol and cyclohexanol [3]. It should, however, be emphasized that these substances are not typical surfactants and that the concentrations tested were large, which ensured immediate achievement of adsorptive equilibrium. A different view of the behaviour of mixed surfactants was presented by Breyer and Bauer [4], who indicated that a mixture of surfactants would yield a peak for the substance with the strongest adsorptive properties. Extensive tensammetric studies of surfactant mixtures have been reported by Jehring [5—7], who showed that under conditions far from adsorptive equilibrium, peaks of individual components of a mixture were formed. Jehring also proved that distance from the adsorptive equilibrium state can be obtained by reduction of drop time or by dilution of solutions.

Some information on the behaviour of surfactant mixtures during accumulation on the HMDE was supplied by experiments on the application of the Kalousek commutator technique [8]. In contrast to tensammetric studies of surfactant mixtures which have mostly been done with a dropping mercury electrode, these measurements followed surfactant accumulation on the HMDE; as far as preconcentration is concerned, these experiments are the same as tensammetry with accumulation on the HMDE. Cosović et al. [8] showed that particular two-component mixtures can behave differently. Some behave in accordance with the model of three condensers connected in parallel (e.g., lecithin/sodium dodecylsulphate and lecithin/albumin). However, most of the mixtures tested (Triton X-100/albumin, sodium dodecylsulphate/albumin, oleic acid/albumin and sodium dodecylsulphate/cholesterol) deviated significantly from that model, which the authors ascribed to horizontal action between molecules or ions. The above considerations and results do not give an unambiguous picture of the behaviour of surfactant mixtures. It is certain that the behaviour of mixtures depends primarily on whether or not the system has attained adsorptive equilibrium. However, further conclusions seem premature in view of the very scanty experimental results presently available.

The present work was designed to extend the understanding of the behaviour of surfactant mixtures under conditions of tensammetric measurement after their accumulation on HMDE from stirred solutions. A main aim was to establish whether or not it is possible to preconcentrate only one component of a mixture of substances having sufficiently different properties, by applying a suitable preconcentration potential. Another aim was to

establish whether or not a mixture of components with very similar properties behaves like a single substance for the purpose of accumulation. Mixtures of two, three and four poly(ethylene glycol)s (PEG) having different m.w. were used as the model system.

The behaviour of individual PEGs under such conditions were described in Part 1 [9]; PEGs with m.w. <1500 do not accumulate on the HMDE to a satisfactory extent and the behaviour of PEGs with m.w. $\geqslant 4000$ is very similar (see Fig. 5 [9]). The behaviour of PEG 1500 is different from that of PEGs with m.w. $\geqslant 4000$: the potential range within which PEG 1500 is adsorbed on the HMDE is noticeably narrower, and the peak for PEG 1500 is smaller and appears at a less negative potential than these features for PEGs with m.w. $\geqslant 4000$ at equal concentrations. As in Part 1 [9], the present studies involved systems containing PEG 20 000, PEG 9000, PEG 6000 and PEG 4000 in different combinations. Systems containing these PEGs and an excess of PEG 1500 were also tested.

It was first established that mixtures of very similar components, e.g., PEG 9000/PEG 20 000 or PEG 6000/PEG 9000/PEG 20 000, form only one additive peak under conditions of tensammetry with accumulation on HMDE. The addition of PEG 4000 to these mixtures changes their behaviour and two nonadditive peaks appear.

A study of PEG mixtures simplifies the general problem because these substances are not subject to significant association, so that results should not display complications connected with surfactant association. A similar system for tensammetric studies of mixtures was adopted by Jehring [6]. The wide application of PEG's, including those with m.w. $\geqslant 1500$, means that the results have a certain practical importance.

EXPERIMENTAL

The apparatus and reagents were identical to those in Part 1 [9]. In all experiments, the base electrolyte was 0.5 M sodium sulphate.

RESULTS

Additive behaviour of mixtures of components with very similar properties

The aim of these investigations was to establish whether a mixture of PEG 9000/PEG 20 000 or a mixture of PEG 6000/PEG 9000/PEG 20 000, in which the components have very similar properties, behaves differently from the individual PEGs or behaves in the same way as the individual PEGs. In such experiments, the influences of the PEG concentration and the preconcentration potential must be considered.

In view of this, tensammetric curves of mixtures of PEG 9000 and PEG 20 000 (1:1) having different total concentrations were studied by examining preconcentration at various potentials. For comparison, analogous experiments were done with PEG 9000 or PEG 20 000 separately. The

concentrations of PEGs were doubled in each successive experiment. The total concentration of the mixture of PEG 9000/PEG 20 000 was the same as the concentration of each of the substances when investigated separately. In all cases, only a single tensammetric peak was obtained. A comparison was made by plotting the peak heights of PEG 9000, PEG 20 000 and their mixture (1:1) as a function of the preconcentration potential (Fig. 1). The results obtained show that although their thresholds were at different levels, the most significant features of all the curves were highly similar. Only the plateau of each successive series increased, because of the increase in the amount of PEGs accumulated on the HMDE. Increasing the preconcentration potential from −1.54 to −1.76 V vs. SCE did not cause any differentiation of the peaks corresponding to the individual PEGs and their mixture. Preconcentration of these PEGs at potentials between −1.76 and −1.80 V vs. SCE caused the appearance of somewhat higher peaks. As a result, surprising maxima were formed in the plots of peak height vs. preconcentration potential. It seems that the most suitable preconcentration potential for analytical purposes is that corresponding to the highest plateau potential, i.e., −1.76 V.

The preconcentration of a mixture of PEG 9000/PEG 20 000 leads to the formation of a peak indistinguishable from those of the individual components (Fig. 2). The height of the tensammetric peak of the PEG 9000/PEG 20 000 mixture (1:1) in the concentration range 0.01—0.10 mg l^{-1} increased proportionally to concentration; the slope of the line was 1.00 μA/0.10 mg l^{-1}, which is very similar to that of PEG 9000 and PEG 20 000.

A mixture of PEG 6000/PEG 9000/PEG 20 000 was also examined at a preconcentration potential of −1.76 V vs. SCE. The ratios of components

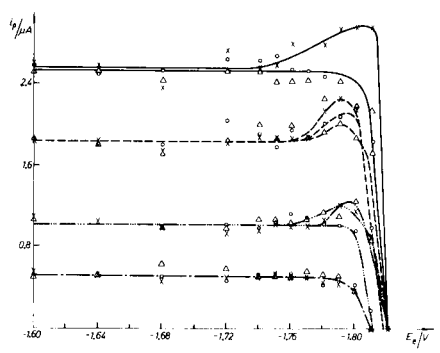

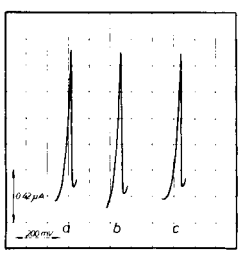

Fig. 1. The dependences of the peak heights of PEG 9000, PEG 20 000 and the additive peak height of their mixture (1:1) upon preconcentration potential. Compounds: (○) PEG 9000; (×) PEG 20 000; (△) 1:1 mixture. Concentration: (—·—) 0.05; (—···—) 0.1; (---) 0.2; (—) 0.4 mg l^{-1}.

Fig. 2. A.c. polarograms: (a) PEG 9000 alone (0.1 mg l^{-1}); (b) 1:1 mixture of PEG 9000 and PEG 20 000 (0.05 mg l^{-1} each); (c) PEG 20 000 alone (0.1 mg l^{-1}). Preconcentration potential −1.76 V vs. SCE; preconcentration time 10 min.

were 2:1:1, respectively. Tensammetric curves were measured for various total concentrations of PEGs from 0.01 to 0.10 mg l^{-1}. In all cases, a single additive peak was obtained. The dependence of peak height on total concentration was linear; the slope of the line was 0.99 μA/0.10 mg l^{-1}, which is similar to that of the individual components.

Nonadditive behaviour of mixtures of components with similar properties

These experiments were intended to establish if, after the introduction of PEG 4000 into a PEG 6000/PEG 9000/PEG 20 000 mixture, the mixture would behave as if it were a single PEG, as in the preceding experiment. Preliminary experiments showed the appearance of two peaks on the tensammetric curves of the mixture of the four PEGs. To detect any possible influence of the preconcentration potential on the appearance of the two peaks and on the proportion between them, the effect of the preconcentration potential (in the range 0 to −1.82 V vs. SCE) on the tensammetric curves of a 1:1:1:1 mixture of the four PEG's at a total concentration of 0.05 mg l^{-1} was studied; measurements were concentrated in the range of the desorption potential. In all the experiments, except those done at preconcentration potentials of −1.81 V and −1.82 V, two nearly overlapping peaks located at −1.812 V and −1.822 V vs. SCE were obtained. With preconcentration at −1.81 or −1.82 V, only one peak appeared. The plots of the peak height vs. preconcentration potential for both peaks are presented in Fig. 3.

When a preconcentration potential of −1.76 V vs. SCE was used, the dependence between the height of the two peaks of the examined mixture and the total concentration of PEGs was studied for the concentration range 0.01—0.10 mg l^{-1}. It was not possible to determine the height of the second peak (−1.822 V) in all cases. The results are presented in Fig. 4(a); typical tensammetric curves for the mixture are shown in Fig. 4(b, c). The ratio of the two peak heights seems to indicate that the less negative peak (−1.812 V) represents the sum of PEG 4000 and PEG 6000, whereas the second peak represents the sum of PEG 9000 and PEG 20 000. The dependences of the peak height on the PEG concentration in the case of both peaks appear to be linear to a first approximation, but the dispersal of the measuring points is very large.

In a further experiment, a 2:1:1 PEG 4000/PEG 9000/PEG 20 000 mixture was examined. Preconcentration was done at −1.76 V vs. SCE; the total concentration of the PEGs was varied over the range 0.01—0.10 mg l^{-1}. In all cases, peaks were obtained at potentials of −1.808 V and −1.827 V vs. SCE. To a first approximation, the heights of these peaks increased linearly with increasing total concentration of the mixture, but again the dispersal of the measuring points was very great. The slope of the plot for the first peak (−1.808 V) was 0.70 μA/0.10 mg l^{-1}, which is more than for PEG 4000. The slope for the second peak was 0.49 μA/0.10 mg l^{-1}, which is close to the slope for the sum of PEG 9000 and PEG 20 000, once their different contents in the mixture have been taken into consideration.

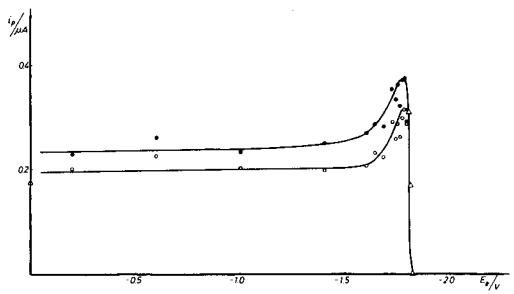

Fig. 3. The dependences of the heights of the two tensammetric peaks of a PEG 4000/PEG 6000/PEG 9000/PEG 20 000 (1:1:1:1) mixture on preconcentration potential: (•) −1.812 V; (○) −1.822 V; (△) single peak. Total concentration of PEGs, 0.05 mg l^{-1}; preconcentration time, 10 min.

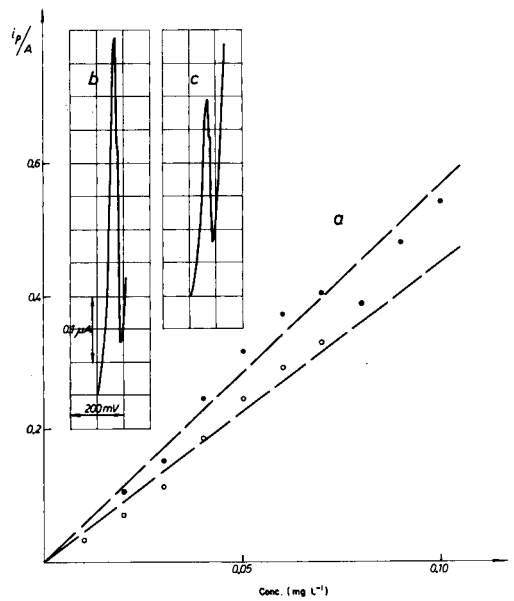

Fig. 4. (a) The dependences of the heights of the two tensammetric peaks of a mixture consisting of PEG 4000, PEG 6000, PEG 9000 and PEG 20 000 on the total concentration of these PEGs: (•) E_p = −1.812 V; (○) E_p = −1.822 V. (b, c). A.c. polarograms of the mixture at various total concentrations of PEGs: (b) 0.09; (c) 0.04 mg l^{-1}. Preconcentration potential, −1.76 V vs. SCE; preconcentration time, 10 min.

The behaviour of mixtures of components with sufficiently different properties

This series of experiments was designed to establish if a suitable choice of preconcentration potential would permit the accumulation of only one component of a mixture. In view of the above results, mixtures of PEGs having very similar properties (i.e., PEG 9000/PEG 20 000 or PEG 6000/PEG 9000/PEG 20 000) were considered as one component of a two-component mix-

ture. As a representative mixture, a system consisting of PEG 9000 and an excess of PEG 1500 was chosen.

When the possibility of determining PEG 1500 and PEG 9000 in admixture was considered, earlier results obtained for PEG 1500 (0.05—500 mg l^{-1}) and for 0.05 mg l^{-1} PEG 9000 solution [9] were placed in a common figure (Fig. 5) to give plots of peak height vs. preconcentration potential. The curve corresponding to 0.05 mg l^{-1} PEG 9000 coincides with the curves corresponding to 50 and 500 mg l^{-1} PEG 1500 solutions and is more negative than the curves corresponding to 0.05, 0.5 and 5 mg l^{-1} PEG 1500 solutions. Thus it is impossible to determine PEG 1500 in the presence of PEG 9000; however, it should be possible to determine PEG 9000 in the presence of PEG 1500 at concentrations not exceeding 5 mg l^{-1}. The range of possible preconcentration potentials for such determinations is marked as the shaded area in Fig. 5.

The complexity of the tensammetric behaviour of mixtures prevents any definite conclusions being reached on the basis of results for individual components. Accordingly, the dependence of the tensammetric peak height vs. preconcentration potential was studied for a mixture consisting of 0.05 mg l^{-1} PEG 9000 and 5 mg l^{-1} PEG 1500. The results are summarized in Fig. 6; for comparison, the corresponding curves for the individual components are included. The results deviate significantly from the values expected on the basis of the behaviour of the individual components. The range of preconcentration potentials corresponding to the simultaneous adsorption of both components is characterized by the appearance of two peaks related to the individual components of the mixture. However, the peak heights differ significantly from those of the individual PEGs measured separately. This is clearly seen in Fig. 7A; the peaks corresponding to PEG 1500 and PEG 9000 are both slightly lower than those obtained for the individual components. The ranges of preconcentration potentials corresponding to the gradual dis-

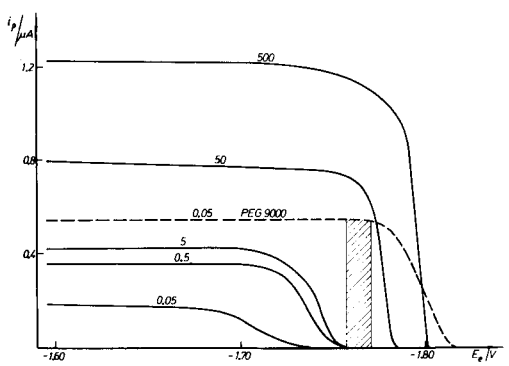

Fig. 5. The influence of an excess of PEG 1500 on the possibility of separate accumulation of PEG 9000. (—) PEG 1500 at the concentrations (mg l^{-1}) indicated on the curves; (---) PEG 9000 at 0.05 mg l^{-1}. The shaded area indicates the anticipated potentials of separate accumulation of PEG 9000 in the presence of 5 mg l^{-1} PEG 1500. Data from [9].

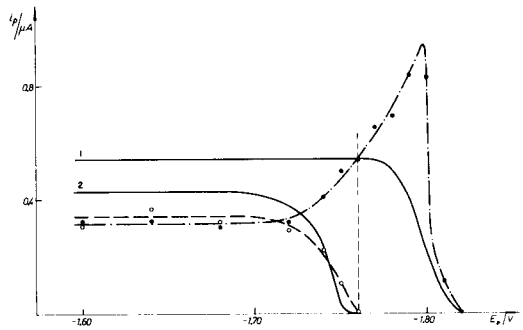

Fig. 6. Dependences of cathodic tensammetric peak height of (•) PEG 9000 and (○) PEG 1500 on preconcentration potential in the case of a mixture (1:100). Curves for the individual dependences: (1) 0.05 mg l^{-1} PEG 9000; (2) 5 mg l^{-1} PEG 1500 (from [9]). Preconcentration time, 10 min.

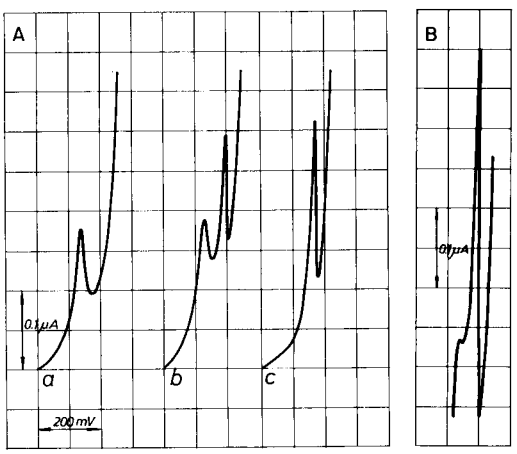

Fig. 7. A.c. polarograms. A, Preconcentration at −1.64 V vs. SCE for 10 min: (a) PEG 1500 alone (0.025 mg l^{-1}); (b) mixture of PEG 1500 and PEG 9000 (0.025 mg l^{-1} each); (c) PEG 9000 alone (0.025 mg l^{-1}). B, Preconcentration at −1.76 V vs. SCE for 10 min for a mixture of 0.04 mg l^{-1} PEG 20 000 and 5 mg l^{-1} PEG 1500.

appearance of the peak from PEG 1500 for a solution containing only PEG 1500 and for a PEG 1500/PEG 9000 mixture coincide. In this range of preconcentration potentials, the peak height of PEG 9000 increased gradually (see Fig. 6). At preconcentration potentials more negative than −1.76 V vs. SCE, only the tensammetric peak of PEG 9000 appeared, and its height continued to increase as the preconcentration potential applied became more and more negative. After a sufficiently negative preconcentration potential had been applied, the peak of PEG 9000 also finally disappeared. This dependence of peak height on preconcentration potential results in formation of a maximum. At the maximum, the dependence of the peak height of PEG 9000 corresponding to the mixture is more than 1.5 times greater than the peak height of individual PEG 9000 under the same accumulation conditions.

The formation of this maximum in the plot of peak height vs. preconcentration potential is not beneficial from the analytical point of view. However, this effect may be eliminated by the proper choice of a preconcentration potential lying on the intersection of the plots of peak height vs. preconcentration potential corresponding to the surfactant mixture and to the individual substances. This value is presented in Fig. 6 as a dashed line and is equal to −1.76 V vs. SCE.

The dependence of the tensammetric peak height of PEG 9000 on the concentration of that PEG was also studied in the range 0.01—0.10 mg l^{-1} in the presence of 5 mg l^{-1} PEG 1500, with a preconcentration potential of −1.76 V. The dependence was linear with a slope of 1.03 μA/0.10 mg l^{-1}, i.e., almost identical to that of PEG 9000 in the absence of PEG 1500. The precision of determination of PEG 9000 in the presence of an excess of PEG 1500 (1:500 and 1:100) was checked in two series of measurements with the results given in Table 1. The precision is satisfactory, the poorer results at the lower concentrations being typical for trace analysis. More than 5 mg l^{-1} PEG 1500 will cause simultaneous adsorption of PEG 9000 and PEG 1500 (cf. Fig. 5) and the result will be erroneous.

Under conditions identical to those above, in the same concentration range, the dependence of the peak height on concentration was studied for the following systems: PEG 4000 with 5 mg l^{-1} PEG 1500; PEG 20 000 with 5 mg l^{-1} PEG 1500; PEG 9000 and PEG 20 000 with 5 mg l^{-1} PEG 1500; and PEG 6000, 9000 and 20 000 with 5 mg l^{-1} PEG 1500. In all these cases, the dependence was linear with a slope similar to those obtained for the individual PEGs. Except for the PEG 4000/PEG 1500 mixture, the precision of determination was checked for all these systems. These results are also presented in Table 1; the precision is again reasonably satisfactory. An example of a tensammetric curve for PEG 20 000 in the presence of 5 mg l^{-1} PEG 1500 is presented in Fig. 7B; curves for PEG 9000 in these mixtures were

TABLE 1

The precision of the determination of PEG 9000, PEG 20 000 or the total concentration of PEGs having m.w. ⩾ 6000 in the presence of 5 mg l^{-1} PEG 1500

Added PEG of m.w.			Ratio of PEG 1500 to other PEGs	Average peak height (mm)[a]	No. of tests	Std. devn. (mm)[a]	S_r
6000 (mg l^{-1})	9000	20 000					
—	0.05	—	100:1	129.5	5	9.5	0.07
—	0.01	—	500:1	26.0	5	5.5	0.21
—	—	0.05	100:1	131.8	5	11.4	0.09
—	—	0.01	500:1	23.4	5	1.5	0.06
—	0.025	0.025	200:1:1	118.6	5	6.0	0.05
0.025	0.0125	0.0125	400:2:1:1	125.0	8	14.0	0.11

[a] 250 mm = 1 μA.

similar. The small bulge at the peak base is a result of some residual influence of PEG 1500, but it does not affect the results of the determination.

DISCUSSION

These model investigations made it possible to distinguish three types of mixtures, differing in their behaviour in tensammetry with accumulation on HMDE.

Mixtures of components having very similar or identical properties

In this case only one additive peak will be obtained. The peak height/concentration relationship of each component in the mixture is identical and the slope of the calibration graph for mixtures is very similar to that of the individual components. This group is represented above by the PEG 9000/PEG 20 000 binary mixture and the PEG 6000/PEG 9000/PEG 20 000 ternary mixture. In more complex mixtures, these mixtures generally behave like individual substances, as shown above when PEG 1500 was also added in relatively high concentration. However, the addition of a substance having slightly different properties into a mixture of this type changes the additive behaviour. For example, the addition of PEG 4000 to the PEG 6000/PEG 9000/PEG 20 000 mixture affected the additive behaviour of that mixture.

It should be emphasized that, in these model investigations, the slopes of the calibration graphs of the individual components (PEG 6000, 9000, 20 000) were very similar. In more general cases, it would be necessary to consider situations in which the mixture components behave additively but the slopes of their calibration graphs are different. This would obviously cause trouble in the evaluation of the results.

Mixtures of components having different properties

In such cases, a suitable choice of preconcentration potential allows the determination of one component, even when the second component is present in excess. Such a possibility is valuable from the analytical point of view. This group is represented above by mixtures of an excess of PEG 1500 with PEG 4000, PEG 9000 or PEG 20 000, individually, or with PEG 9000/PEG 20 000, or PEG 6000/PEG 9000/PEG 20 000. In the last two cases, the higher-molecular-weight PEGs behave like a single component.

The viable amount of any component, the effect of which has been eliminated (PEG 1500 in these experiments), is limited by the negative shift of its desorption potential with increase in concentration. Such a situation is shown in Fig. 5 for PEG 9000 with an excess of PEG 1500. When the amount of PEG 1500 exceeds 100-fold, there is simultaneous adsorption of both components and the determination of PEG 9000 becomes impossible.

As seen in Fig. 6, only one value for the preconcentration potential is suitable for the determination of a particular component in the presence of a large amount of a second component. The application of a less negative

potential leads to simultaneous adsorption of both components; the tensammetric peak is then lower for the component to be measured (PEG 9000) than it would be for the individual component. The application of a potential more negative than the most suitable value produces a peak higher than it should be for the individual component (see Fig. 6). This finding is surprising in view of present knowledge about the dependence of differential capacity on potential. The mixture component present in excess (PEG 1500) beyond its own range of adsorption potential on the HMDE has an increasing effect on the peak of the component to be measured (PEG 9000). This is still more striking because within the range of potential of its own adsorption, PEG 1500 has a decreasing effect on the PEG 9000 peak.

Mixtures of components having similar properties, but nonadditive behaviour

In these cases, the components of the mixture behave too differently for additivity to be possible, but are so similar that one of the components cannot be eliminated by choosing a suitable preconcentration potential. In such cases, two very close peaks will be obtained, but their analytical usefulness is doubtful. Mixtures of PEG 4000, PEG 6000, PEG 9000 and PEG 20 000, and of PEG 4000, PEG 9000 and PEG 20 000 behave in this way.

The conclusions drawn from these model studies cannot be extended uncritically to all surfactant mixtures because PEGs used as the model substances, do not undergo association.

This research was supported by the Committee of Analytical Chemistry of the Polish Academy of Sciences. Part of this paper was presented at Euroanalysis IV, Helsinki, 1981.

REFERENCES

1 B. B. Damaskin and G. A. Tedoradze, Electrochim. Acta, 10 (1965) 529.
2 G. A. Tedoradze, R. A. Arakeljan and E. D. Belokolos, Electrokhimya, 2 (1966) 563.
3 G. A. Dobrenkov and G. D. Shilotkach, Electrokhimya, 7 (1971) 1417.
4 B. Breyer and H. H. Bauer, Alternating Current Polarography and Tensammetry, Interscience, New York, 1963.
5 H. Jehring, Z. Phys. Chem., 225 (1964) 116.
6 H. Jehring, Z. Phys. Chem., 246 (1971) 1; J. Electroanal. Chem., 21 (1969) 77.
7 H. Jehring, Elektrosorptionsanalyse mit der Wechselstrompolarographie, Akademie Verlag, Berlin, 1974.
8 B. Ćosović, N. Batina and Z. Kozarac, J. Electroanal. Chem., 113 (1980) 239.
9 H. Batycka and Z. Łukaszewski, Anal. Chim. Acta, 162 (1984) 207 (Part 1).

Analytica Chimica Acta, 162 (1984) 227—240
Elsevier Science Publishers B.V., Amsterdam — Printed in The Netherlands

AUTOMATED RULE GENERATION FOR THE PROGRAM FOR THE ANALYSIS OF INFRARED SPECTRA (PAIRS)

STERLING A. TOMELLINI* and RICHARD A. HARTWICK

Department of Chemistry, Rutgers University, New Brunswick, NJ 08854 (U.S.A.)

JAMES M. STEVENSON and HUGH B. WOODRUFF

Merck Sharp and Dohme Research Laboratories, P.O. Box 2000, Rahway, NJ 07065 (U.S.A.)

(Received 13th December 1983)

SUMMARY

An automated rule generation program for MISIP, the minicomputer version of PAIRS, has been developed which includes a more mathematical and objective approach to rule generation than that previously employed. Rules are generated in CONCISE, an English-like language. All development work has been done using the MISIP version on a Nicolet 1180 minicomputer. The capabilities of the program were tested by generating rules for the saturated alcohol class using 51 vapor-phase spectra as data. Interpretation rules were also generated by using a limited number of vapor-phase saturated acid spectra. Rules generated by using the program show good predicting power for the tested functionalities and good distinguishing power among subfunctionalities.

Several papers have been published recently on the computerized interpretation of vibrational spectra [1—14]. One of the best known and most widely distributed infrared (i.r.) interpretation programs is the Woodruff and Smith Program for the Analysis of Infrared Spectra (PAIRS) [1]; PAIRS was designed to assist the chemist in determining which functionalities may be present in an unknown compound. Although it was originally designed to interpret only i.r. spectra of condensed-phase (liquid or solid) species, interpretation rules have recently been developed to enable PAIRS to interpret i.r. spectra of vapor-phase species as well [15]. The current interpretation rules indicate the likelihood of presence or absence of over 169 functionalities and subfunctionalities.

Interest in PAIRS has been further enhanced by the development of a version capable of running on an instrument-based minicomputer [2]. This version, known as MISIP (Merck infrared spectral interpretation package) has been optimized for a Nicolet 7199 FTIR system using a Nicolet 1180 minicomputer.

The PAIRS program is considered to be of the heuristic type [1] because it attempts to mimic the normal thought processes involved in interpretation of the i.r. spectrum of an unknown compound. While pattern recognition is

0003-2670/84/$03.00

certainly involved in this process, PAIRS is not representative of pattern recognition programs as generally applied to chemical problems. The abstract, multidimensional mathematical approach taken by most pattern recognition programs is absent in this interpreter. When interpreting the i.r. spectrum of an unknown compound, a spectroscopist uses both his own experience and that of others (from published frequency correlation data) gradually to form a set of "rules" by which to evaluate the presence or absence of functionalities frequently encountered. Rule development, of course, requires constant revision, i.e., a "learning" process. The design of PAIRS allows for this constant revision by treating the rules by which spectra are interpreted as data. Thus, the actual interpretation program which is coded in FORTRAN need not be changed each time the rules are revised. This feature makes rule changes machine-independent, which is essential for a program of this type.

One of the major aims in developing PAIRS was to make the interpretation rules accessible and in a form that is easily understandable and modifiable by the user. To accomplish this goal, a special English-like language known as CONCISE (Computer Oriented Notation Concerning Infrared Spectral Evaluation) was developed [3]. CONCISE has a very small (62 words) and well-defined vocabulary which can be mastered by non-computer-orientated users. It consists of if-then-else logic and begin-done blocking. Once the vocabulary and structure of CONCISE are known, the user is free to create or change interpretation rules at will. Because the interpreter and the CONCISE language are mainly concerned with peak intensity, width and position data, the user can also create interpretation rules for other types of spectra or experiments.

The development of interpretation rules is, however, not necessarily a quick and straightforward process [3]. Adequate correlation data and test spectra are often not available, which severely limits the possibilities of creating interpretation rules for either the user or the computer. Furthermore, even when correlation data are available, they are often of questionable usefulness. For example, peak positions quoted for the absorptions of a given functionality often vary from one reference to another. This variability is very important if one is trying to make a set of interpretation rules. If the created rules allow peaks to fall into an artificially large region, then false positive results (i.e., indicating that a functionality is likely to be present when it is not) will be returned, while an artificially small region will usually result in false negative results being returned. Consideration must also be given to what distinction, if any, will be given to a peak found at the center of the expected range as opposed to one at either extreme. The user must also establish how to use intensity and width data, when available, and what to do if these data cannot be found. Another problem encountered is that few authors define what commonly used i.r. terms such as "sharp", "broad", "strong" and "weak" mean mathematically. Finally, even if good, well-defined peak position, intensity, and width data are available, the user must create rules which in some way numerically reflect the expectation that a given functionality is either present or absent.

This paper reports the development of programs which create CONCISE interpretation rules for PAIRS based on a set of representative spectra in an automated but interactive manner. The programs use peak position, intensity, and width tables produced by an automated peak-picking routine. This method reduces the dependency on published frequency correlation data and enhances the usefulness of data already available. The heuristic approach of PAIRS is maintained, while ease of comprehension and modification of generated rules is given high priority. All work was done using the MISIP version of PAIRS on a Nicolet 1180 minicomputer and programs generated have been optimized for this system.

DESCRIPTION OF EXISTING INTERPRETATION SYSTEM

Both MISIP and PAIRS have been described elsewhere [1—3, 15] and therefore only a cursory description will be given here. The interpretation package available for Nicolet FTIR systems consists of two FORTRAN programs (the interpreter and rule compiler), a set of interpretation rules in the CONCISE language and an integer file containing the compiled rules. The versatility of the interpreter lies partly in that it treats both spectral information and the compiled interpretation rules as data. Thus, changes to the interpretation rules can be made with no knowledge of FORTRAN and little knowledge of the system software for the computer used. Rule changes are machine-independent.

The interpreter program requests as input both spectral and supplemental information. Spectral information includes peak height, width and intensity values. Peak heights are allowed normalized values from 1 to 10, with 10 being the strongest peak in the spectrum. Peak widths are given values of 1, 2 or 3 corresponding to sharp (FWHH < 12 cm^{-1}), average and broad (FWHH > 75 cm^{-1}), respectively. Width values are assigned independently of peak position; thus a peak with FWHH of 80 cm^{-1} is considered broad whether it occurs at 3600 cm^{-1} or 700 cm^{-1}. This is in contrast to many published i.r. data tables which change the criteria for broadness depending on peak position. Peak position values currently are given between 4000 cm^{-1} and 500 cm^{-1}. The present limits are, however, dictated by the interpretation rules and are not a fundamental limitation of the interpreter.

Supplemental information requested by the interpreter includes sample state and empirical formula information. The sample state choices are: oil, neat, salt, CCl_4, $CHCl_3$, vapor or other. Empirical formula information is optional and the entering of partial formula information is allowed. The known presence or absence of a given element can be used, therefore, to disregard functionalities which cannot be present in the compound of interest. If no formula is given, the interpreter assumes all possible elements are present.

The interpreter returns an expectation value calculated according to the interpretation rules for each functionality. The actual interpretation printout

is in descending order by expectation value and a lower limit for the list is requested. Expectation values are allowed to range from a high of 0.99 to a low of 0.01. The underlying philosophy concerning these expectation values is that the interpreter will never return a definite presence (expectation value of 1.00) or absence (expectation value of 0.00) of a given functionality, thereby forcing the user to assess all possibilities and make the final decision.

The compiler, like the interpreter, is written in FORTRAN. It translates the rules from CONCISE to integer strings (the compiled rules) after checking to insure that the logic is correct. Compiled output is not generated if logic or vocabulary errors are encountered, but error messages are printed to assist the user. The compiled output, when generated, is stored in a disk file for future use by the interpreter. Once a set of compiled rules has been created, no further use of the compiler is necessary unless modifications are made in the CONCISE rules.

Because of its availability on an instrument-based minicomputer, the MISIP version of PAIRS has some advantages not found with the original package. Spectra are inherently digitized in FTIR spectroscopy and, therefore, peak position, width and intensity determination can be a relatively straightforward process. Automated peak picking and the ability to have the results of such a routine automatically entered into the interpretation program greatly reduce the time necessary to interpret a spectrum. This speed is useful for both interpreting spectra of unknown compounds and for testing developed interpretation rules with spectra of known compounds. The availability of large libraries containing digitized spectra and the associated programs needed for retrieval also make the testing process much easier. It is for these reasons that the MISIP package as it exists on the Nicolet 7199 system was selected for automated development of interpretation rules for either MISIP or PAIRS.

DEVELOPMENT OF THE AUTOMATED RULE GENERATOR

One of the major hurdles for computerized interpretation programs of the heuristic type to overcome is the massive effort required to develop interpretation rules. Trulson and Munk [14] recognized this fact in their recently reported promising work on a table-driven approach to i.r. spectral interpretation. Rule development and subsequent testing are generally much more time-consuming than either acquiring test spectra or programming the interpretation routines. In order to expand the usefulness of the PAIRS package, automated rule generation must be developed. A further advantage of automated rule generation is that a more mathematical and uniform method of determining expectation values can be developed and used.

If one were to attempt to create interpretation rules in an automated manner by mimicking human thought processes, two problems would arise. First, the thought process may be undefinable and is probably different from one spectroscopist to the next. Different people will probably disagree on

the relative importance of data used and probably even on the amount of data used in the decision-making process. The second problem is that, even if the thought process could be clearly defined, the programming necessary to automate rule generation would most likely be prohibitive in time (both programming and computer) and size (both computer and mass storage). An alternative is to create interpretation rules by a mathematically logical approach in a pseudo-heuristic manner which returns rules in an easily understandable form. The aim is to maintain the user's ability to understand how judgements are based on the data and the capability to modify these data or the resulting rules if misinterpretations result.

In order to complete this version of the automated rule generator, a few underlying principles have been followed. The mathematics involved in generating the expectation values should be as simple as possible. The use of simple mathematics is justified until it is shown that more complicated mathematics are necessary for the generation of better interpretation rules. Correlations between absorptions will thus not be used in determining expectation values. An example of correlation is the relative location of the NH-stretches and NH-bends in amines. Substances with relatively high NH-stretching frequencies have relatively low NH-bending frequencies and vice versa. Disregarding this type of correlation deviates from the thought process of a spectroscopist and, therefore, the heuristic approach, but will be used initially to simplify the mathematics. Every question in the tree will, therefore, produce a mathematical action, not another question. Furthermore, the generation of interpretation rules lacking the ability to make judgements based on correlations will be useful in determining what the actual importance of band correlations is in interpreting i.r. spectra. Knowing the importance of correlations will be of use in the development of future rule generation programs. The output of the rule generator should be interpretation rules in CONCISE. This requirement will force the user to employ the rule compiler as a means of checking the logic and structure of generated rules. It also allows for manual rule changes should the user so desire. The automated rule generator should use peak tables including peak height, position and width as previously designated. It should be able to use these data to determine regions of interest for a particular subclass of compounds and should further be able to return a variety of numerical information regarding the distribution of peaks to the user.

The initial data used for the automated rule generator were vapor-phase spectra. The absence of effects from intermolecular interactions makes vapor-phase spectra easier to interpret. The spectra chosen were of molecules of moderate size and molecular weight so that rotational lines will not be of concern. Over 3300 easily retrievable vapor-phase spectra of 4 cm^{-1} resolution were made available by S. Lowry of Nicolet Analytical Instruments. These spectra, which are part of the vapor-phase library recorded by Sadtler for L. Azarraga of the EPA, can be obtained already baseline-corrected.

The first stage of this work was the development of FORTRAN routines to determine and present distribution information based on the input spectral

data. The spectral data used consisted of tables containing peak position, intensity and width information as previously defined. This peak information was produced from vapor-phase spectra by an automated peak-picking routine now available as part of Nicolet system software. It requires the user to specify threshold and smoothing parameters arising from the variability of noise and baseline among spectra. A 9-point smooth was used for all spectra. A "wiggle" function is included in the distribution routine which allows for the generation of more realistic peak distribution data by taking into account the limits of resolution, peak-picking round-off errors and the limited number of representative spectra generally available for a given class of compounds. An example of a box type of "wiggle" would be the assumption that a peak at position 1700 cm^{-1} would be considered as having equal likelihood of being at 1699 cm^{-1} and 1701 cm^{-1} (a 2 cm^{-1} wiggle). It was decided that a variable "wiggle" should be used depending on the width of the peak. The position "wiggles" used for this study were: a 4 cm^{-1} wiggle for sharp peaks (i.e., 2 cm^{-1} on each side of the peak), an 8-cm^{-1} wiggle for average peaks and a 12 cm^{-1} wiggle for broad peaks. No attempt was made to optimize the position wiggle parameters.

A value called the "occurrence" is defined as the number of peaks in a given wavenumber range divided by the number of spectra in the data base containing the functionality of interest. The range was set to 1 cm^{-1} intervals for this work. A peak position vs. occurrence graph shows areas where peaks exist for a given functionality. The rule generation program determines the peak position vs. occurrence array based on the spectral data input and a cut-off value requested from the user. This cutoff value is used to zero out regions where occurrences are low but not equal to zero. A value of 0.10 was generally used for this work. The program prints out an array in numerical form indicating regions which contain occurrences higher than the limit set by the user. Figure 1 illustrates how the position vs. occurrence distribution is generated.

The program allows the user to generate the interpretation rules in either an automated or manual fashion. Both methods will be described and the automated method is outlined in Table 1. If the program is allowed to generate the rules by the automated method, the user is asked which regions of those listed are important and which are to be disregarded. This distinction allows the user to disregard regions of solvent absorptions and absorptions from other functionalities which are not of interest. The maximum total expectation value allowed for any functionality is 1.0 regardless of the number of absorptions characteristic of that functionality. It was necessary to find a way to use the maximum occurrence value (MOV) for each region to determine the fraction of the total expectation value to allot for that region. The method used is to add together the MOV for each region of interest to get a total MOV (TMOV). The maximum expectation value for each region is then defined as being equal to the MOV for each region divided by the TMOV, thus: MEV = MOV/TMOV.

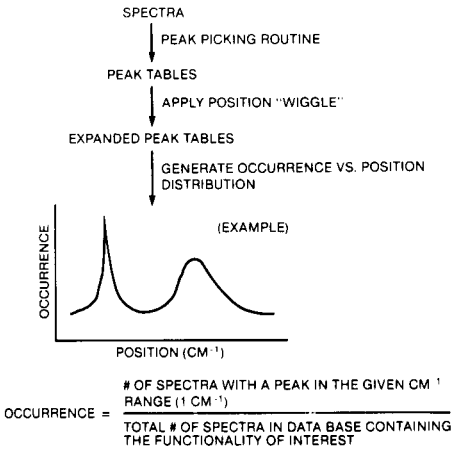

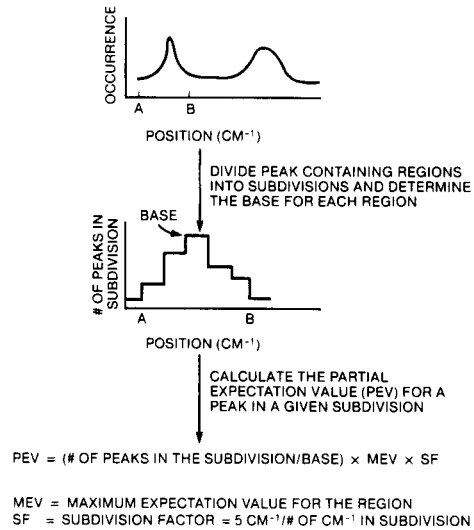

Fig. 1. Generation of occurrence vs. position distribution.

Fig. 2. Determination of partial expectation value (PEV).

TABLE 1

Generalized steps followed by the rule generator in the "auto" mode

1.	Enter peak tables
2.	Apply wiggle functions
3.	Determine occurrence vs. position distribution
4.	Choose regions of interest
5.	Use maximum occurrence value of each region to calculate the maximum expectation value to allot for each region
6.	Divide each region into position subdivisions
7.	Determine width distributions for each region
8.	Calculate a partial expectation value for each position subdivision
9.	Calculate an intensity factor for each intensity interval of each position subdivision
10.	Calculate a final expectation value for a given position subdivision with a given intensity interval and a given width interval
11.	Generate concise rules using the calculated final expectation value
12.	Repeat steps 6 through 11 for each intensity interval of each position subdivision in each region of interest

The manual mode of the rule generator allows the user to classify each region listed as a region of "major" interest, "minor" interest or a region of no interest. The user is then asked the percentage of the total expectation value to allow for the major regions with the percentage to allot to the minor peaks being set equal to whatever is needed to total 100%. The maximum expectation value for each major region is then found by dividing the percentage allocated to the specified major regions of interest by the number of

major peak regions. Similar calculations are done for the regions of minor interest.

Once the regions of interest and the MEV for each region are known, the program requests the name of the functionality for which the interpretation rules are to be created. The name is limited to 20 characters and spaces are not allowed. The program also asks if the rules are to be used alone or combined with other interpretation rules. A control word used by the rule compiler is included in the former case. No further user involvement is permitted and generated rules are output to the terminal or disk file as previously specified by the user.

The regions of interest must be further subdivided to allow for different expectation values to be assigned depending on the position of a peak in the region. The optimum number of subdivisions will have to be determined experimentally but for the present study 5 cm^{-1} subdivisions were employed. Most regions will not contain an integral number of 5 cm^{-1} subdivisions so a subdivision factor (SF) equal to (5 cm^{-1} divided by the number of cm^{-1} in the subdivision) is used to correct for this situation which occurs only on the low frequency end of the region. No attempt was made to center the maximum occurrence value for a region within that region. Instead the regions are divided into 5 cm^{-1} subdivisions starting at the high cm^{-1} end. In order to allot different amounts of the MEV to peaks in different parts of the region, the number of peaks per subdivision is determined. The maximum number of peaks occurring in any subdivision after applying the subdivision factor correction is called the "base" for that region. A partial expectation value (PEV) for a peak in a given subdivision is then calculated by dividing the number of peaks in the subdivision by the base for the region and multiplying by the subdivision factor for that region, thus:

PEV = (Number of peaks in the subdivision/base) × MEV × SF

The PEV is the maximum amount of the expectation value that will be allotted for a peak based solely on position. If a peak is in the most probable subdivision, then PEV = MEV. Figure 2 further illustrates how the PEV is determined for each region.

Width information is also incorporated into the rules by determining width vs. position distributions. Presently, width distributions are being used only to eliminate types of widths not found in a given region. For example, if a region contains only sharp and average width peaks then rules are created asking for only sharp and average peaks. Broad peaks will be disregarded. If, however, sharp and broad peaks are found in a region, then average peaks will be allowed as well. Currently, width information has probably not been used to its fullest potential in the development of interpretation rules. Future versions of the automated rule generator should examine the limits of this potential.

Peak intensity is generally much more important than peak width information in interpreting i.r. spectra. In order to differentiate further between the

peaks in a given region, the distribution of peak intensities in each subdivision is determined. Five peak intensity intervals are considered: 1—2, 3—4, 5—6, 7—8, 9—10. A problem can be encountered if all input spectra contain a band that is in one intensity interval, say 9—10, and none in the 7—8 interval. If interpretation rules are generated so strictly that no value is placed on an intensity of 7—8, then obvious misinterpretations can result for mixtures or compounds with higher or lower molecular weights than the compounds used to generate the rules. It was found that the rules generated could be improved if an intensity wiggle were employed. As in the case of the frequency distribution, this intensity wiggle helps to smooth out the graininess caused by a finite data base.

It was decided that an intensity factor should be determined for each intensity interval in each position subdivision. Thus, if one subdivision contains mostly low intensity peaks, then the rules generated for that subdivision will so reflect this observation. The first step in determining the intensity factors for a subdivision is to count the number of peaks in the subdivision falling into each of the aforementioned five intensity intervals. In order to determine the final intensity factor for any interval it was decided to add the number of peaks in any interval with half the number of peaks in the interval on either side, divide the resulting sum by the total number of peaks in the subdivision and multiply the result by a normalizing factor. The normalizing factor is necessary, in part, because the intervals 1—2 and 9—10 have only one adjacent interval while the others have two adjacent intervals. The normalizing factors (multiplicative) used are 1/2 for the intervals with two adjacent intervals and 2/3 for the end intervals. Thus, for example the intensity factor (IF) for any 7—8 region is: IF = 1/2{[(number of peaks with intensity 7—8) + 1/2(number of peaks with intensity 9—10) + 1/2(number of peaks with intensity 5—6)]/(number of peaks in subdivision)}.

The final expectation value (FEV) for a given intensity interval in a given position interval with a given width interval will be equal to the previously derived partial expectation value multiplied by the intensity factor: FEV = PEV × IF.

It is expected that the above derivation of the final expectation value will need to be revised as knowledge is gained through the generation of interpretation rules and subsequent interpretations. For this reason, the routines used to produce the PEV, IF and FEV are modular and easily modifiable.

All routines of the automated rule generator are written in FORTRAN including the driver routine. One short BASIC program has been written which converts the CONCISE rule file written by the generator into a file suitable for the system editor (DEDIT). The ability to use the editor to modify and combine generated interpretation rules adds great flexibility to the existing interpretation package.

RESULTS AND DISCUSSION

In order to test the rule generating capabilities of the above-described program, the generation of rules for saturated alcohols was undertaken. The object was to create rules for primary, secondary and tertiary alcohols to ascertain the ability of the generated rules to distinguish one subclass from another. It was also of importance in this stage of the project to ascertain the amount of data required to create reasonable interpretation rules.

Spectra of 51 non-α,β-unsaturated alcohols were chosen from the EPA vapor-phase library including 19 primary, 18 secondary and 14 tertiary alcohols. All absorption spectra were of 4 cm^{-1} resolution and were obtained already baseline-corrected. Information on peak position, intensity and width was acquired by using the existing Nicolet peak-picking routine. A 9-point Savitzky -Golay [16] smoothing routine was used to enhance the usefulness of the peak picker. Peak data files which are compatible with both the interpreter and automated rule generator were created by using a previously developed FORTRAN program.

The 19 primary alcohol data files were read into the rule generator. An occurrence threshold of 0.10 was used. The regions chosen as important for this functionality were 3677—3663 cm^{-1} and 1060—1037 cm^{-1}. The maximum expectation values (MEV's) for these regions were 0.61 and 0.39, respectively. Rules were generated in the automated mode as previously described and output to a disk file.

Rules for the secondary and tertiary alcohols were created in exactly the same manner. The regions of interest for the secondary alcohols were 3661—3649 cm^{-1} (MEV of 0.45), 1266—1211 cm^{-1} (MEV of 0.24) and 1151—1128 cm^{-1} (MEV of 0.31). The regions of interest for tertiary alcohols chosen were 3650—3636 cm^{-1} (MEV of 0.50), 1343—1321 cm^{-1} (MEV of 0.18) and 1185—1150 cm^{-1} (MEV of 0.32).

All rule files created by the rule generator were reformatted for use with the system editor (DEDIT) using the simple BASIC program written for this purpose. The resulting DEDIT-compatible files are then combined into one file for use by the CONCISE rule compiler. The CONCISE rules were converted by the rule compiler to an integer string file used by the interpreter routine.

All 51 spectra used as data to generate the interpretation rules were interpreted with the generated rules. The results are listed in Table 2. Compounds 1—19 are primary alcohols, 20—37 are secondary alcohols and 38—51 are tertiary alcohols. Table 2 indicates quite clearly that good interpretation rules can be generated in an automated manner using the program. The intensity and position wiggle functions partially overcome the problems caused by the limited amount of data used to generate the rules. These results are most encouraging and additional development of the rule generation program is warranted.

The generation of rules in an automated and more mathematical and objective manner allows a great deal of information to be learned from an

TABLE 2

Expectation values for 51 alcohols

Compound	Expectation values		
	Primary	Secondary	Tertiary
1 Isobutanol	0.45	0.17	0.01
2 Iso-octanol	0.79	0.01	0.01
3 1-Hexanol, 5-methyl-,	0.83	0.01	0.17
4 1-Hexanol	0.79	0.01	0.01
5 1-Heptanol	0.93	0.01	0.01
6 1-Decanol	0.93	0.01	0.01
7 1-Octanol	0.99	0.01	0.01
8 9-Decen-1-ol	0.93	0.01	0.01
9 Cyclohexaneethanol	0.99	0.01	0.01
10 1-Propanol, 3,3-diphenyl-,	0.80	0.01	0.01
11 9-Octadecen-1-ol	0.99	0.01	0.01
12 Ethanol	0.30	0.34	0.01
13 1-Propanol	0.26	0.10	0.01
14 1-Pentanol, 2-methyl-2-propyl-,	0.84	0.01	0.01
15 Ethanol, 2-bromo-,	0.76	0.01	0.01
16 3-Buten-1-ol, 3-methyl-,	0.38	0.13	0.16
17 1-Pentanol, 2,4,4-trimethyl-,	0.70	0.23	0.01
18 1-Propanol, 2-amino-2-methyl-,	0.35	0.07	0.01
19 1-Tridecanol	0.68	0.01	0.01
20 5-Nonanol	0.01	0.81	0.01
21 2-Nonanol	0.01	0.98	0.01
22 4-Heptanol	0.01	0.81	0.01
23 2-Butanol, 3-methyl-,	0.01	0.93	0.01
24 Cyclohexanol, 2-methyl-, *trans*-,	0.23	0.98	0.01
25 3-Decanol, 6-ethyl-,	0.32	0.61	0.01
26 Cyclohexanol, 2-ethyl-,	0.32	0.80	0.01
27 2-Heptanol, 5-ethyl-,	0.06	0.93	0.01
28 2-Decanol	0.01	0.98	0.01
29 3-Octanol, 6-ethyl-,	0.38	0.41	0.01
30 2-Pentanol, 4-methyl-,	0.32	0.76	0.01
31 2-Heptanol	0.06	0.78	0.01
32 2-Pentanol	0.01	0.93	0.01
33 Cyclohexanol, 4-methyl-,	0.18	0.87	0.01
34 2-Butanol	0.01	0.69	0.01
35 3-Pentanol, 2,2-dimethyl-,	0.32	0.17	0.01
36 Isopropanol	0.01	0.51	0.01
37 4-Heptanol, 2,6-dimethyl-,	0.01	0.58	0.01
38 3-Hexanol, 3,5-dimethyl-,	0.38	0.01	0.73
39 2-Heptanol, 2-methyl-,	0.01	0.06	0.99
40 Cyclohexanol, 1-methyl-, s-	0.25	0.06	0.27
41 3-Pentanol, 3-methyl-,	0.32	0.07	0.73
42 3-Hexanol, 3,4-dimethyl-,	0.01	0.07	0.73
43 Butanol, tert-,	0.01	0.12	0.50
44 3-Pentanol, 3-ethyl-,	0.01	0.06	0.82
45 3-Hexanol, 3,4-diethyl-,	0.01	0.07	0.68
46 2-Octanol, 2-methyl-,	0.01	0.05	0.85
47 4-Penten-2-ol, 2,3-dimethyl-,	0.25	0.01	0.43
48 3-Heptanol, 3,6-dimethyl-,	0.01	0.17	0.99
49 2-Heptanol, 6-amino-2-methyl-,	0.01	0.05	0.61
50 2-Butanol, 2-methyl-4-phenyl-,	0.01	0.09	0.60
51 3-Octanol, 3,7-dimethyl-,	0.15	0.38	0.82

interpretation. For example, the interpretation of spectrum number 7 results in an expectation value of 0.99 for primary alcohol and 0.01 for both secondary and tertiary alcohols. This interpretation indicates that the spectrum is "ideal" for a primary alcohol. Furthermore, the very low expectation values assigned for secondary and tertiary alcohols indicate clearly that absorptions for either of these two functionalities were not present in spectrum number 7. The distinguishing capability of the generated rules in this case is unquestionable.

The interpretation of spectrum number 1 is not quite as clear. An expectation value of 0.45 implies that there are data to indicate the spectrum is that of a primary alcohol but that the data are less than perfect. There is also a smaller amount of data indicating a secondary alcohol and this functionality is assigned a much smaller expectation value of 0.17.

Spectrum number 12 is a case of misinterpretation if one strictly adheres to the values of the assigned expectation values (0.34 for secondary alcohol and 0.30 for primary alcohol). The low values for both functionalities indicate that spectrum number 12 is not ideal for either a primary or secondary alcohol. Furthermore, a difference of 0.04 in expectation values should be treated cautiously until adequate interpretation data indicate that such a small difference can be of importance to the user.

Spectrum number 29, which is actually a secondary alcohol, is assigned the expectation values of 0.41 and 0.38 for secondary and primary alcohols, respectively. Again, the small difference in expectation values (0.03) should not be considered as useful until the amount of data interpreted indicates otherwise. What is important in this case is that the spectrum is not representative of the "best" primary or secondary alcohol as determined by the rule generation program for the spectral data used to generate the rules.

Spectrum number 35 is also a secondary alcohol but has an abnormally high hydroxyl-stretching frequency for this type of alcohol. The interpreter suggests that the compound is most likely a primary alcohol with an expectation value of 0.32. "Secondary alcohol" is assigned a value of 0.17. The interpreter is using the high hydroxyl stretch as positive information for the likelihood for a primary alcohol being present and negative information for the likelihood of a secondary alcohol being present. Again, the user should treat such low expectation values with caution.

Rules were also generated for the saturated acid functionality. Eighteen spectra were chosen from the vapor-phase library, peak-picked and entered into the rule generation program. As with the alcohol rules, an occurrence threshold of 0.10 was used and the rules were generated using the "auto" mode. All 18 spectra used as data for rule generation were then interpreted using the new rules and the results are presented in Table 3. As in the case of the alcohols, the results for the saturated acid class show that good interpretation rules can be generated with a limited number of spectra for data.

The success with which interpretation rules can be generated in an automated fashion has been demonstrated. Both the work of Trulson and Munk

TABLE 3

Expectation values (EV) for 18 acids

Compound	EV	Compound	EV
1 Butyric acid	0.99	10 Undecanoic acid	0.99
2 Pentanoic acid	0.46	11 Octadecanoic acid	0.57
3 Nonanoic acid	0.72	12 Propionic acid, 3-mercapto-,	0.25
4 Cyclohexanepropionic acid	0.99	13 Acetic acid, (*o*-ethoxyphenyl)-	0.77
5 Hexanoic acid, 3,5,5-trimethyl-,	0.52	14 Hexanoic acid, 6-phenyl-,	0.73
6 Butyric acid, 3,3-dimethyl-,	0.62	15 Cycloheptanecarboxylic acid	0.77
7 Butyric acid, 3-methyl-,	0.49	16 10-Undecenoic acid	0.99
8 Caprylic acid	0.77	17 4-Pentenoic acid	0.99
9 Dodecanoic acid	0.99	18 Butyric acid, 2-bromo-,	0.62

[14] on a table-driven approach to infrared spectral interpretation and the present effort on generating interpretation rules in an automated manner show good predicting power for the tested functionalities and good distinguishing power among subfunctionalities. The value of our rule generator as it presently exists lies in its ability to: generate CONCISE interpretation rules very quickly and with limited data, relieve the user who infrequently generates new interpretation rules from the burden of learning the CONCISE language, give a definite meaning to an expectation value approaching 1.00, allow the development of interpretation rules in a mathematically consistent and logical manner, allow the development of interpretation rules for other types of data with only a limited investment of time, and reduce the dependence on frequency correlation tables if spectral data are available. Furthermore, the generation of rules in a mathematically logical, consistent and reproducible method is a first step towards extending the PAIRS and MISIP packages to artificial intelligence.

REFERENCES

1 H. B. Woodruff and G. M. Smith, Anal. Chem., 52 (1980) 2321.
2 S. A. Tomellini, D. D. Saperstein, J. M. Stevenson, G. M. Smith, H. B. Woodruff and P. F. Seelig, Anal. Chem., 53 (1981) 2367.
3 H. B. Woodruff and G. M. Smith, Anal. Chim. Acta, 133 (1981) 545.
4 H. B. Woodruff and M. E. Munk, J. Org. Chem., 42 (10) (1977) 1761; Anal. Chim. Acta, 95 (1977) 13.
5 J. Zupan, Anal. Chim. Acta, 139 (1982) 143; 103 (1978) 273.
6 T. Visser and J. H. Van der Maas, Anal. Chim. Acta, 122 (1980) 337; J. Raman Spectros., 7 (1978) 125, 278.
7 M. Farkas, J. Markos, P. Szepesvary, I. Bartha, G. Szalontai and Z. Simon, Anal. Chim. Acta, 133 (1981) 19.
8 G. Szalontai, Z. Simon, Z. Csapo, M. Farkas and Gy. Pfeifer, Anal. Chim. Acta, 133 (1981) 31.
9 B. Debska, J. Duliban, B. Guzowska-Swider and Z. Hippe, Anal. Chim. Acta, 133 (1981) 303.

10 W-R. Leupold, C. Domingo, W. Niggemann and B. Schrader, Fresenius Z. Anal. Chem., 303 (1980) 337.
11 N. A. B. Gray, Anal. Chem., 47 (1975) 2426.
12 I. E. Frank and B. R. Kowalski, Anal. Chem., 54 (1982) 232R.
13 K. Varmuza, Pattern Recognition in Chemistry, Springer-Verlag, New York, 1980.
14 M. O. Trulson and M. E. Munk, Anal. Chem., 55 (1983) 2137.
15 S. A. Tomellini, J. M. Stevenson and H. B. Woodruff, Anal. Chem., 56 (1984) 67.
16 A. Savitzky and M. J. E. Golay, Anal. Chem., 36 (1964) 1627.

Analytica Chimica Acta, 162 (1984) 241—251
Elsevier Science Publishers B.V., Amsterdam — Printed in The Netherlands

PREDICTION OF WINE QUALITY AND GEOGRAPHIC ORIGIN FROM CHEMICAL MEASUREMENTS BY PARTIAL LEAST-SQUARES REGRESSION MODELING

I. E. FRANK and BRUCE R. KOWALSKI*

Laboratory for Chemometrics, Department of Chemistry BG-10, University of Washington, Seattle, WA 98195 (U.S.A.)

(Received 23rd February 1984)

SUMMARY

A multivariate regression method, PLS, was applied to model the relationship between objective chemical measurements and subjective sensory evaluation of Pinot Noir wine samples. Descriptive and predictive models were calculated according to preset pathways in order to classify the wines according to their geographic origin and to predict several organoleptic characteristics. The importance of inorganic elements in these prediction problems was investigated.

Product quality control is a very important problem in all industrial processes. In most cases, the quality requirements are well defined and there is a narrow range of various measurable characteristics that a "good" product must match. In the food industry, it is a more complex problem. The quality of certain products cannot easily be defined by objective measurements and analytical chemical methods cannot fully replace organoleptic examinations. Wine is one of those interesting chemical mixtures, the overall sensory impression of which is defined by its many organic and inorganic composites in a very complex way.

Recently, a regression method called PLS (partial least squares) was developed [1], which models the relationship among information sources of multiple measurements according to a preset causal path. This method not only describes the connection between variables segregated into blocks, but gives a predictive model for measurements or observations in a response block.

Several studies have been done to explore the relationship between chemical measurements and sensory scores of wine samples [2—5]. Another important question is to identify the geographic origin of wines revealing counterfeits, instability of different types, labels [6—8]. In some other studies [9—11], in which pattern recognition was applied, only one source of information was investigated at a time or all the chemical measurements coming from different analytical methods were treated together, regardless of their natural separation.

0003-2670/84/$03.00

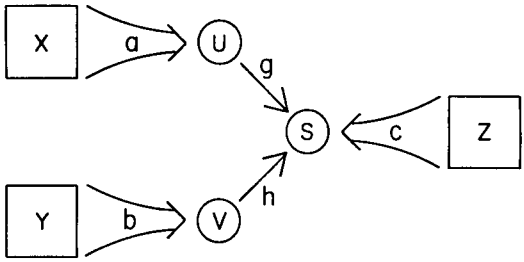

Fig. 1. PLS model with two predictor blocks and a multivariate response block.

In this study, the relationship among elemental, organic composition, sensory evaluation and geographic origin of 40 Vitis Vinifera cv. Pinot Noir from France and the United States is modeled by the PLS method. The PLS model provides useful information about which elements and organic compounds are responsible mainly for the good and bad characteristics of the different wines, about which chemical components differ in the French and American wine regions and about how the overall sensory score is composed of 13 individual organoleptic characteristics of the wine samples.

METHOD

The method applied here to build linear regression models on the data of four blocks is called PLS, which stands for partial least squares referring to the solution of the regression.

The idea behind this method is to describe each block of variables (type of measurement) by a set of latent variables (underlying components) which are linear functions of the original variables in the block. The role of these latent variables is not only to describe their own block (outer relationship), but also to relate to each other according to the preset causal pathway (inner relationship).

The first application in physical sciences [12] used the so-called MODE B algorithm, calculating only one latent variable for each block by multiple regression. The disadvantage of this algorithm is that it does not give a predictive model for the response block. The MODE A algorithm, which calculates several latent variables by single regression to build a predictive model, was applied in several two block chemical systems [13—16]. In the present study the MODE A algorithm was also used and was extended to more than two blocks.

This PLS algorithm describes more than the relationship among the various blocks. By explaining the influence of one block on another, it can predict all the variables in the response block (the block at the end of the causal path) and can establish which predictor block (type of measurement) is the most important as well as which predictor variables have the largest effect on the response variables. A PLS model with two predictor blocks, X and Y,

and one response block, Z, is illustrated in Fig. 1. The relationship between the latent variables and the original variables of the same block (outer relationship) is analogous to an eigenvector expansion. Lesser numbers of latent variables, which are mutually orthogonal, span most of the variance associated with the response block in a predictor block with a higher number of original variables

$$\begin{aligned} u_i^m &= \sum_j a_j^m x_{ij} \\ v_i^m &= \sum_k b_k^m y_{ik} \\ s_i^m &= \sum_l c_l^m z_{il} \end{aligned} \qquad \begin{aligned} &i = 1 \ldots I \\ &j = 1 \ldots J \\ &k = 1 \ldots K \\ &l = 1 \ldots L \\ &m = 1 \ldots M \end{aligned} \tag{1}$$

where i is the sample index, j, k and l are the indices of the variables, m is the index of components, u, v and s are the latent variables, and a, b and c are coefficients calculated by single regressions.

However, there is another criterion in the calculation of these latent variables, namely that they must be maximally correlated to each other, i.e., u and v must explain the maximum variance in s. The relationship among the latent variables is called the inner relationship

$$s_i^m = g^m u_i^m + h^m v_i^m \tag{2}$$

The optimal number (M) of the latent variables for a PLS model of the highest predictive power is determined by Stone-Geisser's cross-validation test [17]. This method estimates prediction error as a function of the number of latent variables by the leave-one-out technique. The model with least predictive error is then chosen. For faster computation, instead of leaving one sample out for prediction from the model and repeating the procedure I times, one-fourth of the samples were omitted and the procedure was repeated four times.

A special case of the PLS model is also used here where there is no Y block and there is only one variable in the Z block. PLS gives a suboptimal solution for the underdetermined system. It mitigates the collinearity problem by regressing the response variable on orthogonal latent variables. In this respect, the PLS regression is similar to the principal component regression. Increasing the number of latent variables to the number of original variables in the predictor block, the PLS solution converges to multiple regression by ordinary least squares. However, by removing some of the later latent variables, which similarly to the principal components describe only variance caused by noise, automatic noise filtering can be achieved. In this case, although the fit of the model is worse than that of the multiple regression solution, the predictive power of the model is increased, as variance caused by random noise is omitted from the model. The coefficients of the resulting linear model can

easily be calculated from the loadings of the latent variables (a_j^m) and the inner relationship coefficients (g^m). The PLS method gives biased estimates for the regression coefficients in contrast to the ordinary least squares solution. However, the variance of PLS estimates is generally smaller than those for least squares, so that often the expected squared error is smaller. This is especially true when $J > I$.

DATA

The 40 Pinot Noir wine samples used in this study, and previously examined by various pattern recognition methods, have been listed elsewhere [9]. The contents of 17 elements were determined by atomic emission spectrometry [9]. The organic components were separated by gas chromatography (g.c.); the mathematical characterization of the chromatograms contained 137 integrated peak areas of organic acids and neutral components [10]. The sensory evaluation was given in terms of 13 individual characteristics and one overall quality score [18]. The geographic categories and their three-digit binary codes are as follows

wines from the Pacific Northwest	1 0 0
wines from California	0 1 0
wines from France	0 0 1

The total of 171 (17 + 137 + 14 + 3) measurements, scores and binary codes, called variables, were segregated into four blocks, each describing a different type of measurement. The data used here are summarized in Table 1. As identification of the 137 chromatographic peaks was not available for this study, the whole chromatogram was used directly as a 137-dimensional measurement vector.

Because of the different scale in each measurement, all variables were scaled to zero mean and unit variance.

RESULTS AND DISCUSSION

The effect of individual sensory parameters on the overall score for wine quality

A PLS regression model was calculated on the sensory evaluation block, trying to explain the variance in the overall quality score from the individual sensory parameters. Three models were built: one on all 40 samples, one on the 26 American wines and one on the 14 French wines. The optimal number of latent variables from prediction point of view was determined by cross-validation. The results are summarized in Table 2. In the overall model, two orthogonal components were found; both describe the "goodness" of the wine (positive correlation to the overall quality). The first, most important component is composed of aroma character and intensity, flavor character and intensity, body and color as positive contributors and undesirable odor

TABLE 1

Data for the wine study

Wine type	Block I Category (3)	Block II Elemental content (17)	Block III G.c. (137)	Block IV Sensory scores (14)
17 from Pacific Northwest	1 0 0	1 Cd	Peaks of organic acids and neutral components	1 Clarity
		2 Mo		2 Color
		3 Mn		3 Aroma intensity
		4 Ni		4 Aroma character
9 from California	0 1 0	5 Cu		5 Undesirable odor
		6 Al		6 Acidity
		7 Ba		7 Sugar
14 from France	0 0 1	8 Cr		8 Body
		9 Sr		9 Flavor intensity
		10 Pb		10 Flavor character
		11 B		11 Oakiness
		12 Mg		12 Astringency
		13 Si		13 Undesirable taste
		14 Na		14 Overall quality
		15 Ca		
		16 P		
		17 K		

and taste as negative contributors. The second, weaker component has positive loadings from clarity, acidity and negative loadings from color, sugar and oakiness. Astringency turned out to be an unimportant parameter according to the panel for predicting the overall quality. If the model is calculated with only one type of wine, cross-validation finds only one predictive component. When the regression coefficients of the American and French model are compared, significant differences can be noted. Although in both models, the highest positive contributors are the aroma and flavor characters and body and the highest negative contributors are the undesirable taste and odor, strangely in the French model, the most negative parameter is clarity; the acidity got a high negative loading while oakiness and sugar became positive in both models. This means that the judges' impression of the overall quality as a function of individual characteristics differs from one type of wine to another. Certain parameters are ignored (low loadings) in the overall and the American model, while in the French model, all the individual scores have high loadings.

The PLS method gives a model with a good fit and prediction accuracy for the overall score, considering the high noise level in sensory evaluation data. However, the regression coefficients differ from those of the Davis scorecard and of the Modified scorecard [18].

TABLE 2

Magnitude of regression coefficients in three different sensory models

Estimated regression coefficients	American and French	American	French	
	Flavor char.	Flavor char.	Flavor char.	+
	Aroma char.	Aroma char.	Aroma char.	
	Body	Body	Body	
	Flavor int.	Color	Color	
	Color	Sugar	Sugar	
	Aroma int.	Oakiness	Aroma int.	
		Flavor int.	Oakiness	
			Astringency	
	Oakiness	Aroma int.		0
	Acidity	Clarity		
	Sugar	Acidity		
	Astringency			
	Clarity			
	Undesirable odor	Astringency	Acidity	−
	Undesirable taste	Undesirable odor	Undesirable odor	
		Undesirable taste	Undesirable taste	
			Clarity	
Error in fit (%)	6	8	4	
No. of latent variables	2	1	1	
Error in prediction (%)	8	10	12	

Prediction of geographic origin

An attempt was made to predict the geographic origin of the wine samples on the basis of one or more information sources by the PLS method. The results are listed in Tables 3 and 4. In previous pattern recognition analyses [9—11] only selected variables were included in the model in order to maintain a high enough sample/variable ratio. With the PLS method, information relevant to the prediction problem from all the variables can be used. Also, in the previous studies, only the goodness of fit of the models was investigated and no result was reported referring to the prediction power of the models calculated by different methods. It is very important in PLS models (and, in general, in any regression model) to choose the number of parameters (variables or components) by cross-validation, which selects the optimal model for prediction.

TABLE 3

Parameters of PLS models predicting geographic origin

Predictor block(s)	Models			
	Sensory	Elemental	G.c.	Elemental + g.c.
No. of components determined by cross-validation	1	4	5	4
Sum of the squared residuals in cross-validation	2.80	0.97	2.11	0.82
Average absolute errors in fit	0.456 0.302 0.253	0.115 0.134 0.116	0.134 0.138 0.176	0.069 0.094 0.081
Misclassification fit: prediction (out of 40 samples)	25:36	0:7	0:10	0:6

TABLE 4

Regression matrix for predicting geographic origin from elemental analysis

	Cd	Mo	Mn	Ni	Cu	Al	Ba	Cr	Sr
Pacific Northwest	1.526	0.381	−0.105	0.722	0.054	0.185	1.333	−5.422	0.105
California	0.760	−0.298	0.110	0.175	−0.250	−0.293	0.112	3.516	0.071
France	−2.287	−0.084	−0.005	−0.898	0.197	0.108	−1.444	1.906	−0.177
	Pb	B	Mg	Si	Na	Ca	P	K	
Pacific Northwest	0.142	−0.107	0.003	−0.003	0.000	0.005	−0.003	−0.000	
California	−0.074	0.057	−0.000	0.013	−0.001	−0.000	0.002	0.000	
France	−0.068	0.049	−0.003	−0.010	0.000	−0.004	0.001	−0.000	

One solution to calculate regression models for category response variables is to introduce as many dummy variables as there are categories to be separated. Each of these dummy variables has two values: 1 if the samples belong to the category described by the variable and 0 if it does not. With the two-block PLS method, all the dummy variables can be incorporated in the model. This means that parallel separation of all three wine types (French, California and Pacific Northwest) can be achieved.

The sensory data do not provide enough information to separate the three wine regions. These data separate only the French wine samples, and the model has practically no predictive power. Both the organic and inorganic compositions provide ample information to separate completely the three wine categories (see Table 3 misclassification in fit), but the prediction power

of the model based on the elemental analysis is much better (see Table 3 misclassification in prediction). Combination of the two chemical blocks as two predictor blocks gives, by far, the best fit (average absolute error in fit), the reported values should be compared on a relative basis with the actual values: 17/40 = 0.43, 9/40 = 0.23 and 14/40 = 0.35.

From the regression coefficient matrix, which in the case of multiple response variables is analogous to the regression coefficient vector, the significance of the predictor variables in separating one particular wine type can be revealed. The regression matrix for the elemental block is given in Table 4. For Californian wines the most characteristic elements are chromium and cadmium; in wines from the Pacific Northwest cadmium, barium and nickel; and in French wines chromium, aluminum and copper. Barium, Cd, Ni and Sr are the best elements in distinguishing between American and French wines (high positive coefficients for the American wines and high negative coefficients for the French wines), while for the separation between the two American types, Al, Cr, Mo and Mn are the most important elements.

In a previous study [9], in two-category separations barium and calcium were selected as variables best separating American and French wines, while aluminum and potassium were best for separating wines from the Pacific Northwest and California.

Prediction of all sensory parameters from chemical measurements

In a previous study [11], an attempt was made to correlate the chemical measurements to the sensory evaluation data. Only two peaks of the gas chromatogram were included in the stepwise regression analysis in order to avoid overfitting, however, many other variables had high correlation to the overall quality score. In the same paper, the first three principal components of the chemical and sensory variables (in the former only g.c. peaks were reported having high loadings) did not show high correlations with one another, so this model failed to capture the relationship between the objective measurements and organoleptic evaluations. The following results show that PLS gives an applicable model, where other multivariate methods failed. With the general two- and three-block PLS method, it is possible to calculate the regression model to predict all the individual and the overall sensory scores together from the chemical composition of the wines. Three causal paths were examined: sensory data prediction from elemental analysis, from gas chromatograms and from both elemental and organic composition. In the first case, three models were built: on all wines, only on American wines and only on French wines.

The American wine model consists of one component of "goodness": positive loadings of positive characteristics and negative loadings of negative ones. The French wine model has one component of "badness": negative loadings of positive characteristics. In the overall model, both components appear. In the French wines, Cd, Mo, Cu and Cr, and in the American wines,

Cd, Pb, Ca, Mo, Ni have a positive influence on the quality. Manganese, Cr, Sr, Mg, K and Ba have negative effects in both regions. The slight differences between the effect of the French and American elemental composition is probably due to the different types of soil that can change the matrix of the elements.

In Fig. 2 goodness of fit for the three models is compared. The values on the horizontal axis are the identification numbers of the sensory characteristics. On average, the French model fits better than the American or the overall model; for most of the sensory parameters the average absolute error is around 10% of the mean of the actual value. A specially bad fit is observed for color (2), undesirable odor (5) and undesirable taste (13). The explanation might be that the undesirable characteristics develop because of organic reactions during the storage time, so that the elemental analysis does not have predictive information about these characteristics.

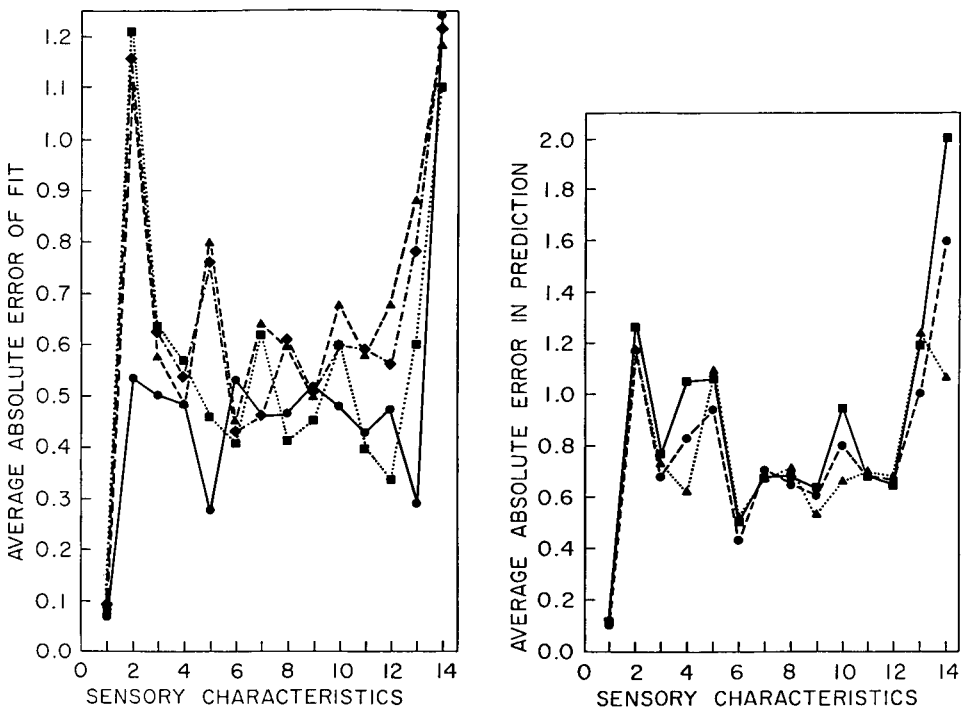

Fig. 2. Goodness of fit of PLS models predicting all the sensory characteristics from elemental analysis. (·—·) All 40 samples; (——) 10% of the mean of the actual value; (— — —) American wine samples; (···) French wine samples.

Fig. 3. Goodness of prediction of PLS models predicting all sensory characteristics from different chemical measurements. (——) G.c.; (— — —) g.c. and elemental analysis; (···) elemental analysis.

As the next step, a predictor model for sensory data on the basis of the chromatographic data was calculated and finally both elemental and organic composition were included in the two predictor block model. The prediction powers of the three models (elemental, organic and elemental and organic) on all 40 samples are compared in Fig. 3.

From the inner relationship coefficients (0.75 of elemental and 0.53 of g.c. block), it is clear that elemental analysis contains more information relevant to the organoleptic characteristics than the organic composition. For certain characteristics, like clarity (1), color (2), acidity (6) and sugar (7), the two chemical blocks have the same predictive power. The prediction based on elemental analysis is better for aroma intensity (3) and character (4), flavor character (9) and intensity (10) and overall judgment (14), while g.c. data give more information about body (8), oakiness (11), astringency (12) and undesirable taste (13) and odor (5). Most of the prediction errors are between 10% and 20%, which is a good result considering the high noise level in sensory evaluation data. Cross-validation chose two components for the elemental analysis and the g.c. plus elemental analysis models and one component for the g.c. model. Because the predictive information from the inorganic and organic composition blocks are highly correlated, the prediction power cannot be increased by using both chemical information sources.

The relationship between the two chemical blocks can be described by a five-component PLS model explaining, for example, the variance in the elemental analysis block from the chromatographic data. The percent error of fit for each element is shown in Table 5. Except for magnesium and copper, all the elements have less than 50% error; the best fit by the PLS model is given for K, Ca, P and Ba.

Conclusion

The aim of this study was to show how the PLS method can be applied to calculate a descriptive and predictive model of the relationship between objective chemical measurements and sensory evaluation data of wine samples. It was demonstrated that the chemical data contain sufficient information to predict the geographic origin, the individual sensory parameters and the overall quality of wines. By segregating chemical variables into blocks coming

TABLE 5

PLS model predicting elemental analysis from organic composition

Element	Cd	Mo	Mn	Ni	Cu	Al	Ba	Cr	Sr
Error in fit (%)	20	31	21	48	82	22	18	25	24
Element	Pb	B	Mg	Si	Na	Ca	P	K	
Error in fit (%)	38	22	120	35	47	11	15	8	

from different analytical measurements, not only the importance of single variables, but the relevance of each block in the prediction problem can be investigated. The composition of latent variables (components) in the PLS model gives quantitative information about which chemical measurements and individual sensory parameters are associated with the quality of the wines.

Because the overall quality score is a different combination of individual parameters in each type of wine, even by the same panel of judges, it is important to develop a model which is able to predict not only the overall sensory judgment, but all the individual quality parameters as well. PLS models predicting response blocks of several variables were calculated successfully to connect inorganic and organic composition with the various sensory parameters.

The PLS method can handle several blocks of multiple measurements, extracting significant components to predict many response variables together. Therefore, it is desirable to include results from several multivariate analytical methods to enable PLS to integrate information from all the relevant sources.

The authors thank the 3M Company for supporting the PLS program development.

REFERENCES

1 K. G. Joreskog and H. Wold (Eds.), Systems Under Indirect Observation, Parts I and II, North Holland, Amsterdam, 1982.
2 R. R. Nelson, T. E. Acree and R. M. Butts, J. Agric. Food Chem., 27 (1979) 1188.
3 A. C. Noble, R. A. Flath and R. R. Forrey, J. Agric. Food Chem., 28 (1980) 346.
4 P. X. Etievant, J. Agric. Food Chem., 29 (1981) 65.
5 H. R. Buser, C. Zainer and H. Tanner, J. Agric. Food Chem., 30 (1982) 359.
6 I. Moret, G. Scarponi, G. Capodaglio, S. Zanin, G. Camaiani and A. Toniolo, Am. J. Enol. Vitic., 31 (1980) 245.
7 G. Scarponi, I. Moret and G. Capodaglio, Riv. Vitic. Enol., 34 (1981) 254.
8 G. Scarponi, I. Moret, G. Capodaglio and P. Cescon, J. Agric. Food Chem., 30 (1982) 1135.
9 W. Kwan, B. R. Kowalski and R. K. Skogerboe, J. Agric. Food Chem., 27 (1979) 1321.
10 W. Kwan and B. R. Kowalski, J. Agric. Food Chem., 28 (1980) 356.
11 W. Kwan and B. R. Kowalski, Anal. Chim. Acta, 122 (1980) 215.
12 R. W. Gerlach, B. R. Kowalski and H. A. Wold, Anal. Chim. Acta, 112 (1979) 417.
13 W. Lindberg, J. Persson and S. Wold, Anal. Chem., 55 (1983) 643.
14 I. E. Frank, J. H. Kalivas and B. R. Kowalski, Anal. Chem., 55 (1983) 1500.
15 M. L. Bisani, D. Faraone, S. Clementi, K. H. Esbensen and S. Wold, Anal. Chim. Acta, 150 (1983) 129.
16 M. Sjöström, S. Wold, W. Lindberg, J. Persson and H. Martens, Anal. Chim. Acta, 150 (1983) 61.
17 M. Stone, J. R. Stat. Soc., Ser. B, 36 (1974) 111.
18 W. Kwan and B. R. Kowalski, J. Food Sci., 45 (1980) 213.

Analytica Chimica Acta, 162 (1984) 253—262
Elsevier Science Publishers B.V., Amsterdam — Printed in The Netherlands

A KALMAN FILTER FOR CALIBRATION, EVALUATION OF UNKNOWN SAMPLES AND QUALITY CONTROL IN DRIFTING SYSTEMS
Part 2. Optimal Designs

P. C. THIJSSEN

University of Nijmegen, Faculty of Sciences, Department of Analytical Chemistry, Toernooiveld, 6525 ED Nijmegen (The Netherlands)
University of Amsterdam, Laboratory for Analytical Chemistry, Amsterdam (The Netherlands)

(Received 27th March 1984)

SUMMARY

It is well known that the optimal design for linear calibration is found at the extremes of the concentration range. For the evaluation of unknown samples, the precision is maximal at the mean value of the calibration standards. If the static model is replaced and stochastic behaviour of the parameters with extension to drift is assumed, only minor differences on these generalizations are obtained. The intelligent analyzer described here integrates on-line procedures for calibration, evaluation, quality control and optimization.

In order to evaluate unknown samples, it is usually necessary to calibrate an analytical instrument. Little attention has been paid to the arrangement of the calibration standards, the usual practice being to distribute the experimental design uniformly. Only if a particular model can be assumed from prior information results on suitable designs will be obtained. For a linear calibration graph, the optimal design comprises replicate standards at two points, which are chosen such that they occur at the extremes of the limited concentration range [1]. For a quadratic graph, the centre of the working range should also be found [2]. More generally, when a polynomial model is used, the optimized calibration pattern is found by taking as many uniformly distributed points as there are parameters [3]. This is analogous to the practice when no model can be assumed from prior information.

An extensive review on optimization of regression designs is available [4]. In the analytical literature, various criteria have been investigated for the optimization procedure. Aarons [2] maximized the final entropy (i.e., the determinant of the covariance matrix) which is directly related to the precision of the estimated parameters. Identical results are obtained by using the imprecision function of an evaluated sample as criterion. Eckschlager [5] introduced this function in information theory in order to derive some practical relations such as the effect of the sensitivity, concentration range

0003-2670/84/$03.00

or noise variance. For the evaluation of unknown analytes, a maximal amount of information is located at the mean value of the preliminary calibration standards, which is of importance for the choice of the concentration range.

Recently, a recursive formulation was suggested for the optimal design computation in least-squares problems with information theory [6]. A similar formulation may be derived for the Kalman filter based on a state space model. Here, the information yield is divided into two parts: a loss of information caused by the prediction and a gain of information as a result of the filtering. For optimal performance of the Kalman filter, the information yield has to be maximized in the measurement sequence.

When the theory proposed in this paper was applied to a calibration problem, i.e., a drifting system involved with dynamic and system noise [7], only small differences were obtained, compared with the traditional results for a linear calibration graph. Although only the calibration problem is investigated, the presented theoretical framework should combine rules-of-thumb on optimization into organized knowledge for a variety of analytical problems, such as sampling and process control.

THEORY

Problem statement

A linear dynamic system is described by the stochastic difference equations

$$\mathbf{x}(k) = F(k)\mathbf{x}(k-1) + \mathbf{w}(k-1) \tag{1}$$

$$z(k) = \mathbf{h}^t(k)\mathbf{x}(k) + v(k) \tag{2}$$

where $z(k)$ is the measurement and $\mathbf{x}(k)$ is the n-dimensional state vector. The n-dimensional system noise vector $\mathbf{w}(k-1)$ and the scalar measurement noise $v(k)$ are defined as gaussian white-noise sequences with zero means and covariance matrices $\mathbf{Q}(k-1)$ and $\mathbf{R}(k)$, respectively. The state $\mathbf{x}(k)$ is normally distributed and independent of the noise, initialized by $\mathbf{x}(0)$ with mean $\hat{\mathbf{x}}(0/0)$ and covariance $\mathbf{P}(0/0)$. Moreover, the $n*n$ transition matrix $\mathbf{F}(k)$ and the $1*n$ measurement vector $\mathbf{h}^t(k)$ have to be known deterministically.

When the state model (1, 2) and the noise covariances $\mathbf{Q}(k-1)$, $\mathbf{R}(k)$ are assumed to be known, the filtered estimates $\hat{\mathbf{x}}(k/k)$ may be determined by the Kalman filter

$$\hat{\mathbf{x}}(k/k-1) = \mathbf{F}(k)\hat{\mathbf{x}}(k-1/k-1) \tag{3}$$

$$\mathbf{P}(k/k-1) = \mathbf{F}(k)\mathbf{P}(k-1/k-1)\mathbf{F}^t(k) + \mathbf{Q}(k-1) \tag{4}$$

$$\hat{\mathbf{x}}(k/k) = \hat{\mathbf{x}}(k/k-1) + \mathbf{k}(k)\{z(k) - \mathbf{h}^t(k)\hat{\mathbf{x}}(k/k-1)\} \tag{5}$$

$$\mathbf{P}(k/k) = \mathbf{P}(k/k-1) - \mathbf{k}(k)\mathbf{h}^t(k)\mathbf{P}(k/k-1) \tag{6}$$

$$\mathbf{k}(k) = \mathbf{P}(k/k-1)\mathbf{h}(k)\{\mathbf{h}^t(k)\mathbf{P}(k/k-1)\mathbf{h}(k) + \mathbf{R}(k)\}^{-1} \tag{7}$$

where $\hat{\mathbf{x}}(k/k-1)$ is the estimate of $\mathbf{x}(k)$ given the measurements $z(1)$, $z(2)$, ..., $z(k-1)$; $\mathbf{k}(k)$ is a $n*1$ filter gain vector. $\mathbf{P}(k/k-1)$ and $\mathbf{P}(k/k)$ are the error covariance matrices of the difference between $\mathbf{x}(k)$ and $\hat{\mathbf{x}}(k/k-1)$ respectively $\mathbf{x}(k)$ and $\hat{\mathbf{x}}(k/k)$, providing statistical measures of the uncertainty in the predicted or estimated state.

The covariance matrix $\mathbf{P}(k/k)$ is affected by the experimental design, in particular the transition matrix $\mathbf{F}(k)$, measurement vector $\mathbf{h}(k)$ and the noise covariances $\mathbf{Q}(k-1)$ and $\mathbf{R}(k)$. The problem of interest is how to select optimal elements in these terms in order to acquire the best performance of the Kalman filter.

Information theory

For a continuous variable $\mathbf{x}$ with a multidimensional probability density $p(\mathbf{x})$, the entropy is defined as

$$\mathbf{H} = -\int_{-\infty}^{+\infty} p(\mathbf{x})\, ld\, \{p(\mathbf{x})\}\, d\mathbf{x} \tag{8}$$

where $d\mathbf{x}$ stands for the volume element.

Assuming linear state dynamics and gaussian distributions for the noise terms and the state, the resulting probability density function for the Kalman filter is also gaussian with the mean $\hat{\mathbf{x}}(k/k)$ and covariance matrix $\mathbf{P}(k/k)$ [8]. As a result the entropy of the n-dimensional normal density is

$$\mathbf{H}(k) = 1/2\, ld\, \{(2\pi e)^n\, |\mathbf{P}(k/k)|\} \tag{9}$$

The information yield $\mathbf{I}(k) = \mathbf{H}(k-1) - \mathbf{H}(k)$ is defined as a change in entropy, obtained by processing the next measurement in the sequence. The total information yield $\mathbf{I}_{tot}(k) = \mathbf{H}(0) - \mathbf{H}(k-1)$, acquired from the start ($k = 0$) up to the measurement k, is the summation of all individual information yields or $\mathbf{I}_{tot}(k) = \sum_{i=1}^{k} \mathbf{I}(i)$.

Straightforward formulation produces for the information yield

$$\begin{aligned}
\mathbf{I}(k) &= 1/2\, ld\, \{|\mathbf{P}(k-1/k-1)|/|\mathbf{P}(k/k)|\} \\
&= 1/2\, ld\{|\mathbf{P}(k-1/k-1)]|/|\mathbf{F}(k)\mathbf{P}(k-1/k-1)]\, \mathbf{F}^t(k) + \mathbf{Q}(k-1)|\} \\
&+ 1/2\, ld\{\mathbf{h}^t(k)\mathbf{P}(k/k-1)]\, \mathbf{h}(k)/\mathbf{R}(k) + 1\} \\
&= \mathbf{I}_{pre}(k) + \mathbf{I}_{fil}(k)
\end{aligned} \tag{10}$$

The information yield of the Kalman filter separates into two parts; one from the prediction and another resulting from the filtering equations. The system noise covariance $\mathbf{Q}(k-1)$ has a direct bearing on the magnitude of the covariance matrix. Less obvious is the effect of the dynamics, i.e., the transition matrix $\mathbf{F}(k)$, on covariance behaviour. Usually the covariance matrix or the uncertainty in the state is increased by the prediction equations (Eqns. 3, 4). The corresponding loss of information is represented by $\mathbf{I}_{pre}(k)$. If the state is not measured, the covariance matrix increases to

infinity. Consequently, the total information yield $I_{tot}(k)$ and also the information loss $I_{pre}(k)$ will tend to zero.

The filter equations (Eqns. 5—7) reduce the uncertainty gradually by means of the information $I_{fil}(k)$ supplied by the new measurement. This term weights the covariance matrix $\mathbf{P}(k/k-1)$ with the measurement vector $\mathbf{h}(k)$ and noise variance $\mathbf{R}(k)$ and should be positive. It may be noted that this part does not involve the calculation of determinants. If the system noise covariances are not zero, the covariance matrix reaches a steady state where an equilibrium is achieved between the information loss $I_{pre}(k)$ and the information gain $I_{est}(k)$. For every measurement processed, less information $I(k)$ is gained and the total information $I_{tot}(k)$ will converge to a fixed level. Finally, no more information can be obtained by the Kalman filter.

The optimal design problem is essentially a sequence of maximized experimental choices with the information yield as a criterion. As a result, the total information yield will also be maximized [6]. For optimal performance, the elements of the noise covariances $\mathbf{Q}(k-1)$ and $\mathbf{R}(k)$ should be minimized in order to obtain maximal information $I_{tot}(k)$. If $\mathbf{R}(k)$ equals zero, an infinite information yield $I(k)$ is acquired. For a zero system noise covariance matrix, the total information yield $I_{tot}(k)$ which can be obtained in the sequence is infinite. In statistical terms, this means that the Kalman filter knows the state $\mathbf{x}(k)$ exactly. More complicated are the effects of the elements in the transition matrix $\mathbf{F}(k)$ and measurement vector $\mathbf{h}(k)$, which depend strongly on the problem investigated. Questions like observability and stability of the model involved have to be considered first to guarantee the existence and uniqueness of an optimal solution. It should be noted that the model structure used embodies in principle all intuitive rules on optimization in estimation problems. As an example, this will be illustrated for the drifting calibration system.

A drifting calibration system

For a linear calibration graph with stochastic drifting parameters, a discrete linear dynamic system (1, 2) has been derived [7]

$$\begin{pmatrix} a(k) \\ b(k) \\ \alpha(k) \\ \beta(k) \end{pmatrix} = \begin{pmatrix} 1 & 0 & 1 & 0 \\ 0 & 1 & 0 & 1 \\ 0 & 0 & 1 & 0 \\ 0 & 0 & 0 & 1 \end{pmatrix} \cdot \begin{pmatrix} a(k-1) \\ b(k-1) \\ \alpha(k-1) \\ \beta(k-1) \end{pmatrix} + \begin{pmatrix} w1(k-1) \\ w2(k-1) \\ w3(k-1) \\ w4(k-1) \end{pmatrix} \tag{11}$$

$$\mathbf{z}(k) = (c, 1, 0, 0) \cdot \begin{pmatrix} a(k) \\ b(k) \\ \alpha(k) \\ \beta(k) \end{pmatrix} + \mathbf{v}(k)$$

The state of the system is determined by measuring standards with known concentrations, that are processed by the Kalman filter. The predicted state

is employed for the evaluation of unknown analytes. After each measurement, a quality control algorithm decides whether to calibrate again or to process the next unknown. The criterion used is based on a preselected precision of the expected results for the evaluation. The decision to recalibrate is followed by selecting which one of the available concentration standards gives the best performance of the Kalman filter.

If the noise covariances are assumed to be constant, the concentration c is the only variable that can be manipulated experimentally. This variable is involved in the filtering part but not in the prediction part of the information yield. Only the information yield $\mathbf{I}_{\mathrm{fil}}(k)$ has to be maximized for an optimal selection, because $\mathbf{I}_{\mathrm{pre}}(k)$ is constant.

If the dual logarithm is omitted and $\mathbf{R}(k)$ is assumed to be constant over the entire graph, the decision on which concentration should be used to calibrate the system is given by

$$\text{maximize } \mathbf{h}^t(k)\mathbf{P}(k/k-1)\mathbf{h}(k)/\mathbf{R}(k) + 1 \tag{12}$$

$$\text{or maximize } c^2 p_{11}/\mathbf{R} + 2cp_{12}/\mathbf{R} + p_{22}/\mathbf{R} + 1$$

where p_{ij} is the i,jth element of the matrix $\mathbf{P}$. This equation has a minimum at $c = -p_{12}/p_{11}$. Because of the limited concentration range, the optimal position in the calibration graph is always found at one of the extremes. Which of the extremes will be chosen depends on the covariance matrix $\mathbf{P}(k/k-1)$, which is influenced by the elements of the system noise covariance $\mathbf{Q}(k-1)$. If the matrix $\mathbf{Q}(k-1)$ equals the zero matrix, the highest and lowest concentration will be repeated. The effect of the concentration range on the covariance matrix is difficult to show. However, if the optimal positions are found at the extremes of the working range, there may still be better concentrations outside this range. Consequently, the concentration range of the calibration standards should be maximized.

In summary: $\mathbf{I}_{\mathrm{fil}}(k)$ is increased if the noise variance $\mathbf{R}(k)$ decreases; $\mathbf{I}_{\mathrm{fil}}(k)$ is increased if the concentration range increases; and $\mathbf{I}_{\mathrm{fil}}(k)$ is maximal at one of the extremes of the working range.

For the imprecision of the evaluated unknowns $\hat{c}(k) = [z(k) - \hat{b}(k)]/\hat{a}(k)$, it is possible to derive the corresponding information yield $\mathbf{I}_{\mathrm{un}}(k)$

$$\mathbf{I}_{\mathrm{un}}(k) = 1/2\ ld\ \{\mathrm{var}(c_0)/\mathrm{var}[\hat{c}(k)]\}$$

$$= 1/2\ ld\ \{\mathrm{var}(c_0)\hat{a}(k)^2/\{\mathbf{h}^t(k)\mathbf{P}(k/k-1)\mathbf{h}(k) + \mathbf{R}(k)\}\} \tag{13}$$

with $\mathrm{var}(c_0)$ equal to the variance of the evaluation before the measurement is processed. If nothing is known in advance, $\mathrm{var}(c_0)$ should be set to 1 initially. If the evaluation of the sample is based on more measurements, $\mathrm{var}(c_0)$ is the precomputed variance.

From Eqn. 13 it follows that: $\mathbf{I}_{\mathrm{un}}(k)$ increases with increasing sensitivity $\hat{a}(k)$; $\mathbf{I}_{\mathrm{un}}(k)$ increases with decreasing noise variance $\mathbf{R}(k)$; $\mathbf{I}_{\mathrm{un}}(k)$ increases if the concentration range is increased; and $\mathbf{I}_{\mathrm{un}}(k)$ has a maximum somewhere within the concentration range. The maximum is located at the mean

value of the used concentration standards, if system noise and drift are not involved. Further, the resulting variance will become smaller for each additional measurement used for the evaluation of an unknown sample. This means that the total information concerning the sample increases. Because of the dynamics and system noise involved, the covariance matrix in the sequence increases and the acquired information will become smaller. However, the information gained should be at least zero.

All these results differ only slightly from the traditional conclusions on optimal designs in calibration problems. For higher-order calibration graphs, similar results can be obtained. In the appendix some equations are given for a linear calibration graph without drift and system noise.

RESULTS

The applicability of the theory presented here is demonstrated on the same simulated example as employed earlier [7]. A Kalman filter was used to process the calibration measurements. The unknowns were evaluated by means of the predicted state of the filter. The quality control algorithm was implemented to decide when to re-calibrate and thereafter to select the concentration standard giving the best performance, by means of the optimization algorithm. For the optimization procedure, the system may choose freely from the available concentration standards 1, 2, 3, 4 and 5.

Figure 1 shows the situation where the samples are used either for calibration or for evaluation by means of the quality control algorithm. The critical imprecision N_{crit} = 5% was used. Figure 1(a) depicts the measurements including drift and noise and Fig. 1(b) shows the concentrations. The measurements and the concentrations are the data used by the Kalman filter to estimate and predict the state of the drifting system (Fig. 1c). The performance of the quality control algorithm to decide whether to take an unknown sample or to calibrate again is shown in Fig. 1(d). When the maximal imprecision N_{max} exceeds the preset limit N_{crit} = 5%, re-calibration is initiated. The system starts with a minimal number of four calibrations with two different concentrations which are chosen suitably for observability.

Figure 2 shows some results of the optimization procedure. Figure 2(a) depicts the information function for the decision on which concentration gives the best performance. When the system is observable ($k \geqslant 4$), a minimum is found somewhere in the concentration range. Therefore the best concentration is always found at one of the extremes; this is confirmed by Fig. 1(b). When the system is not observable ($k < 4$), there is no minimum. However, the system still decides to start calibrating twice with the highest concentration available, followed by taking twice the lowest concentration standard. Hereafter, the lowest and highest concentration are alternated for re-calibration. Figure 2(b) shows the information yield found for the evaluated constituents in the calibration graph. Somewhere in the concentration range, a maximum is found, as it should be. Figure 2(c) depicts

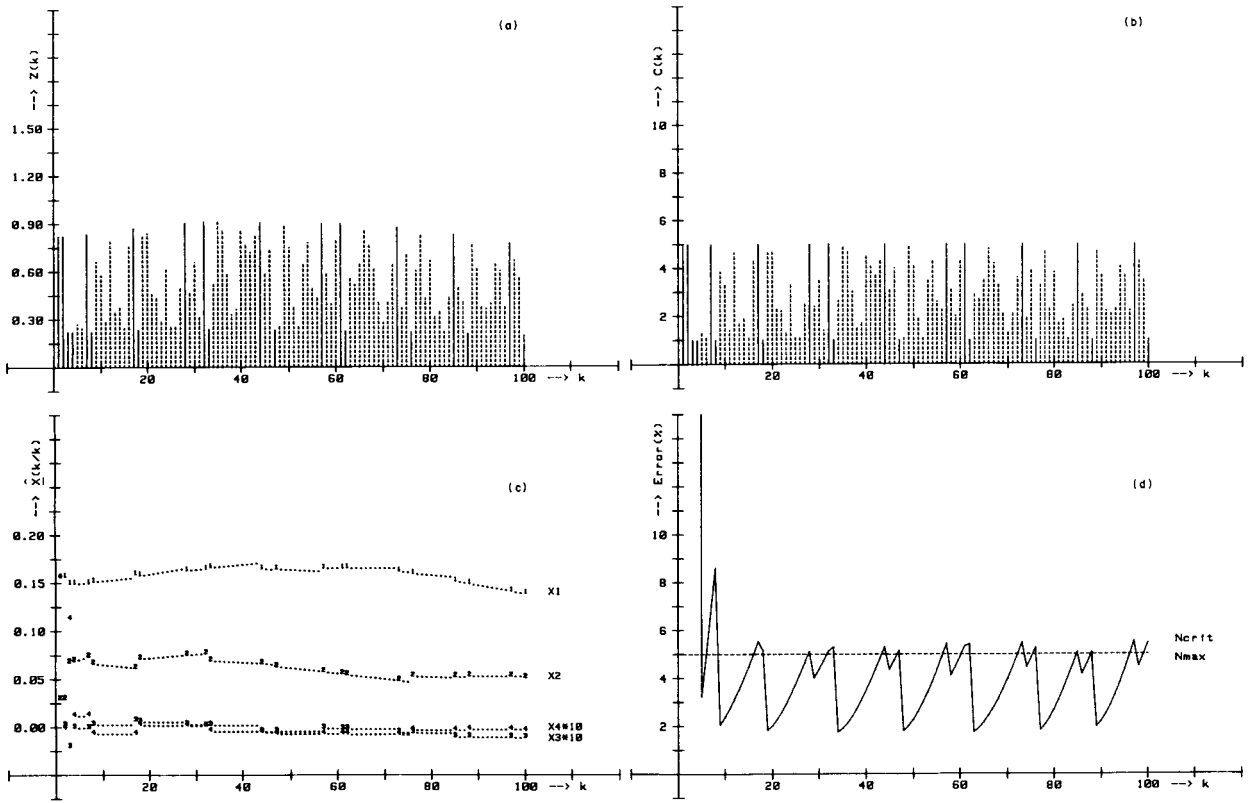

Fig. 1. The situation with samples used for calibration or evaluation. The same drifting system is simulated as before [7]. The quality control algorithm uses a critical imprecision N_{crit} = 5% and is employed with the optimization procedure. (a) Measurements corrupted by noise and drift: (——) used for calibration; (- - -) used for evaluation. (b) Concentrations of the samples: (——) used for calibration; (- - -) estimated from assessment. (c) Estimates and predictions of the state of the system. (1, 2, 3, 4) estimated state based on calibration; (- - -) predicted state used for evaluation. (d) The resulting maximal imprecisions N_{max} used by the quality control algorithm.

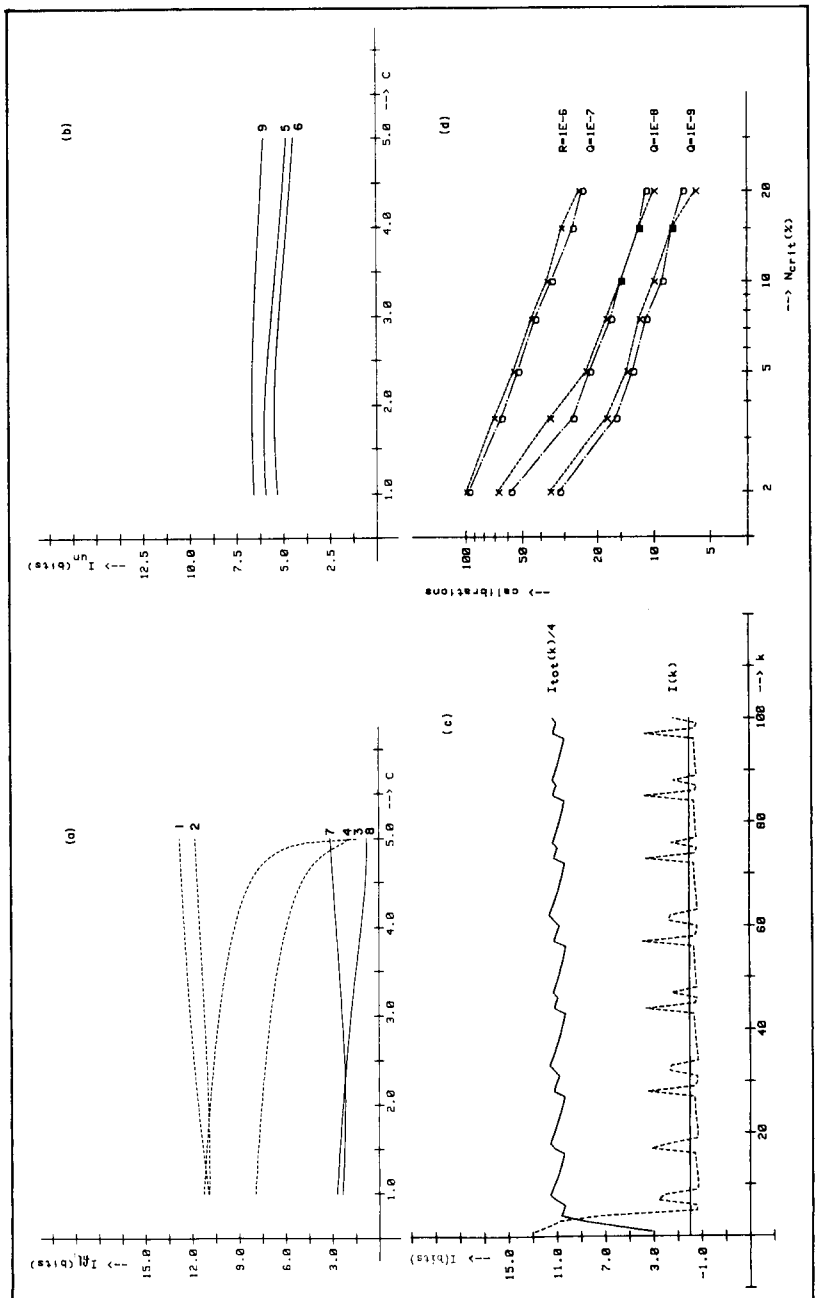

Fig. 2. Results of the optimization algorithm. The procedures for on-line calibration, evaluation and quality control are employed as in Fig. 1. (a) The information function for different indices k (indicated by the numbers on the curves) used to select a concentration standard with the best performance for calibration: (- - -) unobservable system ($k \leqslant 4$); (——) observable system ($k > 4$). (b) The information function found for the evaluation of unknown samples at some indices k. (c) The resulting information yield at every index k: (- - -) information gain or loss; (——) total information. (d) The number of calibrations after 100 samples for various values of the system noise covariances: (×) results for the normal calibration procedure; (○) results for the optimal selection of the concentration standards; the value of $\mathbf{Q}$ represents both $\mathbf{Q}_{33}$ and $\mathbf{Q}_{44}$.

the resulting information yield of the integrated system of calibration, evaluation, quality control and optimization. A positive information value is found when the system re-calibrates. The gain in information is negative when the system evaluates unknown samples. In addition, the total information yield, $I_{tot}(k)$, acquired by the system is given; this is forced to remain above a fixed level by the control procedure applied. The effect of various system noise covariances Q_{33} and Q_{44} is shown in Fig. 2(d) for both the normal and the optimal selection procedures. For the normal procedure, the system re-calibrates twice, initially with the most and least concentrated available standard. When the optimal selection procedure is used, there is a small profit of 0—15% on the number of required calibrations. For different system noise covariances, the savings are similar.

Conclusions

A method is presented for on-line optimization of experimental design in a Kalman filter based on information theory. The information yield comprises a loss caused by the prediction in the sequence and a gain arising from the filtering of the new measurement. For optimal performance of the Kalman filter, the information yield has to be maximized in the measurement sequence. In general, the noise covariances should be minimized. More complicated are the effects of the transition matrix and the measurement vector, which depend greatly on the problem investigated.

For a drifting calibration system, only small differences are obtained in comparison with the traditional results for the linear graph. If the optimization algorithm is integrated in the procedures of calibration, evaluation and quality control, then there is a small profit on the number of calibrations required.

This work was supported by the Netherlands Research Organisation Z.W.O. Special thanks to Prof. Drs. G. Kateman and Dr. H. C. Smit for evaluating the manuscript.

APPENDIX

Results for a linear calibration graph $y_i = ac_i + b$; $i = 1, 2, \ldots, k$, without drift and system noise.

If constant noise variances R_i are assumed and the mean value $\bar{c} = 1/k\Sigma_{i=1}^{k} c_i$ is defined for k calibrations, the resulting entropy H of the experimental design is described by

$$H = 1/2\ ld\ \{[(2\pi e)^2/k]\ [R/\Sigma_{i=1}^{k}(c_i - \bar{c})^2]\}$$

The information yield, I_{fil}, $\{I_{pre} = 0\}$ for a concentration $\tilde{c}$ to be chosen for calibration is

$$I_{fil} = 1/2\ ld\ \{[(\tilde{c} - \bar{c})^2/\Sigma_{i=1}^{k}(c_i - \bar{c})^2] + 1/k + 1\}$$

The information yield, I_{un}, for the evaluation of an unknown sample $\hat{c} = (z_i - \hat{b})/\hat{a}$ with $\mathrm{var}(c_0) = 1$ is

$$I_{un} = -1/2\ ld\ \{(R/\hat{a}^2)\ \{[(\hat{c} - \bar{c})^2/\Sigma_{i=1}^{k}(c_i - \bar{c})^2] + 1/k + 1\}\}$$

It may be noted that I_{fil} has a minimum at $\tilde{c} = \bar{c}$ and I_{un} has a maximum at $\hat{c} = \bar{c}$. Both equations hold only for $k \geqslant 2$.

REFERENCES

1 C. K. Shukla, Technometrics, 14 (1972) 547.
2 L. Aarons, Analyst (London), 106 (1981) 1249.
3 V. V. Fedorov, Theory of Optimal Experiments, Academic Press, New York, 1972.
4 D. M. Steinberg and W. G. Hunter, Technometrics, 26 (1984) 71.
5 G. Eckschlager, Collect. Czech. Chem. Commun., 37 (1972) 137.
6 P. C. Thijssen, G. Kateman and H. C. Smit, Anal. Chim. Acta, 157 (1984) 99.
7 P. C. Thijssen, S. M. Wolfrum, G. Kateman and H. C. Smit, Anal. Chim. Acta, 156 (1984) 87.
8 A. Gelb (Ed.), Applied Optimal Estimation, MIT Press, Cambridge, MA, 1974.

Analytica Chimica Acta, 162 (1984) 263—274
Elsevier Science Publishers B.V., Amsterdam — Printed in The Netherlands

LIGAND EXCHANGE AND FLUORESCENCE QUENCHING STUDIES OF THE FULVIC ACID-IRON INTERACTION
Effects of pH and Light

T. DAVID WAITE[a] and FRANCOIS M. M. MOREL*

Ralph M. Parsons Laboratory, 48-425 Massachusetts Institute of Technology, Cambridge, Massachusetts 02139 (U.S.A.)

(Received 17th February 1984)

SUMMARY

The effects of pH and light on the interaction between fulvic acid and iron have been investigated through studies of the kinetics of exchange of iron between fulvic acid and 1,10-phenanthroline (a strong iron(II) complexing agent), and of the quenching of intrinsic fulvic acid fluorescence by iron in solutions of pH 4.0 and 6.5 containing an excess of fulvic acid. The results enable the iron-fulvic acid interaction to be described in terms of operationally defined iron-fulvic acid groupings, the proportions of which are markedly dependent on pH and light conditions. At pH 4.0, fulvic acid exhibits considerable reducing ability with the result that a substantial portion of iron is present in reduced, unbound form. Irradiation of fulvic acids at this pH markedly increases their reducing ability. Iron that is not reduced is present as small (ultrafilterable), strongly bound iron(III) complexes. Iron bound in this form is an effective quencher of intrinsic fulvic acid fluorescence. At higher pH, essentially all of the iron is relatively strongly bound, with most being in the form of large (non-ultrafilterable) iron(III)—fulvic acid groupings. These groupings are not altered significantly by irradiation and iron bound in this form is not a very effective quencher of intrinsic fulvic acid fluorescence.

The interaction of soil and aquatic fulvic and humic acids with metal ions has been studied extensively over the last twenty years and has resulted in considerable insight into the metal complexation characteristics of these materials. Most attention has been given to divalent trace metals such as Cu^{2+}, Cd^{2+} and Pb^{2+} and to major cations such as Ca^{2+} [1]. Far fewer studies of the interaction of humic substances with metals such as iron and manganese have been published, in part because of the complexity of the aqueous chemistry of these easily hydrolyzed cations. An added complication, and one of particular interest here, is the ability of fulvic and humic acids to reduce these metal ions to a lower valence state [2—4].

The reducing ability of humic and fulvic acids appears to increase on irradiation, resulting in enhanced production of reduced metal ion species. Thus

[a]Present address: Department of Inorganic Chemistry, University of Melbourne, Parkville, Victoria 3052, Australia.

0003-2670/84/$03.00

McMahon [5], Collienne [6], and Miles and Brezonik [7] all observed elevated concentrations of Fe(II) species in the surface waters of highly colored, low pH lakes during daylight hours compared to the concentrations present under dark conditions. In laboratory studies, Sunda et al. [4] observed a photo-enhanced dissolution of colloidal manganese oxides in the presence of marine humic material, a process presumably occurring via reduction of Mn(IV) to Mn(II). Similarly, Waite [8] reported that photo-reductive dissolution of iron oxides is much enhanced under certain conditions in the presence of fulvic acids.

In this paper, the effects of light on the iron-fulvic acid interaction are investigated in solutions of pH 4.0 and pH 6.5. Two approaches, namely the kinetics of ligand exchange and fluorescence quenching, are used to study the changes that occur in the iron-fulvic acid interaction on going from dark to light conditions. The techniques have been applied in investigations on three "model" compounds (catechol, salicylic acid and phthalic acid) possessing some of the characteristics of naturally occurring organic materials and in studies on two fresh-water fulvic acids.

THEORY

The two problems of major interest in this study are to establish which species are present in a mixture of iron and fulvic acid and how the species composition changes on irradiation. Given that information, it becomes possible to rationalize the (photo-redox) chemistry of metal–fulvic acid systems in more general terms.

Species identification by ligand exchange kinetics

For a system that contains A, B, . . ., N iron-containing components that react in a first-order manner with excess of reagent R to form a common product, P, the concentration of product P at any time t is

$$[P]_t = [A]_0[1 - \exp(-k_A t)] + [B]_0[1 - \exp(-k_B t)] + \ldots . + [N]_0[1 - \exp(-k_N t)] + X \quad (1)$$

where $[A]_0$, $[B]_0$, ..., $[N]_0$ are the initial concentrations of the species, X is a time-independent term, and k_A, k_B, . . ., k_N are pseudo first-order rate constants. Many methods (e.g., logarithmic extrapolation and nonlinear regression) are available to resolve initial concentrations and rate constants for two- and three-component mixtures [9, 10].

Identification of species by fluorescence quenching characteristics

The intrinsic near-ultraviolet fluorescence of a wide range of organic compounds is sensitive to many factors that affect the environment of emitting groups. One factor of particular relevance to this study is that of transition

metal complexation. Species with unpaired electron spins are generally found to increase markedly the singlet-to-triplet intersystem crossing rate [11]; thus, paramagnetic transition metal ions such as Cu^{2+}, Fe^{3+}, Ni^{2+} and Co^{2+} which possess *d* levels of energy lower than the excited singlet (or even the triplet) $\pi-\pi^*$ state may strongly quench the ligand fluorescence via intramolecular energy transfer [12]. A good example of this is the lack of fluorescence of transferrin and heme, a phenomenon attributed to energy transfer to a low lying Fe^{3+} *d* level [13]. Disruption of the bond between a quenching cation and a fluorescent ligand or a lowering in the ability of the metal to enhance the rate of intersystem crossing in other ways (such as a change in metal oxidation state) may thus be expected to result in an increase in observed fluorescence. Either or both of these changes may be induced by photolysis or pH change.

The intrinsic fluorescence of isolated fulvic materials is well documented [14] as is the quenching of fluorescence that occurs on complexation with paramagnetic metal ions [15]. Measurement of the fluorescence of fulvic acids before and after iron addition and before and after irradiation should thus provide insight into the nature of the iron—fulvic acid interaction and the changes that occur on photolysis.

EXPERIMENTAL

Materials and instrumentation

Two aquatic fulvic acids extracted from fresh-waters were used in this study. Suwanee River fulvic acid, which was supplied by the U.S. Geological Survey, is the standard aquatic fulvic acid of the International Humic Substances Society and has been characterized in some detail [16]. Grassy Pond fulvic acid was extracted from the surface waters of an acidic central Massachusetts lake by using the methods outlined by Thurman and Malcolm [17].

Unless otherwise noted, all other chemicals used were of analytical-reagent grade. Millipore Q-water was used throughout.

Visible absorbance and fluorescence were measured respectively on a Bausch and Lomb Spectronic 100 and a Perkin-Elmer LS-5 fluorescence spectrometer. Light was supplied by a Kratos/Schoeffel SS-1000 system and provided a reasonably well-collimated, uniform beam. Appropriate filtering produced a spectrum similar to that of 90° elevation noon-day sun. An intensity of approximately 100 mW cm^{-2} was provided by the light source with the total amount of radiation, as determined by ferri-oxalate actinometry [12], being 3×10^{-5} einstein per ml of solution per min.

Procedure

Preliminary studies of the ligand exchange and fluorescence properties of catechol, salicylate and phthalate were done by using 1.0×10^{-4} M solutions

of these compounds containing 5.4×10^{-6} M iron(III) (added from an acidic iron(III) stock solution) and in 0.1 M NaCl buffered to about pH 4 or 6.5. Solutions at pH 4 were obtained by acid addition while the pH 6.5 solutions were obtained by equilibrating a 2×10^{-3} M $NaHCO_3$/0.1 M NaCl solution with a 2.5% carbon dioxide/air mixture. Ligand exchange studies were done by addition of 200 μl of 5×10^{-3} M 1,10-phenanthroline to 5-ml aliquots of the iron-organic mixtures and immediately commencing the monitoring of solution absorbance at 510 nm in closed 10-cm path-length cells. The fluorescence-quenching characteristics of Fe(II) and Fe(III) were investigated by adding micromolar increments of these species to 2.0×10^{-5} M solutions of the organic acids and monitoring the fluorescence after each addition. Similar fluorescence studies were done on two fresh-water fulvic acids at concentrations of 10 mg l^{-1}. The proportion of added iron maintained in small (nonpolymeric) units was determined by ultrafiltration with Amicon PM10 membranes (nominal molecular weight cutoff = 10 000). These membranes were chosen particularly because solute adsorption has been reported to be low [18, 19]. The proportion of iron that passed through a 0.1-μm Nucleopore filter was also determined. The soluble iron(III) stock solution used was labelled with iron-59, enabling the proportion of iron in the filtered fraction to be measured by liquid scintillation.

All studies involving irradiation were done with a 300-ml water-jacketed cylindrical glass container with quartz plate windows at both ends. Solutions of interest were placed in the reaction vessel and continuously stirred and equilibrated at 20°C. The intrinsic fluorescence of the solution was measured prior to addition of approximately 5×10^{-6} M Fe(III). After a 3-h equilibration time under dark conditions, samples were removed from the vessel for ligand exchange study and fluorescence measurement. At this point, photolysis was commenced. After irradiation for approximately 1 h, samples were again removed for ligand exchange study and fluorescence measurement.

RESULTS AND DISCUSSION

Model compound studies

Investigations of ligand exchange, fluorescence quenching, and photodegradability of the chosen model compounds [8] indicate that iron—catechol systems are subject to phenanthroline exchange while iron—salicylate and iron—phthalate mixtures are stable. At pH 6.5, most iron is present initially as $Fe(catechol)_2^-$ with the phenanthroline exchange reaction exhibiting a first-order rate constant of $(3.4 \pm 0.1) \times 10^{-2}$ min^{-1}. At pH 4, catechol reduces iron(III) to iron(II) [20] which, not surprisingly, is very rapidly complexed by phenanthroline. Salicylate, but not catechol or phthalate, fluoresces with the intrinsic fluorescence being quenched on addition of iron(III) at pH 4 [8]. Iron(II) has very little effect on salicylate fluorescence. Fluorescence quenching does not occur at pH 6.5 because the formation of insoluble oxyhydroxides prevents salicylate complexation (as confirmed by the results

of ultrafiltration studies). Iron—salicylate and iron—phthalate complexes are photodegradable while light does not significantly affect the iron—catechol system.

Fulvic acid studies

The results of phenanthroline exchange studies of solutions of 5.4×10^{-6} M total iron at pH 6.5 and pH 3.9 in the presence of 10 mg l^{-1} Suwannee River fulvic acid (average molecular weight 1200) before and after irradiation are shown in Fig. 1. At pH 6.5, approximately 95% of the added iron(III) is converted to $Fe(phen)_3^{2+}$ over the time scale of interest (about 27 h) while at pH 3.9, almost 90% of the added iron(III) is converted to $Fe(phen)_3^{2+}$ in 4 h. The effect of light on the ligand exchangeability of the pH 6.5 system appears to be minor with only a small increase in rate of exchange at early times (Fig. 1A). The effects of light are much more dramatic at the lower pH (Fig. 1B) with a marked increase in the rate of $Fe(phen)_3^{2+}$ formation at early times under light compared to dark conditions. As can be seen from the associated logarithmic plot in Fig. 2, more than one exchangeable component must be postulated to account for these kinetic data. In addition, a portion of the total iron in the system is non-exchangeable. Given these observations, it is useful to separate the total iron present conceptually into four groupings: namely, an instantaneously complexed fraction, Fe(II), a kinetically inert fraction, $Fe(III)L_A$, and two fractions, $Fe(III)L_B$ and $Fe(III)L_C$, that exhibit some degree of phenanthroline exchange on the time scale of interest. (The corresponding pseudo first-order constants are $k_x = \infty$, $k_A = 0$ and $k_B < k_C$.) In accord with the results of Senesi et al. [21], Goodman and Cheshire [22], and Schnitzer and Ghosh [23], who found no Fe(II) binding to fulvics or humics, only iron(III)—fulvic acid entities are postulated. Rate constants and

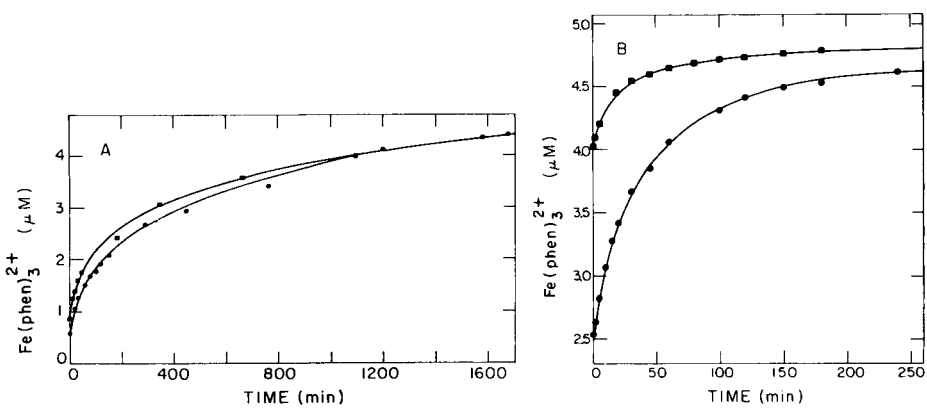

Fig. 1. Concentration of $Fe(phen)_3^{2+}$ formed on addition of excess of phenanthroline to (A) a pH 6.5 solution of 0.1 M NaCl and 2 mM $NaHCO_3$, and (B) a pH 3.9 solution of 0.1 M NaCl, each containing 10 mg l^{-1} Suwannee River fulvic acid and 5.4×10^{-6} M iron: (•) before photolysis; (▪) after photolysis.

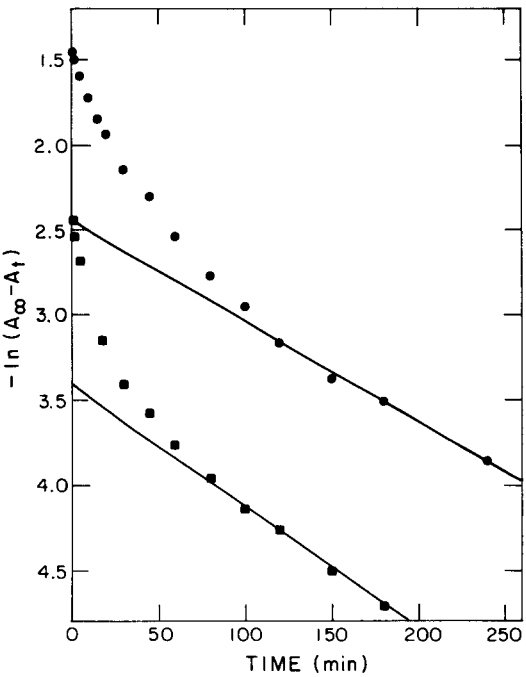

Fig. 2. Data from the dark (•) and light (▪) pH 3.9 phenanthroline exchange study (Fig. 1B) transformed according to the logarithmic extrapolation method. (A is absorbance at 510 nm; the absorbance for 1×10^{-6} M $Fe(phen)_3^{2+}$ was about 0.097.)

zero-time concentrations for the phenanthroline exchangeable components $Fe(III)L_B$ and $Fe(III)L_C$ obtained by fitting an expression of the form of Eqn. 1 to the pH 3.9 and 6.5 data using non-linear least squares regression methods [24] are given in Tables 1 and 2 for the Suwannee River and the Grassy Pond data, respectively. In all cases, initial-parameter estimates were obtained by the logarithmic extrapolation method [10]. A synoptic view of the data is provided in Fig. 3.

The results of the ligand exchange studies indicate that most ($\geqslant 90\%$) of the added iron is phenanthroline-exchangeable at both pH 4 and pH 6.5 and is thus presumably in soluble form. This conclusion is supported by the fact that no iron-59 is lost from solution by settling or by adsorption to the container walls in these iron—fulvic acid mixtures over time. The results of the filtration experiments also tend to confirm this because 72—75% of the iron added to a 10 mg l^{-1} Suwannee River fulvic acid solution passes through a 0.1-μm filter. It is likely that this represents an underestimate of the proportion of soluble iron present because some sorption of iron—fulvic acid complexes to the Nucleopore membrane might be expected. (In fact at pH 4, 92% of the iron passes through the PM-10 membrane.)

TABLE 1

Component concentration and rate constant estimates obtained from nonlinear least-squares regression of Suwannee River phenanthroline exchange data

Parameter[a]	pH 3.9		pH 6.5	
	Dark	Light	Dark	Light
Concentration (10^{-6} M)				
$Fe(III)L_C$	0.81 ± 0.07[b]	0.46 ± 0.02	1.02 ± 0.12	1.05 ± 0.10
$Fe(III)L_B$	1.48 ± 0.07	0.41 ± 0.02	3.41 ± 0.16	3.01 ± 0.10
Fe(II)	2.59	4.15	0.73	1.04
$Fe(III)L_A$	0.52[c]	0.38	0.24	0.30
Rate constant (min^{-1})				
k_C	$(7.7 \pm 0.9) \times 10^{-2}$	$(11.9 \pm 1.3) \times 10^{-2}$	$(2.1 \pm 1.3) \times 10^{-2}$	$(3.3 \pm 0.6) \times 10^{-2}$
k_B	$(13.6 \pm 0.6) \times 10^{-3}$	$(13.9 \pm 2.1) \times 10^{-3}$	$(1.1 \pm 0.2) \times 10^{-3}$	$(1.2 \pm 0.1) \times 10^{-3}$

[a] $Fe(III)L_A$ is kinetically inert, $Fe(III)L_B$ is slowly exchanged, $Fe(III)L_C$ is rapidly exchanged, and Fe(II) is instantaneously exchanged. [b] ± one standard deviation. [c] $[Fe(III)L_A] = [Fe]_T - [Fe(III)L_C] - [Fe(III)L_B] - [Fe(II)]$.

TABLE 2

Component concentration and rate constant estimates obtained from nonlinear least squares regression of Grassy Pond phenanthroline exchange data

Parameter[a]	pH 3.9		pH 6.5	
	Dark	Light	Dark	Light
Concentration (10^{-6} M)				
$Fe(III)L_C$	1.43 ± 0.08[b]	0.44 ± 0.01	0.90 ± 0.04	0.56 ± 0.05
$Fe(III)L_B$	1.26 ± 0.08	0.55 ± 0.01	3.01 ± 0.05	2.45 ± 0.04
Fe(II)	2.26	4.44	0.47	0.75
$Fe(III)L_A$	0.45[c]	−0.03	1.02	1.64
Rate constant (min^{-1})				
k_C	$(4.8 \pm 0.4) \times 10^{-2}$	$(11.6 \pm 0.5) \times 10^{-2}$	$(3.3 \pm 0.3) \times 10^{-2}$	$(6.6 \pm 1.4) \times 10^{-2}$
k_B	$(6.9 \pm 0.6) \times 10^{-3}$	$(10.5 \pm 0.2) \times 10^{-3}$	$(3.1 \pm 0.1) \times 10^{-3}$	$(2.8 \pm 0.1) \times 10^{-3}$

[a–c] See footnotes to Table 1.

Various distinct effects of pH and light on the proportion of iron in each of the kinetically-defined fractions are evident from the results in Fig. 3. The effect of pH on the phenanthroline exchangeability of fulvic acid—iron mixtures under dark conditions is of interest in that there is a distinct pH dependence of the Fe(II) fraction. For Suwannee River fulvic acid, 48% at pH 3.9 and 14% at pH 6.5 are in this category while for Grassy Pond fulvic acid the proportions are 42% and 9%. A similar (though more dramatic) pH dependence of the instantaneously reactable component was observed for catechol, with 94% iron(II) at pH 3.9 and 1.5% iron(II) at pH 6.5. The change in catechol reducing power is related to the change in major species with pH; the labile $Fe(catechol)^+$ species (in dynamic equilibrium with Fe^{2+}) predominates at pH 3.9 and the more stable $Fe(catechol)_2^-$ predominates at pH 6.5. The ligand

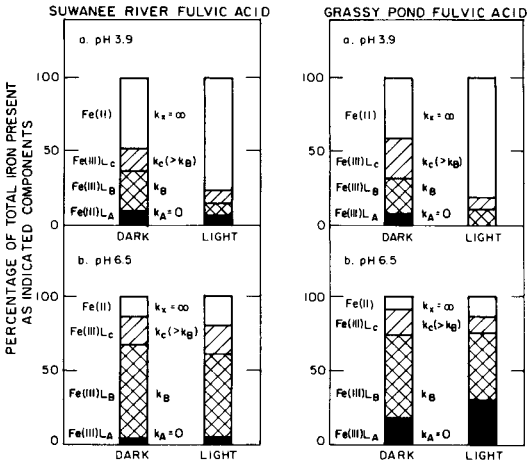

Fig. 3. Pictorial presentation of the effects of pH and light on the proportion of total added iron in each of the kinetically-defined components of Suwannee River and Grassy Pond fulvic acids.

exchange studies for fulvic acid indicate a similar decrease in species lability with increase in pH.

It is interesting to note in Tables 1 and 2 that the decrease in concentration of the Fe(II)-like iron with increase in pH for both fulvic acids (1.86 and 1.79×10^{-6} M for the Suwannee River and Grassy Pond samples, respectively) is almost exactly matched by the increase in concentration of the slowly exchangeable species $Fe(III)L_B$ (respectively, 1.93 and 1.75×10^{-6} M). One conclusion that can be drawn from this correspondence is that a quantitative transfer of iron from the Fe(II) pool to a kinetically more stable entity, $Fe(III)L_B$, occurs as the pH increases. It appears from the results of the ultrafiltration studies that the observed decrease in the concentration of the Fe(II) component with increase in pH is associated with an increase in relatively large-sized groupings because, at pH 4, 92% of the total added iron is ultrafilterable whereas at pH 6.5 only 40% of the iron present passes through a PM-10 membrane though essentially all iron is bound in some form. This observed increase in size with increase in pH (and increase in amount of metal bound) may simply be associated with the unfolding of the fulvic acid molecule as the functional groups become charged and hydrogen bonding is lowered [25]. Alternatively (or in addition), the size increase may be associated with partial hydrolysis of the added iron or may be attributed to increased bridging of fulvic acid molecules by iron(II).

In all cases, the rates of $Fe(phen)_3^{2+}$ formation were observed to decrease with increasing pH. This was particularly obvious for Suwannee River fulvic acid where k_C decreased from 8×10^{-2} min^{-1} at pH 3.9 to 2×10^{-2} min^{-1} at pH 6.5 and k_B changed from 14×10^{-3} min^{-1} to 1×10^{-3} min^{-1} on increasing the pH from 3.9 to 6.5. This decrease in exchange rates is consistent with the

commonly observed increase in stability of metal—fulvic acid complexes with increasing pH [26], a phenomenon no doubt attributable in part to the decreased proton competition at higher pH.

Light was observed to have some effect on almost all the kinetically defined entities with the most distinct changes occurring in the concentrations of the very labile Fe(II) component and the slowly exchanging component, $Fe(III)L_B$. Thus for Suwannee River fulvic acid in pH 3.9 solution, photolysis induces an increase in the Fe(II) component from 48% of total iron in the dark to 77% in the light. A major part of this increased labile pool is gained at the expense of the slowly exchanged component, $Fe(III)L_B$, which decreases from a contribution to total iron of 27% in the dark to only 8% in the light. The effects of light at pH 6.5 are less dramatic but appear to involve the same groupings with the labile Fe(II) component increasing from 13% of the total in the dark to 19% in the light. This is balanced by a decrease in the concentration of $Fe(III)L_B$ from 63% of the total iron in the dark to 57% in the light. Small concentration decreases on irradiation are also observed in $Fe(III)L_C$ (the rapidly exchangeable component) and in $Fe(III)L_A$ (the kinetically inert component) at pH 3.9.

Interestingly, the rate of formation of $Fe(phen)_3^{2+}$ from the slowly exchanged component, $Fe(III)L_B$, appears to be reasonably insensitive to the effects of light while k_C, the rate constant for the formation of $Fe(phen)_3^{2+}$ from $Fe(III)L_C$, consistently increases on photolysis. Thus, light appears to "destabilize" the rapidly exchangeable component $Fe(III)L_C$ but not the more stable component $Fe(III)L_B$, the concentration of which is significantly reduced by light. These observations suggest that $Fe(III)L_B$ is a primary chromophore, as might be expected for an iron(III) salicylate- or phthalate-like binding site, and that $Fe(III)L_C$ is indirectly affected by light, as might be expected for Fe(III) in association with quinone/semiquinone groups.

As in the case of salicylic acid, Fe(II) and Fe(III) exhibit a distinct difference in ability to quench intrinsic fulvic acid fluorescence. This is clearly shown in Fig. 4A where Fe(III), added incrementally to a solution of Suwannee River fulvic acid at pH 3.9, quenches the intrinsic fluorescence significantly more than corresponding additions of Fe(II). A considerably lower quenching ability of Fe(III) is observed at pH 6.5 (Fig. 4B).

The results of studies into the effects of Fe(III) addition and subsequent irradiation on the intrinsic fluorescence of pH 3.9 and pH 6.5 solutions of Suwannee River and Grassy Pond fulvic acids are summarized in Table 3. At pH 3.9, an addition of 5.4×10^{-6} M Fe(III) to 10 mg l^{-1} fulvic acid results in 25—30% quenching of intrinsic fluorescence. The degree of quenching rapidly declines on irradiation with about 18% quenching after 5 min of photolysis and a steady value of about 11% quenching after 10 min. At pH 6.5, the addition of Fe(III) induces a 9—12% decrease in fulvic acid fluorescence but no decrease in quenching ability is observed on irradiation.

It is important to note that a "bleaching" of uncomplexed fulvic acid fluorescence by light also occurs, but the effect of irradiation in decreasing

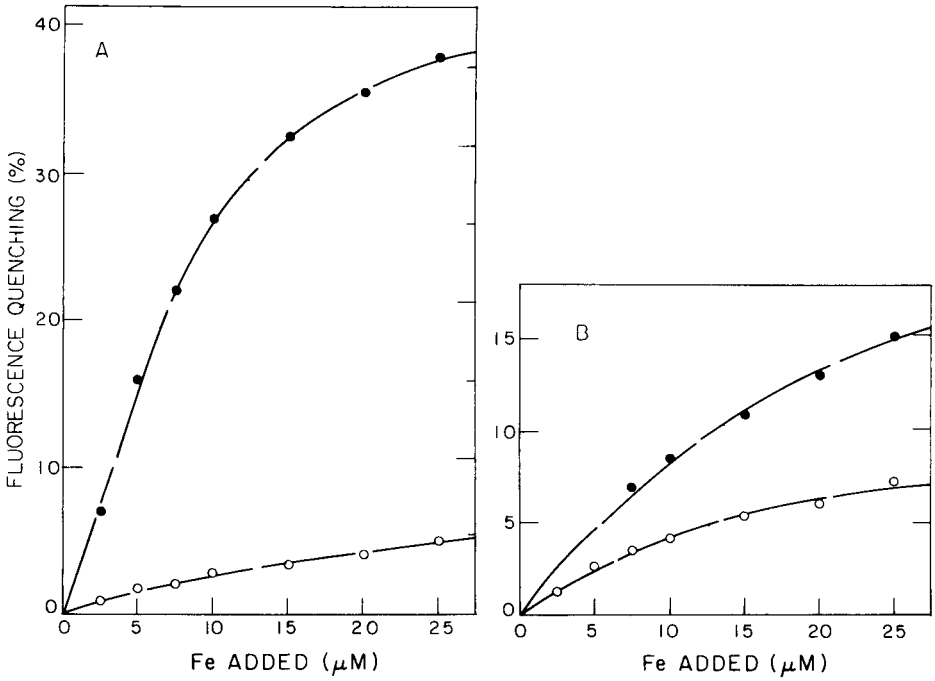

Fig. 4. Quenching of intrinsic Suwannee River fulvic acid fluorescence on addition of (○) Fe(II) and (●) Fe(III) to (A) pH 3.9, and (B) pH 6.5 0.1 M NaCl solutions containing 10 mg l^{-1} fulvic acid. (Excitation wavelength 330 nm, emission wavelength 445 nm).

TABLE 3

Effect of Fe(III) and irradiation on the intrinsic fluorescence of Suwannee River and Grassy Pond fulvic acids at pH 3.9 and pH 6.5 (excitation wavelength 330 nm, emission wavelength 445 nm)

Sample	Photolysis time (min)	Fluorescence quenched (%)	
		pH 3.9	pH 6.4
Suwannee river fulvic acid (SRFA)			
SRFA (10 mg l^{-1})	—	0.0	0.0
SRFA + Fe(III)[a]	—	24.4	12.0
SRFA + Fe(III)	5	17.6	13.5
SRFA + Fe(III)	10	12.4	13.2
SRFA + Fe(III)	30	12.2	14.3
SRFA + Fe(III)	60	12.2	—
Grassy pond fulvic acid (GPFA)			
GPFA (10 mg l^{-1})	—	0.0	0.0
GPFA + Fe(III)[a]	—	30.3	8.7
GPFA + Fe(III)	60	11.3	12.2

[a]In all cases, Fe(III) means addition of 5.4×10^{-6} M Fe(III).

the quenching of fulvic acid fluorescence by ionic iron is rapid in comparison with the time-scale for photo-induced destruction of intrinsic fluorescence. For example, a pH 4 solution of 10 mg l^{-1} uncomplexed Suwannee River fulvic acid exhibited a linear decrease in fluorescence of 3% per hour on irradiation with 3×10^{-5} einstein ml^{-1} min^{-1} (simulated sunlight) compared with a 12% increase in fluorescence in 10 min on irradiation of 10 mg l^{-1} Suwannee River fulvic acid partially complexed with 5×10^{-6} M iron(III).

Interestingly, comparison of the ultrafiltration and quenching results suggests a correspondence between small (ultrafilterable) iron—fulvic complexes and quenched fluorescence. The "dark" results for Suwannee River fulvic acid provide some support for this. At pH 3.9, 92% of the added iron passes through a PM-10 membrane. Of this fraction, 48% is present as Fe(II) while 44% is presumably complexed in small iron—fulvic groups. At pH 6.5, 40% of the total iron is ultrafilterable, 24% of this being attributable to small iron—fulvic groupings. While this decrease by a factor of 1.8 in the proportion of small complexes with pH does not match precisely the observed decrease in fluorescence quenching on increase in pH (a factor of 2.0 from 24.4% to 12.0% at pH 3.9 and pH 6.5, respectively), the correspondence is reasonable. That small, tightly-bound complexes constitute the major fluorescence quenchers in an iron—fulvic acid molecule is to be expected because the metal ion *d* orbitals must be in close proximity to the excited energy levels of the fulvic molecule to allow efficient electron transfer.

Finally, the consistency between results of ligand exchange and fluorescence quenching studies for the two fulvic acids used should be noted. This functional similarity is particularly noteworthy because the fulvic acids were obtained from waters of different nature (in terms of pH, origin, etc.) and the extraction techniques used to obtain these materials separate on the basis of hydrophobicity [27] and not metal-binding character.

This research was supported by NSF Grant No. OCE-8118103 and NOAA Grant No. NA79AA-D-00077.

REFERENCES

1 R. F. Christman and E. T. Gjessing, Aquatic and Terrestrial Humic Materials, Ann Arbor Science, Ann Arbor, MI, 1983.
2 M. Szilágyi, Soil Sci., 111 (1971) 233.
3 R. K. Skogerboe and S. W. Wilson, Anal. Chem., 53 (1981) 228.
4 W. G. Sunda, S. A. Huntsman and G. R. Harvey, Nature, 301 (1983) 234.
5 J. W. McMahon, Limnol. Oceanogr., 24 (1969) 823.
6 R. H. Collienne, Limnol. Oceanogr., 28 (1983) 83.
7 C. J. Miles and P. L. Brezonik, Environ. Sci. Technol., 15 (1981) 1089.
8 T. D. Waite, Ph.D. Thesis. Massachusetts Institute of Technology, 1983.
9 M. K. S. Mak, C. H. Langford and T. R. Khan, J. Ind. Chem. Soc., 54 (1977) 51.
10 H. B. Mark and G. A. Rechnitz, Kinetics in Analytical Chemistry, Interscience-Wiley, New York, 1968.
11 D. M. Hercules, in D. M. Hercules (Ed.), Fluorescence and Phosphorescence Analysis, Interscience Publishers, New York, 1966, pp. 1—40.

12 C. S. Parker, Photoluminescence of Solutions with Application to Photochemistry and Analytical Chemistry, Elsevier, Amsterdam, 1968, pp. 478—481.
13 R. F. Chen, in R. F. Chen and H. Edelhoch (Eds.), Biochemical Fluorescence: Concepts, Vol. 2, M. Dekker, New York, 1976, pp. 573—606.
14 M. Ewald, C. Belin, P. Berger and J. H. Weber, Environ. Sci. Technol., 17 (1983) 501.
15 R. A. Saar and J. N. Weber, Anal. Chem., 52 (1980) 2095.
16 E. M. Thurman and R. L. Malcolm, in R. F. Christman and E. T. Gjessing (Eds.), Aquatic and Terrestrial Humic Materials, Ann Arbor Science, Ann Arbor, MI, 1983, pp. 1—23.
17 E. M. Thurman and R. L. Malcolm, Environ. Sci. Technol., 15 (1981) 463.
18 J. Buffle, P. Deladoey and W. Haerdi, Anal. Chim. Acta, 101 (1978) 339.
19 E. M. Thurman, R. L. Wershaw, R. L. Malcolm and D. J. Pinckney, Org. Geochem., 4 (1982) 27.
20 E. Mentasti, E. Pelizzetti and G. Saini, J. Chem. Soc., Dalton Trans., (1973) 2609.
21 N. Senesi, S. M. Griffith, M. Schnitzer and M. G. Townsend, Geochem. Cosmochim. Acta, 41 (1977) 969.
22 B. A. Goodman and M. V. Cheshire, J. Soil Sci., 30 (1979) 85.
23 M. Schnitzer and K. Ghosh, Soil Sci., 134 (1982) 354.
24 BMDP, BMDP Statistical Software, University of California Press, Ch. 14, 1983.
25 M. Schnitzer and S. U. Khan (Eds.), Soil Organic Matter. Developments in Soil Science, Vol. 8, Elsevier, Amsterdam, 1978.
26 R. A. Saar and J. H. Weber, Can. J. Chem., 57 (1979) 1263.
27 J. A. Leenheer, Environ. Sci. Technol., 15 (1981) 578.

Analytica Chimica Acta, 162 (1984) 275—283
Elsevier Science Publishers B.V., Amsterdam — Printed in The Netherlands

ELIMINATION OF BILIRUBIN INTERFERENCE IN FLUORIMETRIC DETERMINATION OF FLUORESCEIN BY PHASE-RESOLVED FLUORESCENCE SPECTROMETRY

FRANK V. BRIGHT and LINDA B. McGOWN*
Department of Chemistry, Oklahoma State University, Stillwater, OK 74078 (U.S.A.)
(Received 26th March 1984)

SUMMARY

Phase-resolved fluorescence spectrometry is used to eliminate bilirubin interference in the fluorimetric quantitation of fluorescein, despite extensive excitation and emission spectral overlap of the two species. In this method, it is the difference in fluorescence lifetimes of the two species that provides the selectivity parameter. Results are given for a nulling approach and for a multiple phase-angle approach. In the nulling approach, intensity is measured at a detector phase angle at which the intensity for bilirubin is zero. In the multiple phase-angle approach, intensities at several detector phase angles are used to generate a matrix which is solved for the concentrations of fluorescein and bilirubin. Although a steady-state method yielded low results for fluorescein concentration in the presence of bilirubin concentrations above about 3 μM, the phase-resolved methods yielded correct values for fluorescein concentration with bilirubin concentrations up to 10 μM.

Fluorescein is one of the most commonly used fluorescent labels in fluoroimmunoassays and in other biochemical and clinical methods. Measurement of fluorescein in serum samples can be severely hampered by the presence of bilirubin, which has broad fluorescence excitation and emission spectra that overlap the spectra of fluorescein.

The low levels of bilirubin found in normal serum ($\approx 1\ \mu$M) are usually not a problem because of the very low quantum yield of bilirubin fluorescence. However, the high levels of bilirubin found in icteric sera will interfere with the quantitation of fluorescein. The concentration ratios are actually more important than the individual values, because the critical factor in evaluating the extent of interference is the relative fluorescence contributions of fluorescein and bilirubin. A rough estimate of the relative contributions of fluorescein (assuming a quantum yield of 1 and $\epsilon_{490} \simeq 9 \times 10^4$) and albumin-bound bilirubin (quantum yield of 0.001 and $\epsilon_{490} \simeq 3 \times 10^4$) [1], shows that the relative bilirubin (b) contribution will be 1% or more of the fluorescein (f) contribution when $C_b \geqslant 30\ C_f$. Therefore, for $C_b \geqslant 30\ C_f$, a bilirubin blank must be subtracted for conventional (steady-state) fluorimetric determination of fluorescein.

0003-2670/84/$03.00

Free serum bilirubin, i.e., bilirubin not bound to albumin or any other serum species, is not considered in evaluating bilirubin interference because it has a negligible quantum yield (10^{-5}).

An additional problem occurs for bilirubin concentration above about 3 μM (in the sample cuvet). Steady-state fluorescence results indicate that the bilirubin and fluorescein intensities are not additive, resulting in negative errors for fluorescein which increase with increasing bilirubin concentration. These errors become significant for bilirubin concentrations above 3 μM. Additional sample dilutions can be used to lower the bilirubin concentration to non-interfering levels, but this will also dilute the fluorescein concentration.

The phase-resolved fluorescence spectrophotometric technique described here exploits the difference in fluorescence lifetimes of fluorescein and bilirubin to resolve mixtures of the two. In a nulling approach, the signal is measured at the detector phase angle setting required to exactly null the phase-resolved intensity of bilirubin so that only fluorescein intensity is observed. In a multiple phase-angle approach, measurements are made at several detector phase angles and simultaneous equations are solved for the concentrations of the two components. The multiple phase-angle technique extends the tolerable level of bilirubin up to 10 μM. (All concentrations quoted are those in the measurement cuvet.)

THEORY

The theory and instrumentation of phase-resolved fluorescence spectrometry have been described elsewhere [2, 3], and are based on the phase-modulation technique for determination of fluorescence lifetimes [4]. Briefly, the sample is excited with sinusoidally modulated light having an angular frequency ω and intensity $E(t)$ at time t: $E(t) = 1 + m_{ex} \sin \omega t$, where m_{ex} is the degree of modulation. The resulting fluorescence, $F(t)$, of a single component sample with exponential decay will be phase-shifted by angle ϕ and appear as: $F(t) = 1 + m_{ex} \cos \phi \sin (\omega t - \phi)$. For a solution containing two fluorophores, A and B,

$$F(t) = k_A \sin (\omega t - \phi_A) + k_B \sin (\omega t - \phi_B)$$

where k_A and k_B are constants which depend upon the spectral characteristics of the species. If the fluorescence emission is observed with a phase-sensitive detector, the phase-sensitive signal at detector phase ϕ_D will be

$$F(\phi_D) = k_A \cos (\phi_D - \phi_A) + k_B \cos (\phi_D - \phi_B).$$

By choosing ϕ_D to be 90° out of phase with one of the components (e.g., component A; $\phi_D = \phi_A \pm 90°$), that component will be "nulled" and only component B will be observed. If $\phi_D = \phi_B \pm 90°$, only component A will be observed.

Applications of phase-resolved fluorescence spectrometry described in the literature so far have generally involved the selective nulling of one component

in a two-component mixture so that both components in turn can be selectively measured [3, 5]. McGown [6] has recently demonstrated the use of measurements at two phase angles other than the null angles and was able to resolve successfully mixtures of fluorescein and fluorescein isothiocyanate (the former physically adsorbed on albumin and the latter covalently bound to albumin). The use of multiple phase-angle measurements resulting in an overdetermined system has been suggested [7], but does not seem to have been previously demonstrated.

In the multiple phase-angle approach, a solution containing n components is measured at m detector phase angles, where $m \geqslant n$. For example, a solution containing two components A and B is measured at two or more detector phase angles (ϕ_D), and simultaneous equations are solved for the concentrations of the two components

$$\begin{aligned} I_{\phi_{D1}} &= \bar{I}_{A,\phi_{D1}} C_A + \bar{I}_{B,\phi_{D1}} C_B \\ I_{\phi_{D2}} &= \bar{I}_{A,\phi_{D2}} C_A + \bar{I}_{B,\phi_{D2}} C_B \\ &\vdots \\ I_{\phi_{Dm}} &= \bar{I}_{A,\phi_{Dm}} C_A + \bar{I}_{B,\phi_{Dm}} C_B \end{aligned} \qquad (1)$$

The $\bar{I}$ values represent the molar fluorescence intensities of each individual component measured at each detector phase angle using a standard solution of the component. In the work described here, intensities for standard solutions of fluorescein and bilirubin were measured at each detector phase angle to obtain the values of $\bar{I}_f$ and $\bar{I}_b$ at each angle.

EXPERIMENTAL

All fluorescence measurements were made with an SLM 4800S spectrofluorimeter (SLM Instruments, 810 West Anthony Drive, Urbana, IL, 61801), with a 450-W source and photomultiplier tube detection. Excitation at 490 nm and emission at 520 nm were used for all measurements (these are the maximum wavelengths for observation of fluorescein fluorescence).

Unless otherwise noted, three replicate measurements were taken for each solution, each measurement being the average of 100 samplings (this is done internally by the SLM electronics and requires about 30 s per measurement).

Phase-resolved measurements were made at two different modulation frequencies (18 MHz and 30 MHz), in delta phase mode (an instrumental mode which provides simultaneous comparison of the sample beam with a portion of the incident beam that is diverted to a reference PMT after the incident beam has been modulated). For the nulling approach, a standard bilirubin solution was used to locate the null phase angle of bilirubin, and a standard solution of fluorescein was then measured at this phase angle to obtain $\bar{I}_f$.

For the multiple phase-angle approach, intensities for standard solutions of fluorescein and of bilirubin were measured at each phase angle to obtain $\bar{I}_f$ and $\bar{I}_b$ values.

All intensities were measured first at one phase angle and then at the next, and so on, to minimize the effect of any irreproducibility in setting the phase angles.

All steady-state and phase-resolved intensities for all solutions were corrected for any non-negligible background intensity of the HSA-buffer solution by subtracting the intensity of the HSA-buffer measured under the same conditions as the test solution from the measured intensity of the test solution.

Phase angles referred to in the following sections correspond to the detector phase-angle settings subtracted from 360° to compensate for mislabelled controls on the instrument used.

Data were entered by hand into an APPLE IIe microcomputer. The 2×2 matrices were solved by using Cramer's Rule and the overdetermined ($m \times 2$) matrices were solved by a Gaussian—Newton iterative program.

RESULTS

All concentrations quoted below are those in the sample cuvet.

The mixtures of fluorescein and bilirubin used in the following studies contained 1.00 nM fluorescein, to which were added various amounts of bilirubin up to 11 μM, in a total volume of 3.00 ml. The maximum ratio of bilirubin to fluorescein was therefore 11 000:1. This corresponds to an addition of, for example, 30 μl of an icteric serum sample containing 0.1 μM fluorescein and 1 mM bilirubin to the cuvet. Therefore, the bilirubin levels studied correspond to the maximum levels generally encountered in serum, assuming a 100-fold sample dilution. The fluorescein concentration used (1 nM) corresponds to the lower range of concentration of fluorescein-labelled species generally required to obtain a signal-to-noise ratio of 100:1 using conventional fluorescence instrumentation, which has been suggested as the minimum S/N for fluoroimmunoassay procedures [1].

Results will be described for steady-state fluorescence experiments, which were aimed at assessing the extent of bilirubin interference in fluorimetric determination of fluorescein, and for the phase-resolved method with two different modulation frequencies, using both the nulling and the multiple phase-angle approaches.

Steady-state fluorescence

Results for the steady-state determination of 1.00 nM fluorescein in the presence of 1.0—10 μM bilirubin are summarized in Table 1. The results were obtained by measuring the difference in fluorescence intensity of each solution containing bilirubin before and after the addition of 1.00 nM fluorescein (I_b and I_{f+b}, respectively). This difference was then compared to the intensity

TABLE 1

Experimental values of fluorescein concentration[a]

Conditions[b—e]		Average concentration (nM) ± RSD (%)
Steady state[b]	No polarizers, no Triton X-100	0.729 ± 54
	Polarizers	0.897 ± 6.2
	Polarizers and Triton X-100 Trial 1:	0.811 ± 20
	Trial 2:	0.681 ± 52
Phase-resolved[c,d] (18 MHz)	Bilirubin null phase angle (180°)	0.963 ± 12
	2 phase angles (65°, 105°)	1.05 ± 11
	3 phase angles (45°, 65°, 135°)	1.01 ± 8.5
	4 phase angles (45°, 65°, 105°, 135°)	1.06 ± 8.9
Phase-resolved[e] (30 MHz)	Bilirubin null phase angle	0.632 ± 48
	2 phase angles: 159°, 284°	1.00 ± 13
	146°, 284°	1.01 ± 13
	3 phase angles: 146°, 159°, 284°	1.00 ± 13
	159°, 284°, 291°	0.991 ± 12
	146°, 284°, 291°	0.987 ± 14
	4 phase angles: 159°, 284°, 236°, 291°	0.941 ± 16
	6 phase angles (all except bilirubin null angle)	0.912 ± 14
	7 phase angles	0.849 ± 26

[a] 1.00 nM added. [b—e] Based on measurement of one solution at each of [b] 10, [c] 13 (nulling method), [d] 8 (multiple phase-angle method) and [e] 10 different bilirubin concentrations. See text for bilirubin concentration ranges.

of a 1.00 nM fluorescein solution containing no bilirubin (I_f). The resulting error for the determination of fluorescein in the presence of bilirubin is calculated as

$$\text{Error (\%)} = \{[(I_{f+b} - I_b) - I_f]/I_f\} \times 100\%. \quad (2)$$

Large negative errors were found for solutions containing more than 5 μM bilirubin, indicating that the bilirubin and fluorescein intensities are not additive. The null phase-angle studies at 18 MHz (see below and Table 1) indicate that fluorescein intensity is independent of bilirubin concentration. Absorption spectrophotometric studies showed no change in bilirubin absorbance upon addition of as much as 10 nM fluorescein, with Beer's Law being valid for bilirubin up to 10 μM. Therefore, it appears that the non-additivity is due to an effect of fluorescein on the fluorescence of bilirubin rather than a mutual effect.

The use of a polarizer set at 35° in the excitation beam to minimize scattered light improved results (Table 1), but the systematic negative error is still apparent. Polarization was not used in subsequent studies because it did not eliminate the non-additivity and it reduced the intensity of light reaching the sample which decreased the sensitivity for fluorescein determination.

The addition of Triton X-100 to all solutions, combined with polarization, also did not eliminate the systematic negative error. Triton X-100 was added to the solutions for the 18-MHz phase-resolved studies but not used for the 30-MHz studies, and had no apparent effect on the 18-MHz results relative to the 30-MHz results.

Phase-resolved fluorescence spectrometry with 18-MHz modulation frequency

The graphs of phase-resolved intensity vs. detector phase angle for fluorescein and for bilirubin at 18 MHz are shown in Fig. 1A. The detector phase angles at which each component has maximum phase-resolved intensity (i.e., $\phi_D = \phi_f$ or ϕ_b) remained constant for bilirubin up to 5 μM and for fluorescein between 0.5 and 1000 nM, indicating constant lifetimes at these concentrations. A phase-angle difference of 21.2° was found between the peak intensities for the two species, and subtraction of the phase angle at the peak intensity of a scattering solution (measured at 520 nm for both excitation and emission) from the phase angles of each species yielded fluorescence lifetime values of 4.0 ns for fluorescein and 0.48 ns for bilirubin.

Results for the quantitation of 1.00 nM fluorescein in the presence of bilirubin ranging from 0.3 to 7.5 μM bilirubin (Table 1) by means of the nulling approach, indicate the absence of systematic error. This verifies the constancy of the bilirubin null angle at these concentrations, as well as the absence of any effect of the presence of bilirubin on the fluorescein intensity.

Results for the quantitation of 1.00 nM fluorescein using the multiple phase-angle approach are shown in Table 1 for determinations using a total of four detector phase angles, as well as for those combinations of two and three angles yielding the best results. Bilirubin concentrations ranging from 0.5 to 7.0 μM were used in these determinations.

Phase-resolved fluorescence spectrometry with 30-MHz modulation frequency

Plots of the phase-resolved fluorescence intensity for bilirubin and fluorescein are shown in Fig. 1B. The phase-angle difference between the two was 34°. Lifetimes for the two species, calculated as described above for 18 MHz, were 4.0 ns for fluorescein and 0.3 ns for bilirubin. The bilirubin lifetime was harder to determine at 30 MHz than at 18 MHz because of the presence of a significant blank signal from the HSA-buffer solution at 30 MHz.

Determinations of 1.00 nM fluorescein in the presence of 0.55—11 μM bilirubin were done using both the nulling approach and the multiple phase-angle approach with a total of 7 detector phase angles. Results are shown in Table 1, including results for the best combinations of 2, 3, 4 and 6 phase angles. Because of the blank signal, location of the null phase angle was done less directly than at 18 MHz. At the latter frequency, the null phase angle is simply the phase angle at which the phase-resolved intensity of bilirubin is zero. At 30 MHz, the null phase angle of bilirubin is the angle at which the phase-resolved intensity of bilirubin exactly equals that of the HSA-buffer blank, indicating zero contribution from the bilirubin. The source of the

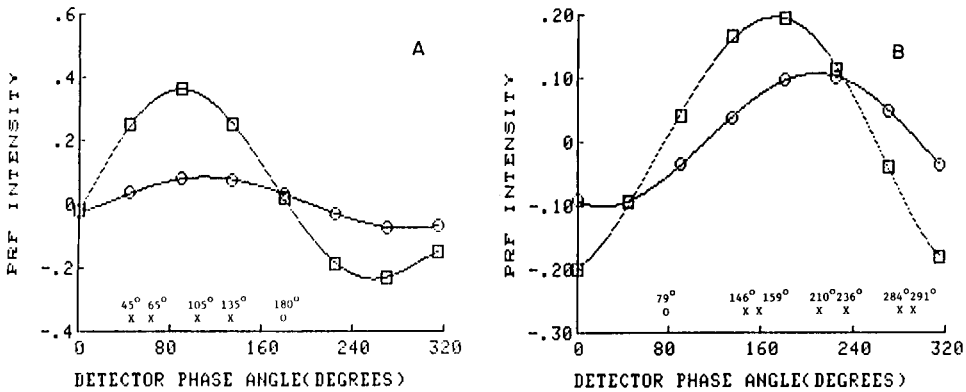

Fig. 1. Phase-resolved fluorescence intensity (relative) as a function of detector phase angle (ϕ_D). Modulation frequency: (A) 18 MHz; (B) 30 MHz. (○) 1.00 nM fluorescein; (□) 4.0 μM bilirubin (A) and 3.0 μM bilirubin (B). Null phase angle of bilirubin and the angles used for multiple phase-angle determinations are indicated by O and X, respectively.

blank signal has not yet been identified. It may be inherent to the HSA-buffer at 30 MHz, perhaps by scattering, or it may be caused by an impurity in the particular batch of reagents used for the 30-MHz studies.

DISCUSSION

Precision of measurement

The average relative standard deviations for replicate measurements on each set of solutions under the measurement conditions used for the set are shown in Table 2. Overall, the best precision was obtained under steady-state conditions. For phase-resolved measurements at 18 MHz, precision data were good at the detector phase angles used for the multiple phase-angle approach, and poor for the null phase-angle measurements. This is to be expected, because the relative noise will be highest at the detector phase angle at which the magnitude of the signal is the lowest, i.e., at the null phase angle of a major contributor to the total signal. Also, the slope of the phase-resolved curve (see Fig. 1) is largest at the null phase angle, resulting in the maximum signal fluctuation with detector phase-angle fluctuation. Best precision was obtained at the two phase angles (105° and 135°) closer to those giving maximum intensities, and was somewhat poorer, although still acceptable, at the two angles (45° and 65°) closer to the null phase angles of the components.

Precision data for the phase-resolved measurements at 30 MHz are best (equalling those for steady-state measurements) at 210°, which is close to the phase angles of both components, and are only slightly less precise at 159°, 146° and 236°. Precision at the null phase angle of bilirubin is not much less than at these angles, because of the presence of the blank signal.

TABLE 2

Imprecision of fluorescence intensity measurements

Conditions[a,b]		RSD (%)	Conditions		RSD (%)
Steady-state	No polarizers, no Triton X-100[a]	1.3	*Phase-resolved* (30 MHz)	78.8° (bilirubin null phase angle)	3.0
	Polarizers (35° excitation)	0.6			
	Polarizers and Triton X-100 (Trial 1)	0.6		146°	2.4
				159°	1.5
Phase-resolved (18 MHz)	180° (bilirubin null phase angle)[b]	20		210°	0.9
				236°	1.2
	45°	4.0		284°	12
	65°	4.1		291°	31
	105°	2.0			
	135°	2.4			

[a,b] Three measurements per solution, except [a] 2 measurements, and [b] 5 measurements.

Poor precisions are obtained at 284° and 291°, which are close to the null angles of fluorescein and of the blank.

Accuracy and precision of the methods

Precision and accuracy at 18 MHz are best for the multiple phase-angle approach using 3 and 4 phase angle combinations. Results at the null phase angle and with two phase angles are similar, and are better than those obtained using steady-state measurements. The substantial improvement obtained in going from two to three phase angles warrants the additional time and effort. Three phase angles are adequate for resolving fluorescein and bilirubin and additional angles are not needed.

It is expected that 30-MHz modulation should have better resolving power for bilirubin and fluorescein than 18 MHz because of the short fluorescence lifetimes involved. This is indeed the case, as evidenced by the fact that excellent accuracy is obtained at several two-angle combinations, with no noticeable improvement when three phase angles are used. A loss of accuracy results when more than three angles are used, because of the locations of the particular angles included in the group of seven. The use of more phase angles chosen from an optimal location on the fluorescence curve (Fig. 1B) should improve method precision.

Extended tolerable bilirubin range

Because it is the non-additivity of the bilirubin signal that causes non-linear response for fluorescein in the steady-state method, and because the bilirubin signal is zero in the nulling approach, it is clear why the nulling approach yields correct results for fluorescein concentration. It is easily shown why the same is true for the multiple phase-angle approach.

For the case of two phase angles, ϕ_{D1} and ϕ_{D2}, using Cramer's Rule to solve the square 2 × 2 matrix

$$I_{\phi_{D1}} = \bar{I}_{f,\phi_{D1}} C_f + \bar{I}_{b,\phi_{D1}} C_b ; I_{\phi_{D2}} = \bar{I}_{f,\phi_{D2}} C_f + \bar{I}_{b,\phi_{D2}} C_b \quad (3)$$

the solution for fluorescein is

$$C_f = (I_{\phi_{D1}} \bar{I}_{b,\phi_{D2}} - I_{\phi_{D2}} \bar{I}_{b,\phi_{D1}}) / (\bar{I}_{f,\phi_{D1}} \bar{I}_{b,\phi_{D2}} - \bar{I}_{f,\phi_{D2}} \bar{I}_{b,\phi_{D1}}) \quad (4)$$

with an analogous equation for bilirubin. The $\bar{I}_b$ values are dependent on both C_b and C_f, and because both $\bar{I}_b$ values ($\bar{I}_{b,\phi_{D1}}$ and $\bar{I}_{b,\phi_{D2}}$) are simple sine-function multiples of the steady-state $\bar{I}_b$, they will remain in the same proportion to each other despite any variation in the steady-state value of $\bar{I}_b$. Therefore, any changes in the phase-resolved $\bar{I}_b$ values caused by changes in the steady-state $\bar{I}_b$ will cancel in Eqn. 4, leaving C_f unchanged. The same would not be true for C_b, because the $\bar{I}_b$ terms do not cancel in the analogous equation for C_b. However, in eliminating bilirubin interference, it is not necessary to obtain a correct value for C_b, but only to separate its contribution from that of fluorescein to yield correct values for C_f.

The authors gratefully acknowledge partial support for this research from the Department of Health and Human Services via a grant from the National Institute on Drug Abuse, DA03479-01, and from a Grant-in-Aid of Research from Sigma Xi, the Scientific Research Society. We are also grateful to Dr. J. P. Chandler of the Computer and Information Science Department at Oklahoma State University for providing the Gaussian—Newton iterative program.

REFERENCES

1 D. S. Smith, M. Hassan and R. D. Nargessi, in E. L. Wehry (Ed.), Modern Fluorescence Spectroscopy, Vol. 3, Plenum Press, New York, 1981, pp. 157, 168, 170—174.
2 T. V. Veselova, A. S. Cherkasov and V. I. Shirokov, Opt. Spectrosc., 29 (1970) 617.
3 J. R. Lakowicz and H. Cherek, J. Biochem. Biophys. Methods, 5 (1981) 19.
4 R. D. Spencer and G. Weber, Ann. N.Y. Acad. Sci., 158 (1969) 361.
5 J. R. Lakowicz and H. Cherek, J. Biol. Chem., 256 (1981) 6348.
6 L. B. McGown, Anal. Chim. Acta, 157 (1984) 327.
7 J. R. Knutson, D. G. Walbridge and L. Brand, Biochemistry, 21 (1982) 4671.

Analytica Chimica Acta, 162 (1984) 285—291
Elsevier Science Publishers B.V., Amsterdam — Printed in The Netherlands

SPECTROPHOTOMETRIC DETERMINATION OF LITHIUM ION WITH THE CHROMOGENIC CROWN ETHER, 2″,4″-DINITRO-6″-TRIFLUOROMETHYLPHENYL-4′-AMINOBENZO-14-CROWN-4

Y. P. WU and G. E. PACEY*
Department of Chemistry, Miami University, Oxford, OH 45056 (U.S.A.)
(Received 10th February 1984)

SUMMARY

A spectrophotometric method of determining alkali metal ions with a chromogenic crown ether reagent was found to be more selective and sensitive than an ion-pairing method based on the same size of crown ether cavity. It is shown that in the ion-pairing method, the sensitivity toward lithium ion was 5.685×10^{-4} absorbance/mg l^{-1}, with sodium interfering at 300 mg l^{-1}. The chromogenic crown ether, 2″,4″-dinitro-6″-trifluoromethylphenyl-4′-aminobenzo-14-crown-4, was much superior to benzo-14-crown-4. The sensitivity of the chromogenic crown ether was 1.69×10^{-3} absorbance/mg l^{-1}. This represents a three-fold increase in sensitivity and less reagent is needed (2×10^{-4} M for the chromogenic method versus 1.4×10^{-3} M for ion-pairing). Interference from sodium decreased to 3000 mg l^{-1}. The reagent was used to determine lithium ion in treated blood serum samples in both a batch and flow injection method and results were compared with data obtained with atomic absorption; excellent agreement was obtained in all cases.

The design and synthesis of new analytical reagents for alkali metal ions is pursued not for application to a batch method, but for use in selective method in automated chemistry, ISFETs, optrodes or test strip papers. The most important criterion for these reagents is selectivity. Therefore, the crown ethers are excellent candidates for synthetic modification to produce selective and sensitive analytical reagents for the determination of alkali metals.

Very few colorimetric reagents that complex alkali metal ions are known. This is due to the low tendency of these cations to form complexes with ordinary anionic or dipolar ligands. The discovery of crown ethers and cryptands with their potential affinity for alkali metal ions made it possible to design reagents that could selectively complex alkali metal ions and produce a color change. Recently, researchers have shown that monobasic chromophoric crown ethers exhibit very selective extraction behavior, thus making them useful as analytical organic reagents [1—4]. The chromogenic crown ethers were synthesized by reacting a chromophore with a 4′-aminobenzo crown ether. An investigation into this type of system, rather than the azo type of linkage previously reported [5], seemed to be preferred, because the monobasic amine linkage has a greater aqueous solubility, as well as

0003-2670/84/$03.00

significantly larger intervals between the wavelengths of maximum absorption for the protonated and deprotonated species.

Reagents for the determination of lithium ion are of particular interest; there is a need for a selective reagent for lithium ion. In particular, people suffering from manic depression are placed on lithium carbonate therapy. The control of the level of lithium in the body is critical. With too little or too much lithium, the patient is still a manic depressive. The control of lithium levels, using a self-administered test, would provide a considerable upgrading of mental health to the patient. The first step of this research is to develop selective lithium ion reagents. Therefore, it was decided to modify benzo-14-crown-4 into a chromogenic crown ether for use in lithium determinations. A comparison is made between the chromogenic crown ether and an ion-pairing technique, utilizing benzo-14-crown-4 with picrate as the counter ion.

EXPERIMENTAL

Reagents and apparatus

The two crown ether reagents investigated were benzo-14-crown-4 (**I**) and 2″,4″-dinitro-6″-trifluoromethylphenyl-4′-aminobenzo-14-crown-4 (**II**). The synthesis of these compounds has been reported elsewhere [6]. All the solvents for the extraction studies were of spectroscopic grade. All alkali salts were at least 99.0% pure.

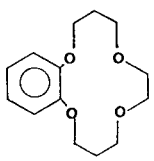

I

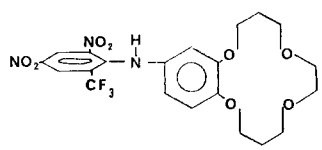

II

Spectra were measured with a Hewlett-Packard Model 8450A spectrophotometer. A Corning Model 12 pH meter was used for pH measurements.

Procedures

Ion-pair extraction. The ion-pairing extraction behavior of benzo-14-crown-4 was investigated with dichloromethane. The percentage extraction of picrate was measured by mixing 10 ml each of alkali hydroxide (0.1 M) and picric acid (7×10^{-4} M) in an aqueous phase (pH 11.3) with an equal volume of benzo-14-crown-4 (7×10^{-4} M) in organic phase. After shaking for 10 min on a multi-wrist shaker, the concentration of the picrate/crown/alkali metal ion-pair complex was measured spectrophotometrically. The extraction constants and partition coefficients were determined by the procedures described elsewhere [7].

The linear range was determined by mixing 10 ml of 1.4×10^{-3} M benzo-14-crown-4 in dichloromethane with 10 ml of a solution of a varying con-

centration (0—700 mg l^{-1}) of lithium ion which contained a constant amount of rubidium hydroxide as a pH controller. A constant pH of 11.3 in the aqueous phase was maintained throughout. Interferences from sodium and potassium ions were studied by determining a constant concentration of lithium ion while increasing the concentration of the interfering ion.

Chromogenic crown ether. The u.v.-visible spectra were obtained by dissolving a dried and weighed quantity of the chromogenic crown ether in 40% acetone/60% water that contained a fixed concentration of lithium chloride (0.1 M). Two spectra were recorded, one at pH 2 and the other at a pH suitable for complete dissociation of the amine proton.

The extraction constants and complex stoichiometry were evaluated as follows. A 10 ml aliquot of 0.1 M alkali metal solution was extracted with 10 ml of 1,2-dichloroethane containing varying amounts (5×10^{-5}—8×10^{-4} M) of crown ether. Rubidium hydroxide was used to maintain a constant pH of 12.6 in the aqueous phase. The absorption spectrum of the 1,2-dichloroethane was recorded between 200 and 800 nm. The extraction constant, K_{ex}, and the apparent change in molar absorptivity, $\Delta\epsilon$, were then calculated by using previously reported methods [2]. A second experiment, in which the pH and the metal ion concentration were constant and the concentration of the crown ether in the organic phase was varied, produced the data that were needed to calculate the ratio of crown ether to metal in the complex [2].

The acidity constants, K_a and K'_a, of the crown ether and the formation constants, K_{ML} and K_{MHL}, for lithium ion in 10% dioxane were evaluated spectrophotometrically. Several milligrams of the reagent were dissolved in 2.5 ml of dioxane in a 25-ml volumetric flask. Lithium chloride or other alkali metal salt was added and the solution was diluted to 25 ml with water. The rubidium hydroxide solution was then added, after which the absorbance and pH of the solution were measured. The ionic strength was in the range 0.07—0.15. When the effect of alkali metal ion on the proton dissociation process was to be excluded, rubidium hydroxide was used at the proper concentration to maintain the desired pH.

The linear range was evaluated by mixing 10 ml of a solution of varying concentration (0—700 mg l^{-1}) of lithium ion. Rubidium hydroxide was used in all extractions to maintain a constant pH of 13.2 in aqueous phase. Sodium ion interference was studied by holding a constant concentration of lithium ion while increasing the sodium concentration from 0 to 3500 mg l^{-1}.

The flow-injection system used for the automation of the method was as described previously [8]. The blood serum samples were prepared by using 10 ml of blood serum with 2 ml of water and heating in boiling water for 15 min. After 10 min of centrifugation, the precipitated proteins were collected on the bottom of the tube, allowing for the sampling of a deproteinated solution. Obviously, the amount of serum prepared would be 500 times more than this flow-injection method requires.

RESULTS AND DISCUSSION

Ion-pair extraction behavior of benzo-14-crown-4

Ion-pair extraction was based on the complex formation with alkali metal ions, followed by liquid—liquid extraction of the ion-pair of the crown complex and a highly colored anion. In this type of study, the detection was based on the intermolecular ion-pair extraction. As can be seen in Table 1, the sequence of the percentage extraction of the picrate/crown/alkali metal ion-pair was $Li^+ > Na^+ > K^+$. It is interesting that benzo-14-crown-4 extracts lithium most efficiently among the alkali metal ions, while benzo-12-crown-4 totally eliminates the Li^+ from the extraction process [7]. The reason may be that lithium ion is the most strongly hydrated among the alkali metal ions. Therefore, lithium ion would favor the slightly larger cavity of benzo-14-crown-4 (cavity radius of 0.6—0.75 Å) over the benzo-12-crown-4 (0.5—0.65 Å). Another interesting point observed in this study was the spectral change of the alkali metal picrates. The maximum of the main absorption band for the alkali metal ions (Li^+, Na^+, K^+) was found to be at 356 nm (in water). However, the maximum absorption bands were at 358 nm for Li^+, 368 nm for Na^+, and 375 nm for K^+ in dichloromethane. This observation could be attributed to the different interaction between cations and counterions in the crown complexes which caused the bathochromic shifts of the spectrum. In the case of lithium ion, which has the greatest polarization power of all the alkali metal ions, the interaction is more covalent. This results in a localized negative charge on the picrate ion and the bathochromic shift is not as large. In contrast, the ion—ion interaction is more favored when the potassium ion is complexed. This ion-pair interaction results in a delocalized negative charge of the picrate; therefore, a large bathochromic shift is observed. The partition coefficient has been calculated as 6.0×10^{-4}. The extraction constants, dissociation constants, and stoichiometric ratio between the crown ether and the metal ion were evaluated as described earlier [7]. These results are summarized in Table 2.

A calibration graph was prepared for standard solutions of lithium chloride. It was linear over the range of 14—695 mg l^{-1} lithium ion for measurements at 358 nm with a sensitivity of $5.685 \times 10^{-4} \pm 1.232 \times 10^{-5}$ (absorbance/mg l^{-1}). The correlation coefficient was 0.999.

TABLE 1

Extraction of alkali metals with benzo-14-crown-4 as the ligand, dichloromethane as the solvent and picrate as the counter ion

[Crown]/[Pic]	Extraction (%)		
	Li^+	Na^+	K^+
1.0	1.89	0.56	0.09
1.5	2.83	0.68	0.18
2.0	3.61	1.00	0.40

TABLE 2

Extraction and dissociation constants of alkali metal ion complexes[a] with benzo-14-crown-4 as the ligand, picrate as the counter-ion and dichloromethane as the solvent

Metal	Li	Na	K
$\log K_{ex}$	2.77 ± 0.02	2.17 ± 0.04	1.65 ± 0.05
$\log K_d$	−4.78	−5.38	−5.94

[a]All stoichiometric ratios were 1:1 (metal ion/crown ether).

Interferences were studied for benzo-14-crown-4 method. An increase in absorbance was observed when the sodium ion concentration exceeded 300 mg l^{-1}. Potassium ion had essentially no effect until its concentration exceeded 4000 mg l^{-1}. The low tolerance of the method to sodium ion indicates that the method is of little value where sodium is a dominant species.

Complex formation and extraction with the chromogenic crown compound

The complexation and extraction of alkali metal ions by 2″,4″-dinitro-6″-trifluoromethylphenyl-4′-aminobenzo-14-crown-4 was shown to be markedly different. The color of the compound in an aqueous solution turned from orange (λ_{max} = 380 nm, ϵ = 12 000 l mol^{-1} cm^{-1}) to blood-red (λ_{max} = 462 nm, ϵ = 20 000 l mol^{-1} cm^{-1}) on dissociation of the amine proton. This is due to the increased conjugation of the chromophoric system.

During the extraction and complexation of aqueous alkali metals, a complex equilibrium is established [2]. The protonated crown ether species, HL, originally in the organic phase will distribute itself between the organic phase and the aqueous phase. The aqueous phase, having been adjusted to the proper pH, will cause HL to dissociate. Another possibility is that complexation can occur without deprotonation forming MHL^+ species which can dissociate to ML. The complexed crown ether species, ML, in the aqueous phase then distributes between the organic and aqueous phases. Depending on the diameter of the crown cavity and the alkali metal cation, a 2:1 ligand:metal complex, ML · HL, can be formed.

From the plots of log [metal ion distribution ratio] vs. log $[HL]_0$, the stoichiometry of the complex was evaluated. The $[HL]_0$ values for the plot were obtained from the total concentration of HL in the original organic solution, $[HL]_t$, after correction for the fraction converted into ML and ML · HL or distributed into the aqueous phase. The slope for Li^+ was close to 1, indicating that Li^+ was extracted only in the form of ML. The slope for K^+ was close to 2, thus K^+ was extracted only in the form of the complex ML · HL. An upward curvature with varying slopes between 1 and 1.8 was obtained for Na^+, the value being higher at high concentration of HL. This indicates that Na^+ was extracted in the form of both ML and ML · HL with

ML prevailing at lower concentrations of HL and ML · HL dominating at the higher concentrations of HL. These results are interesting when compared to the values reported for the stoichiometric ratio of benzo-14-crown-4 to the alkali metal ions (Li^+, Na^+, K^+), under ion-pairing conditions, (1:1, in each case). It is believed that this change in the stoichiometric ratio is due to the addition of the chromophore which increases the rigidity of the compound. Thus, it would reduce the ability of the polyether ring to distort and accommodate those cations which have radii larger than the cavity of the crown ether. In addition, it seems very probable that the chromophoric compound formed an intramolecular ion-pair. Therefore, the space above the cavity is not occupied by a counter-ion as is the case for ion-pairing.

The extraction constants for Li^+, Na^+, K^+ were obtained by plotting log [metal distribution ratio] against log $[HL]_0$ [2]. These results are summarized in Table 3. These values are quite low, which might result from a rather large charge separation in the complex structure. The values of Na^+ and K^+ also indicate a 2:1 crown-to-metal complex was preferred. These data imply that a 2:1 crown complex is only significant when there is an excess of crown reagent. Thus, lithium selectivity can be increased if the crown ether reagent is used at low concentrations.

The pK_a of the crown ether reagent was found to be 9.99. The pK_a' was 9.6. The aqueous formation constants for the complex with lithium ion were calculated as $\log K_{ML} = 1.18$ and $\log K_{MHL} = 0.78$.

It was found that deprotonation is a necessary requirement for measuring the extraction of alkali metal ions. The buffer system necessary to attain proper deprotonation can be prepared by using an amine with a pK_a greater than the pK_a of the reagent. However, when chloroform was combined with the triethylamine, which was the commonly used solvent/buffer system in previous work, the system was totally useless because deprotonation of the crown ether was instantaneous. Trials of other solvent systems showed that 1,2-dichloroethane was the most efficient solvent for the extraction in this case. Unfortunately, triethylamine could not be used in 1,2-dichloroethane because, even in the absence of metal ions, some of the reagent dissociated. Thus, pure 1,2-dichloroethane was used and the pH of the aqueous phase was adjusted to assure the occurrence of deprotonation. The pH adjustment was made by the addition of rubidium hydroxide because it was shown earlier to exhibit no complexation with the crown ether reagent.

Because the extraction constants showed that this reagent is rather selective for lithium ion, a calibration graph for lithium was constructed. The

TABLE 3

Extraction constants of the alkali metal ions in the chromogenic crown ether system

Metal	Li^+	Na^+	K^+
pK^{ex}_{ML}	11.00	11.43	—
$pK^{ex}_{ML \cdot HL}$	—	8.69	9.72

TABLE 4

Comparison of batch and flow-injection methods based on the chromogenic crown ether with the atomic absorption (a.a.s.) method for the determination of lithium ion in blood serum[a]

Sample	Li^+ concentration (mg l^{-1})			
	Added	Batch[b]	F.i.a.[c]	A.a.s.[d]
1	25	24.7 ± 1.3	24.8 ± 0.5	25 ± 0.7
2	50	49.1 ± 2.5	50 ± 0.4	49.8 ± 0.5
3	100	98.0 ± 5.0	99.7 ± 0.8	99.0 ± 0.9
4	250	240 ± 9.0	245 ± 2.1	230 ± 4.0

[a]Blood serum was doped with lithium carbonate and deproteinized before use. [b]Triplicate samples. [c]Ten samples. [d]Five measurements of the same sample. Dilution was necessary to bring the samples into the linear range.

reagent blank, the organic phase when lithium ion is not involved, has a λ_{max} value of 380 nm while the complexed species (LiL) exhibited a wavelength shift. When the concentration of lithium ion was high enough, λ_{max} = 464 nm was observed. By plotting the net absorbance at 464 nm vs. the lithium concentration, a calibration curve was obtained. Linearity was shown from 14 to 560 mg l^{-1} with a sensitivity of $1.69 \times 10^{-3} \pm 2.20 \times 10^{-5}$ absorbance/mg l^{-1}. The interference by sodium on lithium determinations was studied with a constant lithium concentration of 280 mg l^{-1} while the sodium concentration was increased in the range 0—3500 mg l^{-1}. There was no major increase in absorbance until sodium concentrations exceeded 3000 mg l^{-1}.

Table 4 shows the results obtained for the determination of lithium ion in blood serum which was doped with a known amount of lithium carbonate using the chromogenic reagent in a batch method, the chromogenic reagent in a flow-injection method and by atomic absorption spectrometry. The comparison between the results is good. The automated extraction flow-injection procedure provided excellent results. One additional point is that the atomic absorption method required dilution of samples whereas the flow-injection system operated with the samples directly. The savings in time and reagents make the flow-injection method superior.

REFERENCES

1 M. Takagi, H. Nakamura and K. Ueno, Anal. Lett., 10 (1977) 1115.
2 H. Nakamura, M. Takagi and K. Ueno, Talanta, 26 (1978) 921.
3 G. E. Pacey, B. P. Bubnis and Y. P. Wu, Analyst (London), 106 (1981) 636.
4 B. P. Bubnis, J. L. Steger, Y. P. Wu, L. A. Meyers and G. E. Pacey, Anal. Chim. Acta, 137 (1983) 307.
5 J. P. Dix and F. Vogtle, Angew. Chem., 90 (1978) 893.
6 Y. P. Wu and G. E. Pacey, Tetrahedron, (1984).
7 Y. P. Wu and G. E. Pacey, Talanta, 31 (1984) 165.
8 B. Karlberg and S. Thelander, Anal. Chim. Acta, 98 (1978) 1.

Analytica Chimica Acta, 162 (1984) 293—304
Elsevier Science Publishers B.V., Amsterdam — Printed in The Netherlands

SURFACTANT EFFECTS ON THE SPECTROPHOTOMETRY OF THE GADOLINIUM—CHROME AZUROL S COMPLEX

GARY J. KLOPF and KELSEY D. COOK*

Department of Chemistry, University of Illinois, 1209 W. California St., Urbana, IL 61801 (U.S.A.)

(Received 10th April 1984)

SUMMARY

Increased molar absorptivities and red-shifted absorbance maxima were noted only upon the addition of cetylpyridinium chloride (CPC), a cationic surfactant. A 1:2:4 gadolinium/chrome azurol S/CPC complex was formed but dissociated at [CPC]/[Gd^{3+}] > 4 apparently because gadolinium(III) was displaced from this complex by additional surfactant monomers. Ternary complexes having different stoichiometries formed in the presence of excess dye. Sodium dodecyl sulfate (SDS), an anionic surfactant, induced dissociation of the binary complex at micellar concentrations, suggesting that dissociation resulted from adsorption of Gd^{3+} cations on the negatively charged micellar surface. Addition of Triton X-100, a nonionic surfactant, had little effect at either micellar or submicellar concentrations. These results confirm that complex stability is an important factor in the use of surfactants as sensitizers in quantitative spectrophotometry.

Triphenylmethane dyes have been used extensively for the spectrophotometric determination of lanthanide metal ions (Ln^{3+}) [1]. The metal-dye complexes formed have molar absorptivities (ϵ) typically in the range $1—5 \times 10^4$ l mol^{-1} cm^{-1}. The sensitivity of these spectrophotometric determinations is often enhanced by adding certain organic reagents to solutions of the metal—dye complex [2—5]. The resultant sensitization is characterized by an increase in molar absorptivity and frequently a red shift in the wavelength of maximum absorbance of the complex. For example, Ganago and Alinovskaya [2] reported that the addition of 1,10-phenanthroline to the praseodymium(III)/chrome azurol S (CAS) complex resulted in a three- to four-fold increase in the molar absorptivity and a red shift of approximately 40—50 nm. They established that a ternary complex having a specific 1:1:3 (Pr: CAS: 1,10-phenanthroline) stoichiometry was formed.

Surfactants have also been used to increase the sensitivity of spectrophotometric determinations [6—9]. These amphiphilic species (consisting of a non-polar hydrophobic "tail" and a polar hydrophilic "head") will form micelles when their concentration exceeds the critical micelle concentration (CMC). Therefore, in solution they can interact with the metal—dye complex as individual molecules or as aggregates. Both surface adsorption and core solubilization of the complex have been proposed to explain micellar sen-

*Present address: Department of Chemistry, University of Tennessee, Knoxville, TN 37996.

0003-2670/84/$03.00

sitization [6]. Monomer interactions may involve ternary complexes similar to those formed with other sensitizers. For example, Poluektov et al. [10] reported sensitization of the lanthanum(III) and erbium(III) complexes of methyl thymol blue (MTB) by the cationic surfactant cetyltrimethylammonium bromide (CTAB) and attributed the spectral changes noted to the formation of a 1:2:4 (M^{3+}/MTB/CTAB) complex. Svoboda and Chromy [11] reported similar results for the lanthanum/xylenol orange/cetylpyridinium bromide (CPB) system. However, because their work was done at CPB concentrations both above and below the CMC, the possibility that not only surfactant monomer, but also micellar interactions could be involved cannot be ruled out. Thus, as in most cases, it has not been clearly established whether surfactant monomer or micellar interactions are responsible for sensitization. In fact, a recent study in this laboratory [12] found that for some systems both can be involved.

Several lanthanide(III)/triphenylmethane dye complexes are included among those reported to be sensitized by surfactants [6—8, 13—15]. As for other metal ions, studies of these sensitized lanthanide systems often do not include consideration of mechanistic details. For example, Chernova [8] and Vekhande and Munshi [16], found that the addition of cationic surfactants to Ln^{3+}—CAS complexes induces sensitization. However, no details of the spectroscopy of the complex as a function of surfactant concentration were presented [8, 16].

To characterize these sensitized lanthanide systems better, this study focuses on a careful examination of the spectrophotometric behavior of a representative lanthanide/triphenylmethane dye complex, the gadolinium—CAS complex, as the concentration and class of surfactant (cationic, anionic and nonionic) are varied. This study extends the previous examination of metal/CAS/surfactant complexes to the class of lanthanide metal ions, providing some opportunity to investigate the effect of different metal ions. The general intention of this study and others presently underway in this laboratory is to improve the understanding of those mechanisms underlying surfactant sensitization so that a model useful in predicting the behavior of these and other metal/dye/surfactant complexes can be developed.

EXPERIMENTAL

Apparatus

Absorbances were measured with either a GCA/McPherson Model EU-707 or a Hewlett-Packard Model 8450A spectrophotometer. Most measurements were made with 1-cm matched quartz cuvettes. For samples with absorbances that would have exceeded an absorbance of 2.5 in these cells, a 1-mm pathlength quartz sample cell was substituted. For convenience and uniform presentation, data in the figures are therefore reported as absorbance per cm of pathlength rather than simply the measured absorbances. The reference cell contained a distilled-deionized water blank in all cases because neither

neither buffer nor any of the surfactants showed any absorbance from 400 to 700 nm. The pH values were measured with an Orion Model 701A pH meter equipped with a Model 91-01 glass electrode and a Model 90-01 reference electrode. Surface tensions reported for each solution were measured with a du Nuoy platinum ring tensiometer and represent the average of three replicate measurements. The tensiometer was calibrated using a series of solvents with known surface tensions.

Reagents

All solutions were prepared with distilled-deionized water. Stock solutions of Gd^{3+} (10^{-3} M) were prepared from either Gd_2O_3 (Sigma, 99.9% purity) or $GdCl_3 \cdot 6H_2O$ (Aldrich, Gold Label). When the gadolinium oxide was used, the appropriate amount of compound was first dissolved in a slight excess ($[Cl^-]/[Gd^{3+}] > 3:1$) of 6.0 M hydrochloric acid (prepared from Baker, trace analysis grade) before diluting to volume with water. In either case, the concentration of the stock solution was confirmed by complexiметric titration with EDTA.

Chrome azurol S (Eastman, practical grade) was recrystallized three times using a procedure described by Vekhande and Munshi [16a] for the purification of eriochrome azurol B. Stock solutions of CAS (10^{-3} M) were prepared by dissolving CAS in sufficient 0.1 M sodium hydroxide (Mallinckrodt, reagent grade) to give a final sodium hydroxide concentration of 3×10^{-3} M.

Reagent-grade cetylpyridinium chloride (CPC; Sigma) was recrystallized three times from ethanol and diethyl ether. The sodium dodecyl sulfate (SDS; 99% specially pure material; BDH Biochemicals) was used without additional purification. Reagent-grade Triton X-100 (octylphenoxypolyethoxyethanol; Sigma) was used as received. An average molecular weight of 624 g mol^{-1} [17] was assumed for calculating Triton X-100 concentrations.

The pH 6.70 ± 0.10 hexamethylenetetramine (HMT)/hydrochloric acid buffer nor any of the surfactants showed any absorbance from 400 to 700 nm. The pH values were measured with an Orion Model 701A pH specified above) and then diluting to 1 l with water. The final solution was 1.00 M in HMT and approximately 0.017 M in hydrochloric acid.

Procedure

All solutions were prepared for spectrophotometric measurements by pipetting the appropriate volume of each stock solution into 50-ml volumetric flasks. The reagents were added in the following order: buffer, metal ion, dye and surfactant. Each solution was then diluted to volume and allowed to develop for 30 min prior to spectrophotometric measurements (maximum absorbances were achieved within 30 min, and no changes were observed during the subsequent 2—3 h required to record a set of spectra). All solutions contained sufficient buffer to be 0.10 M in HMT. This concentration was found to maintain the solution pH at 6.70 ± 0.10 except when SDS concentrations exceeding $5—6 \times 10^{-3}$ M were used. Readjusting the pH

of those solutions to 6.70 ± 0.10 by adding 6.0 M hydrochloric acid was found to have no effect on the experimental results.

RESULTS AND DISCUSSION

The Gd^{3+}—CAS complex

The spectra of uncomplexed CAS and the Gd^{3+}—CAS complex are shown in Fig. 1 for comparison with those involving surfactant. The broad absorption maximum from 550 to 610 nm can be assigned to the binary complex and consists of two strongly overlapping bands centered at approximately 556 nm and 605 nm. The absorbance caused by excess of uncomplexed CAS appears red-shifted (λ_{max} = 440 nm) from its value without Gd^{3+} present (425—430 nm) because the free dye and complex absorbances overlap substantially. A 1:1 Gd^{3+}—CAS stoichiometry, in agreement with other reports [18—20], was confirmed for the binary complex at pH 6.70 by using Job's method of continuous variations and the mole ratio method. The molar absorptivity of this complex, $1.84 \times 10^4 \pm 240$ l mol^{-1} cm^{-1} at 556 nm and pH 6.7, was evaluated from the average slope of two working curves and is in good agreement with that previously reported by Horiuchi and Nishida [18] at 560 nm and at pH 9.4. The standard deviation reported is the pooled value [21] for the two working curves.

Effect of cationic surfactants

Most reports of surfactant sensitization involve cationic surfactants. Figure 1 illustrates the effects of 2×10^{-4} M cetylpyridinium chloride (CPC), a representative cationic surfactant, on the spectroscopy of the Gd^{3+}—CAS system. The addition of CPC is accompanied by increased sensitivity and by a red-shifted λ_{max} (625—630 nm, Fig. 1). Both Job's method and the mole ratio method showed that the Gd^{3+}:CAS stoichiometry changed from 1:1 to 1:2 upon the addition of CPC.

To establish whether these changes are due to interactions with micelles or surfactant monomers, the dependence of the complex absorbance (625 nm) on CPC concentration was assessed for three different binary complex concentrations (Fig. 2). If micellar interactions were involved, the onset of sensitization should occur at the CMC regardless of the binary complex concentration. Surface tension measurements established that the critical micelle concentration of CPC is lowered from 1×10^{-3} M to $3—5 \times 10^{-4}$ M by the addition of the HMT/HCl buffer. Addition of the binary complex could lower the CMC further [22—24] in which case increasing the binary complex concentration should lower the amount of CPC necessary for sensitization. Sensitization occurred at CPC concentrations as low as 1×10^{-5} M, but it was found that the concentration of CPC required for sensitization increased as the binary complex concentration increased, inconsistent with micellar sensitization. Further evidence for monomer interactions comes from the fact that maximum sensitization for each complex con-

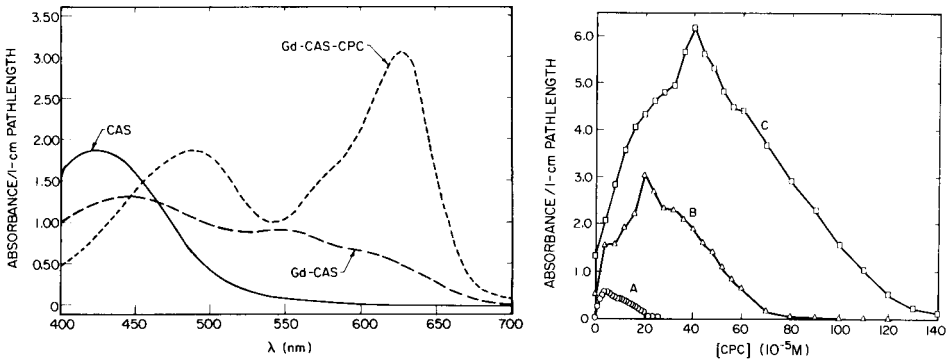

Fig. 1. Absorption spectra of CAS ([CAS] = 1×10^{-4} M); Gd^{3+}—CAS ([Gd^{3+}] = 5×10^{-5} M, [CAS] = 1×10^{-4} M); and Gd^{3+}—CAS—CPC ([Gd^{3+}] = 5×10^{-5} M, [CAS] = 1×10^{-4} M, [CPC] = 2×10^{-4} M).

Fig. 2. Dependence of absorbance (at 625 nm) of Gd^{3+}—CAS ([CAS]/[Gd^{3+}] = 2) on CPC concentration. Gd^{3+} concentration: (A) 1×10^{-5} M; (B) 5×10^{-5} M; (C) 1×10^{-4} M.

centration occurred at a 4:1 stoichiometric [CPC]/[Gd^{3+}] ratio (Fig. 3). This suggests that a 1:2:4 Gd^{3+}/CAS/CPC ternary complex is responsible for sensitization. Identical stoichiometries have been reported for other Ln^{3+}/triphenylmethane dye/cationic surfactant complexes [7].

Two additional features of the mole ratio plots (Fig. 3) should be noted. First, the complex absorbance at 625 nm exhibits a discontinuity for [CPC]/[Gd^{3+}] ratios between two and three, especially noticeable at the highest concentration of Gd^{3+}. This reflects the formation of a precipitate which redissolves at higher [CPC]/[Gd^{3+}] ratios. Similar behavior has been reported for CAS complexes of Be^{2+}, Cu^{2+} and Al^{3+} [12]. Tikhonov [7] attributed this phenomenon to the stepwise formation of ternary complexes. Apparently, for the system studied here, a stoichiometry is reached at which the complex is uncharged and insoluble. As more surfactant monomers are added, the stoichiometry of this complex evidently changes, and the precipitate redissolves. The absorbance then continues to increase until the 4:1 [CPC]/[Gd^{3+}] ratio is reached. If additional interactions did not take place, excess of surfactant should have no additional effect, and the absorbance of the ternary complex should level off at higher surfactant concentrations. This is clearly not the case. In fact, careful examination of the absorbance spectra (Figs. 4 and 5) as the [CPC]/[Gd^{3+}] ratio increases reveals that a complicated series of events is occurring. The initial formation of the ternary complex as CPC is added to solutions of the Gd^{3+}—CAS complex is evident from Fig. 4. The absorbance of the ternary complex at 490 nm and 625 nm increases until a 4:1 [CPC]/[Gd^{3+}] ratio is reached while the absorbance at 420 nm decreases (Figs. 4 and 6a) because free dye is consumed (the [CAS]/[Gd^{3+}] ratio for the complex increases

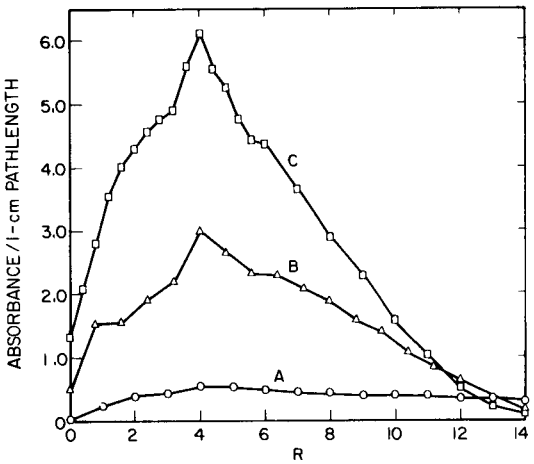

Fig. 3. Dependence of absorbance (at 625 nm) of Gd^{3+}—CAS ([CAS]/[Gd^{3+}] = 2) on R ([CPC]/[Gd^{3+}]). Gd^{3+} concentration: (A) 1×10^{-5} M; (B) 5×10^{-5} M; (C) 1×10^{-4} M.

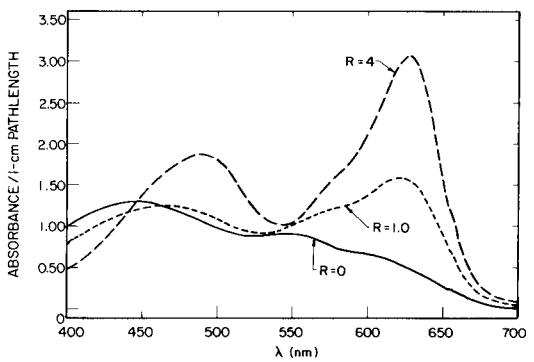

Fig. 4. Absorption spectra of Gd^{3+}—CAS ([Gd^{3+}] = 5×10^{-5} M, [CAS] = 1×10^{-4} M) for several R ([CPC]/[Gd^{3+}]) values.

from 1:1 to 2:1). Once the 4:1 [CPC]/[Gd^{3+}] stoichiometry has been exceeded, the 1:2:4 Gd^{3+}/CAS/CPC complex evidently begins to dissociate. Increasing the [CPC]/[Gd^{3+}] ratio from 4:1 to 8:1 induces a marked decrease in the absorbance at 625 nm (Figs. 5 and 6a). However, not until an 8:1 [CPC]/[Gd^{3+}] ratio is reached does the absorbance at 490 nm begin to decrease substantially (Fig. 6a). Thus absorbances at 490 and 625 nm evidently arise from at least two distinct species with overlapping spectra, rather than from two transitions of a single species.

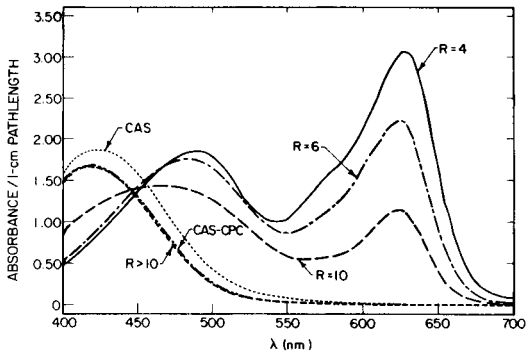

Fig. 5. Absorption spectra of Gd^{3+}—CAS ($[Gd^{3+}] = 5 \times 10^{-5}$ M, [CAS] = 1×10^{-4} M) for several R ([CPC]/$[Gd^{3+}]$) values; CAS ([CAS] = 1×10^{-4} M); and CAS/CPC ([CAS] = 1×10^{-4} M, [CPC] = 1.2×10^{-3} M).

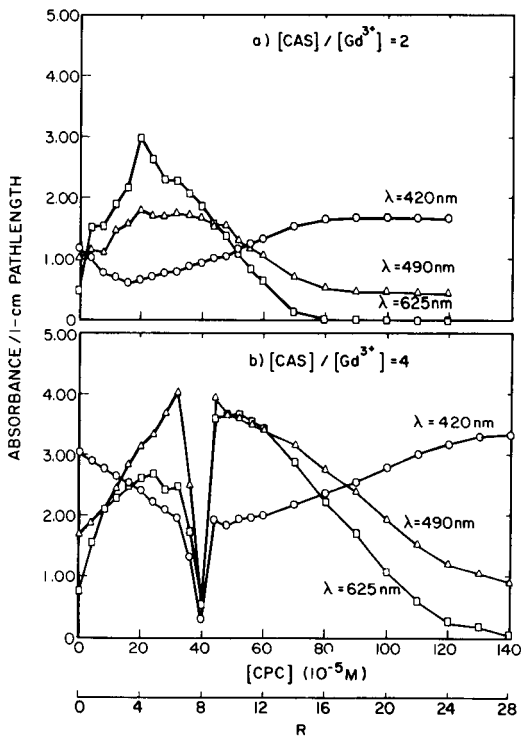

Fig. 6. Dependence of absorbance of Gd^{3+}—CAS ($[Gd^{3+}] = 5 \times 10^{-5}$ M) on both CPC concentration and R ([CPC]/$[Gd^{3+}]$). (a) [CAS] = 1×10^{-4} M, (b) [CAS] = 2×10^{-4} M.

As the absorbance at 490 nm decreases, the free dye absorbance at 420 nm increases, and an isosbestic point appears at approximately 440 nm (Fig. 5). At large $[CPC]/[Gd^{3+}]$ ratios, the absorption spectrum resembles that of CAS in the presence of CPC indicating that dissociation of the ternary complex has been completed and that only CAS—CPC interactions remain. Figure 5 illustrates that these interactions have only a small effect on the CAS spectrum.

Similar dissociation of ternary complexes at high surfactant-to-metal ratios has been reported [14, 25—28]. In other investigations in this laboratory [12], less extensive dissociation was observed for M^{n+}/CAS/CTAB complexes of Cu^{2+} and Al^{3+}. The Be^{2+}/CAS/CTAB complex did not dissociate. Apparently, the stability of the complex varies significantly in these and other ternary systems.

The mechanism responsible for dissociation has not been characterized previously. The onset of micellization may be responsible because of competition for the anionic dye (CAS) between the cationic micellar surface and the metal cation. Alternatively, if the ternary complex formation constant is small, excess of surfactant monomer may displace the metal. For the same reasons that suggest monomer sensitization, the data of Fig. 2 support the latter (monomer) dissociation model.

Either dissociation mechanism would lead to a prediction that increasing the amount of free dye should increase the surfactant concentration required for dissociation because excess of surfactant could first interact with uncomplexed dye. Thus, dissociation of the ternary complex should not begin until the excess free dye is consumed. As seen in Fig. 6(b), addition of excess of dye does delay the onset of dissociation. In fact, increasing the $[CAS]/[Gd^{3+}]$ ratio from 2 to 4 increases the $[CPC]/[Gd^{3+}]$ ratio required to initiate dissociation from approximately 4 to 10. However, additional changes occur which should be noted. In the presence of excess of dye, the absorbance at 625 nm still reaches a local maximum at approximately a 4:1 $[CPC]/[Gd^{3+}]$ ratio, whereas the absorbance at 490 nm (now greater than that at 625 nm) continues to increase until approximately a 6:1 $[CPC]/[Gd^{3+}]$ ratio is reached. At $[CPC]/[Gd^{3+}]$ ratios near 8:1, a precipitate is formed, and the absorbance of the ternary complex decreases substantially. As the $[CPC]/[Gd^{3+}]$ ratio is increased further, the precipitate redissolves, and the absorbance at 625 nm reaches a new maximum exceeding that noted before precipitation occurred. However, at $[CPC]/[Gd^{3+}]$ ratios greater than 10, the absorbances of the ternary complex decrease while that attributed to free dye increases as the complex begins to dissociate. These changes noted on the addition of excess of CAS suggest that another ternary complex capable of incorporating additional surfactant monomers has formed. The composition of the complex has not yet been established. Additional work is presently underway to characterize this system better.

Effect of anionic surfactants

Initial investigations with sodium dodecyl sulfate (SDS, a representative anionic surfactant) showed no measurable sensitization of the Gd^{3+}—CAS complex. However, dissociation of the binary complex was observed as the SDS concentration was increased. Surface tension measurements showed that the CMC of the SDS used was lowered from 7×10^{-3} M to $3\text{—}4 \times 10^{-3}$ M by the addition of buffer. Both a decrease in the binary complex absorbance at 556 nm and 605 nm and a corresponding increase in the uncomplexed CAS absorbance at 425 nm were observed to coincide with SDS micellization (indicated by surface tension data) suggesting that the formation of SDS micelles was responsible for dissociation of the binary complex (Fig. 7).

The onset of dissociation was also found to coincide with the CMC ($3\text{—}4 \times 10^{-3}$ M) for two additional binary complex concentrations, 2×10^{-5} M and 1×10^{-4} M. This provides additional support for the micellar hypothesis because dissociation in each case is coincident with micellization rather than with a specific $[SDS]/[Gd^{3+}]$ ratio. Chernova [8] reported that anionic surfactants either break down anionic metal—dye complexes or have no effect, but she did not include specific examples of representative systems. The role of micelles may be explained if the anionic micellar surface and the negatively charged dye compete for the metal cation. The extent of this competition evidently varies with the metal ion involved. In similar studies with CAS complexes of Be^{2+} and Cu^{2+} [12], dissociation by SDS was substantially less extensive than that observed here (in fact, SDS sensi-

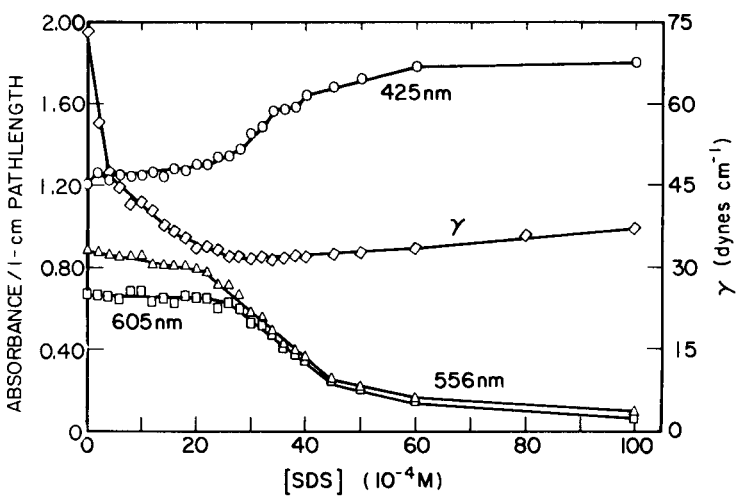

Fig. 7. Dependence of surface tension (γ) and absorbance (complex at 556 nm and 605 nm, and free CAS at 425 nm) of solutions of Gd^{3+}—CAS ($[Gd^{3+}] = 5 \times 10^{-5}$ M, $[CAS] = 1 \times 10^{-4}$ M) on SDS concentration.

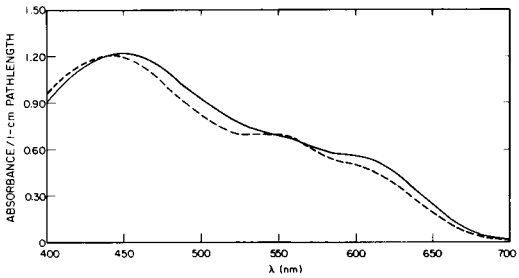

Fig. 8. Absorption spectra: (- - -) Gd^{3+}—CAS ([Gd^{3+}] = 5×10^{-5} M, [CAS] = 1×10^{-4} M); (—) Gd^{3+}—CAS with Triton X-100 ([Gd^{3+}] = 5×10^{-5} M, [CAS] = 1×10^{-4} M, [Triton X-100] = 8×10^{-4} M).

tized the Be^{2+}—CAS complex in solutions of high ionic strength). It is likely that both the stability of the complexes and the strength of metal ion binding at the micellar surface are important in determining the degree of dissociation.

Effect of nonionic surfactants

Savvin et al. [9] attributed sensitization induced by nonionic surfactants to strictly micellar solubilization of the metal—dye complex. Chernova [8] suggested that nonionic surfactants selectively solubilize only certain metal—dye complexes. Rare-earth complexes are among those upon which nonionic surfactants had no significant effects [8]. To verify this observation, a representative nonionic surfactant, Triton X-100, was added to solutions of the Gd^{3+}—CAS binary complex. Although the Triton X-100 concentrations used ($4—80 \times 10^{-5}$ M) spanned the measured CMC ($2—3 \times 10^{-4}$ M), only small changes in the absorbance intensities at 555—560 nm and 605—610 nm were noted (Fig. 8). These small spectral changes result either from weak surfactant—binary complex interactions or from slight changes in solvent polarity caused by the added surfactant.

CONCLUSIONS

This study has shown that at low surfactant concentrations, the Gd^{3+}—CAS complex exhibits spectroscopic behavior consistent with that of other metal—CAS complexes previously examined [12]. At submicellar levels, sensitization occurs only with cationic surfactants and can be attributed to the formation of a ternary complex involving interactions between surfactant monomer and the negatively charged binary complex. In contrast with the behavior of other metal ions [12], high concentrations of either anionic or cationic surfactants can induce complete dissociation of the Gd^{3+}—CAS complex. Micellar levels of the nonionic surfactant Triton X-100, however, were found to have very little effect on the spectroscopy of this complex.

Most surfactant-sensitized spectrophotometric methods employ micellar surfactant concentrations to attain increased sensitivity. A previous investigation [29] established that the degree of sensitization attained can depend on the presence of inorganic salts. This study has demonstrated that another factor which must be considered is the stability of the ternary complex. Micellar-sensitized determinations can produce inaccurate results unless the formation constant of the complex is relatively large. For example, the determination of Gd^{3+} concentrations with CAS and micellar levels of CPC could yield erroneous results because dissociation in this system occurs at large [CPC]/[Gd^{3+}] ratios. However, the existence of surfactant-sensitized quantitative procedures based on similar ternary systems [6] suggests that accurate working curves can be attained if an appropriate surfactant:dye ratio is chosen and if the dye concentration is well in excess of that of the analyte.

If the potential sources of inaccuracy are recognized and taken into consideration, surfactant-sensitized spectrophotometric methods can be used successfully for quantitative work. However, the maximum analytical utility of these methods will not be realized until the composition of the metal—dye—surfactant complexes, the nature of the interactions involved, and the factors influencing the degree of sensitization attained are more thoroughly examined.

Acknowledgment is made to the donors of the Petroleum Research Fund, administered by the American Chemical Society, for partial support of this research. Support from the University of Illinois Campus Research Board and Biomedical Research Committee (funded by N.I.H.) is also gratefully acknowledged.

REFERENCES

1 E. B. Sandell and N. Onishi, Colorimetric Determination of Trace Metals, Vol. 1, 4th edn., Wiley-Interscience, New York, 1979.
2 L. I. Ganago and L. A. Alinovskaya, Zh. Anal. Khim., 25 (1969) 904.
3 L. I. Ganago and L. A. Alinovskaya, Zh. Anal. Khim., 28 (1973) 494.
4 L. A. Alinovskaya and L. I. Ganago, Zh. Anal. Khim., 28 (1973) 661.
5 P. B. Granovskaya and M. K. Akhmedli, Zh. Anal. Khim., 37 (1982) 405.
6 W. L. Hinze, in K. L. Mittal (Ed.), Solution Chemistry of Surfactants, Vol. 1, Plenum Press, New York, 1979, pp. 79—127.
7 V. N. Tikhonov, Zh. Anal. Khim., 32 (1977) 1435.
8 R. K. Chernova, Zh. Anal. Khim., 32 (1977) 1477.
9 S. B. Savvin, R. K. Chernova and L. M. Kudryavtseva, Zh. Anal. Khim., 34 (1979) 66.
10 N. S. Poluektov, L. A. Ovchar and R. S. Lauer, Zh. Anal. Khim., 28 (1973) 1958.
11 V. Svoboda and V. Chromy, Talanta, 13 (1966) 237.
12 J. H. Callahan and K. D. Cook, Anal. Chem., 56 (1984) 1632.
13 H. Shih, H. Ho, J. Chang and Y. Fang, Fen Hsi Hua Hsueh, 8 (1980) 38.
14 S. Sun, Gaodeng Xeuxiao Huaxue Xuebao, 3 (1982) 314.
15 Y. Ci, K. Hu, Z. Liu and L. Wen, Hua Hsu Hsueh Pao, 39 (1981) 341.

16 C. Vekhande and K. N. Munshi, Indian J. Chem., 14A (1976) 189.
16a C. Verkhande and K. N. Munshi, Microchem. J., 23 (1978) 28.
17 E. A. Dennis, A. A. Ribeiro, M. F. Roberts and R. J. Robson, in K. L. Mittal (Ed.), Solution Chemistry of Surfactants, Vol. 1, Plenum Press, New York, 1979, pp. 175—194.
18 Y. Horiuchi and H. Nishida, Bunseki Kagaku, 17 (1968) 1233.
19 S. N. Sinha, S. P. Sangal and A. K. Dey, Proc. Nat. Acad. Sci., India, 38A (1968) 289.
20 L. G. Anisomova and L. D. Shapovalova, S. B. Nauch. Soobshch. Dagestan. Univ. Kafedra Khim., 6 (1969) 39; (Chem. Abstr. 77: 28 522k (1972)).
21 D. P. Shoemaker, C. W. Garland and J. I. Steinfeld, Experiments in Physical Chemistry, 3rd edn., McGraw-Hill, New York, 1974, p. 37.
22 M. J. Rosen, Surfactants and Interfacial Phenomena, Wiley, New York, 1978, p. 104.
23 H. Sato, M. Kawasaki and K. Kasantani, J. Phys. Chem., 87 (1983) 3759.
24 K. Mandal and J. N. Demas, Chem. Phys. Lett., 84 (1981) 410.
25 L. I. Ganago and N. N. Ishenko, Zh. Anal. Khim., 35 (1980) 1718.
26 Z. Marczenko and H. Kalowska, Mikrochim. Acta, (II) (1979) 507; Anal. Chim. Acta, 123 (1981) 279.
27 L. I. Ganago and N. N. Ishenko, Zh. Anal. Khim., 37 (1982) 1636.
28 Y. Horiuchi and H. Nishida, Bunseki Kagaku, 17 (1968) 1486.
29 J. H. Callahan and K. D. Cook, Anal. Chem., 54 (1982) 59.

Analytica Chimica Acta, 162 (1984) 305—313
Elsevier Science Publishers B.V., Amsterdam — Printed in The Netherlands

SPECTROFLUORIMETRIC DETERMINATION OF TERBIUM AS ITS TERNARY COMPLEX WITH EDTA AND TIRON
Compositional Studies, Optimization of Fluorescence Output and Conversion to a Flow System

SAMUEL J. LYLE* and NIDAL A. ZA'TAR

The Chemical Laboratory, University of Kent at Canterbury, Kent CT2 7NH (Great Britain)

(Received 5th March 1984)

SUMMARY

The spectrofluorimetric determination of terbium(III) as its ternary complex with EDTA and Tiron was studied further with regard to composition of the complex and the procedure was optimized by a simplex method. The results suggest a 1:1 molar ratio of terbium to Tiron for the ternary complex. The optimization study indicated that the three chosen variables (pH, and EDTA and Tiron concentrations) are not interactive. The method was converted for use in a segmented-flow system with basic Technicon units and a spectrophotofluorimeter as detector. This procedure is satisfactory for the determination of terbium(III) in the range 0.03—0.24 μg ml^{-1} at a sampling rate of 30 h^{-1}. Results were satisfactory for the determination of terbium in lanthanide oxides, mixed oxides, the mineral bastnasite and a green phosphor ($Gd_{0.96}Ce_{0.02}Tb_{0.02}F_3$).

An earlier paper [1] dealt with a comparative study of some published methods recommended for the spectrofluorimetric determination of terbium in aqueous solution. The comparison was made to select the method most satisfactory for the determination of terbium in the presence of other lanthanides and yttrium. From the methods examined, that published by Poluektov et al. [2] who used EDTA and Tiron (disodium-1,2-dihydroxybenzene-3,5-disulphonate) was considered to be the best.

The work described here can be divided into two parts. The first part deals with compositional studies, optimization of fluorescence output, and more detailed studies concerning the effect of pH and of reagent excess on fluorescence output, while the second is concerned with the development of an automatic spectrofluorimetric method for the determination of terbium(III) as its ternary complex with EDTA and Tiron.

EXPERIMENTAL

Chemicals

All chemicals used were of analytical-reagent grade, unless stated otherwise. The disodium salt of EDTA was used to prepare a 0.02 M solution in

0003-2670/84/$03.00

water. The 0.01 M Tiron (97% pure; Lancaster Synthesis, Lancaster, England) was prepared in water from the salt recrystallized from ethanol.

Sodium-1-methoxy-2-hydroxybenzene monosulphonate (MPSA) was synthesized by the method of Abarenkova and Cuman [3] and was characterized by its n.m.r. spectrum and elemental analysis. (Required for $C_7H_7O_5SNa$, 37.2% C, 3.1% H, 14.2% S, 10.2% Na; found 34.4%C, 3.3% H, 13.9% S, 9.8% Na.) A 1.0×10^{-3} M solution was prepared in water.

For the buffer solution, 70 ml of diethylamine (standard laboratory reagent, 99% pure) was added to 400 ml of water and the pH was adjusted to 12 by the addition of concentrated hydrochloric acid.

The 10^{-3} M terbium(III) and other solutions of metal ions were prepared as described previously [1].

Equipment

Manual spectrofluorimetric measurements were done with a Perkin-Elmer MPF3 spectrophotofluorimeter with a quartz cell (1 × 1 cm cross-section). Absorption spectra were obtained with a Unicam SP800 spectrophotometer and pH was measured with a Radiometer PHM62 standard pH meter fitted with a glass/silver/silver chloride combined electrode system.

The apparatus for automatic spectrofluorimetric analysis consisted of a Technicon Sampler II and Pump I, with an Aminco-Bowman spectrophotofluorimeter as detector and measuring device, the output from which was fed to a pen recorder. Solvaflex tubing was used in manifold construction. Glass mixing coils, 1.6 mm i.d. (Technicon Instruments) were used in the manifold construction. The excitation and emission wavelengths were 320 and 545 nm, respectively, and the excitation and emission slits were 5.0 and 0.5 mm, respectively.

The flow-through detector cell was constructed from a fluorimeter cell (Hellma (England) Ltd., Westcliff-on-Sea, Essex), which had internal dimensions 4 mm × 10 mm (cross-section) × 45 mm (height). The volume of the cell was reduced to 0.12 ml by insertion of a tight-fitting PTFE block (4 mm × 10 mm cross-section) into the cell. The block had two holes (each 1 mm diameter) drilled vertically through it to act as inlet and outlet for the sample-bearing solution. The cell was aligned with the light beam in the cell-holder of the spectrophotofluorimeter and with inlet and outlet channels connected to the flow system (Fig. 1).

Procedures

Flow system. The flow system is set out in Fig. 1. The sample, containing terbium(III) concentrations in the range 0.03—0.24 $\mu g\ ml^{-1}$, is pumped into the system at a sampling rate of 30 samples per hour, using a sample-to-wash ratio of 1:5. The wash liquid is water. The sample is mixed with EDTA and Tiron and segmented with air at a K4 Technicon-type junction. The segmented solution passes through the first two mixing coils to meet the buffer solution; and the combined stream then passes through a third mixing coil

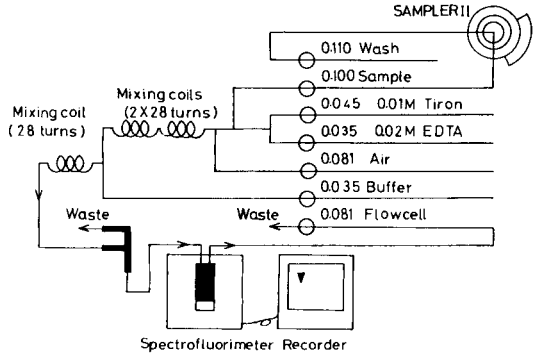

Fig. 1. Flow system for automatic spectrofluorimetric determination of terbium(III) as its ternary complex with EDTA and Tiron. (Numbers on the pump manifold refer to the internal diameters (in inches) of the pumping lines.)

to a debubbler at which air and surplus liquid goes to waste. The remaining liquid passes into the detector cell of the spectrophotofluorimeter. The time interval from aspiration of the sample to recording the corresponding peak on the chart is 5 min.

Sample preparation. Preparation of samples for manual spectrofluorimetric measurements has been described previously [1]. For automated spectrofluorimetric determination of terbium(III) in oxides of other lanthanides or yttrium, the sample is dissolved in the minimum amount of hot hydrochloric acid. The solution is evaporated to dryness on a water bath, and the residue is dissolved in water so that the total concentration of metal ion does not exceed 200 $\mu g\ ml^{-1}$ [1]. Cerium(IV) oxide requires more drastic treatment; it can be taken up in concentrated sulphuric acid with the addition of a few drops of 30% hydrogen peroxide [4]; the solution is evaporated to dryness and the residue dissolved in water so that the total amount of cerium does not exceed 150 μg. Lanthanide or yttrium fluorides are decomposed by the method described by Woyski and Harris [4]; a well-ground sample of the fluoride is taken into solution by treating it with concentrated nitric acid and boric acid. The solution is evaporated to dryness on a water bath and the residue taken up in water.

RESULTS AND DISCUSSION

Optimization of the general procedure

The absorption of terbium-free and terbium-containing solutions prepared according to the directions described previously [1] were studied at pH 12, over the wavelength range 250—400 nm. Typical spectra are presented in Fig. 2. The spectrum of a mixture of terbium—EDTA complex and Tiron at pH 12.0 differs significantly from those of terbium—EDTA and Tiron separately at the same pH indicating ternary complex formation. The absorbance

of the mixture at 320 nm (the excitation wavelength for maximum emission from terbium(III) as its ternary complex with EDTA and Tiron) was higher than those of terbium—EDTA and Tiron separately.

The effect of pH on terbium(III) emission as its ternary complex with EDTA and Tiron was studied using solutions prepared as described in the earlier general procedure [1]. The EDTA and Tiron concentrations were kept fixed (2.3×10^{-5} M and 4.0×10^{-5} M, respectively), and the solution was given an ionic strength of 0.2 in sodium perchlorate. The variation of fluorescence output of a mixture of terbium(III), EDTA and Tiron as a function of the pH of the solution is presented in Fig. 3. The fluorescence appears only above pH 8.5; maximum terbium(III) emission occurs in the pH range 10.75—12.25. In this pH range, EDTA will be fully dissociated with pK_a values for carboxylic group proton dissociation of 6.61 and 10.23 [5], giving the species designated HY^{3-} and Y^{4-}, respectively, where H_4Y represents EDTA. For Tiron, one of the phenolic groups will be fully dissociated with a pK_a value of 7.60 [5], giving the species designated HT^{3-} where H_4T represents the fully protonated reagent. The TbY^- ion by itself gives negligible emission at the above-mentioned concentrations. At pH values higher than 12.25, terbium(III) emission decreases sharply. The decrease could be due to dissociation of the second phenolic group to give T^{4-} ($pK_a \approx 12.48$ [5]).

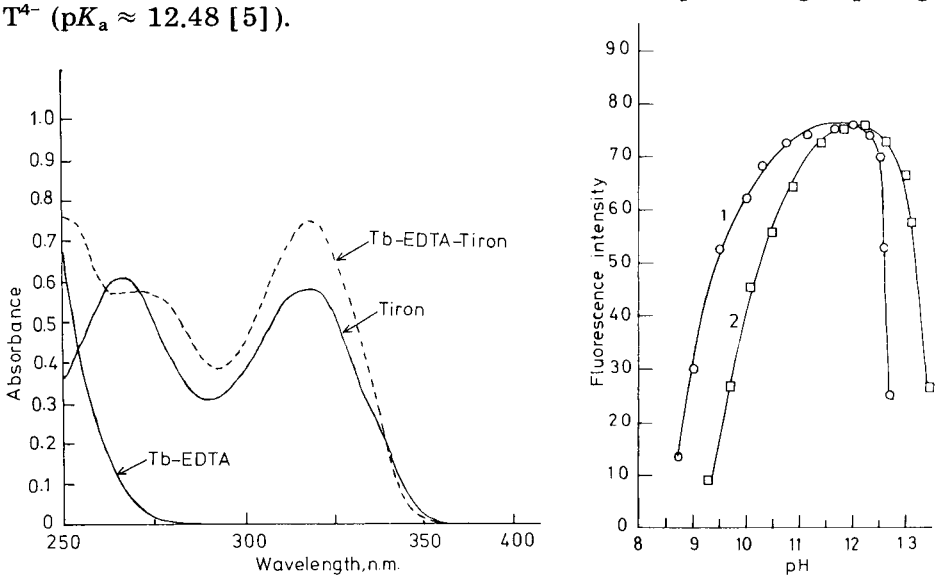

Fig. 2. Absorption spectra for combinations of 1.5×10^{-4} M terbium, 8.0×10^{-3} M EDTA and 2.0×10^{-4} M Tiron at pH 12.0.

Fig. 3. Effect of pH on terbium emission: (1) as its ternary complex with EDTA and Tiron; (2) as its ternary complex with EDTA and MPSA. Conditions: 4.61×10^{-6} M terbium(III), 4.00×10^{-5} M EDTA, 2.30×10^{-5} M Tiron or MPSA, and ionic strength of 0.2 in sodium perchlorate; excitation and emission wavelengths were 320 nm and 545 nm, respectively.

In further experiments, the effect of pH on terbium(III) emission was studied for the ternary complex with EDTA and MPSA, which has a methoxy group instead of the second phenolic group in Tiron. The solutions were prepared in the same way as for the Tiron ternary system. The pK_a for the phenolic group dissociation in MPSA was measured spectrophotometrically and found to be 8.8. The variation of fluorescence intensity as a function of pH is presented in Fig. 3. It is similar in profile to that of the Tiron system. Maximum terbium(III) emission occurs in the pH range 11.5—12.5. The sharp decrease in intensity beyond pH 12.5 cannot be attributed to a change in proton dissociation of the secondary ligand in this case. It can be concluded that breakdown of the ternary complexes by the increasing hydroxyl ion concentration of the medium in both systems is the most likely explanation for the decreased emission intensity.

The absorbance of terbium-free (Tiron and EDTA) and terbium-containing solutions was studied at 320 nm (the excitation wavelength for maximum emission from terbium(III) as its ternary complex with EDTA and Tiron) and pH 12.0 as a function of Tiron concentration. The results are presented in Fig. 4. For terbium-free solutions containing a fixed amount of EDTA (8.0×10^{-3} M), a rectilinear relation was observed between absorbance and Tiron concentration up to at least 2.4×10^{-4} M. From curve 1 (Fig. 4) the molar absorptivity for the species HT^{3-} was calculated to be 3.61×10^3 l mol^{-1} cm^{-1}. For solutions containing fixed amounts of terbium(III) and EDTA, a non-linear relation was observed between absorbance and Tiron concentration up to a terbium:Tiron mole ratio of 1:1, beyond which a rectilinear relation was observed (curves 2 and 3). The non-linear increase in absorbance as a function of Tiron concentration in terbium-containing solution indicates the presence of a new absorbing species (the ternary complex). The concentration of this species is increased by increasing the Tiron concentration and extrapolation of the linear parts of curves 2 and 3 suggest a terbium/Tiron ratio of 1:1 in the complex. The rectilinear increase in absorbance with increasing Tiron beyond "complete" ternary complex formation is due to the increase in free Tiron concentration only. Thus the ternary complex probably has a Tb:EDTA:Tiron mole ratio of 1:1:1.

A mole ratio study in which the EDTA and Tiron concentrations were fixed at 8.0×10^{-3} M and 4.0×10^{-4} M, respectively, and the terbium concentration was varied, supported the 1:1 ratio of metal ion to Tiron in the complex.

The effect of excess of Tiron on the emission from 4.61×10^{-6} M terbium solution was studied. The results obtained are presented in Fig. 5. It was found that keeping the EDTA concentration fixed (8.0×10^{-3} M) and changing the concentration of Tiron produced an increase in terbium emission up to a terbium/Tiron mole ratio of 1:4; any further increase resulted in a decrease in the terbium emission. The decrease in emission can be attributed to the inner filter effect resulting from Tiron absorption (Fig. 2) attenuating the intensity of the excitation light beam as it passes through

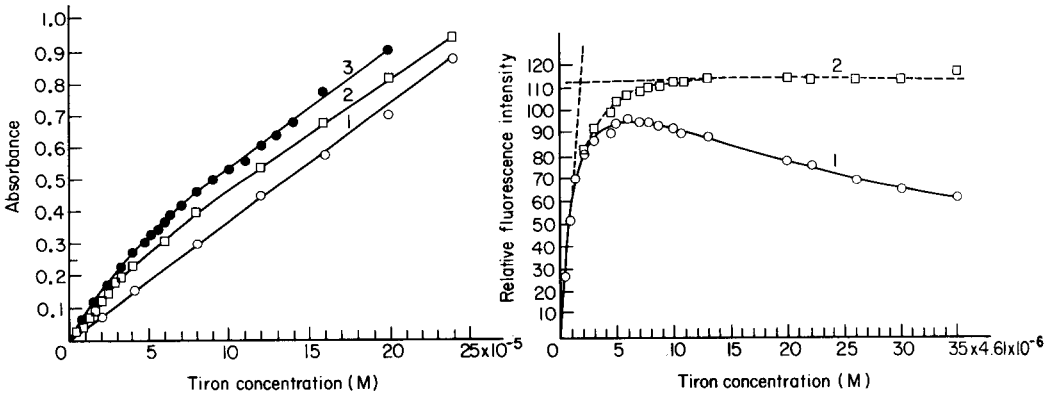

Fig. 4. Absorbance at 320 nm of terbium-free and terbium-containing solutions all at pH 12.0 as a function of Tiron concentration. The solutions were prepared according to the directions given in the earlier general procedure [1]. Conditions: (1) 8.0×10^{-3} M EDTA; (2) 3.0×10^{-5} M terbium(III) and 8.0×10^{-3} EDTA; (3) 6.0×10^{-5} M terbium(III) and 8.0×10^{-3} M EDTA.

Fig. 5. Effect of Tiron concentration on terbium(III) emission as its ternary complex with EDTA and Tiron at pH 12.0 following the general procedure [1]. Conditions: 4.61×10^{-6} M terbium(III) and 8.0×10^{-3} M EDTA. Curves: (1) observed terbium(III) emission; (2) values corrected for the inner filter effect.

the solution. The observed terbium emission can be corrected [6] for this effect with the results presented in curve 2, Fig. 5. Satisfactory corrected results were obtained up to a Tiron concentration of 1.6×10^{-4} M, beyond which the correction became inaccurate. A 1:1 ratio of terbium to Tiron is again suggested for the ternary complex from this study.

The effect of temperature on the emission from 1.0×10^{-6} M terbium as its ternary complex with EDTA and Tiron was studied. Temperature changes within the range 15—35°C do not significantly affect fluorescence output but further increases in temperature cause a progressive decrease in fluorescence output.

The method described for spectrofluorimetric determination of terbium as its ternary complex with EDTA and Tiron [2] was optimized by using the modified simplex method [7]. The above and other preliminary experiments showed that both the EDTA and Tiron concentrations as well as the pH had a pronounced influence on terbium emission. The ternary complex system reaches its equilibrium within 1 min, and the fluorescence output remains stable for more than an hour. It follows that the parameters to be optimized are the concentrations of EDTA and Tiron, and the pH. These parameters were optimized previously [1] by varying one factor at a time. As three parameters have to be optimized, the simplex is represented by a tetrahedron. The solutions were prepared as in the general procedure [1]. A high value of 1.6×10^{-4} M was chosen for the Tiron concentration, because at higher concentrations the correction needed for the inner filter effect becomes inaccurate. A high value of 12.5 for pH was set because above this

TABLE 1

Results of the simplex optimization for 4.61×10^{-6} M terbium (instrumental response is corrected for the inner filter effect)

Vertex number	Simplex (vertex number)	Variables			Response
		pH	Tiron:Tb	EDTA:Tb	
1		9.60	0.00	1.00	1
2		9.00	5.00	2.00	34
3		10.00	0.00	3.00	5
4	1, 2, 3, 4	10.50	1.00	1.00	18
5	2, 3, 4, 5	10.00	4.00	3.00	60
6	2, 3, 4, 6	10.29	6.00	4.00	63
7	2, 4, 6, 7	9.86	8.00	1.60	40
8	2, 6, 7, 8	8.93	11.66	4.06	15
9	2, 6, 7, 9	10.10	3.66	1.76	53
10	6, 7, 9, 10	11.16	6.77	2.90	71
11[a]	6, 7, 9, 11	7.91	7.65	3.35	−1
12	6, 9, 10, 12	11.17	2.90	4.17	70
13	6, 10, 12, 13	11.64	6.78	5.62	73
14	6, 10, 12, 14	12.41	8.34	7.55	65
15	10, 12, 13, 15	12.35	4.96	4.46	70
16	10, 13, 15, 16	12.26	9.44	4.48	71
17	10, 13, 15, 17	11.98	7.80	4.39	73

[a]Vertex lies outside the boundary.

value the ionic strength of the solution was affected at higher pH. The results (Table 1) indicate that vertex 13 is persistently retained and yields the highest response, its ordinates giving the optimal values of the parameters to be optimized. The final response (17) is the same; thus there is no pronounced maximum on the response surface and the optimal conditions are not critical. Further contractions or reflections were not warranted, because the differences in fluorescence output were no longer significant.

Flow system

The flow system set out in Fig. 1 was used for the spectrofluorimetric determination of terbium. A rectilinear calibration graph of fluorescence intensity as a function of terbium(III) concentration was obtained for the range 0.03—0.24 μg ml^{-1} terbium(III) with a sample-to-wash ratio of 1:5. A maximum of 30 samples per hour can be processed. The relative standard deviation for 0.10 μg ml^{-1} terbium(III) was 3.0% for 15 measurements.

The method was applied for the determination of terbium in synthetic samples containing dysprosium(III) or gadolinium(III) (Table 2) and in mixed oxides of the lanthanides, the mineral bastnasite and green phosphor, $Gd_{0.96}Ce_{0.02}Tb_{0.02}F_3$ (Table 3). It should be stressed that the EDTA/Tiron reagent system should preferably be used only after a group separation of lanthanides and yttrium from other elements which may be present [1].

TABLE 2

Determination of terbium(III) in synthetic samples containing different amounts of gadolinium(III) or dysprosium(III) (the expected terbium(III) concentration was 0.183 $\mu g\ ml^{-1}$ for each sample)

Other metal added ($\mu g\ ml^{-1}$)		No. of measurements	Terbium(III) found ($\mu g\ ml^{-1}$)	Relative standard deviation (%)
Gd(III)	Dy(III)			
50	—	5	0.183	3.5
100	—	5	0.183	2.9
150	—	4	0.178	2.9
200	—	5	0.175	3.1
250	—	7	0.165	2.8
300	—	7	0.158	3.5
—	10	5	0.183	3.2
—	40	3	0.183	3.0
—	80	3	0.180	2.7
—	150	5	0.185	2.7
—	200	7	0.187	2.6
—	250	7	0.192	2.4
—	300	8	0.195	2.7

Under the conditions set out in Fig. 1, and by following the directions given for preparing the samples, a minimum terbium(III) concentration of 0.03 $\mu g\ ml^{-1}$ can be detected. However, from the interference study [1] it was concluded that other lanthanides or yttrium can be tolerated only up to concentrations of 200 $\mu g\ ml^{-1}$. Thus terbium can only be determined down to about 150 $\mu g\ g^{-1}$ in other lanthanides or yttrium.

TABLE 3

Applications to the determination of terbium(III)

Substance	Sample size (μg)	Volume of solution (ml)	No. of detns.[a]	Terbium(III) present		Relative standard deviation (%)
				Expected	Found	
Heavy earth concentrate[b]	2000	100	5 (4)	(0.57 ± 0.02)%[c]	0.641%	3.0
Bastnasite[d]	3000	25	10 (6)	(750 ± 40) $\mu g\ g^{-1}$ [c]	719 $\mu g\ g^{-1}$	3.4
Green phosphor[e]	300	20	10 (1)	826 $\mu g\ g^{-1}$	834 $\mu g\ g^{-1}$	3.0

[a]Number of determinations on each of the number of independent samples given in parentheses. [b]From Johnson, Matthey & Co., Reading, England. [c]Determined by neutron activation analysis at the Universities Research Reactor Centre, Warrington, England. [d]From Union Molycorp, CA, U.S.A. [e]Prepared from weighed amounts of the components.

The provision of samples of rare earth concentrate and bastnasite by Johnson, Matthey & Co., and Union Molycorp, respectively, is gratefully acknowledged. One of us (N.A.Z.) thanks the Arab-British Chamber Charitable Foundation for financial assistance.

REFERENCES

1 S. J. Lyle and N. A. Za'tar, Anal. Chim. Acta, 153 (1983) 229.
2 N. S. Poluektov, M. A. Tishchenko and M. A. Alakaeva, Tr. Khim. Khim. Tekhnol., 5 (1973) 104.
3 E. A. Abarenkova and A. K. Cuman, Tr. Leningr. Inzh. Ekon. Inst., 46 (1963) 92.
4 M. M. Woyski and R. E. Harris, in I. M. Kolthoff and P. J. Elving (Eds.), Treatise on Analytical Chemistry, Vol. 8, Part II, Interscience, New York, 1963, pp. 78 and 41.
5 L. G. Sillen and A. E. Martell, Stability Constants of Metal-Ion Complexes, The Chemical Society, Spec. Publ., No. 17, London (1964).
6 C. A. Parker, Photoluminescence of Solutions, Elsevier, Amsterdam, 1968, p. 222.
7 S. L. Morgan and S. N. Deming, Anal. Chem., 46 (1974) 1170.

Analytica Chimica Acta, 162 (1984) 315—321
Elsevier Science Publishers B.V., Amsterdam — Printed in The Netherlands

SPECTROPHOTOMETRIC TITRATION OF CRYPTANDS AND COMPLEXIMETRIC TITRATION OF BARIUM WITH CRYPTAND (2.2.2)

JANE A. DRUMHILLER, JOHN L. LAING and RICHARD W. TAYLOR*
Department of Chemistry, University of Oklahoma, Norman, OK 73019 (U.S.A.)
(Received 6th January 1984)

SUMMARY

A spectrophotometric titration of cryptands (2.2.1), (2.2.2), (2_B.2.2) and (2_B.2_B.2) in aqueous medium is described. Titration of the cryptands with standard lead(II) perchlorate allows these cryptands to be quantified down to 1.0×10^{-5} M. The complexiметric titration of barium(II) with cryptand (2.2.2) using metalphthalein indicator is described and compared with a similar method with EDTA as titrant.

The macrobicyclic polyoxa-diamines, or cryptands, synthesized by Lehn and coworkers [1, 2], are of considerable interest to workers in diverse areas of chemistry because of their ability to form stable complexes with alkali, alkaline earth, and heavy metal cations [3—5], to solubilize salts in nonpolar media [6, 7], to transport cations across natural [8, 9] and artificial membranes [10, 11], and to enhance elimination of toxic heavy metal ions [12, 13]. Titrimetric methods for the determination of the cryptand concentration based on neutralization with HCl or by standard addition of calcium or barium ions have been reported by Heumann and Schiefer [14] and a gravimetric method has been described by Müller and Beaumatin [15]. These methods are useful for cryptand solutions in the 10^{-2}—10^{-3} M range. The gravimetric procedure requires approximately 12 h and the neutralization titration is sensitive to interference by other bases. The present paper describes a spectrophotometric titration method in which lead(II) is used for

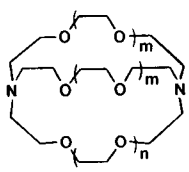

(2.2.1) m = 1, n = 0
(2.2.2) m = 1, n = 1
(2_B.2.2) m = 1, n = 1 with 
(2_B.2_B.2) m = 1, n = 1 with 

determination of cryptands (2.2.1), (2.2.2), (2_B.2.2), and (2_B.2_B.2) at 10^{-4}—10^{-5} M and the application of cryptand (2.2.2) for the complexiметric determination of barium ion using metalphthalein indicator.

0003-2670/84/$03.00

EXPERIMENTAL

Reagents and stock solutions

Cryptands (2.2.1), (2.2.2), (2_B.2.2) and (2_B.2_B.2) were purchased from PCR and used without further purification. Stock lead solutions (≈0.01 M) were prepared from lead perchlorate (G. F. Smith Chemical Co.) and standardized by titration with EDTA (Aldrich, Gold Label) [16]. 2-(*N*-Morpholino)ethanesulfonic acid, MES, and piperazine-*N*,*N*′-bis(2-ethanesulfonic acid), PIPES (Sigma), barium chloride (Aldrich, Gold Label) and metalphthalein (Sigma) were used as received. Tetraethylammonium perchlorate was prepared from tetraethylammonium hydroxide (Aldrich) and perchloric acid (J. T. Baker) and recrystallized four times from water. All solutions were prepared with doubly distilled water.

Stock solutions of the cryptands were prepared by dissolving 0.0813, 0.9253, 0.1058 and 0.0720 g of cryptand (2.2.1), (2.2.2), (2_B.2.2) and (2_B.2_B.2), respectively, in freshly-boiled water to a total volume of 250 ml. A second stock solution of cryptand (2.2.2) was prepared from 0.9485 g of cryptand dissolved to make 250 ml of solution. Cryptand solutions were routinely kept under refrigeration after preparation. The cryptand stock solutions were stable for weeks to months when kept out of direct light and stored under nitrogen in a refrigerator. Stock buffer solutions consisted of 0.05 M MES or 0.05 M PIPES.

Instrumentation

All spectrophotometric measurements were made with a Hitachi 100-80 double-beam instrument. pH Measurements were made with a Fisher 420 pH meter equipped with a glass electrode (Corning 476024) and a reference electrode (Fisher 13-639-51) used in conjunction with a Fisher remote reference electrode (13-639-55) filled with 0.1 M tetraethylammonium perchlorate to prevent introduction of potassium ions to the test solutions. Because potassium and sodium ions form stable complexes with cryptands [3], these cations are generally replaced by the larger tetraalkylammonium ions which do not form stable cryptates [3]. Microliter syringes (Hamilton 75 NCN and 701 NCH) with a Chaney adapter were used to deliver the lead(II) titrant.

Spectrophotometric determination of cryptands

Cryptand (2.2.2) sample solutions were prepared by transferring various amounts of stock cryptand (1.0—10.0 ml) and 100 ml of MES buffer to a 1-l volumetric flask and diluting to volume with water. Sample solutions of cryptands (2.2.1) and (2_B.2.2) and (2_B.2_B.2) were prepared by transferring 2 or 4 ml of cryptand and 5 ml of MES or PIPES buffer to a 25-ml volumetric flask and diluting to volume. The pH of the sample solutions was adjusted to the following values: 6.4 for (2.2.2) and (2_B.2.2); 7.0 for (2.2.1) and (2_B.2_B.2). The pH values were chosen to minimize formation of lead

hydroxide during titrant addition while providing complete and reasonably rapid complex formation.

A portion (3 ml) of the appropriate sample solution was transferred to a 1-cm quartz cuvette equipped with a teflon stopper. The titration was done by adding aliquots of standardized lead solution to the cuvette with a microliter syringe. The solution in the cuvette was shaken and placed in the spectrophotometer and a time interval of 2—15 min was allowed for the reaction to go to completion. Absorbance readings were taken at the following wavelengths: 255 nm for (2.2.1); 249 nm for (2.2.2); 255 nm for (2_B.2.2); and 240, 250, 267 nm for (2_B.2_B.2).

The wavelengths chosen correspond to the peak maxima for the respective lead cryptates. Three wavelengths were utilized for $Pb(2_B.2_B.2)^{2+}$ to ascertain the effect of the large background absorbance of the ligand in the 260—285 nm region (see inset, Fig. 1). All readings were made against a distilled water blank. The lead titrant solution was prepared to be approximately 100 times the concentration of the cryptand in the sample solution. The titration was continued until the absorbance readings reached a constant value. Several additional readings were made at lead concentrations past the spectrophotometric end-point.

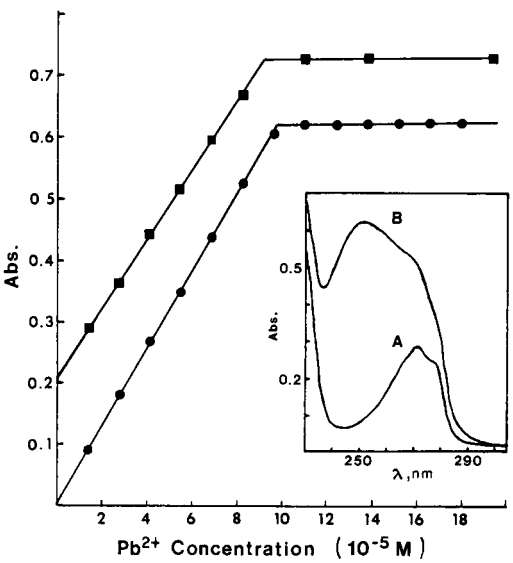

Fig. 1. Titrations of cryptands (2.2.2) and (2_B.2_B.2) with 0.01036 M $Pb(ClO_4)_2$; (▪) 9.39 × 10^{-5} M (2_B.2_B.2) at 250 nm; (•) 9.88 × 10^{-5} M (2.2.2) at 249 nm. In the upper trace, the *y*-axis is offset by +0.1 absorbance for clarity. The inset shows the spectra of 9.39 × 10^{-5} M cryptand (2_B.2_B.2) at pH 7.0: (A) without lead present; (B) with a total lead concentration of 1.04 × 10^{-4} M; b = 1 cm.

Complexometric titration of barium

A stock solution of barium was prepared by dissolving 1.0416 g of dried barium chloride in freshly boiled water to make 500 ml of solution. Additional test solutions were prepared by making (1 + 1), (1 + 4), and (1 + 9) dilutions of the stock solution. Metalphthalein indicator stock solution was prepared by dissolving 0.18 g of the solid indicator in several milliliters of concentrated ammonia and diluting to 100 ml; this solution was stored under refrigeration when not in use.

For a titration, 5 ml of barium test solution was transferred to a 125-ml Erlenmeyer flask and 50 ml of water was added. The solution was heated to the boiling point and allowed to cool under an ascarite filter. Then 3 ml of concentrated ammonia and 0.5 ml of indicator solution were added and the pH was adjusted to 10.8—11.0 with concentrated tetraethylammonium hydroxide. The solution was then titrated rapidly with either standardized EDTA or cryptand (2.2.2) solutions until the indicator changed from violet to a pale pink color [17].

Results and discussion

The cryptands investigated form 1:1 complexes with lead with stability constants ranging from 2.0×10^{11} ($2_B.2_B.2$) to 1.3×10^{13} (2.2.1) [4, 5]. The formation of the lead cryptate is accompanied by the appearance of a broad peak centered at wavelengths of 250—260 nm with $\Delta\epsilon$ ($\epsilon_{PbC} - \epsilon_C$) values in the range 6000—7000 (see inset, Fig. 1). The absorbance is most likely caused by a charge-transfer process involving lead and the bridgehead nitrogens [18] because lead complexes with saturated crown ethers do not exhibit similar absorbance peaks. At the pH values used, the cryptands exist as a mixture of the mono- and di-protonated forms. However, the large values of the stability constants provide quantitative (>99%) conversion of the cryptands to the corresponding cryptates under these conditions at concentrations as low as about 1×10^{-5} M.

Figure 1 shows a plot of absorbance vs. total Pb^{2+} concentration for the titration of cryptands (2.2.2) and ($2_B.2_B.2$). Table 1 lists the results of spectrophotometric determinations of all four cryptands in the concentration ranges studied. The precision may be improved by use of repetitive type syringes for addition of the titrant. An alternative procedure, obviating the use of microliter syringes, would involve preparation of a series of solutions with identical amounts of cryptand and buffer and increasing amounts of standard lead. After the pH of each solution had been adjusted to the proper value and a 10—15 min reaction interval had been allowed, the absorbance would be read at the appropriate wavelength. At low cryptand concentrations and near the equivalence point, the complex formation reactions are slow and a time interval of 3—15 min was allowed between titrant additions. This problem may be alleviated somewhat by raising the pH of the analyte solution. The rate of complex formation increases as the pH is raised because of the increasing fraction of the more reactive mono-

TABLE 1

Spectrophotometric titration of cryptands

Cryptand	No. of detns.	Cryptand conc. found[a] (10^{-5} M)	Stock soln. conc. (10^{-4} M)	
			Calculated	Added
(2.2.1)	3	8.08 ± 0.08	10.10	9.78
(2.2.2)	4	1.97 ± 0.15	98.8[b]	98.3
	5	3.96 ± 0.07		
	7	9.89 ± 0.10		
(2.2.2)[c]	3	0.997 ± 0.015	99.5[d]	100.8
	4	9.93 ± 0.04		
(2_B.2.2)	4	15.4 ± 0.2	9.65	9.96
(2_B.2_B.2)	3[e]	9.51 ± 0.07	5.97[h]	6.09
	4[f]	9.60 ± 0.17		
	4[g]	9.59 ± 0.19		

[a]Uncertainty given as 1 std. dev. [b]Average of 16 determinations at 3 dilutions. [c]A second stock solution of cryptand (2.2.2) was prepared from 0.9485 g of (2.2.2) dissolved to make 250 ml. [d]Average of 7 determinations at 2 dilutions. [e]240 nm. [f]250 nm. [g]267 nm. [h]Average of 11 determinations at 3 wavelengths.

and unprotonated forms of the cryptand [3]. For cryptands (2_B.2_B.2) and (2.2.1), it was necessary to raise the pH of the samples to approximately seven in order to keep the reaction times less than 15 min. For cryptand (2.2.2), serial dilutions made from the stock solutions were titrated and the calculated concentrations of the stock solution of this and other cryptands are shown in Table 1. The relative precision for replicate determinations of each cryptand is generally about 1.8% or less. The relative error, based on the difference between the stock cryptand concentration determined by titration and calculated from the weight of cryptand used, ranges from +0.5 to −2.0% for cryptands (2.2.2) and (2_B.2_B.2), respectively. The larger values for cryptands (2.2.1) and (2_B.2.2), +3.2% and −3.1%, respectively, may be related to the fact that both of these compounds are viscous oils and are difficult to dry and weigh.

The logarithmic values of the stability constants for the Ba^{2+}, Sr^{2+}, Ca^{2+} and Mg^{2+} cryptates of (2.2.2) are 9.6, 8.0, 4.4, and 2.0, respectively [3]. Although the stability constant for $Ba(2.2.2)^{2+}$ is similar to the values for the barium complexes of EDTA, log K = 7.8, and diethylenetriaminepentaacetic acid, DTPA, log K = 8.8 [19], the selectivity order is reversed for the alkaline earth series. Thus (2.2.2) has a selectivity for barium ion over calcium ion of approximately 1.6×10^5 while the corresponding values for EDTA and DTPA are about 1.3×10^{-3} and 0.016, respectively. The Ba^{2+}/Sr^{2+} selectivities for 2.2.2, EDTA, and DTPA are about 40, 0.16 and 0.12, respectively. Several reports have been published describing the deter-

mination of Mg^{2+}, Ca^{2+} and Sr^{2+} with cryptands (2.2.1) and (2.2.2) by a flow-injection method [20, 21], but the dissociation kinetics of the $Ba(2.2.2)^{2+}$ complex are too slow, $t_{1/2} \approx 4 \times 10^{-4}$ s [22], for that method. However, barium ion may be determined by conventional complexim etric titration techniques. Table 2 shows the results for the determination of barium ions by titration with cryptand (2.2.2) and with EDTA for comparison [17]. The indicator color change at the end-point is not particularly sharp for either titrant and it is important carefully to control the pH and indicator concentration. It is also helpful to match the end-point color with a known solution. The results presented in Table 2 show that titrations using cryptand (2.2.2) as the titrant have essentially the same accuracy and relative precision as those using EDTA.

Support for this work was provided by the Petroleum Research Fund administered by the American Chemical Society (Grant 10167G-3,4) and the OU Associates Summer Research Participation program (J.A.D.).

TABLE 2

Complexim etric titration of barium ions with cryptand (2.2.2) or EDTA[a]

Ba^{2+} taken[b] (10^{-3} M)	Ba^{2+} found (10^{-3} M)[c]					
	N	Found with (2.2.2)	RSD (%)	N	Found with EDTA	RSD (%)
1.00	6	0.99 ± 0.01	1.0	6	1.00 ± 0.01	1.0
2.00	5	1.98 ± 0.02	1.0	6	1.96 ± 0.02	2.0
5.00	4	5.04 ± 0.03	0.6	6	5.01 ± 0.06	1.1
10.00	5	10.04 ± 0.07	0.7	3	9.96 ± 0.15	1.5

[a]Stock [(2.2.2)] = 9.88×10^{-3} M; stock [EDTA] = 1.00×10^{-2} M. [b]$[Ba^{2+}]$ calculated from the weight of solid $BaCl_2$ taken. [c]Uncertainty given as 1 std. dev.

REFERENCES

1 B. Dietrich, J. M. Lehn and J. P. Sauvage, Tetrahedron Lett., (1969) 2885, 2889.
2 B. Dietrich, J. M. Lehn, J. P. Sauvage and J. Blanzat, Tetrahedron, 29 (1973) 1629.
3 J. M. Lehn and J. P. Sauvage, J. Am. Chem. Soc., 97 (1975) 6700.
4 G. Anderegg, Helv. Chim. Acta, 58 (1975) 1218.
5 F. Arnaud-Neu, B. Spiess and M. J. Schwing-Weill, Helv. Chim. Acta, 60 (1977) 2633.
6 B. Dietrich and J. M. Lehn, Tetrahedron Lett., (1973) 1225.
7 M. Cinquini, F. Montanari and P. Tundo, Gazz. Chim. Ital., 107 (1977) 11.
8 B. Tümmler, G. Maass, W. Müller and W. Lamprecht, Biochem. Biophys. Acta, 508 (1978) 122.
9 R. Günther, O. Hauswirth and R. Ziskoven, J. Physiol., 284 (1978) 145P.
10 M. Kirch and J. M. Lehn, Angew. Chem. Int. Ed. Engl., 14 (1975) 555.
11 J. M. Lehn, Pure Appl. Chem., 51 (1979) 979.
12 W. H. Müller and W. A. Müller, Naturwissenschaften, 61 (1974) 455.
13 Ph. Baudot, M. Jacque and M. Robin, Toxicol. Appl. Pharmacol., 41 (1977) 113.

14 K. G. Heumann and H.-P. Schiefer, Fresenius Z. Anal. Chem., 298 (1979) 358.
15 W. H. Müller and J. Beaumatin, Anal. Chem., 46 (1974) 2218.
16 J. Körbl and R. Pribil, Collect. Czech. Chem. Commun., 23 (1958) 873.
17 G. Schwarzenbach, Complexometric Titrations, Interscience, New York, 1957, p. 72.
18 B. G. Cox, J. Garcia-Rosas and H. Schneider, J. Am. Chem. Soc., 104 (1982) 2434.
19 A. Ringbom, Complexation in Analytical Chemistry, Wiley, New York, 1963, p. 332.
20 D. Espersen and A. Jensen, Anal. Chim. Acta, 108 (1979) 241.
21 H. Kagenow and A. Jensen, Anal. Chim. Acta, 114 (1980) 227.
22 B. G. Cox and H. Schneider, J. Am. Chem. Soc., 99 (1977) 2809.

Analytica Chimica Acta, 162 (1984) 323—331
Elsevier Science Publishers B.V., Amsterdam — Printed in The Netherlands

AN ULTRAVIOLET DIFFERENCE SPECTROPHOTOMETRIC METHOD FOR DETERMINATION OF DRUG-BINDING PARAMETERS

SAMIA NOUR and JOSEPH J. VALLNER*

Department of Pharmaceutics, College of Pharmacy, University of Georgia, Athens, GA 30602 (U.S.A.)

(Received 23rd January 1984)

SUMMARY

Ultraviolet (u.v.) difference spectrophotometry is a direct technique to probe ligand/macromolecule interactions. The difference technique is very sensitive to the interactions that occur and can be used with ligands of limited solubility. A method for reducing the binding data gathered from the u.v. difference technique is now described. Data from the literature as well as obtained in these laboratories were reduced by using a plot of change in absorbance difference versus added perturbant concentration. Deviation from initial linearity enables the concentrations of free and bound ligand to be determined and hence the binding parameters can be calculated by standard techniques. Literature and laboratory binding data are calculated for phenylbutazone, oxyphenbutazone, sulindac, diclofenac, ethacrynic acid, and sulfadimethoxine.

The determination of the binding parameters of a drug to human serum albumin is of considerable importance. The extent of protein-binding affects the distribution and elimination of the drug in the body, and hence affects the therapeutic regimen [1]. The determination of numbers of binding sites (n) and the corresponding association constants (K) lead to information concerning the nature of the binding forces and possible clinical complications associated with competitive displacement of one drug by a concomitantly administered drug [2].

Binding data obtained from numerous techniques are usually represented graphically and analyzed as suggested by Klotz [3], Scatchard [4] or Scott [5]. In spite of the shortcomings existing in these treatments and the varied deficiencies that have been extensively discussed in the literature [6—8], the classical graphical analysis of binding data has the advantage of being simple. In addition, it is not seriously biased if there is only one single class of binding sites. To determine the binding parameters by either graphical or computer methods [9, 10], the data should be in terms of the concentrations of free and bound drug, most often provided by subtractive methods (e.g., equilibrium dialysis, ultrafiltration, etc.).

Methods for the determination of equilibrium (affinity) constants based on examination of intensive parameter changes have been developed from the original equation of Benesi and Hildebrand [11]. Some workers have

0003-2670/84/$03.00

suggested ways to determine the equilibrium constant from u.v. difference data [12—14]; however, each of these methods required that considerable constraints be upheld or some fractional saturation measurement be made. Reviews of these methods are available [15—17].

Rosen [18] has suggested a method for reducing binding data derived from circular dichroism measurements. In this method, successive additions of perturbant are made and allowed to interact with a constant concentration of protein. Rosen calculated the amount of free and bound drug from the induced ellipticity versus concentration curves and used the concentrations subsequently to estimate n and K.

In the work reported here, the method of Rosen [18] has been extended to u.v. difference binding data. Previous binding data for phenylbutazone [19], oxyphenbutazone [19] and sulindac [20] are used. Experimental verification of the method was done with interaction of the perturbants diclofenac, ethacrynic acid and sulfdimethoxine with human serum albumin (HSA).

EXPERIMENTAL

Materials

The human serum albumin fraction V (Miles, Research Products Division, Elkhart, IN) used had been previously investigated for purity. Diclofenac sodium (Ciba-Geigy), ethacrynic acid (Merck Sharp & Dohme Research Laboratories) and sulfadimethoxine (Hoffman—La Roche) were used as supplied. Other materials were reagent grade and were used as received. Deionized water was used for preparation of pH 7.4 isotonic Tris and phosphate buffers.

Method and data treatment

The binding of diclofenac sodium, ethacrynic acid and sulfadimethoxine to human serum albumin (HSA) was investigated by difference spectrophotometry (Cary 118C spectrophotometer). The tandem cell technique was used in the split beam mode [21]. Four semimicro 10-mm matched cuvettes were used. Concentration of HSA was 1.45×10^{-5} M in the case of ethacrynic acid binding and 0.58×10^{-5} M for the other drugs studied. Microliter aliquots of the test drugs were added to the buffer cell in the reference beam and the protein cell in the sample beam (at equal concentration) to give a final concentration of the drug ranging from 2.48×10^{-6} M to 5.32×10^{-5} M in the case of diclofenac sodium, 1.63×10^{-6} M to 1.63×10^{-4} M with ethacrynic acid, and 7.90×10^{-7} M to 6.71×10^{-6} M in the case of sulfadimethoxine. The resulting difference spectra were recorded, the protein and drug concentration being kept equivalent in both beams throughout the experiments [22]. Concentrations of ligands and protein were low enough to permit light scattering and fluorescence to be ignored.

The association of the drugs with protein was evaluated from the difference

absorption spectra. Each of the spectra is characterized by positive peaks and negative troughs. These appear at wavelengths that differ from those of the maximum absorption of the drugs.

Change in absorption (ΔA) vs. concentration curves were then generated by plotting the change in absorbance, ΔA, measured as the difference in intensity of the peak and trough vs. the concentration of the drug added. Increasing concentrations of the drug initially produced a linear increase in absorbance change which later began to deviate from linearity. The data were collected in order to obtain such a curved plot of ΔA vs. concentration. The tangent to the curve at the origin was drawn and the distance from the ordinate to the tangent at a given ΔA was taken as the concentration of bound drug, while that from the tangent to the curve gave the free drug present [18]. The data were then plotted as described by Scatchard [4] and the primary association constant (K_1) as well as the number of high affinity binding sites (n_1) were determined.

RESULTS AND DISCUSSION

Phenylbutazone and oxyphenbutazone have been shown to bind to HSA by many workers [14, 18, 19] using various protein binding techniques. Abd Elbary et al. [19] used equilibrium dialysis as well as difference spectrophotometry to study the binding of both drugs to HSA. They calculated the binding parameters from their equilibrium dialysis data and simply used the difference spectral data to show a ligand–protein interaction. The suggested data reduction method given here was applied to their u.v. difference binding data [19] and similar results were obtained. For phenylbutazone, the K_1 calculated by application of the Rosen method was 4.63×10^5 compared to 5.06×10^5 reported from their equilibrium dialysis results. The number of primary binding sites was equivalent in each case and equal to 1.25. Table 1 shows values of K_1 and n_1 for phenylbutazone/HSA binding from other sources; it is clear that the method suggested for reduction of u.v. difference data is in good agreement.

For oxyphenbutazone, the K_1 and n_1 values obtained by Abd Elbary et al. are the same as the values calculated (Table 1). Figures 1 and 2 are representative of how the literature data were taken to generate the corresponding curves and Scatchard plots for these two drugs.

It should be noted that the assumption made by Rosen is that the change in ellipticity (from circular dichroism spectra) is directly proportional to the amount of drug bound. While this may be true in the case for which only one site per molecule of protein is involved, it needs more justification when there is more than one site with more than one association constant. The first association constant would then be more accurately determined than the second [18].

The absorbance difference vs. concentration curve of sulindac was plotted from u.v. difference data reported by Shams-Eldeem et al. [20] (Fig. 3). The

TABLE 1

Comparison of the methods used to examine to binding of some drugs to HSA at pH 7.4

Drug	Binding parameters		Method of protein-binding determinations[a]	Temp (°C)	Ref.
	K_1	n_1			
Phenylbutazone[b]	6.50×10^5	1.00	FQ	27.5	[14]
	6.50×10^5	0.89	DS	28	[14]
	2.37×10^5	1.14	CD	—	[18]
	5.06×10^5	1.25	ED	25	[19]
	4.63×10^5	1.25	DS	25	This study
Oxyphenbutazone[b]	3.53×10^5	1.3	ED	25	[19]
	5.03×10^5	1.3	DS	25	This study
Diclofenac sod.[b]	2.07×10^6	+	DS	25	Unpublished work
	3.09×10^6	1.98	DS	25	This study
Ethacrynic acid[c]	4.3×10^3	3.9	ED	30	[23]
	2.92×10^5	1.0	DS	25	This study
Sulfadimethoxine[c]	1.8×10^5	1.0	ED	25	[26]
	5.46×10^6	0.5	DS	25	This study

[a]CD, circular dichroism; ED, equilibrium dialysis; FQ, fluorescence quenching; DS, difference spectrophotometry. [b]Phosphate buffer. [c]Phosphate—Tris buffer.

line obtained was curved towards the ordinate. It was not possible to calculate the amount of free and bound drug from this curve. This finding may support the cooperative binding phenomenon of sulindac with HSA that was suggested earlier [20] solely on the basis of equilibrium dialysis data. Alternatively there may exist more than a single class of binding site, with different absorptivities for each, and with equilibrium constants such that both sites may be filling simultaneously.

For diclofenac sodium, difference absorption spectra were obtained for the association of drug with HSA. The spectra were characterized by an isosbestic point at 265 nm, a positive peak at 290 nm, and a negative trough at 256 nm. The u.v. absorption spectrum of diclofenac sodium at pH 7.4 showed a maximum absorption band at 274 nm. Figure 4 depicts u.v. difference spectra of the diclofenac/HSA interaction at a HSA concentration of 1.45×10^{-5} M. The calculations of the amounts of free and bound diclofenac were done using an absorbance difference vs. concentration curve derived from u.v. difference spectra at an HSA concentration of 0.58×10^{-5} M. This was done for two reasons: first, to obtain binding information covering a wider range of D/P ratio (1.26—9.16) and second, to get a curve having more data points in the initial linear portion that indicates one-to-one binding of diclofenac sodium to HSA over this concentration range. This linear portion of the curve may eliminate the inaccuracies inherent in drawing a tangent to the origin that Rosen mentioned as a difficulty in his method

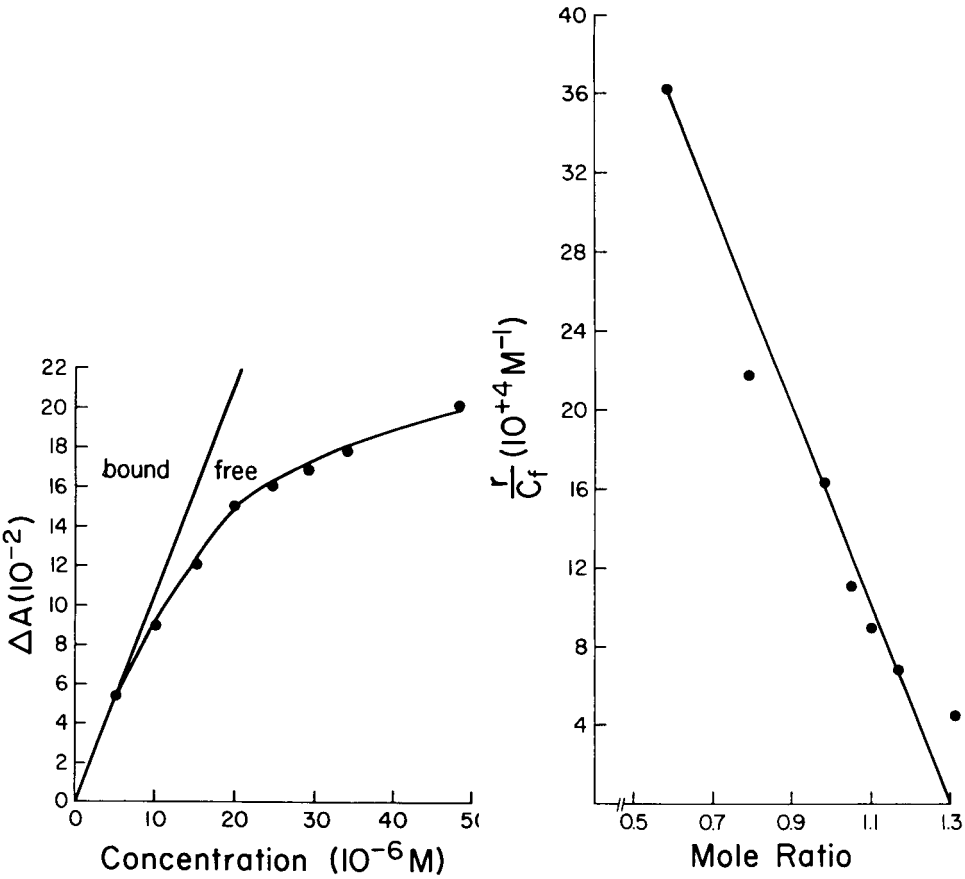

Fig. 1. Ultraviolet absorbance difference (ΔA) of oxyphenbutazone [20] binding to HSA (1.45×10^{-5} M), in pH 7.4 isotonic phosphate buffer, as a function of the concentration of the drug.

Fig. 2. Scatchard representation of u.v. difference data obtained for oxyphenbutazone/HSA interaction in pH 7.4 isotonic phosphate buffer. (r = moles of bound drug per mole of HSA; C_f = molar concentration of free drug.)

[18]. Plotting the data as described by Scatchard resulted in a curved plot (Fig. 5A). The K_1 and n_1 calculated via the absorbance difference vs. concentration method for the binding of diclofenac were found to be 3.09×10^6 and 1.98, respectively. These values are comparable with those calculated in a recently concluded study of diclofenac binding. The binding parameters in the prior study were calculated as described by Gorman and Darnall [12] taking into consideration the elimination of most of the sources of error suggested in the literature [15—17]. This method assumes 1:1 stoichiometry and the K value was calculated to be 2.07×10^6.

Ethacrynic acid was shown to bind to HSA by difference spectrophoto-

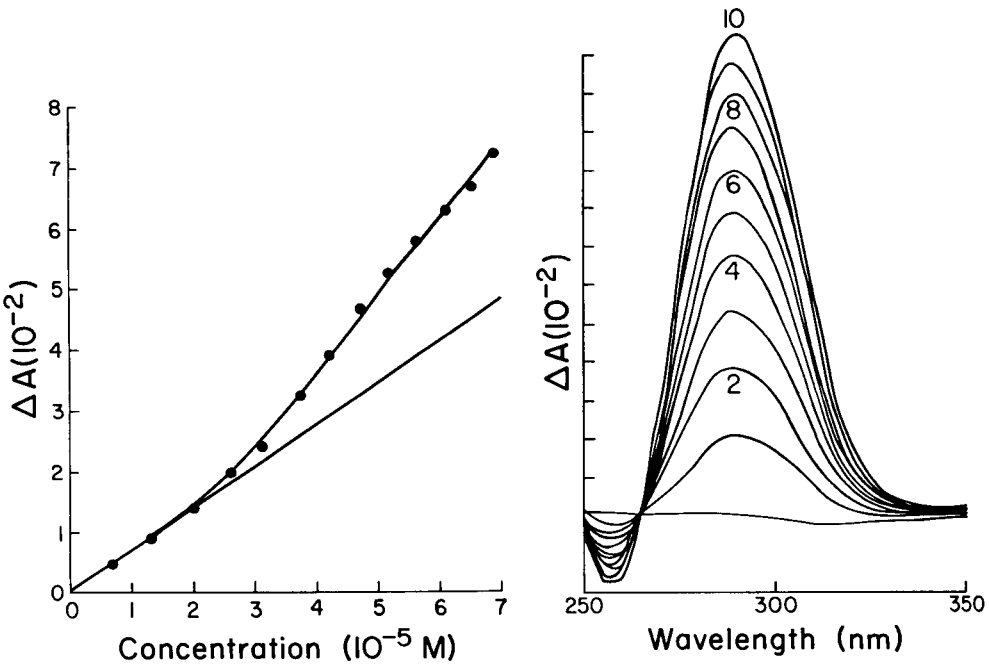

Fig. 3. Ultraviolet absorbance difference (ΔA) of sulindac [20] binding to HSA (1.45×10^{-5} M) in pH 7.4 isotonic phosphate buffer, as a function of the concentration of the drug.

Fig. 4. Difference spectrophotometry after addition of diclofenac to 1.45×10^{-5} M HSA. Each curve represents the addition of 25-μl increments of 2×10^{-4} M diclofenac sodium to buffer in the reference compartment and to protein in the sample compartment. The numbers 1—10 indicate the number of increments added.

metry. Difference spectra were obtained for the association of the drug with protein at D/P ratios of 0.57 to 8.28. The spectra were characterized by positive peaks at 279 nm and 288 nm with a shoulder at 298 nm, a negative trough at 317 nm, and an isosbestic point at 309 nm. The u.v. absorption spectrum of ethacrynic acid is characterized by a maximum absorption band at 277 nm. A curve was generated by plotting the change in absorbance (measured as the difference in intensities of the 279 nm peak and the trough) vs. the concentration of ethacrynic acid added. Increasing concentration of the drug produced increasing absorbance changes that deviated from linearity at very low D/P ratio (0.57).

When the Rosen method was adapted for the difference spectrophotometric data, a K_1 of 2.92×10^5 with n_1 of 1.5 was found; the Scatchard plot from which these data were derived is given in Fig. 5B. Nakano et al. [23] in their work on the binding of diuretics to HSA gave values of 4.3×10^3 and 3.9 for K_1 and n_1 for the ethacrynic acid/HSA interaction. They used an equilibrium dialysis technique, a 2×10^4 M HSA solution, D/P ratios

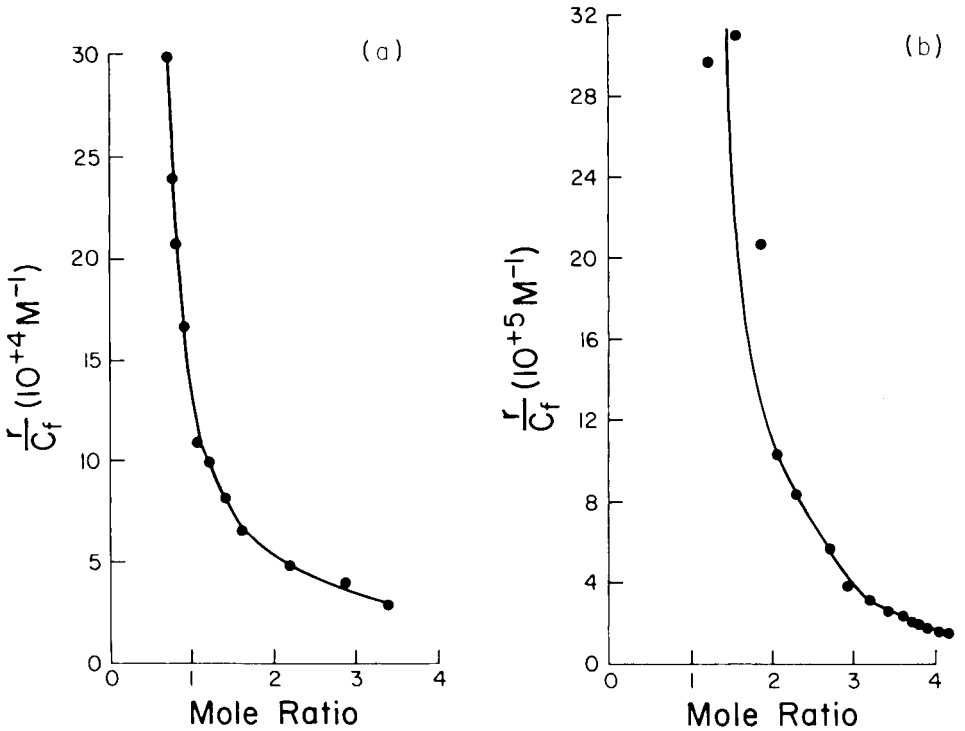

Fig. 5. Scatchard representation of u.v. difference data obtained for (a) the diclofenac sodium/HSA interaction and (b) the ethacrynic acid/HSA interaction in pH 7.4 isotonic Tris buffer.

of 0.5—5 and a temperature of 30°C. The free drug was quantified spectrophotometrically and this has been shown by some authors to present some difficulty for obtaining accurate results at low mole ratios (i.e., r) [24, 25].

For sulfadimethoxine, values of 5.44×10^6 and 0.9 for K_1 and n_1 were calculated from u.v. difference spectrophotometric results. This compares to values of 1.8×10^5 and 1 (for K_1 and n_1) that were given by Elofsson et al. [26] based on equilibrium dialysis information.

Although the primary binding parameters reported here for ethacrynic acid and sulfadimethoxine are not in agreement with those in the literature, the combination of different experimental conditions and equilibrium dialysis may be responsible. Some studies based on equilibrium dialysis as the method are void of valid data points at low molar ratios (low r values). At low molar ratio, especially if the drug is highly bound to protein, errors in free drug determination arise if the assay procedure is insensitive. This is reflected in the Scatchard plot with a smaller K_1 value than would be normal and a higher n_1 value. The Scatchard plot is then compromised and in many cases misused in determining the primary binding sites and affinities;

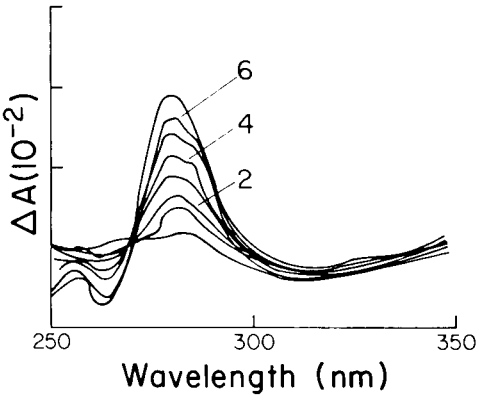

Fig. 6. Difference spectrophotometry after addition of sulfadimethoxine to 5.8×10^{-6} M HSA. Each curve represents the addition of 5 μl (curves 1—4) or 10 μl (curves 5—7) of 8.1×10^{-5} M sulfadimethoxine to buffer in the reference compartment and to protein in the sample compartment.

what is obtained may be an average value of binding parameters, not only at the primary binding sites but the other sites of lower affinities as well.

The difference absorption spectra of the sulfadimethoxine/HSA interaction are characterized by a positive peak at 280 nm, a negative trough at 264 nm, and an isosbestic point at 268 nm (Fig. 6). The u.v. absorption spectra of this drug are characterized by a maximum absorption band at 266 nm.

In summary, ultraviolet difference spectrophotometry has been used by some workers to demonstrate binding of drugs to albumin. This method is considered to be accurate, reproducible and suitable for drugs of limited solubilities, and provides valuable information on the protein interaction. However, there was a belief that, in contrast to equilibrium dialysis and other similar techniques, this method did not yield specific binding parameter information. Reduction of the binding data according to the method of Rosen [18] requires that a plot of ΔA vs. concentration be obtained and deviation from linearity be followed over a range of D/P ratios. It does not necessitate the saturation of the protein sites. When this procedure was adopted here, amounts of free drug as low as 10^{-8} M were calculated, which would perhaps be too low to be detected if a subtractive technique were used. Furthermore, subtractive techniques are always open to errors in separation of the free drug from the complexed drug even when radioactive tracers are used.

This method does have a disadvantage in that inaccuracies in determining the tangent to the absorbance difference vs. concentration curve may be open to error [18]. Starting the addition to the HSA with a low concentration of the drug may give an accurate linear portion from which the tangent may be best drawn.

This work was supported in part by an Amideast Fellowship (1982—83) awarded to S. N.

REFERENCES

1 B. K. Martin, Nature, 207 (1965) 27.
2 J. J. Vallner, J. H. Perrin and S. Wold, J. Pharm. Sci., 65 (1976) 1182.
3 I. M. Klotz, Arch, Biochem., 9 (1946) 109.
4 G. F. Scatchard, Ann. N.Y. Acad. Sci., 51 (1949) 660.
5 R. L. Scott, Rec. Trav. Chim., 75 (1956) 787.
6 B. S. Madsen and J. S. Robertson, J. Pharm. Pharmacol., 28 (1974) 807.
7 H. G. Weder, J. Schildknecht, R. A. Lutz and P. Kesselring, Eur. J. Biochem., 42 (1974) 475.
8 I. M. Klotz, Science, 217 (1982) 1247.
9 I. M. Klotz and D. L. Hunston, J. Biol. Chem., 250 (1975) 3001.
10 J. E. Fletcher, A. A. Spector and J. D. Ashbrook, Biochemistry, 9 (1970) 4580.
11 H. A. Benesi and J. H. Hildebrand, J. Am. Chem. Soc., 71 (1949) 2703.
12 E. G. Gorman and D. W. Darnall, Biochemistry, 20 (1981) 38.
13 P. C. Huang and S. Gabay, Biochem. Pharmacol., 23 (1974) 957.
14 V. Maes, J. Hoebeke, A. Vercruysse and L. Kanarek, Mol. Pharmacol., 16 (1979) 147.
15 W. B. Person, J. Am. Chem. Soc., 87 (1965) 167.
16 D. A. Deranleau, J. Am. Chem. Soc., 91 (1965) 4044.
17 K. J. Bergeron and W. R. Roberts, Anal. Biochem., 90 (1978) 844.
18 A. Rosen, Biochem. Pharmacol., 19 (1970) 2075.
19 A. Abd Elbary, J. J. Vallner and C. W. Whitworth, J. Pharm. Sci., 71 (1982) 241.
20 M. A. Shams-Eldeen, J. J. Vallner and T. E. Needham, J. Pharm. Sci., 67 (1978) 1077.
21 A. S. Brill and H. E. Sandberg, Biophys. J., 8 (1968) 664.
22 J. J. Vallner, L. A. Sternson and D. L. Parsons, J. Pharm. Sci., 65 (1976) 873.
23 M. Nakano, K. Fujii and S. Goto, Chem. Pharm. Bull., 27 (1979) 101.
24 T. J. Benya and J. G. Wagner, Can. J. Pharm. Sci., 11 (1976) 71.
25 K. M. Giacomini, A. Abang and T. F. Blaschke, Br. J. Clin. Pharmacol., 14 (1982) 752.
26 R. Elofsson, S. O. Nilsson and A. Agren, Acta. Pharm. Suec., 7 (1970) 473.

Analytica Chimica Acta, 162 (1984) 333—338
Elsevier Science Publishers B.V., Amsterdam — Printed in The Netherlands

DETERMINATION OF ORGANOPHOSPHORUS COMPOUNDS BY DYE-ASSISTED CHROMATOGRAPHY

ANDRES TRUJILLO, T. GNANASAMBANDAN and HENRY FREISER*

Strategic Metals Recovery Research Facility, Department of Chemistry, University of Arizona, Tucson, AZ 85721 (U.S.A.)

(Received 23rd January 1984)

SUMMARY

The application of dye-assisted reversed-phase liquid chromatography for the determination of several organophosphorus compounds is demonstrated for mobile phases containing 10^{-4} M Brilliant Green in a mixed solvent of water and methanol, acetonitrile and 1,4-dioxane. This method, based on the interactions between a dye and analyte molecules, offers good detection limits for compounds which have weak chromophores. Detection limits are in the submicrogram range for aromatic pesticides, and in the low microgram range for non-chomophoric aliphatic compounds.

Organophosphorus compounds are commonly used in agriculture as insecticides [1], and in industry as extractants for the recovery of metals [2]. As insecticides, these compounds have the advantage of having low toxicity toward mammals and also of being degraded easily into less toxic compounds.

The preferred method for the separation, quantitation, and identification of organic phosphorus compounds has been gas chromatography (g.c.) with photometric or with mass spectrometric detection [3, 4]. A problem associated with the g.c. method is the thermal decomposition of the sample. This problem can be overcome by using other chromatographic techniques such as thin-layer, ion-exchange, and high-performance liquid chromatography (h.p.l.c.) which use milder conditions for separation [3]. Of the previous chromatographic techniques, h.p.l.c. seems to be the most promising for the rapid separation and quantitation of neutral organic phosphorus compounds because of its high resolving power and the capacity to preconcentrate and cleanup samples using practically the same hardware [5, 6]. A serious drawback of h.p.l.c. with photometric detection is the lack of sensitivity for compounds having weak chromophores [3].

Efforts to improve photometric detection of non-absorbing ionic compounds has been successful to a considerable extent using ion-pair chromatography [7—9]. This technique, however, can be applied only for the more easily ionizable organophosphorus acids and amines. This study deals with the photometric detection of neutral nonabsorbing aliphatic phosphorus compounds as well as the enhanced detection of neutral aromatic phosphorus

0003-2670/84/$03.00

compounds using reversed-phase h.p.l.c. with a dye-containing mobile phase. The method consists in the equilibration of a reversed-phase column with a mobile phase containing a dye. Once equilibration has been achieved, the sample is injected on the column and the same mobile phase is used for elution. Detection of neutral nonchromophoric analytes is possible because of the interaction between the analyte and the dye molecules which cause an increase in the molar absorptivity of the dye at several wavelengths. The interaction between the analyte and the dye is fairly general, and several families of neutral compounds including alcohols, ketones, esters and nitriles, can also be detected with this method [10, 11].

EXPERIMENTAL

Apparatus

Two chromatographic systems were used in this study. The first consisted of an Altex pump (model 110 A), a 10-μl loop rotary valve injector (Spectra-Physics, SP-419-0410), and a Whatman Partisil ODS-2 (10 μm, 25 cm $\times$ 0.46 cm) column. The second chromatographic system consisted of a dual-pump Spectra-Physics liquid chromatograph (SP-3500B) equipped with another 10-μl loop rotary-valve injector, and a slurry-packed Spherisorb S5-ODS-2 column (5 μm, 25 cm $\times$ 0.46 cm).

The detectors used were a Spectra-Physics SP-8200 u.v./visible selectable wavelength detector equipped with a 254-nm or 436-nm filter, and a refractive index detector (Showa Denko KK Shodex RI Model SE-11).

Mobile phase. The mobile phases contained 0.10×10^{-3} M Brilliant Green and various concentrations of water and organic solvent. Cleaning and equilibration of the columns were as described previously [10]. The flow rate was maintained at 1.0 ml min^{-1}. The temperature was maintained at 30° C. The volume of the mobile phase was taken as the breakthrough volume.

Chemicals and stock solutions

The organophosphorus compounds used in this study were obtained from several sources, and were used without further purification. The presence of trace impurities in these compounds was established by inspection of chomatograms obtained for each compound studied and were found to be noninterfering (i.e., peaks are small and completely resolved from the main component). Deionized water was degassed under vacuum at 50° C. Reagent-grade methanol and acetonitrile were used as received. 1,4-Dioxane was refluxed over sodium metal for three days and then distilled from glass before use. Brilliant Green hydrogen sulfate (94% pure; Eastman) was used as received.

Stock solutions of organophosphorus compounds were prepared by carefully weighing the compound in a volumetric flask and then diluting it with dioxane or, in some cases, with mobile phase. Standards prepared in aqueous solutions were used within one day. Calibration graphs were prepared by replicate injection of 10 μl of standard. Five standards were used for every compound.

RESULTS AND DISCUSSION

The dye used here was the hydrogensulphate salt of Brilliant Green. This dye is strongly adsorbed by the reversed-phase column and exhibits high sensitivity for the detection of nonchromophoric neutral substances. The selection of Brilliant Green was based on the requirements of water solubility, sensitivity, and stability towards decomposition. Other dyes meeting the above requirements are Methylene Blue, Nile Blue A, and Acridine Orange.

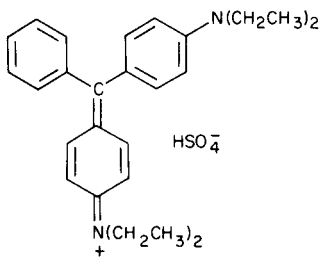

The wavelength of detection used was not always that of maximum sensitivity. For convenience, 254 or 436 nm was selected when the Spectra-Physics detector was used. The wavelength of maximum sensitivity can be obtained by comparing the spectra of the mobile phase in the absence and presence of analyte [12, 13].

The analytes used in this study were members of the phosphates, phosphites, phosphonates, phosphorothionates, and phosphorodithionates family. Aliphatic as well as aromatic compounds were included in order to compare the detection sensitivity for both nonabsorbing and strongly absorbing compounds. Because the compounds used were widely different in molecular weight and functionalities, it was necessary to study them for different mobile-phase compositions. Capacity factors for several organic phosphorus compounds including pesticides are listed in Tables 1—3. Table 1 shows the capacity factors for several compounds of low molecular weight eluted with methanol or dioxane in the mobile phase. Elution with dioxane-water gives good results for the separation, but its utility for the elution of compounds of higher molecular weight (e.g., aromatics) was limited by the increased back-pressure produced by this highly viscous solvent. Instead of continuing working with dioxane in the mobile phase, methanol and acetonitrile-water mixture were considered.

Capacity factors for compounds of low molecular weight obtained with different methanol-water mobile phases are shown in Table 1. The capacity factors obtained with methanol as organic modifier are considerably higher than those obtained with 10% dioxane-water. Thus, the solvent strength of the former is expected to be ineffective for the elution of the phosphorus compounds with higher molecular weight. For the elution of the more hydrophobic compounds, acetonitrile-water mixtures were found to be appropriate.

TABLE 1

Capacity factors (k') obtained with methanol or dioxane in the mobile phase[a]

Compound	Methanol (%)				Dioxane (%)
	10	15	30	40	10
Dimethyl methylphosphonate	1.8	1.6	0.7	—	0.8
Diethyl phosphite (DEPI)	5.0	3.9	1.8	1.4	2.5
Hexamethylphosphoramide (HMP)	10.4	7.9	4.5	2.8	3.5
Diethyl ethylphosphonate (DEEPO)	13.0	9.4	4.5	3.5	6.9

[a]Mobile phase: 0.10 mM Brilliant Green and x % methanol or dioxane (v/v). Partisil ODS-2 column with detection at 254 nm.

TABLE 2

Capacity factors obtained with 50% acetonitrile

Compound	k'[a]	Compound	k'[a]	Compound	k'[a]
Methyl parathion	4.5	Dibutyl butylphosphonate	9.6	EPN	17.6
Triphenyl phosphate	9.2			Tri-(*o*-tolyl) phosphate	28.9
Ethyl parathion	9.5	Fenthion	9.7		
Tributyl phosphate	9.5	Coumaphos	11.5	Ethion	35.0
Diazinon	9.6	Phorate	12.4	Carbophenothion	40.5

[a]Mobile phase was 0.10 mM dye, 2.0 mM ammonium phosphate, and 50% acetonitrile-water. Spherisorb S5-ODS-2 column.

In Table 2, capacity factors for some phosphorus compounds having molecular weights greater than 200 are shown. Elution with 50% acetonitrile-water was not effective for the separation of all the compounds shown in Table 2. Thus, although separation of methyl and ethyl parathion was possible, resolution of dibutyl butylphosphonate from its analog, tributyl phosphate, was impossible under the present conditions.

The effect of the dye on the retention of the organic phosphorus compounds was investigated by comparing the capacity factors of the compounds eluted in the presence (k') and absence (K'') of dye. From the results obtained (Table 3), a linear relationship having a correlation coefficient (r) of 0.9998 and regression equation: $k' = (1.02 \pm 0.01)\,K'' + (0.82 \pm 0.04)$, was obtained. Thus, the net effect of the dye on retention is to increase the capacity factor by 0.82 units. Analogous relationships have been obtained before for aliphatic alcohols [10]. The increase in capacity factors caused by the dye, both

TABLE 3

Comparison of capacity factors in presence and absence of dye[a]

Compound	K'' (0.0 mM)[a]	k' (0.10 mM)[b]
Dibutyl phosphite	0.5	1.3
Dibutyl butylphosphonate	2.3	3.2
Tributyl phosphate	2.3	3.2
Tri-(*o*-tolyl) phosphate	4.7	5.6

[a]Mobile phase was 75% (v/v) methanol-water; Partisil ODS-2 column; refractive index detector. [b]System as for preceding column but with 0.10 mM dye added, and u.v.-visible detection at 436 nm.

adsorbed in the column and in the mobile phase, may be ascribed to the increased interaction of the analyte and the adsorbed dye and the possible formation of a dye-analyte adduct having a larger partition coefficient favoring retention, as proposed earlier [10]. Further work is necessary to elucidate the actual mechanism of retention.

The sensitivity of the method was investigated by preparing various calibration plots for several representative pesticides and aliphatic phosphorus compounds. In both cases, the calibration plots were prepared by replicate injection of a mixture of compounds that was completely resolved. For the pesticides, standards containing 0.1, 0.5, 1.0, 5.0, and 10.0 μg were used. Plots of amount injected vs. peak height, in absorbance, were found to be linear (r = 0.9991—0.9999) over the range studied. The detection limits, defined as three times the peak-to-peak noise, are tabulated together with the regression equations [14] in Table 4. The highest sensitivity was obtained with methyl parathion because this compound is aromatic and has a chromophore in the ultraviolet region. Phorate, being aliphatic, showed the lowest sensitivity. The sensitivity in the absence of the dye is lower for compounds having an absorbing chromophore, and is practically zero for compounds without chromophores.

Calibration plots for other aliphatic compounds were prepared as mentioned before. Standards containing 70, 200, 300, 500, and 700 μg were injected. The calibration plots obtained (Table 4) are linear (r = 0.976—0.998) over the concentration ranges studied. The sensitivity is about the same for all three compounds because these compounds themselves do not absorb. Thus the response measured is exclusively due to the dye-analyte interaction.

The limit of detection for the aliphatic compounds are about one hundred times larger than the corresponding detection limits obtained with the aromatic compounds (Table 4). This difference is attributed to the contribution of the absorbing chromophores in the aromatic compounds.

Even though the sensitivity obtained with the present method is modest, it is still comparable to that of other h.p.l.c. methods reported recently in which optimum detection conditions were used [6, 15].

TABLE 4

Calibration plots for organic phosphorus compounds[a]

Compound	Slope (m) ± s.d.	Intercept (b) ± s.d.	Detection limit (μg)	Std. error (× 10)
Pesticides[b]				
Ethyl parathion	17.71 ± 0.20	1.36 ± 0.91	0.10	1.98
Coumaphos	9.58 ± 0.05	−0.21 ± 0.23	0.20	0.50
Methyl parathion	44.24 ± 0.64	4.88 ± 2.93	0.10	6.39
Diazinon	6.83 ± 0.17	1.16 ± 0.84	0.20	1.67
Phorate	2.88 ± 0.08	0.18 ± 0.19	0.50	0.76
Aliphatic compounds[c]				
DEPI	8.11 ± 0.28	3.64 ± 1.28	37.0	0.03
HMP	7.40 ± 0.45	9.98 ± 1.90	40.0	0.04
DEEPO	5.28 ± 0.68	16.5 ± 2.89	57.0	0.07

[a]Mobile phase containing 0.10 mM dye, 2.0 mM ammonium phosphate and 50% (v/v) acetonitrile—water (for pesticides) or 30% (v/v) methanol—water (aliphatics). Detection at 254 nm. H is peak height in milliabsorbance; C is the amount of sample injected in μg, and s.d. is the standard deviation. [b]Regression eqn.: $H = mC + b$. [c]Regression eqn.: $H = mC/100 + b$.

This research was supported by a grant from the Office of Naval Research.

REFERENCES

1 M. Eto, Organophosphorus Pesticides: Organic and Biological Chemistry, CRC Press, Cleveland, OH, 1974.
2 Y. Marcus, A. S. Kertes and E. Yanir, Equilibrium Constants of Liquid—Liquid Distribution Reactions, Butterworth, London, 1974.
3 J. Sherma and G. Zweig, Anal. Chem., 55 (1983) 57R.
4 J. Sherma, CRC Rev. Anal. Chem., 3 (1973) 299.
5 D. C. Paschal, R. Bicknell and D. Dresbach, Anal. Chem., 49 (1977) 1551.
6 A. Otsuki and T. Takaku, Anal. Chem., 51 (1979) 833.
7 M. Denkert, L. Hackzell, G. Schill and E. Sjogren, J. Chromatogr., 218 (1981) 31.
8 Y. Askemark, K. G. Wahlund and G. Schill, Anal. Chem., 51 (1979) 976.
9 J. Dinunzio and H. Freiser, Talanta, 26 (1979) 587.
10 T. Gnanasambandan and H. Freiser, Anal. Chem., 54 (1982) 2379.
11 T. Gnanasambandan and H. Freiser, Anal. Chem., 54 (1982) 1282; 53 (1981) 909.
12 E. Rabinowitch and L. Epstein, J. Am. Chem. Soc., 63 (1941) 69.
13 E. Schnabel, H. Nother and H. Kuhn, in T. S. Gore, B. S. Joshi, S. V. Sunthankar and B. D. Tilak (Eds.), Recent Progress in the Chemistry of Natural and Synthetic Colouring Matters and Related Fields, Academic Press, New York, 1962, p. 561.
14 D. M. Hirst, Mathematics for Chemists, Macmillan, London, 1976, p. 259.
15 C. E. Parker, C. A. Haney and J. R. Hass, J. Chromatogr., 237 (1982) 233.

Analytica Chimica Acta, 162 (1984) 339—346
Elsevier Science Publishers B.V., Amsterdam — Printed in The Netherlands

PREPARATION OF MACRORETICULAR CHELATING RESINS CONTAINING MERCAPTO GROUPS FROM 2,3-EPITHIOPROPYL METHACRYLATE/DIVINYLBENZENE COPOLYMER BEADS AND THEIR ADSORPTION CAPACITY

HIRONORI MAEDA*

Department of Industrial Chemistry, Kumamoto Institute of Technology, Ikeda, Kumamoto 860 (Japan)

HIROAKI EGAWA

Department of Industrial Chemistry, Faculty of Engineering, Kumamoto University, Kurokami, Kumamoto 860 (Japan)

(Received 31st January 1984)

SUMMARY

Macroreticular chelating resins containing mercapto groups were prepared by the reaction of 2,3-epithiopropyl methacrylate/divinylbenzene macroreticular copolymer beads with ethanolic potassium hydrogensulfide solution for 1 h at 50°C. The adsorption capacities of this resin for Ag^{+}, Hg^{2+}, Cu^{2+}, Pb^{2+} and Cd^{2+} were determined at various pH values. In the acidic region, the resin shows a high affinity for Ag^{+} and Hg^{2+} and high resistance against air oxidation. Cadmium is readily eluted with 1 mol dm^{-3} hydrochloric acid; silver, mercury and copper ions can be eluted with 1 mol dm^{-3} hydrochloric acid containing 5% (w/v) thiourea. The proposed resin appears to be useful for the removal of As^{3+} from aqueous solutions.

Various polymers containing mercapto groups have been studied as reversible reducing agents and chelating agents [1—12], but the preparation of a chelating resin containing mercapto groups from macroreticular polymer beads does not seem to have been investigated. Previous papers [13, 14] dealt with the preparation of some macroreticular chelating resins containing mercapto groups and their adsorption capacity for heavy metal ions. These macroreticular resins are more practical than gel-type resins for the selective removal and recovery of heavy metal ions from industrial wastes because of their physical stability and fast adsorption rate. In this paper, the preparation of a macroreticular chelating resin containing mercapto groups from 2,3-epithiopropyl methacrylate/divinylbenzene copolymer beads is described and its adsorption capacity for heavy metal ions is discussed. The adsorption of arsenic(III) ion on the resin from aqueous solution was also investigated.

0003-2670/84/$03.00

EXPERIMENTAL

Synthesis of 2,3-epithiopropyl methacrylate and preparation of the macroreticular resins

2,3-Epithiopropyl methacrylate (ETMA) monomer was prepared by adding 325 g of ammonium thiocyanate to a mixture of 500 cm^3 of glycidyl methacrylate monomer, 0.05 g of hydroquinone monomethyl ether, and 250 cm^3 of methanol with cooling (5—10°C) [15]. The mixture was kept overnight at 5°C. The mixture was washed with water, the product was distilled, and the fraction at 61—63°C (3 mm Hg) was collected.

The macroreticular ETMA/divinylbenzene copolymer beads were synthesized by suspension polymerization in the presence of 2,2,4-trimethylpentane as diluent. Copolymer beads with the desired diameter were selected with a sieve (32—60 mesh). The copolymer beads (1 g) were treated with ethanolic potassium hydrogensulfide solution (6 cm^3) at 50°C for definite times to introduce mercapto groups. The resulting resin was washed with 1 mol dm^{-3} ammonia, and with deionized water until the wash water became neutral.

Procedures

Measurement of sulfur content. The resins were first purified by Soxhlet extraction with methanol for 10 h. Weighed portions (5 mg) were decomposed by the Schöniger flask method, the products being absorbed in 3% hydrogen peroxide solution. The resulting sulfuric acid was determined by conductometric titration, and the sulfur content of the resin was calculated.

Measurement of adsorption capacity for metal ions. In a glass-stoppered Erlenmeyer flask were placed 0.125 or 0.25 g of the resin and 50 cm^3 of buffered metal ion solution (0.01 mol dm^{-3}) and the mixture was left at room temperature (about 25°C) for 48 h with occasional shaking. The amount of metal ion adsorbed on the resin was calculated from the result of complexiметric titration of the metal ion in the supernatant liquid. The metal ions adsorbed on the resin were then removed by shaking 0.25 g of the resin with 50 cm^3 of 1 mol dm^{-3} hydrochloric acid, or 1 mol dm^{-3} hydrochloric acid containing 5% (w/v) thiourea, at 30°C for 1 h. The amount of metal ion desorbed was quantified by atomic absorption spectrometry.

Measurement of adsorption capacity for arsenic(III) ion. The resin (0.125 g) and 50 cm^3 of sodium arsenite solution (3 mg dm^{-3} or 200 mg dm^{-3} arsenic) were shaken in a glass-stopped Erlenmeyer flask at 30° C for 24 h. The amount of arsenic(III) ion adsorbed was calculated from the result of quantifying arsenic(III) in the supernatant liquid by means of the spectrophotometric procedure based on silver diethyldithiocarbamate [16]. The arsenic(III) adsorbed on the resin was removed by shaking the resin with sodium hydroxide solution at 30°C for 1 h (see Table 3). This arsenic was also quantified spectrophotometrically.

RESULTS AND DISCUSSION

Preparation of the macroreticular chelating resins

The macroreticular chelating resins containing mercapto groups were prepared by the route in Scheme 1.

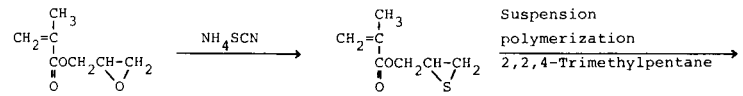

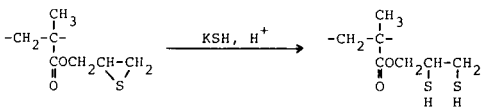

Chelating resins containing mercapto groups have also been prepared by reaction of poly(glycidyl methacrylate) polymer beads with a methanolic solution of ammonium thiocyanate, followed by reaction of the products with ethanolic potassium hydrogensulfide [13]. However, the resins which were prepared by that method from glycidyl methacrylate (GMA)/divinylbenzene (DVB) copolymer beads, in order to increase their physical stability, showed a poor affinity for mercury ion. The adsorption capacity of those resins for mercury ion decreased greatly as the DVB content increased. For example, the mercury adsorption capacity of the mercapto-containing GMA/DVB (5% v/v) copolymer beads was about 0.3 mmol g^{-1} of resin.

In order to prepare macroreticular resins containing mercapto groups, which would have high physical stability and high adsorption capacity for certain metal ions, attention was turned to the reaction of ETMA/DVB (5% v/v) copolymer beads with ethanolic potassium hydrogensulfide solution.

Figures 1 and 2 show the infrared (i.r.) spectrum and the Hg^{2+} capacity of the resin obtained, respectively. In the i.r. spectrum (Fig. 1), a characteristic band at 615 cm^{-1} corresponding to the episulfide ring (νC—S) in spectrum A disappeared after the reaction with potassium hydrogensulfide (spectrum B), while a weak sharp band at 2550 cm^{-1} corresponding to mercapto groups (νS—H) appeared (spectrum B). Thus the introduction of mercapto groups into this cross-linked resin was readily achieved by treatment of the ETMA/DVB (5% v/v) resin with potassium hydrogensulfide for 1 h at 50°C. Figure 2 shows that the Hg^{2+} capacity of this treated resin was high in comparison with that of the mercapto-containing GMA/DVB resin. Figure 2 also shows that the sulfur content of the treated resin is high. These results indicate that the macroreticular chelating resins having mercapto groups can be prepared easily from ETMA/DVB copolymer beads.

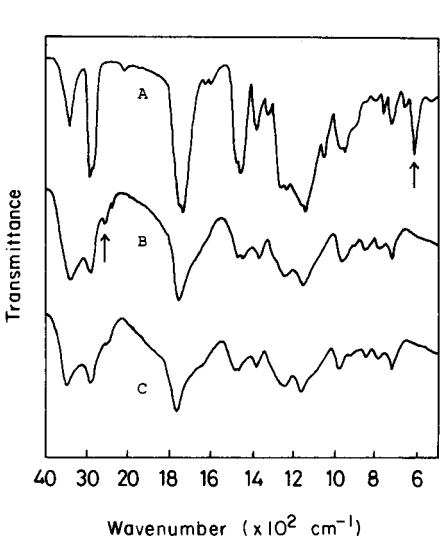

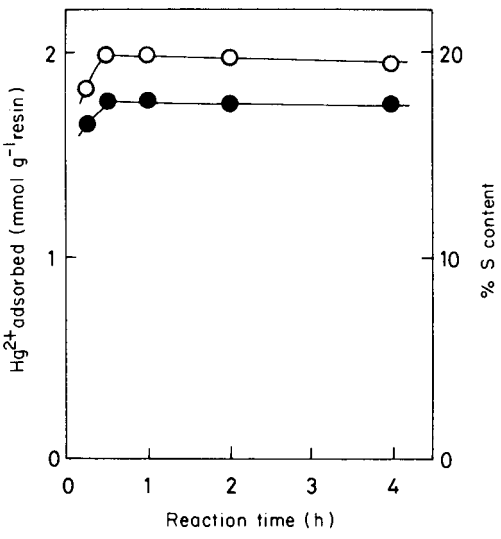

Fig. 1. Infrared spectra of the resin beads: (A) ETMA/DVB (5% v/v) copolymer beads; (B) these resin beads treated with hydrogensulfide; (C) after adsorption of Hg^{2+}.

Fig. 2. Effect of reaction time with potassium hydrogensulfide on the adsorption of Hg^{2+} and the sulfur content: (○) Hg^{2+} adsorbed; (●) sulfur content. Reaction temperature 50°C.

Effect of porosity of the resins on the adsorption capacity for metal ions

The effect of macropore structure (porosity) of the resin on the adsorption of mercury ion was investigated. Resins with different porosities were prepared from the ETMA/DVB copolymer beads which were obtained by suspension polymerization with different amounts of diluent (2,2,4-trimethylpentane; TMP) varying from 10% (v/v) to 100% (v/v) relative to the monomer consisting of ETMA (91—99% v/v) and DVB (1—9% v/v). The pore characteristics (pore volume, specific surface area, and average pore radius) of those resins are shown in Table 1.

Figures 3 and 4 show the capacity for metal ions in relation to the DVB content and the diluent volume, respectively. As shown in Fig. 4, resin 8 (Table 1) provides the highest affinity for metal ions, whereas resins 5, 6 and 7 which had insufficient porosity (specific surface area) had a poor affinity for metal ions. Clearly, the adsorption capacity of these resins for metal ions is greatly affected by their porosity.

Resistance of the resin to oxidation

The resistance of the resin containing mercapto groups was tested by measuring the mercury adsorption capacity of samples exposed to air. The capacities (at pH 2) of resins exposed to air for 0, 30, 60, 120 and 150 days were 1.85, 1.81, 1.79, 1.76 and 1.72 mmol g^{-1} of resin, respectively. Although low-molecular-weight compounds containing mercapto groups are readily

TABLE 1

Pore structure of the ETMA/DVB copolymer beads prepared

No.	DVB[a] (% v/v)	TMP[a] (% v/v)	Pore volume (ml g^{-1})	Specific surface area (m^2 g^{-1})	Average pore radius (nm)
1	1	50	0.34	0.65	750.0
2	3	50	0.35	2.97	180.0
3	7	50	0.44	19.38	35.0
4	9	50	0.51	26.55	32.0
5	5	10	0.04	0.00	—
6	5	30	0.17	2.77	53.1
7	5	40	0.31	4.20	32.0
8	5	50	0.36	16.20	60.0
9	5	75	0.81	0.89	1068.3
10	5	100	1.17	0.74	1935.8

[a]These values represent % (v/v) of DVB in monomer and % (v/v) of 2,2,4-trimethylpentane (TMP) per monomer mixture, used in the synthesis of the resin.

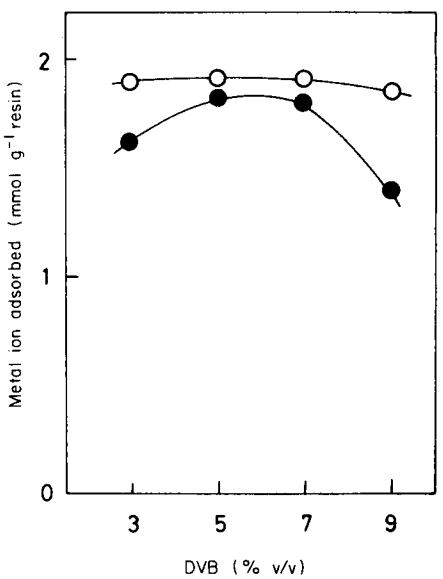

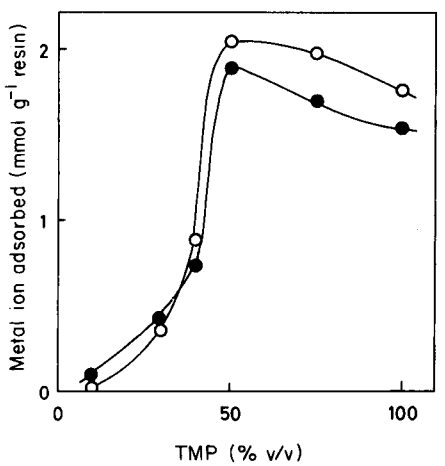

Fig. 3. Effect of cross-linking on the adsorption of metal ions on the treated resin (50% v/v TMP). Metal: (○) Ag^+; (●) Hg^{2+}.

Fig. 4. Effect of pore structure on the adsorption of metal ions on the treated resin (5% v/v DVB): (○) Ag^+; (●) Hg^{2+}.

oxidized to form the corresponding disulfide, the adsorption ability of the treated resins for mercury ion decreased very little after exposure to air for 150 days. These resins are therefore considered to be sufficiently stable to air oxidation for use in industry.

Adsorption behavior of the resins for various metal ions

The adsorption capacities of the proposed resin for Ag^{+}, Hg^{2+}, Cu^{2+}, Pb^{2+}, Cd^{2+} and Ca^{2+} ions were measured at various pH values with the results given in Fig. 5. In the acidic region, the resin shows a high affinity for Ag^{+} and Hg^{2+}, but little affinity for the other metal ions studied. The order of affinity is $Ag^{+} > Hg^{2+} \gg Pb^{2+} > Cu^{2+} \geqslant Cd^{2+} > Ca^{2+}$. These results may be interpreted on the basis of Pearson's concept of hard and soft acids and bases [17], i.e., Ag^{+} and Hg^{2+} are soft acids which prefer soft ligand atoms. From the result shown, separation of Ag^{+} or Hg^{2+} ions from the other metal ions studied is possible at about pH 1.

Table 2 shows the recoveries of the metal ions adsorbed on the proposed resin. The metal ions adsorbed on the resin can be eluted easily, except for lead, by treating with 1 mol dm^{-3} hydrochloric acid or 1 mol dm^{-3} hydrochloric acid solution containing 5% (w/v) thiourea. Elution of lead with acetic acid solutions was also unsatisfactory.

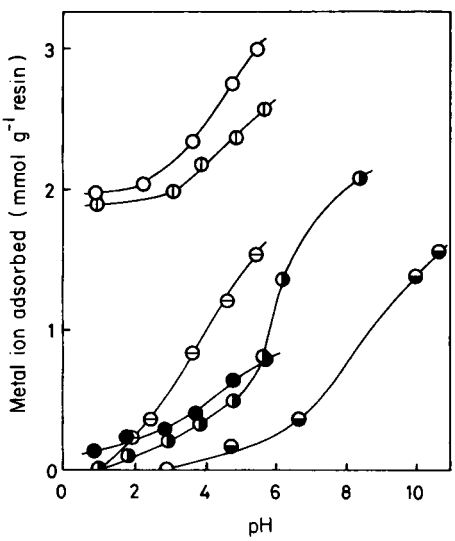

Fig. 5. Effect of pH on the adsorption capacity for various metal ions: (○) Ag^{+}; (◑) Hg^{2+}; (⊖) Pb^{2+}; (●) Cu^{2+}; (◑) Cd^{2+}; (◒) Ca^{2+}.

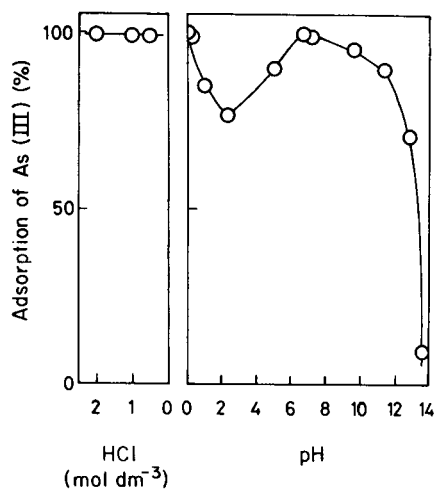

Fig. 6. Effect of concentration of hydrochloric acid and pH on the adsorption of As^{3+} on the resin (see Experimental).

TABLE 2

Elution of metal ions adsorbed on the proposed resin[a]

Metal ion	Eluent[b]	Metal added (mg)	Metal eluted (mg)	Recovery[c] (%)
Cd^{2+}	HCl	36.64	36.53	99.7
Ag^{+}	HCl	52.01	0.32	0.6
Hg^{2+}	HCl	76.03	20.66	27.2
Cu^{2+}	HCl	16.38	5.46	33.3
Pb^{2+}	HCl	35.11	12.02	34.2
Ag^{+}	Thiourea/HCl	52.01	51.68	99.4
Hg^{2+}	Thiourea/HCl	75.63	75.23	99.5
Cu^{2+}	Thiourea/HCl	15.11	14.80	97.9
Pb^{2+}	Thiourea/HCl	28.94	2.77	9.6

[a]Adsorption conditions: 50 cm^3 of 0.01 mol dm^{-3} metal ion solution per 0.25 g of resin, room temperature, 48 h. [b]Elution conditions: 50 cm^3 of 1 mol dm^{-3} HCl or 5% (w/v) thiourea in 1 mol dm^{-3} HCl, 30°C, 1 h. [c]Results are the average of two runs. Linear ranges were not evaluated.

TABLE 3

Elution of As^{3+} adsorbed on the resin with sodium hydroxide solutions[a]

NaOH eluent[b] (mol dm^{-3})	As^{3+} added (mg)	As^{3+} eluted (mg)	Recovery (%)
0.5	3.35	1.81	54.0
1	3.26	2.55	78.2
2	3.33	2.76	82.9

[a]Adsorption conditions: 50 cm^3 of 200 mg dm^{-3} As(III) solution per 0.125 g of resin, 30°C, 24 h. [b]Elution conditions: 50 cm^3 of sodium hydroxide solution, 30°C, 1 h.

The adsorption of the proposed resin for arsenic(III) ion in aqueous solution was investigated at various pH values with the results shown in Fig. 6. The pH of the solutions was adjusted with hydrochloric acid or sodium hydroxide without buffering. Obviously, the proposed resin has a high affinity for arsenic(III) ions in almost neutral solutions and in acidic solutions (0.5—2 mol dm^{-3} HCl). As shown in Table 3, As^{3+} can be eluted by treating the resin with sodium hydroxide solutions. The results suggest that the resin should be useful for the removal of arsenic(III) ions from aqueous solutions. Application for the removal and recovery of arsenic(III) ions from a geothermal power wastewater is under investigation.

REFERENCES

1 H. P. Gregor, D. Dolar and G. K. Hoeshele, J. Am. Chem. Soc., 77 (1955) 3675.
2 Y. Nakamura, Kogyo Kagaku Zasshi, 58 (1955) 269.
3 C. G. Overberger and A. Leborits, J. Am. Chem. Soc., 77 (1955) 3675; 78 (1956) 4792.
4 Y. Hamamura, M. Tachikawa and S. Uno, Nippon Nougei Kagaku Kaishi, 29 (1955) 194.
5 J. R. Parrish, Chem. Ind., (1956) 137.
6 M. Okawara, T. Nakagawa and E. Imoto, Kogyo Kagaku Zasshi, 60 (1957) 73.
7 Y. Hamamura, H. Uejima, N. Ishikawa, S. Iguchi and K. Hayashiya, Nippon Nougei Kagaku Kaishi, 31 (1957) 703.
8 M. Okawara and Y. Sumitomo, Kogyo Kagaku Zasshi, 61 (1958) 1508.
9 M. Okawara, Y. Onishi and E. Imoto, Kogyo Kagaku Zasshi, 64 (1961) 226.
10 M. Okawara, E. Haruki and E. Imoto, Kogyo Kagaku Zasshi, 64 (1961) 229.
11 E. Bayer, H. Fiedler, L. L. Hock, D. Otterbach, G. Schenk and W. Voelter, Angew. Chem., 76 (1964) 76.
12 M. J. Benes, J. Stamberg, J. Peska, M. Tichy and M. Cikrt, Angew. Makromol. Chem., 44 (1975) 67.
13 H. Egawa, Y. Jogo and H. Maeda, Nippon Kagaku Kaishi, (1979) 1760.
14 H. Maeda and H. Egawa, Nippon Kagaku Kaishi, (1983) 578.
15 H. Egawa and T. Nonaka, Kobunshi Ronbunshu, 35 (1978) 21.
16 ASTM. Standard Methods for the Examination of Water and Wastewater, 13th edn., 1971, p. 62.
17 R. G. Pearson, J. Am. Chem. Soc., 85 (1963) 3533.

Analytica Chimica Acta, 162 (1984) 347—356
Elsevier Science Publishers B.V., Amsterdam — Printed in The Netherlands

THE LIQUID—LIQUID EXTRACTION OF PLATINUM IN THE PRESENCE OF TIN(II) CHLORIDE FROM DILUTE HYDROCHLORIC ACID INTO 4-METHYL-2-PENTANONE

NAZIR AHMED and KLAUS R. KOCH*

Department of Analytical Science, University of Cape Town, Rondebosch, Cape Town 7700 (South Africa)

(Received 20th February 1984)

SUMMARY

The distribution of complexes of type $[Pt(SnCl_3)_nCl_{4-n}]^{2-}$ ($n = 1—4$) and $[Pt(SnCl_3)_5]^{3-}$ between 1.5—3.5 M hydrochloric acid and 4-methyl-2-pentanone is discussed in detail. Platinum can be quantitatively extracted into the organic phase from hydrochloric acid solutions containing tin(II) chloride when the mole ratio Sn^{2+}: $Pt^{2+} \geqslant 5$. In the presence of sufficient tin(II) chloride, the $[Pt(SnCl_3)_5]^{3-}$ anion is the predominant species extracted into the organic phase. Similar results pertain to starting solutions of either $PtCl_4^{2-}$ or $PtCl_6^{2-}$, although Pt^{4+} is rapidly reduced to Pt^{2+}. Small amounts of Co^{2+}, Ni^{2+}, Fe^{3+} and Cu^{2+} do not interfere.

The characteristic reaction between tin(II) chloride and platinum(II)/(IV) chlorides in dilute hydrochloric acid solution has long been known [1]. Such reactions continue to attract attention as indicated by the appearance of recent reports concerning structural aspects of platinum complexes containing the trichlorostannato moiety as ligand [2, 3]. The intense red of solutions containing complex anions of type $[PtCl_{4-n}(SnCl_3)_n]^{2-}$ ($n = 1—4$) and $[Pt(SnCl_3)_5]^{3-}$ has been exploited analytically for the determination of micro-amounts of platinum [4, 5]. Furthermore, the interesting catalytic effect of tin(II) chloride on the liquid—liquid extraction of platinum by sulphoxides [6], substituted thioureas [7], tributylphosphate [8] and triphenylphosphine [9, 10] has enjoyed much attention. Khattak and Magee [11] used high-molecular-weight amines to extract platinum in the presence of tin(II) chloride, while Gorbanev et al. [12] presented an extraction study of "cluster" compounds involving inter alia some platinum complexes containing the $SnCl_3^-$ ligand. The latter study, however, dealt largely with spectroscopic details of precipitated "cluster" compounds, while reporting few details of their extractive behaviour.

The results of a detailed investigation of the liquid—liquid extraction of platinum(II) chlorides in the presence of significant amounts of tin(II) chloride, from dilute hydrochloric acid solutions into 4-methyl-2-pentanone (methyl isobutyl ketone, MIBK) are reported in this paper.

0003-2670/84/$03.00

EXPERIMENTAL

All solutions were prepared with boiled-out, glass-distilled water, which was cooled and stored under nitrogen. Concentrated hydrochloric acid (analytical-reagent grade) was saturated with nitrogen, by passing the gas through the acid for at least 15 min. Commercially available tin(II) chloride dihydrate, potassium tetrachloroplatinate(II) and potassium iodate (analytical-reagent grade) were used without further purification.

All extractions were done under nitrogen at room temperature (23 ± 2°C) using specially prepared 25-cm^3 separatory funnels equipped with an adaptor to allow for the introduction of solutions under an atmosphere of nitrogen. Generally, 5 cm^3 of aqueous phase of the desired composition (6×10^{-3} mol dm^{-3} Pt^{2+} and the required amount of Sn^{2+}) was pre-equilibrated by means of vigorous mechanical shaking (20 min). The organic phase (of equal volume) of desired composition was then added, taking care to exclude air, followed by shaking for the desired time interval. For each set of extractions, a blank experiment was done in which a given aqueous phase was shaken with pure hexane, and subsequently treated as the rest of the batch. Percentage extraction was then calculated from the relation $[M]_B - [M]_S/[M]_B \times 100$ where $[M]_B$ and $[M]_S$ are the metal concentrations in the blank and sample, respectively. Separate experiments confirmed mass balance for the system, leading to some typical percentage platinum recoveries as follows (the organic phase composition for each case is given in parentheses): (0% MIBK) 99.0%; (40% MIBK) 99.0%; (50% MIBK) 101.4%; (60% MIBK) 100.9%; (75% MIBK) 101.6%; (100% MIBK) 99.0%.

For all extractions, solutions were freshly prepared and used within 3—5 days of preparation. This is important in the case of tin(II) chloride solutions, which are sensitive to oxidation by traces of air. Solutions were assayed for tin(II) content by means of a conventional titration with potassium iodate, from which generally a 90—95% Sn(II) content was deduced.

Atomic absorption spectrometry (a.a.s.) was used to quantify both platinum and tin in the aqueous phase; a Perkin-Elmer 5000 spectrometer was used with an air—acetylene flame. Attention was paid to possible interferences, particularly in the case of platinum. It was found that 0.2% (w/v) lanthanum nitrate served as a satisfactory "releasing" agent, allowing the measurement of the concentration of platinum to an accuracy of better than ±2.5%. In general, all results were obtained by preparing matched matrix standards containing 0.2% lanthanum nitrate.

The determination of tin by a.a.s. proved satisfactory when a fuel-rich air—acetylene flame was used without interference suppressors. In general, the aqueous phase only was analysed because of the difficulty of preparing suitable standard solutions in the organic phase.

Other metals such as Cu, Fe, Ni and Co were also determined by a.a.s. in the standard flame mode. No difficulties were experienced, as matched matrix standards were also prepared in each case.

RESULTS AND DISCUSSION

Previous studies [10] showed that the reaction between K_2PtCl_4 and $SnCl_2 \cdot 2H_2O$ in dilute hydrochloric acid reached steady state at room temperature (23 ± 2°C) relatively rapidly. On the basis of these observations, we chose to equilibrate freshly prepared aqueous solutions containing the desired amounts of hydrochloric acid, chloroplatinate(II) and tin(II) chloride under nitrogen for at least 20 min before use.

Preliminary experiments led to the following observations. Virtually no platinum (<1%) was extracted from hydrochloric acid (1.5—4.0 mol dm^{-3}) into MIBK in the absence of tin(II) chloride. It was necessary to conduct all experiments under nitrogen, in order to prevent oxidation of tin(II) by dissolved oxygen. All solvents were thus degassed and stored under nitrogen. Platinum(IV) is reduced by tin(II), either concomitant with, or prior to, complex formation with the $SnCl_3^-$ moiety. Kinetic data have been interpreted in terms of relatively slow complex formation subsequent to reduction [13]. Consequently, potassium tetrachloroplatinate(II) was used for this work unless otherwise indicated. In the presence of significant amounts of tin(II) chloride (measured in terms of the molar Sn(II):Pt(II) ratio, R), platinum was virtually quantitatively extracted by pure MIBK phases; extraction was accompanied by complete transfer of the red-orange colour from the aqueous to the organic phase. Further, tin(II) chloride was found to distribute between the aqueous phase and the organic phase in the absence of platinum, although this distribution differed significantly in the presence of platinum. Some of these aspects were then studied in greater detail.

The effect of contact time

Pre-equilibrated 2.4 mol dm^{-3} hydrochloric acid solutions containing 6×10^{-3} mol dm^{-2} platinum(II) and tin(II) in a molar ratio Sn:Pt of 5:1, were shaken with a 40% MIBK/hexane (v/v) mixture for 2—20 min. Table 1 shows that the extraction process is relatively rapid, so that for a contact time in excess of 5 min, the percentages of platinum and tin extracted remains essentially constant. An extraction time of 10 min was arbitrarily chosen for all subsequent experiments unless otherwise stated.

The effect of the Sn(II):Pt(II) ratio

As a consequence of the preliminary observations, the extraction of only tin(II) chloride was first examined as a function of the initial acid concentra-

TABLE 1

Variation of % Pt extracted as a function of contact time (20 min pre-equilibration, 2.4 mol dm^{-3} HCl, R = 5:1)

Time (min)	2	4	6	8	10	15	20
Pt (%)	71	69	68	68	68	68	68

tion and the organic phase composition. Figure 1 shows some results in which the percentage of tin (as percent of the initial amount in the aqueous phase) is plotted as a function of the organic phase composition for various acid concentrations. Significant amounts of tin are extracted, particularly at higher acid concentrations with organic phases tending to neat MIBK. This observation is expected to render interpretation of possible platinum/trichlorotin complex stoichiometry in the organic phase difficult.

However, the non-extractability of $PtCl_4^{2-}$ in the absence of tin(II) chloride into even pure MIBK, is in sharp contrast to the observation that in the presence of relatively small amounts of tin(II) chloride, significant amounts of platinum become extractable. Figure 2 shows the amount of platinum

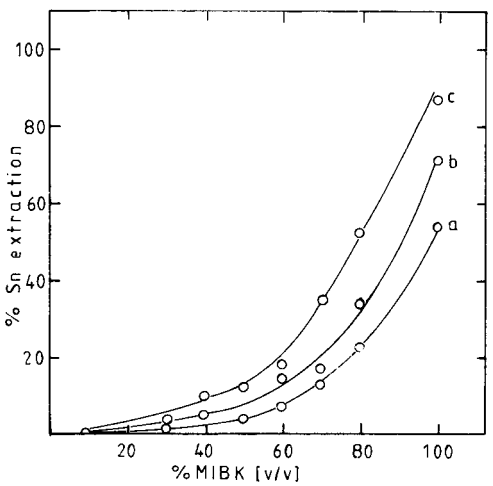

Fig. 1. The extraction of tin(II) chloride from (a) 1.4, (b) 2.4 and (c) 3.4 mol dm^{-3} HCl as a function of volume percent MIBK in hexane.

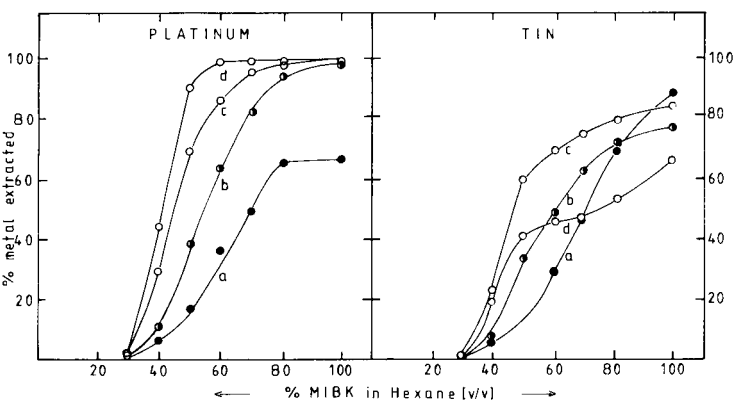

Fig. 2. The % Pt and % Sn extracted from 1.4 mol dm^{-3} HCl solutions as a function of organic phase composition at molar Sn(II):Pt(II) ratios of (a) 2:1, (b) 4:1, (c) 5:1 and (d) 10:1. (Initial $[Pt^{2+}] = 6 \times 10^{-3}$ mol dm^{-3}.)

extracted as a function of the organic phase composition at various values of R from 1.4 mol dm^{-3} hydrochloric acid (qualitatively similar trends were obtained for initial acid concentrations of 2.4 and 3.4 mol dm^{-3}). The large increase in the amount of platinum so extracted is accompanied by an equally significant increase in the amount of co-extracted tin (compare Fig. 1), which must clearly be associated with the platinum complex species in the organic phase. Inspection of Fig. 2 shows that the general trend for the tin co-extracted depends on the initial value of R, so that at $R = 10$ there is a noteworthy difference in the amount of tin extracted compared to solutions with $R \leqslant 5$.

The significance of the initial Sn:Pt ratio to the extraction of platinum may further be emphasized by a plot of the percentage of platinum extracted as a function of R (Fig. 3). For organic phases consisting of 40—60% MIBK/hexane mixtures, a definite increase in extraction of platinum was observed for R in the range 4—6, the maximum increase occurring at $R \approx 5$. This suggests that the extracted platinum-trichlorotin species may have a preferred stoichiometry of 5:1 with respect to the Sn:Pt ratio. On the basis of such preferential extraction of platinum complex species containing tin in the molar ratio of 5 Sn:1 Pt, the trends in the amount of tin extracted in Fig. 2 may be explained. Figure 2 shows that the percentage of tin extracted from solutions with R of 2, 4 and 5, steadily increases as the organic phase compositions increases from 40 to 80% MIBK in hexane, as does the percentage of platinum extracted. For solutions with $R = 10$, however, the extraction of tin levels off around the 50% mark, with corresponding quantitative extraction of platinum. As the organic phase becomes even richer in MIBK, the amount of tin extracted again increases gradually. This further increase in extraction of tin is reminiscent of the general trends observed in Fig. 1, and

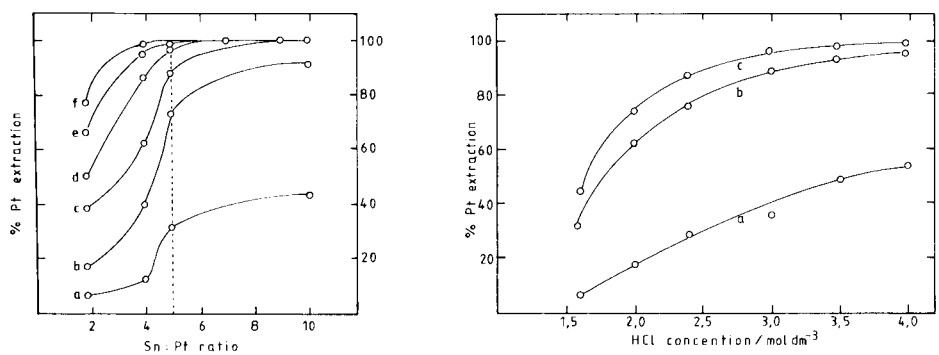

Fig. 3. The % Pt extracted as a function of the initial value of R at 1.4 mol dm^{-3} HCl and with MIBK concentrations of (a) 40%, (b) 50%, (c) 60%, (d) 70%, (e) 80% and (f) 100% (v/v). There is a discontinuity of trend for curves (a), (b) and (c) at $R = 5$.

Fig. 4. The effect of the initial HCl concentration on the % Pt extracted under conditions of deliberately poor extraction for values of R of (a) 2, (b) 5 and (c) 10. (Organic phase 40% (v/v) MIBK in hexane.)

may thus be ascribed to tin not associated with platinum, which tin is co-extracted with any platinum complex species (results were similar for solutions with 2.4 and 3.4 mol dm^{-3} hydrochloric acid initially).

If it is assumed that whenever possible, the extracted platinum complex species has associated with it five mole-equivalents of tin, and if allowance is made for some inevitable co-extraction of tin (as in Fig. 1), then it is possible to estimate the expected Sn:Pt ratio, R_{calc}, in the organic phase. Table 2 lists a comparison between the calculated and observed ratios (obtained from analysis of the organic phase).

The general agreement between R_{calc} and R_{obs} is remarkable, considering the crude method of calculating R_{calc} (i.e., ignoring any possible synergic effects, and errors introduced by oxidation of tin(II) as well as other experimental errors).

Thus, it seems reasonable to postulate that the platinum is preferentially extracted as the trigonal bipyramidal $[Pt(SnCl_3)_5]^{3-}$ anion, although other anionic species containing fewer $SnCl_3^-$ moieties, are evidently also extractable. Although no detailed information about the distribution of complex platinum-trichlorotin species is available, synthetic studies [14], as well as a recent multinuclear n.m.r. investigation [15], indicate that red solutions containing Pt(II) and Sn(II) chlorides in 3 mol dm^{-3} hydrochloric acid, appear to consist of a mixture of predominantly red $[Pt(SnCl_3)_5]^{3-}$ and yellow $[PtCl_2(SnCl_3)_2]^{2-}$ anions.

The effect of the hydrochloric acid concentration

Preliminary experiments showed that the hydrochloric acid concentration had an important influence on the amount of platinum extractable in the presence of a given amount of tin(II) chloride. Thus for acid concentrations less than about 0.5 mol dm^{-3}, extensive hydrolysis of the chloro(trichlorostannato)platinum(II) species occurs [16], so that less platinum is extracted. High hydrochloric acid concentrations favour the extraction of platinum,

TABLE 2

Comparison of the observed and calculated Sn:Pt ratio in the organic phase for various initial HCl concentrations and an initial Sn:Pt ratio of 10:1

MIBK (%)	1.4 mol dm^{-3} HCl		2.4 mol dm^{-3} HCl		3.4 mol dm^{-3} HCl	
	R_{obs}	R_{calc}[a]	R_{obs}	R_{calc}[a]	R_{obs}	R_{calc}[a]
50	5.37	5.02	4.95	5.01	5.23	5.03
60	5.47	5.04	5.13	5.02	5.27	5.05
70	5.80	5.11	5.75	5.13	6.24	5.45
80	6.46	5.34	6.77	5.60	7.10	6.11
100	8.01	6.65	8.95	7.85	9.65	9.08

[a] R_{calc} based on the amount of Pt extracted, and the assumption that, if possible, the ion extracted is $[Pt(SnCl_3)_5]^{3-}$ (see text).

but if the acidity exceeds 5 mol dm^{-3}, then the MIBK becomes considerably more soluble in the aqueous phase, resulting in undesirable phase changes as well as excessive atomic absorption signal enhancements, rendering accurate results impossible. Furthermore, at high acidity, the rate of oxidation of tin(II) chloride by unavoidable traces of dissolved oxygen increases in proportion to $([Sn^{2+}][H_3O^+])^{1/2}$ [17]. For these reasons, this study was limited to 1.0—4.5 mol dm^{-3} hydrochloric acid.

Figure 4 shows the effect of hydrochloric acid concentration on the partitioning of platinum between the aqueous and organic phases under deliberately chosen conditions of poor extraction. Evidently, the higher acidities favour the transfer of platinum into the organic phase. This trend may be understood in terms of the known partition behaviour of hydrochloric acid in the water/HCl/MIBK system as described in detail by Widmer [18]. Thus, the concentration of the solvated HCl ion-pair in the organic phase increases with the concentration of HCl in the aqueous phase. Consequently, one may expect a larger amount of the anionic chloro(trichlorostannato)platinum(II) species to be exchangeable for chloride ions in the organic phase according to the general scheme

$$[PtL_nCl_{4-n}]^{2-} + \overline{2(MIBK{-}H^+)Cl^-} \rightleftharpoons \overline{[PtL_nCl_{4-n}]^{2-}(MIBK{-}H^+)_2} + 2Cl^-$$

(for $n = 1$—4)

$$[PtL_5]^{3-} + \overline{3(MIBK{-}H^+)Cl^-} \rightleftharpoons \overline{[PtL_5]^{3-}(MIBK{-}H^+)_3} + 3Cl^-$$

where $L = SnCl_3^-$ and the bar denotes ion-pair formation in the organic phase.

The overall effect of the concentration of hydrochloric acid must be considered in terms of the H_3O^+ and Cl^- ions. According to the proposed scheme, higher H_3O^+ concentrations should favour the extraction of chloro(trichlorostannato)platinum(II) species, while higher Cl^- concentrations should hinder the transfer of platinum to the organic phase. These expectations were confirmed experimentally as shown in Fig. 5. It is clear that under a given, com-

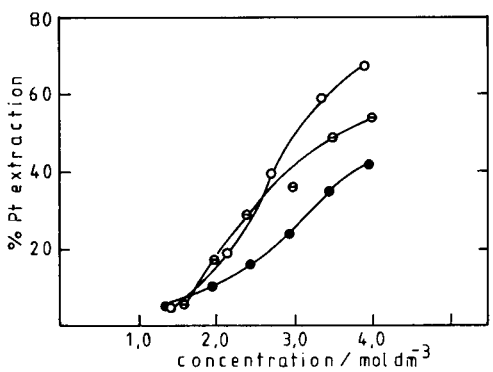

Fig. 5. The effects of H_3O^+ and Cl^- ions on the amount of Pt extracted from solutions of Sn:Pt ratio 2:1: (○) effect of H_3O^+ concentration at fixed $[Cl^-] = 1.4$ mol dm^{-3}; (⊖) effect of HCl concentration; (●) effect of Cl^- concentration at fixed $[H^+] = 1.4$ mol dm^{-3}.

parable set of conditions, the relative amount of platinum extracted increases in the order $[Cl^-] < [HCl] < [H^+]$, in accordance with mechanism of extraction postulated above.

The relative value of R appears to be significant in such comparisons, because at $R \geqslant 5$ only a marginal difference exists between the effect of increased hydrochloric acid concentration and the effect of increasing H_3O^+ concentration (added as perchloric acid) for a fixed chloride concentration. At lower values of R, differences are more marked. For a fixed H_3O^+ concentration of 1.4 mol dm^{-3}, increasing the chloride concentration (added as ammonium chloride) still results in more platinum being extracted, although to a lesser extent than for corresponding increases of hydrochloric acid or H_3O^+ concentrations. This suggests marked hydrophobicity of the pentakis-(trichlorostannato)platinum(II) ion, which is probably the predominant species extracted given sufficient tin(II) chloride. The rather unusual trigonal bipyramidal geometry of this anion, and its high relative charge and size must all result in much more favourable solvation by MIBK in the organic phase than in the case of the chloride, thus providing the driving force for this extraction of platinum. The favourable solvation of the $[Pt(SnCl_3)_5]^{3-}$ and possibly $[Pt(SnCl_3)_nCl_{4-n}]^{2-}$ ($n \leqslant 4$) anions in the organic phase is evidently the dominant factor, rendering small changes in hydrochloric acid concentration of little significance, particularly for MIBK-rich phases. Platinum may thus be quantitatively extracted from aqueous solutions which are $\geqslant 1.0$ mol dm^{-3} in hydrochloric acid by using pure MIBK in the presence of sufficient tin(II) chloride.

The effect of the formal oxidation state of platinum and a preliminary interference study

In the presence of sufficient tin(II) chloride, platinum may be extracted irrespective of its formal oxidation state (II or IV). Presumably any Pt(IV) is reduced by tin(II) rapidly during the initial equilibration period allowed, followed by complex formation. Undoubtedly, in the present system, the platinum exists in the formally divalent state on extraction. Thus, in principle, for $R \geqslant 6$, it is possible to extract $PtCl_4^{2-}$ or $PtCl_6^{2-}$ quantitatively into a pure MIBK phase.

The utility of any liquid—liquid extraction scheme depends on its selectivity for a desired metal species. The distribution of various transition metals between dilute ($\leqslant 5$ mol dm^{-3}) hydrochloric acid and MIBK has been previously studied [19, 20]. In the present study, the two likely sources of interference are redox processes between various metal species and tin(II), and partial or complete co-extraction of other metals. Accordingly, a preliminary interference study was conducted by extracting platinum(II) in the presence of various transition metals likely to be associated with platinum, excluding other platinum group metals such as palladium and rhodium. Although iron(III) would be expected to co-extract into the MIBK phase at relatively high acidities (>4 mol dm^{-3} HCl), Ni(II), Co(II/III) and Cu(II)

TABLE 3

The effect of base metals on the extraction of platinum from 1.4 mol dm^{-3} HCl, with R = 10:1 and 6 × 10^{-3} mol dm^{-3} metal ion for various organic phase compositions

MIBK (%)	Metal extracted (%)				
	Pt	Co	Ni	Fe	Cu
50	91	0	0	0	0
60	—	0	0	0	0
70	95	0	0	0	≈2
80	98	0	0	0	≈8
100	100	0	0	0	≈35

should not co-extract into a MIBK-rich phase at low acidities. Table 3 shows some data obtained for the extraction, in the presence of tin(II), of platinum and equimolar amounts of Fe(III), Co(II), Ni(II) and Cu(II).

It is evident that the amount of platinum extracted is essentially unaffected by the presence of the base metals. No cobalt, nickel or iron was co-extracted, but a significant amount of copper does enter the pure MIBK phase. Clearly, the reduction of iron(III) by tin(II) prevents extraction of iron and large amounts of iron(III) would interfere seriously by consuming the tin(II) chloride. According to Boswell and Brooks [19] and Wickbold [20], copper is extractable into pure MIBK only from ⩾4 mol dm^{-3} hydrochloric acid to an extent of 3—6%. In the present system, about 35% of the copper co-extracted with the platinum from 1.4 mol dm^{-3} hydrochloric acid with Sn(II):Pt(II) = 10:1. The reason for this discrepancy is not clear; there may be some synergic effect from the presence of tin(II) or platinum(II) chloride, or Cu(II) may be partially reduced to Cu(I). The possibility of inter-platinum group metal separations based on a tin(II) chloride scheme is under investigation. To date, platinum has been separated easily from palladium and ruthenium.

We are grateful to the University of Cape Town and the Council for Scientific and Industrial Research for generous financial support. One of us (N.A.) gratefully acknowledges a fellowship from the Council for Mineral Technology.

REFERENCES

1 L. Wöhler, Chem. Ztg., 31 (1907) 938.
2 J. H. Nelson and N. W. Alcock, Inorg. Chem., 21 (1982) 1196.
3 A. Albinati, R. Nägeli, H. Rüegger and P. S. Pregosin, Angew. Chem. Int. Ed. Engl., 21 (1982) 284.
4 E. B. Sandell, Colorimetric Determinations of Traces of Metals, Interscience, New York, 1944, p. 721.
5 G. H. Ayres and A. S. Meyer, J. Am. Chem. Soc., 77 (1955) 2671.

6 P. G. Antonov, Yu. N. Kukushkin, A. N. Shan'ko and L. V. Konovalov, J. Gen. Chem. USSR, 46(2) (1976) 412.
7 A. Diamantatos and A. A. Verbeek, Anal. Chim. Acta, 91 (1977) 287.
8 E. W. Berg and W. L. Senn Jr., Anal. Chim. Acta, 19 (1958) 12.
9 M. Mojski, Talanta, 27 (1980) 7.
10 K. R. Koch and J. E. Yates, Anal. Chim. Acta, 147 (1983) 235.
11 M. A. Khattak and R. J. Magee, Talanta, 12 (1965) 733.
12 A. I. Gorbanev, V. P. Sergeev, B. E. Dzevitskii and V. B. Margulis, Proc. Int. Solv. Extr. Conf., Lyon, France, Vol. (1) (1974) 19.
13 K. G. Moodley and M. J. Nicol, J. Chem. Soc., Dalton Trans., (1977) 239.
14 J. F. Young, R. D. Gillard and G. Wilkinson, J. Chem. Soc., (1964) 5176.
15 J. H. Nelson, V. Cooper and R. W. Rudolph, Inorg. Nucl. Chem. Lett., 16 (1980) 263.
16 Yu. N. Kukushkin, P. G. Antonov and K. I. Dubonos, Russ. J. Inorg. Chem., 21(9) (1976) 1348.
17 S. J. Lachman and F. C. Tompkins, Trans. Faraday Soc., 40 (1944) 136.
18 H. M. Widmer, J. Phys. Chem., 74(17) (1970) 3251.
19 C. R. Boswell and R. R. Brooks, Mikrochim. Acta, 5 (1965) 814.
20 R. Wickbold, Z. Anal. Chem., 244 (1969) 372.

Analytica Chimica Acta, 162 (1984) 357—362
Elsevier Science Publishers B.V., Amsterdam — Printed in The Netherlands

Short Communication

BISQUATERNARY-DRUG MEMBRANE ELECTRODES WITH HIGH SENSITIVITY

VASILE V. COŞOFREŢ[a] and RICHARD P. BUCK*
Department of Chemistry, University of North Carolina, Chapel Hill, NC 27514 (U.S.A.)
(Received 27th March 1984)

Summary. The construction and performance characteristics of ion-selective plastic membrane electrodes for succinylcholine, hexamethonium and decamethonium are described. The electrodes, based on ion-pair complexes with triphenylstilbenyl borate (TPSB), show near-Nernstian responses over the range 10^{-2}—10^{-6} M or less, with very low limits of detection at around 10^{-7} M. The responses are not affected by pH in the range 2—10. The selectivity relative to some inorganic ions, amino acids, neurotransmitters, drugs and various drug excipients is reported.

Many ion-selective membrane electrodes sensitive to various drugs have been reported [1, 2], but not all of them provide acceptable sensitivity and selectivity for the drug of interest. Among them, various electrodes sensitive to quaternary ammonium ions show relatively high sensitivity [3—7]. This communication deals with the construction, characterization and analytical evaluation of ion-selective membrane electrodes highly sensitive to bisquaternary compounds of pharmaceutical interest, such as succinylcholine, hexamethonium and decamethonium. It is well known that the number of methylene groups in the central chain between the two cationic heads in α,ω-bis(trimethylammonium)alkanes has a significant effect on pharmacological activity [8]. Hexamethonium (six methylene groups) is a very effective ganglionic blocking agent, while decamethonium (ten methylene groups) is one of the most potent curare-like agents known. Succinylcholine, a decamethylene compound with ester groups in the chain, has proven to be a potent neuromuscular blocking agent and has become prominent as a short-acting muscle relaxant and curarizing agent.

Here, a new ion-pairing agent, triphenylstilbenyl borate (TPSB) is reported. It has great selectivity for the above-mentioned bisquaternary drugs, relative to amino acids, neurotransmitters, drug excipients and common inorganic cations, and provides very low limits of detection. The potentiometric procedure described permits the determination of these drugs at levels of $\geqslant 0.3\ \mu g\ ml^{-1}$ in both pure and pharmaceutical samples.

[a] On leave from Institute of Chemical and Pharmaceutical Research, Bucharest, Romania.

0003-2670/84/$03.00

Experimental

Reagents and materials. All reagents, except TPSB, were of analytical-reagent grade and were used as received. Succinylcholine chloride, hexamethonium bromide and decamethonium bromide were purchased from Sigma (St. Louis, MO). 2-Nitrophenyloctyl ether (Fluka) and poly(vinyl chloride) (Aldrich) were used. Triphenylstilbenyl borate (potassium salt) was kindly donated by Dr. D. Daniels (Kodak, Rochester, MY). Injectable succinylcholine chloride solutions (USP quality) were purchased from a local drugstore. All solutions were prepared with distilled water in a Tris—HCl buffer of pH 7.0. Succinylcholine solutions contained 0.05% (w/v) methyl-*p*-hydroxybenzoate as stabilizer.

Electrode preparation and handling. The membrane electrodes were constructed as described previously [9] except that the electroactive material used was TPSB. The internal reference solutions were 10^{-3} M of the respective drug at pH 7.0 (0.1 M Tris—HCl buffer). The TPSB in the polymer membranes was converted to the bisquaternary-drug form by soaking the electrodes in the appropriate 10^{-2} M drug for 24 h. When not in use, the electrodes were stored in the same solution as the internal solution.

E.m.f. measurements. All electrode potentials were measured vs. an Orion 91-01 double-junction reference electrode with 10% (w/v) sodium sulfate solution in the outer compartment, using an Orion digital pH/mV meter (Model 701A). Potentials were recorded when stable readings were obtained (normally within 15 s). The pH values were measured with an Orion 91-02 glass combination electrode.

Direct potentiometric measurement of bisquaternary-drugs in the microgram range. Immerse the appropriate bisquaternary-drug electrode and the reference electrode in the aqueous sample solution (25.0 ml) at pH 7.0 (0.1 M Tris-HCl buffer). Allow them to equilibrate by stirring, and record the e.m.f. value. Check the figure obtained by the standard addition method. For this purpose, add 1.0 ml of a 10^{-4} M standard solution of the bisquaternary drug. Record the change in mV reading (accuracy ±0.1 mV) and use this reading to calculate the concentration of the drug.

Direct potentiometric assay of succinylcholine in injectable solutions. Pipet 1.0 ml of injectable solution from one vial into a 250-ml volumetric flask. Add 12.5 ml of 1% (w/v) methyl-*p*-hydroxybenzoate and dilute to the mark with 0.1 M Tris—HCl buffer solution of pH 7.0 (solution A). Pipet a 50-ml aliquot into a 100-ml beaker. Immerse the relevant electrodes, stir and take the steady e.m.f. reading. To check the value obtained, add 5.0 ml of a 10^{-2} M standard solution of succinylcholine chloride, record the change in reading as above, and use it to calculate the concentration of succinylcholine. The result for succinylcholine chloride is obtained from the equation: succinylcholine chloride (mg ml^{-1} of vial solution) = $C_s \times 9032.5 \times (1.10 \times 10^{\Delta E/S} - 1)^{-1}$, where C_s is the concentration of the standard solution, ΔE is the change in mV reading caused by the standard addition, and S is the electrode slope, which must be evaluated very accurately before each series of measurements.

Results and discussion

Membrane material. It is well known that bisquaternary-, as well as monoquaternary compounds and various amino derivatives, react with tetraphenylborate and similar compounds to form stable ion-pair complexes. Triphenylstilbenyl borate (TPSB) was found to be very suitable as an ion-pairing agent for bisquaternary drugs with which it forms very insoluble compounds; very low limits of detection are thus obtained. The TPSB complexes were prepared in situ, by soaking the TPSB (potassium salt)/PVC membranes in the appropriate bisquaternary solution. Of the plasticizers tested, 2-nitrophenyloctyl ether (NPOE), dioctylphthalate, di-iso-butylphthalate, nitrobenzene, 2-nitro-*p*-cymene, NPOE showed the best behavior in terms of response time and reproducibility. The membrane compositions were 3.2% (w/w) TPSB, 64.5% (w/w) NPOE and 32.3% (w/w) PVC.

Calibration data. The critical response characteristics of the TPSB-based bisquaternary-drug membrane electrodes are summarized in Table 1. Calibrations were done at constant pH and ionic strength, provided by using Tris—HCl buffer, pH 7.0. The highest concentrations of bisquaternary drugs used for calibrations were 10^{-2} M. All the electrodes can be used in the concentration range 10^{-2}—10^{-7} M, a linear relationship E(mV) vs. concentration being obtained down to 10^{-6} M. Detection limits of $\leqslant 10^{-7}$ M indicate the feasibility of using these electrodes to determine traces of bisquaternary drugs in various samples. The very similar values of the detection limits indicate that TPSB forms complexes of much the same solubility with the various bisquaternary derivatives. The calibration curves for the individual electrodes were found to be reproducible from day to day provided that the electrodes were stored in the appropriate bisquaternary-drug solution between measurements.

Effect of pH. To study the pH dependence of the electrode potentials, the pH values of the initial solutions were adjusted carefully with sodium hydroxide and/or hydrochloric acid solutions. The potentials were almost independent of pH in the range 2.0—10.5, even for the succinylcholine

TABLE 1

Response characteristics for bisquaternary-drug membrane electrodes

Parameter	Succinylcholine electrode	Hexamethonium electrode	Decamethonium electrode
Slope[a] (mV/log *a*)	29.05 ± 0.35	28.03 ± 0.44	29.45 ± 0.29
Intercept (mV)	157 ± 1.8[b]	147 ± 2.2	152 ± 2.1
Linear range (M)	10^{-2}—10^{-6}	10^{-2}—2.5×10^{-7}	10^{-2}—2.5×10^{-7}
Usable range (M)	10^{-2}—10^{-7}	10^{-2}—5.0×10^{-8}	10^{-2}—10^{-7}
Detection limit (M)	1.58×10^{-7}	3.16×10^{-8}	1.12×10^{-7}
(ng ml^{-1})	46	6.4	29

[a]Average values calculated for 10^{-3}—10^{-5} M range with standard deviation of average slope value for multiple calibration (5—7).
[b]Standard deviation of values recorded during one month.

electrode, when 0.05% (w/v) methyl-*p*-hydroxybenzoate was added to the succinylcholine chloride solutions. In this case, at pH > 10.5, a significant potential decrease was recorded. The decrease was time-dependent and was caused by hydrolysis of succinylcholine to choline; in the absence of any stabilizer, hydrolysis proceeded very quickly at pH > 8.

Selectivity of the electrodes. The interference of various substances on the electrode responses was studied by the mixed solution method and the respective selectivity coefficients, $K_{i,j}^{pot}$, were calculated from the equation

$$K_{i,j}^{pot} = (10^{\Delta E/S} - 1)[Q^{2+}]/[j^{z+}]^{2/z} \quad (1)$$

where ΔE is the change in potential in the presence of interfering ion, j^{z+}; S is the slope of the calibration graph for the bisquaternary primary ion (i), and $[Q^{2+}]$ and $[j^{z+}]$ are the concentrations of the primary and the interfering ions, respectively, at the same pH and ionic strength. The selectivity coefficients obtained are listed in Table 2. The results show that the decamethonium electrode has a higher degree of selectivity than either the hexamethonium or succinylcholine electrode. The greater selectivity of the decamethonium electrode over the hexamethonium electrode is caused by decamethonium having four methylene groups more than hexamethonium. All the TPSB-based electrodes exhibit negligible interferences from common inorganic cations or from some amino acids and neurotransmitters. Glucose, lactose, corn starch, maltose, mannitol and sugars do not interfere. Choline, acetylcholine and quaternary ammonium compounds interfere in the electrode responses; as expected by inspection of the bisquaternary-drug structures, the greatest interference was observed in the case of the succinylcholine electrode.

TABLE 2

Selectivity coefficients for the TPSB-based bisquaternary membrane electrodes

Interfering species, j	$[Q^{2+}]/[j^{z+}]$	Selectivity coefficient		
		Succinylcholine	Hexamethonium	Decamethonium
K^+, Na^+, Ca^{2+}, Mg^{2+}	10^{-4}	$<10^{-4}$	$<10^{-4}$	$<10^{-4}$
Succinylcholine	10^{-3}	(1)	3.6×10^{-2}	2.9×10^{-3}
Hexamethonium	10^{-3}	3.3×10^{-1}	(1)	1.4×10^{-2}
Decamethonium	10^{-3}	7.3	1.7	(1)
Pentamethonium	10^{-3}	2.4×10^{-1}	5.4×10^{-2}	7.3×10^{-3}
Arginine	10^{-4}	8.2×10^{-4}	2.7×10^{-4}	1.5×10^{-4}
L-Histidine	10^{-4}	4.8×10^{-4}	4.6×10^{-4}	4.0×10^{-4}
Isoniazid	10^{-4}	6.5×10^{-4}	6.5×10^{-4}	4.2×10^{-4}
L-Epinephrine	2×10^{-2}	1.5×10^{-2}	3.2×10^{-2}	1.0×10^{-2}
γ-Aminobutyric acid	10^{-4}	1.7×10^{-4}	8.1×10^{-3}	1.3×10^{-3}
Dopamine	10^{-4}	5.7×10^{-3}	2.5×10^{-3}	4.0×10^{-4}
Choline	10^{-3}	4.7	1.68	7.6×10^{-1}
Carbamylcholine	10^{-3}	1.2	5.6×10^{-1}	2.4×10^{-1}
Acetylcholine	10^{-3}	77.8	15.4	1.62

TABLE 3

Determination of the bisquaternary drugs in the microgram range in pure solutions by the standard addition method[a]

Drug	Range taken (μg)	Range of concentration of sample solution before std. addn. (μg ml^{-1})	Recovery[b] (%)
Succinylcholine chloride	7.2—18.0	0.288—0.720	100.4 ± 1.9
Hexamethonium	7.2—18.0	0.288—0.720	99.8 ± 2.0
Decamethonium	8.4—21.0	0.336—0.840	99.5 ± 1.6

[a]See Experimental. [b]Mean recovery for 4 determinations over the specified range with standard deviation.

Response times. The electrodes provided stable e.m.f. readings within 15 s in the linear ranges of the respective calibration curves. In very dilute solutions ($\geqslant 10^{-7}$ M), response times were 1—2 min.

Analytical applications. All these TPSB-based electrodes proved useful in the determination of the bisquaternary drugs when the standard addition method was used. Results for measurements of the pure drug solutions at <1.0 μg ml^{-1} are shown in Table 3. In all cases, the standard deviation was $<2.0\%$. Succinylcholine was also determined in injectable solutions with good precision and an average recovery of 100.5% (Table 4).

Conclusions. The bisquaternary-drug membrane electrodes can be applied successfully for the potentiometric determination of the respective drugs down to 0.5 μg ml^{-1} concentrations without prior treatment if the standard addition method is used. When the official method [10] is used, about 2 h is required for assay. Here, an electrode assay can be accomplished within a maximum of 15 min.

TABLE 4

Determination of succinylcholine chloride in injectable solutions[a] with the TPSB-based succinylcholine membrane electrode by the standard addition method[b]

Product	Sample	Recovery (% of nominal content)[c]
Anectine	1	100.7 ± 0.84
	2	100.9 ± 0.55
	3	100.5 ± 0.71
	4	99.9 ± 0.99
	5	100.5 ± 1.00

[a]A sterile solution for intravenous injection (10-ml multiple dose vial, 20 mg ml^{-1}, Burroughs Welcome Co.) made isotonic with sodium chloride; pH adjusted with hydrochloric acid and preserved with 0.1% methylparaben. [b]See Experimental. [c]All values are average of five determinations with standard deviation.

REFERENCES

1 V. V. Coşofreţ and R. P. Buck, Ion Select. Electrode Rev., 6 (1984) 59.
2 V. V. Coşofreţ, Ion Select. Electrode Rev., 2 (1980) 159; Membrane Electrodes in Drug-Substances Analysis, Pergamon Press, Oxford, 1982.
3 R. Scholer and W. Simon, Helv. Chim. Acta, 55 (1972) 1801.
4 S. S. Davies and O. Olejnik, J. Pharm. Pharmacol., 31 (1979) 19; Anal. Chim. Acta, 132 (1981) 51.
5 C. R. Martin and H. Freiser, Anal. Chem., 53 (1981) 902.
6 L. Cunningham and H. Freiser, Anal. Chim. Acta, 132 (1981) 43.
7 C. J. Coetzee and A. J. Basson, Anal. Chim. Acta, 126 (1981) 217.
8 J. B. Stenlake, in Burger's Medicinal Chemistry, M. E. Wolff, (Ed.), 4th edn., Part III, Ch. 46, Wiley, New York, 1981.
9 V. V. Coşofreţ and R. P. Buck, J. Pharm. Biomed. Anal., (1984) in press; Analyst (London) (1984) in press.
10 United States Pharmacopeia, XX Rev., U.S. Pharmacopeial Convention Inc., Rockville, MD, 1980.

Analytica Chimica Acta, 162 (1984) 363—367
Elsevier Science Publishers B.V., Amsterdam — Printed in The Netherlands

Short Communication

HOMOGENEOUS ENZYME-LINKED ASSAYS MEDIATED BY ENZYME ANTIBODIES; A NEW APPROACH TO ELECTRODE-BASED IMMUNOASSAYS

SUSAN B. BRONTMAN and M. E. MEYERHOFF*
Department of Chemistry, The University of Michigan, Ann Arbor, MI 48109 (U.S.A.)
(Received 30th March 1984)

Summary. A new homogeneous enzyme—immunoassay system is described. The assay employs an ammonia-liberating enzyme covalently coupled to protein antigens along with two antibodies. An anti-enzyme antibody inhibits the enzyme. However, an antibody selective for the antigen reverses the inhibition process. When samples containing free antigen are present in the assay mixture, there is competition for anti-antigen antibody sites and protection against the anti-enzyme antibodies is diminished. The extent of the enzymatic reaction is monitored with an ammonium ion-selective electrode. Preliminary data demonstrating the feasibility of this approach for human serum albumin are presented.

The development of novel non-isotopic competitive binding immunoassays for the detection of antigens in physiological fluids has become an important area of bioanalytical research. Such assays offer attractive alternatives to the more traditional radioimmunoassay methods. Enzymes have emerged recently as effective labels for immunoassay methods [1—3]. This communication describes a new homogeneous enzyme immunoassay arrangement.

The proposed assay (see Fig. 1) utilizes the enzyme, adenosine deaminase (ADA), which catalyzes the hydrolysis of adenosine to inosine and ammonia [4]. The enzyme is covalently coupled to an analyte protein. Also, two antibody reagents are required, one selective for the protein to be measured and a second one directed toward the active site of the enzyme. When antibodies selective for the antigen are first added to the enzyme conjugate, these antibodies partially protect the enzyme from inhibition when the enzyme antibodies are added, thereby increasing the catalytic activity observed. When samples containing free antigen are present in the assay mixture, a competition for the anti-antigen antibody sites occurs and protection against the anti-enzyme antibodies is diminished. The extent of the enzymatic reaction can be monitored with an ammonium ion-selective electrode.

The feasibility of this new assay approach is demonstrated by developing an assay for the model protein, human serum albumin (HSA). The factors which limit sensitivity and speed of the assay are discussed as are prospects for improving the overall quantitative characteristics of the technique.

0003-2670/84/$03.00

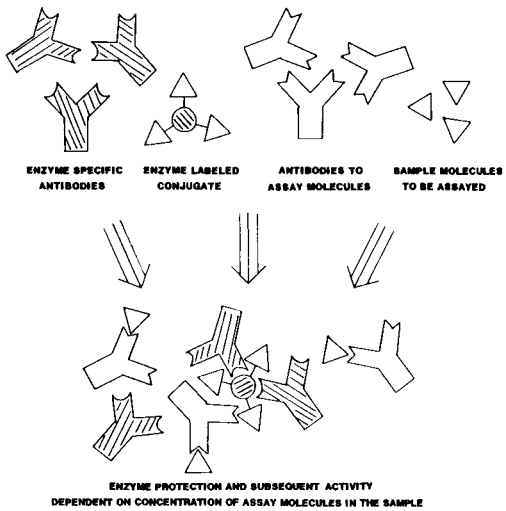

Fig. 1. Representation of reagents used and processes that take place in the proposed assay.

Experimental

Apparatus. Potentiometric measurements were made with a tubular flow-through ammonium ion-selective electrode based on nonactin [5] in an autoatic continuous flow arrangement. Fractions obtained from size-exclusion chromatography of ADA—HSA conjugates were collected with an ISCO model 1850 fraction collector with continuous photometric monitoring of the effluent. All incubations for the enzyme immunoassays were performed in 3-ml borosilicate glass tubes.

Reagents. Reagents obtained from Sigma Chemical Company were adenosine deaminase (ADA) type III from calf intestinal mucosa, human serum albumin (HSA) fraction V, adenosine, tris(hydroxymethyl)aminomethane (Tris), Sephadex G-100, and glutaraldehyde (grade I, aqueous 25% solution). All other chemicals were reagent grade. Standards and working buffer solutions were prepared with distilled-deionized water.

A 0.01 M Tris/sulfuric acid buffer, pH 7.5, containing 0.5 mM ethylenediaminetetraacetic acid [4] was used as the working buffer. A 0.1 M phosphate buffer, pH 7.0, was used when preparing ADA—HSA conjugates via the glutaraldehyde cross-linking reaction.

Antisera were prepared and provided by the Unit for Laboratory Animal Medicine at the University of Michigan. For working antibody reagents, each antiserum lot was subjected to an ammonium sulfate fractionation to isolate the γ-globulin components of the serum [6].

Preparation and purification of ADA—HSA conjugates. The ADA was cross-linked to HSA by a glutaraldehyde reaction [7]. The conjugate was prepared by mixing 2 mg of HSA and 0.20 mg of ADA in 2 ml of phosphate buffer. The protein solution was dialyzed extensively against three 1-l

volumes of the phosphate buffer. The solutions were then placed in a glass test tube and gently stirred as 150 μl of 1% glutaraldehyde was added in 50-μl increments over the first 2 h of the reaction. After 4 h, the reaction mixture was centrifuged at 2200 *g* for 15 min at 4° C. The supernatant solutions were then dialyzed against the Tris working buffer. These conjugates were then partly purified as follows: a fraction of the conjugate was passed through a Sephadex G-100 size-exclusion column and the effluent was continuously monitored at 280 nm. As protein began to elute, 0.5-ml fractions were collected.

Determination of relative ADA activity. Aliquots (10 μl) of ADA or ADA—HSA conjugates (from the fractions) were added to 1.49 ml of working buffer in test tubes and 50 μl of 5 mM adenosine solution was added to initiate the reaction. After 15 or 60 min (depending on the absolute activity of the ADA in the sample), 50 μl of 0.02 M silver nitrate was added to the tube to stop the enzymatic reaction. Ammonium ions produced were quantified and corrected for amounts produced in a similar blank reaction.

Only fractions from the size-exclusion column with highest protection characteristics were used in subsequent assays by the proposed method.

Procedure for calibration curves for HSA. Assays were run in triplicate. First, 1.10 ml of working buffer was added to each tube followed by 100 μl of an HSA standard solution and 100 μl of diluted HSA antibody. After 20 min, 100 μl of diluted HSA—ADA conjugate was added and the mixture was incubated at room temperature for another 20 min. Subsequently, 100 μl of the diluted ADA antibody reagent was added and after another 20 min of incubation, 50 μl of adenosine solution was added and silver nitrate was added after 1 h. The ammonium content was determined as described above.

Calibration curves were constructed by arbitrarily assigning the amount of ammonium ions produced from the "protected" enzyme conjugate as 100% activity and that level produced from the inhibited conjugate as 0%.

Results and discussion

The pure ADA used here was inhibited up to a maximum of 72% even in the presence of excess of the anti-ADA antibody preparation. Nearly maximum inhibition (70%) could be achieved using a 1:100 dilution of this antibody. Fractions of the ADA—HSA conjugate most effective for the proposed type of assay were also generally inhibited up to 70% with the same 1:100 dilution of the antibody preparation. Thus, the covalent attachment of HSA to the enzyme apparently does not preclude inhibition of the enzyme by anti-ADA antibodies. None of the ADA—HSA fractions obtained from the size-exclusion procedure exhibited full activity in the presence of anti-HSA antibodies. The ADA—HSA conjugates prepared to date are activated (protected) up to 32% (e.g., from 70% to 38% inhibition) in the presence of anti-HSA antibodies. Despite this rather narrow range of enzyme modulation, the conjugates prepared were useful to demonstrate the principle of the new method.

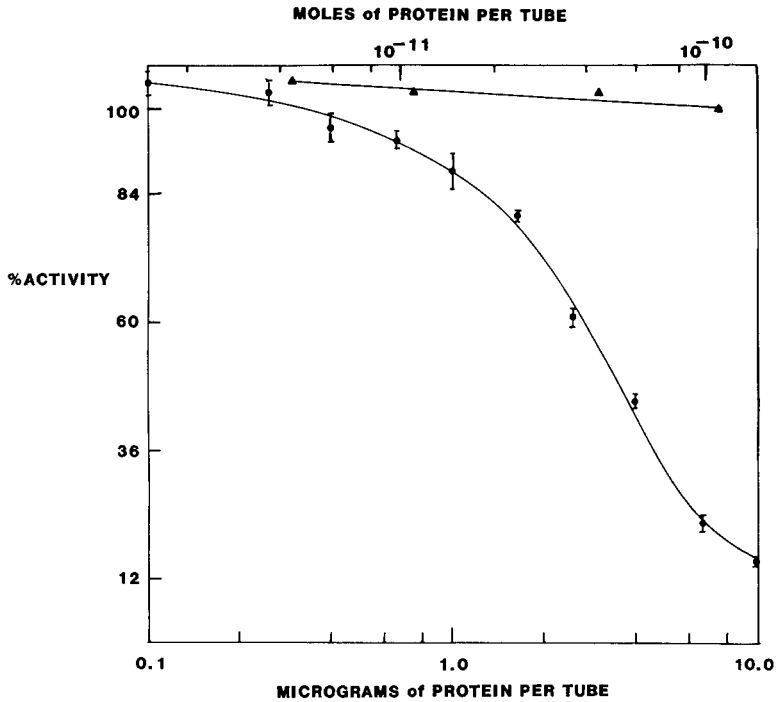

Fig. 2. Calibration curve obtained for detection of free HSA (•); data points shown are average of triplicate measurements with standard deviation. Also shown is the response of the system to varying free myoglobin levels (▲).

Figure 2 shows a typical calibration curve obtained when free HSA concentrations were varied with an ADA—HSA conjugate fraction that can be protected up to 32%. It can be seen that the reproducibility is quite good for triplicate samples; slightly less than 1 μg of HSA protein could be detected, which is similar to the detection limit of another homogeneous enzyme immunoassay [8]. Figure 2 also shows that increasing concentrations of myoglobin did not significantly affect the ability of anti-HSA antibodies to protect the ADA—HSA conjugate.

The use of a new, more controllable cross-linking reagent, *N*-succinimidyl 3-(2-pyridyldithio)propionate [9], may permit detection limits and assay times to be reduced by producing an ADA—HSA conjugate that is more fully protected; work in this direction is currently under way. In addition, size-exclusion chromatography with gels possessing larger fractionation ranges should also aid in obtaining a more suitable conjugate.

Data presented here demonstrate the feasibility of the proposed approach. It is expected to be applicable with other enzymes, other antigens, and other types of detectors. Modifications of the experimental system would be required for clinical samples.

The authors gratefully acknowledge the National Science Foundation for supporting this work (Grant CHE-8118817).

REFERENCES

1 G. B. Wisdom, Clin. Chem., 22 (1976) 1243.
2 S. L. Sharpe, W. M. Cooreman, W. J. Blumme and G. M. Leekeman, Clin. Chem., 22 (1976) 733.
3 A. H. W. M. Schuurs and B. K. Van Weeman, Clin. Chim. Acta, 81 (1977) 1.
4 Biochemica Information I, Boehringer—Mannheim, 1975, p. 24.
5 Y. M. Fraticelli and M. E. Meyerhoff, Anal. Chem., 53 (1981) 992.
6 D. H. Campbell, J. S. Garvey, N. E. Cremer and D. H. Sassdorf, Immunology, W. A. Benjamin, New York, 1964, pp. 118—120.
7 S. Avrameas, Immunochem., 6 (1969) 43.
8 I. Gibbons, C. Skold, G. L. Rowley and E. F. Ullman, Anal. Biochem., 102 (1980) 167.
9 D. Pain and A. Surolia, J. Immunol. Methods, 40 (1981) 219.

Analytica Chimica Acta, 162 (1984) 369—371
Elsevier Science Publishers B.V., Amsterdam — Printed in The Netherlands

Short Communication

GUANIDINIUM-SELECTIVE PVC MEMBRANE ELECTRODES BASED ON CROWN ETHERS

MARIA BOCHEŃSKA and JAN F. BIERNAT*

Institute of Inorganic Chemistry and Technology, Polytechnical University, 80952 Gdańsk (Poland)

(Received 13th October 1983)

Summary. Guanidinium-selective membrane electrodes were constructed with dibenzo-24-crown-8, dibenzo-27-crown-9, tribenzo-27-crown-9 or dibenzo-30-crown-10. The detection limits and selectivity coefficients towards different interfering ions, such as Li^+, Na^+, K^+, NH_4^+, Mg^{2+} and Ca^{2+} were determined. The electrode with dibenzo-27-crown-9 shows linear response over the range 10^{-1}—10^{-4} M, with selectivity coefficients about 10^{-2} for most alkali and alkaline earth metal ions.

Pedersen [1] first reported crystalline complexes of organic molecules such as thiourea with crown ethers. Their nature is complex. The size of the cavity of the crown, and the ability of the crown framework to adapt itself to the shape of the guest molecule, are significant. Hydrogen bonding may also increase the stability of such complexes.

Complexes of the guanidinium ion with crown ethers, in which the guanidinium ion may form six hydrogen bonds with oxygen atoms of the crown, can be very stable. Madan and Cram [2] obtained stable and crystalline complexes of the guanidinium cation with benzo-27-crown-9, tribenzo-27-crown-9 and dibenzo-18-crown-6. Lehn et al. [3, 4] studied the effect of guanidine substitution on the stability of guanidinium complexes with aliphatic hexacarboxyamide-27-crown-9. In the work described here, guanidinium-sensitive membrane electrodes based on crown ethers as the active material were examined. The crown ethers tested were dibenzo-30-crown-10 (1), dibenzo-27-crown-9 (2), tribenzo-27-crown-9 (3) and dibenzo-24-crown-8 (4). Selectivity coefficients of the membrane electrodes towards different interfering ions (Li^+, Na^+, K^+, NH_4^+, Mg^{2+} and Ca^{2+}) were measured. The best and most selective was the electrode with dibenzo-27-crown-9 as the active phase.

Experimental

Crown ethers 1 and 4 were synthesized as described by Pedersen [5]. Compounds 2 and 3 were prepared by the methods of Izatt et al. [6] and Madan and Cram [2], respectively. The ^{1}H-n.m.r. spectra and the mass spectra of all four compounds confirmed their structure and purity; melting points agreed with those previously reported.

0003-2670/84/$03.00

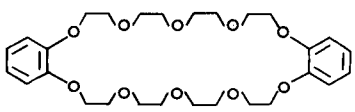

1

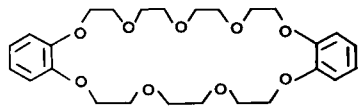

2

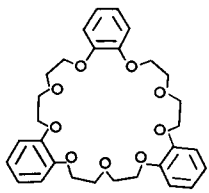

3

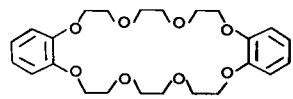

4

The poly(vinyl chloride) membranes were prepared conventionally [7, 8]; their composition was 1:2:0.1 PVC-S-72/plasticizer/active material (by weight). Di-n-butyl phthalate was the best plasticizer tested. Tetrahydrofuran was used as the solvent. The discs obtained (8 mm diameter, 0.5 mm thick) were incorporated into Ag/AgCl electrode bodies, with 10^{-2} M KCl as the internal electrolyte.

A double-junction reference electrode of the ERM-10-00 type (Ag/AgCl, KCl) was used with 0.1 M tetraethylammonium nitrate in the bridge. All potentials were measured at 25 ± 0.1°C using a N517 (MERA ELWRO) pH-meter equipped with a V541 digital voltmeter, which allowed reading to ±0.1 mV.

The detection limits of the electrodes for guanidinium ion were evaluated as recommended by Cammann [8]. Selectivity coefficients, $K_{i,j}^{pot}$, were evaluated by the standard [8, 9] mixed-solution method from potential measurements in solutions containing a fixed amount (10^{-2} M) of cations j: Li^+, Na^+, K^+, NH_4^+, Mg^{2+} and Ca^{2+} and a varying amount of guanidinium ions (10^{-6}—10^{-1} M).

The tolerable pH range was evaluated by measuring the potential in solutions with a fixed (10^{-2} or 10^{-1} M) amount of guanidinium ions at varying pH adjusted by adding small amounts of 1 M hydrochloric acid or tetraethylammonium hydroxide.

Results and discussion

The ion-selective properties of the PVC membrane electrodes based on crowns **1**—**4** were investigated. The selectivity coefficients towards different interfering ions with respect to guanidinium ion are summarized in Table 1. Electrodes in use for over five months were still functional. The e.m.f. readings were nearly constant in the pH range 4—10; at lower pH values, there were irreversible changes in the properties of the electrode membranes.

The selected crown ethers **1**—**4** have different types of cavity, and differ in flexibility and overall electron density of the donating oxygen atoms. The cavity of dibenzo-30-crown-10 (**1**) is quite large compared with the radius

TABLE 1

Selectivity coefficients, slopes, ranges of linear responses and detection limits of guanidinium-selective membrane electrodes with ligands 1—4

Ligand	Selectivity coefficients						Slope mV/pG[a]	Linear range (pG[a])	Detection limit (M)
	Li^+	Na^+	K^+	NH_4^+	Mg^{2+}	Ca^{2+}			
1	5×10^{-2}	1.2×10^{-1}	1	4×10^{-2}	1.3×10^{-1}	1×10^{-1}	51	1—4	10^{-5}
2	1×10^{-2}	2.2×10^{-2}	1×10^{-1}	3×10^{-2}	7.9×10^{-3}	1.8×10^{-2}	50	1—4	10^{-5}
3	3.5×10^{-2}	3.5×10^{-2}	2.8×10^{-1}	7.9×10^{-2}	1.1×10^{-2}	3.1×10^{-2}	51	1—3.5	2×10^{-5}
4	3.1×10^{-2}	1.6×10^{-2}	1.7×10^{-1}	8×10^{-2}	2.8×10^{-2}	5.6×10^{-2}	49	1—3.5	10^{-4}

[a] pG is the negative logarithm of the guanidinium concentration.

of the guanidinium ion and the macrocycle is very flexible. This compound forms a very stable complex with potassium ion, so that the selectivity for the guanidinium ion is bad. The cavity of dibenzo-24-crown-8 (4) is not big enough for the guanidinium ion and the selectivity is again unsatisfactory. The best fit for the guanidinium ion was provided by dibenzo-27-crown-9 (2) and tribenzo-27-crown-9 (3). The electrode based on 2 exhibits the best selectivity. Compound 3 is more rigid than 2; 2 has a slightly larger cavity and a higher overall electron density of oxygen. All these factors are probably decisive for the improved selectivity of the membrane electrode based on dibenzo-27-crown-9.

Financial support of this work by MR-1.11 project is gratefully acknowledged.

REFERENCES

1 C. J. Pedersen, J. Org. Chem., 36 (1971) 1690.
2 K. Madan and D. J. Cram, J. Am. Chem. Soc., 99 (1977) 2564.
3 J. M. Lehn, P. Vierling and R. C. Hayward, J. Chem. Soc. Chem. Commun., (1979) 296.
4 J. M. Lehn, Pure Appl. Chem., 50 (1978) 871.
5 C. J. Pedersen, J. A. Chem. Soc., 89 (1967) 7017.
6 R. M. Izatt, R. E. Terry, D. P. Nelson, Y. Chan, D. J. Eatough, J. S. Bradshaw, L. D. Hansen and J. J. Christensen, J. Am. Chem. Soc., 98 (1976) 7626.
7 J. Petranek and O. Ryba, J. Electroanal. Chem., 44 (1973) 425; Anal. Chim. Acta, 72 (1974) 375.
8 K. Cammann, Working with Ion Selective Electrodes, Springer-Verlag, Berlin, 1979.
9 Sh. K. Norov, A. K. Tashmukhamedova and N. Zh. Saifullina, Z. Anal. Chem. USSR, 37 (1982) 222.

Analytica Chimica Acta, 162 (1984) 373—377
Elsevier Science Publishers B.V., Amsterdam — Printed in The Netherlands

Short Communication

ION-SELECTIVE ELECTRODES IN TITRATIONS INVOLVING AZO-COUPLING REACTIONS
Part 3. Indirect Determination of Slowly Reacting Components

K. VYTŘAS*, T. ČAPOUN[a] and J. KALOUS

Department of Analytical Chemistry, College of Chemical Technology, 532 10 Pardubice (Czechoslovakia)

(Received 3rd February 1984)

Summary. Compounds that react slowly with arenediazonium salts can be determined by back-titration. When 1-naphthalene- or 4-bromo-1-naphthalenediazonium chloride is used, the excess is back-titrated with sodium tetraphenylborate or 2,4-diaminotoluene, the titration being monitored with a PVC membrane electrode plasticized with 2-nitrophenyl 2-ethylhexyl ether. Disodium 2-naphthol-3,6-disulfonate (R-salt), 2-naphthol-7-sulfonic acid, acetylacetone, and 1-(2′,5′-dichloro-4′-sulfophenyl)-3-carboxy-5-pyrazolone were determined without systematic errors in times shorter than needed for direct titration.

It has been shown [1, 2] that ion-selective electrodes with plastic membranes are useful for monitoring titrations based on azo-coupling reactions. If the arenediazonium ion used as titrant is sufficiently lipophilic, these electrodes follow its concentration changes and the potentiometric titration curves are well developed. However, the reactions of some compounds tested [2] with arenediazonium ions are so slow that the titrations become impractical in terms of time. Indirect titrations were therefore studied as described below.

Experimental

Solutions and instrumentation. 1-Naphthalenediazonium chloride and 4-bromo-1-naphthalenediazonium chloride solutions (both 0.01 M) were prepared and standardized with sodium tetraphenylborate or purified 2,4-diaminotoluene as described previously [2].

Stock solutions (0.01 M) of the compounds tested were prepared from accessible specimens of 2-naphthol-7-sulfonic acid, acetylacetone and 1-(2′,5′-dichloro-4′-sulfophenyl)-3-carboxy-5-pyrazolone, and from a standard sample of disodium 2-naphthol-3,6-disulfonate (R-salt). Concentrated Britton-Robinson buffers [1, 2] were used to adjust the pH value of the solutions titrated.

---

[a]Present address: Research Institute of Civil Defence, 113 84 Prague (Czechoslovakia).

0003-2670/84/$03.00

Instrumentation was the same as described previously [2]. The indicator electrode, with a membrane made from poly(vinyl chloride) plasticized with 2-nitrophenyl 2-ethylhexyl ether, was conditioned in a stirred aqueous suspension of the appropriate arenediazonium tetraphenylborate.

General procedure. Direct titrations of passive compounds with arenediazonium salt solutions were done as described earlier [2]. For back-titrations, an appropriate volume of the sample solution (usually 5 ml of 0.01 M solution) and 70 ml of buffer were measured into a 150-ml beaker, cooled externally with ice to 0° C, and the arenediazonium chloride solution was added (usually 10 ml of 0.01 M solution). The mixture was stirred magnetically and, after the potential of the electrodes had stabilized, the solution was titrated with either 0.01 M sodium tetraphenylborate or 0.01 M 2,4-diaminotoluene.

Results and discussion

When 1-naphthalenediazonium chloride solution is used for indirect titrations, the results depend on time. After the addition of the diazonium salt to the sample, the electrode potential must reach a constant value as a result of a fully completed azo-coupling reaction; this can take 15—20 min. This time needed to reach a stable potential must then be maintained in later titrations. With shorter times, the azo-coupling reaction is not complete and the titrant (sodium tetraphenylborate or 2,4-diaminotoluene) consumption is higher than it should be. Yet if final the titration is started after a long delay, the titrant consumption decreases owing to partial decomposition and auto-azo-coupling reaction of the 1-naphthalenediazonium salt.

As 4-bromo-1-naphthalenediazonium chloride solutions are much more stable, similar problems with time dependences do not arise. The excess of diazonium salt can be titrated immediately after the potential has stabilized (about 10 min).

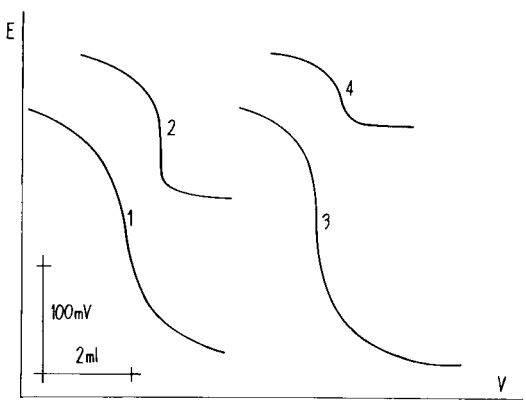

Fig. 1. Titration of excess of 4-bromo-1-naphthalenediazonium chloride in indirect determinations of (1,2) disodium 2-naphthol-3,6-disulfonate (R-salt) and (3,4) acetylacetone with (1,3) sodium tetraphenylborate or (2,4) 2,4-diaminotoluene.

Both sodium tetraphenylborate and 2,4-diaminotoluene can be recommended for back-titrations of the excess of arenediazonium salt solution. Although the overall potential change is higher in back-titrations with $NaBPh_4$, 2,4-diaminotoluene usually gives more reproducible results because the potential break is sharper (see Fig. 1).

As shown in Table 1, indirect determinations of slowly reacting compounds are always shorter than the direct titration with the same arene-

TABLE 1

Characteristic values for potentiometric titrations of slowly reacting compounds (ca. 0.05 mmol) with 0.01 M arenediazonium salts

Substance determined	Titration procedure	pH	Titration curve		Titration time (min)
			Overall potential change (mV)	Steepness near end-point (mV per 0.1 ml)	
With 1-naphthalenediazonium salt					
Disodium 2-naphthol-3,6-disulfonate (R-salt)	D.T.[a]	8	98	3	180
		9	107	8	130
		10	104	13	90
	$NaBPh_4$ [b]	10	213—235	31—41	10
2-Naphthol-7-sulfonic acid	D.T.	10	121—130	9—11	90
	$NaBPh_4$	10	158—177	7—9	25
	DAT	10	99—126	14—25	25
Acetylacetone	D.T.	10	133—148	13—17	60
	$NaBPh_4$	10	179—205	14—21	15
	DAT	10	95—112	21—26	15
With 4-bromo-1-naphthalenediazonium salt					
Disodium 2-naphthol-3,6-disulfonate (R-salt)	D.T.	8	171	19	180
		9	173	22	90
		10	174—183	21—38	60
	$NaBPh_4$	10	262—269	27—38	15
	DAT	10	107—138	30—44	15
2-Naphthol-7-sulfonic acid	D.T.	8	242	8	200
		9	212	14	170
		10	209—230	36—49	60
	$NaBPh_4$	10	230—263	26—43	15
Acetylacetone	D.T.	8	184	7	120
		9	178	8	80
		10	170—196	14—31	60
	$NaBPh_4$	10	272—281	50—62	15
	DAT	10	57—68	10—16	15
1-(2',5'-Dichloro-4'-sulfophenyl)-3-carboxy-5-pyrazolone	D.T.	9	165—178	44—56	40
	$NaBPh_4$	9	208—230	32—37	5

[a]Direct titration. [b,c]Back-titration of excess of arenediazonium salt with 0.01 M sodium tetraphenylborate or 0.01 M 2,4-diaminotoluene (DAT).

diazonium salt, despite the larger number of operations involved. During a back-titration, the potential value is stabilized almost immediately after each titrant addition, and the results do not contain systematic errors (Table 2). Obviously, the addition of excess of arenediazonium ion favours the formation of the reaction product. It is also advantageous that the diazonium salt is standardized against the same titrant as is used for back-titrations, thus reducing possible errors.

Finally, in titrations with sodium tetraphenylborate, the concentration of electroactive substance in the electrode membrane is regenerated and the electrode is thus reconditioned on the basis of the extraction of arenediazonium tetraphenylborate into the membrane plasticizer. Accordingly, the use of the coated-wire type of electrodes is possible [3]. The indirect

TABLE 2

Statistical evaluation of titration results

Substance determined	Titration procedure[a]	pH	Taken (mg)	Found[b] (mg)	Testing values[c]	
					Tab.	Calc.
With 1-naphthalenediazonium salt						
Disodium 2-naphthol-3,6-disulfonate	$NaBPh_4$	10	17.413	17.385 ± 0.181(4)	0.72	0.11[e]
2-Naphthol-7-sulfonic acid	D.T.	10	11.211[d]	11.127 ± 0.143(4)	—	—
	$NaBPh_4$	10		11.174 ± 0.155(4)	0.41	0.11[f]
	DAT[c]	10		11.174 ± 0.032(4)	0.41	0.19[f]
Acetylacetone	D.T.	10	5.016[d]	3.764 ± 0.084(4)	—	—
	$NaBPh_4$	10		3.779 ± 0.035(4)	0.41	0.09[f]
	DAT	10		3.782 ± 0.014(4)	0.41	0.13[f]
With 4-bromo-1-naphthalenediazonium salt						
Disodium 2-naphthol-3,6-disulfonate	D.T.	10	17.413	17.110 ± 0.231(4)	0.72	0.94[e]
	$NaBPh_4$	10		17.445 ± 0.270(4)	0.72	0.09[e]
	DAT	10		17.433 ± 0.043(4)	0.72	0.33[e]
2-Naphthol-7-sulfonic acid	D.T.	10	10.200[d]	10.150 ± 0.143(5)	—	—
	$NaBPh_4$	10		10.120 ± 0.133(5)	0.31	0.08[f]
Acetylacetone	D.T.	10	4.930[d]	3.712 ± 0.011(5)	—	—
	$NaBPh_4$	10		3.713 ± 0.009(5)	0.31	0.03[f]
	DAT	10		3.727 ± 0.020(5)	0.31	0.25[f]
1-(2',5'-Dichloro-4'-sulfophenyl)-3-carboxy-5-pyrazolone	D.T.	9	17.656[d]	16.685 ± 0.022(4)	—	—
	$NaBPh_4$	9		16.782 ± 0.223(4)	0.41	0.28[f]

[a]See footnote to Table 1. [b]Given as a reliability interval $\bar{x} \pm u_0 R$ ($\bar{x}$ is the arithmetic mean, R the range, and u_0 the critical value for the given number of replications (in parentheses) and the significance level $\alpha = 0.05$). [c]Tabulated critical values (Tab.) and calculated values (Calc.) are given for the u_0-test or the u-test, calculated from the formulae $u_0' = (|\bar{x} - \mu|)/R$, or $u' = (|\bar{x}_A - \bar{x}_B|)/(R_A + R_B)$, respectively, where μ is the amount taken and indices A, B denote the respective values for the first and second compared methods of determination. [d]The sample was not pure. [e]The u_0-test. [f]The u-test.

determination with 4-bromo-1-naphthalenediazonium salt can be recommended for monitoring slowly reacting passive compounds used in production of azo dyestuffs.

REFERENCES

1 K. Vytřas, J. Kalous, Z. Kalábová and M. Remeš, Anal. Chim. Acta, 141 (1982) 163 (Part 1).
2 K. Vytřas, J. Kalous and T. Čapoun, Anal. Chim. Acta, 162 (1984) 141 (Part 2).
3 K. Vytřas, M. Remeš and H. Kubešová-Svobodová, Anal. Chim. Acta, 124 (1981) 91.

Analytica Chimica Acta, 162 (1984) 379—383
Elsevier Science Publishers B.V., Amsterdam — Printed in The Netherlands

Short Communication

DIFFERENTIAL PULSE POLAROGRAPHIC DETERMINATION OF PYRIDOXINE IN MULTIVITAMIN TABLETS

E. JACOBSEN* and T. M. TOMMELSTAD
University of Oslo, Institute of Pharmacy, P.O. Box 1068, Blindern, Oslo 3 (Norway)
(Received 13th March 1984)

Summary. Pyridoxine (vitamin B_6) is easily oxidized to pyridoxal by active manganese dioxide. Pulse polarograms recorded from alkaline media (pH 12—13) containing pyridoxal are very well-defined. The current is diffusion-controlled and the peak current is proportional to the concentration of pyridoxine. This provides a simple determination of pyridoxine in multivitamin tablets. There is no interference from other vitamins; nicotinamide can be determined simultaneously from the same polarogram. The method is not applicable to tablets containing the colloids Methocel 4000 or Kollidon, which are strongly adsorbed on the electrode and inhibit the electroreduction of pyridoxal.

Numerous chemical methods have been proposed for the determination of pyridoxine (vitamin B_6) in tablets. The methods include gas chromatography [1], spectrophotometry [2], fluorescence spectrometry [3] and voltammetry at a carbon paste electrode [4]. All these methods are time-consuming and separation or derivatization prior to the actual measurement is required. The object of the present work was to investigate the application of differential pulse polarography in a simple and relatively rapid determination of pyridoxine in multivitamin tablets.

Experimental

Instrumentation. D.c. and differential pulse polarograms were recorded with a Princeton Applied Research Model 174 Polarographic Analyzer connected to a Houston Omnigraph 200 XY recorder. Conventional types of dropping mercury electrode and of electrolysis cell were used. Phase-sensitive a.c. polarograms were recorded with a Metrohm Polarecord E-506 connected to an E-505 polarographic stand. An Ag/AgCl/saturated KCl electrode was used as reference electrode and a platinum wire served as auxiliary electrode in all experiments. All experiments were done at 25 ± 0.1°C. Dissolved air was removed from the solutions by bubbling oxygen-free nitrogen through the cell for 5 min and passing it over the solution during the electrolysis.

Chemicals. All vitamins (pharmaceutical grade), multivitamin tablets and placebos were obtained from Collett-Marwell Hauge A/S and from A/S Apothekernes Laboratorium for Specialpraeparater (Oslo, Norway).

0003-2670/84/$03.00

Pyridoxal and manganese dioxide ("aktiv gefällt") were from Merck. Phosphate buffer of pH 6.8 was prepared by dissolving 7.16 g of disodium hydrogenphosphate ($12\,H_2O$) and 2.8 g of potassium dihydrogenphosphate in 1 l of distilled water. Stock solutions of pyridoxine hydrochloride were prepared by dissolving an appropriate amount in distilled water. All other chemicals were of reagent grade and used without further purification.

Recommended procedure for pyridoxine in vitamin tablets. Transfer one multivitamin tablet to a centrifuge tube, add 20.00 ml of phosphate buffer, pH 6.8, and crush the tablet with a glass rod. Add 2.1 g of active manganese dioxide and shake the suspension for 1 h in a rotary shaker. Remove the excess of manganese dioxide by centrifugation at 5000 rpm. Transfer 15.00 ml of the solution to a polarographic cell and add 5.00 ml of 2.5 M sodium hydroxide. Remove dissolved air with oxygen-free nitrogen and record a differential pulse polarogram (drop time 1 s, pulse amplitude 50 mV and scan rate 5 mV s^{-1}) in the potential range −0.8 to −1.5 V vs. Ag/AgCl/saturated KCl. Measure the peak current and determine the amount of pyridoxine from a calibration graph prepared by the same procedure from pyridoxine standards in the presence of a placebo. The polarogram must be recorded within 30 min after the addition of sodium hydroxide.

Results and discussion

According to Lingane and Davis [5], pyridoxine gives two d.c. polarographic waves when tetramethylammonium bromide is used as supporting electrolyte. Experiments showed that the first of these waves is due to reduction of hydrogen ions produced by the pyridoxine hydrochloride and the second wave ($E_{1/2}$ = 2.0 V vs. SCE) is too close to the reduction wave of the supporting electrolyte to be of any practical analytical value. Hence, in order to quantify pyridoxine by polarography, the drug must be oxidized to pyridoxal prior to the electroreduction.

Polarographic behaviour of pyridoxal. The d.c. polarographic behaviour of pyridoxal has been investigated by Volke [6] and Manoušek and Zuman [7, 8]. These authors showed that polarograms of pyridoxal recorded from acidic or neutral media exhibit a small kinetic wave. The limiting current of the wave increases with increasing pH of the supporting electrolyte and reaches a limiting value above pH 10. Above this pH value, the current is diffusion-controlled and two electrons are involved in the electrode reaction.

The above results were confirmed here. However, differential pulse polarograms of pyridoxal are better defined and the peak current is much larger than the d.c. current (Fig. 1). Obviously, pulse polarography is a more suitable method for the determination of this drug.

The best-defined peaks were obtained from supporting electrolytes with pH 12—13. In this pH region, the peak width at half-height is 85 mV (pulse amplitude 50 mV), indicating an almost reversible one-electron reduction. The reversibility was confirmed by phase-sensitive a.c. polarography. Very well-defined fundamental and second-harmonic a.c. polarograms were

obtained. In contrast, d.c. polarography indicates that the reduction is irreversible (Fig. 1) and that two electrons are involved in the overall electrode reaction [7]. Hence, the electroreduction of pyridoxal probably occurs in two steps

$$R{-}C\begin{matrix}=O\\ \diagdown H\end{matrix} + H^+ + e^- \overset{\text{fast}}{\rightleftharpoons} R\overset{*}{C}\begin{matrix}\diagup OH\\ \diagdown H\end{matrix}$$

$$R{-}\overset{*}{C}\begin{matrix}\diagup OH\\ \diagdown H\end{matrix} + H^+ + e^- \overset{\text{slow}}{\rightarrow} R{-}CH_2OH$$

Only the first step is measured by differential pulse and a.c. polarography, whereas the overall two-electron reduction is observed by the much slower d.c. polarographic method.

Differential pulse polarograms recorded from 0.1 M sodium hydroxide with various amounts of pyridoxal present showed that the peak height increased linearly with concentration in the range 10^{-5}—5×10^{-4} M. The peak potential of pyridoxal recorded from this electrolyte was —1.22 V vs. Ag/AgCl/saturated KCl. The peak potentials of riboflavin and nicotinamide determined in the same electrolyte were —0.68 and —1.70 V, respectively. No other vitamins are reduced in this potential range. Hence, it should be possible to determine pyridoxal by differential pulse polarography without any interference from other vitamins.

Determination of pyridoxine in multivitamin tablets. Pyridoxine is easily oxidized to pyridoxal by shaking with active manganese dioxide [9]. Experiments showed that the oxidation is complete when phosphate buffer, pH 6.8—7.0, is used as solvent. At higher pH values, the oxidation is incomplete and at pH 13 only 10% of the drug is oxidized. In subsequent experiments, pyridoxine was oxidized at pH 6.8—7.0 (rotary shaker) for 1 h and the pH was then increased to 13 by addition of strong alkali before the polarogram was recorded.

The oxidation of pyridoxine must, of course, be done with an excess of active manganese dioxide great enough to oxidize all vitamins (ascorbic acid, thiamine, etc.) present in the actual tablet. However, the excess of manganese dioxide should not be too great. Experiments showed that if the amount of manganese dioxide per tablet in 20 ml of buffer exceeded 2.5 g, the peak current of pyridoxal decreased; in the presence of 5 g of manganese dioxide, about 50% of the pyridoxal was removed from the solution probably by adsorption to the excess of manganese dioxide.

Differential pulse polarograms of pyridoxine in the absence and in the presence of other vitamins were recorded after oxidation with manganese dioxide and adjustment of the pH to 13 with sodium hydroxide. All polarograms of such synthetic mixtures were well-defined and reproducible. Polarograms of actual multivitamin tablets, however, were more reproducible if the excess of manganese dioxide was removed by centrifugation prior to recording the polarogram. Obviously, the tablets contain surfactants which are adsorbed on the excess of active manganese dioxide and thus removed

from the solution by the centrifugation. Pyridoxal is not stable in strongly alkaline media. Hence, the polarogram must be recorded as soon as possible and not later than 30 min after the addition of sodium hydroxide.

The procedure recommended in the Experimental section is based on the above results. The results of the determinations of pyridoxine in Collett multivitamin tablets with a nominal pyridoxine content of 2 mg by this procedure were satisfactory. The tablets contained vitamins A, B_1, B_2, C, D, nicotinamide and pantothenate, and excipients such as sugars, titanium dioxide, magnesium stearate and wax. The mean result from the analysis of 10 separate tablets was 1.92 mg/tablet (range 1.81—2.02 mg) with a relative standard deviation of 3.1%.

Differential pulse polarograms of nicotinamide recorded from strong alkaline media are very well defined [10]. Experiments showed that the treatment with active manganese dioxide had no effect on the polarographic wave of nicotinamide. Hence, the nicotinamide content in multivitamin tablets can be determined in the same solution prepared for the determina-

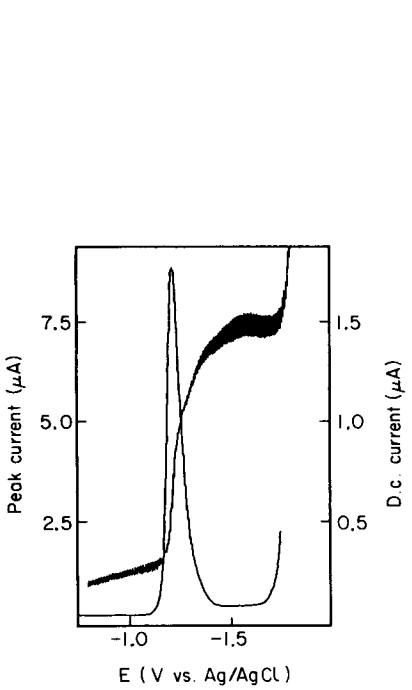

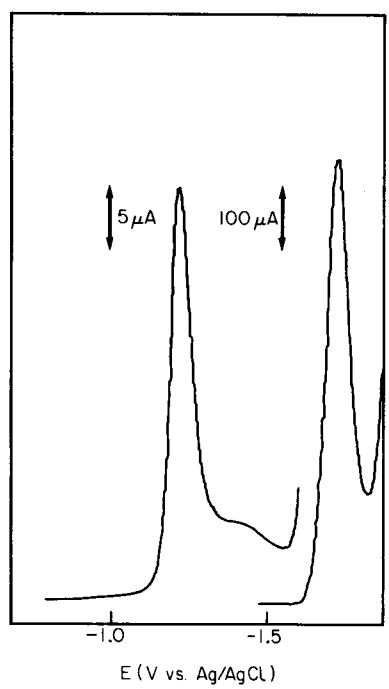

Fig. 1. D.c. and differential pulse polarograms of 10^{-4} M pyridoxal in 0.1 M sodium hydroxide.

Fig. 2. Differential pulse polarogram of pyridoxine (E_p = −1.22 V) and of nicotinamide (E_p = −1.70 V) in a Collett multivitamin tablet oxidized with active manganese dioxide and recorded after addition of sodium hydroxide to pH 13. Drop time 1 s, pulse amplitude 50 mV and scan rate 5 mV s^{-1}.

tion of pyridoxine simply by adjusting the sensitivity and continuing the recording from −1.5 to −1.8 V vs. Ag/AgCl/saturated KCl (Fig. 2).

Effect of surfactants. The above procedure was also used in an attempt to determine pyridoxine in Vitaplex multivitamin tablets. However, only a small peak of pyridoxal was observed on the polarograms and the reproducibility was poor. Further experiments showed that this problem was caused by the presence of methylcellulose (Methocel 4000) in these tablets. Methocel is surface-active, being strongly adsorbed on the electrode, and the adsorbed film inhibits the electroreduction of pyridoxal. Most of the Methocel is probably adsorbed on the excess of manganese oxide and removed by centrifugation prior to the electrolysis, but a small amount remains in the solution and causes a large decrease in the peak current of pyridoxal.

Because Methocel was found to inhibit the electroreduction of pyridoxal, the effect of other chemicals which are often present in tablets was studied in a series of experiments. These tests showed that the presence of even large amounts of the following chemicals did not cause any interference in the determination of pyridoxine by the recommended procedure: sucrose, glucose, lactose, sorbitol, titanium dioxide, talc, saccharin sodium, starch (*amylum solani*), magnesium stearate, glycerol, ricinus (castor) oil, oil of orange, white beeswax and Sunset Yellow dye. However, the presence of only 2.5 mg of Methocel 4000 or 7.5 mg of Kollidon (polyvinylpyrrolidone) in 20 ml of supporting electrolyte caused complete inhibition of the electroreduction of 10^{-4} M pyridoxal. The presence of even very small amounts of one of these two surfactants resulted in a large decrease of the peak current of pyridoxal. Consequently, the proposed method is not applicable to the determination of pyridoxine in tablets containing one of these two surfactants.

Methocel 4000 and Kollidon are not adsorbed on the electrode in the potential range where nicotinamide is reduced and they do not affect the polarographic determination of this vitamin.

REFERENCES

1 L. T. Sennello and C. J. Argoudelis, Anal. Chem., 41 (1969) 171.
2 K. Paczek and H. Wardynska, Acta Pol. Pharm., 27 (1970) 573.
3 M. M. Polansky, R. T. Camarra and E. W. Toepfer, J. Assoc. Offic. Agric. Chem., 47 (1964) 827.
4 P. Söderhjelm and J. Lindquist, Acta Pharm. Suec., 13 (1976) 201.
5 J. J. Lingane and O. L. Davis, J. Biol. Chem., 137 (1941) 567.
6 J. Volke, Z. Phys. Chem., Sonderheft, (1958) 268.
7 O. Manoušek and P. Zuman, J. Electroanal. Chem., 1 (1959—60) 324.
8 O. Manoušek and P. Zuman, Collect. Czech. Chem. Commun., 27 (1962) 486.
9 I. Kruse, Tartu Riikliku Ulikooli Toim, 270 (1971) 143.
10 E. Jacobsen and K. B. Thorgersen, Anal. Chim. Acta, 71 (1974) 175.

Analytica Chimica Acta, 162 (1984) 385—387
Elsevier Science Publishers B.V., Amsterdam — Printed in The Netherlands

Short Communication

ELIMINATION OF IRON INTERFERENCE IN THE DIFFERENTIAL PULSE ANODIC STRIPPING VOLTAMMETRY OF COPPER

J. J. CAMPION

Department of Chemistry, SUNY New Paltz, New Paltz, New York 12561 (U.S.A.)

(Received 24th October 1983)

Summary. The interference of iron(III) on the quantitation of copper(II) in citrate media by differential-pulse anodic stripping voltammetry can be completely removed by lowering the pH to 1.5 with 70% perchloric acid.

Because of the proximity of the copper(II) and iron(III) peak potentials in an ammonium citrate (pH 5) medium, the presence of iron can cause positive errors in the quantitation of copper by differential-pulse anodic stripping voltammetry (d.p.a.s.v.) [1]. Though Bonelli et al. [1] were unable to eliminate or mask the interference chemically, they were able to compensate for it; the corrected signal for copper for a given deposition time was obtained by subtracting the iron signal for zero deposition time. It would be preferable to eliminate the interference chemically, because a decrease in the relative size of the copper/iron signal reduces the accuracy of the subtraction method, unless the deposition time is inconveniently long. The present communication shows that a simple pH adjustment can completely remove the iron interference.

Experimental

Stripping voltammetry was done with conventional instrumentation and a three-electrode cell containing a hanging mercury drop electrode (HMDE), a platinum counter electrode, and either a Ag/AgCl (saturated KCl) or a Ag/0.01 M silver nitrate reference electrode. All chemicals were reagent grade. Distilled water was passed through a Millipore Milli Q purification system.

A 10-ml sample of the citrate buffer was deaerated with nitrogen. A deposition potential of −0.75 V vs. Ag/AgCl or −1.25 V vs. Ag/0.01 M silver nitrate was held for 60 s. After an equilibration period, the potential was scanned anodically at 5 mV s^{-1}. Concentrations of copper(II) were determined by the method of standard additions.

Chloride concentrations as low as 4×10^{-5} M can suppress the copper stripping peak in an acetate buffer [2], and in a citrate (pH 3.1) medium the chloride oxidation wave and iron wave are close. For these reasons,

0003-2670/84/$03.00

and because of the possible influence of chloride on the iron wave, the Ag/AgCl electrode was eventually replaced with a Ag/0.01 M silver nitrate electrode when chloride leakage was first confirmed. Though potentials in this paper are referred to the Ag/AgCl electrode, the voltammograms were actually obtained with a Ag/0.01 M silver nitrate electrode.

Results and discussion

Because the half-wave potential of iron(III) in a citrate medium is very pH-dependent [3], a 0.2 M ammonium citrate (pH 3.1) medium was chosen to establish if there was a greater separation between the copper and iron peaks. In this medium, the peak potentials of copper and iron are −0.01 and +0.12 V, respectively, vs. Ag/AgCl. Figure 1 shows a voltammogram of a citrate solution with a residual concentration of 5.0 $\mu g\ l^{-1}$ copper(II) (60 s deposition) in the presence of 1.0 mg l^{-1} iron(III). Though the peaks differ by 0.13 V, the resolution is not very good, and the interference would be magnified at lower copper(II) concentrations.

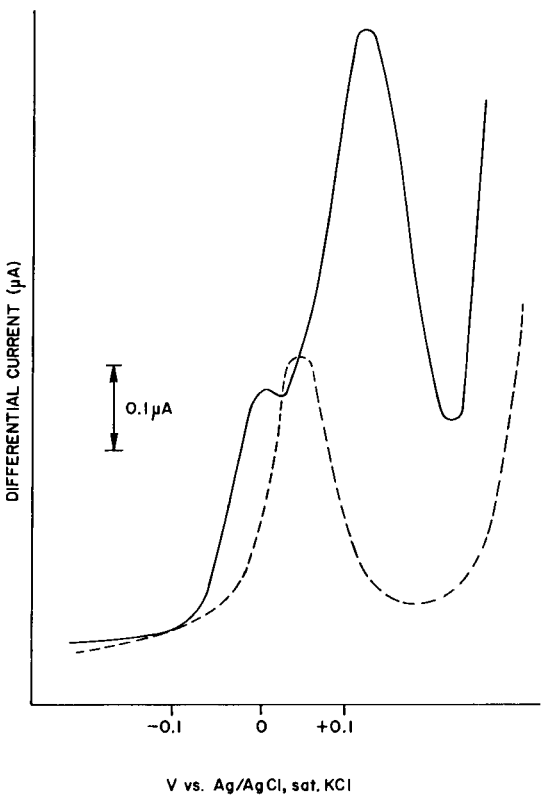

Fig. 1. D.p.a.s. voltammogram of 5.0 $\mu g\ l^{-1}$ Cu(II) and 1.0 mg l^{-1} Fe(III) in citrate media: (—) pH 3.1; (- - -) pH 1.5. 60-s deposition at −0.75 V.

Figure 1 also shows that the addition of 150 μl of 70% perchloric acid to the electrolysis cell containing 10 ml of the citrate (pH 3.1) buffer, completely removes the interference. The added 150 μl of perchloric acid lowers the pH to 1.5, causing a +0.04-V shift of the copper peak and, most significantly, a shift of the iron peak beyond the dissolution of mercury. The quantity of perchloric acid added does not appear to be critical; the 150-μl aliquot per 10 ml solution was approximately the minimum required to shift all traces of the iron wave beyond the dissolution of mercury. To minimize contamination, no more than the smallest required volume of perchloric acid should be added.

Two additional changes were observed. The steeply rising portion of the voltammogram, corresponding to the dissolution of mercury, was shifted positively, and the size of the copper peak (after accounting for the copper from the perchloric acid itself) was increased by 13%. The most reasonable explanation for these changes is the protonation of the citrate ion; in its protonated form the citrate ion is less likely to complex with both Hg(II) and Cu(II).

Data obtained with a freshly prepared buffer showed that the peak height of a fixed copper(II) concentration is constant over a range of iron(III) concentrations (0—10 mg l^{-1}) in the citrate (pH 1.5) medium. Peak height varied linearly with copper(II) concentration (0—50 μg l^{-1}) at a fixed iron(III) concentration (5.0 mg l^{-1}) in the freshly prepared citrate buffer (residual Cu(II) = 2.3 μg l^{-1}).

The simplicity of the citrate acidification method makes it an attractive alternative to using the subtraction method or to changing the medium between the deposition and stripping steps.

The author is grateful to Dr. A. V. Patsis of this department and to Dr. E. Lifshin of General Electric for arranging the sabbatical leave at the General Electric Research and Development Center, Schenectady, N.Y. Thanks are also due to Dr. J. C. Carnahan for the use of his laboratory facilities at G.E., Ms. R. B. Rohling for her technical assistance, and Dr. A. A. Bregman (Department of Biology, SUNY New Paltz) for his critical reading of this manuscript.

REFERENCES

1 J. E. Bonelli, R. K. Skogerboe and H. E. Taylor, Anal. Chim. Acta, 101 (1978) 437.
2 T. M. Florence and G. E. Batley, J. Electroanal. Chem., 75 (1977) 791.
3 L. Meites, Handbook of Analytical Chemistry, McGraw-Hill, New York, 1963, p. 563.

Analytica Chimica Acta, 162 (1984) 389—392
Elsevier Science Publishers B.V., Amsterdam — Printed in The Netherlands

Short Communication

A SIMPLE PRETREATMENT OF URINE FOR THE DIRECT DIFFERENTIAL-PULSE ANODIC STRIPPING VOLTAMMETRIC DETERMINATION OF LEAD

ALAN M. BOND* and JUERG B. REUST[a]

Division of Chemical and Physical Sciences, Deakin University, Victoria 3217 (Australia)

(Received 21st October 1983)

Summary. Lead can be determined directly in urine at the $\mu g\ l^{-1}$ level after a simple clean-up procedure consisting of an adsorptive removal of parts of the organic matrix on an apolar chromatographic medium followed by a filtration step.

The determination of lead and other heavy metals in body fluids, such as urine, has become a matter of wide interest, because of the toxicity of these metals and their influence in controlling the course of biological processes [1]. In principle, electrochemical methods such as stripping voltammetry in its various forms [2—9] would be very suitable as they offer high sensitivity combined with the possibility of a simultaneous determination of other metals such as copper, thallium and cadmium. However, the matrix in urine may cause significant problems, particularly with stripping voltammetry, and whilst a direct determination in urine has been reported [6], at the trace level found with persons not suffering from lead exposure, the methodology normally would have to include a pretreatment step (e.g., wet digestion [7]) which is time-consuming and expensive and introduces a high risk of contamination or losses of the analyte. A simple pretreatment procedure without these disadvantages is therefore very desirable. Recently, Sep-Pak C_{18} cartridges have been developed by Waters Associates, and these may enable the matrix problem to be eliminated. These cartridges are small columns (ca. 1 cm × 1 cm) containing an octadecylsilane bonded-phase packing retained between filters. The material adsorbs a wide variety of organic compounds from water-based solutions. In particular, it has been used for sample purification and steroid determinations in urine [10—12] and as a preconcentration step in the determination of metals [13]. However, the Sep-Pak cartridges have not so far been examined as a clean-up procedure for metal determinations by anodic stripping voltammetry. This possibility is investigated in the present communication.

[a]Present address: Analytical Research and Development, SANDOZ L.t.d., CH-4002 Basle, Switzerland.

0003-2670/84/$03.00

Experimental

Chemicals. Acids were analytical-reagent grade. Metal stock solutions (1000 mg l^{-1} Ionenstandard; Fluka AG, Buchs, Switzerland) were diluted daily. The water used was prepared in a Nanopure system (Barnsted Sybron Corp., Boston, MA), which delivered high-purity water of a similar quality as indicated earlier [14]. All glassware and plastic ware were cleaned in (1 + 9) nitric acid, (1 + 9) hydrochloric acid and finally 0.01 M hydrochloric acid.

Electrochemical instrumentation and procedure. The electrochemical instrumentation consisted either of a system with dual-microprocessor control [15] or an EG & G PAR (Princeton, NJ) Model 384 Polarographic Analyzer. The working electrode was a rotating glassy carbon electrode (type EA290; Metrohm, Herisau, Switzerland) with a mercury film formed in situ ($[Hg^{2+}] = 10^{-5}$ M). The instrumental conditions were as follows: E(deposition) = −1000 mV vs. SCE, E(final) = +20 mV, E(pulse) = +50 mV, scan rate = 7 mV s^{-1}, t(deposition) = 150 s, rotation speed = 1200 rpm, t(rest) = 30 s. All experiments were done at 21 ± 1°C.

Urine pretreatment. All urine samples were characterized by their medical urine status. Samples were collected by a clean-catch midstream method and examined as follows: (i) visual inspection for colour and turbidity; (ii) microscopic inspection for cells, bacteria, crystals and pathological changes; (iii) analysis for pH, density, protein concentration, glucose concentration, ketone concentration, bilirubin concentration and urobilinogen concentration.

The urine sample was made 10^{-2} M in hydrochloric acid. A cartridge containing the apolar C_{18} material (Sep-Pak, Waters Associates, Milford, MA) was attached with a short length of flexible tubing to the end of a 10-cm diameter glass funnel. The funnel was then filled with the urine sample and the treated urine was collected from the outflow of the Sep-Pak cartridge in a beaker. Some of the treated sample was then sucked through a disposable 0.45-μm filter (Millex; Millipore Corp., Bedford, MA) into a syringe, and a 10-ml portion was transferred from the syringe to the electrochemical cell.

Results and discussion

The attempted direct electrochemical determination of lead in untreated urine leads to erroneous results because of adsorption of constituents of the matrix on the electrode surface, complexation of the metal, and electrochemical reaction of matrix constituents. Such effects can result in totally useless voltammetric curves. Figure 1(a) shows that reliable peak-height or peak-area evaluation is impossible. Furthermore, these effects are not reproducible; for the same urine sample examined at different times, a completely different curve can be obtained as shown in Fig. 1(b), presumably because of modified adsorption effects on the electrode surface. In contrast, with the pretreatment recommended above, the voltammograms show the characteristics expected for successful determination of lead (Fig. 1c). Apparently the pretreatment method removes enough of the interfering apolar matrix con-

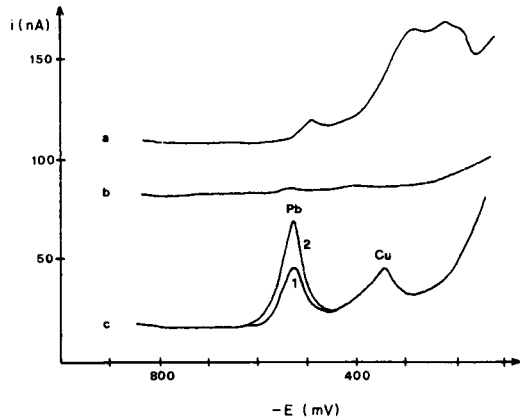

Fig. 1. Differential pulse anodic stripping voltammograms of 10 $\mu g\ l^{-1}$ lead in 10 ml of urine. (a) Untreated sample, measurement 1; (b) untreated sample, measurement 2. (c) Untreated sample: (1) 10 $\mu g\ l^{-1}$ lead; (2) standard addition to give a total of 20 $\mu g\ l^{-1}$ lead. All samples were taken from the same batch of urine.

stituents to enable interference-free measurements to be obtained provided that the method of standard additions is used. After the pretreatment, the response signal for the same lead concentration is much larger (cf. Fig. 1a, b) and the requirement of a linear signal vs. concentration relationship is fulfilled (in the investigated concentration range between 10 and 400 ng ml^{-1} lead added, coefficients of correlation for linear regression were always >0.994).

Recently, a new approach for detecting interferences has been developed here [15]. The method requires the simultaneous measurement of the differential pulse stripping response at pulse widths of 20, 40, 60, 80 and 100 ms. The time dependence, in addition to peak position and half-width, is used as a criterion for absence of interference. Untreated urine samples always showed a time dependence characteristic of systems with a high amount of interference, whereas the time dependence for treated samples was as expected for an interference-free determination. The peak potential of the stripping peak is more negative than that expected for uncomplexed lead, so that the simple pretreatment method involved is appropriate for analytical work but clearly does not remove all the complexing agents present. Consequently, the method of standard additions must be used rather than direct calibration.

Presently, an extensive research program requiring the examination of workers with possible exposure from lead smelting is being undertaken in these laboratories. The method described above has proved to be suitable for this work because it covers the range critical for lead poisoning in humans, as indicated in references [16] and [17]: 80 or 65 ng ml^{-1}, respectively, is normal, 80 or 65—150 ng ml^{-1} acceptable, 150—200 ng ml^{-1} excessive and

>250 ng ml^{-1} dangerous. Preliminary studies also show that the method is applicable for the determination of cadmium in urine.

The authors are indebted to Mrs. V. Reust and Mr. R. W. Knight for experimental assistance with the medical characterization, and the preparation of the samples, respectively. They also gratefully acknowledge the financial support of the Australian Research Grants Scheme and the Swiss National Science Foundation.

REFERENCES

1 M. Piscator and B. Pettersson, in S. S. Brown (Ed.), Clinical Chemistry and Chemical Toxicology of Metals, Elsevier, Amsterdam, 1977, pp. 143—154.
2 B. Searle, W. Chan and B. Davidow, Clin. Chem., 19 (1973) 76.
3 T. R. Copeland, J. H. Christie, R. Osteryoung and R. K. Skogerboe, Anal. Chem., 45 (1973) 2171.
4 W. Kisser, Arch. Toxicol., 34 (1975) 237.
5 J. T. Kinard, Anal. Lett., 10 (1977) 1147.
6 W. Lund and R. Erikson, Anal. Chim. Acta, 107 (1979) 37.
7 J. Golimowski, P. Valenta, M. Stoeppler and H. W. Nuernberg, Talanta, 26 (1979) 649.
8 M. A. Schreiber and T. A. Last, Anal. Chem., 53 (1981) 2095.
9 M. T. Watts, B. J. Poulson, L. L. Szabo, M. A. Kenny and W. Y. Lee, J. Anal. Toxicol., 5 (1981) 231.
10 C. H. L. Shackleton and J. O. Whitney, Clin. Chim. Acta, 197 (1984) 231.
11 R. Heikkinen, T. Fotsis and H. Adlercreutz, Clin. Chem., 27 (1981) 1186.
12 L. C. Ramirez, C. Millot and B. F. Maume, J. Chromatogr., 229 (1982) 267.
13 A. M. Bond and G. G. Wallace, Anal. Chim. Acta, 164 (1984) in press.
14 J. B. Reust and V. R. Meyer, Analyst (London), 107 (1982) 673.
15 A. M. Bond, H. B. Greenhill, I. D. Heritage and J. B. Reust, Anal. Chim. Acta, 165 (1984) in press.
16 Br. Med. J. (1968) 5629.
17 Swiss National Accident Insurance Fund, Suva, Occupational Diseases, Guideline No. 6, 2869/MB 6, 1977.

Analytica Chimica Acta, 162 (1984) 393—398
Elsevier Science Publishers B.V., Amsterdam — Printed in The Netherlands

Short Communication

FITTING TABULATED CURRENT FUNCTIONS TO LINEAR-SWEEP VOLTAMMOGRAMS

JAMES F. RUSLING
Department of Chemistry (U-60), University of Connecticut, Storrs, CT 06268 (U.S.A.)
(Received 26th March 1984)

Summary. A procedure is described for fitting tabulated theoretical current functions to linear-sweep voltammograms. The method, suitable for a small microcomputer, employs linear extrapolation between current function values, and non-linear regression for minimizing deviations between experimental and theoretical currents. Examples of its use for confirmation of simple electrode reaction mechanisms and estimation of electrochemical parameters are described.

The shapes of current—potential (i—E) curves in linear-sweep voltammetry (l.s.v.) depend on the mechanism of the electrode reaction. A primary difficulty in analyzing l.s.v. curve shapes lies in the solution of the relevant differential equations; even for the simplest mechanisms it is not possible to obtain a closed-form expression for i in terms of E, and numerical solutions must be sought [1]. An elegant way of fitting theoretical models is to use finite difference techniques coupled to parameter optimization [2, 3]. However, such methods require moderately large computers and long times for proper convergence, and may not always be practical when only a confirmation of the electrode mechanism is needed.

Numerical solutions for many electrochemical mechanisms are available [4, 5] as tabulated dimensionless current functions vs. a potential function, usually defined in terms of $(E - E^{0\prime})n$, where $E^{0\prime}$ is the standard formal potential and n is the number of electrons transferred per molecule. These tables can be used to calculate voltammograms by estimating the values of $E^{0\prime}$, n, and D, the diffusion coefficient, that give the theoretical $i - E$ curve with the "best" graphical fit to experiment. Such a procedure is tedious, and by no means guarantees the statistical best fit or accurate values of parameters. However, a rapid, statistically sound fit results if the deviations of current functions from experiment are minimized by using non-linear regression. This communication describes such a procedure, appropriate for a microcomputer, developed as a BASIC subroutine to be used with an existing general program for non-linear regression [6, 7].

0003-2670/84/$03.00

Computations

Potential functions of the form $E_j^N = (E_j - E^{0'})n$ and their respective theoretical current functions (F_j) [4, 5] for the mechanism to be fitted to the experimental data are stored in DATA statements, and read into memory at the beginning of the program. The maximum F_j is identified and set equal to F_{max}. Subsequently, experimental i_j, E_j pairs are read into memory. In the present work, 12—28 data points equally spaced (usually 10 mV) on the E-axis were used. The first i_j was generally 3—6% of i_p, the peak current, expressed as a positive quantity. Potentials are ordered such that the E_j increase in a positive direction as the i_j increase. Thus, for reductions the signs of the E_j would be changed before entering into the program. This makes the computation general for both oxidations and reductions. The program also has a provision for linear background correction. If such a correction is desired, the program requires input of baseline slope, S_b, and the baseline current (i_b) at an arbitrary potential E', well before the rise of the peak. The corrected values of the current are computed from

$$i_j' = i_j - S_b(E_j - E') - i_b \tag{1}$$

A general non-linear regression program [6] is used to minimize the sum of dev^2. Initial estimates of the parameters are required. In the present case, $\text{dev}_j = i_j' - i(\text{calc})_j$, and a subroutine to compute $i(\text{calc})_j$ from the F_j is required. The parameters in this routine are $E^{0'}$, n, and i_p. The subroutine begins by computing values of P_j^N corresponding to the experimental values of E_j, from

$$P_j^N = (V_1 - E_j)V_2 \tag{2}$$

where V_1 and V_2 are the initial or existing estimates of $E^{0'}$ and n, respectively, A test is made on calculation of each P_j^N to establish if it falls within the potential range of the tabulated E_j^N values. If a P_j^N is out of range, $i(\text{calc})_j$ is computed from $i(\text{calc})_j = 1.5\, i(\text{calc})_j$, where the i_j on the right-hand side is its existing value. This procedure increases dev_j^2 so that the offending P_j^N will be brought into the correct range on succeeding cycles. If a P_j^N is within range, however, the tabulated values of E_j^N immediately above and below P_j^N are located. The larger of the two is denoted $E^N(k-1)$ and the smaller $E^N(k)$. The extrapolated current function, C_j, is then computed from the corresponding tabulated current functions $F(k)$ and $F(k-1)$, by using

$$C_j = F(k-1) + [F(k) - F(k-1)]\,[E^N(k-1) - P_j^N]\,/\,[E^N(k-1) - E^N(k)] \tag{3}$$

The current is then calculated from

$$i(\text{calc})_j = V_3 C_j / F_{max} \tag{4}$$

where V_3 is the peak current parameter. The subroutine then returns to the beginning to compute the next P_j^N. Once $i(\text{calc})_j$ have been obtained for each E_j, the program computes the sum of dev_j^2 and then adjusts the parameters

V_1, V_2 and V_3 in order to minimize this sum. The entire process is repeated until preset conditions for convergence [6] are reached, yielding the best values of $E^{0\prime}$, n and i_p.

Values of $E^{0\prime}$ and i_p are directly measurable from the voltammogram [1] and can be compared with the computed ones. The peak current is used in Eqn. (4) to scale the current functions to the experimental conditions used. Effectively, n is a peak width parameter. Considering a two-electron reversible reduction, for example, a value of $n < 2$ for the theoretical voltammogram defines a peak wider than the $n = 2$ peak; a value of $n > 2$ defines a peak narrower than the theoretical $n = 2$ peak. For fast multielectron reactions, the computed value of V_2 or n has some diagnostic value, as will be shown below.

The program described above was written in Level II BASIC and computations were done on a Radio Shack Model I microcomputer with 48K memory. A typical fit took 20—60 min, depending on the size of the data set.

Experimental

Linear-sweep voltammograms were obtained with three-electrode cells, using a PARC Model 170 or a Bioanalytical Systems BAS-100 Electrochemistry System and standard procedures described previously [8—10]. The working electrode was either a hanging-drop mercury electrode (HDME), a carbon paste electrode, or a glassy carbon electrode (GCE). Solid electrodes were resurfaced prior to each scan [9]. A platinum wire served as the counter electrode, and as reference either a saturated calomel electrode (SCE, for aqueous solutions) or a Ag/Ag^+ (0.001 M) electrode (acetonitrile—water) was used. All chemicals were the best grade available commercially [8—10] and were used as received.

Results and discussion

The fitting procedure was tested with systems representing simple reversible and quasireversible electron transfers and fast electrodimerization reactions. These examples included both oxidations and reductions under a variety of experimental conditions. The procedure gave excellent fits of current functions to voltammograms for these known redox systems. Relative standard deviations (standard deviation of regression/i_p) were less than 2% (Table 1). Computed and measured values of E^0 and i_p were in excellent agreement. Replicate fits begun with widely different initial values of parameters gave nearly identical final results. Graphically, computed values of currents were almost indistinguishable from experiment (Fig. 1). Acceptable agreement was obtained even for 1,2,3,4-tetrahydrocarbazole (THC), where overlap of the primary l.s.v. peak with a secondary peak necessitated the use of a truncated data set (Fig. 2).

Several additional uses of the fitting procedure can be identified. Ferriheme (iron(III) protoporphyrin), under conditions in Table 1, undergoes a fast EE or ECE reduction [10]. The width of the l.s.v. peak is governed by the

TABLE 1

Results of fitting current functions (CF) to l.s.v. data

Species	Conc. (mM)	Electrolyte	WE[a]	Mech.[b] [Ref.]	CF [Ref.]	v ($V\ s^{-1}$)	$E^{0'}$ (mV)		n		i_p (μA)		RSD (%)
							Meas.	Calc.	Theory	Calc.	Meas.	Calc.	
Tl(I)	0.20	0.1 M KCl	HDME	Rev. Red. [9]	Rev. [4]	0.10	−497[c]	−498	1	0.98	3.06	3.07	0.46
Ferrocene	0.77	0.2 M $LiClO_4$ CH_3CN/H_2O, 9:1	GCE	Rev. Ox. [9]	Rev. [4]	0.10	104[d]	102	1	1.01	27.5	27.7	0.74
Ferriheme	0.60	0.1 M NaOH	HDME	EE Red. [10]	Rev. [4]	0.01	−700[c]	−695	2	1.12	0.680	0.678	1.40
$Fe(CN)_6^{4-}$	0.5	0.5 M KNO_3	GCE[g]	QR Ox. [9]	Rev. [4]	0.50	245[c]	249	1	0.67	21.2	21.6	1.9
Homarine[h]	0.77	pH 12.3 phosphate	HDME	DIM Red. [12]	DIM [5]	0.20	−1339[e]	−1340	1	0.93	8.25	8.26	1.9
THC	1.8	MeCN/H_2O, 9:1	GCE	DIM Ox. [8]	DIM [5]	0.20	525[f]	526	1	0.94	135	136	1.3

[a]Working electrodes: HDME, hanging drop mercury electrode; GCE, glassy carbon. [b]Mechanisms: Rev., reversible; QR, quasireversible; DIM, electrodimerization; EE, fast two-electron transfer; Red., reduction; Ox, oxidation. [c]mV vs. SCE, as E at $i = 0.852\ i_p$. [d]mV vs. Ag/Ag^+ (0.001 M), as E at $i = 0.852\ i_p$. [e]mV vs. SCE, as E at $i = 0.93\ i_p$. [f]mV vs. Ag/Ag^+ (0.001 M), as E at $i = 0.93\ i_p$. [g]Electrode pretreated [11] and allowed to stand 1—2.5 h in air before use. [h]1-Methyl-2-carboxypyridinium ion.

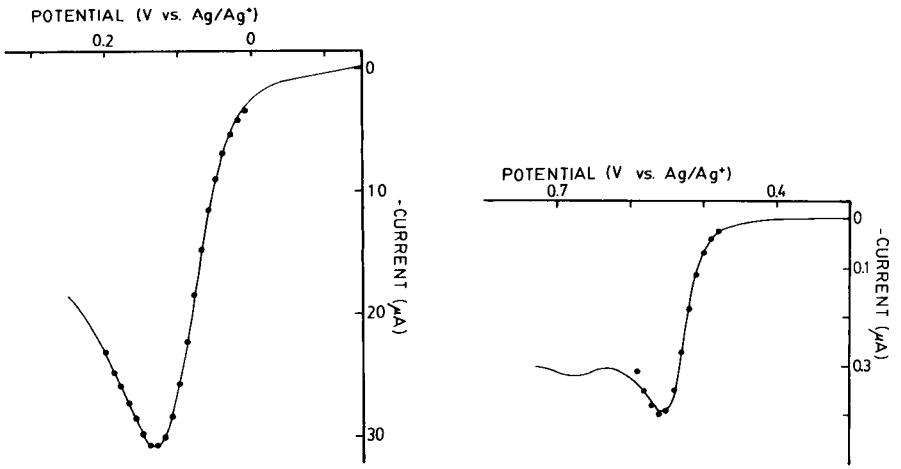

Fig. 1. Linear-sweep voltammogram at 0.1 V s^{-1} for oxidation of 0.77 mM ferrocene in 0.2 M $LiClO_4$ in acetonitrile/water (9:1) at a glassy carbon electrode. Solid line is experimental data; points are computed from reversible current function [4] by using non-linear regression.

Fig. 2. Linear-sweep voltammogram at 2.0 V s^{-1} for oxidation of 1.8 mM 1,2,3,4-tetrahydrocarbazole in 0.2 M $LiClO_4$ in acetonitrile/water (9:1) at a carbon paste electrode. Solid line is experimental data; points are computed from electrodimerization current function [5] by using non-linear regression.

separation in E^0 values of the two consecutive electron transfers. This width is reflected by the computed value of V_2 of 1.12, similar to the previously reported V_2 of 1.19, estimated graphically [10]. The computed V_2 can be used to estimate the standard potential of the intermediate in the second electron transfer. Table 1 also illustrates that data for quasireversible reactions (e.g., the hexacyanoferrate(II) redox couple at air-oxidized glassy carbon [11]) can be fitted reasonably well with the reversible current function. In such cases, V_1 and V_2 have no theoretical significance, and can be considered peak position and shape parameters, respectively.

Deviation plots [7], which have been previously used for discrimination between different mechanisms [9], were not useful for this purpose with the present fitting procedure. Such plots of residuals vs. E_j were non-random when data were fitted with the correct current functions, presumably because of neglect of electrode sphericity or edge effects and small systematic errors from the approximation of a curve with a straight line in the extrapolations. The relative standard deviation (RSD) of the regression was also useless for distinguishing between mechanisms because of variable resolution in the different tabulated current functions. Inspection of fits of wrong current functions to selected sets of data (Table 2), indicated that the best parameter for distinguishing between mechanisms was V_2 or n. Computed values of n obtained by using the wrong current function were in error by 20% or more,

TABLE 2

Results of fitting wrong current function (CF) to l.s.v. data[a]

Data set	Mech.	CF	$E^{0\prime}$ (mV)		n		i_p (μA)		RSD (%)
			Meas.	Calc.	Theor.	Calc.	Meas.	Calc.	
Tl(I)	Rev.	DIM	−505[e]	−507	1	0.68	3.06	3.05	0.34
Ferrocene	Rev.	DIM	110[f]	111	1	0.70	27.5	27.5	0.58
Ferriheme	EE	DIM	−701[e]	−703	2	0.78	0.680	0.673	1.3
Homarine	DIM	Rev.	−1331[c]	−1334	1	1.30	8.25	8.28	2.7
THC	DIM	Rev.	515[d]	514	1	1.37	135	137	1.7

[a]See Table 1 for footnotes.

while n values obtained with the correct current function were within about 7% of the correct value in most cases for reversible and electrodimerization reactions.

Although good fits of tabulated current functions can be obtained, the diagnostic power of the fitting procedure by itself is limited, and its utility will be enhanced by supplementary data, such as an independent value of n, product identities, and dependences of changes in peak current and potential upon varying scan rate and other experimental conditions. For electrode reactions in which the magnitude of a chemical rate constant influences peak shape, more complex procedures must be used. The main usefulness of the fitting procedure described is to provide rapid confirmatory evidence for presumed simple electrode reaction mechanisms.

This work was supported in part by U.S. PHS Grant No. CA33195 awarded by the National Cancer Institute, Dept. of Health and Human Services. The author thanks Barry J. Scheer and Geoffrey N. Kamau for contributing l.s.v. data.

REFERENCES

1 A. J. Bard and L. R. Faulkner, Electrochemical Methods, Wiley, New York, 1980.
2 J. J. O'Dea, J. Osteryoung and R. A. Osteryoung, J. Phys. Chem., 87 (1983) 4725.
3 M. K. Hanafey, R. L. Scott, T. H. Ridgway and C. N. Reilley, Anal. Chem., 50 (1978) 116.
4 R. S. Nicholson and I. Shain, Anal. Chem., 36 (1964) 706.
5 R. S. Nicholson, Anal. Chem., 37 (1965) 667.
6 L. Meites, The General Non-linear Regression Program CFT4A, privately published, 1983.
7 L. Meites, CRC Crit. Rev. Anal. Chem., 8 (1979) 1.
8 C. L. Kulkarni, B. J. Scheer and J. F. Rusling, J. Electroanal. Chem., 140 (1982) 57.
9 J. F. Rusling, Anal. Chem., 55 (1983) 1719.
10 J. F. Rusling and M. Y. Brooks, J. Electroanal. Chem., 163 (1984) 277.
11 J. F. Rusling, Anal. Chem., 56 (1984) 575.
12 J. F. Rusling, J. Electroanal. Chem., 125 (1981) 447.

Analytica Chimica Acta, 162 (1984) 399—402
Elsevier Science Publishers B.V., Amsterdam — Printed in The Netherlands

Short Communication

AN IMPROVED COMPUTER PROGRAM FOR CALCULATING FORMATION CONSTANTS OF LIGAND COMPLEXES FROM pH DATA

JOHN P. CHANDLER

Department of Computing and Information Sciences, Oklahoma State University, Stillwater, OK 74078 (U.S.A.)

RICHARD E. THOMPSON[a], H. OLIN SPIVEY* and EDWIN L.-F. LI[b]

Biochemistry Department, Oklahoma State University, Stillwater, OK 74078 (U.S.A.)

(Received 5th August 1983)

Summary. Several improvements are made to available computer programs for calculating formation constants from pH data. The most important features are wide portability of program among computers, ability to optimize any parameter in the model equations and to fix any parameters (including stepwise formation constants) to a constant, and options to allow for variations in thermodynamic activity of ions and to fit pH after fitting the volume of added reagent. The latter feature was used with synthetic data to explore the effects of random errors in either reagent volume or pH or both. Whereas fits to reagent volume will usually be more accurate for systems with pK_a values near 7, this is not the case for systems with pK_a values which differ by ≥ 2.0 from 7.

For determining acidity constants (K_a) and metal-complex formation constants, pH data can be especially valuable for several systems and conditions. The model equations are often so complex, however, that elaborate computer programs are needed for data analysis. The most powerful of these are based on the SCOGS program [1]. Its most impressive features are its general applicability to equilibria of polynuclear species, and its ease of use. It can derive the appropriate mathematical model from the chemical model provided by the user. A good comparison of these programs and their features has been given by Zuberbuhler and Kaden [2].

Some desirable features are still missing from these programs, however, and a program, which overcomes several of these deficiencies is described here. The feature of using analytical rather than numerical derivatives [2] in the minimization routine is not included. The implicit equations needed to permit calculation of ion activities appears to preclude this possibility. No problems have been encountered with the use of numerical derivatives.

---

[a]Present address: Abbott Labs, Irving, TX 76061, U.S.A.
[b]Present address: 5 San Romanoway, Downsview, Ontario M3N 2Y4, Canada.

0003-2670/84/$03.00

Methods

The FORTRAN program was tested with both real and synthetic data. The first set of synthetic data simulated adenosine triphosphate (1 mM) in aqueous 0, 1.0 and 20.0 mM magnesium chloride solutions. The complex species and logarithms of the thermodynamic over-all formation constants assumed were: HL^{3-} (7.70), H_2L^{2-} (12.20), MgL^{2-} (5.00), $MgHL^{-}$ (10.40) and NaL^{3-} (2.40), where L represents this hypothetical ligand. A second set of synthetic data was generated with acidity constants (K_a), approximately 2.0 pH units lower. No supporting electrolyte was used; thus activity coefficients varied throughout the experiments. Normally distributed errors were calculated [3] and added to the exact values of pH or reagent volume to generate sets of data with different but realistic extents of random error in either or both variables.

Results and discussion

The program SCOGS2 contains the following capabilities and changes to SCOGS [1]. Whereas SCOGS only allows least-squares minimization of the cumulative ("over-all") formation constants, SCOGS2 allows any constant in the resulting equilibrium equations to be minimized. Any of the adjustable parameters (J) may be declared variable (MASK(J) = 0) or fixed (MASK(J) = 1) during a given fit. This change, for example, enabled best-fit values to be found for initial ligand concentration and the number of displaceable protons initially added with the ligand in a study of 5-phosphoribosyl-1-pyrophosphate (PRPP) [4]. The best-fit values of these two parameters were obtained with high precision, exceeding that known from other measurements in this case. Optimizing the number of displaceable protons also compensated exactly for strong acid impurities as discussed by Briggs and Stuehr [5]. Their program, however, was limited to single pK_a systems. To evaluate the effects of other impurities with PRPP, the number of different ligands and metal ions allowed was increased from 2 each to 4 each.

Constraints of equality may be added by the user to SCOGS2, which, e.g., permit selected stepwise formation constants or microscopic formation constants to be held constant. This enables certain stepwise formation constants, k, to be fixed during optimization of all other cumulative formation constants. This is desirable whenever independent data establish certain constants better than the data being analyzed, or the consequence of assuming a given stepwise formation constant is sought. In programs such as SCOGS, which optimize the cumulative formation constants, this cannot be achieved by fixing any of the cumulative formation constants unless the complex is formed in one step from the free ligand and metal or proton. In SCOGS2, however, addition of E(2) = E(1) + 0.65, for example, to the problem-dependent subroutine fixes the log of the second stepwise formation constant equal to 0.65 because the E's are the logarithms of the cumulative formation constants 1 and 2. No constraints other than those desired are added by this method.

Improved algorithms for minimizing the sum of squared residuals are added, giving SCOGS2 improved convergence properties. The least-squares algorithm is now a separate program module rather than being an integral part of the program. As a result, the Marquardt gradient algorithm [6] can easily be replaced by a compatible direct search minimization procedure such as STEPIT [7]. Such a replacement might be desirable if slow convergence of the Marquardt method were found or if one wished to explore the parameter space more thoroughly to avoid local minima. Neither slow convergence nor local minima were found here, but it is preferable to use STEPIT to test for the latter more thoroughly.

If requested, SCOGS2 allows for variations in thermodynamic activities of ions and reports the ionic strength at each reagent-addition point. Activity coefficients are calculated with the empirical extension of the Debye-Hückel equation suggested by Davies [8]. This is done by adding the equation for ionic strength to the COGSNR subroutine of Sayce [1], which solves the simultaneous equations by the Newton—Raphson algorithm. The resulting ionic strength is used to calculate the Debye—Hückel factor and all ion activities at each iteration of the Newton—Raphson procedure, which continues until convergence criteria are satisfied.

If requested, SCOGS2 fits to pH after completing the fit to reagent volume. It would also be possible [9, 10] to fit simultaneously to reagent volume and pH, although this capability has not yet been added to SCOGS2. Fitting to pH permits one to evaluate the consequences of random errors in measured pH values rather than, or in addition to, reagent volume.

To explore the consequences of such errors, synthetic data sets were used with random errors of specified standard deviations in one or both variables. Standard deviations in the pH were approximately 0.01, 0.035 and 0.10; standard deviations in reagent volume were 0.001, 0.035 and 0.010 ml. The sum of squares of the normalized residuals after convergence of the least-squares fits were within one standard deviation of the expected values for all fits. For the system with a pK_a value of 7.70, the errors in calculated constants were most often less when fits were made to reagent volume rather than pH. Even when data errors were confined to pH, parameter errors were not significantly higher with fits to reagent volume than with fits to pH. Systems with pK_a values further from 7 however, would be expected to be much more sensitive to pH errors. This was confirmed with the data for the system with pK_a = 5.0. For pH errors of $\geqslant$0.035, fits to pH gave significantly more accurate constants than fits to reagent volume. In general, errors in formation constants increase as the number of species in the complex increases. When, for example, errors in reagent volume are $\geqslant$0.003 ml and fits to pH are made, errors in the formation constant of $MgHL^-$ are especially large, and the linear estimates of the errors are very poor. The sensitivity of a formation constant, especially that of $MgHL^-$, to errors is difficult to predict. With the ability to fit to either reagent volume or pH,

however, it is possible to generate synthetic data comparable to the experimental system under study, to test the consequences of errors, and thereby design the experiments and data evaluations to minimize the errors in derived constants.

Some of the generality of SCOGS2 was achieved by allowing the user to add FORTRAN code to the package in certain places, an example of which was given above in discussing constraints of equality. However, an attempt was made to restrict all problem-dependent code to a single subroutine called PROBD, which is called from several places in SCOGS2. Other modifications permit setting maximum and minimum allowable values on any parameter, and specification of standard deviations in experimental reagent volume or pH to provide proper statistical weighting of the data points. The names of the variables in the program were also changed to identify their function more clearly.

The program is written in 1966 A.N.S.I. Standard FORTRAN to permit maximum portability. A copy of the program (about 3700 FORTRAN lines) can be purchased from the authors.

This work was supported in part by a grant from the National Institutes of Health (GM 16916).

REFERENCES

1 I. G. Sayce, Talanta, 15 (1969) 1397.
2 A. D. Zuberbuhler and T. A. Kaden, Talanta, 29 (1982) 201.
3 G. Marsaglia and T. A. Bray, SIAM Rev. 6 (1964) 260; Commun. A.C.M., 11 (1968) 757.
4 R. E. Thompson, E. L.-F. Li, H. O. Spivey, J. P. Chandler, A. J. Katz and J. R. Appleman, Bioinorg. Chem., 9 (1978) 35.
5 T. N. Briggs and J. E. Stuehr, Anal. Chem., 46 (1974) 1517.
6 D. W. Marquardt, SIAM J. Appl. Math., 11 (1963) 431.
7 J. P. Chandler, STEPIT, QCPE distribution no. 307, Quantum Chemistry Program Exchange, Indiana University Chemistry Department, Program 66, 1971.
8 C. W. Davies, Ion Association, Butterworths, London, 1962, p. 41 (Eqn. 3.14).
9 P. A. P. Moran, J. Multivar. Anal., 1 (1971) 232.
10 D. R. Powell and J. R. Macdonald, Comput. J., 15 (1972) 148.

Analytica Chimica Acta, 162 (1984) 403—407
Elsevier Science Publishers B.V., Amsterdam — Printed in The Netherlands

Short Communication

BURNT-GAS COMPOSITION OF THE HELIUM—OXYGEN—ACETYLENE FLAME

ANNA YUEN and GARY M. HIEFTJE*
Department of Chemistry, Indiana University, Bloomington, IN 47405 (U.S.A.)

(Received 10th April 1984)

Summary. The burnt gas composition of a potentially important atom reservoir, the He—O_2—C_2H_2 flame, is calculated. This flame, compared to the air—acetylene flame, provides a slightly more reducing and a much less quenching environment.

Several years ago, the helium—oxygen—acetylene flame was introduced and its characteristics were compared to those of other flames [1—3]. It was reported that the use of helium, a gas with high thermal conductivity, enabled this flame to have atom formation capabilities intermediate between those of air—C_2H_2 and N_2O—C_2H_2 mixtures [3]. The maximum safe operating temperature for the helium-diluted flame was reported to be 2760 K, also between that reported for the other two flames. The spectral background of the He—O_2—C_2H_2 flame was shown to be relatively unstructured, like that of the air—C_2H_2 flame, but low in comparison to other high-temperature flames [2]. However, the most distinctive and perhaps useful characteristic of the new flame is that it contains a relatively low concentration of excited-state quenching species, making it attractive as an atom cell for atomic fluorescence spectrometry.

To understand better this interesting and potentially important atom reservoir, calculations were done to determine the composition of the burnt gases in the secondary combustion zone most often used for atomic measurements. The flame gas composition should be useful in understanding the physical (e.g., thermal conductivity, temperature) and chemical (stoichiometry, presence of reducing species) properties of the flame and also in calculating quenching cross-sections and quantum efficiencies for analyte atoms introduced into it. Finally, knowledge of the burnt-gas composition should allow additional comparisons between the He—O_2—C_2H_2 flame and the commonly used air—C_2H_2 and N_2O—C_2H_2 flames.

The burnt-gas composition, expressed as partial pressures of CO_2, CO, H_2O, O_2, H_2, OH, O, N, and He, was calculated as in the Damköhler and Edse method [4], but with slight modification. The results suggest that the He—O_2—C_2H_2 flame, compared to the air—C_2H_2 mixture, provides a slightly more reducing and a much less quenching environment.

0003-2670/84/$03.00

Method of calculation

The Damköhler and Edse method [4] allows the calculation of burnt-gas compositions of flames with fuels that are comprised of molecules containing C, H, O and N. In order to use this method with the He—O_2—C_2H_2 flame, it must be slightly modified because of the absence of nitrogen and presence of helium. Calculations were done on an intelligent terminal (Model 4051, Tektronix, Beaverton, OR).

The temperature of the He—O_2—C_2H_2 flame is 2735 K in the commonly-used quantitative zone (1 cm above burner top) with gas flow rates of 1.94 l min^{-1} C_2H_2, 8.4 l min^{-1} He and 2.4 l min^{-1} O_2 [5]. These flow rates describe the flame represented by

$$C_2H_2 + 2.37\ O_2 + 8.295\ He \rightarrow \text{burnt gases} \tag{1}$$

The Damköhler and Edse method takes into consideration the ratios of the input flame gases in Eqn. 1. These ratios are expressed in terms of the number of atoms of element j (n_j) relative to the number of atoms of hydrogen (n_H) available. For a flame consisting of C, H, O and N, the three ratios of interest would be n_C/n_H, n_O/n_H, and n_N/n_H. Because the present flame contains no nitrogen but does contain helium, the three ratios to consider are n_C/n_H, n_O/n_H, and n_{He}/n_H. According to Eqn. 1, the values of these three ratios are $n_C/n_H = 1.00$, $n_O/n_H = 2.37$, and $n_{He}/n_H = 4.15$. Obviously, n_C, n_H, n_O, and n_{He} can be expressed as sums of partial pressures (P_i) of the burnt gases (i)

$$n_C = k_1(P_{CO_2} + P_{CO}) \tag{2}$$

$$n_H = k_2(2P_{H_2} + P_H + P_{OH} + 2P_{H_2O}) \tag{3}$$

$$n_O = k_3(2P_{CO_2} + P_{CO} + P_{H_2O} + 2P_{O_2} + P_{OH} + P_O) \tag{4}$$

$$n_{He} = k_4(P_{He}) \tag{5}$$

where the k's are proportionality constants.

The Damköhler and Edse method also takes into account the six equilibria of Table 1. Because the present flame contains no nitrogen, only the first five equilibria of Table 1 need be considered. Conveniently, it can be safely assumed that helium is unreactive in the flame and serves simply as a diluent.

Using the first five equilibria in Table 1 and their equilibrium constants at 2735 K, the three ratios (n_C/n_H, n_O/n_H, and n_{He}/n_H) from Eqn. 1, and Eqns. 2—5, one can calculate the partial pressures of He, CO_2, CO, H_2O, O_2, H_2, OH, O and H according to the sequence of steps listed in Table 2 and described in more detail below.

The Damköhler and Edse method is basically iterative. As indicated in step 1 of Table 2, assumed values of P_{CO_2}/P_{CO} and P_{H_2O} are needed for each iteration. For the first iteration, reasonable values for P_{CO_2}/P_{CO} and P_{H_2O} are near 1.4 and 0.06, respectively [4]. For later iterations, values for P_{CO_2}/P_{CO} and P_{H_2O} are selected, the results of previous iterations serving as a guide. Once values of P_{CO_2}/P_{CO} and P_{H_2O} are supplied, the rest of the iteration

TABLE 1

Equilibria used in the Damköhler and Edse method and their equilibrium constants

Equilibria	Equilibrium constants at 2735 K[a]
(1) $CO_2 \rightleftharpoons CO + \frac{1}{2}O_2$	$K_1 = 0.116$
(2) $H_2O \rightleftharpoons H_2 + \frac{1}{2}O_2$	$K_2 = 0.0169$
(3) $H_2O \rightleftharpoons \frac{1}{2}H_2 + OH$	$K_3 = 0.0176$
(4) $\frac{1}{2}H_2 \rightleftharpoons H$	$K_4 = 0.0652$
(5) $\frac{1}{2}O_2 \rightleftharpoons O$	$K_5 = 0.0422$
(6) $\frac{1}{2}N_2 + \frac{1}{2}O_2 \rightleftharpoons NO$	—

[a]Reference 4.

TABLE 2

Steps in calculating the burnt-gas composition of a $He—O_2—C_2H_2$ flame[a]

Steps for each iteration	Variables calculated	Equations used	Comments
1	P_{CO_2}/P_{CO}, P_{H_2O}	—	Assumed values
2	P_{O_2}	$P_{O_2} = [K_1(P_{CO_2}/P_{CO})]^2$	Definition of K_1
3	P_O	$P_O = K_5(P_{O_2})^{1/2}$	Definition of K_5
4	P_{H_2}	$P_{H_2} = K_2P_{H_2O}/(P_{O_2})^{1/2}$	Definition of K_2
5	P_H	$P_H = K_4(P_{H_2})^{1/2}$	Definition of K_4
6	P_{OH}	$P_{OH} = K_3P_{H_2O}/(P_{H_2})^{1/2}$	Definition of K_3
7	n_H/k_2	$n_H/k_2 = 2P_{H_2} + P_H + P_{OH} + 2P_{H_2O}$	Eqn. 3
8	n_C/k_1	$n_C/k_1 = (n_H/k_2)(n_C/n_H)$	—
9	P_{CO}	$P_{CO} = (n_C/k_1)/[1 + (P_{CO_2}/P_{CO})]$	Eqn. 2
10	P_{CO_2}	$P_{CO_2} = (n_C/k_1) - P_{CO}$	Eqn. 2
11	n_{He}/k_4	$n_{He}/k_4 = (n_H/k_2)(n_{He}/n_H)$	—
12	P_{He}	$P_{He} = n_{He}/k_4$	Eqn. 5
13	n_O/k_3	$n_O/k_3 = 2P_{CO_2} + P_{CO} + P_{H_2O} + 2P_{O_2} + P_{OH} + P_O$	Eqn. 4
14	n_O/n_H	$(n_O/k_3)/(n_H/k_2)$	Calculated n_O/n_H ratio
15	P_{Total}	$P_{Total} = P_{CO_2} + P_{CO} + P_{H_2O} + P_{O_2} + P_{H_2} + P_{OH} + P_O + P_H + P_{He}$	Total partial pressures of all burnt gases

[a]Variables: K_e = equilibrium constants at 2735 K (Table 1) where e = 1, 2, 3, 4, 5. n_j = number of gram-atoms of element j (Eqns. 2—5) where j = C, N, O, He. n_C/n_H = 1.00, n_{He}/n_H = 4.15. P_i = partial pressures of flame species i, where i = CO_2, CO, H_2O, O_2, H_2, OH, O, H or He.

(steps 2 through 15) can be done according to the equation given in each step. At the end of each iteration, P_{Total}, or the sum of the partial pressures of all burnt gases (step 15) and the n_O/n_H ratio (step 14) are calculated. Understandably, the calculated P_{Total} and n_O/n_H ratio depend mainly on the initially assumed values of P_{H_2O} and P_{CO_2}/P_{CO}, respectively. Therefore, after

each iteration, the calculated value of P_{Total} is compared to its true value (1 Atm.). If the calculated P_{Total} is too high (low), then the initial value of P_{H_2O} was too high (low). Also after each iteration, the calculated n_O/n_H ratio is compared to the actual n_O/n_H ratio which, according to Eqn. 1, is 2.37. If the calculated n_O/n_H ratio is too high (low), then the initial value of P_{CO_2}/P_{CO} was too high (low). Therefore, these two comparisons permit improved values of P_{CO_2}/P_{CO} and P_{H_2O} to be assumed and used in the next iteration. When the calculated P_{Total} and n_O/n_H ratio equal their true values (within ± 0.00001 for P_{H_2O}, $\pm$ 0.0003 for n_O/n_H ratio), the partial pressures calculated from the last iteration are taken to be the burnt gas composition of the He—O_2—C_2H_2 flame.

Results and discussion

The calculated burnt-gas composition for the He—O_2—C_2H_2 flame conditions given earlier is listed in column 2 of Table 3. Also listed for comparison in Table 3 are the burnt-gas compositions of several air—C_2H_2 flames. Column 3 lists the burnt-gas composition calculated here for an air—C_2H_2 flame which has input gas flow rates similar to those for the He—O_2—C_2H_2 flame. Columns 4 and 5 list the composition of air—C_2H_2 flames reported by others.

The major difference between the burnt-gas compositions of the He—O_2—C_2H_2 and air—C_2H_2 flames (columns 2 and 3 of Table 3) is that the partial pressure of nitrogen in the air—C_2H_2 flame has been replaced by helium. This

TABLE 3

Calculated burnt-gas compositions for the air—C_2H_2 and He—O_2—C_2H_2 flames

Burnt-gas component	Partial pressure (Atm.)			Mole fraction
	He—O_2—C_2H_2 [a] 2735 K	Air—C_2H_2 [b] 2475 K	Air—C_2H_2 [c] 2523 K	Air—C_2H_2 [d] 2421 K
N_2	—	0.726	0.73	0.622
He	0.705	—	—	—
CO_2	0.097	0.120	0.12	0.053
H_2O	0.068	0.078	0.07	0.097
CO	0.073	0.055	0.04	0.171
H_2	0.007	0.006	0.00	0.052
O_2	0.024	0.005	0.02	—
OH	0.014	0.005	0.01	0.001
NO	—	0.003	0.01	0.000
H	0.006	0.002	0.00	0.004
O	0.007	0.001	0.00	0.000

[a]Gas flow rates: 1.94 l min^{-1} C_2H_2, 8.4 l min^{-1} He, 2.4 l min^{-1} O_2. [b]Gas flow rates: 1.94 l min^{-1} C_2H_2, 10.8 l min^{-1} Air which leads to 8.42 l min^{-1} N_2 and 2.27 l min^{-1} O_2. [c]Reference 4. [d]Reference 6.

substitution is desirable because of the higher thermal conductivity and lower quenching cross-section of helium compared to nitrogen; as a result, the $He—O_2—C_2H_2$ flame exhibits higher atom formation efficiencies [3] and less excited-state quenching [5].

Another important difference between the flames is that the predicted partial pressures of both carbon monoxide and oxygen are higher in the $He—O_2—C_2H_2$ flame. Because carbon monoxide is an important reductant, its presence is desirable in order to promote atom formation; in contrast, the larger amount of oxygen, a quencher and oxidizer, is undesirable. Fortunately, the effect caused by 0.024 atmosphere of oxygen would not be expected to be large enough to offset the gain realized by substituting helium for nitrogen. Therefore, compared to the air—C_2H_2 flame, the $He—O_2—C_2H_2$ flame is expected to provide a slightly more reducing and less quenching environment.

This research was funded by the National Science Foundation through grants CHE-83-14121 and CHE-83-20053 and by the Office of Naval Research.

REFERENCES

1 N. C. Clampitt and G. M. Hieftje, Anal. Chem., 46 (1974) 382.
2 K. A. Saturday and G. M. Hieftje, Anal. Chem., 49 (1977) 2013.
3 K. A. Saturday and G. M. Hieftje, Anal. Chem., 52 (1980) 786.
4 A. G. Gaydon and H. G. Wolfhard, Flames, Wiley, New York, 1979, pp. 323—339.
5 K. A. Saturday, Ph.D. Thesis, Indiana University, Bloomington, IN, 1979.
6 B. V. L'Vov, L. P. Kruglikova, L. K. Polzik and D. A. Katskov, J. Anal. Chem. USSR, 30(5) (1975) 715.

Analytica Chimica Acta, 162 (1984) 409—411
Elsevier Science Publishers B.V., Amsterdam — Printed in The Netherlands

Short Communication

MOLECULAR EMISSION CAVITY ANALYSIS
Part 26. Determination of Total Phosphate in Detergents

O. OSIBANJO[a] and S. A. AL-TAMRAH[b]

Chemistry Department, University of Birmingham, PO Box 363, Birmingham B15 2TT (Great Britain)

ALAN TOWNSHEND*

Chemistry Department, University of Hull, Hull HU6 7RX (Great Britain)

(Received 6th March 1984)

Summary. Total phosphate is determined in dry-ashed detergents by dissolution in 0.3 M sulphuric acid, injection of a 5-μl aliquot into a carbon cavity, and measurement of the HPO emission at 528 nm in a hydrogen-based flame.

Inorganic phosphates are important builders in detergents. Their reactions with certain metal ions such as calcium and magnesium ions soften the water. The commonest builder is sodium tripolyphosphate.

Molecular emission from cool hydrogen-based flames has been applied to the determination of phosphorus in detergents [1]. A cool aluminium surface was used to enhance the green HPO emission, which was measured at 525.2 nm. The HPO emission has also been used for determination of phosphorus in lubricating oils [2]. In both applications, the sample was ashed, and the solution obtained was freed from depressive cationic interferences by passing down a cation-exchange column. Inorganic [3, 4] and organic [3, 5] phosphorus compounds have been determined by molecular emission cavity analysis (m.e.c.a.) [6] also by measuring the intensity of their HPO emissions; nanogram amounts of phosphorus were determined by injecting 5-μl samples into aluminium or silica-lined cavities. As with the conventional emission technique, cations depressed the HPO emissions [3], but these could be eliminated by treatment with a cation-exchange resin [4]. Such a procedure has been applied to the determination of phosphorus in rocks [7]. The depressive effect of cations can also be removed by adding perchloric acid, or preferably sulphuric acid, to the phosphate solution [3].

There remains a requirement for a relatively simple, reliable method for the determination of total phosphate in detergents. El-Hag [4] confirmed that acidic solutions of most polyphosphates gave the same m.e.c.a. response

Present addresses: [a]Chemistry Department, University of Ibadan, Ibadan, Nigeria. [b]Chemistry Department, King Saud University, Riyadh, Saudi Arabia.

0003-2670/84/$03.00

as orthophosphate, because hydrolysis to orthophosphate occurred rapidly when an acidified solution was heated in the cavity by the flame. This communication describes a procedure for the determination of total phosphate in detergents, based on the injection of a sulphuric acid solution of dry-ashed detergent, which does not require ion-exchange pretreatment.

Experimental

Apparatus. An Evans Electroselenium EEL 240 atomic absorption spectrometer, modified as described previously [8], was fitted with a carbon cavity, 4 mm deep and 4 mm in diameter. The peak height emission intensity was recorded at 528 nm, via a 3-nm spectral slit-width. A hydrogen (6.0 l min^{-1})/nitrogen (6.4 l min^{-1})/air (3.8 l min^{-1}) flame was used. This gave the greatest intensity.

Reagents. A 1000 mg l^{-1} phosphorus solution was prepared by dissolving 5.03 g of analytical-grade sodium dihydrogenphosphate in 50 ml of distilled water and diluting to exactly 1 l with distilled water. Commercial detergent powders (Omo, Daz and Drive) were purchased from a local supermarket.

Procedure. Weigh accurately about 0.2 g of the dry detergent sample into a porcelain crucible. Heat in a muffle furnace at 520° C for 20 min to destroy organic matter, allow to cool, dissolve in distilled water, and dilute to 100 ml with that solvent. Transfer 1 ml of this solution to a 10-ml volumetric flask, add exactly 1 ml of 3 M sulphuric acid, and complete to volume with distilled water. Inject 5 μl of this solution into the carbon cavity and ignite the flame. Measure the green phosphorus emission intensity (second peak) at 528 nm. Prepare calibration solutions (100—500 mg l^{-1} phosphorus) by appropriate dilution of the 1000 mg l^{-1} sodium dihydrogenphosphate solution with 0.3 M sulphuric acid, so that the final sulphuric acid concentration is 0.03 M.

Results

Injection of 5 μl of an aqueous solution (0.1 g l^{-1}) of dry-ashed "Daz" into a stainless steel cavity, and insertion into the hydrogen/nitrogen/air flame, gave no measurable HPO emission, because of intense cavity incandescence. No improvement was obtained with samples to which sulphuric acid had been added. However, the use of a carbon cavity, which does not become incandescent under the flame conditions used, allowed intense reproducible HPO emissions to be obtained from 0.03 M sulphuric acid solutions of the ashed detergent. All three detergents, under these conditions, gave two peaks at 528 nm. The first (t_m = 6 s [6]) is from the S_2 emission from sulphuric acid, the band spectrum of which extends to this wavelength [9]. The second (t_m = 10 s) is due to HPO emission, and is the peak that should be measured for phosphate determinations. The second peak appears at exactly the same t_m value as that for sodium dihydrogenphosphate under the same conditions, showing that all condensed phosphates had been converted to orthophosphate before emitting species were generated.

TABLE 1

Determination of total phosphate in some commercial detergents

Detergent	Total phosphate found (% P)	
	M.e.c.a.	Quinoline molybdate[a]
Daz	7.5, 7.45	7.6
Drive	9.6, 9.6	9.6
Omo	8.3, 8.2	8.15

[a]Mean of two results.

A linear calibration graph was obtained up to at least 2.5 μg of phosphorus in the 5-μl solution injected. The total phosphate concentrations measured for the three detergents are shown in Table 1. The results are compared with those obtained by the quinoline molybdate titrimetric procedure [10], and are found to be in good agreement.

Conclusions

The determination of total phosphate in detergents by the proposed method is accurate and reasonably rapid. Time-consuming pre-hydrolysis of the condensed phosphates is not necessary, as it is in the quinoline molybdate and similar methods, and in spectrophotometric methods based on molybdenum blue formation [10]. The m.e.c.a. method is also very sensitive, and does not require the removal of interfering cations.

REFERENCES

1 A. Syty, Anal. Lett., 4 (1971) 531.
2 W. N. Elliott, C. Heathcote and R. A. Mostyn, Talanta, 19 (1972) 359.
3 O. Osibanjo, Ph.D. Thesis, University of Birmingham (1976); Proc. Anal. Div. Chem. Soc., 13 (1976) 127.
4 I. H. El-Hag, Ph.D. Thesis, University of Birmingham (1982); Anal. Proc., 19 (1982) 320.
5 R. Belcher, S. L. Bogdanski, O. Osibanjo and A. Townshend, Anal. Chim. Acta, 84 (1976) 1.
6 M. Burguera, S. L. Bogdanski and A. Townshend, CRC Crit. Rev. Anal. Chem., 10 (1981) 185.
7 A. C. Calokerinos and T. P. Hadjiioannou, Anal. Chim. Acta, 157 (1984) 171.
8 R. Belcher, S. L. Bogdanski and A. Townshend, Anal. Chim. Acta, 67 (1973) 1.
9 R. W. B. Pearse and A. G. Gaydon, The Identification of Molecular Spectra, 4th edn., Chapman and Hall, London, 1976, p. 293.
10 W. J. Williams, Handbook of Anion Determination, Butterworths, London, 1979, pp. 461 and 466.

Analytica Chimica Acta, 162 (1984) 413—417
Elsevier Science Publishers B.V., Amsterdam — Printed in The Netherlands

Short Communication

SOME OBSERVATIONS ON THE ATOMIC ABSORPTION SPECTROMETRY OF GALLIUM WITH ELECTROTHERMAL ATOMIZERS

P. VASILE BOTHA and JÁNOS FAZAKAS*

Institute for Soil Science and Agrochemistry, and Center for Analytical Spectrochemistry, Bd. Mărăsti 61, R-71331 Bucharest 32 (Rumania)

(Received 23rd September 1983)

Summary. Signal strength can be doubled in normal graphite furnaces compared to pyrolytically coated ones, thus proving the essential role of carbon in the atomization of gallium. Platform vaporization enhances both peak height and area signals. The use of ascorbic acid as matrix modifier improves sensitivity considerably, with enhancements being more pronounced in pyrolytically coated furnaces.

Previous papers [1—3] have described the use of non-resonance lines for the determination of volatile and slightly volatile elements. For palladium, the use of wall or platform vaporization [1] allowed detection of absorption at the non-resonance lines. The best sensitivity achieved for the 340.5-nm non-resonance line of palladium (originating at 6670 cm^{-1} above the ground state) is only 2.1 times poorer than that obtained at the most sensitive resonance line. Calibration graphs were also found to be much more linear at the non-resonance line than at the resonance line. Studies of the influence of purge gas flow rate [2] on the resonance and non-resonance lines showed that the latter are influenced more than the former, possibly owing to the cooling effect of the purge gas which will obviously have more influence on the non-resonance transitions. Thus, for palladium at the non-resonance line studied, the population of the excited states is partly thermally controlled [2]. The palladium resonance lines are affected adversely by pressure [3] whereas the sensitivity of the non-resonance lines is enhanced.

Later work with volatile and non-volatile elements confirmed the results obtained with palladium. However, for some volatile elements with non-resonance lines originating above 7000 cm^{-1} (lead and thallium), only platform vaporization ensured a suitable sensitivity when non-resonance lines were used. The present communication extends the investigation of the analytical potential of non-resonance lines to gallium.

Experimental

A Pye-Unicam SP-9 spectrometer (time resolution 20 ms) and an electrothermal atomizer (heating rate 2000°C s^{-1}) were used. An ashing temperature of 900°C was used as recommended by the manufacturer. The atomization temperature for wall vaporization was found to be optimal at 1800°C for pyrolytically coated furnaces. However, for normal graphite a sensitivity plateau was reached only at 2200°C. With platform vaporization, the atomization temperature giving the best sensitivity was similar to that for wall vaporization. Above 600°C, the atomizer was operated in the temperature-control mode (radiational feedback). Argon was used as purge gas at ca. 2 l min^{-1}. A Varian hollow-cathode gallium lamp was operated at 5 mA. A spectral bandwidth of 0.2 nm was used for all wavelengths investigated. Some data on the spectral transitions studied are given in Table 1.

The gallium stock solution was obtained by dissolving 0.1 g of the metal in the minimum amount of aqua regia and diluting to 100 ml with water. Working solutions were prepared daily and were made 0.05% in nitric acid to prevent hydrolysis. All chemicals used in the interference studies were of reagent grade and were shown not to contain any detectable amount of gallium.

Results and discussion

Influence of vaporization surface and some interference effects. For economic reasons, normal graphite furnaces were used in this investigation. Unexpectedly, an almost twofold signal enhancement was observed, compared to pyrolytically coated furnaces. This was contrary to literature data [5, 6] and to previous experience of the present authors with other elements. The sensitivity enhancements observed are shown in Table 2. It is difficult fully to clarify the reasons for the phenomena observed, but is quite obvious that carbon plays an important role in the atomization of gallium. The sensitivity difference persists with platform vaporization. That it is the atomization surface that is important and not the nature of the atom reservoir is proved by the fact that when vaporization was done from a pyrolytic platform in a normal furnace, the inhibition effect of the pyrolytically coated surface was just as apparent as in a pyrolytically coated furnace. On

TABLE 1

Some characteristics of the most important spectral transitions of gallium

Wavelength (nm)	Spectral term values (cm^{-1})	gf value [4]
287.42	0—34 782	0.74
294.36	826—34 782	1.5
294.42	826—34 782	0.24
403.30	0—24 789	0.24
417.21	826—24 789	0.53

TABLE 2

Comparison of gallium peak-height signals under various conditions

Matrix	Normal graphite with vaporization from different surfaces			Pyrographite with vaporization from different surfaces	
	Wall	Normal platform[a]	Pyroplatform[a]	Wall	Pyroplatform[a]
Aqueous solution[b]	100	130	100	50	65
3% Ascorbic acid	130	170	—	100	130
1% HNO_3	180	230	—	115	150

[a]Platform mass 90 mg. [b]In 0.05% nitric acid.

the assumption that when a pyrolytically coated surface is present, gallium is partly vaporized as an oxide, it would be expected that platform vaporization would minimize differences between the two types of graphite. This was not the case, so that the phenomenon observed is definitely a surface effect. The presence of active sites in normal carbon furnaces may promote the formation of a more easily atomized form of gallium.

It follows, therefore, that the presence of a matrix modifier that can provide free carbon in the system will enhance the gallium signal in pyrolytically coated furnaces. Indeed, as shown in Table 2, the addition of 3% ascorbic acid enhances considerably the gallium signal in such furnaces. As shown in Table 2, some enhancement is also evident for normal furnaces though not as large as for the coated ones. No attempt was made to optimize the amount of ascorbic acid used as matrix modifier; the concentration used is probably far from optimal.

Given the above results, it is recommended that normal graphite furnaces and platforms be used instead of pyrolytically coated ones for the determination of gallium. Vaporization from a platform yields a considerable enhancement of the gallium signal (see Table 2). When gallium is to be determined in organic matrices (that may yield free carbon during pyrolysis), matrix matching of samples and standards is mandatory. Alternatively, ascorbic acid in high concentration should be added to both samples and standards.

The considerable enhancement of gallium signals by nitric acid has been already noted by Alder and Hickman [7]. As shown in Table 2, this was also noted here. In view of the experiments with ascorbic acid, the enhancement by nitric acid could be due to the activation of some carbon sites by the acid. It is also possible that the presence of nitric acid promotes the formation of higher oxides of gallium with greater thermal stability [7]. If this is true, then the presence of nitric acid should allow the use of higher ashing temperatures.

All the results obtained with ascorbic and nitric acids indicate a decisive role for carbon in the atomization of gallium. If this is true, then carbide-forming elements should depress the gallium signal by binding some of the

active carbon sites. However, the addition of a 100-fold excess of molybdenum did not depress the gallium signal but provided a slight enhancement. This is difficult to explain. It should be mentioned, however, that Suzuki and Ohta [8] determined gallium with good sensitivity in a molybdenum microtube atomizer.

The analytical potential of non-resonance lines. As shown in Table 1, gallium has several non-resonance lines originating at 826 cm^{-1} above the ground state. Considering the rather high oscillator strength of these non-resonance lines [4], considerable analytical sensitivity would be expected. The 294.36/294.42-nm non-resonance line was found to be ca. 30% more sensitive than the 287.42-nm resonance line for a spectral bandwidth of 0.2 nm. When bandwidths of 0.5 nm were used as recommended by some manufacturers (see, e.g. [6]), these two lines were of almost equal sensitivity. The other two gallium lines investigated (403.30 and 417.21 nm) had the relative sensitivity mentioned previously [6].

The calibration graphs for the 294.36/294.42-nm non-resonance line pair and for the 287.42-nm resonance line based on peak height and area are shown in Fig. 1. The non-resonance line gives less linear calibrations than was expected, probably owing to the inability of the spectrometer to isolate the non-resonance doublet. The 403.30- and 417.21-nm lines (not shown in Fig. 1) gave calibration graphs that were linear up to an absorbance of ca. 1.2. Because of the much higher intensity of the longer wavelengths emitted by the hollow-cathode lamp, the photomultiplier voltage can be significantly reduced. This should result in an improvement of precision.

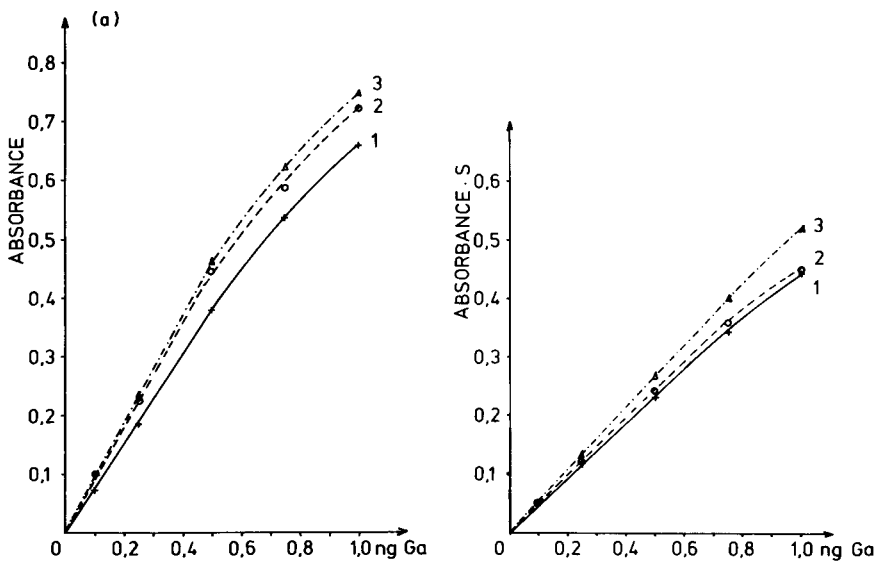

Fig. 1. Calibration graphs for gallium, with atomization from a normal platform in a normal graphite furnace: (a) peak height; (b) peak area. Curves: (1) 287.42 nm, atomization at 1800°C; (2) 294.36/294.42 nm, atomization at 1800°C; (3) 294.36/294.42 nm, atomization at 2200°C.

Atomization temperatures have very little influence on the relative sensitivity of the gallium non-resonance lines. It seems that for elements that have their non-resonance levels below ca. 4000 cm^{-1}, there is little influence of atomization temperature on non-resonance lines irrespective of the volatility of the element; this was shown for tin and indium in other work. For elements with such relatively "low-lying" non-resonance levels, wall vaporization yields analytically useful signals. With elements with non-resonance lines originating above 4000—5000 cm^{-1}, wall vaporization gives analytically useful signals only for elements of low volatility (e.g., palladium) [1—3]. For the more volatile elements (lead and thallium), other work showed that platform vaporization must be used to obtain useful sensitivities.

Parsons et al. [9] have forecast the temperature-intensity dependence of the gallium non-resonance lines, as well as suggesting that the sensitivity of the resonance lines will be adversely affected by increasing temperature. This was explained by the gradual depletion of the ground-state atomic population (47.5% at 2000 K vs. 42.0% at 3200 K). In the present investigation, the sensitivity of the resonance line was not found to be influenced by atomization temperature. In a recent paper [8], the 294.36-nm non-resonance line was mistakenly identified as a resonance line.

The authors thank Mr. David Tyreman (Pye-Unicam) for the provision of some of the graphite tubes used in the present work.

REFERENCES

1 J. Fazakas, Anal. Lett., 14 (1981) 535; 15 (1982) 245; Fresenius Z. Anal. Chem., 312 (1982) 227.
2 J. Fazakas, Spectrosc. Lett., 15 (1982) 21.
3 J. Fazakas, Spectrochim. Acta, Part B, 37 (1982) 921.
4 R. Mavrodineanu and H. Boiteux, Flame Spectroscopy, Wiley, New York, 1965.
5 C. W. Fuller, Electrothermal Atomization in Atomic Absorption Spectrometry, Royal Society of Chemistry, London, 1977.
6 T. C. Dymott, Atomic Absorption with Electrothermal Atomization, Pye Unicam, Cambridge, 1981.
7 J. F. Alder and D. A. Hickman, At. Abs. Newsl., 16 (1977) 110.
8 M. Suzuki and K. Ohta, Prog. Anal. At. Spectrosc., 6 (1983) 49.
9 M. L. Parsons, B. W. Smith and P. M. McElfresh, Appl. Spectrosc., 27 (1973) 471.

Analytica Chimica Acta, 162 (1984) 419—422
Elsevier Science Publishers B.V., Amsterdam — Printed in The Netherlands

Short Communication

DETERMINATION OF BORON IN ENGINE COOLANTS BY DIRECT CURRENT PLASMA ATOMIC EMISSION SPECTROMETRY

NOEL M. POTTER*

Analytical Chemistry Department, General Motors Research Laboratories, Warren, MI 48090 (U.S.A.)

RONALD R. LOVELACE

Pontiac Motor Division, General Manufacturing Laboratory, 1 Pontiac Plaza, Pontiac, MI 48053 (U.S.A.)

(Received 24th April 1984)

Summary. Boron in unused engine coolants is determined by direct current plasma atomic emission spectrometry with a relative standard deviation of approximately 1%. Ethane-1,2-diol is added to calibration solutions to match the concentrations in the samples being analyzed. Results obtained are within 1% of the amount of boron in an engine coolant of known composition. The time needed for a batch of 10 samples is approximately 3 h.

Engine coolants typically contain ethylene glycol (ethane-1,2-diol) for freeze protection as well as several additives to prevent corrosion of the ferrous and nonferrous alloys used in the cooling system. A borate salt is commonly added to provide buffering action so that the coolant solution remains buffered at a high pH even after extended use.

Boron in automotive engine coolants is often determined by the classical mannitol—boric acid titration [1, 2]. Although accurate, this method is subject to interferences from phosphate, mercaptobenzothiazole and tolyltriazole, which are present in many coolant formulations. In addition, the method is time-consuming. Several spectrophotometric methods have been used to determine boron in a variety of materials [2, 3]. Carminic acid has been successfully applied for the determination of boron in engine coolants [1] but, like most other spectrophotometric methods for boron, it is slow and cumbersome.

With the availability of plasma atomic emission spectrometers, several new methods have been developed for the determination of boron in various materials [4—6], but not in engine coolants. In view of the success of direct current plasma (d.c.p.) atomic emission spectrometry in determining boron in glass [7] and after some experience with the d.c.p. in determining boron in a ferrous alloy, this study was initiated to develop a d.c.p. method for determining boron in unused engine coolants.

0003-2670/84/$03.00

Experimental

Apparatus and operating parameters. A SpectraSpan-V d.c. plasma atomic emission spectrometer (Spectrametrics, Andover, MA) was used with the operating conditions listed in Table 1.

Standards and reagents. All chemicals were ACS reagent grade unless stated otherwise. A boron standard solution (100 μg ml^{-1}, boron) was prepared by dissolving boric acid (0.5720 g) in deionized water (1 l). This solution was stored in a plastic bottle. Acetic acid and ethane-1,2-diol (J. T. Baker, Phillipsburg, NJ) were used to prepare sample and calibration solutions.

Procedure. Glassware and plasticware were cleaned with (1+1) nitric acid and rinsed with deionized water prior to use. Samples were mixed thoroughly by shaking. Weighed portions of sample (2 g) were put into 200-ml plastic volumetric flasks. Water (100 ml) and acetic acid (10 ml) were added. The contents of the flasks were then diluted to volume and mixed prior to measurement. (Sample weighing was easily accomplished by weighing an aliquot of the sample contained within a 3-ml plastic syringe, injecting a portion into the 200-ml volumetric flask, and reweighing the plastic syringe and contents.)

Calibration solutions containing 3, 5, and 10 μg ml^{-1} boron were prepared by adding aliquots of the boron stock solution to 200-ml volumetric flasks. Water (100 ml), ethane-1,2-diol (4 ml), and acetic acid (10 ml) were added. The contents of the flasks were then diluted to volume and mixed prior to measurement.

The boron resonance line at 249.678 nm was used. The instrument was calibrated with the 3 and 10 μg ml^{-1} calibration solutions as recommended by the manufacturer. Calibration plots were linear over this range. At least two measurements were made on each sample. The calculated concentration values were averaged to obtain the reported concentration.

To compensate for instrumental drift, favorable integration times (30 s) and frequent calibration solution measurements were used. Calibration solutions most closely approximating sample solutions were measured before and after every two sample solutions. The amount of drift in the response of the calibration solutions was calculated, and the sample solution response was corrected with this value. If the drift was greater than 4% relative, the instrument was recalibrated before proceeding.

TABLE 1

Operating conditions

Wavelength	249.678 nm	Sleeve argon pressure	3.4 atm.
Entrance slit	50 × 300 μm	Nebulizer argon pressure	1.9 atm.
Exit slit	50 × 300 μm	Sample flow rate	$\approx$2 ml min^{-1}
Integration time	30 s		

Results and discussion

Boron was quantified in various production lots of the formulation shown in Table 2 [8]. The method was not applied to other formulations.

No differences in boron concentrations were noted for calibration solutions contained within borosilicate glass up to 48 h. Engine coolant samples were placed in plastic volumetric flasks because the coolants are basic and hence could leach boron from borosilicate glass. Sample solutions were stable for several days.

Spectral interferences. No spectral interferences for boron were noted at 249.678 nm with these engine coolants. Wavelength scans were made in the vicinity of 249.678 nm with solutions containing ethane-1,2-diol and acetic acid; in addition, these solutions contained engine coolant additives at concentrations of 10 times the levels normally encountered (Table 2). These scans showed no differences when compared to scans made with deionized water. The boron line at 208.893 nm was not used because ethane-1,2-diol increased the background response in its vicinity. Other boron lines were not examined.

Nonspectral interferences. Chemical and vaporization effects also may be troublesome in d.c.p. atomic emission spectrometry. Acetic acid (10 ml) was added to all sample and calibration solutions (200 ml) to maintain similar acid concentrations. (Most engine coolants are basic.) Ethane-1,2-diol had to be added to calibration solutions because it increases the boron response signal; the increase is about 6% without acetic acid and is about 3% with acetic acid. The effect of ethane-1,2-diol on the boron response signal is constant for concentrations between 1 and 4% (v/v).

All other additives, except the foam suppressor (Pluronic L-61), at concentrations 10 times those normally encountered (Table 2) had no effect on the boron response signal. Foam suppressor concentrations at 10 and 20

TABLE 2

Composition of automotive engine coolant concentrate[a]

Constituent	% (w/w)	Constituent	% (w/w)
Ethylene glycol	95.56	Sodium mercaptobenzo-thiazole (50% soln.)	0.50
Sodium nitrate ($NaNO_3$)	0.10		
Sodium molybdate ($Na_2MoO_4 \cdot 2H_2O$)	0.20	Sodium tolyltriazole (50% soln.)	0.20
Sodium tetraborate ($Na_2B_4O_7 \cdot 5H_2O$)	0.40	Sodium hydroxide	0.235
		Water	2.30
Sodium silicate solution (40% Na_2SiO_3)	0.30	Foam suppressor (Pluronic L-61)	0.05
Phosphoric acid (85% H_3PO_4)	0.15	Green dye (fluorescein or alizarin cyanone green B extra)	0.005

[a]Ref. 8.

times that specified reduced the boron response signal by about 4%, but the concentrations normally encountered (Table 2) had no effect. It is presumed that the foam suppressor affects the sample nebulization characteristics. Hence, for other coolant formulations the effect of foam suppressors (or other surfactants), which may affect sample nebulization rates, should be investigated before application of this method.

Method evaluation. To evaluate this method, an engine coolant of known composition was prepared according to the formulation in Table 2. For 0.0600% boron added, values of 0.0602, 0.0595, and 0.0603% were obtained with the proposed d.c.p., spectrophotometric, and the titrimetric methods, respectively. All boron concentrations found were within 1% of that added to the formulation.

Several lots of the engine coolant containing near 0.06% boron were processed by this method. The boron concentrations found were compared to results obtained by the mannitol—boric acid titration [1]. The d.c.p. results obtained in duplicate exhibited an average relative deviation of 2.15% from the titrimetric method. The relative standard deviation calculated from 15 results on one sample was 1.0%.

Finally, this d.c.p. method offers an attractive alternative to the mannitol—boric acid titration because samples can be processed rapidly. Only about 3 h (including preparation of sample and calibration solutions) are required to determine boron in 10 samples, whereas approximately one day is needed for the titration method excluding the time required to determine correction factors.

The authors thank H. E. Vergosen III and D. Blossfeld for preparing coolant formulations and providing data, and R. B. Loranger for helpful discussions.

REFERENCES

1 R. B. Loranger, H. E. Vergosen, III, D. P. Krause and N. M. Potter, Methods for the Chemical Analysis of a Formulated Antifreeze, General Motors Research Laboratories, Warren, MI, Research Publication GMR-4266, February 1983.
2 R. S. Braman, in I. M. Kolthoff and P. J. Elving (Eds.), Treatise on Analytical Chemistry, Part II, Vol. 10, Wiley, New York, 1978, pp. 1—101.
3 A. A. Nemodruk and Z. K. Karalova, Analytical Chemistry of Boron, Daniel Davey and Co., New York, 1965.
4 J. W. Owens, E. S. Gladney and D. Knab, Anal. Chim. Acta, 135 (1982) 169.
5 E. Grallath, P. Tschöpel, G. Kölblin, U. Stix and G. Tölg, Z. Anal. Chem., 302 (1980) 40.
6 G. F. Wallace, At. Spectrosc., 2 (1981) 61.
7 R. A. Burdo and M. L. Snyder, Anal. Chem., 51 (1979) 1502.
8 L. C. Rowe, R. L. Chance and M. S. Walker, Mater. Perform., No. 6, 22 (1983) 17.

Analytica Chimica Acta, 162 (1984) 423—426
Elsevier Science Publishers B.V., Amsterdam — Printed in The Netherlands

Short Communication

X-RAY FLUORESCENCE DETERMINATION OF TRACE ELEMENTS IN SOIL

IRENE M. ZSOLNAY*, JONATHAN M. BRAUER and STANLEY A. SOJKA

Occidental Chemical Corporation, Grand Island Research Center, Long Road, Grand Island, NY 14072 (U.S.A.)

(Received 2nd February 1984)

Summary. Trace elements in soil are quantified by a direct X-ray fluorescence method. Gallium is used as an internal standard to compensate for variations in sample matrix, instrumental operating characteristics, and sample preparation. At the 50-mg kg^{-1} level, V, Cr, Ni, Cu, Zn and As can be determined within a precision and accuracy of ± 20% or less. Sample preparation is less elaborate than for some other methods.

The ability to determine selected trace metals efficiently in large numbers of soil samples is important from an environmental protection point of view. An expeditious method was needed to assess trace metal contaminants in soils. There are several analytical methods available to quantify trace elements, but most of these methods require samples in solution form. Few methods have been described for solid samples [1, 2].

This communication describes an X-ray fluorescence spectrometric method to determine V, Cr, Ni, Cu, Zn and As at trace levels in soil with the aid of an internal standard. The use of an internal standard efficiently corrects for a variety of instrumental and operational variations and for differences in the soils. To select a suitable internal standard, it is necessary to fulfil several requirements. The standard should be different from the common major components of the soil (Si, Al, Ca, Mg, Ti, Fe, etc.) and should have similar X-ray absorption characteristics to the elements of interest. The X-ray peak of the internal standard should not overlap any of the elements of interest or with the matrix elements in the soil. For these reasons, gallium was chosen in this work.

Experimental

X-ray fluorescence analysis. All measurements were done with a Siemens SRS-1 X-ray fluorescence spectrometer equipped with a PDP-8E computer and a ten-position sample chamber. A lithium fluoride analyzing crystal and a scintillation detector were used with a chromium target X-ray tube for Ni, Cu, Zn and As, and with a gold target X-ray tube for Cr and V. Counts were collected for 100 s for each element at the peak position along with a

0003-2670/84/$03.00

background count to calculate the net peak intensities. For the internal standard, counts were collected for 100 s using both instrument settings.

For the pulse height analyzer, the window width was set to 0.80 V and the baseline to 0.85 V. The collimator setting was 0.40 mm.

Reagents. Reagents were purchased from Alpha Ventron (Chromatography Grade) as 1000 mg l^{-1} solutions of V, Cr, Ni, Cu, Zn, As and Ga. Reagent-grade anhydrous sodium carbonate and reagent grade silicon dioxide were purchased from J. T. Baker Chemicals.

Preparation of standards for calibration. To 3-g portions of the synthetic mixture (1:1 mixture of silica and sodium carbonate) were added 50, 100, 250 and 500 $\mu g\, g^{-1}$ of the six elements to prepare standard calibration curves. The standard mixtures were dried at 110° C. The dried mixtures were ground in a mortar and pestle. Portions (2 g) of the ground mixture were pressed into discs with 10 000 psi, using a hydraulic press, in a 30-mm diameter dye. The plots of intensity vs. concentration were linear for all six elements in the 1—500 $\mu g\, g^{-1}$ range (Fig. 1).

For the soil samples, one standard was prepared as follows. To a 3-g portion of the synthetic mixture was added 50 $\mu g\ g^{-1}$ amounts of the six elements together with 50 $\mu g\ g^{-1}$ gallium as internal standard. The mixture was again treated as described above. A 2-g portion of the synthetic mixture was pressed in the same manner to be used as blank.

Sample preparation and processing. From a well homogenized soil sample, a 10-g portion was crushed to 1—2 mm particle size and dried at 110° C. The dried sample was further ground to about 120 mesh in a tungsten carbide ball mill. A 2-g portion of the powder was taken and pressed for final processing. To a 3-g portion of the same sample, 50 $\mu g\ g^{-1}$ gallium was added as internal standard, together with some deionized water to make a thick paste. The well-mixed sample was then dried again for 15 min at 110° C, reground, and a 2-g portion was pressed for analysis. The synthetic mix blank, the

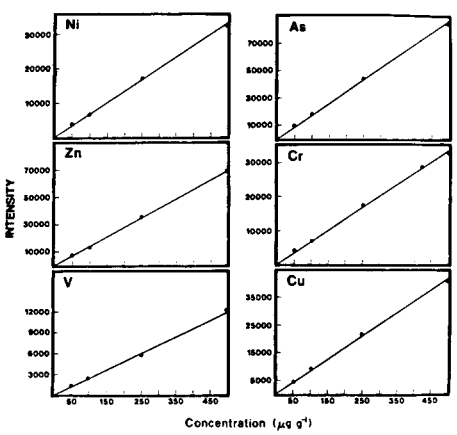

Fig. 1. Peaks of intensity vs. concentration for 6 elements.

synthetic mix plus all elements (including 50 $\mu g\ g^{-1}$ Ga) and the sample discs with and without the gallium addition were measured to obtain the matrix correction factor. A 100-s counting time was used for each peak and background.

The matrix correction factor (F_s) was calculated by dividing the net counts of Ga in the sample by the net counts of the Ga in the synthetic mixture. Data were processed by the usual internal standard method.

X-ray peak overlap correction. The vanadium K_α peak is superimposed on the titanium K_β peak. Generally, soil samples contain 0.1—2% titanium. To correct for the K_β counts of the titanium, the counts are collected at the titanium K_α position to measure the titanium concentration present. The intensity ratio K_β:K_α is calculated from a vanadium free standard. To achieve the net vanadium counts, the Ti K_α counts, multiplied by this ratio, is subtracted from the vanadium value. This number is used in the further steps of the calculation. Likewise, the arsenic K_α peak occurs at the same position as the lead L_α peak and a similar procedure is used to correct the arsenic intensity. If the major components of the soil matrix have wide variations, the K_β:K_α ratio should be measured to establish its proper value.

Furthermore, for the calculation of the arsenic concentration, a background adjustment is introduced in the equation. This adjustment factor corrects for the differences of the slopes of the X-ray spectrum for the sample vs. synthetic standard, which may be significant at the low 2θ angle area.

The synthetic mixture was used to generate matrix correction factors to collect data for the evaluation of precision and accuracy and to evaluate sensitivity.

If the iron concentration in the soil matrix is 2% or less, the stated approach is valid. If the iron concentration is significantly above 2%, then an additional correction will be necessary. For these soils, synthetic standards must be prepared which reflect the amount of iron in the unknown. The soils used in this work all contained iron concentrations of 2% or less.

Results and discussion

The matrix correction factors were further tested in soil samples, purified soils, and synthetic mixtures. It was found that, within a 95% confidence limit, the F_s may be used as a general correction factor for all tested elements with a precision of ±20%.

The precision of the method was assessed by examining the reproducibility of sample preparation, the counting process, and results for a known mixture. Thus, seven discs of a soil sample with known amounts of the elements and gallium were prepared and processed. Statistical analysis showed that sample preparation leads to a ±2% variation. The X-ray counting reproducibility was addressed by multiple measurements on one sample; the variation was within ±2%.

The correction factor gives results within ±1—5% for the elements Zn, Cu, Ni and As.

Results obtained for chromium and vanadium were less accurate, with

errors being 15—20% of the expected value. To select a more effective internal standard for V and Cr is difficult. All the nearby elements are common components of the soil (K, Ca or Ti) and a 50 $\mu g\ g^{-1}$ addition would not significantly change the intensities.

The accuracy of the method was tested by determining the recovery of 50 $\mu g\ g^{-1}$ additions of the six elements in a known sample and with one NBS (SRM 1645 River Sediment) standard. The results are summarized in Tables 1 and 2, respectively. As the tables show, all results are within ±20% of the actual value. Thus, each element can be detected at the $\mu g\ g^{-1}$ level with an imprecision of ±20% or less and a relative inaccuracy of ±20% or less. Duplicate randomly selected soil samples were prepared for a large number of samples for quality assurance purposes. The imprecision varied between 0.5 and 10%.

We gratefully acknowledge the support and encouragement of D. L. Eichler.

TABLE 1

Recoveries measured from a known sample

Element	V	Cr	Ni	Cu	Zn	As
Recovery ($\mu g\ g^{-1}$)[a]	55.6	59.8	50.0	56.0	44.4	47.6

[a]50 $\mu g\ g^{-1}$ added.

TABLE 2

Results for NBS SRM 1645 River Sediment[a]

Element	Concentration ($\mu g\ g^{-1}$)		Difference (%)
	Certified	This work	
V	23.5 ± 29.3%	26	+9.6
Ni	45.8 ± 6.3%	48	+4.6
Cu	109 ± 17.5%	128	+14.8
Zn	1720 ± 9.8%	1695	−1.5
As	66	75	+12.0

[a]The Cr content is 2.96%, which is beyond the range of this method.

REFERENCES

1 D. Sommer and K. Z. Ohls, Anal. Chem., 304 (1980) 97.
2 J. B. Headridge, Spectrochim. Acta, Part B, 35 (1980) 785.

Analytica Chimica Acta, 162 (1984) 427—430
Elsevier Science Publishers B.V., Amsterdam — Printed in The Netherlands

Short Communication

ANOMALOUS INFRARED SPECTRA OF DIAZEPAM IN POTASSIUM BROMIDE PELLETS PREPARED FROM CHLOROFORM SOLUTIONS

HIROMITSU KANAI*, VERONICA INOUYE and REGINALD GOO[a]

Chemistry Section, Laboratories Branch, Hawaii State Department of Health, Honolulu, HI 96813 (U.S.A.)

(Received 24th February 1984)

Summary. When diazepam in chloroform was incorporated into a KBr pellet, its infrared (i.r.) spectrum showed an anomalous spectral phenomenon at 836 cm^{-1}. Examination of i.r. spectra of diazepam obtained by the solution, multiple-internal-reflectance, and KBr-pellet techniques suggest that this spectral characteristic is due to the orientation effect of diazepam in KBr pellets.

Although there are some limitations [1], in forensic science the KBr pellet method is preferred for identification of drug samples by i.r. spectrometry [2, 3]. However, unlike other tranquilizers of the 1,4-benzodiazepin-2-one class, diazepam incorporated in chloroform solution in a KBr pellet was found here to produce an anomalous spectral phenomenon at 836 cm^{-1}. On one occasion there was a shoulder and in another experiment there was a band at 836 cm^{-1}. Furthermore, the relative intensity of the 836 cm^{-1} band with respect to the 816 cm^{-1} band was variable. This did not occur when chloroform was replaced by petroleum ether to recrystallize the diazepam.

The orientation effects of solid analytes on i.r. spectra have been described by several authors [4—6]. The orientation effects of waxy analytes on the i.r. spectra of solids have been explained [7]. It was considered that this spectral property of diazepam could be related to this effect. To study this problem, the i.r. spectral characteristics of diazepam were investigated by several i.r. techniques (KBr pellet, solution, and multiple internal reflection). Further, the effects of pressure applied to prepare the pellet, variations in the diazepam concentration in the KBr pellet, and the effect of both thermal and kinetic relaxation of the KBr pellet were also studied.

Experimental

The rapid KBr pellet method [8] was used. All the KBr pellet samples and multiple-internal-reflectance samples were scanned from 4000 cm^{-1} to

[a]Present address: Dept. of Public Works, City and County of Honolulu, HI 96813.

0003-2670/84/$03.00

400 cm^{-1} on a Perkin-Elmer model 467 i.r. spectrometer. A sample of 3% diazepam in chloroform was scanned from 4000 cm^{-1} to 600 cm^{-1}. A 5 mg ml^{-1} diazepam solution in chloroform was applied to both surfaces of the KR-5 internal reflecting crystal and after evaporation of chloroform, the waxy diazepam was analyzed with the multiple-internal-reflectance accessory set at an angle of 30°.

Results and discussion

Figure 1 shows the relevant portions of the i.r. spectra for diazepam obtained by the chloroform, multiple internal reflection, and KBr pellet techniques, respectively. Although there is a shoulder for the diazepam monitored with the multiple-internal-reflection method, the i.r. spectra of diazepam in both the solution and multiple-internal-reflectance methods do not show a band at 836 cm^{-1}. In addition, there is a broad band at 750 cm^{-1} in the KBr pellet spectrum which is not present in the other spectra. Although both the multiple-internal-reflectance and KBr-pellet techniques detected the diazepam which was in the waxy form, the former method detected it as a

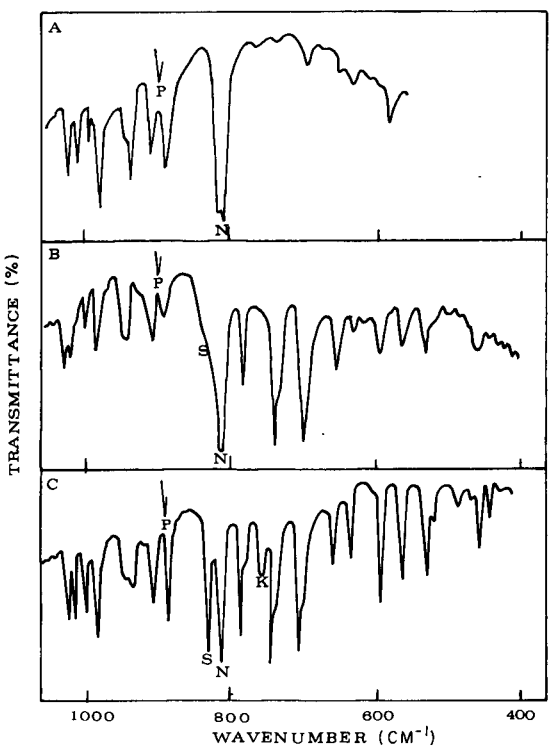

Fig. 1. The effect of the physical states of diazepam on the i.r. spectrum: (A) in chloroform; (B) by multiple internal reflection; (C) KBr pellet. P, polystyrene film calibration at 906.5 cm^{-1}; S, 836 cm^{-1} band; N, 816 cm^{-1} band; K, broad band at 750 cm^{-1}.

waxy film, whereas in the latter method the analyte was in the restricted environment of the KBr crystals. Therefore, these bands at 836 cm^{-1} and 750 cm^{-1} can probably be attributed to an orientation effect of the diazepam in the KBr pellet.

If this suggestion is correct, then any changes in the diazepam concentration and in the pressure applied to prepare the KBr pellet should show an effect at 836 cm^{-1}. Because of the waxy nature of diazepam, some of it will partition from the KBr crystals and move towards the surface of the pellet. The amount that can partition will depend on the pressure applied to prepare the pellet. As shown in Fig. 2A—C when the pressure of the hydraulic press was maintained at 15 000 psi, the 1% sample exhibited no peak at 836 cm^{-1} but both the 2% and 5% samples showed an intense band at 836 cm^{-1} immediately after pellet preparation. Although there was no time-dependent change in the intensity of the 836 cm^{-1} absorption of the 2% and 5% samples of diazepam, the 1% sample showed a strong band at this wavenumber when

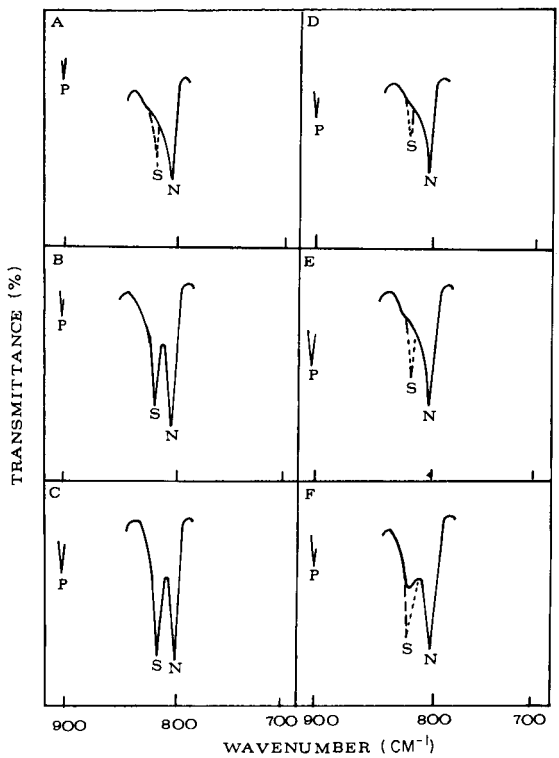

Fig. 2. The effect of diazepam concentration and of the pressure applied to prepare the KBr pellet on the i.r. spectra. Diazepam concentration: (A, D) 1%; (B, E) 2%; (C, F) 5%. Pressure applied: (A—C) 15 000 psi; (D—F) 24 000 psi. The solid lines represent spectra obtained immediately after preparation; the dotted lines represent spectra obtained after 30 min. P, S and N as in Fig. 1.

the sample was rescanned after 30 min. The intensity of the 836 cm^{-1} band relative to the 816 cm^{-1} band became greater as the diazepam concentration increased. As shown in Fig. 2D—F, when the pressure was increased to 24 000 psi, the 1% and 2% samples had a shoulder and the 5% sample showed a weak band at 836 cm^{-1} immediately after the pellet was prepared. After 30 min, these samples all showed a band at 836 cm^{-1}. The intensity of the 836 cm^{-1} band of the pellet prepared at 24 000 psi was less intense than that of pellets pressed at 15 000 psi.

To study the effect of thermal relaxation of a diazepam-coated KBr pellet on the i.r. spectrum, a waxy film of diazepam was applied to an approximately 2-mm thick KBr pellet which had been pressed at 24 000 psi. The spectrum of this pellet was recorded immediately. Spectral characteristics similar to those shown in the reflectance study were obtained. There was a shoulder at 836 cm^{-1} and a strong band at 816 cm^{-1}. The sample was then placed on a wooden block and heated in a 35°C oven for 2 h; after it had cooled to room temperature, the spectrum was recorded as before; a moderate band at 836 cm^{-1} appeared. Later, the diazepam was scraped from the surface of this pellet and the spectrum was recorded again. Although there was a moderate band at 836 cm^{-1}, the intensity of the 816 cm^{-1} band in the remaining sample had decreased. These observations suggest that part of the diazepam molecules moved into a space created by the thermally relaxed KBr crystals as shown by the appearance of the 836 cm^{-1} band. However, a portion of the diazepam remained near the surface of the KBr pellet; when this portion was removed, the intensity of the 816 cm^{-1} band decreased. The ratios of the transmittances of the bands at 836 cm^{-1} and 816 cm^{-1} at various concentrations of diazepam in the KBr pellet were compared. Although the ratios were constant for the pellet of diazepam in petroleum ether, there was a concentration dependence of the ratio for diazepam in chloroform.

Based on the evidence presented above, the anomalous i.r. spectral characteristics of diazepam in KBr pellets obtained from chloroform solution can be attributed to an orientation effect of diazepam in the pellet.

REFERENCES

1 G. Duyckaerts, Analyst (London), 84 (1959) 201.
2 J. A. Heagy, Anal. Chem., 42 (1970) 1459.
3 A. G. Allen, D. A. Cooper, W. O. Kiser and R. D. Cottrell, J. For. Sci., 26 (1981) 12.
4 A. L. Smith, Applied Infrared Spectroscopy, Wiley, New York, 1979, p. 162.
5 G. Turrell, Infrared and Raman Spectra of Crystals, Academic Press, New York, 1972, p. 277.
6 H. E. Hallam, Vibrational Spectroscopy of Trapped Species, Wiley, New York, 1971, p. 300.
7 N. B. Colthup, L. H. Daly and S. E. Wiberley, Introduction to Infrared and Raman Spectroscopy, Academic Press, New York, 1964, p. 89.
8 C. E. Meloan, Elementary Infrared Spectroscopy, Macmillan, New York, 1963, p. 29.

Analytica Chimica Acta, 162 (1984) 431—436
Elsevier Science Publishers B.V., Amsterdam — Printed in The Netherlands

Short Communication

A SAMPLE-DRYING TECHNIQUE FOR ROOM-TEMPERATURE PHOSPHORESCENCE

DAVID L. McALEESE and R. BRUCE DUNLAP*
Department of Chemistry, University of South Carolina, Columbia, SC 29208 (U.S.A.)
(Received 7th February 1984)

Summary. The sample-drying procedure described improves the precision, decreases the time needed and reduces the expense of the solid-surface room-temperature phosphorescence technique. Samples are dried in a glovebag apparatus interfaced to the sample compartment of the spectrophotophosphorimeter. The samples are treated with sodium citrate to prevent moisture quenching the phosphorescence emission. The relative standard deviations of measurements are reduced to less than 2% for large sets of samples. The total time required for 37 samples is only 5.5 h compared to 20 h by a conventional technique.

Room-temperature phosphorescence (r.t.p.) is gaining recognition as a selective and sensitive luminescence technique for the determination of important organic and biological compounds [1, 2]. Molecules exhibit the phenomenon when adsorbed on a suitable solid substrate. Cellulose filter papers are credited as the most applicable r.t.p. supports to date [2]. Samples are prepared by application of a few microliters of analyte solution to the supports. Because moisture quenches r.t.p. emission, the samples require desiccation prior to the measurement step.

During the past decade, sample desiccation has been accomplished in various ways: with heating systems (infrared lamps, hot air blowers and ovens), with vacuum desiccators or vacuum ovens, and with dry argon, nitrogen and air. In most of the 18 publications which report precision values for r.t.p. [3—15], a flow of dry gas in the sample compartment of the phosphorimeter was the last step or the only method of desiccation for samples adsorbed on cellulose paper. The other four procedures [16—19] utilized oven or vacuum desiccation of samples followed by exposure of the samples to atmospheric humidity during measurement. It was shown here that these methods account for a considerable lack of precision in the r.t.p. technique because they fail to dry the samples reproducibly.

Therefore, a new sample-drying procedure was developed which not only improves the precision, but also reduces the time needed and the expense of the r.t.p. technique. A sample-drying chamber was devised that isolated the samples from moisture throughout the drying and measurement procedures. Furthermore, a protecting agent was added to the samples to prevent phosphorescence quenching from any incidental moisture introduced in the system.

0003-2670/84/$03.00

Experimental

Instrumentation. Room-temperature phosphorescence intensity measurements and excitation/emission spectra were obtained on an Aminco-Bowman spectrophotofluorimeter equipped with a 150-W xenon arc light source, a phosphoroscope, a laboratory-constructed sample holder [2] and 1P21 photomultiplier tube detector. Excitation and emission slits were excluded [20] and the photomultiplier slit was set at 5 mm. Excitation and emission data were not corrected for variations in lamp, grating, and detector response.

Chemicals. All phosphors were reagent grade and were used without any further purification. Solutions of the analytes were refrigerated in the dark to prevent degradation.

Drying apparatus. A model SS-1 plastic glovebag (Instruments for Research and Industry) was interfaced to the sample compartment of the spectrophotofluorimeter. This was done by attaching one of the glovebag sleeves to the sample compartment lid. In the sample compartment, the light baffle farthest from the excitation and emission monochromators was removed and two containers of blue-indicating Drierite were placed in adjacent slots. Immediately after the addition of Drierite to the sample compartment, the lid was connected to the instrument. The sample compartment was then exposed only to the interior of the glovebag. A Bacharach humidity gauge and a box containing a 5-pound bed of Drierite were placed inside the glovebag. The sample compartment and glovebag chamber were allowed to dry and equilibrate for several hours to near 0% humidity.

Sample preparation. Ethanol or aqueous (pH 7) solutions of the phosphors were deposited on 3.2-mm diameter circles of Whatman No. 3MM chromatography paper with Analtech 2-μl micro-pipettes. The pipet tips were inserted through a small hole in the glovebag and placed in contact with the center of the supports whereupon the solutions freely drained onto the supports. The samples were dried for 30 min inside the glovebag followed by a 2-μl application of an aqueous (pH 7) 1 M sodium citrate solution. It has been shown that sodium citrate inhibits moisture and oxygen quenching of the r.t.p. emission of dried samples [18]. The samples were mounted on the sample holder and processed consecutively after a final 2-h desiccation period.

Instrument modification. The excitation monochromator of the Aminco-Bowman spectrophotofluorimeter was optically modified by shifting the collimating mirror closest to the light source towards the plane grating. This increased the vertical image of the excitation beam incident on the sample. As described elsewhere [20], the samples were subjected to total front surface illumination.

Results

From the present investigation and from an analysis of reported data [3—19], it is clear that the drying procedures previously used account for a substantial lack of precision in the r.t.p. technique. In our experiments, drying procedures which used oven or vacuum desiccation followed by a

flow of dry gas (argon or nitrogen) in the sample compartment or by a flow of dry gas alone typically resulted in relative standard deviations of 5—10% for r.t.p. measurements of large sets of samples. The precision was in this range or worse for samples dried only by oven or vacuum desiccation and subsequently exposed to atmospheric humidity during measurement. The phosphorescence drying curves of samples dried with a flow of argon at 8000 ml min^{-1} became flat after 20 min of desiccation for pre-dried samples and 30 min for wet samples. However, the intensities of samples prepared with sodium citrate or other agents (salts and sugars) continued to increase after 2 h of desiccation with dry argon. None of these methods dried the samples adequately; this was confirmed in initial experiments with the glove-bag method, which provided higher sample intensities than any of the other procedures.

With the glovebag procedure, r.t.p. intensities and drying times were optimized for *p*-aminobenzoic acid (PABA) and 4-biphenylcarboxylic acid (4BPCA), two compounds which phosphoresce intensely but differ structurally. The effect of sodium citrate concentration on the r.t.p. intensities of these compounds is illustrated in Fig. 1; the dependence of the phosphorescence of both compounds on the amount of sodium citrate applied to the support is very similar. Approximately 0.5 mg of sodium citrate produced the highest phosphorescence emission for both compounds, so this quantity was selected for the drying studies.

The effect of drying time on the r.t.p. emission of the two compounds is shown in Fig. 2. In the upper curve of Fig. 2A, the intensities of the samples prepared with sodium citrate became constant after 1.5 h of desiccation in

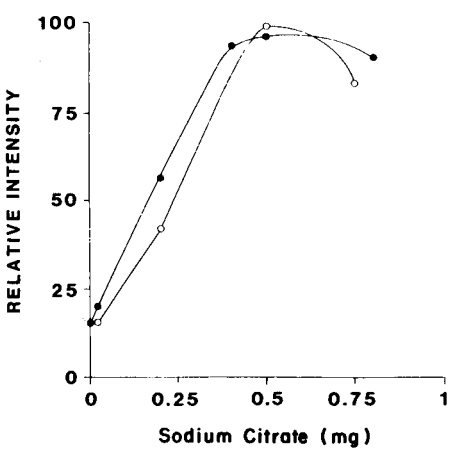

Fig. 1. Relative phosphorescence intensity plotted as a function of the amount of sodium citrate: (•) for 54.9 ng of PABA; (○) for 50 ng of 4BPCA, adsorbed on paper. 4BPCA intensities are adjusted for easier comparison of the curves. Samples were dried for 3 h before measurement.

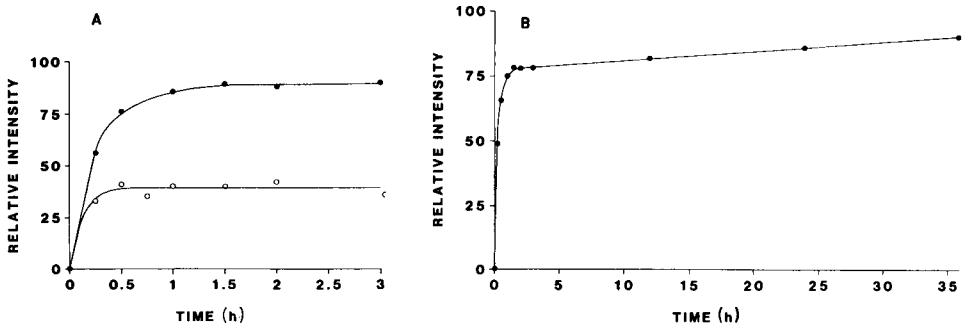

Fig. 2. Relative phosphorescence intensity plotted as a function of drying time. (A) 50-ng 4BPCA samples with (•) and without (○) 0.5 mg of sodium citrate; (B) 54.9-ng PABA samples containing 0.5 mg of sodium citrate. Each point represents a different sample.

the glovebag apparatus; the relative standard deviation (RSD) of the last three intensities was 1.1%. The lower curve of Fig. 2A resulted from 4-biphenylcarboxylic acid samples prepared without sodium citrate and dried with a flow of dry argon (8000 ml min^{-1}) in the sample compartment of the instrument. The phosphorescence emission of these argon-dried samples increased to a constant intensity after 30 min of desiccation. The RSD of the last six intensities was 6.8%. The effect of prolonged desiccation time on the r.t.p. intensities of *p*-aminobenzoic acid samples dried in the glovebag is shown in Fig. 2B. The increase in intensity of these sodium citrate samples during the first 3 h was similar to that of the 4-biphenylcarboxylic acid samples. However, the curve continued a gradual upward trend from 1.5 to 36 h of desiccation. Because the average increase in emission over the last 34.5 h was only 0.4% h^{-1}, a 2-h desiccation period was chosen for the precision studies.

The reproducibility of the glovebag technique was tested by the measurement of r.t.p. intensities from replicate phosphor samples (Table 1). The intensities of samples prepared with sodium citrate were about 2-fold higher and substantially more reproducible than their unprotected counterparts. Yet the increase in intensity did not provide an increase in detection limit because the salt produced a 1.9-fold increase in the background signal compared to a 1.8-fold increase in the *p*-aminobenzoic acid phosphorescence. The average RSD of all sets of background and phosphorescent samples containing sodium citrate was 1.4%.

It was observed that the average r.t.p. intensities varied among different sets of samples containing the same amount of phosphor when samples were processed at different times. However, the sample-to-background signal ratios were similar (<3% RSD) among separate sets of data.

Data for 37 samples of 4-biphenylcarboxylic acid were obtained consecutively over a span of 2 h. The intensities of four samples that differed significantly from the others were excluded from any calculations. The relative

TABLE 1

Typical results for selected compounds

Compound	$\lambda_{ex}/\lambda_{em}$ (nm)	Mass (ng)	Number of samples	Average reading (μA)	RSD (%)
—	286/422	0[b]	6	0.87	3.62
—	286/422	0	5	1.65	1.93
p-Aminobenzoic Acid	286/422	50[b]	8	106	5.19
p-Aminobenzoic Acid	286/422	50	5	193	1.01
p-Aminobenzoic Acid	286/422	100	10	184	1.32
4-Biphenylcarboxylic Acid	289/482	100	10	146	1.06
1-Naphthoic Acid	297/518	100	10	36.9	1.12
L-Tryptophan	282/450	100	10	7.20	1.44
9-Cyanophenanthrene	311/503	100	10	3.03	1.79

[a]Samples contained 0.5 mg of sodium citrate. [b]Samples prepared without sodium citrate.

standard deviations of the sets of replicates varied from 0.54% to 2.50% with an overall average of 1.53%. A least-squares fit of log intensity vs. log concentration produced a line with a slope of 0.898 ± 0.0383 and a correlation coefficient of 0.995 for 30 samples. The calculated limit of detection based on a signal-to-noise ratio of 2 was 32 pg. The total working time for these 37 samples was only 5.5 h compared to 20 h for the conventional argon drying technique.

Discussion

Results in Table 1 are typical of what can be accomplished routinely with this drying technique. Because the increase in sample intensity beyond 1.5 h of desiccation was extremely slow, large sets of samples normally requiring long times were conveniently dried simultaneously and measured consecutively. The glovebag apparatus housed a large number of samples, in contrast to other drying methods that restrict the numbers of samples [3—5, 8, 9, 11—17, 19].

After use, the glovebag apparatus was detached from the sample compartment and stored as an intact unit. The sealed glovebag chamber remained dry in storage for several months. Experiments were resumed simply by adding fresh Drierite to the sample compartment and connecting the lid to the instrument. Sample application could be initiated immediately because the glovebag chamber was dry. Flushing the glovebag with dry oxygen produced no loss in r.t.p. intensity.

Others have attempted to improve r.t.p. precision with the use of internal standards [13] or by solving sample positioning problems [14], but nobody has previously succeeded in reducing the average precision below 5% for large sets of samples on paper supports.

These investigations were supported by NIH Grant CA 15645 from the National Cancer Institute. R. Bruce Dunlap is the recipient of a Faculty Research Award (FRA-144) from the American Cancer Society.

REFERENCES

1 R. T. Parker, R. S. Freedlander and R. B. Dunlap, Anal. Chim. Acta, 119 (1980) 189.
2 R. T. Parker, R. S. Freedlander and R. B. Dunlap, Anal. Chim. Acta, 120 (1980) 1.
3 S. L. Wellons, R. A. Paynter and J. D. Winefordner, Spectrochim. Acta, Part A, 30 (1974) 2133.
4 T. Vo-Dinh, E. L. Yen and J. D. Winefordner, Anal. Chem., 48 (1976) 1186.
5 E. M. Schulman and R. T. Parker, J. Phys. Chem., 81 (1977) 1932.
6 T. Vo-Dinh, G. L. Walden and J. D. Winefordner, Anal. Chem., 49 (1977) 1126.
7 T. Vo-Dinh and J. D. Winefordner, Appl. Spectrosc. Rev., 13 (1977) 261.
8 C. G. de Lima and E. M. de M. Nicola, Anal. Chem., 50 (1978) 1658.
9 T. Vo-Dinh and J. R. Hooyman, Anal. Chem., 51 (1979) 1915.
10 E. L. Yen-Bower and J. D. Winefordner, Appl. Spectrosc., 33 (1979) 9.
11 R. T. Parker, R. S. Freedlander, E. M. Schulman and R. B. Dunlap, Anal. Chem., 51 (1979) 1921.
12 T. Vo-Dinh, R. B. Gammage and P. R. Martinez, Anal. Chim. Acta, 118 (1980) 313.
13 M. W. Warren, J. P. Avery and H. V. Malmstadt, Anal. Chem., 54 (1982) 1853.
14 J. L. Ward, R. P. Bateh and J. D. Winefordner, Analyst (London), 107 (1982) 335.
15 R. P. Bateh and J. D. Winefordner, Anal. Lett., 15 (1982) 373; J. Pharm. Sci., 72 (1983) 559.
16 R. M. A. Von Wandruszka and R. J. Hurtubise, Anal. Chem., 48 (1976) 1784.
17 C. D. Ford and R. J. Hurtubise, Anal. Chem., 51 (1979) 659.
18 D. L. McAleese, R. S. Freedlander and R. B. Dunlap, Anal. Chem., 52 (1980) 2443.
19 R. A. Dalterio and R. J. Hurtubise, Anal. Chem., 54 (1982) 224.
20 D. L. McAleese and R. B. Dunlap, Anal. Chem., 56 (1984) 836.

Analytica Chimica Acta, 162 (1984) 437—442
Elsevier Science Publishers B.V., Amsterdam — Printed in The Netherlands

Short Communication

THE SPECTROPHOTOMETRIC DETERMINATION OF COBALT BY EXTRACTION OF TRIPHENYLSULPHONIUM TETRATHIOCYANATOCOBALTATE(II)

D. THORBURN BURNS* and S. KHEAWPINTONG

Department of Analytical Chemistry, The Queen's University of Belfast, Belfast, BT9 5AG (Northern Ireland)

(Received 16th March 1984)

Summary. Cobalt (0—130 μg) can be determined spectrophotometrically at 625 nm after its extraction as triphenylsulphonium tetrathiocyanatocobaltate(II) into 1:4 acetone/1,2-dichloroethane at pH 7. The effects of pH, diverse ions and masking studies are reported. The method is applied to the determination of cobalt (0.2—10.0%) in high-speed tool steels without prior separation of iron, and in vitamin B12.

Various onium cations have been proposed for the extraction of complex anions of transition metals [1]. Among these anions, the tetrathiocyanatocobaltate(II) ion has been widely studied [2—7]. Little analytical work has been reported on the triphenylsulphonium anion since it was first prepared in 1933 by Courtot and Tung [8]. Potratz and Rosen [9] noted that triphenylsulphonium tetrathiocyanatocobaltate(II) extracted into chloroform, but, although the partition coefficient has been measured [10], no quantitative applications have been developed. Precipitation reactions with the triphenylsulphonium cation may be followed polarographically; those with mercury and bismuth are quantitative [11].

Certain onium salts have become more readily available because of their application by organic chemists as "naked anions" in phase-transfer reactions and related synthetic methods [12]. Triphenylsulphonium chloride has been used as a phase-transfer catalyst in organic oxidations [13—15] and as a stabilizer in polyester polymers [16], and has been proposed for the control of iron chlorosis in plants [17] and for soil conditioning [18]. Its application in extraction-spectrophotometry for the determination of cobalt in tool steels and in vitamin B12 is reported here.

Experimental

Apparatus. Pye-Unicam SP8-400 and SP6-550 u.v.-visible spectrophotometers were used for recording absorption spectra and for routine absorbance measurements, respectively, with quartz 2-cm matched cells.

Reagents and solutions. Triphenylsulphonium chloride (Fluka, practical grade, aqueous 50% solution) was purified by shaking with activated carbon.

0003-2670/84/$03.00

A 0.003 M stock solution was made by dissolving 0.4 ml of purified reagent in 250 ml of distilled water. The solution was stored in a brown glass bottle, covered with aluminium foil. A stock solution of 1000 mg l^{-1} cobalt(II) was prepared by dissolving 2.630 g of anhydrous cobalt(II) sulphate (analytical grade dried to constant weight at 400° C) in 1 l of distilled water. More dilute standard solutions were prepared as required. A pH 7 buffer was prepared by mixing 30.5 ml of 0.2 M disodium hydrogenphosphate and 19.5 ml of 0.2 M sodium dihydrogenphosphate and diluting to 100 ml with distilled water. Dichloroethane was distilled twice and the fraction with b.p. 82—83° C was collected for use. All other reagents were of analytical grade. Twice-distilled water was used throughout.

General procedure. Place a 2-ml aliquot containing ca. 40 μg of cobalt(II) in a 100-ml separating funnel. Add 3.0 ml of 5 M ammonium thiocyanate, 4 ml of pH 7 buffer and 2 ml of 0.003 M triphenylsulphonium chloride solution, and dilute to 15 ml with water. Add 2 ml of acetone and mix. Extract with 8-ml and 1-ml portions of dichloroethane. Filter the separated organic phases through a Whatman No. 1 paper, previously moistened with solvent, into a 10-ml volumetric flask. Wash through with solvent and make up to volume. Measure the absorbance of the extract at 625 nm against 1,2-dichloroethane.

Procedure for steel samples. For steel samples containing 2—10% or 0.2—1% cobalt, dissolve accurately weighed 0.05- or 0.5-g samples, respectively, in a mixture of 5 or 50 ml of distilled water, 3 or 30 ml of concentrated hydrochloric acid and 1 or 10 ml of concentrated nitric acid, in 250-ml conical flasks. Warm to aid dissolution. Boil to near dryness, cool, add 1 or 10 ml of concentrated hydrochloric acid and evaporate to near dryness. Cool, add 50 ml of distilled water and warm to dissolve the solids. Cool and filter through a Whatman No. 1 paper into a 100-ml volumetric flask. Wash the residual solids (silica, tungstic acid) with a small volume of hot 2% (v/v) hydrochloric acid followed by water, and make up to volume. Mix well and dilute 1:5 with distilled water. Transfer 5- or 10-ml aliquots of this solution, containing 10—60 μg of cobalt, into 100-ml beakers. Add 5 ml of saturated ammonium D-tartrate solution (in the case of a steel sample containing copper, add 3 ml of 0.2 M sodium thiosulphate after the addition of the tartrate), 3 ml of 5 M ammonium thiocyanate, and 4 ml of pH 7 buffer. Mix thoroughly, check the pH, and if necessary readjust to 7.0 with 5 M ammonia. Transfer to a 100-ml separating funnel. Add 3 ml of 0.003 M triphenyl sulphonium chloride and 2 ml of acetone, and continue as in the general procedure.

Prepare a calibration graph for the range 0—150 μg of cobalt after adding 10 ml of iron(III) nitrate solution, containing an equivalent amount of iron as the steel samples to the sample aliquots.

Examination of main experimental variables

A variety of solvents including alcohols, ketones, esters, ethers and chlorinated and aromatic hydrocarbons were examined for extraction efficiency,

using 40 μg of cobalt(II) in the general procedure. Nitrobenzene, propylene carbonate and acetone/1,2-dichloroethane (1:4) were the most efficient extractants. Nitrobenzene was rejected because of its toxicity, and propylene carbonate produced a higher blank than the acetone/dichloroethane mixture which was therefore selected.

The pH of the aqueous phase was adjusted before extraction by addition of 5 M hydrochloric acid or 5 M ammonia. The absorbance of the extract was constant over the pH range 6—8. Below pH 6 a slight increase in sensitivity was noted but the solutions were unstable, whilst above pH 8 the sensitivity decreased. In subsequent work, the aqueous phase was buffered at pH 7; of the various buffers tested, disodium hydrogenphosphate/sodium dihydrogenphosphate gave the lowest blank.

The effects of varying the amounts of the reagents (ammonium thiocyanate, triphenylsulphonium chloride, buffer) were examined for 40-μg amounts of cobalt(II) in solution. In each case, the absorbance of the extract increased up to a constant value with increase in amount of reagent. Convenient amounts in the plateau regions are specified in the general procedure. The extent of extraction was found to be unaffected by ionic strength, provided that the pH remained at 7, and by phase-volume ratios, with undetectable amounts of cobalt(II) remaining in the aqueous phases.

The composition of the complex was established spectrophotometrically by Job's method of continuous variations [19] to be $((C_6H_5)_3S)_2[Co(SCN)_4]$. Organic elemental analysis of the precipitate formed in the absence of solvent was consistent with the same composition: required for $(C_{18}H_{15}S)_2[Co(CNS)_4]$, 58.7%C, 3.7%H, 6.9%N; found 59.0%C, 3.5%H, 6.7%N.

Results and discussion

A linear calibration graph was obtained over the range 0—100 μg of cobalt at 625 nm (molar absorptivity = 407 l mol^{-1} cm^{-1}). For the determination of 40 μg of cobalt, the coefficient of variation was 1.03% (7 results).

The possible interferences of various cations and anions on the extraction of 40 μg of cobalt were examined. Decreased extraction occurred (—3.1% for 4 mg and —3.5% for 40 mg of iron), when 5 ml of saturated ammonium tartrate was used as masking agent for iron(III). These interfering effects in the determination of cobalt in steel and that of the blank were compensated for by addition of an equivalent amount of iron to the standards. The results of the interference and masking study are summarized in Table 1. The only ions which interfered significantly and are of interest in the analysis of steels, were iron(III) (500:1), niobium and tin (300:1) and copper (100:1). The interferences of iron(III), niobium and tin can be masked by ammonium fluoride and that of copper by sodium thiosulphate. Alternatives to ammonium fluoride were sought to avoid attack on glassware, and addition of 1.5 ml of saturated ammonium tartrate solution was found to be satisfactory to mask 5 mg of copper(II) or iron(III), 1 mg of tin(IV) or 1 mg of niobium in the determination of 40 μg of cobalt. Under the conditions of the above

TABLE 1

Effect of various ions on the determination of cobalt(II)

Ion[a]	Ratio to Co(II) (w/w)	Change in absorbance (%)	Ion[a]	Ratio to Co(II) (w/w)	Change in absorbance (%)
Pd^{2+}	100	—	Cr(III)	500	+15
Fe^{2+}	300	+69		500[c]	—
	10	+10	Cu^{2+}	100	+50
	300[b]	—		100[d]	—
Fe^{3+}	500	+54	Sn(IV)	300	−73
	300	—		10	—
	500[c]	—		300[c]	—
	500[e]	+4	Nb(V)	300	−12
Bi(III)	300	−19		300[c]	—
	300[c]	—	SiO_3^{2-}	2500	−23
Hg^{2+}	500	+15		50	—
	100	—	WO_4^{2-}	2500	−27
	500[b]	—		500	—
U(IV)	500	−27	CN^-	2500	−108
	100	−7		25	−100
	500[c]	—	EDTA	2500	−100
Zn^{2+}	500	−89		25	−100
	10	—			

[a]Cations added as chloride, sulphate or nitrate; anions added as sodium salts, except ascorbate added as ascorbic acid. [b]Hydrazine hydrate added. [c]Ammonium fluoride added. [d]Sodium thiosulphate added. [e]Saturated ammonium tartrate solution added.

procedure, the following cations in the weight ratio 500:1 were without appreciable effect: Al^{3+}, Ca^{2+}, Cd^{2+}, K^+, Mg^{2+}, Mn^{2+}, Na^+, NH_4^+, Ni^{2+}, Pb^{2+} and Zr(IV). Other cations which interfered significantly were Cr^{3+}, U(IV), Hg^{2+} and Zn^{2+} at 500:1 ratios, and Bi(III) and Fe^{2+} at 300:1 ratios. The effects of iron(II) and mercury(II) were overcome by the addition of hydrazine hydrate, and Bi(III) and Cr^{3+} can be masked by ammonium fluoride. Among the anions that do not interfere are ascorbate, carbonate, chloride, citrate, fluoride, hydrogenphosphate, molybdate, nitrate, sulphate, thiosulphate and vanadate. Cyanide and EDTA should be absent.

The results for the determination of cobalt in seven British Chemical Standard steel samples (Table 2) are in excellent agreement with the certificate values.

Triphenylsulphonium chloride may also be used as an alternative to (ethoxycarbonylpentadecyl)trimethylammonium bromide [20] and hexamethylphosphoramide [21] for the extraction-photometric determination of cobalt in Vitamin B12 following wet oxidation with nitric/perchloric acid [22]. The results (Table 3) obtained by standard addition and direct calibration based on the above procedure are in excellent agreement, although below the theoretical value (4.34%), owing to sample impurity.

TABLE 2

Analysis of high-speed tool steels

BCS Steel No.	Cobalt in steel (% w/w)		
	Certified value	Certified range	Found[a]
220/2	0.32	0.31—0.33	0.311 ± 0.004
241/2	5.70	5.66—5.73	5.73 ± 0.114
481	0.21	0.19—0.22	0.211 ± 0.003
482	0.24	0.21—0.27	0.251 ± 0.002
483	1.94	1.90—1.99	1.960 ± 0.030
484	10.20	10.10—10.39	10.27 ± 0.047
485	5.06	5.00—5.11	5.115 ± 0.038

[a]Mean ± standard deviation (7 results).

TABLE 3

Results for cobalt(II) in vitamin B12 after standard addition

Co added (μg)	0	10	30	50
Co found (% w/w)[a]	3.924 ± 0.007	3.949 ± 0.068	3.964 ± 0.097	3.935 ± 0.125

[a]95% confidence limits (7 results) for cobalt in vitamin B12.

The absorbances of extracts of triphenylsulphonium tetrathiocyanatocobaltate(II) were stable for at least 6 h in diffuse daylight and 3 h in direct sunlight, although the reagent is said to be photochemically unstable [23].

REFERENCES

1 A. J. Bowd, D. Thorburn Burns and A. G. Fogg, Talanta, 16 (1969) 719.
2 C. Calzolari and L. Favretto, Analyst (London), 93 (1968) 494.
3 N. Gundersen and E. Jacobsen, Anal. Chim. Acta, 42 (1968) 330.
4 A. J. Bowd and D. Thorburn Burns, Mikrochim. Acta, (1965) 1151.
5 H. E. Affsprung, N. A. Barnes and H. A. Potratz, Anal. Chem., 23 (1951) 1680.
6 K. W. Ellis and N. A. Gibson, Anal. Chim. Acta, 9 (1953) 275.
7 D. Thorburn Burns, P. Hansprasopwattana and B. P. Murphy, Anal. Chim. Acta, 134 (1982) 397.
8 C. Courtot and T. Y. Tung, Compt. Rend., 197 (1933) 1227.
9 H. A. Potratz and J. M. Rosen, Anal. Chem., 21 (1949) 1276.
10 R. Bock and C. Hummel, Z. Anal. Chem., 198 (1963) 176.
11 M. Shinagawa, H. Matsuo and N. Maki, Jpn. Analyst, 5 (1956) 80.
12 W. E. Keller, Compendium of Phase-Transfer Reactions and Related Synthetic Methods, Fluka, Buchs, Switzerland, 1979.
13 O. Katsutoshi, Y. Tokio and K. Fukui, Bull. Chem. Soc. Jpn., 42 (1969) 1800.
14 K. Fukui, K. Kanai, T. Takezono and H. Kitana, Kogyo Kagaku Zasshi, 67 (1964) 1131.
15 K. Kanai, K. Okubo, H. Katano and K. Fukui, Bull. Jpn. Pet. Inst., 7 (1965) 52.
16 I. M. Abrams, L. L. Benezra and R. D. Goold, U.S. Patent 3,028-361, April 3 1962; Chem. Abstr., 57 (1962) 2411f.

17 J. Antognini, R. Curtis and H. M. Day, Symposium on Metal Chelates in Plant Nutrition, Seattle, 1956, p. 61; Chem. Abstr., 52 (1958) 5565f.
18 A. L. Pugh, J. A. Vomocil and T. R. Nielson, Agron. J., 52 (1960) 399.
19 P. Job, Ann. Chim. (Paris), 9 (1928) 113.
20 I. Blazis and M. Malat, Chem. Listy, 75 (1981) 312.
21 P. Bruno, Anal. Lett., 14 (1981) 1493.
22 T. T. Gorsuch, The Destruction of Organic Matter, Pergamon, Oxford, 1970.
23 C. M. J. Stirling, The Chemistry of the Sulphonium Group, Part I. Wiley, Chichester, 1981.

Analytica Chimica Acta, 162 (1984) 443—446
Elsevier Science Publishers B.V., Amsterdam — Printed in The Netherlands

Short Communication

THE SPECTROPHOTOMETRIC DETERMINATION OF SULPHATE AFTER ITS EXTRACTION WITH METHYLTRICAPRYLAMMONIUM CHLORIDE INTO CYCLOHEXANE

D. THORBURN BURNS* and M. BUSHRA

Department of Analytical Chemistry, The Queen's University of Belfast, Belfast, BT9 5AG (Northern Ireland)

(Received 9th March 1984)

Summary. Improvements are described to Flynn's procedure for the extraction of sulphate with Aliquat-336 and its subsequent determination as sulphuric acid. A single-point photometric measurement with sodium 2,4-dinitrophenate is applied to the determination of sulphate (ca. 10 mg kg^{-1}) in soils, and also to sulphur in organic compounds after oxygen flask combustion.

The sulphate ion in small amounts is normally determined nephelometrically, turbidimetrically or by indirect spectrophotometric methods. The indirect methods are based on the displacement of a chromogenic species from a relatively insoluble compound or by the determination of the excess of a compound or ion that reacts with sulphate [1, 2]. The only direct spectrophotometric method is that based on the formation of $FeSO_4^+$; in brines it is necessary to make corrections based on the concentrations of the major constituents [3].

The sulphate ion is difficult to extract into organic solvents because it is highly hydrophilic. Flynn [4] extracted sulphate with methyltricaprylammonium chloride (Aliquat-336) into cyclohexane containing 5% phenol [4]. The sulphate was back-extracted into hydrochloric acid. After evaporation to dryness to remove volatile acids the residual sulphuric acid was determined by measuring the hydrogen ion concentration using cresol red as indicator. This communication describes the adaptation of the method, using sodium 2,4-dinitrophenate as indicator, and its application in the analysis of soils and organic materials.

Experimental

Apparatus and reagents. A Pye-Unicam SP8-400 and an SP6-550 u.v.-visible spectrophotometer were used for recording spectra and for routine absorbance measurements, respectively, with 0.2- or 1-cm quartz cells. An Aliquat-336 extraction solution was prepared by diluting 200 ml of Aliquat-336 (methyltricaprylammonium chloride; Fluka) to 1.0 l with cyclohexane containing 5% (w/v) phenol. A 0.01 M sodium 2,4-dinitro-

0003-2670/84/$03.00

phenate solution was prepared by diluting 1.84 g of 2,4-dinitrophenol (purified by recrystallization from 70% ethanol) in 100 ml of 0.1 M sodium hydroxide in a 1-l volumetric flask; 250 ml of ethanol was added and the solution was diluted to volume with water. All other reagents were of analytical grade. Double-distilled water was used throughout.

Procedure. Place an aliquot of sample containing about 1 mg of sulphate in a 250-ml beaker, adjust the pH to 4 (pH meter) with dilute hydrochloric acid or sodium hydroxide as required. Dilute to 100 ml with water. Evaporate to 10 ml on a hot plate, transfer to a water-bath and evaporate to apparent dryness. Add 20 ml of water and quantitatively transfer to a 500-ml separating funnel containing 100 ml of 20% Aliquat solution. Make up to within 2 ml of total capacity with distilled water. Shake, with repeated inversion, for 2 min, and allow the phases to separate. Discard the aqueous phase. Wash the organic phase with 25 ml of 0.01 M hydrochloric acid by gentle shaking for 1 min, allow the phases to settle and discard the aqueous phase. Strip the sulphate from the organic phase into 3 M hydrochloric acid as follows. Add 25 ml of 3 M hydrochloric acid and shake gently for 2 min, allow the phases to separate, and collect the aqueous phase in a clean 100-ml separating funnel. Repeat with a further 25 ml of 3 M hydrochloric acid. Wash the combined acid extracts with 25 ml of di-isopropyl ether. After phase separation, collect the aqueous phase in a 100-ml beaker. Place the beaker on a boiling water-bath until the ether has evaporated, and then on a hot plate to reduce the volume to about 10 ml. Evaporate the remainder on the water-bath to residual sulphuric acid and leave for 30 min to ensure that all the hydrochloric acid has evaporated. Transfer the residual acid quantitatively to a 100-ml volumetric flask containing 10 ml of 0.01 M sodium 2,4-dinitrophenate solution. Dilute to volume, mix carefully and measure the absorbance at 450 nm in a 2-mm quartz cell against water. Prepare a calibration graph by using aliquots (0—10 ml) of 0.005 M sulphuric acid treated as the "residual acid" above.

Results and discussion

Problems were encountered when cresol red indicator was used as described by Flynn [4]. It was considered that, because of its pK_a value, most of the indicator would be present as the acid form over the acid concentration range of interest [5]. More acidic indicators [5] were examined which also avoided problems from atmospheric carbon dioxide; 2,4-dinitrophenol was found to be satisfactory. However, better results were obtained when the indicator was converted to its sodium salt for use as the reagent. The extent of reaction is determined by the disappearance of the phenate anion, measured at 450 nm. The calibration graph was linear over the range $0—5 \times 10^{-4}$ M sulphate in the final solution, with a negative slope; the relative standard deviation ($n = 5$) was 4% at 1 mg of total sulphate.

Flynn's previous study [4] indicated that the method was remarkably free from interference. This was confirmed for ions of interest in the analysis

of soils. No interference on the measurement of 1 mg of sulphate was observed from 4 mg of carbonate, nitrate, chloride, phosphate, acetate, fluoride or perchlorate or from 1-mg amounts of magnesium, cobalt(II), manganese(II), zinc, copper(II), iron(III), nickel, lead, calcium or ammonium ions. However, when Morgan's solution [6] (10% w/v sodium acetate and 3% v/v acetic acid, pH 4.8) was used to extract sulphate from soil [7], linear but lower recoveries were found. Therefore, it is necessary to add this solution to sulphate standards when a calibration graph is prepared for the determination of sulphate in soils.

Air-dried samples (10 g) of low sulphate soils (from the Ministry of Agriculture, Northern Ireland) plus 0.3 g of decolourizing charcoal were shaken for 1 h with 30 ml of Morgan's solution and filtered. The solutions were extracted with Aliquat-336 and then treated as in the procedure above. The calibration graph was prepared by extraction of sodium sulphate solutions in the presence of 30 ml of the acetate buffer as for the samples. The samples were also analysed turbidimetrically [8]. The results are shown in Table 1.

The photometric finish can also be applied to systems which allow direct formation of sulphuric acid, e.g., oxygen flask combustion of organic com-

TABLE 1

Sulphate content of low-sulphate soil samples

Sample	Sulphate found (mg kg^{-1})[a]	
	Proposed method	Turbidimetric method
A	9.6 ± 0.4	10.1 ± 0.2
B	10.6 ± 0.4	10.1 ± 0.2
C	10.0 ± 0.4	9.6 ± 0.2

[a]Mean ± standard deviation, $n = 5$.

TABLE 2

Results for organic sulphur compounds

Compound	Sulphur (%)	
	Calculated	Found[a]
S-Benzylthiouronium chloride[b]	15.82	15.73 ± 0.16
Phenylthiourea[b]	21.07	20.8 ± 0.20
Bis(triphenylphosphine)copper trifluoromethanesulphonate (BCR research compound)	4.35	4.35 ± 0.04

[a]Mean ± standard deviation, $n = 6$. [b]Microanalytical reagent.

pounds. The combustion procedure used was similar to that applied for the analysis of halogenated samples [9]; sample weights were such as to contain 1 mg of sulphur, and the absorbent was 0.05 ml of hydrogen peroxide (100 vol) in 10 ml of water carefully neutralized to pH 7. After being shaken (15 min), and allowed to stand (15 min), the contents were transferred to a 100-ml beaker and evaporated to residual sulphuric acid, and the procedure was completed as before. Typical results are shown in Table 2.

The results confirm that, after extraction of sulphate with Aliquat-336, the photometric finish to determine acidity, based on the sodium salt of an indicator as reagent, is more reliable than when the weak acid form of an indicator is used to measure pH.

REFERENCES

1 W. J. Williams, Handbook of Anion Determination, Butterworths, London, 1979.
2 F. D. Snell, Photometric and Fluorimetric Methods of Analysis. Nonmetals, Wiley, New York, 1981.
3 R. Goguel, Anal. Chem., 41 (1969) 1034.
4 W. W. Flynn, Anal. Chim. Acta, 90 (1977) 343.
5 E. Bishop, Indicators, Pergamon, Oxford, 1972.
6 M. F. Morgan, Conn. Agric. Exp. Stn, Bull. Nos., 392, 129, 1937.
7 S. E. Allen (Ed.), Chemical Analysis of Ecological Materials, Blackwell, Oxford, 1974.
8 L. Chesnin and C. H. Yien, Proc. Soil Sci. Soc. Am., 15 (1950) 149.
9 D. T. Burns and B. K. Maitin, Analyst (London), 108 (1983) 452.

Analytica Chimica Acta, 162 (1984) 447—449
Elsevier Science Publishers B.V., Amsterdam — Printed in The Netherlands

Short Communication

AUTOMATIC SPECTROFLUORIMETRIC METHOD FOR THE DETERMINATION OF DYSPROSIUM AS ITS TERNARY COMPLEX WITH EDTA AND TIRON

SAMUEL J. LYLE* and NIDAL A. ZA'TAR

The Chemical Laboratories, University of Kent at Canterbury, Kent CT2 7NH (Great Britain)

(Received 5th March 1984)

Summary. The automatic method is based on the ternary complex formed with EDTA and Tiron. The method is satisfactory for quantifying 0.1—1.2 $\mu g\ ml^{-1}$ dysprosium under conditions similar to those used for terbium. The effect of other lanthanides, yttrium, thorium, and dioxouranium(VI) on the fluorescence intensity is described; the main interference is from terbium(III).

Poluektov et al. [1] described a method for the simultaneous spectrofluorimetric determination of terbium(III) and dysprosium(III) as ternary complexes with EDTA and Tiron (disodium-1,2-dihydroxybenzene-3,5-disulphonate). This method has been studied in detail and optimized to provide an automatic method for the determination of terbium(III) [2]. Here, an adaptation is reported for the determination of dysprosium(III).

Experimental

The reagents and apparatus were the same as those described previously [2]. For the standard dysprosium(III) solution, dysprosium(III) oxide (99.9% Dy_2O_3; Rare Earth Products, Widnes, England) was ignited at dull red heat and cooled in a small desiccator; about 0.168 g of it was weighed out accurately and dissolved in the minimum volume of hydrochloric acid. The solution was evaporated to dryness on a water bath and the residue was dissolved in 1 l of water.

Results and discussion

The use of 0.6 M sodium tungstate solution [3] is reported to be satisfactory for the determination of 0.01—0.1 $\mu g\ ml^{-1}$ dysprosium, but the sensitivity is low and other lanthanides and yttrium markedly quench the fluorescence from dysprosium even at the 1 $\mu g\ ml^{-1}$ level [3]. The determination of dysprosium as its complex with anisaldehyde [4] has been reported to be satisfactory for 0.13—1.6 $\times\ 10^3\ \mu g\ ml^{-1}$; other lanthanides and yttrium were merely stated to quench the energy-transfer process in relation to their concentration

0003-2670/84/$03.00

by collisional competition between dysprosium and the other lanthanides. Tishchenko et al. [5] examined some pyrazolone derivatives and reported that other lanthanides and yttrium produced some quenching during the determination of dysprosium; it was necessary to quantify dysprosium by the method of standard additions. A method based on iminodiacetic acid and Tiron is satisfactory for the determination of 8×10^{-4}—1.6×10^{2} $\mu g\ ml^{-1}$ dysprosium but the effects of other lanthanides and yttrium were not reported [6].

In the present work, the effects of other lanthanide(III), yttrium, thorium and dioxouranium(VI) ions on the determination of dysprosium by the Tiron/EDTA procedure [7] were examined. The results are listed in Table 1. The concentration levels at which interference becomes significant are very similar to those found for the terbium determination [7] except that terbium interferes seriously with the dysprosium method, whereas the reverse does not apply. Both thorium and dioxouranium(VI) interfere at considerably lower concentrations than in the terbium determination.

The effects of changing the reagent/metal ion ratio, temperature and pH were not studied in detail. The conditions found satisfactory for the determination of dysprosium were similar to those described for terbium [1]. The Tiron/EDTA procedure is easier and faster than the liquid/liquid extraction methods [4, 5]. The system with iminodiacetic acid and Tiron [6] is somewhat less sensitive than the EDTA/Tiron system although probably otherwise as attractive.

When the conditions recommended for the automatic spectrofluorimetric determination of terbium [2] were used, except that the fluorescence output was measured at 582 nm with a 2.0-mm slit on the emission side of the cell, a rectilinear calibration graph was obtained over the range 0.1—1.2 $\mu g\ ml^{-1}$ dysprosium. The relative standard deviation for 0.93 $\mu g\ ml^{-1}$ dysprosium was

TABLE 1

Effect of other lanthanide ions, thorium, and uranium(VI) on fluorescence emission from 0.49 $\mu g\ ml^{-1}$ dysprosium at 582 nm in the automatic Tiron/EDTA system

Metal ion	Amount ($\mu g\ ml^{-1}$)	Dy found ($\mu g\ ml^{-1}$)	Quenching[a] (%)	Metal ion	Amount ($\mu g\ ml^{-1}$)	Dy found ($\mu g\ ml^{-1}$)	Quenching[a] (%)
La^{3+}	210	0.475	4.0	Ho^{3+}	230	0.470	5.4
Ce^{3+}	105	0.450	8.0	Er^{3+}	205	0.470	5.4
	75	0.480	2.7	Tm^{3+}	200	0.470	5.4
Pr^{3+}	210	0.470	5.4	Yb^{3+}	185	0.470	5.4
Nd^{3+}	200	0.475	4.0	Lu^{3+}	190	0.475	4.0
Sm^{3+}	200	0.475	4.0	Th^{4+}	232	0.465	5.6
Eu^{3+}	210	0.470	5.4	UO_2^{2+}	80	0.455	8.0
Gd^{3+}	190	0.475	4.0		60	0.480	2.7
Tb^{3+}	0.24	0.470	5.4	Y^{3+}	180	0.445	6.7

[a]Mean of 10 measurements in each case.

2.8% for 15 measurements. This procedure is about three times less sensitive than the method for terbium and the linear range is narrower.

Because of the large difference in the emission wavelengths for terbium and dysprosium, a simultaneous automatic spectrofluorimetric determination of the two ions is possible by measuring the emission of terbium at 545 nm and that of dysprosium at 582 nm. The proposed method can be applied to the determination of dysprosium in lanthanide oxides, mixtures and minerals. From the interference study (Table 1), it can be concluded that the limitations on application of the method will usually be similar to those found for the terbium determination [2]. However, cerium(III) and terbium(III) can be tolerated only up to concentrations of 75 and 0.24 μg ml^{-1}, respectively.

REFERENCES

1 N. S. Poluektov, M. A. Tishchenko and L. A. Alakaeva, Tr. Khim. Khim. Tekhnol., 5 (1973) 104.
2 S. J. Lyle and N. A. Za'tar, Anal. Chim. Acta, 162 (1984) 305.
3 G. Alberti and M. A. Massucci, Anal. Chem., 38 (1966) 214.
4 W. J. McCarthy and J. D. Winefordner, Anal. Chem., 38 (1966) 849.
5 M. A. Tishchenko, L. I. Kononenko, R. A. Vitkun and N. S. Poluektov, Ukr. Khim. Zh., 32 (1966) 508.
6 M. A. Tishchenko, G. I. Gerasimenko and N. S. Poluektov, Zavod. Lab., 40 (1974) 935.
7 S. J. Lyle and N. A. Za'tar, Anal. Chim. Acta, 153 (1983) 229.

Analytica Chimica Acta, 162 (1984) 451—455
Elsevier Science Publishers B.V., Amsterdam — Printed in The Netherlands

Kurze Mitteilung

VERGLEICHENDE UNTERSUCHUNGEN ZUR TITRIMETRISCHEN, PHOTOMETRISCHEN UND IONEN-CHROMATOGRAPHISCHEN HYDROGENCARBONAT-BESTIMMUNG IN TRINK- UND MINERALWÄSSERN

DA-REN YAN, B. RÖSSNER und G. SCHWEDT*[a]

Institut für Anorganische Chemie der Universität, Tammannstr. 4, D-3400 Göttingen (F.R.G.)

(Eingegangen den 16 Januar 1984)

Summary. (A comparison of titrimetric, spectrophotometric and ion-chromatographic methods for the determination of hydrogencarbonate in drinking and mineral waters.) A photometric method for hydrogencarbonate determination in various natural waters is presented, based on measurements with methyl red. Accuracy of the results is demonstrated by comparison with titrimetric and ion-chromatographic methods. The photometric method is suitable for contents in the range of 1—2000 mg l^{-1}. The linear range of the continuous flow method varies from 6—60 mg l^{-1} to 12—90 mg l^{-1} depending on conditions.

Zusammenfassung. Es wird ein photometrisches, automatisierbares Analysenverfahren für Hydrogencarbonat-Bestimmungen in verschiedenen Wasserarten vorgestellt, das auf Messungen mit Methylrot basiert. Richtigkeit der Ergebnisse werden an Vergleichen mit Titrations- und einem ionen-chromatographischen Verfahren gezeigt. Das photometrische Verfahren eignet sich für Bestimmungen im Bereich von 1—2000 mg l^{-1}.

Im Unterschied zur Analytik anderer anorganischer Anionen sind in der neueren Literatur nur wenige Verfahren für das Hydrogencarbonat neben dem üblichen Titrationsverfahren der Carbonathärte-Bestimmung zu finden. Eine Umwandlung des gesamten anorganischen Kohlenstoffs in Kohlendioxid mit anschließender Abtrennung und quantitativer Analyse in einem IR-Gasanalysator [1] bzw. mit photometrischer Bestimmung nach Absorption des Kohlendioxids in einer Phenolphthalein-Lösung [2] ermöglicht automatisierbare, apparativ jedoch relativ aufwendige Bestimmungen in Wässern. Für die klinisch-chemische Analytik wurde bereits 1968 ein ebenfalls photometrisches Verfahren beschrieben [3], das ohne Freisetzung von Kohlendioxid auskommt. Es beruht auf der Erhöhung des pH-Wertes einer alkoholischen KH_2PO_4-Lösung durch Zugabe von Hydrogencarbonat, die mittels eines pH-Indikators gemessen wird. In der vorliegenden Arbeit wird über die

[a]Neue Anschrift: Institut für Lebensmittelchemie der Universität, Pfaffenwaldring 55, D-7000 Stuttgart 80, F.R.G.

0003-2670/84/$03.00

Anwendung dieses photometrischen Verfahrens in manueller und automatischer ("continuous-flow") Ausführung in Trink-, Oberflächen- und Mineralwässern im Vergleich zur pH-Titration (der Carbonathärte) und zur ionen-chromatographischen Analytik berichtet. Die Anforderungen der Feldanalytik am Ort der Probenahme werden in die Untersuchungen mit einbezogen.

Experimenteller Teil

Carbonathärte-Titration. Zur Titration werden 100 ml einer Wasserprobe mit 3 Tropfen einer 0,1%igen methanolischen Methylorange-Lösung versetzt und mit 0,02 mol l^{-1} HCl auf den Farbton einer Lösung aus 100 ml destillierten Wasser, 3 Tropfen Methylorange-Lösung und einer Spatelspitze Kaliumhydrogenphtalat titriert. Eine weitere Methode ist die Endpunktbestimmung mit einem pH-Meter bei dem pH-Wert von 4,40. Sie wird in gleicher Weise wie oben beschrieben durchgeführt und wird bei Anzeige von pH 4,40 beendet.

Photometrische Hydrogencarbonat-Bestimmung. Hier kommen ein manuelles und ein Continuous-flow-Verfahren zur Anwendung.

Zur Durchführung des manuellen Verfahrens wird eine Eichung wie folgt durchgeführt: man pipettiert in eine Reihe trockener 25 ml-Meßkolben 0-, 0,25-, 0,50-, 0,75-, 1,00-, 1,25-ml einer $2{,}00 \times 10^{-2}$ mol l^{-1} $NaHCO_3$-Standardlösung und je 5 ml 0,25 mol l^{-1} $KH_2PO_4/10^{-3}$ mol l^{-1} Methylrot-Reagenz und füllt mit bidestillierten CO_2-freiem Wasser auf 25 ml auf. Die photometrischen Messungen erfolgen mit einem Filterphotometer Nanocolor (Macherey-Nagel, Düren) 25 bzw. 50 D bei 520 nm und 570 nm. Der Nullpunkt wird mit einem Reagenzienblindwert eingestellt, der anstelle der $NaHCO_3$-Lösungen bidestilliertes CO_2-freies Wasser enthält.

Die Wasseranalysen werden wie bei der Eichung beschrieben hergestellt. Statt der $NaHCO_3$-Standardlösung werden 20 ml der Wasserprobe (Gehalte unter 100 mg l^{-1}), bei Mineralwasserproben 0,5 bis 5 ml (Gehalte über 1000 bzw. 100 mg l^{-1}) eingesetzt.

Das Continuous-flow-Verfahren wird mit einem Spectrophotometer (Cecil CE373), welches mit einer 70 μl-Durchflußzelle (Typ 179.10-QS, Fa. Hellma; Schichtdicke 10 mm, Zentrummaß 15 mm) versehen ist, einer peristaltischen Schlauchpumpe (Gilson-4-Kanal-Pumpe), einer Mischspirale (14 W, i.D. 2,4 mm) und folgenden Schläuchen durchgeführt. Der Probenschlauch hat den i.D. 1,65 mm. Der Reagenzschlauch (i.D. 2,06 mm) fördert das $KH_2PO_4/4 \times 10^{-5}$ mol l^{-1} Methylrot-Reagenz in Methanol-Wasser. Die Optimierung und die Möglichkeiten der Wahl von Nachweisgrenze und Linearitätsbereich durch Änderung der KH_2PO_4-Konzentration und des Methanolgehaltes im Reagenz sind aus Tabelle 3 ersichtlich. Der Schlauch für die Luftförderung zur Luftsegmentierung hat den i.D. 1,02 mm, der Gesamtförderschlauch i.D. 2,06 mm. Die Pumpengeschwindigkeit beträgt 600 skalanteile (skt), die Probensaugzeit 15 s. Eine Spülzeit von 45 s zwischen zwei Proben (mit bidest. Wasser, CO_2-frei) ist notwendig. Die Wellenlänge für die Messung wird auf

520 nm festgesetzt. Der Meßwert der Waschlösung (Blind-Lösung: bidest. Wasser CO_2-frei) wird mit einem Potentiometer am Photometer auf $E = 0{,}5$ eingestellt. Zur Aufzeichnung der Signale dient ein Schreiber oder Integrator.

Ionen-chromatographische Bestimmungen. Es wird ein System bestehend aus einer KNAUER-HPLC-Pumpe und -Leitfähigkeitsdetektor, einem SP4100 Computing Integrator (Spectra-Physics) und einer Wescan-Anionen-Trennsäule (Nr. 269-001) eingesetzt. Ein Rheodyne-Probenaufgabeventil mit 200 µl Probeschleife dient zur Probeninjektion. Die mobile Phase besteht aus einer 4×10^{-3} mol l^{-1} Kaliumhydrogenphtalat-Lösung, die mit KOH auf pH 4,5 eingestellt wird. Die Flußrate beträgt 3 ml min^{-1}, der Druck 125 bar und die Detektor-Empfindlichkeit 500 Skalenteile.

Ergebnisse und Diskussion

Hydrogencarbonat-Ionen reagieren mit den Dihydrogenphosphat-Ionen der Reagenzlösung unter Verringerung der Wasserstoffionen-Konzentration, der pH-Wert der Meßlösung nimmt mit steigender HCO_3^--Konzentration zu, die Extinktion des Indikators Methylrot bei 520 bzw. 570 nm dagegen nimmt ab [3]. Die Konzentrationen an Methylrot und für KH_2PO_4 in der Reagenzlösung wurden optimiert. Die Extinktionsmessungen ergeben bei 570 nm (mit Filtern) eine etwas geringere Steigung als bei 520 nm (Eichfunktion: $E(520) = -0{,}445\,c + 0{,}956$, $r = 0{,}9983$; $E(570) = -0{,}315\,c + 0{,}64$, $r = 0{,}9996$ mit c in mmol l^{-1}). Die Linearität ist bei 570 nm etwas besser, sie reicht von 1×10^{-4} bis 4×10^{-2} mol l^{-1} (bzw. 5,2 bis 208 mg l^{-1} HCO_3^-).

Der Vergleich der Analysenergebnisse nach vier verschiedenen Analysenverfahren zeigt eine gute Übereinstimmung untereinander (Tabelle 1).

TABELLE 1

Methodenvergleiche zur Hydrogencarbonat-Bestimmung (Trinkwasserproben 1—6: Sösetalsperre u. deren Zuflüsse im Oberharz/BRD)

Verfahren	Hydrogencarbonat-Gehalt (mg l^{-1})					
	1	2	3	4	5	6
Am Ort der Probenahme						
Photometrisch[a] 520 nm	25,9	20,1	36,0	22,9	28,1	13,0
570 nm	26,8	20,1	35,8	22,9	29,9	13,7
Titrimetrisch mit Indikator	29,05	19,0	36,1	21,25	31,4	13,7
Titrimetrisch mit pH-Meter[a]	27,4	19,8	35,8	23,9	29,9	14,0
Im Labor (2 Tage später)						
Titrimetrisch mit Indikator	28,2	19,8	34,5	20,3	29,2	14,4
Titrimetrisch mit pH-Meter	28,1	20,1	37,2	22,6	30,5	13,4
Photometrisch 520 nm	25,9	20,1	36,0	22,9	28,1	13,0
570 nm	26,8	20,1	35,8	22,9	29,9	13,7
Ionen-chromatographisch	28,3	23,3	32,6	22,9	23,6	17,4

[a]Mit batteriebetriebenen Meßgeräten.

Deutliche Unterschiede treten nur bei zwei Proben zwischen dem ionenchromatographischen Verfahren (nach [4]) und den titri- sowie photometrischen Verfahren auf. In bezug auf die Analysenzeit und auch auf die Reproduzierbarkeit ist das photometrische Verfahren dem titrimetrischen überlegen; die relativen Standardabweichungen liegen je nach Konzentration und Stabilität der Probe zwischen 0,5 und 3,0%. In Tabelle 2 sind die Ergebnisse für Oberflächen-, Trink- und Mineral-wässer im Vergleich zwischen

TABELLE 2

Hydrogencarbonat-Bestimmungen in Fluß-, Trink- und Mineralwässern

Wasserprobe		Hydrogencarbonat-Gehalt (mg l^{-1})[a]			
		Photometrisch 520 nm	570 nm	pH-Titration	Titration mit Indikator
Flußwasser (Oberflächen-)	I	37,4	38,1	38,9	39,3
	II	5,3	6,0	5,3	6,1
	III	90,0	91,5	88,5	92,7
	IV	11,2	9,7	11,4	11,0
Trinkwasser (Göttingen)		74,4	74,2	75,7	75,8
Mineralwässer					
"Salzschliefer"[b]		147,4	149,5	145,4	—
"Wildberg-Quelle"[c]		1440	1434	1476	1473
"Caldener"[d]		1475	1535	1515	—

[a]Mittelwert aus 3 Parallelbestimmungen. [b]Soll: 148,5. [c]Soll: 1448. [d]Soll: 1519.

TABELLE 3

Daten zur Optimierung des "Continuous-flow"-Verfahrens

KH_2PO_4 (mol l^{-1})	Methanol (%)	Steigung der Eichgeraden	Korrelationskoeffizient	Linearitätsbereich (mg l^{-1})
Abhängigkeit der Extinktionsmessungen[a] *von der KH_2PO_4-Konzentration*				
0,125	20	1,238	0,9973	12—90
0,100	20	1,653	0,99996	6—60
0,075	20	2,045	0,9958	3—60
0,050	20	2,941	0,9996	3—36
0,025	20	5,481	0,9985	1,5—24
Abhängigkeit der Extinktionsmessungen[a] *von der Methanol-Konzentration in der Reagenzlösung*				
0,100	2	0,829	0,9991	12—72
0,100	10	1,572	0,9953	6—60
0,100	20	1,658	0,9967	6—60
0,100	30	1,756	0,9995	6—60

[a]Messung der Signalhöhen: jeweils 4×10^{-5} mol l^{-1} Methylrot.

photometrischen und titrimetrischen Verfahren zusammengestellt. Eine Veränderung der Hydrogencarbonat-Gehalte innerhalb von zwei Tagen nach der Probenahme wurde nicht festgestellt (Tabelle 1).

Das photometrische Verfahren läßt sich auch automatisieren. Als "Continuous-flow"-Verfahren sind mindestens 60 Proben pro Stunde meßbar. Der Linearitätsbereich ist geringer als beim manuellen Verfahren. Die Ergebnisse aus der Optimierung von KH_2PO_4- und Methanol-Konzentration in der Reagenzlösung sind in Tabelle 3 aufgeführt. Die Nachweisgrenze des Verfahrens liegt bei 0,75 mg l^{-1} Hydrogencarbonat (bzw. 1.25×10^{-5} mol l^{-1}).

LITERATUR

1 K. Salonen, Water Res., 15 (1981) 403.
2 J. Crowther und W. B. Moody, Anal. Chim. Acta, 120 (1980) 305.
3 Y. A. Sinnema, Pharm. Weekbl. Ned., 103 (1968) 837.
4 T. A. Jupille, D. W. Togami und D. E. Burge, Chromatographia, 16 (1982) 312.

Analytica Chimica Acta, 162 (1984) 457
Elsevier Science Publishers B.V., Amsterdam — Printed in The Netherlands

Erratum

D. Littlejohn, I. Duncan, J. Marshall and J. M. Ottaway, Analytical Evaluation of Totally Pyrolytic Graphite Cuvettes for Electrothermal Atomic Absorption Spectrometry.

Anal. Chim. Acta, 157 (1984) 291—302.

p. 292, last line before Table 1 should read:

"TPG has the lowest value of ρD"

p. 299, lines 4 and 5 should read:

". . . measurement, the peak area sensitivity for the TPG cuvette is approximately twice that for the pyro coated cuvette".

Corrected.
280118
Au.

ANALYTICA CHIMICA ACTA, VOL. 162 (1984)

AUTHOR INDEX

Ahmed, N.
— and Koch, K. R.
The liquid—liquid extraction of platinum in the presence of tin(II) chloride from dilute hydrochloric acid into 4-methyl-2-pentanone 347
Alder, J. F., see Fielden, P. R. 85
Alder, J. F., see McCallum, J. J. 75
Al-Tamrah, S. A., see Osibanjo, O. 409
Åström, O., see Nordin-Andersson, I. 9

Batycka, H.
— and Łukaszewski, Z.
Tensammetry with accumulation on the hanging mercury drop electrode. Part 1. The influence of preconcentration potential on the accumulation of poly(ethylene glycols) with various molecular weights 207
Batycka, H.
— and Łukaszewski, Z.
Tensammetry with accumulation on the hanging mercury drop electrode. Part 2. The behaviour of mixtures of poly(ethylene glycols) as an example of surfactant mixtures 215
Biernat, J. F., see Bochéńska, M. 369
Bocheńska, M.
— and Biernat, J. F.
Guanidinium-selective PVC membrane electrodes based on crown ethers 369
Boef, G. den, see Schothorst, R. C. 1
Bond, A. M.
— and Reust, J. B.
A simple pretreatment of urine for the direct differential-pulse anodic stripping voltammetric determination of lead 389
Boniforti, R.
—, Ferraroli, R., Frigieri, P., Heltai, D. and Queirazza, G.
Intercomparison of five methods for the determination of trace metals in sea water 33
Botha, P. V.
— and Fazakas, J.
Some observations on the atomic absorption spectrometry of gallium with electrothermal atomizers 413
Brauer, J. M., see Zsolnay, I. M. 423
Bright, F. V.
— and McGown, L. B.
Elimination of bilirubin interference in fluorimetric determination of fluorescein by phase-resolved fluorescence spectrometry 275
Brinkman, U. A. Th., see Kok, W. Th. 19
Brontman, S. B.
— and Meyerhoff, M. E.
Homogeneous enzyme-linked assays mediated by enzyme antibodies; a new approach to electrode-based immunoassays 363
Buck, R. P., see Coşofreţ, V. V. 357
Burns, D. T.
— and Bushra, M.
The spectrophotometric determination of sulphate after its extraction with methyltricaprylammonium chloride into cyclohexane 443
Burns, D. T.
— and Kheawpintong, S.
The spectrophotometric determination of cobalt by extraction of triphenylsulphonium tetrathiocyanatocobaltate(II) 437
Bushra, M., see Burns, D. T. 443

Cacho, J.
—, Garnica, A. and Nerín, C.
Critical study of metallochromic indicators for calcium 133
Caletka, R.
— and Krivan, V.
Substoichiometric extraction of tantalum with diantipyrylmethane 67
Campion, J. J.
Elimination of iron interference in the differential pulse anodic stripping voltammetry of copper 385
Čapoun, T., see Vytřas, K. 141, 373
Cedergren, A., see Nordin-Andersson, I. 9
Chandler, J. P.

—, Thompson, R. E., Spivey, H. O. and Li, E. L.-F.
An improved computer program for calculating formation constants of ligand complexes from pH data 399
Cicognini, M., see Mussini, T. 103
Cook, K. D., see Klopf, G. J. 293
Coşofreţ, V. V.
— and Buck, R. P.
Bisquaternary-drug membrane electrodes with high sensitivity 357
Covington, A. K., see Mussini, T. 103

Dauyotis, V. E., see Moorhead, E. D. 161
den Boef, G., see Schothorst, R. C. 1
Dewald, H. D., see Wang, J. 189
Drumhiller, J. A.
—, Laing, J. L. and Taylor, R. W.
Spectrophotometric titration of cryptands and complexiметric titration of barium with cryptand (2.2.2) 315
Dunlap, R. B., see McAleese, D. L. 431

Egawa, H., see Maeda, H. 339
Esprit, M.
—, Vandecasteele, C. and Hoste, J.
Determination of fluorine in geological materials by fast neutron activation based on the $^{19}F(n, 2n)^{18}F$ reaction 57

Fazakas, J., see Botha, P. V. 413
Feng, X.
— and Ryan, D. E.
Combination collectors in adsorption colloid flotation for multielement determination in waters by neutron activation 47
Ferraroli, R., see Boniforti, R. 33
Fielden, P. R.
—, McCallum, J. J., Stanios, T. and Alder, J. F.
Detection of toluene diisocyanate with a coated quartz piezoelectric crystal. Part 4. A portable automatic detector with humidity correction 85
Fielden, P. R., see McCallum, J. J. 75
Frank, I. E.
— and Kowalski, B. R.
Prediction of wine quality and geographic origin from chemical measurements by partial least-squares regression modeling 241
Frei, R. W., see Kok, W. Th. 19
Freiser, H., see Trujillo, A. 333
Frigieri, P., see Boniforti, R. 33

Gábor-Klatsmányi, P., see Kopytin, A. V. 123, 133
Garnica, A., see Cacho, J. 113
Gnanasambandan, T., see Trujillo, A. 333
Goo, R., see Kanai, H. 427
Guilbault, G. G., see Suleiman, A. 97

Hartwick, R. A., see Stevenson, J. M. 227
Heltai, D., see Boniforti, R. 33
Hieftje, G. M., see Yuen, A. 403
Hoste, J., see Esprit, M. 57

Ilyin, E. G., see Kopytin, A. V. 133
Inouye, V., see Kanai, H. 427
Izvekov, V. P., see Kopytin, A. V. 123, 133

Jacobsen, E.
— and Tommelstad, T. M.
Differential pulse polarographic determination of pyridoxine in multivitamin tablets 379

Kalous, J., see Vytřas, K. 141, 373
Kalvoda, R.
Adsorptive stripping voltammetry of electroactive organic compounds 197
Kanai, H.
—, Inouye, V. and Goo, R.
Anomalous infrared spectra of diazepam in potassium bromide pellets prepared from chloroform solutions 427
Kheawpintong, S., see Burns, D. T. 437
Klopf, G. J.
— and Cook, K. D.
Surfactant effects on the spectrophotometry of the gadolinium—chrome azurol S complex 293
Koch, K. R., see Ahmed, N. 347
Kok, W. Th.
—, Brinkman, U. A. Th. and Frei, R. W.
On-line electrochemical reagent production for detection in liquid chromatography and continuous flow systems 19
Kopytin, A. V.
—, Gábor-Klatsmányi, P., Izvekov, V. P., Pungor, E. and Ilyin, E. G.
Investigation of ion-selective electrodes based on quaternary phosphonium salts. Part 3. An ion-selective electrode for hexafluorophosphate 133
Kopytin, A. V.
—, Gábor-Klatsmányi, P., Izvekov, V. P.,

Pungor, E. and Yagodin, G. A.
Investigation of ion-selective electrodes based on quaternary phosphonium salts. Part 2. A tetrachlorothallate(III) ion-selective electrode 123
Kowalski, B. R., see Frank, I. E. 241
Krivan, V., see Caletka, R. 67

Laing, J. L., see Drumhiller, J. A. 315
Li, E. L.-F., see Chandler, J. P. 399
Longhi, P., see Mussini, T. 103
Lovelace, R. R., see Potter, N. M. 419
Łukaszewski, Z., see Batycka, H. 215
Lyle, S. J.
— and Za'tar, N. A.
Spectrofluorimetric determination of terbium as its ternary complex with EDTA and tiron. Compositional studies, optimization of fluorescence output and conversion to a flow system 305
Lyle, S. J.
— and Za'Tar, N. A.
Automatic spectrofluorimetric method for the determination of dysprosium as its ternary complex with EDTA and Tiron 447

Maeda, H.
— and Egawa, H.
Preparation of macroreticular chelating resins containing mercapto groups from 2,3-epithiopropyl methacrylate/divinylbenzene copolymer beads and their adsorption capacity 339
McAleese, D. L.
— and Dunlap, R. B.
A sample-drying technique for room-temperature phosphorescence 431
McCallum, J. J., see Fielden, P. R. 85
McCallum, J. J.
—, Fielden, P. R., Volkan, M. and Alder, J. F.
Detection of toluene diisocyanate with a coated quartz piezoelectric crystal. Part 3. Practical coatings for a humidity-corrected detector 75
McGown, L. B., see Bright, F. V. 275
Meyerhoff, M. E., see Brontman, S. B. 363
Moorhead, E. D.
—, Dauyotis, V. E. and Stephens, M. M.
Evaluation of electrochemical charge-transfer rates by using (real) laplace space analysis. Single-potential-step chronoamperometry of hexacyanoferrate(III)/(II) and europium(III)/(II) couples 161
Morel, F. M. M., see Waite, T. D. 263
Mussini, T.
—, Cicognini, M., Longhi, P., Rondinini, S. and Covington, A. K.
Standard pH values for potassium hydrogenphthalate reference buffer solutions in 10, 30 and 50% (w/w) 1,4-dioxane/water mixed solvents at temperatures from 288.15 to 318.15 K 103

Nagashima, K.
— and Suzuki, S.
Solid-state electrochemical detector for carbon monoxide at sub-mg l^{-1} concentrations 153
Nerín, C., see Cacho, J., 113
Nordin-Andersson, I.
—, Åström, O. and Cedergren, A.
Determination of water by flow injection analysis with the Karl Fischer reagent. Minimization of effects caused by differences in physical properties of the samples 9
Nour, S.
— and Vallner, J. J.
An ultraviolet difference spectrophotometric method for determination of drug-binding parameters 323

O'Brien, G. E., see Reardon, P. A. 175
Osibanjo, O.
—, Al-Tamrah, S. A. and Townshend, A.
Molecular emission cavity analysis. Part 26. Determination of total phosphate in detergents 409

Pacey, G. E., see Wu, Y. P. 285
Potter, N. M.
— and Lovelace, R. R.
Determination of boron in engine coolants by direct current plasma atomic emission spectrometry 419
Pungor, E., see Kopytin, A. V. 123, 133

Queirazza, G., see Boniforti, R. 33

Reardon, P. A.
—, O'Brien, G. E. and Sturrock, P. E.
A swept-potential electrochemical detector for flow streams 175
Reust, J. B., see Bond, A. M. 389
Rondinini, S., see Mussini, T. 103

Rössner, B., see Yan, D.-R. 451
Rusling, J. F.
Fitting tabulated current functions to linear-sweep voltammograms 393
Ryan, D. E., see Feng, X. 47

Schothorst, R. C.
—, van Son, M. and den Boef, G.
The application of strongly reducing agents in flow injection analysis. Part 4. Uranium(III) 1
Schwedt, G., see Yan, D.-R. 451
Sojka, S. A., see Zsolnay, I. M. 423
Son, M. van, see Schothorst, R. C. 1
Spivey, H. O., see Chandler, J. P. 399
Stanios, T., see Fielden, P. R. 85
Stephens, M. M., see Moorhead, E. D. 161
Stevenson, J. M.
—, Woodruff, H. B., Tomellini, S. A. and Hartwick, R. A.
Automated rule generation for the program for the analysis of infrared spectra (pairs) 227
Sturrock, P. E., see Reardon, P. A. 175
Suleiman, A.
— and Guilbault, G. G.
A coated piezoelectric crystal detector for phosgene 97
Suzuki, S., see Nagashima, K. 153

Taylor, R. W., see Drumhiller, J. A. 315
Thijssen, P. C.
A Kalman filter for calibration, evaluation of unknown samples and quality control in drifting systems. Part 2. Optimal designs 253
Thompson, R. E., see Chandler, J. P. 399
Tomellini, S. A., see Stevenson, J. M. 227
Tommelstad, T. M., see Jacobsen, E. 379
Townshend, A., see Osibanjo, O. 409
Trujillo, A.
—, Gnanasambandan, T. and Freiser, H.
Determination of organophosphorus compounds by dye-assisted chromatography 333

Vallner, J. J., see Nour, S. 323
Vandecasteele, C., see Esprit, M. 57
van Son, M., see Schothorst, R. C. 1
Volkan, M., see McCallum, J. J. 75
Vytřas, K.
—, Čapoun, T. and Kalous, J.
Ion-selective electrodes in titrations involving azo-coupling reactions. Part 3. Indirect determination of slowly reacting components 373
Vytřas, K.
—, Kalous, J. and Čapoun, T.
Ion-selective electrodes in titrations involving azo-coupling reactions. Part 2. Titrations with diazonium salts derived from 1-aminonaphthalenes and 1-amino-9,10-anthraquinone 141

Waite, T. D.
— and Morel, F. M. M.
Ligand exchange and fluorescence quenching studies of the fulvic acid-iron interaction. Effects of pH and light 263
Wang, J.
— and Dewald, H. D.
Theoretical and experimental aspects of the response of stripping voltammetry in flow injection systems 189
Woodruff, H. B., see Stevenson, J. M. 227
Wu, Y. P.
— and Pacey, G. E.
Spectrophotometric determination of lithium ion with the chromogenic crown ether, 2″,4″-dinitro-6″-trifluoromethylphenyl-4′-aminobenzo-14-crown-4 285

Yagodin, G. A., see Kopytin, A. V. 123
Yan, D.-R.
—, Rössner, B. and Schwedt, G.
Vergleichende untersuchungen zur titrimetrischen, photometrischen und ionenchromatographischen hydrogen-carbonat-bestimmung in trink- und mineralwässern 451
Yuen, A.
— and Hieftje, G. M.
Burnt-gas composition of the helium—oxygen—acetylene flame 403

Za'tar, N. A., see Lyle, S. J. 305, 447
Zsolnay, I. M.
—, Brauer, J. M. and Sojka, S. A.
X-ray fluorescence determination of trace elements in soil 423

ACA announcements

ANNOUNCEMENTS OF MEETINGS

21st INTERNATIONAL SYMPOSIUM ON ADVANCES IN CHROMATOGRAPHY, OSLO, NORWAY, JUNE 3–6, 1985

The above symposium will be held at the Hotel Scandinavia in Oslo, Norway. The scope of the meeting will cover papers, poster sessions and informal discussion groups by outstanding researchers from throughout the world in all fields of chromatography. In particular, new developments in gas, liquid, supercritical fluid and thin-layer chromatography will be included. There will also be a commercial exhibition of the latest instrumentation and books. Participation in the symposium will be on the basis of invited papers as well as unsolicited contributions. Authors desiring to present papers or posters must submit 200-word abstracts by December 1st, 1984. Complete manuscripts of accepted authors will be due on June 3rd, 1985 at the meeting in Oslo. All correspondence pertaining to the symposium and exhibition space should be directed to: Prof. A. Zlatkis, Chemistry Department, University of Houston, Houston, TX 77004, U.S.A. Tel.: (713) 749-2623.

2nd INTERNATIONAL SYMPOSIUM ON THE SYNTHESIS AND APPLICATIONS OF ISOTOPICALLY LABELLED COMPOUNDS, KANSAS CITY, MO, U.S.A., SEPTEMBER 3–7, 1985

The above symposium will be held at the new Vista Hotel, Kansas City, MO, U.S.A.

The object of the symposium is to provide a forum for the exchange of information between leading scientists involved in the synthesis and applications of isotopically (radioactive and stable) labeled compounds. The symposium will include a scientific exhibit. Topics will encompass synthesis, analysis, purification, and storage of isotopically labeled compounds and their applications in biomedical, clinical and environmental studies as well as metabolism, pharmacokinetics and toxicology.

Further information regarding submission of papers and registration can be obtained from Dr. Donald Wilk, Symposium Coordinator, School of Pharmacy, 5100 Rockhill Road, Kansas City, MO 64110, U.S.A. Tel.: (816) 276-1616.

30th INTERNATIONAL CONGRESS OF PURE AND APPLIED CHEMISTRY, MANCHESTER, U.K., SEPTEMBER 9–13, 1985

The 30th IUPAC Congress is being organised by the Royal Society of Chemistry, on behalf of IUPAC. Eight sections form the basis for the congress: (1) Analytical: Current Progress in Analytical Chemistry; (2) Education; (3) Industrial: Chemical Industry-Year 2001; (4) Inorganic; (5) Organic: Organic Chemistry as a Life Science; (6) Organic: Dyestuffs-Past, Present and Future; (7) Physical: Advances in Physical and Theoretical Chemistry; (8) Physical/Analytical: New Electrochemical Sensors.

Those persons who have already accepted invitations to give main lecturers have been announced. All sections are seeking posters, for which ample space will be available, and oral (shorter) contributions are sought for sections 2, 7 and 8. Persons wishing to offer an oral contribution or poster must submit a title and short synopsis (not more than 100 words) indicating the section concerned not later than 31 October 1984 for oral contributions; and not later than 28 February 1985 for posters.

For further information, please contact: Dr. John. F. Gibson, 30th IUPAC Congress, Royal Society of Chemistry, Burlington House, London W1V 0BN, U.K.

2nd SYMPOSIUM ON HANDLING OF ENVIRONMENTAL AND BIOLOGICAL SAMPLES IN CHROMATOGRAPHY, FREIBURG, F.R.G., OCTOBER 24–25, 1985

The organisation of this second event – the first was held in Lausanne, Switzerland in November 1983 – is in the hands of the International Association of Environmental Analytical Chemistry and sponsored by national bodies. A strong industrial participation is planned. It is the intention to bring together specialists in this field who can give a good account of the state-of-art in their respective specialty and to present first-hand experience in sample handling. Continuous flow extraction techniques, solid surface sample handling with pre-column technology (on-line and off-line), pre-chromatographic use of derivatization techniques, column-switching methodology for handling of complex samples are some of the topics that will be treated and extensively discussed. Special emphasis will be placed on techniques with automation potential and actually automated procedures suitable for ruitine handling of larger series of samples. Much of this methodology and "philosophy" can be applied to different types of matrices and problem solving but it is the intention to concentrate on applications to biological (urine, blood, tissue, plant material) and environmental samples (water, waste water, air) with drugs (pharmaceuticals) and priority pollutants as the analytes.

Further information from: Workshop Office IAEAC, M. Frei-Hausler, Postfach 46, CH-4123 Allschwil 2, Switzerland.

CALENDAR OF FORTHCOMING MEETINGS

Nov. 13–16, 1984 New York, NY, U.S.A.	**23rd Annual Eastern Analytical Symposium** Contact: Dr. S. David Klein, EAS Publicity, Merck & Co., Inc., P.O. Box 2000/R80L-106, Rahway, NJ 07065, U.S.A. Tel.: (201) 846-1582. (Further details published in Vol. 157, No. 1.)
Nov. 19–24, 1984 Barcelona, Spain	**EXPOQUIMIA 84 – Salón Internacional de la Quimica** Contact: EXPOQUIMIA, Feria de Barcelona, Barcelona 4, Spain.
Nov. 21–23, 1984 Barcelona, Spain	**14th Annual Symposium on Analytical Chemistry of Pollutants** Contact: 3rd International Congress on Analytical Techniques in Environmental Chemistry/EXPOQUIMIA, Av. Reina Ma. Christina, Palacio No. 1, Barcelona 4, Spain. Tel.: 223.31.01; telex: 50458 FOIMB-E.
Nov. 21–23, 1984 Barcelona, Spain	**3rd International Congress on Analytical Techniques in Environmental Chemistry** Contact: 3rd International Congress on Analytical Techniques in Environmental Chemistry/EXPOQUIMIA, Av. Reina Ma. Christina, Palacio No. 1, Barcelona 4, Spain. Tel.: 223.31.01; telex: 50458 FOIMB-E. (Further details published in Vol. 157, No. 1.)
Dec. 10–12, 1984 Baltimore, MD, U.S.A.	**4th International Symposium on HPLC of Proteins, Peptides, and Polynucleotides** Contact: Shirley E. Schlessinger, Symposium Manager, Fourth International Symposium on HPLC of Proteins, Peptides, and Polynucleotides, 400 East Randolph, Chicago, IL 60601, U.S.A. Tel.: (312) 527-2011.
Jan. 7–11, 1985 Leysin, Switzerland	**1985 European Winter Conference on Plasma Spectrochemistry** Contact: Prof. J.M. Mermet, Plasma Conference, Service Central d'Analyse, CNRS, B.P. 22, F-69390 Vernaison, France. (Further details published in Vol. 159.)

Feb. 25–March 1, 1985 New Orleans, LA, U.S.A.	**36th Pittsburgh Conference and Exposition on Analytical Chemistry and Applied Spectroscopy** Contact: Linda Biggs, Pittsburgh Conference, 437 Donald Road, Dept. J-005, Pittsburgh, PA 15235, U.S.A.
April 15–19, 1985 Pretoria, South Africa	**IUPAC Symposium on Analytical Chemistry in the Exploration, Mining and Processing of Materials** Contact: The Symposium Secretariat, S. 328, CSIR, P.O. Box 395, Pretoria 0001, South Africa. Tel.: (012) 86-9211.4412 or (012) 86-9211.2077. Telex: 3630 SA.
April 28–May 3, 1985 Miami Beach, FL, U.S.A.	**189th National Meeting of the American Chemical Society** Contact: Meetings Department, American Chemical Society, 1155 Sixteenth Street, NW, Washington, DC 20036, U.S.A.
June 3–6, 1985 Oslo, Norway	**21st International Symposium on Advances in Chromatography** Contact: Prof. A. Zlatkis, Chemistry Department, University of Houston, Houston, TX 77004, U.S.A. Tel.: (713) 749-2623. Telex.: 762878
June 9–15, 1985 Frankfurt am Main, F.R.G.	**ACHEMA 85, 21st Exhibition-Congress on Chemical Engineering** Contact: DECHEMA, Organisation ACHEMA, Postfach 970146, D-6000 Frankfurt am Main 97, F.R.G. Tel.: (06 11) 75 64-0241/242. Telex: 412 490 dcha d.
June 19–21, 1985 Snowmass, CO, U.S.A.	**Silanes, Surfaces and Interfaces** Contact: Mail Stop CO2430, Dow Corning Corporation, Midland, MI 48640, U.S.A.
July 1–5, 1985 Edinburgh, Scotland, U.K.	**9th International Symposium on Column Liquid Chromatography** Contact: J.H. Knox, Department of Chemistry, University of Edinburgh, Edinburgh EH9 3JJ, Scotland, U.K.
Sept. 3–7, 1985 Kansas City, MO, U.S.A.	**2nd International Symposium on the Synthesis and Applications of Isotopically Labeled Compounds** Contact: Dr. D. Wilk, Symposium Coordinator, School of Pharmacy, 5100 Rochill Road, Kansas City, MO 64110, U.S.A. Tel.: (816) 276-16160.
Sept. 5–8, 1985 Birmingham, U.K.	**Flow Analysis III – An International Conference on Flow Analysis** Contact: Flow Analysis III, Dr. A.M.G. Macdonald, Department of Chemistry, The University, P.O. Box 363, Birmingham B15 2TT, U.K. (Further details published in Vol. 159.)
Sept. 8–13, 1985 Chicago, IL, U.S.A.	**190th National Meeting of the American Chemical Society** Contact: Meetings Department, American Chemical Society, 1155 Sixteenth Street, NW, Washington, DC 20036, U.S.A.
Sept. 9–13, 1985 Manchester, U.K.	**30th International Congress of Pure and Applied Chemistry** Contact: The Royal Society of Chemistry, Burlington House, London W1V 0BN, U.K. (Further details published in Vol. 155.)
Sept. 15–21, 1985 Garmisch-Partenkirchen, F.R.G.	**Colloquium Spectroscopicum Internationale XXIV** Contact: CSI XXIV, Organisationsbüro, Institut für Spektrochemie und angewandte Spektroskopie, Postfach 778, D 4600 Dortmund 1, F.R.G.
Sept. 16–19, 1985 Bradford, U.K.	**Particle Size Analysis 1985** Contact: Dr. T. Allen, School of Powder Technology, University of Bradford, Bradford, West Yorkshire BD7 1DP, U.K. Tel.: (0274) 733466 ext. 382/380.

Oct. 24–25, 1985 Freiburg, F.R.G.	**2nd Symposium on Handling of Environmental and Biological Samples in Chromatography** Contact: Workshop Office IAEAC, M. Frei-Hausler, Postfach 46, CH-4123 Allschwil 2, Switzerland.
Nov. 11–16, 1985 Yalta, U.S.S.R.	**5th Danube Symposium on Chromatography** Contact: Dr. L.N. Kolomiets, The Scientific Council of Chromatography, Academy of Sciences of the U.S.S.R., Institute of Physical Chemistry, Lenin-Prospect 31, Moscow 117312, U.S.S.R.
Jan. 3–10, 1986 Maui, HI, U.S.A.	**1986 Winter Conference on Plasma Spectrochemistry** Contact: 1986 Winter Conference, c/o ICP Information Newsletter, Department of Chemistry, GRC Towers, University of Massachusetts, Amherst, MA 01003-0035, U.S.A. Tel.: (413) 545-2294.
July 20–26, 1986 Bristol, U.K.	**SAC 86 – International Conference and Exhibition on Analytical Chemistry** Contact: Miss P.E. Hutchinson, Royal Society of Chemistry, Analytical Division, Burlington House, London W1V 0BN, U.K. Tel.: (01) 734-9971.
Aug. 25–29, 1986 Antwerp, Belgium	**10th International Symposium on Microchemical Techniques** Contact: Dr. R. Dewolfs, University of Antwerp (UIA), Department of Chemistry, Universiteitsplein 1, B-2610 Wilrijk, Belgium. Tel.: 03/828.25.28 (ext. 204). Telex: 33646

SCIENTOMETRICS

(Including the Journal of Research Communication Studies)

An International Journal for All Quantitative Aspects of the Science of Science, Communication in Science, and Science Policy

Aims and Scope:
This periodical aims to provide an international forum for communications dealing with the results of research into the quantitative characteristics of science. Emphasis is placed on investigations in which the development and mechanism of science are studied by means of mathematical (statistical) methods.

Since Vol. 4 No. 4, SCIENTOMETRICS incorporates the *Journal of Research Communication Studies*, the aim of which was to serve as a medium of communication for authors, editors, publishers, conference organizers and all others involved in the transfer of research information.

The fields covered by both journals are relatively new but their growing importance is becoming increasingly recognized. Furthermore, it has become clear that studies on the nature of scientific research and its effects on the world in which we live are inextricably linked with the methods of dissemination of the knowledge resulting from that research. It therefore seemed appropriate for the two journals to combine forces and merge editorial boards; the scope of the new SCIENTOMETRICS has been extended to bring the results of research investigations together in one place, in such a form that they will be of use not only to the investigators themselves but also to the research workers who form the object of these studies.

Some Recently Published Articles...

A Quantitative Analysis of Indian Science and Technology Manpower Employment and Economic Development,
A.R. Rajeswari (India)

Citation Analysis of Physics Journals: Comparison of Subfields of Physics,
N. Midorikawa (Japan)

The "Rank Distortion" Effect and Non-Gaussian Nature of Scientific Activities,
S.D. Haitun (USSR)

The Author Cocitation Structure of Macroeconomics,
Katherine W. McCain (U.S.A.)

Condensed Matter Physics Journals,
R. Todorov (Bulgaria)

A Classification of Citation Roles for the Social Sciences and Related Fields,
Bluma C. Peritz (Israel)

Citation Study of a Scientific Revolution: Sudden Infant Death Syndrome. 1. The New Paradigm,
J.G. Gregory (New Zealand)

Are Methodological Papers more Cited than Theoretical or Empirical Ones? The Case of Sociology,
B.C. Peritz (Israel)

Stochastic Model for Innovation and Resulting Skew Distribution for Technological Concentration with Verification in Japanese Industry,
H. Eto, K. Makino (Japan)

Language Use Patterns in the Fisheries Periodical Literature,
R.B. Baldauf, Jr. B.H. Jernudd (U.S.A.)

Migration of Physicist to other Academic Disciplines: Situation in The Netherlands,
J. Van Houton, H.G. Van Vuren, C. Le Pair, G. Dijkhuis (The Netherlands)

Subscription Information
1984: Vol. 6 (6 issues)
US $ 81.25/Dfl. 211.00.
including postage.

ELSEVIER

P.O. Box 211,
1000 AE Amsterdam,
The Netherlands

P.O. Box 1663,
Grand Central Station,
New York, NY 10163

The Dutch guilder price is definitive. US $ prices are subject to exchange rate fluctuations.

(*Continued from inside back cover*)

Short Communications

Bisquaternary-drug membrane electrodes with high sensitivity
V. V, Coşofreţ and R. P. Buck (Chapel Hill, NC, U.S.A.) . . . 357
Homogeneous enzyme-listed assays mediated by enzyme antibodies; a new approach to electrode-based immunoassays
S. B. Brontman and M. E. Meyerhoff (Ann Arbor, MI, U.S.A.) . . . 363
Guanidinium-selective PVC membrane electrodes based on crown ethers
M. Bocheńska and J. F. Biernat (Gdańsk, Poland) . . . 369
Ion-selective electrodes in titrations involving azo-coupling reactions. Part 3. Indirect determination of slowly reacting components
K. Vytřas, T. Čapoun and J. Kalous (Pardubice, Czechoslovakia) . . . 373
Differential pulse polarographic determination of pyridoxine in multivitamin tablets
E. Jacobsen and T. M. Tommelstad (Oslo, Norway) . . . 379
Elimination of iron interference in the differential pulse anodic stripping voltammetry of copper
J. J. Campion (New Paltz, NY, U.S.A.) . . . 385
A simple pretreatment of urine for the direct differential-pulse anodic stripping voltammetric determination of lead
A. M. Bond and J. B. Reust (Deakin, Victoria, Australia) . . . 389
Fitting tabulated current functions to linear-sweep voltammograms
J. F. Rusling (Storrs, CT, U.S.A.) . . . 393
An improved computer program for calculating formation constants of ligand complexes from pH data
J. P. Chandler, R. E. Thompson, H. O. Spivey and E. L.-F. Li (Stillwater, OK, U.S.A.) . . . 399
Burnt-gas composition of the helium–oxygen–acetylene flame
A. Yuen and G. M. Hieftje (Bloomington, IN, U.S.A.) . . . 403
Molecular emission cavity analysis. Part 26. Determination of total phosphate in detergents
O. Osibanjo, S. A. Al-Tamrah (Birmingham, Great Britain) and A. Townshend (Hull, Great Britain) . . . 409
Some observations on the atomic absorption spectrometry of gallium with electrothermal atomizers
P. V. Botha and J. Fazakas (Bucharest, Rumania) . . . 413
Determination of boron in engine coolants by direct current plasma atomic emission spectrometry
N. M. Potter (Warren, MI, U.S.A.) and R. R. Lovelace (Pontiac, MI, U.S.A.) . . . 419
X-ray fluorescence determination of trace elements in soil
I. M. Zsolnay, J. M. Brauer and S. A. Sojka (Grand Island, NY, U.S.A.) . . . 423
Anomalous infrared spectra of diazepam in potassium bromide pellets prepared from chloroform solutions
H. Kanai, V. Inouye and R. Goo (Honolulu, HI, U.S.A.) . . . 427
A sample-drying technique for room-temperature phosphorescence
D. L. McAleese and R. B. Dunlap (Columbia, SC, U.S.A.) . . . 431
The spectrophotometric determination of cobalt by extraction of triphenyl-sulphonium tetrathiocyanatocobaltate(II)
D. T. Burns and S. Kheawpintong (Belfast, Northern Ireland) . . . 437
The spectrophotometric determination of sulphate after its extraction with methyltricaprylammonium chloride into cyclohexane
D. T. Burns and M. Bushra (Belfast, Northern Ireland) . . . 443
Automatic spectrofluorimetric method for the determination of dysprosium as its ternary complex with EDTA and Tiron
S. J. Lyle and N. A. Za'Tar (Canterbury, Great Britain) . . . 447
Vergleichende untersuchungen zur titrimetrischen, photometrischen und ionen-chromatographischen hydrogencarbonat-bestimmung in trink- und mineralwässern
D.-R. Yan, B. Rössner und G. Schwedt (Göttingen, West Germany) . . . 451

Erratum . . . 457

Author Index . . . 459

(*Continued from outside back cover*)

Evaluation of electrochemical charge-transfer rates by using (real) laplace space analysis. Single potential-step chronoamperometry of hexacyanoferrate(III)/(II) and europium(III)/(II) couples
E. D. Moorhead, V. E. Dauyotis and M. M. Stephens (Lexington, KY, U.S.A.) . . . 161
A swept-potential electrochemical detector for flow streams
P. A. Reardon, G. E. O'Brien and P. E. Sturrock (Atlanta, GA, U.S.A.) . . . 175
Theoretical and experimental aspects of the response of stripping voltammetry in flow injection systems
J. Wang and H. D. Dewald (Las Cruces, NM, U.S.A.) . . . 189
Adsorptive stripping voltammetry of electroactive organic compounds
R. Kalvoda (Prague, Czechoslovakia) . . . 197
Tensammetry with accumulation on the hanging mercury drop electrode. Part 1. The influence of preconcentration potential on the accumulation of poly(ethylene glycols) with various molecular weights
H. Batycka and Z. Łukaszewski (Poznań, Poland) . . . 207
Tensammetry with accumulation on the hanging mercury drop electrode. Part 2. The behaviour of mixtures of poly(ethylene glycols) as an example of surfactant mixtures
H. Batycka and Z. Łukaszewski (Poznań, Poland) . . . 215

Computer Methods and Applications
Automated rule generation for the program for the analysis of infrared spectra (pairs)
J. M. Stevenson, H. B. Woodruff (Rahway, NJ, U.S.A.), S. A. Tomellini and R. A. Hartwick (New Brunswick, NJ, U.S.A.) . . . 227
Prediction of wine quality and geographic origin from chemical measurements by partial least-squares regression modeling
I. E. Frank and B. R. Kowalski (Seattle, WA, U.S.A.) . . . 241
A Kalman filter for calibration, evaluation of unknown samples and quality control in drifting systems. Part 2. Optimal designs
P. C. Thijssen (Nijmegen, The Netherlands) . . . 253

Optical Methods
Ligand exchange and fluorescence quenching studies of the fulvic acid-iron interaction. Effects of pH and light
T. D. Waite and F. M. M. Morel (Cambridge, MA, U.S.A.) . . . 263
Elimination of bilirubin interference in fluorimetric determination of fluorescein by phase-resolved fluorescence spectrometry
F. V. Bright and L. B. McGown (Stillwater, OK, U.S.A.) . . . 275
Spectrophotometric determination of lithium ion with the chromogenic crown ether, 2",4"-dinitro-6"-trifluoromethylphenyl-4'-aminobenzo-14-crown-4
Y. P. Wu and G. E. Pacey (Oxford, OH, U.S.A.) . . . 285
Surfactant effects on the spectrophotometry of the gadolinium–chrome azurol S complex
G. J. Klopf and K. D. Cook (Urbana, IL, U.S.A.) . . . 293
Spectrofluorimetric determination of terbium as its ternary complex with EDTA and tiron. Compositional studies, optimization of fluorescence output and conversion to a flow system
S. J. Lyle and N. A. Za'tar (Canterbury, Great Britain) . . . 305
Spectrophotometric titration of cryptands and complexiметric titration of barium with cryptand (2.2.2)
J. A. Drumhiller, J. L. Laing and R. W. Taylor (Norman, OK, U.S.A.) . . . 315
An ultraviolet difference spectrophotometric method for determination of drug-binding parameters
S. Nour and J. J. Vallner (Athens, GA, U.S.A.) . . . 323

Separations
Determination of organophosphorus compounds by dye-assisted chromatography
A. Trujillo, T. Gnanasambandan and H. Freiser (Tucson, AZ, U.S.A.) . . . 333
Preparation of macroreticular chelating resins containing mercapto groups from 2,3-epithiopropyl methacrylate/divinylbenzene copolymer beads and their adsorption capacity
H. Maeda and H. Egawa (Kumamoto, Japan) . . . 339
The liquid–liquid extraction of platinum in the presence of tin(II) chloride from dilute hydrochloric acid into 4-methyl-2-pentanone
N. Ahmed and K. R. Koch (Rondebosch, South Africa) . . . 347

(Continued on facing pag

CONTENTS

(Abstracted, Indexed in: Anal. Abstr.; Biol. Abstr.; Chem. Abstr.; Curr. Contents Phys. Chem. Earth Sci.; Life Sci.; Index Med.; Mass Spectrom. Bull.; Sci. Citation Index; Excerpta Med.)

General Analytical Chemistry

The application of strongly reducing agents in flow injection analysis Part 4. Uranium (III)
R. C. Schothorst, M. van Son and G. den Boef (Amsterdam, The Netherlands) 1

Determination of water by flow injection analysis with the Karl Fischer reagent. Minimization of effects caused by differences in physical properties of the samples
I. Nordin-Andersson, O. Åström and A. Cedergren (Umea, Sweden) 9

On-line electrochemical reagent production for detection in liquid chromatography and continuous flow systems
W. Th. Kok, U. A. Th. Brinkman and R. W. Frei (Amsterdam, The Netherlands) 19

Intercomparison of five methods for the determination of trace metals in sea water
R. Boniforti (La Spezia, Italy), R. Ferraroli, P. Frigieri, D. Heltai and G. Queirazza (Milan, Italy) 33

Combination collectors in adsorption colloid flotation for multielement determination in waters by neutron activation
X. Feng and D. E. Ryan (Halifax, Nova Scotia, Canada) 47

Determination of fluorine in geological materials by fast neutron activation based on the $^{19}F(n,2n)^{18}F$ reaction
M. Esprit, C. Vandecasteele and J. Hoste (Gent, Belgium) 57

Substoichiometric extraction of tantalum with diantipyrylmethane
R. Caletka and V. Krivan (Ulm-Donau, West Germany) 67

Detection of toluene diisocyanate with a coated quartz piezoelectric crystal Part 3. Practical coatings for a humidity-corrected detector
J. J. McCallum, P. R. Fielden, M. Volkan and J. F. Alder (Manchester, Great Britain) 75

Detection of toluene diisocyanate with a coated quartz piezoelectric crystal Part 4. A portable automatic detector with humidity correction
P. R. Fielden, J. J. McCallum, T. Stanios and J. F. Alder (Manchester, Great Britain 85

A coated piezoelectric crystal detector for phosgene
A. Suleiman and G. G. Guilbault (New Orleans, LA, U.S.A.) 97

Standard pH values for potassium hydrogenphthalate reference buffer solutions in 10, 30 and 50% (w/w 1, 4-dioxane/water mixed solvents at temperatures from 288.15 to 318.15 K
T. Mussini, M. Cicognini, P. Longhi, S. Rondinini (Milan, Italy) and A. K. Covington (Newcastle upon Tyne, Great Britain) 103

Critical study of metallochromic indicators for calcium
J. Cacho, A. Garnica and C. Nerín (Zaragoza, Spain) 113

Electrometric Methods

Investigation of ion-selective electrodes based on quaternary phosphonium salts Part 2. A tetrachlorothallate (III) ion-selective electrode
A. V. Kopytin, P. Gábor-Klatsmányi, V. P. Izvekov, E. Pungor (Budapest, Hungary) and G. A. Yagodin (Moscow, U.S.S.R.) 123

Investigation of ion-selective electrodes based on quaternary phosphonium salts Part 3. An ion-selective electrode for hexafluorophosphate
A. V. Kopytin, P. Gábor-Klatsmányi, V. P. Izvekov, E. Pungor (Budapest, Hungary) and E. G. Ilyin (Moscow, U.S.S.R.) 133

Ion-selective electrodes in titrations involving azo-coupling reactions Part 2. Titrations with diazonium salts derived from 1-aminonaphthalenes and 1-amino-9, 10-anthraquinone
K. Vytřas, J. Kalous and T. Čapoun (Pardubice, Czechoslovakia) 141

Solid-state electrochemical detector for carbon monoxide at sub-ppm concentrations
K. Nagashima and S. Suzuki (Tokyo, Japan) 153

(Continued on inside back cover)